The supramolecular chemistry of handcuff rotaxanes and deteriorating leather

Marysia Tarnowska

January 2023

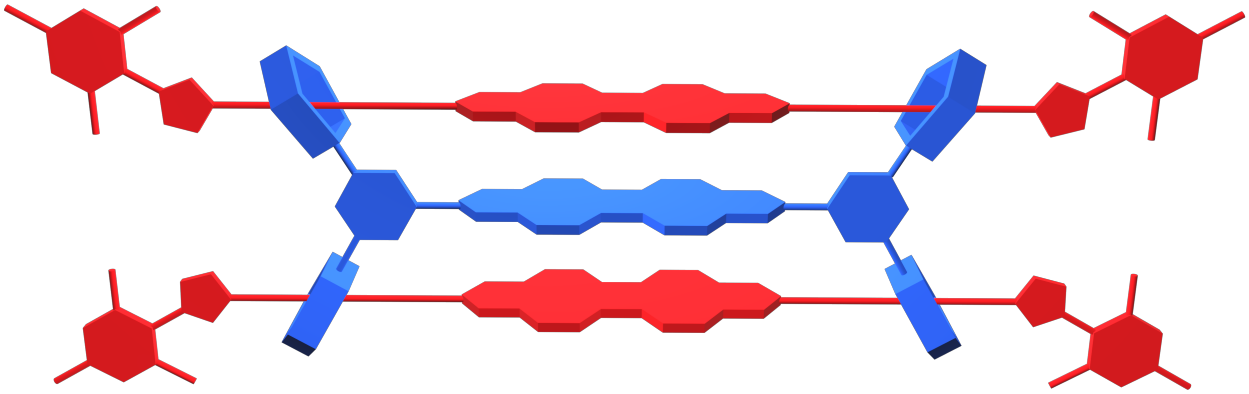

Thesis submitted to the University of Nottingham for the Degree of Doctor of Philosophy

Declaration

I declare that all of the work in this thesis is my own other than when explicitly acknowledged. This work has not previously been used to obtain any other academic qualification than this one.

The research into handcuff rotaxanes was funded through the University of Nottingham scholarships and the research into leather was funded through a separate EPSRC IAA grant I won specifically for this purpose and conducted in collaboration with the Natural History Museum.

Marysia Tarnowska

Acknowledgements

Many thanks to Neil Champness for his supervision and support in the early and middle stages of the handcuff project, for designing and developing such an interesting project to work on, and for our many enjoyable discussions about both the chemistry and the world in general.Thank you also to Ben Pilgrim for taking over the supervisory role in the later stages of the project, and especially for helping redesign aspects of the handcuff project to be more tractable following the disruption of the pandemic and my medical leave.

Much of the work done on the handcuff project was elevated and enriched by discussions and interactions with members of both the Champness and Pilgrim groups, especially Nic Pearce, Georgia Orton, Mark Newman, Arjun Patel and Martin Black, or through comparison with previous work by Phil Langer.

I thank Rosie Young and Stephen Argent for teaching me about and helping me with X-ray crystallography. I also would like to thank Stephen Davies for all his help with the spectroelectrochemistry. It would truly not have been possible without him. Meanwhile, Nick Kindon was invaluable when it came to organic synthesis and purification troubleshooting.

The leather part of this thesis comes with a whole new set of wonderful people I'd like

to thank. This project would not have even begun without Nick Bennett and his help with winning the EPSRC IAA grant for it or his advice about how to lead it. My collaborators at the Natural History Museum: Wren Montgomery, Konstantina Konstantinidou and Innes Clatworthy have made the sample collection and sample analysis possible and were also a joy to work with. I also received lots of help and additional samples from Graham Lampard of the Museum of Leathercraft, Rosie Bolton and Arianne Panton of the Leather Conservation Centre and Annie Lama and Stefan Davis of the University of Northampton.

I'd like to also thank Claire Housley for her unending support during and following the Champness group's departure from Nottingham, as well as Vihanga Munasinghe and Suzanne Jansze for making the WISC Mentoring experience so warm and supportive.

Finally, I'd like to thank Chris, my partner, and Gabi, an old friend, both of whom supported me the entire time.

Abstract

Supramolecular chemistry deals with systems made of distinct chemical species which, when put together, have different properties than each individual component. These species are often not bonded in a covalent or ionic sense, but are based on host-guest chemistry. Mechanically interlocked molecules (MIMs) and handcuff rotaxanes in particular, which are systems containing multiple covalently bonded macrocycles, through which a rod is threaded then stoppered, are an example of such species. MIMs have wide ranging applications in nanoscale electronics, systems which mimic biology, and many others. Since its recent discovery, pillar[5]arene has been used extensively in MIMs due to its interesting host-guest properties, and this work deals with handcuff rotaxanes containing it, as well as perylene diimide (PDI), tetrazine, and imidazole groups.

The feasibility of the synthesis of a three-membered PDI cofacial stack or a 'triple decker handcuff rotaxane', using a templated, clipping method, utilising interactions between PDI cores and between pillar[5]arenes and imidazole groups, is investigated. The difficulty in this lies in the synthesis of a 'linker' that can connect two pillar[5]arene macrocycles and also the PDI core of the macrocycle based component of the handcuff rotaxane. Various methods of amine alkylation, amide coupling and ether synthesis were explored to connect the functionalised pillar[5]arenes together, but due to the difficulties with pillar[5]arene syntheses and purifications they were all unsuccessful in either of those steps. However, novel pillar[5]arene-based species were successfully synthesised in this part of the project and fully or partially characterised.

Next, a simpler cofacial stack of a PDI and a tetrazine based on handcuff rotaxane topology was attempted but was unsuccessful due to the low solubility of pillar[5]arene-based species in solvents required for the tetrazine forming reaction. However, during this part of the project two new functionalised pillar[5]arenes were synthesised and characterised and attempts at optimising these syntheses were made.

Finally, a handcuff rotaxane containing only one PDI species was successfully synthesised and characterised. Its properties were probed using cyclic voltammetry, spectroelectrochem-

istry and electron paramagnetic resonance spectroscopy and compared with similar handcuff rotaxanes previously synthesised in the group. The lack of stacking species in this handcuff proved a previously postulated hypothesis that the synthesis method here described only requires templating between the host's macrocycles and the threading guest. This does however, lower the yields relative to species with additional molecular recognition sites.

The thus far described part of this work explored and celebrated the organic synthesis of supramolecular structures, while the second part focuses on spectroscopic analysis of supramolecular systems. The systems in question are the collagen-tannin matrices found in leather, and more specifically in deteriorated leather book bindings from the Natural History Museum. As such the two parts of this thesis are only related due to dealing with supramolecular structures and should be interpreted separately.

This second project explored a leather acidic deterioration process known to conservators as red rot. Red rot affects leather book bindings from the late 19^{th} and early 20^{th} centuries and causes them to become dry and reddish, or in advanced stages crumble into a dark powder.

This project set out to explore health and safety aspects of red rot dust using various spectroscopic techniques and suggest further necessary tests. This was evaluated using Inductively Coupled Plasma analysis (Optical Emission Spectroscopy and Mass Spectrometry), in comparison with permissible heavy metal content in samples as defined by a commercial certification body, OEKO TEX. For the tested samples, it was found that arsenic, cadmium and lead were not within the permissible limits and hence caution when handling these items is recommended.

Furthermore, this work aimed to understand more about the red rot deterioration process by comparing undeteriorated and deteriorated leather samples with Fourier Transform Infrared spectroscopy and Scanning Electron Microscopy. No features present in red rot but absent in other types of deterioration were found, however, this work recommends gas chromatography as another technique that might achieve this.

Finally, this work attempts to quantify the degree of deterioration of bindings suffering from red rot through an FTIR peak ratios. Such a ratio is explored and found to relate to

visually assessed levels of degradation. However it is not certain that this is a red rot specific ratio and not a general degradation ratio.

This work allowed for health and safety recommendations to be made to the museum, as well as for a deeper understanding of the red rot deterioration process to be obtained.

List of abbreviations and acronyms

18C6 - 18-crown-6

ATR-FTIR - attenuated total reflectance - fourier transform infrared

BPP34C10 - bisparaphenylene-34- crown-10

Boc - *tert*-butoxycarbonyl protecting group

BrP24C8 - bromopyrido[24]crown-8

CBPQT - cyclobis(paraquat-p- phenylene)

CDI - carbonyldiimidazole

COSY - ^{1}H–^{1}H correlated spectroscopy

CV - cyclic voltammetry

DB24C8 - dibenzo[24]crown-8

DBB224C82 - dibenzobicyclo[2.2.2]octane-bridged macrotricyclic [24]crown-8 dimer

DCE - dichloroethane

DMF - N, N-dimethylformamaide

DOSY - diffusion ordered spectroscopy

DP24C8 - dipyrido[24]crown-8

EDC - 1-Ethyl-3-(3-dimethylaminopropyl)carbodiimide

EDX - energy dispersive X-ray

EPR - electron paramagnetic resonance

ESI - electrospray ionisation

Fc - ferrocene

ICP - inductively coupled plasma

IDDA - inverse demand Diels-Alder

LCC - Leather Conservation Centre

LOD - limit of detection

LOQ - limit of quantification

MALDI - matrix-assisted laser desorption/ionisation

MIM - mechanically interlocked molecule

MOF - metal-organic framework

MS - mass spectrometry

MoL - Museum of Leathercraft

NDI - naphthalene diimide

NHM - Natural History Museum

NMR - nuclear magnetic resonance

NOESY - nuclear Overhauser effect spectroscopy

OES - optical emission spectroscopy

PDI - perylene-3,4,9,10-tetracarboxylic diimide

PPE - personal protective equipment

PTCDA - perylene-3,4,9,10-tetracarboxylic dianhydride

SEM - scanning electron microscopy

SW - square wave

TA24C82 - triptycene/anthracene-bridged macrotricyclic [24]crown-8 dimer

TBAI - tetrabutylammonium iodide

TEA - triethylamine

THF - tetrahydrofuran

TLC - thin layer chromatography

TOF - time of flight

TTF - tetrathiafulvalene

UON - University of Northampton

UV - ultra violet

VOC - volatile organic compound

XRC - X-ray crystallography

r.t. - room temperature

vis - visible

Contents

1 Introduction **1**

1.1 Mechanical bond . . . 1

1.2 Catenanes . . . 1

1.2.1 Statistical and directed methods . . . 3

1.2.2 Templating methods . . . 4

1.2.3 Magic ring methods . . . 6

1.3 Rotaxanes . . . 6

1.4 Handcuff Rotaxanes . . . 9

1.4.1 Simple [2]handcuff rotaxanes . . . 11

1.4.2 Applications: Redox Activity . . . 16

1.4.3 [n]handcuff rotaxanes where n>2 . . . 19

1.5 Chemical species utilised in this work . . . 21

1.5.1 Pillar[5]arenes and their host-guest properties . . . 21

1.5.2 Perylene diimides . . . 23

1.5.3 Tetrazines . . . 24

2 Synthesis of [3]handcuff rotaxane **25**

2.1 Introduction . . . 25

2.2 Synthesis of triple decker handcuff body . . . 27

2.2.1 Synthesis of substituted pillar[5]arene . . . 27

2.2.2 Linker for pillar[5]arene macrocycles . . . 28

2.2.3 The synthesis of an amino bis-pillar[5]arene species . . . 29

2.2.4 The synthesis of an amido bis-pillar[5]arene species . . . 33

2.2.5 The synthesis of an ether bis-pillar[5]arene species . . . 40
2.3 Conclusions and future work . . . 49
2.3.1 Other linkers . . . 49
2.3.2 Proposed assembly of triple decker handcuff . . . 51
2.3.3 Conclusions . . . 52

3 Synthesis of [2]handcuff rotaxane **54**
3.1 Synthesis of tetrazine handcuff . . . 54
3.1.1 Synthesis of nitrile substituted pillar[5]arene . . . 55
3.2 Synthesis of the alkene handcuff . . . 62
3.2.1 Synthesis of substituted pillar[5]arene . . . 63
3.2.2 Synthesis of the handcuff body . . . 69
3.2.3 Synthesis of the handcuff rod . . . 73
3.2.4 Alkene handcuff synthesis . . . 74
3.2.5 Synthesis of a [3]rotaxane through alkene metathesis . . . 84
3.3 Conclusions . . . 85

4 Introduction to leather **86**
4.1 Leather . . . 86
4.2 Tanning process . . . 87
4.2.1 Tannins . . . 88
4.2.2 Effects of tanning on skins . . . 90
4.3 Book Binding . . . 91
4.4 Leather Deterioration . . . 92
4.4.1 Red Rot . . . 93

4.5 Analytical techniques . . . 95
4.5.1 FTIR . . . 95
4.5.2 SEM . . . 99
4.5.3 ICP-OES and ICP-MS . . . 100

5 Exploration of red rot **102**

5.1 Aims . . . 102
5.2 Reference and deteriorated samples . . . 102
5.2.1 Sample naming conventions . . . 102
5.2.2 Sample metadata . . . 104
5.3 ATR-FTIR . . . 104
5.3.1 ATR-FTIR of reference samples . . . 106
5.3.2 ATR-FTIR of deteriorated samples . . . 113
5.3.3 Conclusion . . . 124
5.4 SEM . . . 127
5.4.1 SEM of reference samples . . . 128
5.4.2 SEM-EDX of reference samples . . . 130
5.4.3 SEM of deteriorated samples . . . 132
5.4.4 SEM-EDX of deteriorated samples . . . 136
5.4.5 Conclusion . . . 139
5.5 ICP Analysis . . . 140
5.5.1 ICP-OES . . . 140
5.5.2 ICP-MS . . . 143
5.5.3 Conclusion . . . 146

5.6 Conclusions and future work 147

6 Experimental **149**

6.1 General equipment 149

6.2 1-(4-bromobutoxy)-4-methoxybenzene (**1**) 150

6.3 4-bromobutane-pillar[5]arene (**2**) 151

6.4 *N*-Boc-ethylenediaminobutane-pillar[5]arene (**3.1**) 152

6.5 Attempt at *N*-Boc-ethylenediamino-bis-hexane (**4**) 153

6.6 4-phthalimidobutane-pillar[5]arene (**5**) 153

6.7 4-aminobutane-pillar[5]arene (**6**) 154

6.8 Boc-5-aminoisophthalic acid (**7**) 155

6.9 Attempt at amido bis-pillar[5]arene (**8**) 155

6.10 Attempts at amido bis-octane (**9**) 156

6.11 Ether tris-pillar[5]arene (**10.3**) 157

6.12 Attempt at ether bis-pillar[5]arene analogue (**11**) 158

6.13 Benzonitrile-pillar[5]arene (**12**) 159

6.14 3-butene-substituted pillar[5]arene (**13**) 160

6.15 Attempts at nitrile-methoxybenzene (**14**) 161

6.16 1-(but-3-en-1-yloxy)-4-methoxybenzene (**15**) 162

6.17 Alkene handcuff body (**17**) 163

6.18 N-(8-bromooctyl)phthalimide (**18**) 163

6.19 N-(8- imidazolyloctyl)phthalimide (**19**) 164

6.20 8-(1H-imidazol-1-yl)octan-1-amine (**20**) 164

6.21 Alkene handcuff rod (**21**) 165

6.22 2,4,6- trimethylbenzyl iodide (**22**) 165

6.23 Alkene handcuff (**23**) 166

A Appendix **168**

A.1 Index 168

A.2 NMR Peak ratio calculation 169

A.3 ^{1}H NMR spectra 170

A.4 Crystallography 214

A.5 Reproduced data for pillar[5]arene (**16**) 215

A.6 Electronic Appendices 243

A.6.1 Artefact Data 243

A.6.2 Photos of Samples 243

A.6.3 FTIR 243

A.6.4 SEM 244

A.6.5 ICP 244

A.6.6 Loose .py files 244

A.6.7 Abbreviations in file names 245

A.7 Additional SEM and SEM-EDX 246

1 Introduction

Supramolecular chemistry has been described as "chemistry beyond the molecule".[1] It deals with distinct chemical species, which when put together form a system with properties different to the sum of the individual components. Such systems are often based on host-guest chemistry, where the host and guest are selectively bound by reversible intermolecular interactions. Today, the field of supramolecular chemistry deals with mechanically interlocked molecules (MIMs),[2] molecular machines,[3] systems which mimic biology,[4] and many others.[5,6] This field has been steadily expanding since the 1960s and has two Nobel prizes associated with it. In 1987 Cram,[7] Pedersen,[8] and Lehn[9] received one for the founding of and contributions to the field, and in 2016 Sauvage,[10] Stoddart,[11] and Feringa[12] received the second Nobel prize for their work on molecular machines.

1.1 Mechanical bond

The study of MiMs is based on the concept of the mechanical bond, or a special architectural feature which results from the entanglement of the component parts of interlocked molecules. When two or more distinct species are so entangled as to make their separation impossible without breaking or distorting some of their chemical bonds, this entanglement is called the mechanical bond. Due to this, the strength of the mechanical bond depends directly on the strength of the chemical bonds in the components and the mechanical bond can never be stronger than the weakest chemical bond in a given molecule.[13]

1.2 Catenanes

Catenanes are structures made of two or more mechanically interlocking macrocycles. These macrocycles are not chemically bonded together, but to separate them one of the macrocycles has to be opened (a chemical bond has to be broken). The nomenclature for catenanes is based on how many components they are made of; a [2]catenane is comprised of two interlocking rings shown in Figure 1.1, while a [3]catenane is comprised of three.

There are multiple ways a catenane may be prepared, shown in Figure 1.2. These are:

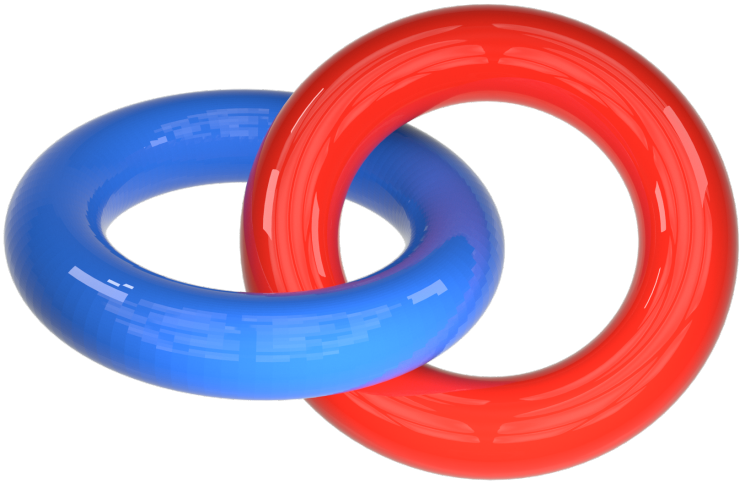

Figure 1.1: A model of a [2]catenane prepared in Blender.

(i) clipping, which involves a macrocycle threading onto a 'rod', then joining the ends of this 'rod' to form a second macrocycle; (ii) double clipping, which involves two 'rods' coming together, then joining the ends of each 'rod'; and (iii) magic ring synthesis where all or some macrocycles can open and re-close resulting in the catenane.

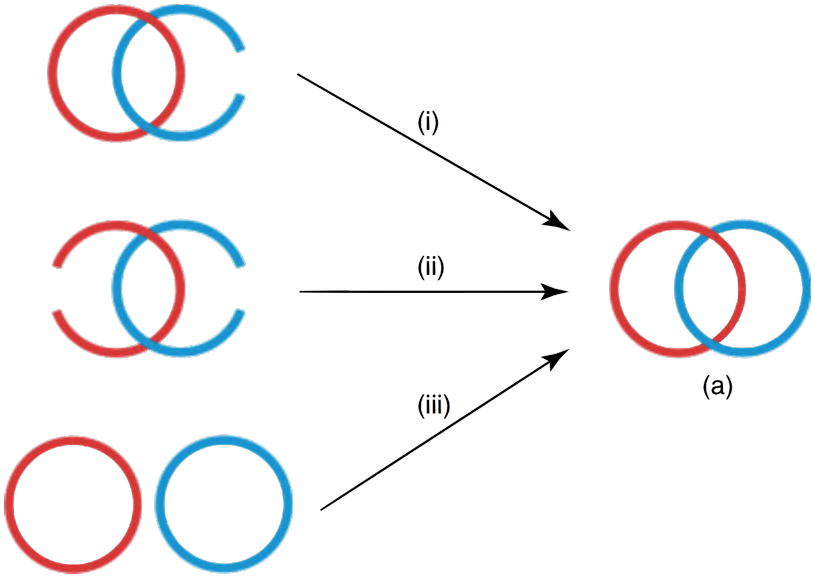

Figure 1.2: Examples of different catenanes and their syntheses: (a) [2]catenane, (i) clipping, (ii) double clipping, (iii) magic ring synthesis.[14]

It is also important to consider chemical topology when talking about catenanes. They are an example of a topologically non-trivial species which means they cannot be turned into another isomer of themselves by deformation of bonds. The macrocycles of a catenane cannot be separated without breaking a bond; the catenane (shown in Figure 1.2a) and its non-interlocked component macrocycles (shown in Figure 1.2 as the starting material of the magic ring synthesis (iii)) are hence topological isomers.[2]

1.2.1 Statistical and directed methods

The first artificial catenane, synthesised by Wasserman[15] in 1960, used the clipping method by threading a diester rod through a macrocycle and cyclising it with a condensation of diesters as shown in Scheme 1.1(a). This method was statistical in that it relied on the rod threading through the macrocycle by chance, resulting in a very poor yield ($\sim 0.0001\%$) of the desired catenane.

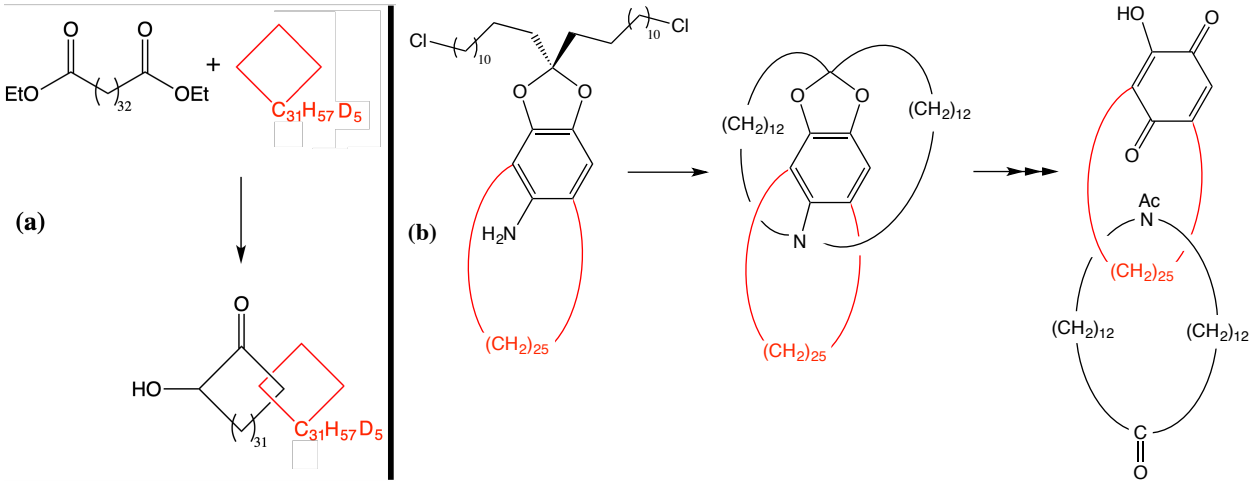

Scheme 1.1: (a) The first synthesis of a catenane by Wasserman in 1960[15]. (b) The first directed covalent synthesis of a catenane by Schill and Lüttringhaus in 1964.[16] Diagram adapted from publication by Beer and Evans[14]

The first improvement on this statistical method came in the form of directed covalent synthesis. Schill and Lüttringhaus synthesised a macrocycle with two long alkyl chains protruding above and below the macrocycle's plane, capped with chlorine atoms. These could be attacked by an amine group that was situated inside the macrocycle to give an interlocked, but also covalently bonded species shown in Scheme 1.1(b). Once the necessary

bonds were cleaved this structure resulted in a [2]catenane. This synthesis also falls under the category of clipping.

1.2.2 Templating methods

These early statistical and directed methods were both overshadowed by Sauvage's templating methods, which involve the use of a template around which the supramolecular structure can form and afford much greater yields. Templation arises from molecular recognition between the chemical species that will become components of an interlocked molecule. These are non-covalent interactions such as donor-acceptor, hydrophobic, hydrogen-bonding, etc. interaction.[13]

In 1983 he reported[17] the synthesis of a [2]catenane using a tetrahedral d^{10} Cu(I) cation as a template for two phenanthroline (phen) ligands, giving tetrahedral complexes shown in Scheme 1.2. These phen ligands can be (i) double clipped and (ii) clipped respectively to give the [2]catenane, which is coordinatively bonded to a metal centre. Such a catenane is often called a 'catenate'. The synthesised catenate can be demetallated to give a catenane which is not bonded to a metal centre any longer. Such a catenane is often called a 'catenand'. The crystal structure of this catenand can also be seen in Scheme 1.2. It was determined that the two macrocycles within the synthesised catenand can move freely around each other.

Another templating method, developed by Stoddart, involves the use of π-π interactions. His earliest work on this topic, in 1989, involved a [2]catenane containing cyclobis(paraquat-p-phenylene) cyclophane ($CBPQT^{4+}$), an electron-poor macrocycle, and bisparaphenylene-34-crown-10 (BPP34C10), an electron-rich macrocycle, shown in Scheme 1.3. The pyridinium and hydroquinone moieties are attracted to each other through electrostatic forces resulting in π-π stacking, allowing these species to template around each other. These pyridinium species can then be clipped to give a [2]catenane.[20]

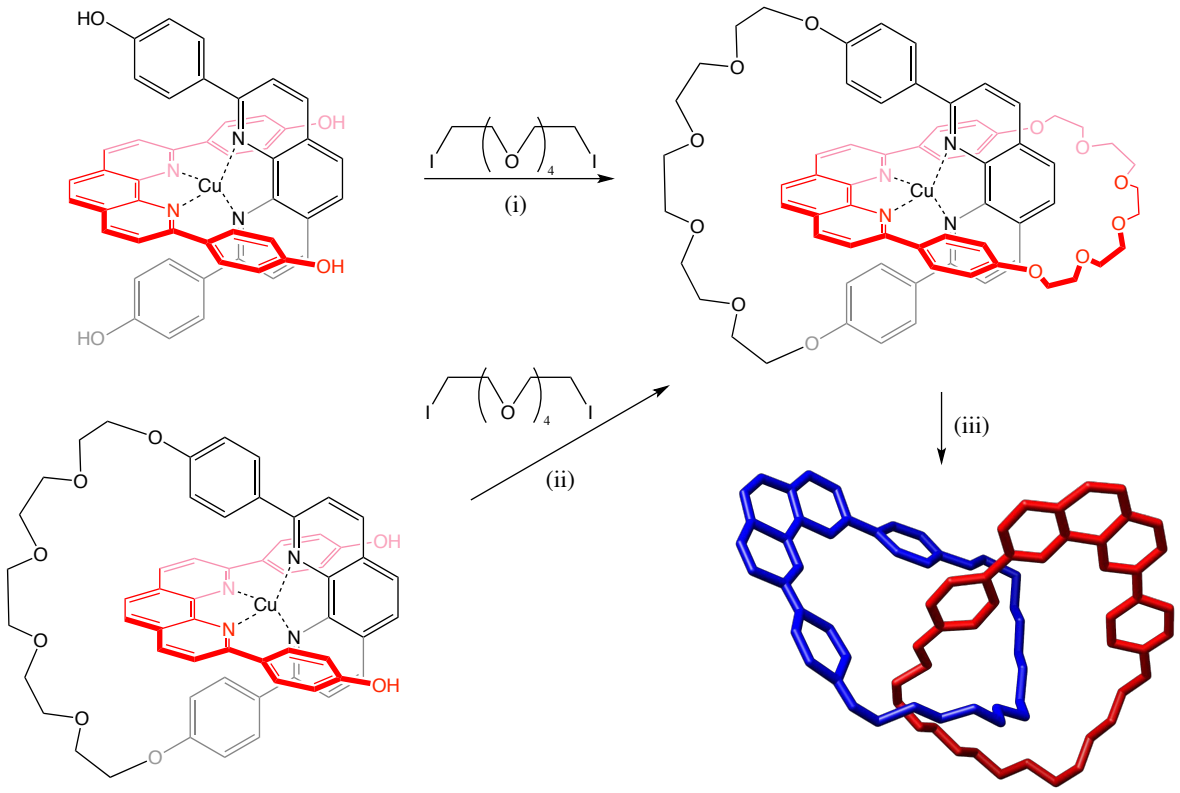

Scheme 1.2: Sauvage's templated synthesis.[17] The phen ligands of the upper complex can be double clipped (i), while the phen ligand of the lower complex can be clipped (i) to give the desired [2]catenate. The catenate can then be demetallated (iii) to give the catenand. Diagram adapted from publication by Leigh *et al.*[18] and from crystallographic data.[19]

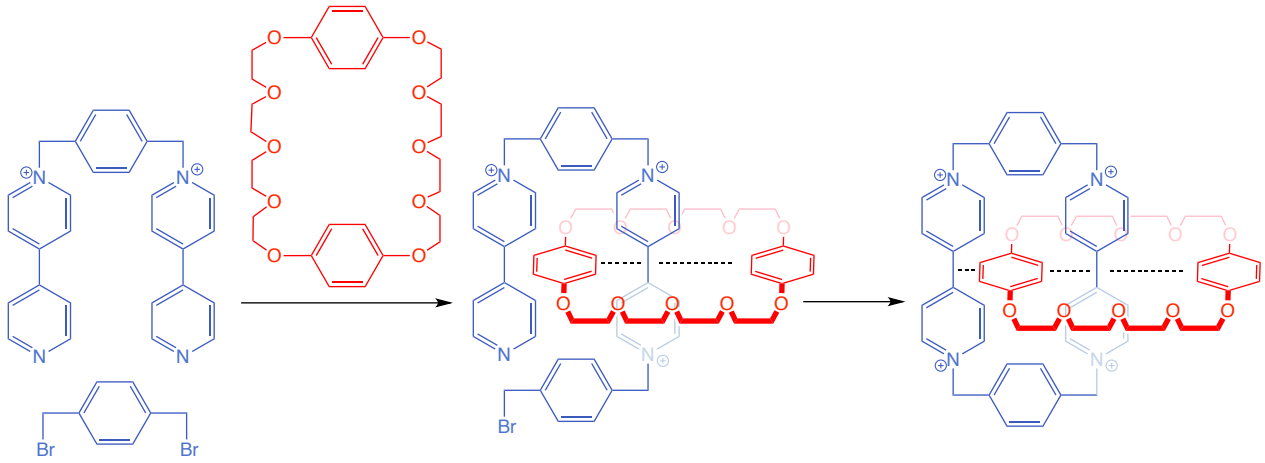

Scheme 1.3: Scheme showing the templated synthesis of Stoddart's [2]catenane based on π-π interactions (shown as dotted lines) between $CBPQT^{4+}$ (shown in blue) and BPP34C10 (shown in red) macrocycles.[20]

1.2.3 Magic ring methods

More recently, catenanes have been synthesised using a 'magic ring' approach. In 1994, Fujita synthesised a [2]catenane from two entirely closed macrocycle complexes based on a square planar Pd centre and ethylenediamine and pyridyl ligands, shown in Scheme 1.4. Due to the lability of the Pd-pyridyl bonds, the macrocycles can open, interlock and then close, forming the [2]catenane, driven by hydrophobic interactions. At low concentrations, the macrocycle remains a monomer, but at high concentrations the two macrocycles interlock, filling each other's cavities thus minimising hydrophobic interactions with the solvent.[21]

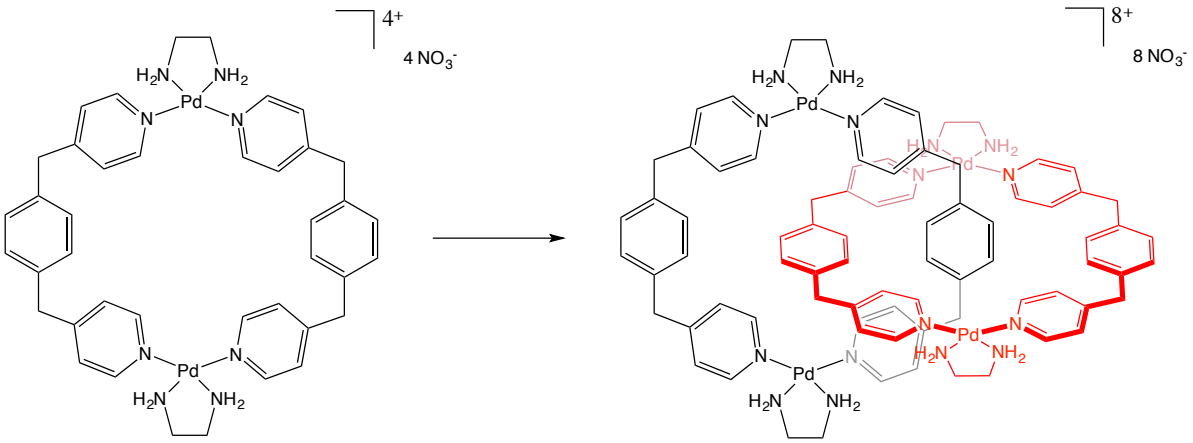

Scheme 1.4: A reaction scheme showing a [2]catenane formed from two entirely whole macrocycles through magic ring synthesis due to hydrophobic interactions. Diagram adapted from publication by Stoddart *et al.*[22]

1.3 Rotaxanes

Rotaxanes are another type of MIM, made of a rod-like molecule threaded through a macrocycle and stoppered with bulky groups on each end to prevent the macrocycle from de-threading. If the stopper groups are not present, that species is called a pseudo rotaxane instead. The nomenclature for rotaxanes works similarly to that of catenanes in that a [2]rotaxane is comprised of two components - a stoppered rod and a macrocycle, and a [3]rotaxane is comprised of three - either a stoppered rod and two macrocycles or a macrocycle and two stoppered rods. A model of the simplest [2]rotaxane is shown in Figure 1.3. Unlike catenanes, rotaxanes are considered topologically trivial, as the ring (if stretched) could 'slip off' the rod without breaking any bonds, affording two topologically trivial components.

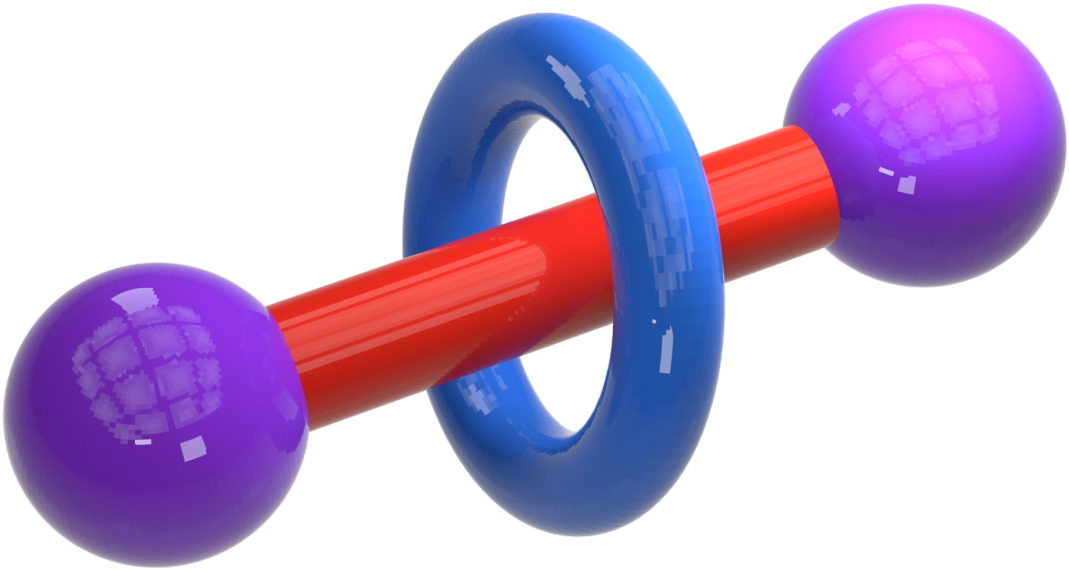

Figure 1.3: A model of a [2]rotaxane prepared in Blender with the macrocycle shown in blue, rod in red and stoppers in purple.

General synthetic strategies include: (i) capping, where the ring threads onto the rod, which is then stoppered with bulky groups to give the final rotaxane; and (ii) clipping, where a section of the ring threads onto the stoppered rod and is then clipped to form the final rotaxane shown in Figure 1.4.

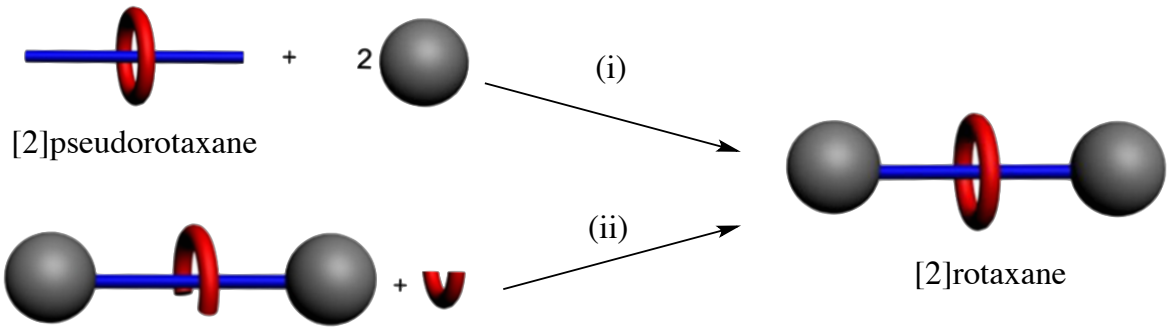

Figure 1.4: The main synthetic strategies for rotaxanes: (i) capping a pseudo rotaxane with bulky stopper groups; (ii) clipping a ring already positioned over the stoppered rod. The [2]rotaxane contains a rod (in blue), a ring (in red) and stopper groups (in grey). Diagram adapted from a publication by Xue *et al.*[23]

The first ever rotaxane was synthesised using the capping method by Harrison and Harrison in 1967.[24] They used statistical methods similar to those in Wasserman's catenane synthesis described in Section 1.2.1. To make isolation possible, the authors attached the macrocycle to a resin and passed a solution containing the rod and stopper repeatedly over it. Statistically speaking, the rod would react with the stoppers while threaded through the macrocycle some of the time, giving the desired, capped rotaxane. After seventy repetitions the rotaxane was cleaved from the resin and purified, affording a 6% yield. Following the innovations in catenane synthesis, next came the directed covalent methods of Schill *et al.*[25], but this method also suffered from poor yields due to the large number of steps required.

As with catenane synthesis, next came templating methods. Ogino used hydrophobic interactions to direct a diamine-alkyl rod through the hydrophobic cavity of a cyclodextrin macrocycle, before stoppering the rod with a bulky cobalt complex. This improved the yields of the synthesised rotaxanes to 19%.[26] Templating methods using π-π stacking were also repurposed for the synthesis of rotaxanes by Stoddart *et al.* The first such [2]rotaxane, synthesised in the much higher yield of 32% through a clipping method, contained the previously discussed $CBPQT^{4+}$ macrocycle and a hydroquinone based rod with triisopropylsilyl stoppers,[27] as shown in Figure 1.5. Templating methods based on Cu(I), analogous to those used by Sauvage for catenane synthesis, were also implemented for rotaxane synthesis, for example by Gibson *et al.*[28] shown in Figure 1.5, again improving the yield to 42%.

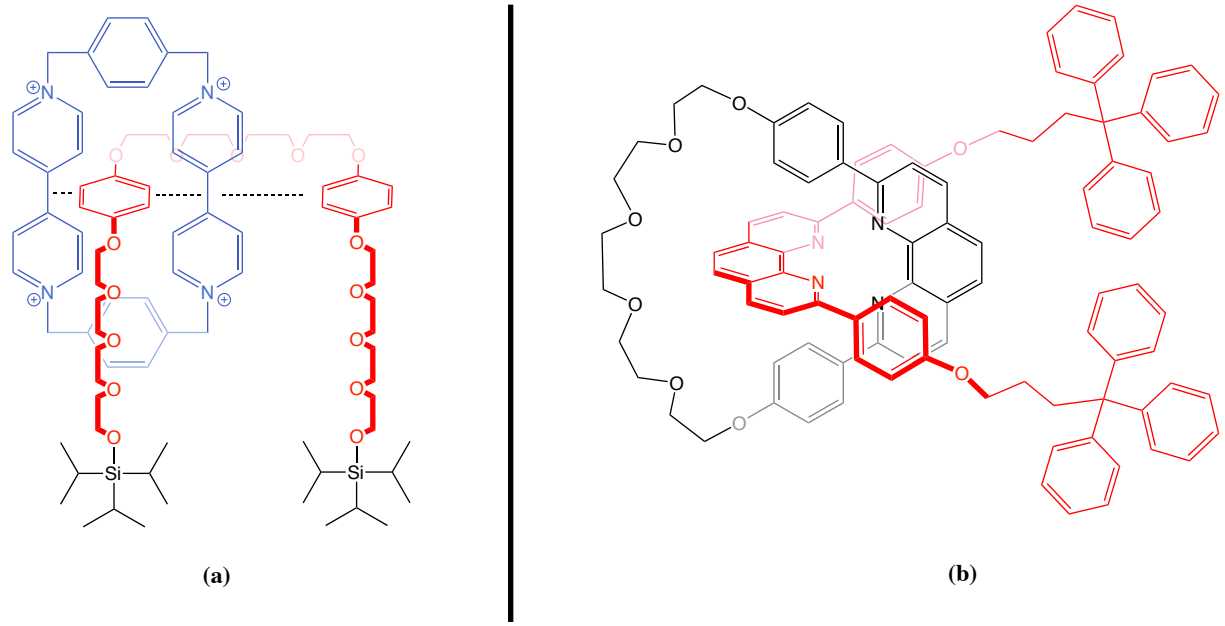

Figure 1.5: (a) A [2]rotaxane synthesised by Stoddart *et al.*[27] containing a $CBPQT^{4+}$ macrocycle (shown in blue) and a hydroquinone based rod (shown in red) with triisopropylsilyl stoppers (shown in black), π-π interactions are shown as dotted lines. (b) A [2]rotaxane synthesised by Gibson *et al.*[28] based on templating methods involving Cu(I) tetrahedral cations developed by Sauvage.

1.4 Handcuff Rotaxanes

A more extensive review of handcuff rotaxanes (as well as handcuff catenanes and related structures) than what follows here, can be found in a published review article by the author of this thesis in collaboration with other members of the Champness and Pilgrim groups.[29] This review is attached in Appendix A.5. This author's contributions to it include researching and writing the handcuff rotaxane section, drawing all of the chemical structures within it and making many of the 3D models in Blender. The majority of the following section is a repurposing of the author's contributions to this review, as this work was undertaken within the scope of the Ph.D degree as an alternative activity during the time when the pandemic-related closure of the university prevented progress on the project's primary experimental component.

Expanding on the concept of rotaxanes and catenanes, more complex MIMs such as handcuff rotaxanes and catenanes have been made. This work will focus on handcuff rotaxanes. A handcuff rotaxane is a mechanically bonded system made of a rod (aka axle, thread, dumbbell), which threads through both macrocycles of a bis-macrocyclic body. A handcuff catenane is when the rod of the handcuff rotaxane is also joined at the ends, creating a third macrocycle threading through both of the other macrocycles. They are named so because the body looks like a pair of real life handcuffs as shown in Figure 1.6.

Figure 1.6: A diagram showing the origin of the name handcuff (left) rotaxane and (right) catenane prepared in Blender.

For a species to be considered a handcuff rotaxane, it should be clear that any templating interactions between the individual parts aren't essential to the compound's integrity once the synthesis is finished. The only interaction that is crucial to that integrity should be the mechanical bond. A model of the simplest handcuff rotaxane is shown in Figure 1.7. The colour scheme is deliberate to aid understandability of the structural depictions of the complex molecules within this thesis. The colour blue was chosen for the body and red for the rod.

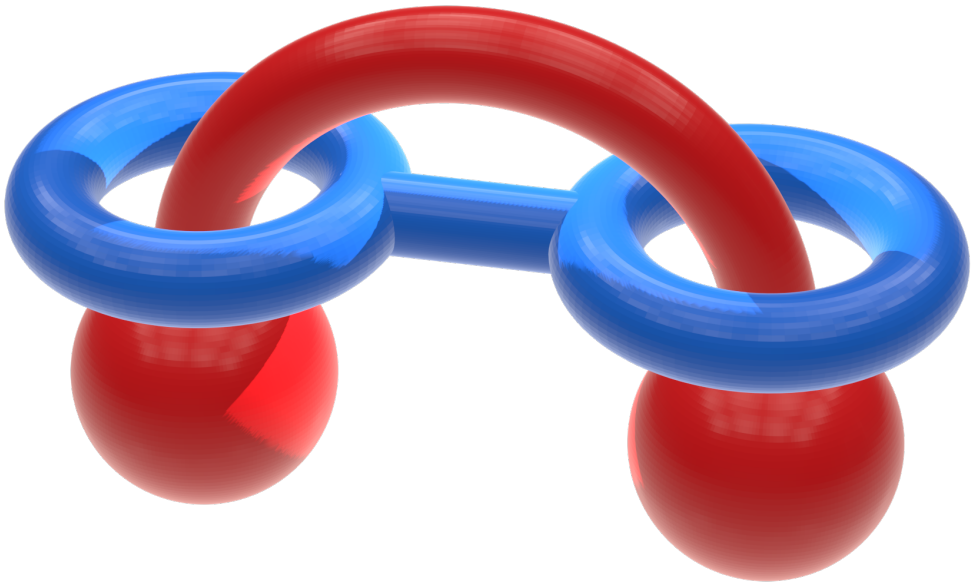

Figure 1.7: A diagram showing a model of the simplest [2]handcuff rotaxane prepared in Blender.

1.4.1 Simple [2]handcuff rotaxanes

Handcuff rotaxanes also vary in how they are put together. Takata's example, based on two functionalised dibenzo[24]crown-8 macrocycles (DB24C8) and a bis(dialkylammonium) rod[30], involves making a [3]rotaxane by threading the rod through both macrocycles and stoppering both of its ends. This threading is possible due to interactions between the π-donating DB24C8 macrocycles and the π-accepting dialkylammonium ions on the rod. Once the [3]rotaxane is made, its two macrocycles are then bridged to give the handcuff rotaxane as shown in Scheme 1.5. Such a synthesis method will henceforth be referred to as a linking synthesis, as linking of the pre-threaded macrocycles is the last non-trivial step involved in making such a handcuff rotaxane.

Another type of linking synthesis, where each half-component of a rod stoppered on one end, are first threaded through each macrocycle of the bis-macrocyclic species, then linked in the final step, can be observed in Iwamoto's handcuff as shown in Scheme 1.5.[31,32]

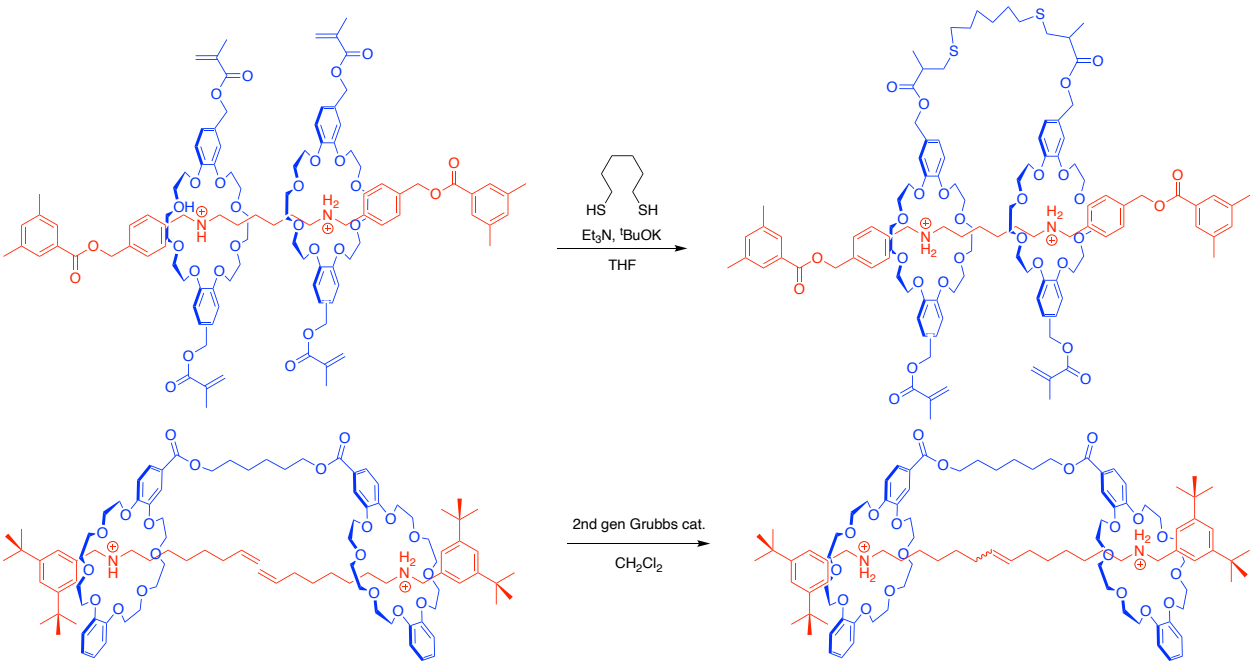

Scheme 1.5: Top: the bis(methacrylate) functionalised DB24C8 macrocycles of the [3]rotaxane are bridged with hexanedithiol using a Michael addition reaction. Bottom: the linking synthesis of the two rod components, utilising olefin metathesis, to give the final handcuff rotaxane.

A different type of synthesis, which is here called a threading synthesis, involves threading a rod through a complete bis-macrocyclic handcuff body and stoppering it, as is displayed in the work of Gaeta and Neri.[33] Their bis(alkylbenzylammonium) rod threads through both macrocycles of their calix[6]arene based bis-macrocyclic species due to similar donor-acceptor π-π interactions to those shown in both of the previous examples. The pseudo rotaxane species was subsequently stoppered at both ends to give the handcuff rotaxane as shown in Figure 1.8.

Since calix[6]arene is an asymmetrical macrocycle, two additional isomers of this handcuff rotaxanes were structurally possible, but this isomerism was avoided due to the asymmetrical shape of the aklylbenzylammonium recognition units and only the Tail-to-Tail isomer (illustrated on same Figure) was made.

Another very similar example based on donor-acceptor π-π interactions between a handcuff body based on tetralactam macrocycles and a bis(diamide) rod has been synthesised using a threading synthesis by Schalley[34] as shown in Scheme 1.6.

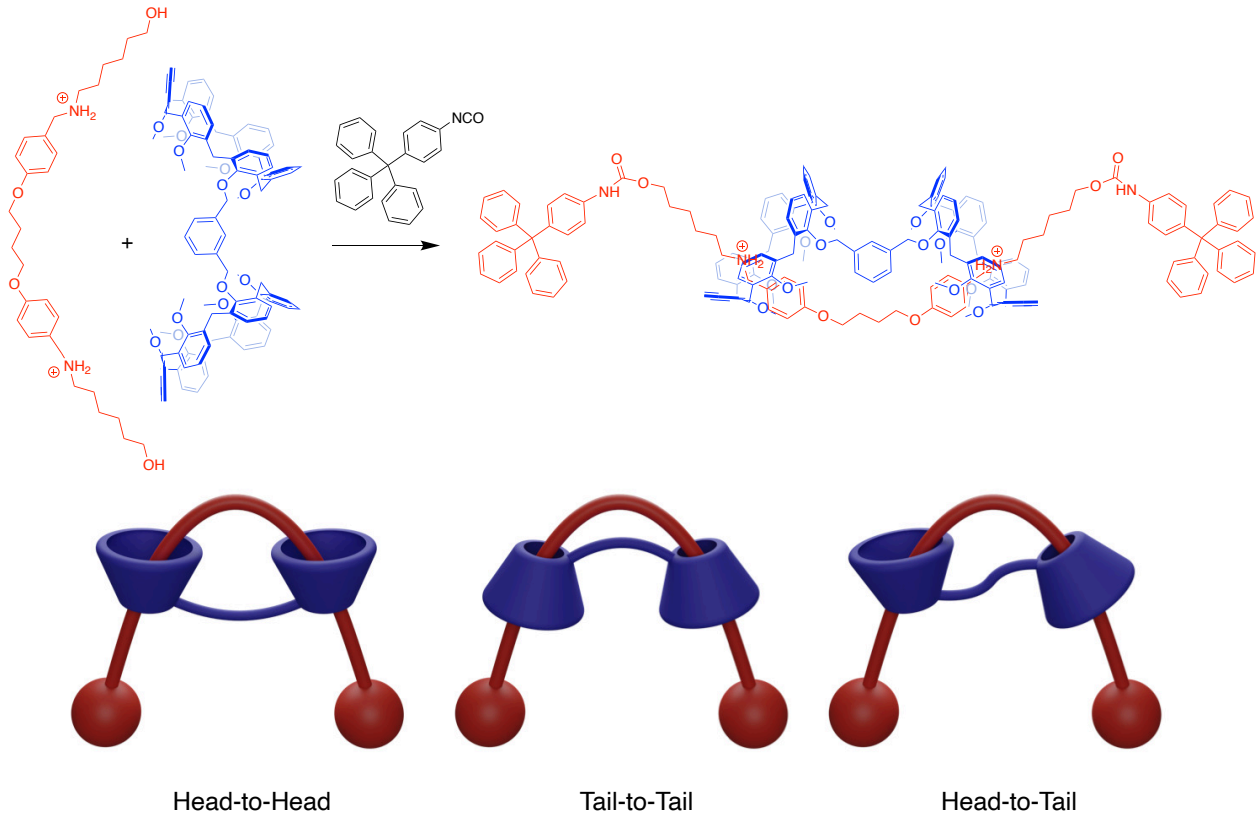

Figure 1.8: The bis(alkylbenzylammonium) rod threads through the calix[6]arene based handcuff body and is stoppered with p-tritylphenylisocyanate in a threading synthesis. The possible isomers are shown as models prepared in Blender.

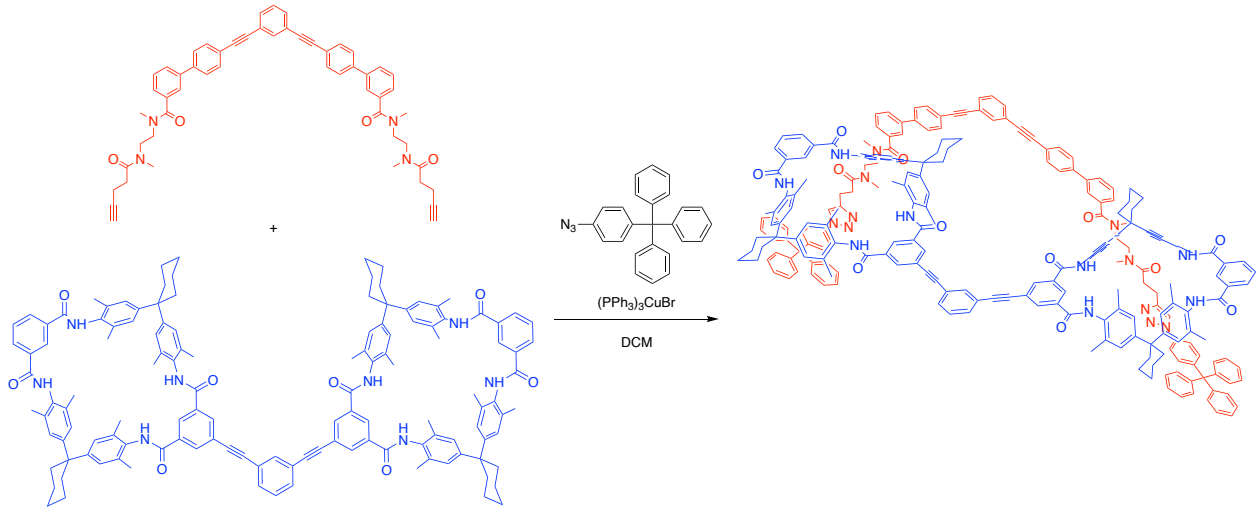

Scheme 1.6: The bis(diamide)rod threads through the tetralactam based handcuff body and is stoppered with an azide-functionalized trityl phenyl species in a threading synthesis.

These three types of handcuff syntheses (linking macrocycles, linking rods, and threading) are visually summarised in Figure 1.9.

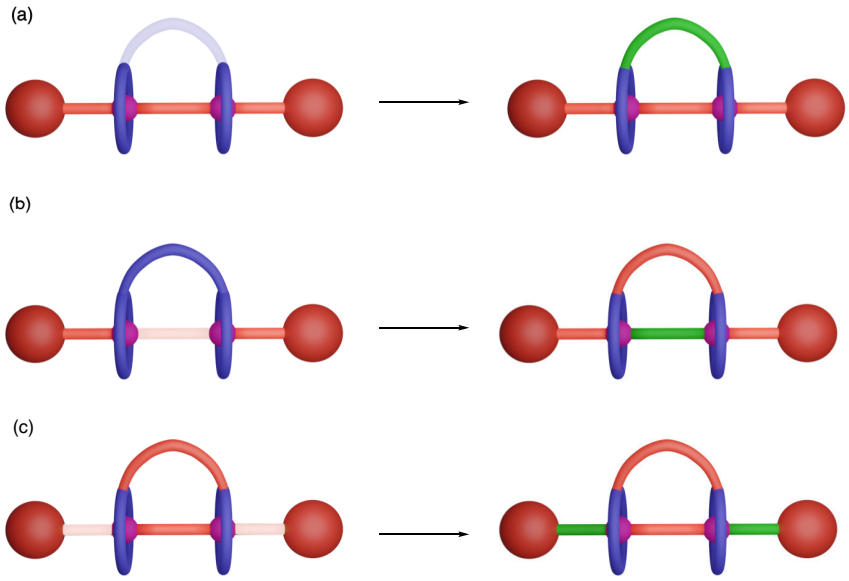

Figure 1.9: A visual summary of handcuff syntheses prepared in Blender; (a) linking macrocycles, (b) linking rods, (c) threading.

On the other hand the first ever handcuff rotaxane, synthesised by Vögtle[35] in 2006 did display isomerism. The two asymmetrical trilactam monosulfonamide macrocycles were threaded with a benzylic amide rod, utilising the hydrogen bonding interactions between the lactam amide groups of the macrocycle and the amide carbonyl groups of the rod. This pseudo rotaxane was then stoppered, and the macrocycles were bridged with oligomethylene, oligoxylene or oligoether linkers in another example of a linked synthesis. When the two macrocycles are threaded onto the achiral rod, they display cyclodirectionality with respect to each other depending on the clockwise or counterclockwise sequence of the sulfonamide and amide groups. This leads to the synthesis of a pair of enantiomer handcuffs and a diastereoisomer handcuff as shown in Figure 1.10. The synthesis of these handcuff rotaxanes had been attempted by the Vögtle group a few years earlier, when they called them bonnanes, but their results remained unpublished until more efficient methods of enantioseparation were available.[36]

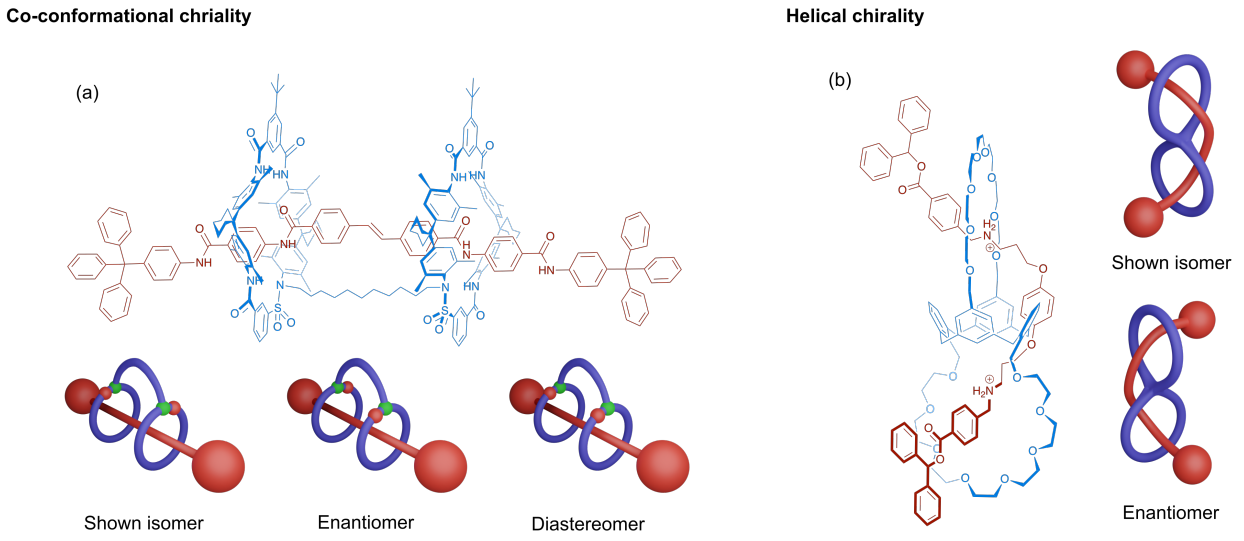

Figure 1.10: Various modes of handcuff isomerism shown on the examples of: (a) Vögtle's handcuff rotaxane, (b) Tokunaga's handcuff rotaxane.

A more recent example of a chiral handcuff comes from the Tokunaga group.[37] It is comprised of two achiral components; a handcuff body based on two crown ether macrocycles on a calix[4]arene frame and a bis(dialkylammonium) handcuff rod. The rod first threads through the macrocycles utilising the crown ether - dialkylammonium recognition motif and is then stoppered with diphenyldiazomethane. This threading synthesis gives the handcuff rotaxane. The handcuff's chirality arises from the possibility of the rod threading the second macrocycle from its either side giving two enantiomers where the rod can be in either of the two helically opposite positions as shown in Figure 1.10.

1.4.2 Applications: Redox Activity

Aside from being interesting examples of complex supramolecular architectures in their own right, handcuff rotaxanes have been used to study redox properties of species which are held near each other due to mechanical bonds but are separate compounds with some degree of free movement. Schalley's system brought together a tetrathiafulvalene (TTF) and naphthalene diimide (NDI) species to study their electronic interactions, utilising the crown ether - dialkylammonium recognition motif[38]. In similar studies, the Champness group brought together two perylene diimide (PDI) species and a PDI and a naphthalene species utilising π-π stacking between those species and the interactions of a pillar[5]arene π-donor and an imidazolium π-acceptor[39,40] as shown in Figure 1.11. All of these examples used the threading type synthesis.

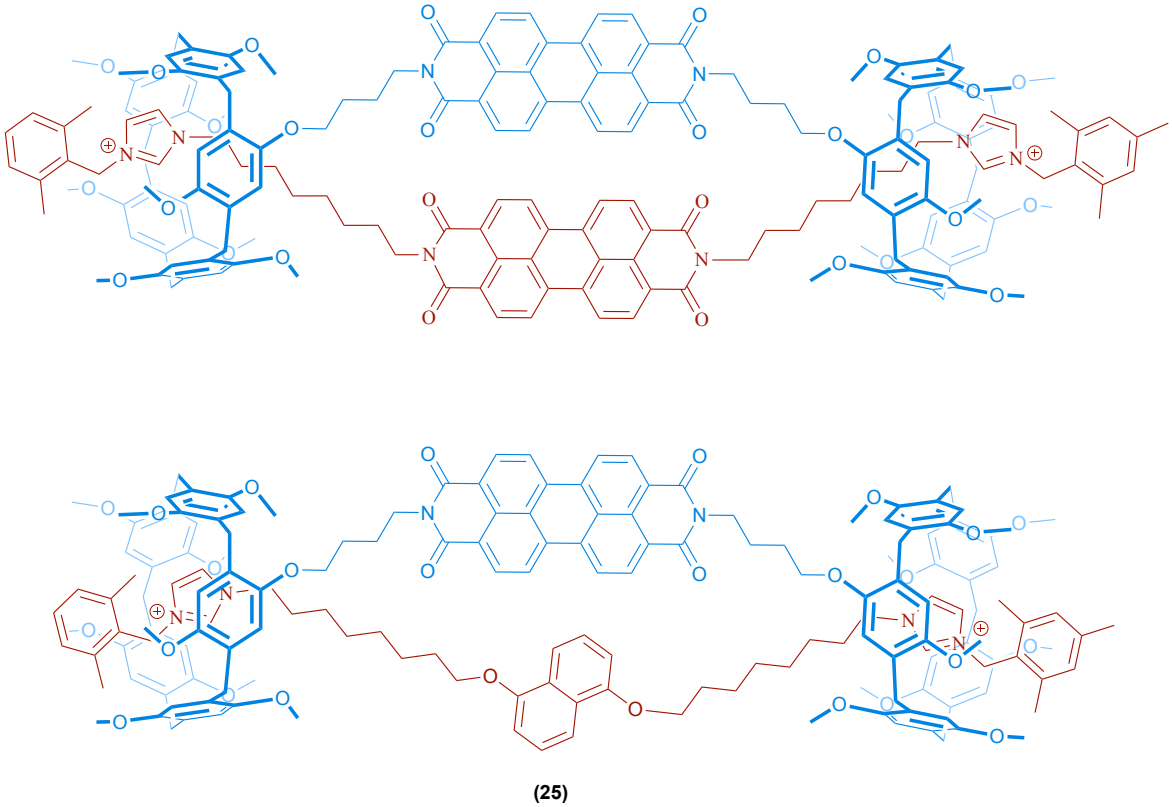

Figure 1.11: Handcuff rotaxanes used to bring two species together to study their redox properties. Top: PDI-PDI, and bottom: PDI-naphthalene handcuffs.

The nature of interactions between the two PDIs was investigated using cyclic voltammetry (CV) and electron paramagnetic resonance spectroscopy (EPR). The PDI-PDI handcuff

can accept four electrons during CV. The first two reversible reductions are two single electron processes. At this stage, a new molecular orbital spanning the two PDI cores is observed, which slightly stabilises the doubly reduced handcuff relative to the equivalent doubly reduced body and rod. The last reduction is assigned as a two-electron process and the molecular orbital spanning the two PDI cores is no longer observed. This is shown in Figure 1.12.

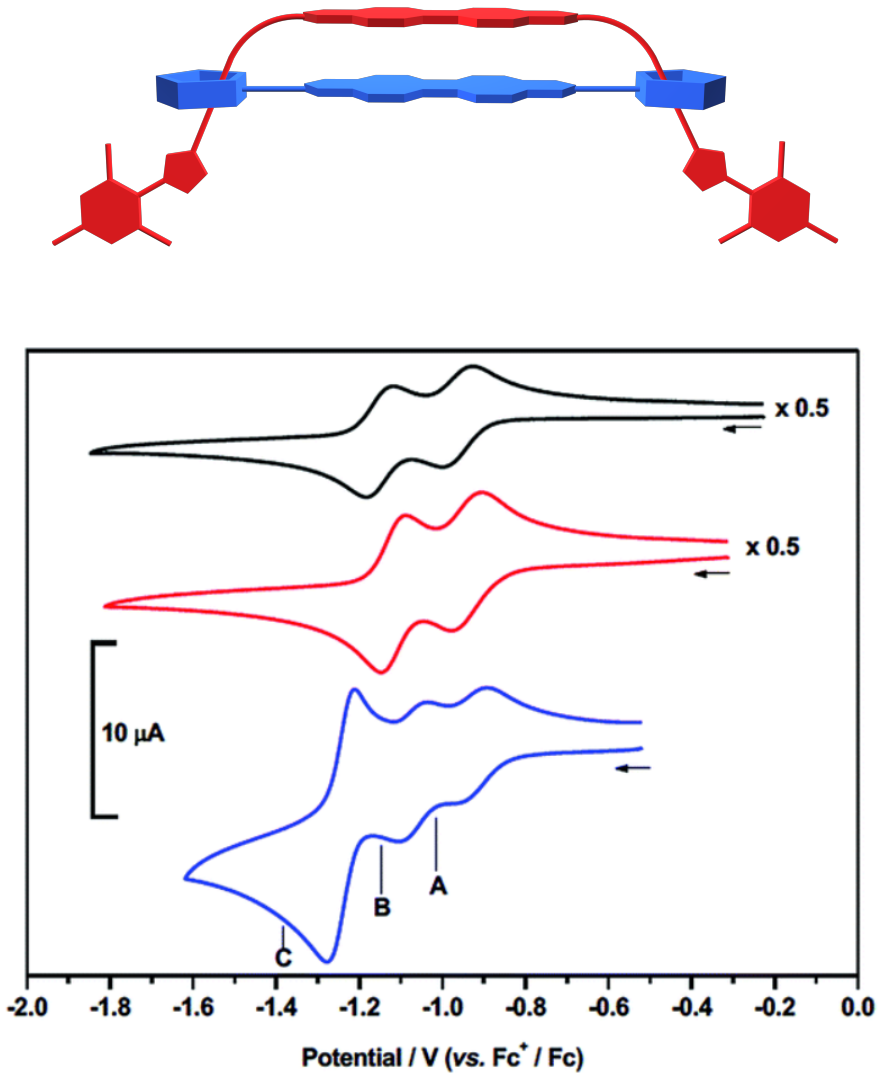

Figure 1.12: CV for the PDI-PDI handcuff rotaxane and its individual components. Black: handcuff body, red: handcuff rod, blue: handcuff. The reductions are labelled A: first one-electron reduction, B: second one-electron reduction, C: third two-electron reduction. Adapted from Langer *et al.*[39]

EPR spectroscopy was then used to investigate the localisation of charge in the singly and doubly reduced handcuff. The results for the singly reduced handcuff were consistent with the unpaired electron being either fully delocalised or hopping between the two PDI moieties on the EPR timescale, while for the doubly reduced handcuff, a loss of signal is observed, which further supports the theory that a molecular orbital spans the two PDI cores. This is shown in Figure 1.13.

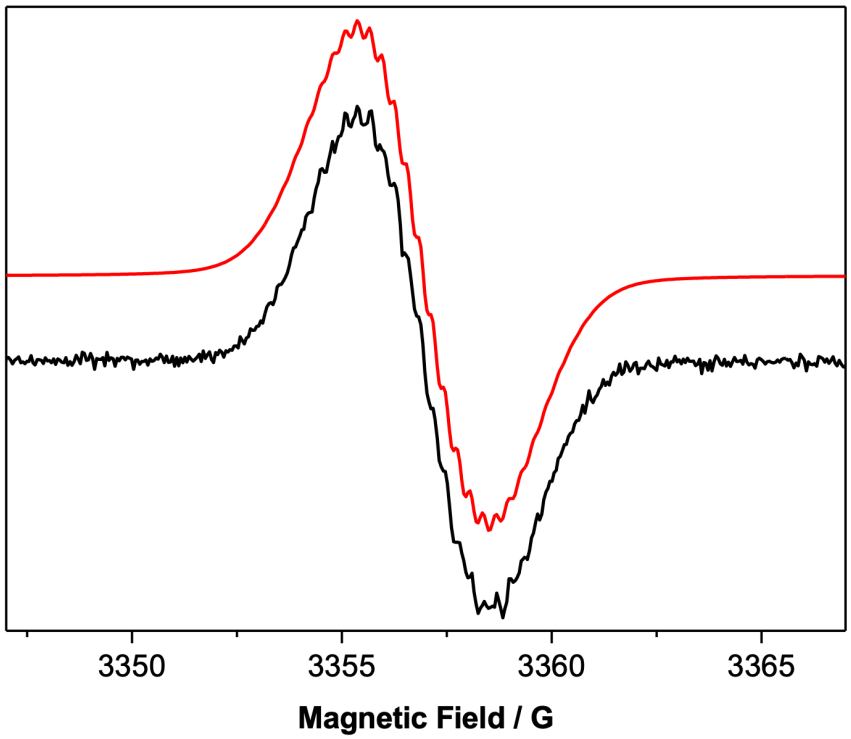

Figure 1.13: Experimental (black) and simulated (red) X-band EPR spectra of the singly reduced PDI-PDI handcuff rotaxane. The sample was electrogenerated at 273 K from the parent molecule in CH_2Cl_2 with $[^nBu_4N][BF_4]$ (0.4 M) as the supporting electrolyte. The simulated spectrum was generated using g_{iso} of 2.0034, a_{iso} of 0.835 (8H), 0.281 (8H), 0.061 (8H), 0.267 (4N) x 10^{-4} cm^{-1}, a line-width of 0.30 G and a Lorentzian line-shape. Adapted from Langer *et al.*[39]

1.4.3 [n]handcuff rotaxanes where n>2

Many examples of higher order [n]rotaxanes where n>2 due to the presence of multiple macrocycles or rods have been synthesised,[13] and this concept can be extended to handcuff rotaxanes as well. Sauvage has made a [3]handcuff rotaxane containing a tetrakis-macrocyclic body and two rods[41] analogous to two simple [2]handcuff rotaxanes fused together by their macrocycle bridges as shown in Figure 1.14(a). This system is based on a pyridine - copper recognition motif and utilises metal templating to achieve a threading synthesis. This structure is, however, never demetallated, making it technically a handcuff rotaxanate, though this terminology is rarely invoked.[13]

Tanaka synthesised a [3]handcuff rotaxane[42] in the form of a porphyrin stack. The [3]handcuff rotaxane is based on a bromopyrido[24]crown-8 (BrP24C8) and alkylbenzylammonium recognition motif and was made using a threading synthesis as shown in Figure 1.14(b). First, a bis(alkylbenzylammonium) rod was threaded through a handcuff body based on BrP24C8 macrocycles. That handcuff body was then functionalised with two alkylbenzylammonium species on opposite sides of its porphyrin core to make it also function as a second handcuff rod. This new rod was used to thread through an additional handcuff body, giving a trimer joined entirely through handcuff interactions. This methodology could be extended to give larger stacks, and the porphyrin cores can be different on each species making this a versatile method of studying porphyrin oligomers.

The two ideas in this section that seemed worth exploring further, were tetrakis-macrocycle handcuff bodies and stacking within [n]handcuff rotaxanes where n>2. When combined with the chemical species that have been previously utilised within the group, the idea for this project - a [3]handcuff rotaxane utilising a triple stack of PDIs (1.5.2) and a tetrakis-pillar[5]arene (1.5.1) body was born. The knowledge that would be gained by making these molecules and its importance is detailed in Section 2.1.

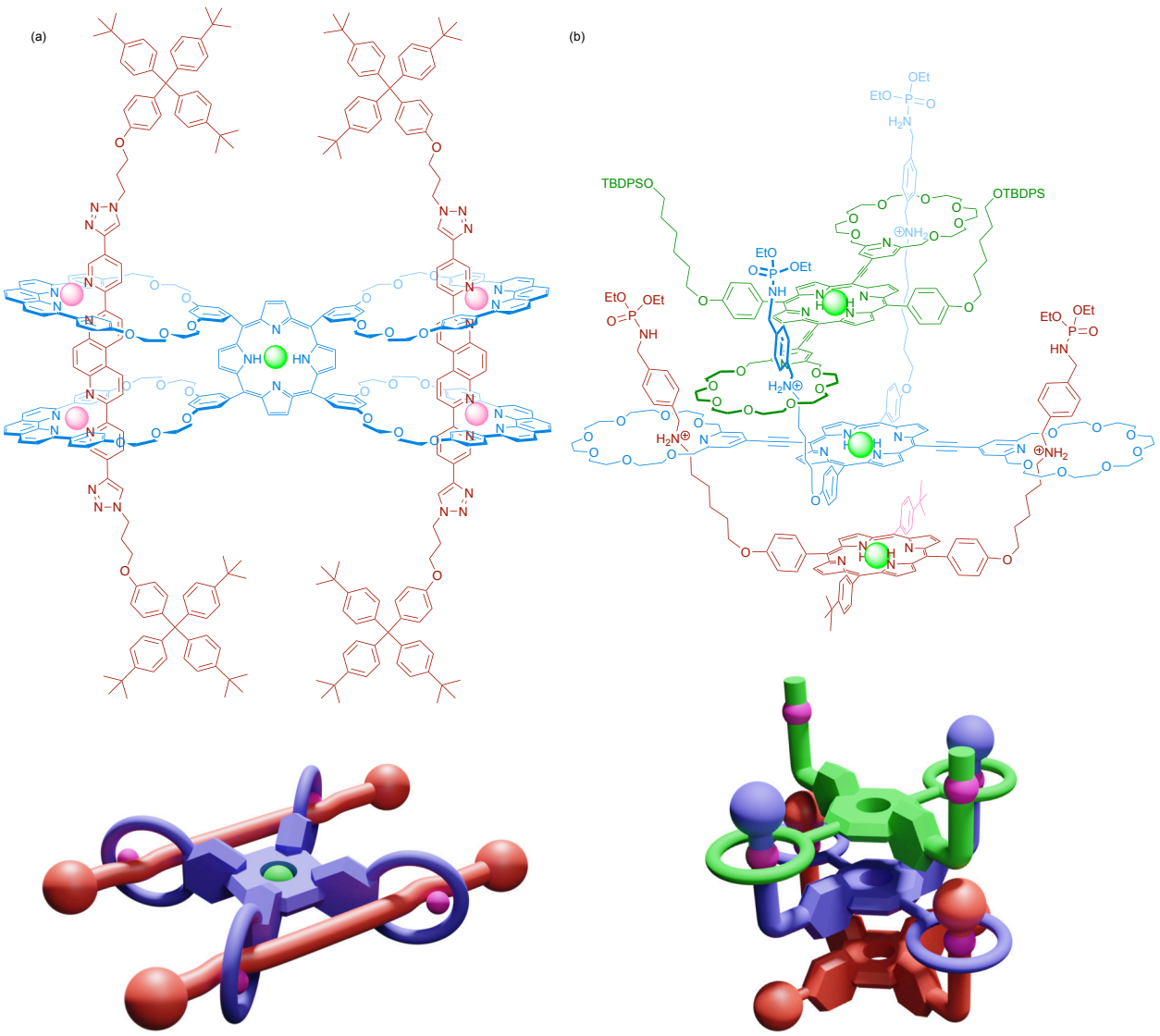

Figure 1.14: A [3]handcuff rotaxane made of a tetrakis macrocyclic body and two rods made using a threading synthesis.

1.5 Chemical species utilised in this work

Now that handcuff rotaxanes and the ideas behind this project have been explained, it is time to focus on the chemical species that will be used to explore it.

1.5.1 Pillar[5]arenes and their host-guest properties

Pillar[n]arenes are macrocyclic structures made of n hydroquinone units (where n is usually 5 – 10) linked with methylene bridges at the 2 and 5, or *para*, positions, giving a symmetrical pillar-like structure. The pillar is hollow, with a π-electron rich cavity that allows for a rod to thread through it. This is unlike calixarenes which are similar macrocyclic structures made of phenolic units, but linked at the 3 and 5, or *meta*, positions resulting in a chalice-like cavity that can accommodate guest molecules rather than allow threading, though exceptions exist.[43]

The first pillar[5]arene, and the one that is important to this thesis, is the dimethoxy-pillar[5]arene, from here on termed pillar[5]arene, synthesised in 2008 by Ogoshi *et al.*[44], shown in Figure 1.15, along with the structure of a general calixarene for comparison.

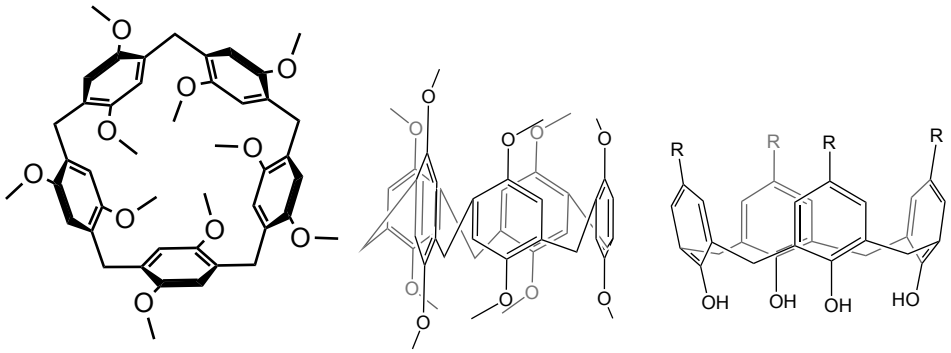

(16)

Figure 1.15: From left to right: the structure of pillarene viewed from the top, the structure of pillar[5]arene viewed from the side and the structure of a general calixarene viewed from the side for comparison of the pillar and chalice structures.

The synthesis of pillar[5]arene involves the Friedel-Crafts cyclo-oligomerisation of 1,4-dimethoxybenzene with paraformaldehyde and a catalyst such as iron chloride. This reaction operates under an equilibrium, resulting in high yields of the thermodynamically stable product - the cyclopentamer, with low yields of the cyclohexamer, as well as polymeric chains.

The cyclopentamer is more stable than other cyclo-oligomers due to the fact that it has the lowest bond angle strain across its methylene bridges; the Ar-CH_2-Ar bond angle is very close to the ideal sp^3 hybridisation angle.[45] The crystal structure of pillar[5]arene is shown in Figure 1.16.

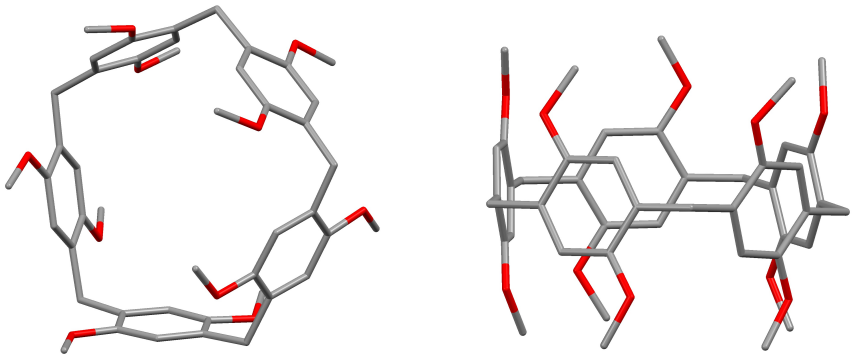

Figure 1.16: The crystal structure of pillar[5]arene. Left: view showing the pentagonal nature of the cavity. Right: view showing the pillar-like structure of the cyclopentamer.

Pillar[5]arene has only moderate solubility in organic solvents such as chloroform due to strong packing interactions. To improve its solubility in organic solvents its methoxy groups can be demethylated to alcohol groups through a reaction with boron tribromide[44] shown in Scheme 1.7. This compound can then be further functionalised at the alcohol positions to achieve various property changes, for example, introducing carboxylate anions makes it water soluble.[46]

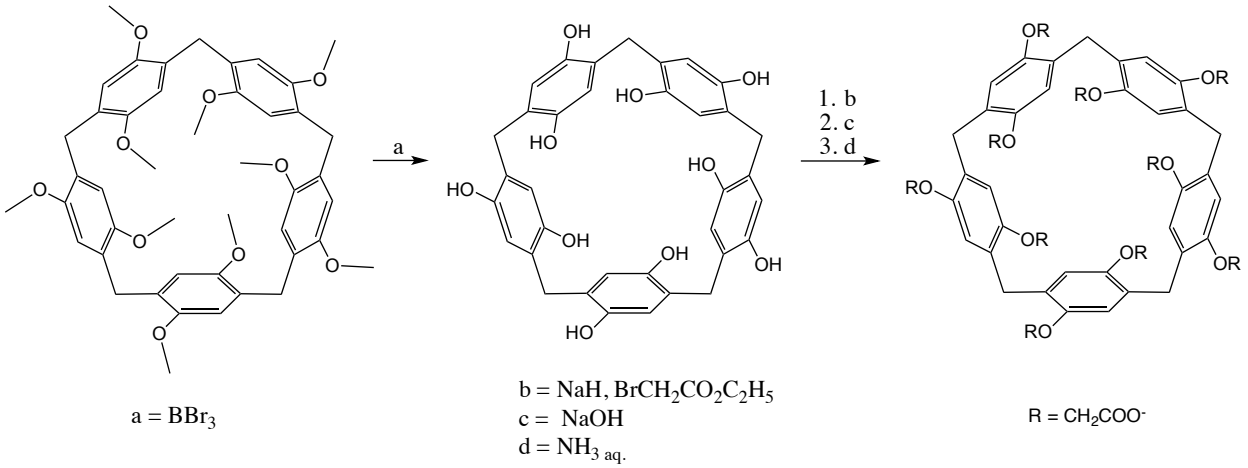

Scheme 1.7: Functionalisation of pillar[5]arene.

Pillar[5]arene can also be monofunctionalised so that only one of the macrocycle's

methoxy groups is replaced with another chemical species. There are two methods for such functionalisation - deprotection of one of the methoxy groups to an alcohol group using boron tribromide, which then can be further functionalised as desired[47] or cocyclisation of one already functionalised monomer with four non-functionalised monomers using boron trifluoride to give the functionalised pillar[5]arene[48].

Both of these methods give quite low yields (up to 30%), so an improved cocyclisation synthesis method with a 1:16 ratio of the substituted methoxybenzene to unsubstituted methoxybenzene using iron chloride was developed.[49] This method claimed yields between 50–85% for a range of substituted pillar[5]arenes and is important for this work.

1.5.2 Perylene diimides

Rylene diimides are flat, aromatic structures consisting of naphthalene units joined at the *peri* positions and an imide group connected to positions one and eight on the terminal naphthalene units. Due to their interesting electronic and optical properties as well as their thermal stability[50] they have been widely used in organic electronics[51], fluorescent standards[52] and in dyes[53].

The rylene diimide relevant to this work is perylene-3,4,9,10-tetracarboxylic diimide here referred to as PDI and shown in Figure 1.8. It can be synthesised from the corresponding anhydride, perylene-3,4,9,10-tetracarboxylic dianhydride (PTCDA) and a desired alkylamine or aniline.

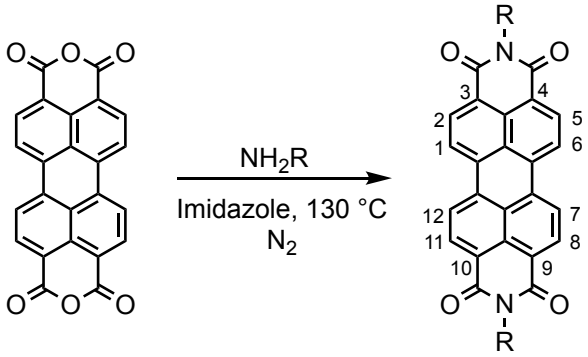

Scheme 1.8: Reaction scheme showing the synthesis of PDI from PTCDA.

PDIs contain a planar πsystem, which allows for intermolecular π- πinteractions between

separate PDI molecules. These interactions can lead to supramolecular self-assemblies such as stacks of PDIs with a separation from 3.34 to 3.55 Å[54]. Functionalisation of PDIs can tailor their properties to be useful for many different supramolecular assemblies[50].

1.5.3 Tetrazines

Tetrazines are six membered aromatic rings, which contain four nitrogen atoms. The 1,2,4,5-tetrazine, or s-tetrazine is important for this work and is shown in Scheme 1.9. Tetrazines have the highest proportion of N atoms within a single ring that is still stable.[55] They exhibit fluorescence and electrofluorochromism[56] and hence are interesting for their optical properties, and they can participate in Inverse Electron-Demand Diels-Alder (IEDDA) reactions, which makes them interesting in the synthesis of further compounds.[55]

Their synthesis was first discovered by Pinner in 1893 utilising a condensation of hydrazine and nitrile and subsequently an oxidation of the produced dihydrotetrazine.[57] It has since been improved in various ways (e.g. by the modified Pinner synthesis[58]) as shown in Scheme 1.9 along with an example IEDDA reaction.

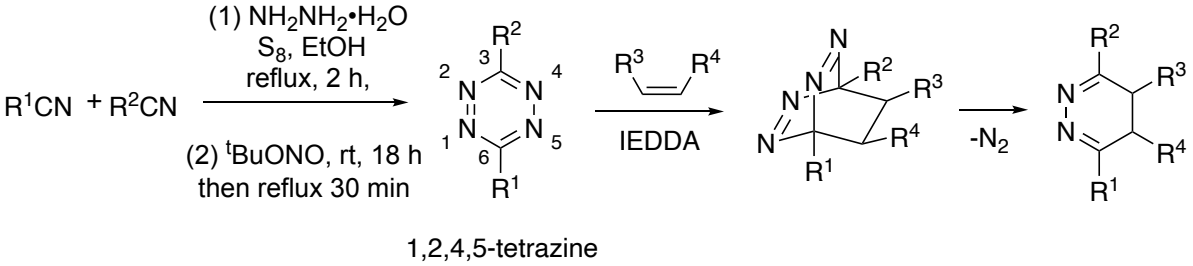

Scheme 1.9: Reaction scheme showing the synthesis of a tetrazine and its subsequent IEDDA reaction.

2 Synthesis of [3]handcuff rotaxane

2.1 Introduction

The use of perylene diimides (PDIs) in organic semiconductors[59–61] has driven an interest in studying their intermolecular properties.[50] A key interaction for all rylene diimides is their π-πstacking, which can influence their redox properties and hence the conductivity of the material.

Stacks of PDIs can be achieved using a few different methods to 'fix' them in place. For example, covalently bonding on one imide terminal,[62–64] on both terminals,[65–67] hydrogen bonding,[68,69] and mechanically bonding[39] PDI-PDI 'stacks' have been studied. The last of which is the PDI-PDI handcuff rotaxane previously synthesised within the group, discussed in the Introduction 1.4.2.

Understanding PDI aggregates beyond two-membered stacks is also desirable as a way of better understanding the bulk properties and trimers have been used in modelling to that end.[70] These are harder to synthesise, but some attempts at covalent trimers have been made: e.g. non-stacked planar trimers[71,72], macrocyclic trimers,[73] or stacks covalently bonded on one imide terminal.[74–76] The aim of this project was therefore to synthesise a mechanically bonded, three-membered PDI cofacial stack or a 'triple decker handcuff rotaxane', as an extension of the study into PDI stacks using the 'oligomer approach' (using stacks with a small number of components to mimic the structure-property relationships of larger ones).[77] No such species was found in the literature.

Studying PDI stacks using a handcuff rotaxane approach allows for these species to be in close proximity to each other and even oriented in specific ways (e.g. co-facially), yet still remain distinct species with potentially separate properties and the potential for motion or separation. This is likely more analogous to the behaviours of freely stacked molecules, than what is possible when utilising rigid covalent bonds or other interlocked structures such as catenanes.[39] However, due to the architectural complexity of handcuff rotaxanes and the numerous synthetic steps required to make them, these structures are difficult to synthesise.

The design of the handcuff rotaxane devised for this project was based on three PDI containing components: the central 'handcuff body' and two identical threaded 'handcuff rods' shown as a model in Figure 2.1.

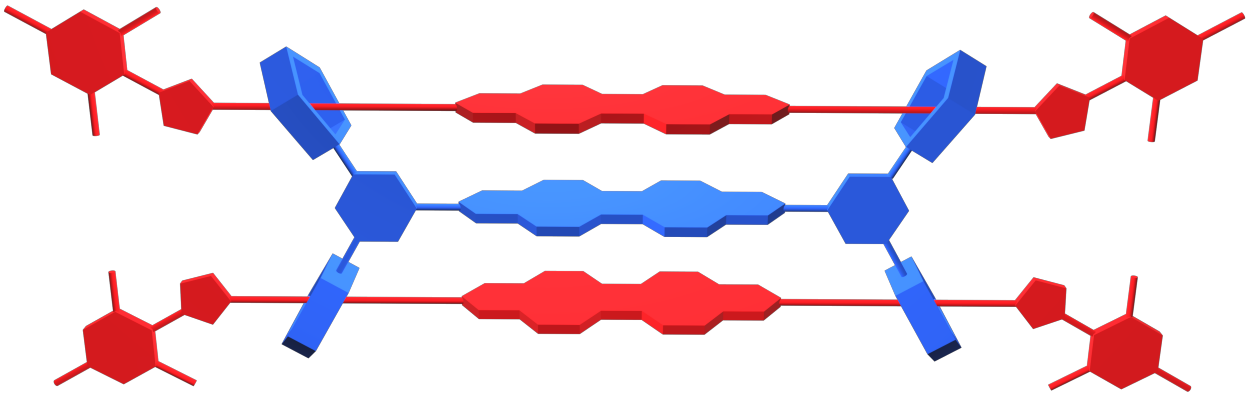

Figure 2.1: Model of the triple decker handcuff with PDI cores.

To accommodate two rods, the body needed to contain four macrocyclic species. These were chosen to be pillar[5]arenes as they contain a sizeable electron rich cavity needed for threading. Moreover, their synthesis and functionalisation is well established, which makes them good candidates for a wide range of potentially successful synthetic strategies. To maximise templating between the macrocycles and rods, the rods would then need to contain a small, electron poor species, such as an imidazole unit. This pattern of PDI cores, pillar[5]arene (**16**) macrocycles and imidazole units was chosen for this project, as it has been successfully utilised before[39,40,78] allowing for comparisons of the properties of interlocked species.

Since PDIs have a strong affinity for π-stacking with each other, the individual components of this proposed handcuff could possibly interact in this manner, organising rods and bodies close enough to each other for the imidazole-pillar[5]arene recognition motif to begin the threading process and for favourable entropic effects of displacing solvent molecules from the pillar[5]arene cavity to further drive mechanical bonding. The threaded rods and body can then be stoppered to prevent dethreading.

2.2 Synthesis of triple decker handcuff body

2.2.1 Synthesis of substituted pillar[5]arene

To synthesise a handcuff body containing pillar[5]arene macrocycles, their basic design must be altered so that one methoxy group is substituted for a pendant group which can be attached to other chemical species. For this work, a four-carbon aliphatic chain with a bromide leaving group was chosen and this substituted pillar[5]arene will here be called 4-bromobutane-pillar[5]arene. Its synthesis is shown in Scheme 2.1.

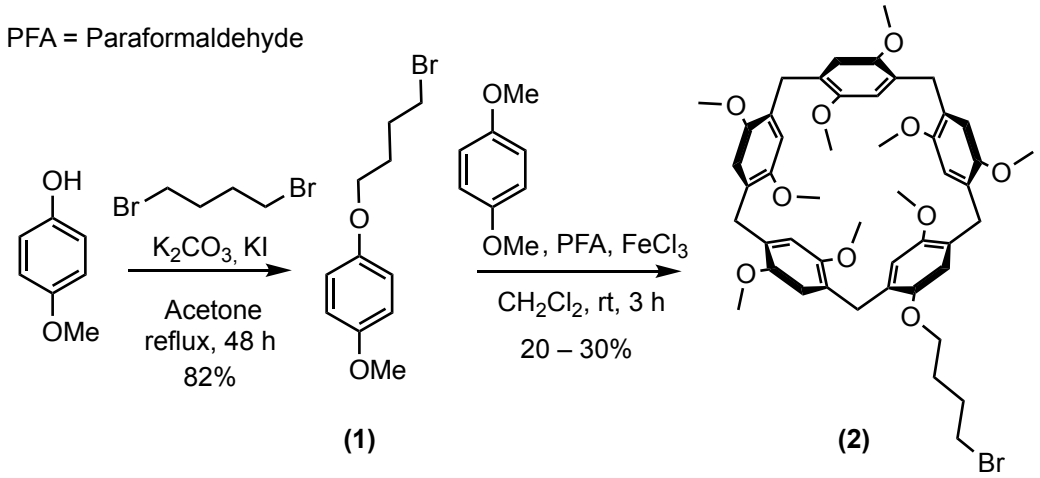

Scheme 2.1: Reaction scheme for the synthesis of the 4-bromobutane-pillar[5]arene (**2**).

Commercially available 4-methoxyphenol was combined with 1,4-dibromobutane in the presence of potassium carbonate and reacted to give 1-(4-bromobutoxy)-4-methoxybenzene (**1**).[79] Its synthesis was confirmed by ^{1}H NMR spectroscopy shown in the Appendix in Figure A.1 and Figure A.2. It was then co-cyclised with 1,4-dimethoxybenzene by reaction with paraformaldehyde in the presence of iron(III) chloride to give the 4-bromobutane-pillar[5]arene (**2**) according to the improved pillar[5]arene synthesis method[49] discussed in the Introduction (1.5.1). The product's presence was confirmed by ^{1}H NMR spectroscopy shown in the Appendix in Figure A.3 and Figure A.4.

Yields in the range of 20–30% were obtained for this reaction across many repetitions, in line with typical yields reported in the literature.[80–82] A more detailed explanation of the side products involved in a similar pillar[5]arene reaction and the purification method

developed for these types of compounds is given in Chapter 3.2.1.

2.2.2 Linker for pillar[5]arene macrocycles

In order to synthesise the handcuff body, a unit capable of connecting to two pillar[5]arene macrocycles and also to the PDI core is required, which will be referred to as a 'linker'. The linker function is to connect to the PDI core by reaction through an amine functional group and also to act as a bridge that connects to two pillarene moieties. Reaction of two such 'bis-pillar[5]arenes' with the PDI core will provide the necessary four pillar[5]arene units for the handcuff body. This naming convention is shown in Figure 2.2.

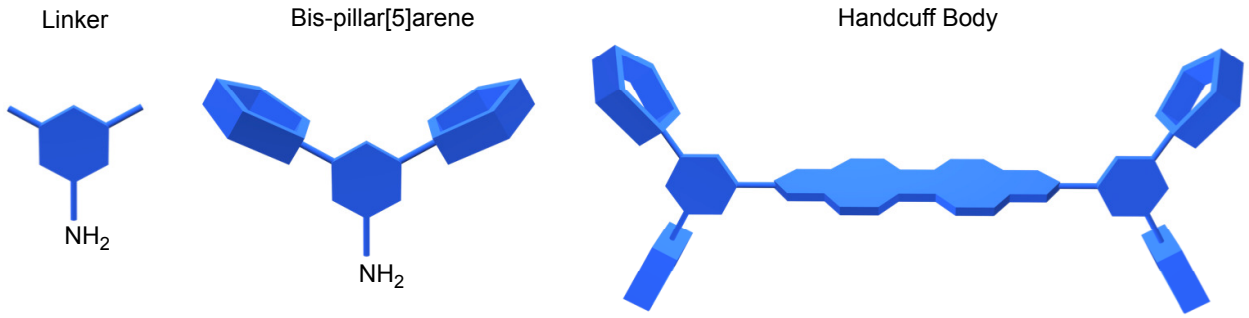

Figure 2.2: Naming convention showing a model of a linker, a bis-pillar[5]arene species and a handcuff body.

In previous syntheses of rotaxanes within the group a linker was not necessary, because a single pillar[5]arene macrocycle can be functionalised with an amine group and thus react with one side of a PDI core. However, for this work, a linker is crucial to make the addition of four macrocycles possible.

One complication of this synthesis is that simple PDIs have poor solubility[50] due to their strong stacking. Combining perylenetetracarboxylic dianhydride (PTCDA) with the linker first, to give a PDI with two reactive sites for macrocycle attachment to them is unlikely to disrupt the intermolecular π-stacking enough to improve solubility,[83] making the subsequent addition of the macrocycles to it quite difficult. Combining PTCDA with the bis-pillar[5]arene species, which is large and 'floppy' enough to disrupt the aggregation of the resultant PDIs is therefore a preferred order of reactions. This solubility allows for the PDI

based handcuff body to be dissolved with the handcuff rod during the final threading and stoppering reaction of the handcuff synthesis.

Many possibilities for the linker design exist, and three were explored in this work. The first one utilised amine alkylation (2.2.3), the second amide coupling (2.2.4) and the third ether synthesis (2.2.5).

2.2.3 The synthesis of an amino bis-pillar[5]arene species

The linker chosen to connect the macrocycles to the core for the handcuff body was ethylenediamine, a readily available species. It was chosen for a few reasons. Its flexibility should be advantageous in achieving a conformation where all of the macrocycles can be threaded by the rods. *N*-Boc-ethylenediamine, where only one of the amine groups is free to react with the macrocycles, reducing the possibility of side products, is commercially available. The free amine group is also nucleophilic, and should become more nucleophilic still with the first macrocycle substituted onto it, which could drive the formation of the bis-alkylated product. Meanwhile, the possibility of the quaternary product being formed was deemed unlikely without forcing conditions or very reactive alkylating agents. The structure of the proposed triple decker handcuff is shown in Figure 2.3.

Furthermore, if this type of reaction succeeded it would be easy to vary the length (with longer alkyl groups) or the structure of the chain (e.g. inserting ethers) between the two amine groups to better match the size of the handcuff rod or to improve solubility. Alternatively, since the substituted macrocycles would act as electron withdrawing groups, if that were to make the subsequent PDI reaction less efficient, this possible variability in chain structure could be useful to put more distance between those electron withdrawing groups and the amine that will react with PTCDA.

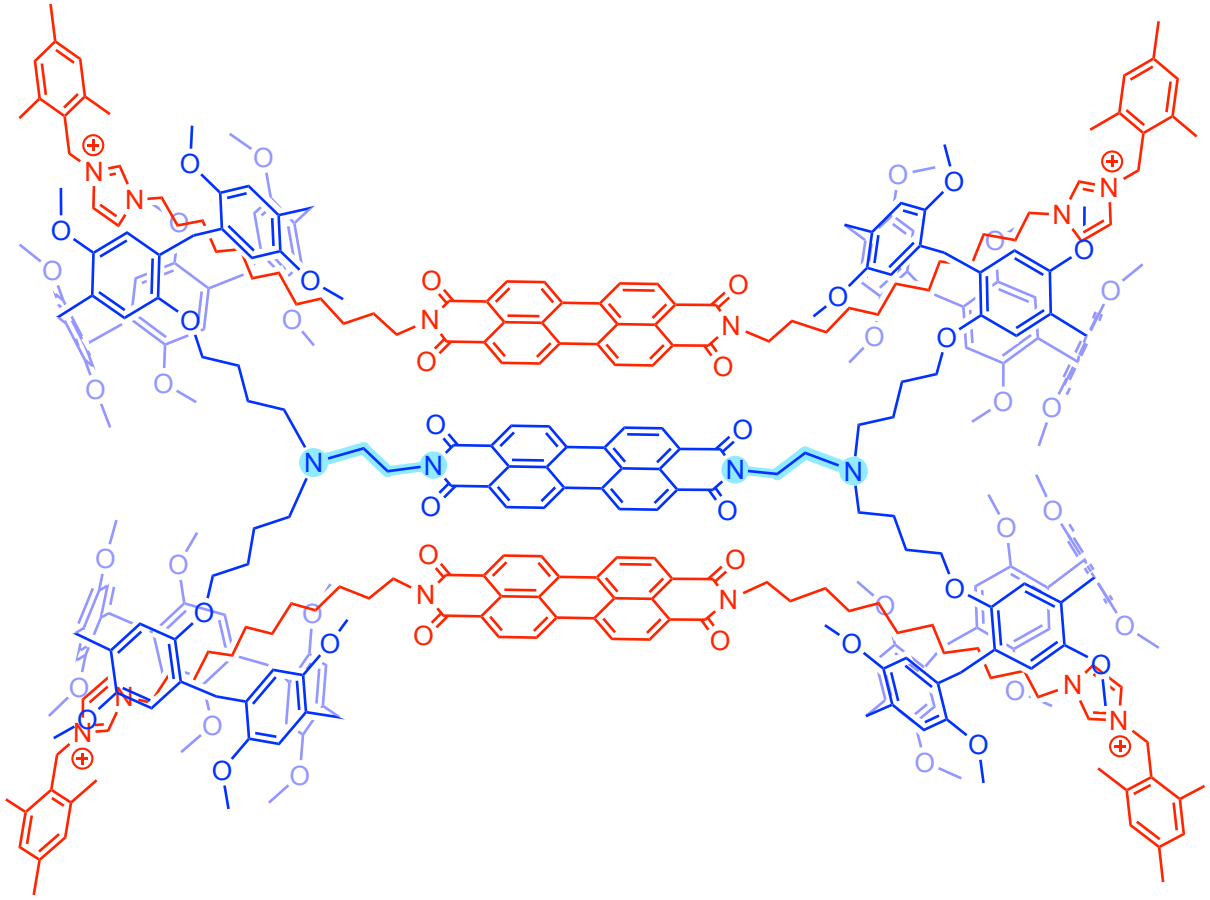

Figure 2.3: Proposed structure of a triple decker handcuff with PDI cores, pillar[5]arene macrocycles and imidazole units. The ethylenediamine linker is highlighted in blue.

Reactions of ethylene diamine or similar amines with bromoalkanes have been widely reported in the literature.[84–87] Following these literature examples, an attempt was made to join together two of the macrocycles using this linker before joining it with PTCDA to give the PDI based handcuff body. *N*-Boc-ethylenediamine was used in the presence of potassium carbonate as shown in Scheme 2.2.

To avoid the aforementioned forcing conditions, the heating was initially kept to 80 °C, but was raised to 135 °C when no reaction was observed. After heating, this reaction yielded only the mono-alkylated product (**3.1**). Some amount of it being formed was expected, but the total absence of the bis-alkylated amine species (**3.2**) was disappointing. This was confirmed by ^{1}H NMR spectroscopy shown in the Appendix in Figure A.5 and Figure A.6 and the yield of (**3.1**) was very low at 3%. Efforts to remove water and grease

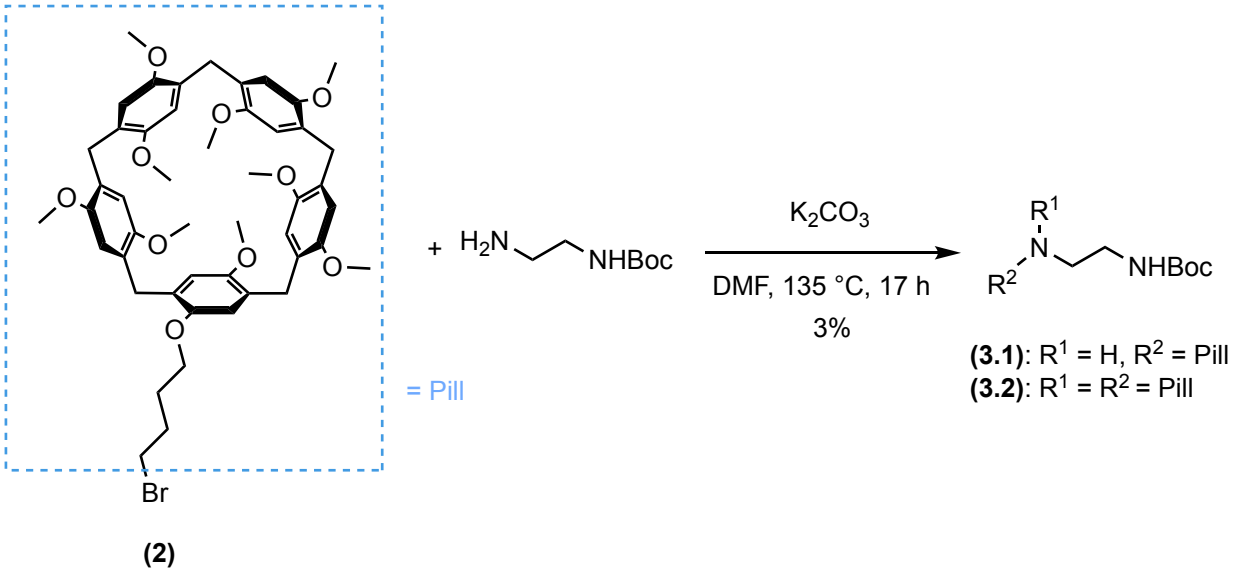

Scheme 2.2: Reaction scheme showing the synthesis of amino bis-pillar[5]arene (**3**) with the yield of the mono-substituted product (**3.1**) reported. Conversion of starting material or yield were not obtained for this reaction due to difficulty interpreting the ^{1}H NMR spectrum

contaminants (that were originally thought to be hexane) culminating in heating the sample under reduced pressure were made, but these extreme conditions led to the decomposition of the mono-alkylated amine (**3.1**) into a substituted pillar[5]arene species which resembles the 4-bromobutane-pillar[5]arene (**2**) starting material, as shown on the ^{1}H NMR spectrum in the Appendix in Figure A.7.

To conserve the pillar[5]arene starting material in the face of this extremely low yield, the next attempt was performed on an analogue, 1-bromohexane, and *N*-Boc-ethylenediamine under the same conditions as shown in Scheme 2.3.

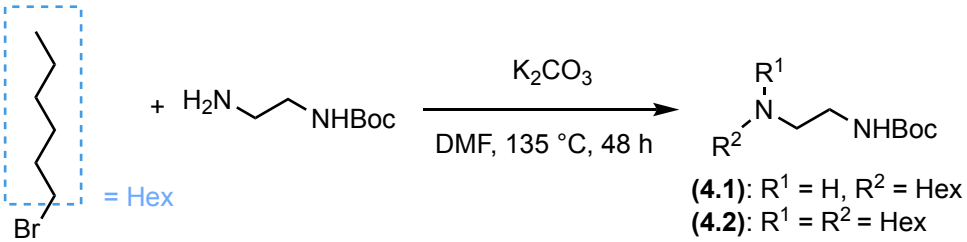

Scheme 2.3: Reaction scheme showing the synthesis of the analogue (**4**).

Unlike the previous reaction, electrospray ionisation mass spectrometry (ESI-MS) showed the mono- (**4.1**) and bis-alkylated (**4.2**) products at (m/z calc'd for $[M+H]^+$ (245.2224);

found (245.2208)) and (m/z calc'd for $[M+H]^+$ (329.3163); found (329.3169)) respectively. The pillar[5]arene containing (**3.1**) and (**3.2**) species might have been too large for the ESI-MS. The reaction was stopped when *N*-Boc-ethylenediamine and (**4.1**) was no longer detectable using ESI-MS. ^{1}H NMR spectra of the crude product were taken after extraction with CH_2Cl_2 and are shown in the Appendix in Figure A.8 and A.9. They show many of the expected peaks, but also ones that are difficult to identify. The ^{1}H NMR spectrum also exhibits signs of many possible side products being present. This reaction could have led to the formation of the quaternary amine product in addition to the mono- and bis-substituted ones, and the mono-substituted product's non-protected amine could attack the *N*-Boc's carbonyl to form a cyclic side product (imidazolin-2-one).[88]

To avoid at least the quaternary amine side product, an aldehyde substituted pillar[5]arene could be considered in a sequential reductive amination with *N*-Boc-ethylenediamine. An oxybenzaldehyde-substituted pillar[5]arene has been reported previously as the product of a reaction between 4-bromobutane-pillar[5]arene (**2**) and 4-hydroxybenzaldehyde in the presence of potassium carbonate and potassium iodide in good yields of 70–80%.[89,90] Unfortunately, other authors report much lower yields of 20–30%,[79,91,92] which seem more realistic after the low yields and difficulties with separations in a similar reaction that will be discussed in the next chapter in section 3.1.1. Furthermore, it is not certain that adding two oxybenzaldehydes to an amine would be sterically possible.

Due to the somewhat disappointing results with the amino linker, work on that linker was paused while another linker was explored.

2.2.4 The synthesis of an amido bis-pillar[5]arene species

The second linker chosen was the readily available 5-aminoisophthalic acid, with the expectation that an amide coupling with an amine substituted pillar[5]arene would prove to be a more reliable reaction. The proposed structure of the triple decker handcuff rotaxane that utilises this linker s shown in Figure 2.4

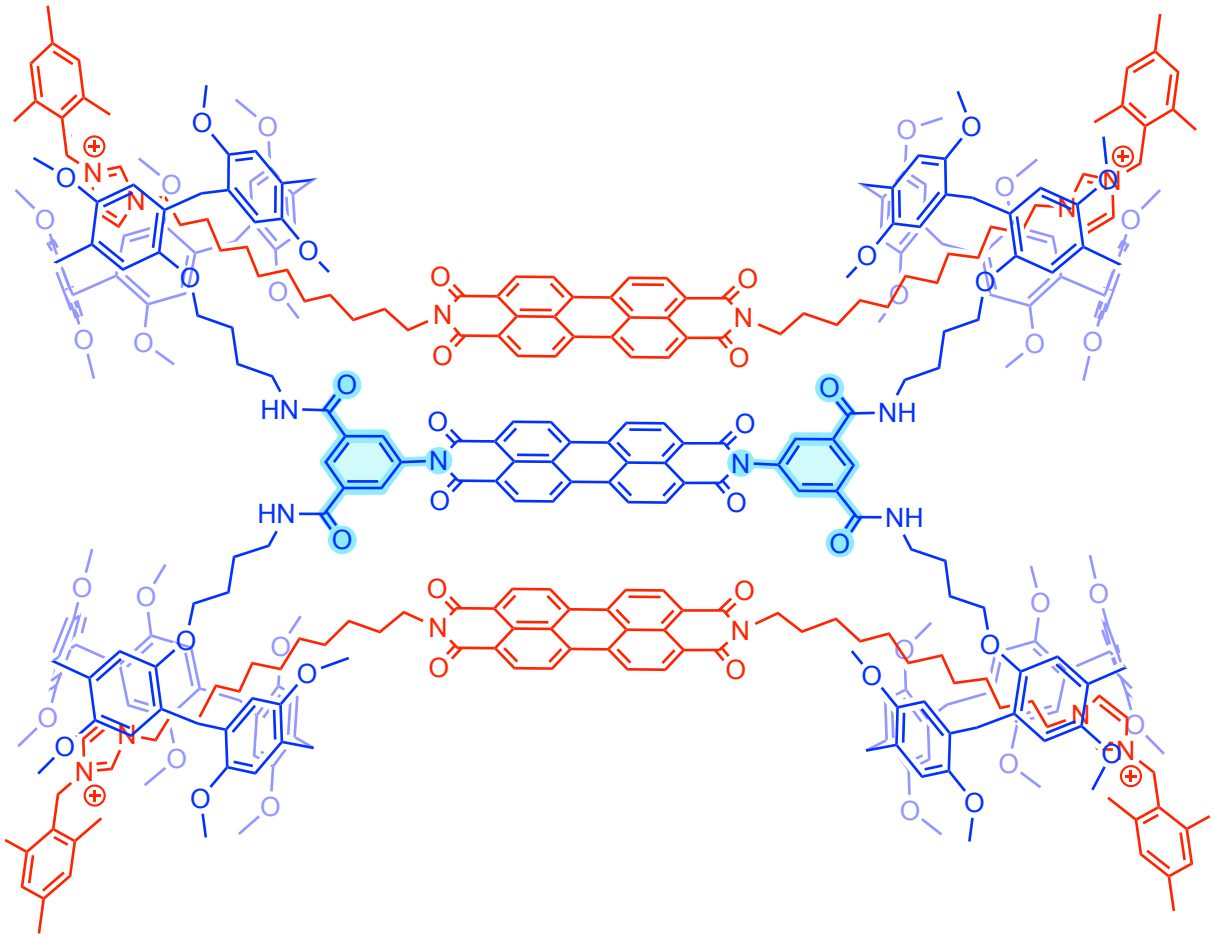

Figure 2.4: Proposed structure of a triple decker handcuff with PDI cores, pillar[5]arene macrocycles and imidazolium units. The linker is highlighted in blue.

The abundance of amide coupling agents should make it possible to find favourable conditions for this reaction. The final amide should also prove more stable to heat and hence avoid accidental decomposition as was the case for amino bis-pillar[5]arene (**3**). In this case the chosen linker was rigid, which could be advantageous for keeping the macrocycles in positions that make threading more likely. Finally, the reaction between isophthalic acid

and PTCDA has been widely reported in the literature,[93–96] confirming the feasibility of making the handcuff body with this amido bis-pillar[5]arene.

First, 4-aminobutane-pillar[5]arene (**6**) is needed for this amide coupling. It can be produced from 4-bromobutane-pillar[5]arene (**2**) through the Gabriel synthesis[97] shown in Scheme 2.4. Using 4-phthalimidobutane-pillar[5]arene (**5**) as an intermediate avoids multiple aminations.

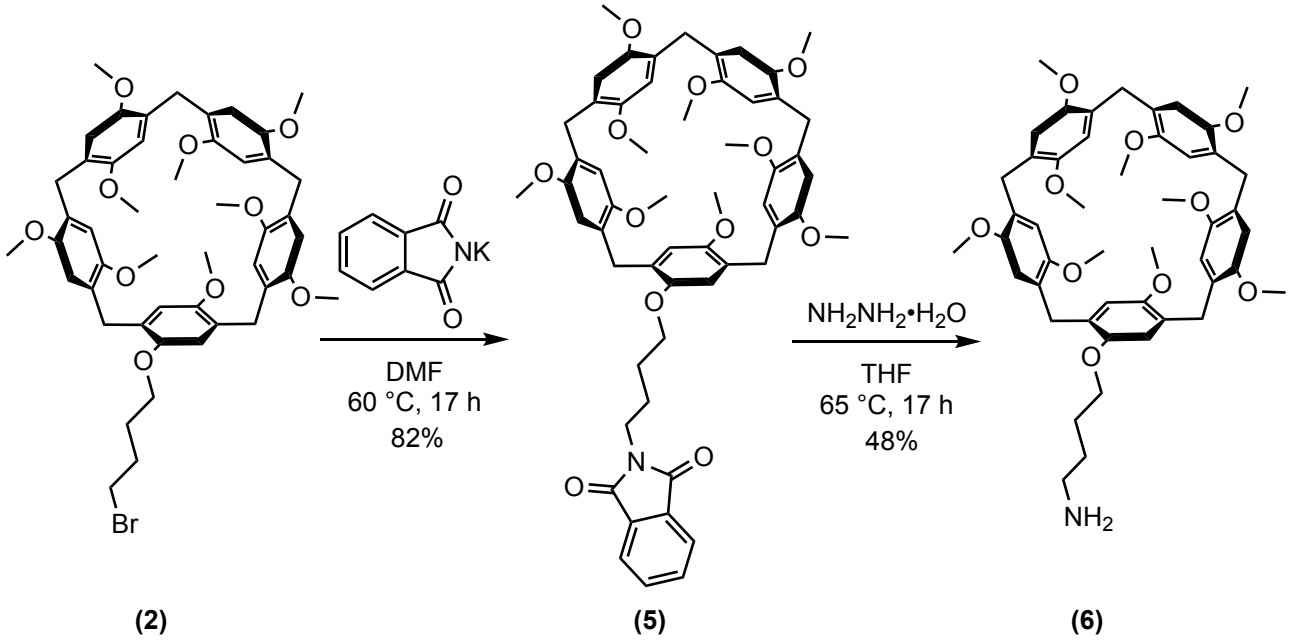

Scheme 2.4: Reaction scheme for the Gabriel synthesis of 4-aminobutane-pillar[5]arene (**6**) with 4-phthalimidobutane-pillar[5]arene (**5**) as an intermediate.

4-bromobutane-pillar[5]arene (**2**) and potassium phthalimide were mixed together to give 4-phthalimidobutane-pillar[5]arene (**5**). Its presence was confirmed by ^{1}H NMR spectroscopy shown in the Appendix in Figure A.10 and Figure A.11. It then reacted with hydrazine to give 4-aminobutane-pillar[5]arene (**6**). Its presence was confirmed by ^{1}H NMR spectroscopy shown in the Appendix in Figure A.12 and Figure A.13.

Before two 4-aminobutane-pillar[5]arene (**6**) macrocycles can be joined using the 5-aminoisophthalic acid linker, the linker itself needed to have its amine group protected[98] as shown in Scheme 2.5 giving Boc-5-aminoisophthalic acid (**7**). This was to avoid side reactions between the acid group of one and amine group of another linker molecule.

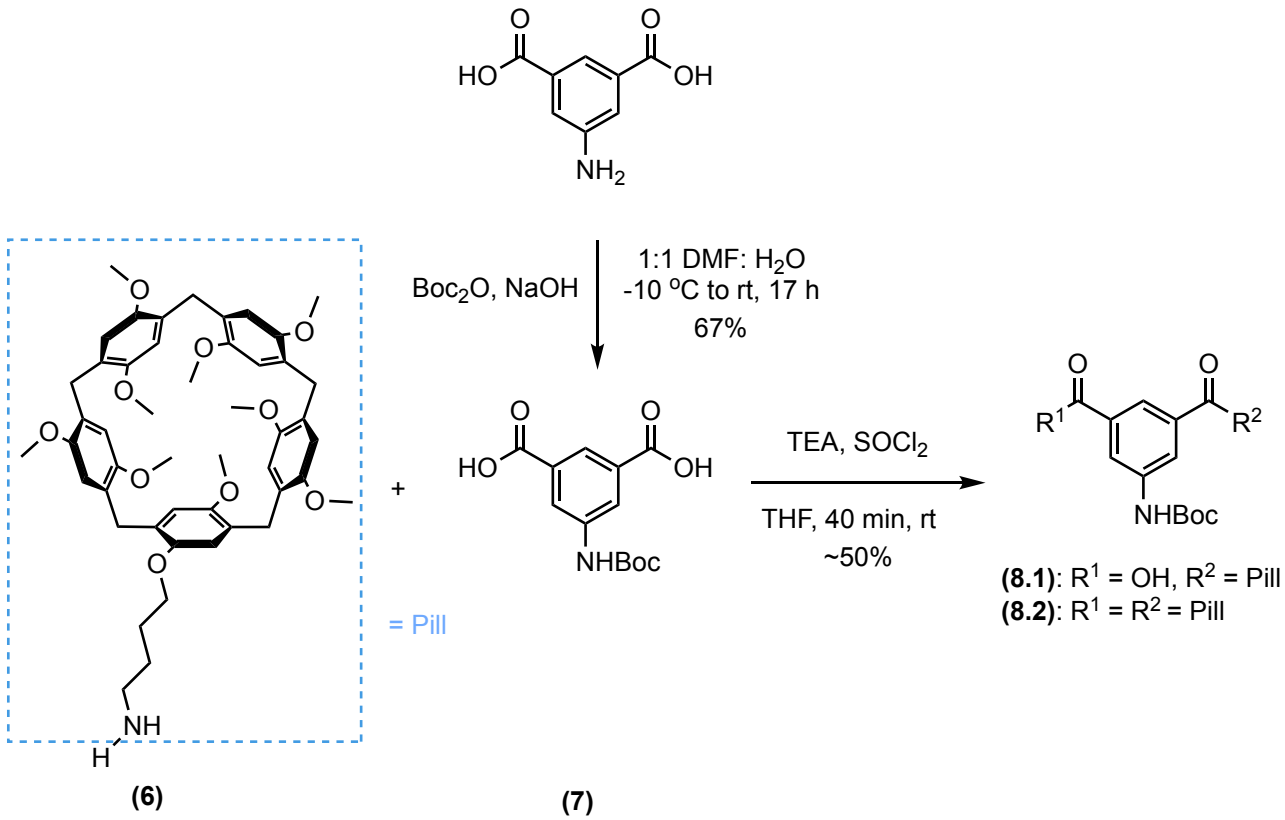

Scheme 2.5: Reaction scheme for the synthesis of the amido bis-pillar[5]arene (**8**) from Boc-5-aminoisophthalic acid (**7**) and 4-aminobutane-pillar[5]arene (**6**). ∼50% is the lower estimated conversion rate of (**6**) according to ^{1}H NMR as the mono- (**8.1**) and bis-substituted (**8.2**) products were not definitively separated.

The protected linker B, Boc-5-aminoisophthalic acid (**7**), was then mixed with 4-aminobutane-pillar[5]arene (**6**) and thionyl chloride. The mono-substituted version of the desired product (**8.1**) was detected using ESI-MS (m/z calc'd for $[M+H]^+$ (1069.4703); found (1069.4675)), but the desired bis-substituted product (**8.2**) was not. Another aliquot of thionyl chloride and 4-aminobutane-pillar[5]arene (**6**) was added to promote the second amide formation. The desired product was still not detected using ESI-MS, but to ensure that this was due to the molecule's absence rather than its large size or fragility, the reaction mixture was also tested using MALDI-TOF MS. Both the mono- and bis-substituted products were detected using MALDI-TOF MS, as shown in Figure 2.5, so the reaction mixture was purified.

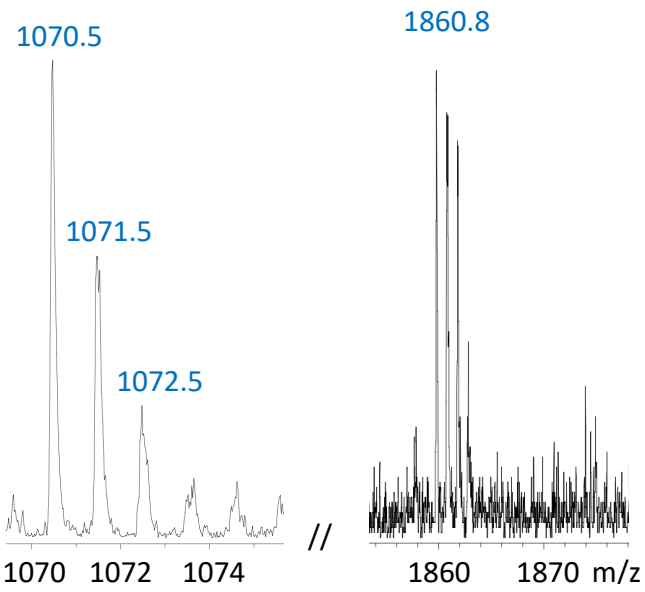

Figure 2.5: Zoom of the MALDI-TOF MS of (**8.1**): MALDI m/z calc'd for [M] (1069.4703); found (1070.467),and (**8.2**): MALDI m/z calc'd for [M] (1759.8129); found (1860.781)

The ^{1}H NMR of this reaction mixture after purification is shown in Figure 2.6(b). The starting material, Boc-5-aminoisophthalic acid (**7**), is not soluble in chloroform or CH_2Cl_2 so was assumed to be entirely removed during purification. This means that the Boc (1.55 ppm), aromatic isophthalic (7.98 ppm) and amide (7.17 ppm) peaks should belong to the mono- (**8.1**) and bis- (**8.2**) substituted products and are hence useful diagnostic peaks. The amide hydrogens can undergo hydrogen-deuterium exchange and are therefore unreliable, the Boc group peak appears in a region with a lot of other peaks, hence its integration might also be unreliable, leaving the aromatic isophthalamide peaks as the most reliable diagnostic peaks. All other peaks are here integrated against those isophthalamide aromatic peaks.

For the desired (**8.2**), the ratio of aromatic isophthalamide peaks to the pillar[5]arene aromatic peaks (6.77 ppm) should be 3:20 (3:10 for mono- (**8.1**)). In this case, it is 3:30. The higher pillar[5]arene integrations are therefore likely due to unreacted 4-aminobutane-pillar[5]arene (**6**), which has ten aromatic hydrogens. If we assume that this mixture contained only (**8.2**) and no (**8.1**), that would give us a lower estimate of ∼50% unreacted starting material. A pure (**8.1**), would give us ∼67% unreacted starting material. In either case, the conversion rate of starting material is quite low for a multistep synthesis.

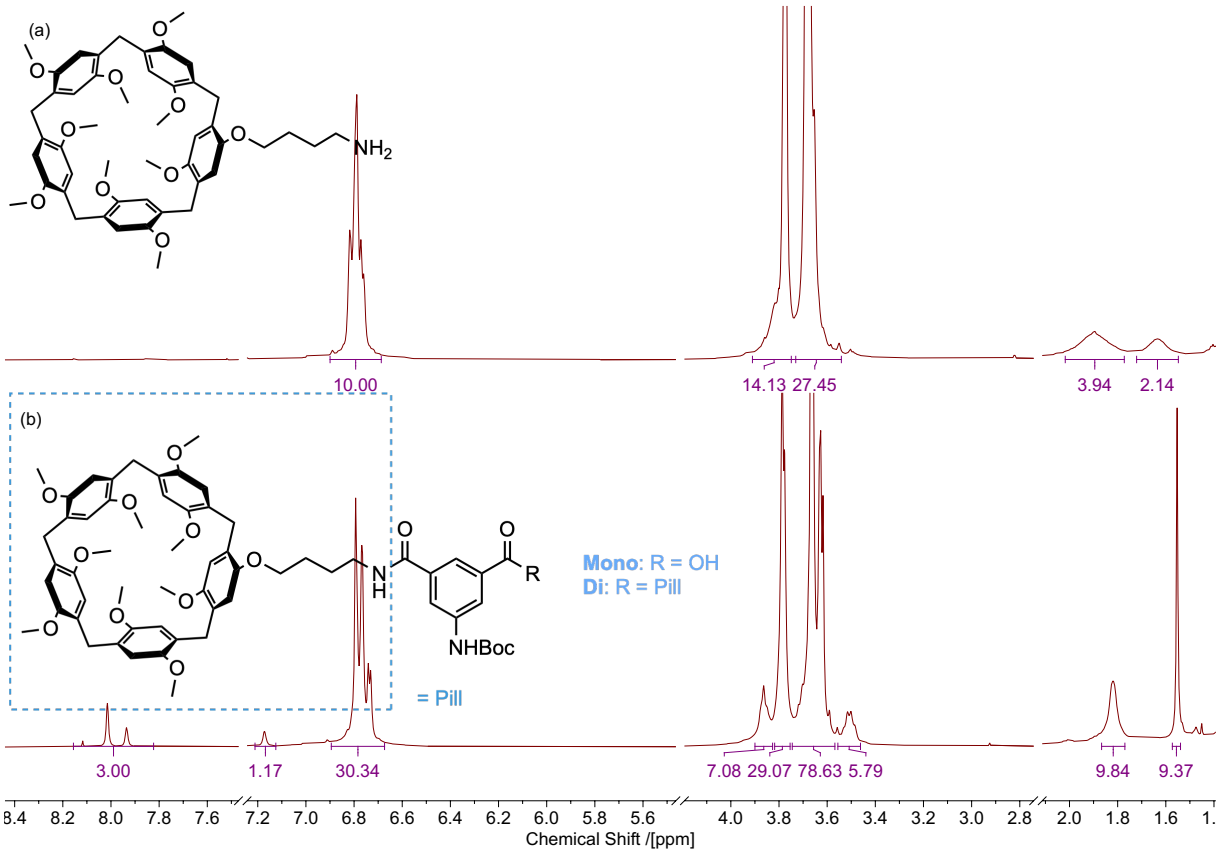

Figure 2.6: ^{1}H NMR Spectrum of (a) 4-aminobutane-pillar[5]arene (**6**) and (b) amido bis-pillar[5]arene (**8**).

It is harder to estimate the ratios of (**8.1**) to (**8.2**) present in this mixture from the ^{1}H NMR spectrum, as the only peak which would allow us to do so is the unreliable amide peak, as it is different for the two products (1 for (**8.1**), 2 for (**8.2**)), and also not present in 4-aminobutane-pillar[5]arene (**6**). If no exchange was happening, then the ratio of 3:1 observed here would clearly signify this to be majority (**8.1**), but without further evidence, this is not at all certain.

Attempts at further purification did not yield better results or definitively remove one of the products from the potential mixture. The possible presence of both the desired and side product, the difficulty in separating them and the overall low conversion of the starting material for this reaction suggested that trying a different coupling agent would be beneficial.

To conserve 4-aminobutane-pillar[5]arene (**6**) the next attempt of this synthesis was on an analogue, which was chosen to be 1-octylamine as shown in Scheme 2.6. For the first attempt, the conditions were kept the same as for the amido bis-pillar[5]arene (**8**) reaction to have a good comparison.

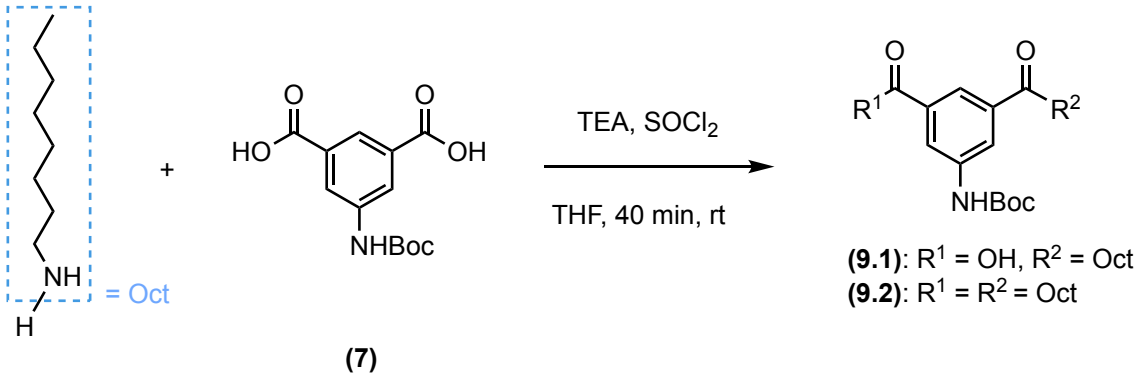

Scheme 2.6: Reaction scheme for the synthesis of the analogue species (**9**). Conversion of starting material or yield were not obtained for this reaction due to difficulty interpreting the ^{1}H NMR spectrum.

The reaction was monitored using ESI-MS as the mono-substituted product (**9.1**) was easily visible (m/z calc'd for $[M+H]^+$ (393.2384); found (393.2385)). The bis-substituted product (**9.2**) was sometimes visible (m/z calc'd for $[M+H]^+$ (504.3796); found (504.3777)). This time, additional equivalents of amine and thionyl chloride were added three times over the course of the reaction aiming to drive the reaction to completion. Unfortunately this did not succeed. An aliquot of the reaction mixture was worked up and subjected to ^{1}H NMR spectroscopy, shown in the Appendix Figure A.17.

Without the pillar[5]arene peaks obscuring the aromatic region, two sets of aromatic isophthalic peaks are visible (7.97 and 7.84 ppm) and (6.98 and 6.87 ppm). Two aliphatic quartets at 3.43 ppm and 3.14 ppm (-C**H**$_2$-NHC=O-) appear similarly duplicated. Finally, the *t*-Bu peak is also duplicated at 1.43 and 1.42 ppm. These duplicated peaks are shown in Figure 2.7. Such duplication could signify the presence of both (**9.1**) and (**9.2**).

As with amido bis-pillar[5]arene (**8**), thionyl chloride was deemed an unsuitable coupling agent for this reaction. One reason that conversion of starting material to product could be suffering is if the HCl given off during the formation of the intermediate acid chloride was

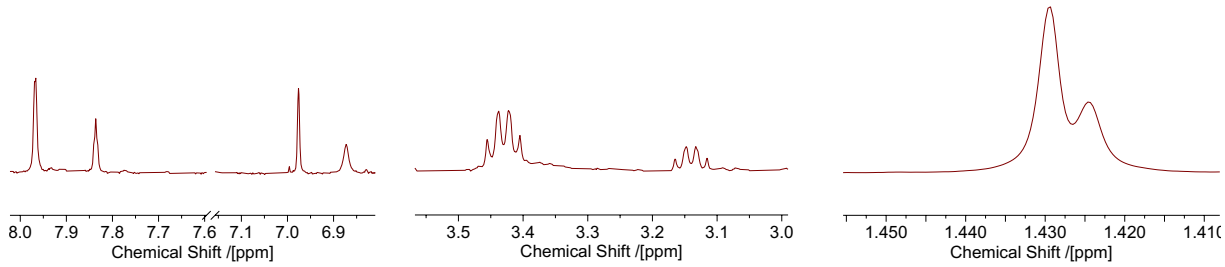

Figure 2.7: Duplicated peaks in the ^{1}H NMR spectrum of the (**9**) reaction mixture.

protonating the amine and hence making it non-nucleophilic, stopping its reaction with the acid chloride. The TEA added to the reaction mixture should quench the HCl, but was perhaps insufficient. Increasing the amount of TEA in this reaction to improve conversion could be worthwhile.

The next attempt to synthesise the analogue (**9**) was performed using carbonyldiimidazole (CDI) as a coupling agent.[99] This attempt was even less successful; TLC monitoring of the reaction did not show any progression and ESI-MS only found the mono-substituted product (**9.1**) (m/z calc'd for $[M+Na]^{+}$ (415.2209); found (415.2203)) very rarely. Some of the difficulty could be explained by CDI's instability towards atmospheric moisture.[100]

When looking back at these syntheses during the writing of this thesis, it became apparent that EDC is a more promising coupling agent that should have been explored. This coupling agent has been used for similar coupling reactions with pillar[5]arene substrates.[101,102]

2.2.5 The synthesis of an ether bis-pillar[5]arene species

The next linker chosen for these experiments was 5-aminobenzene-1,3-diol. This is another rigid linker like 5-aminoisophthalic acid, but it would rely on a substitution reaction between the alcohol groups of the linker and the bromide from 4-bromobutane-pillar[5]arene (**2**), allowing us to sample a different chemical space with the aim of finding better yielding reactions. This was also an attempt to avoid problems with doubly substituting an amine encountered with amino bis-pillar[5]arene (**3**). The proposed structure of this triple decker handcuff is shown in Figure 2.8.

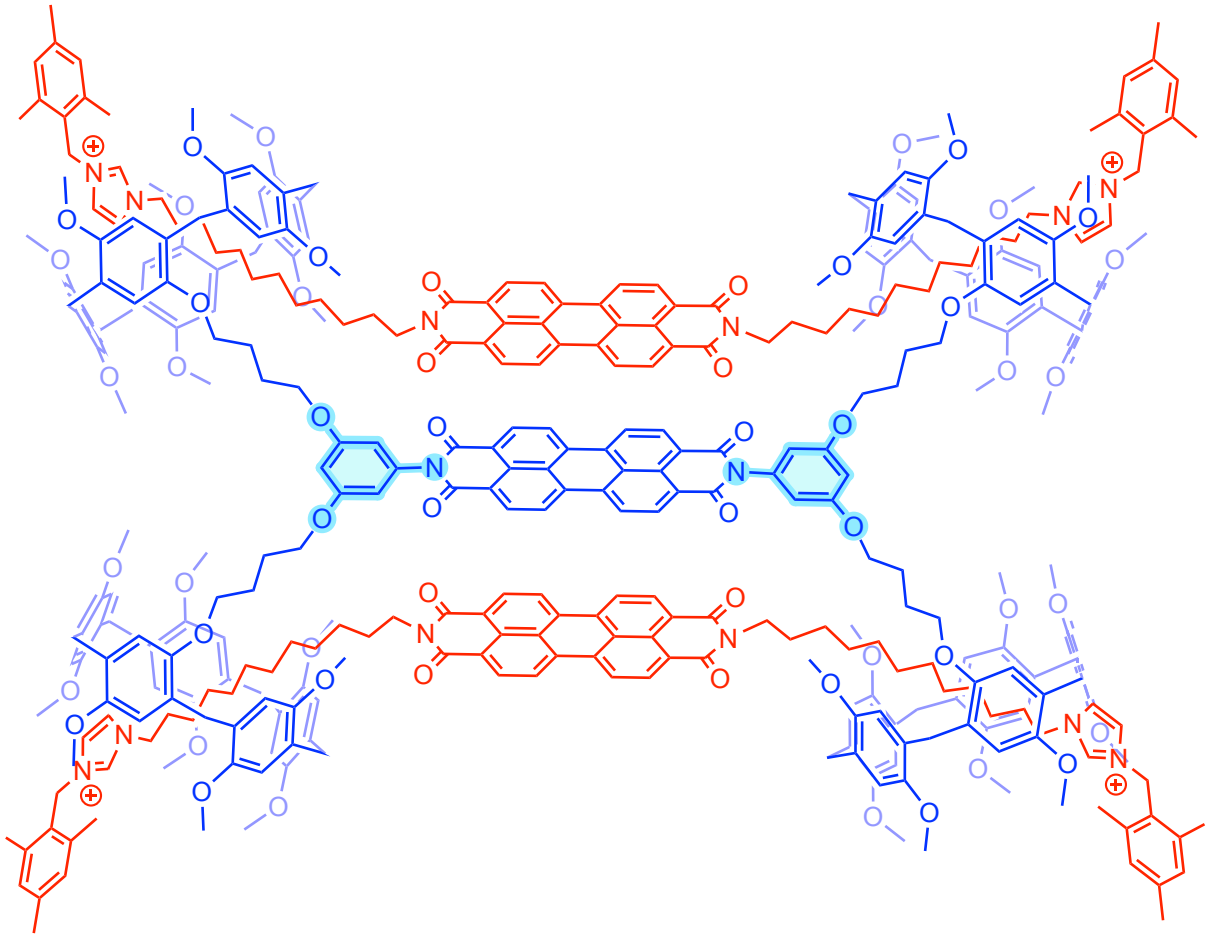

Figure 2.8: Proposed structure of a triple decker handcuff with PDI cores, pillar[5]arene macrocycles and imidazolium units. The linker is highlighted in blue.

Due to limiting costs of 5-aminobenzene-1,3-diol, the reaction was first explored with phloroglucinol (benzene-1,3,5-triol) as an analogue. The first attempt following literature methods[103–105] was therefore between phloroglucinol and 4-bromobutane-pillar[5]arene (**2**) as shown in Scheme 2.7.

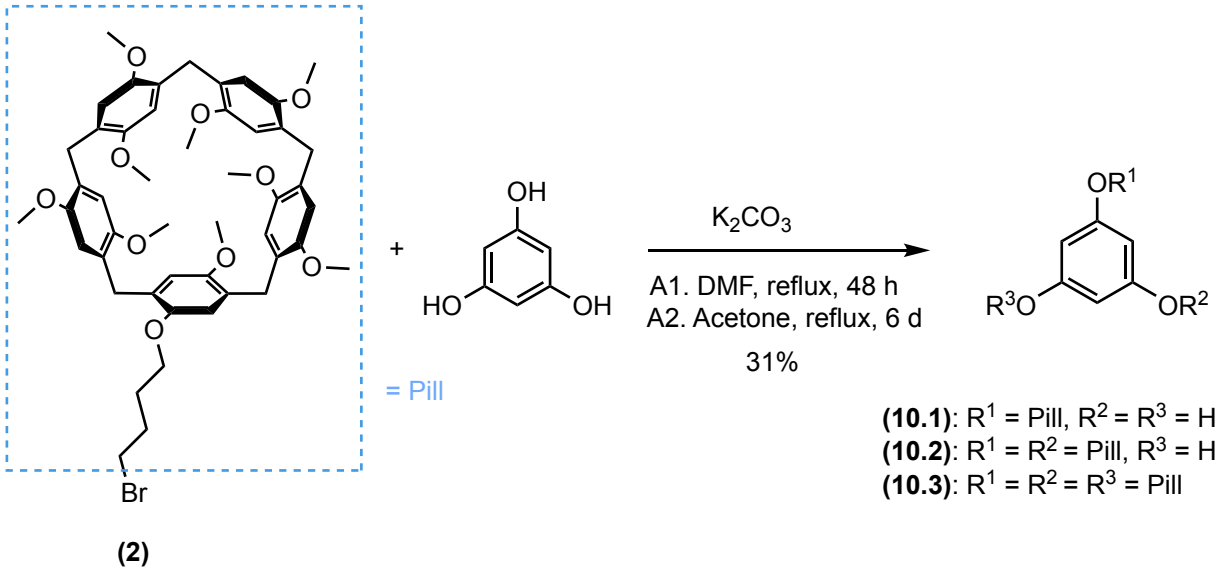

Scheme 2.7: Reaction scheme for the synthesis of ether bis-pillar[5]arene (**10**). The yield quoted here is for the tris-substituted product (**10.3**) isolated during the second attempt (A2) at this synthesis.

A mixture of mono- (**10.1**), bis- (**10.2**), and tris-substituted (**10.3**) products was expected during the reflux of three equivalents of 4-bromobutane-pillar[5]arene (**2**) with one equivalent of phloroglucinol, and an excess of potassium carbonate. However, after 24 h none of the possible products were detected using ESI-MS, so the reaction was continued for another day. All three products were detected after 48 h with MALDI-TOF MS as shown in Figure 2.9, however the signal for the bis-substituted (**10.2**) product was rather weak. The reaction was stopped at this point to evaluate its success.

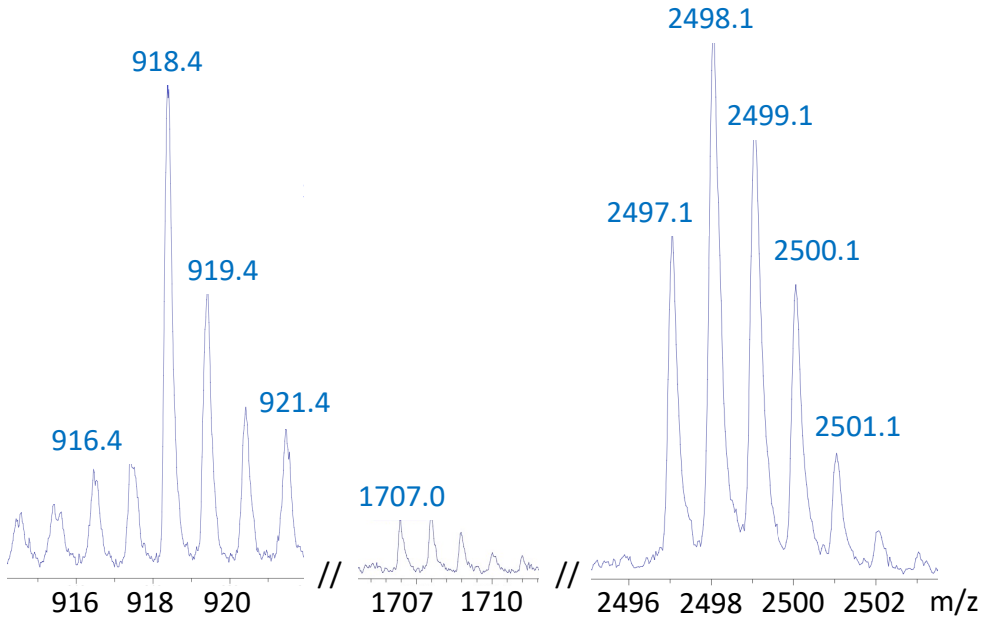

Figure 2.9: Zoom of the MALDI-TOF MS of (**10.1**): MALDI m/z calc'd for [M] (916.4034); found (916.450). (**10.2**): MALDI m/z calc'd for [M] (1706.7751); found (1706.956). (**10.3**): MALDI m/z calc'd for [M] (2497.1468); found (2497.052).

After multiple flash column chromatography purifications, a white solid was obtained. The MALDI-TOF MS spectrum still confirmed the presence of all three species (**10.1**), (**10.2**), and (**10.3**), as well as the starting material (**2**). The ^{1}H NMR spectrum (shown as (b) in Figure 2.10) provides supporting evidence for this solid being a mixture of products and starting material. The integral ratio of the aromatic pillar[5]arene peaks at 6.83 – 6.74 ppm to the aromatic phloroglucinol peaks at 6.18 – 6.09 ppm would be 10:3 for (**10.1**), 20:3 for (**10.2**) and 30:3 for (**10.3**). (**10.3**) would also only have single aromatic phloroglucinol peak. For any mixture of just those three compounds that integral ratio would be below 30:3 in line with the exact amounts of each of those compounds present. For this mixture, that ratio is 36:3. The ratios of the rest of the peaks relative to the aromatic core peaks are also higher than possible for (**10.3**).

The two aromatic core peaks at 6.14 (rather than one peak) suggest that there are also significant amounts of (**10.1**) or (**10.2**) or both, present, which should bias all the ratios to be lower than those of pure (**10.3**). With that in mind, the higher than expected integrations can only be explained by the presence of a significant amount of the starting material (**2**)

in this mixture as well. This could also explain the three multiplets in the shifted aliphatic region at 3.95 ppm (For any pure ether bis-pillar[5]arene (**10**) this should be two peaks and for (**2**) it is one peak).

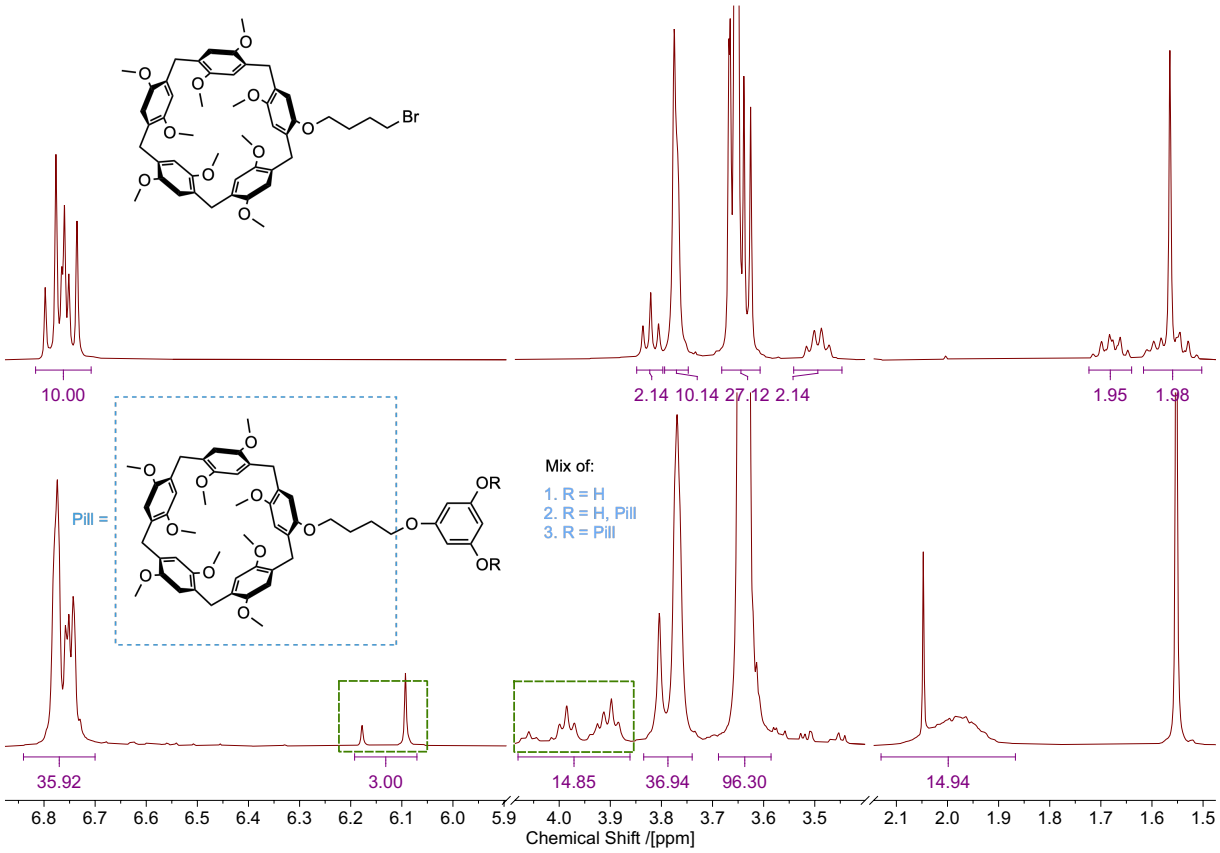

Figure 2.10: ^{1}H NMR spectra of (a) 4-bromobutane-pillar[5]arene (**2**), (b) Mixture of mono- (**10.1**), bis- (**10.2**), and tris-substituted (**10.3**) products.

DMF can decompose to dimethylamine when heated near its boiling point or in the presence of acidic or basic materials.[106] In this reaction it was both heated for a long time and in the presence of potassium carbonate, which could have led to an appreciable quantity of dimethylamine being formed. Dimethylamine can react with 4-bromobutane-pillar[5]arene (**2**) and hence interfere with its desired reaction with phloroglucinol, which might be why the yield for this reaction was so low. Due to this, a solvent change was deemed necessary for further exploration.

For the second attempt, acetone was used as a solvent instead of DMF and the reaction was also left to continue for a longer period of six days, which could improve conversion of starting materials to products. Furthermore, this time two equivalents of 4-bromobutane-pillar[5]arene (**2**) were mixed with one equivalent of phloroglucinol (instead of three and one). The new ratio of starting materials was intended to cause less of the tris-substituted product (**10.3**) to form.

The MALDI-TOF MS of the purified reaction mixture did not show (**10.1**) or (**10.2**), but did show the starting material (**2**) and the tris-substituted product (**10.3**). Its ^{1}H NMR is assigned in the Appendix in Figure A.18. The integral ratios of the aromatic phloroglucinol core peaks to the rest of the peaks were much closer to the expected ratios for the tris-substituted product (**10.3**). It also confirms the lack of (**10.1**) and (**10.2**) observed by MALDI-TOF MS, as the extra aliphatic and aromatic peaks present in the mixture are not present here. Based on this it can be concluded that these new conditions led to a majority tris-substituted product (**10.3**) being formed with much less of the starting material still present. This might be due to the extended reaction time which should favour the more substituted product, or due to the solvent change. The yield for this new set of conditions was however still poor at 31%.

Despite not being the desired product in this reaction, this novel tris-pillar[5]arene species could have uses of its own. If paired with a tri-armed rod species, a threefold interlocked handcuff rotaxane (sometimes called molecular bundle) could be formed. These have been used as elevators where a platform moves between stations.[34,107–114] More similarly to this novel compound, other tris-pillar[5]arene species have been previously synthesised and have varied applications such as: nanofibres, spherical vesicles, sheet superstructures[102] or can transform from 0D to 3D assemblies based on concentration changes.[115]

To conserve 4-bromobutane-pillar[5]arene (**2**), the next attempt at synthesis was performed on the substituted monomer unit (**1**) as shown in Scheme 2.8. Different conditions for ether synthesis were found (as described in Section 3.1.1) and used here with the expectation of better yields.

Two equivalents of (**1**) were mixed with one equivalent of phloroglucinol in the presence of

sodium hydride and 18-crown-6 (18C6).[116] An aliquot of the reaction mixture was removed after 24 h to monitor progress via ESI-MS, which detected the mono- (**11.1**) (m/z calc'd for $[M+Na]^+$ (327.1203); found (327.1215)) and bis-substituted (**11.2**) products (m/z calc'd for $[M+Na]^+$ (505.2197); found (505.2207)), but not the tris-substituted (**11.2**) product.

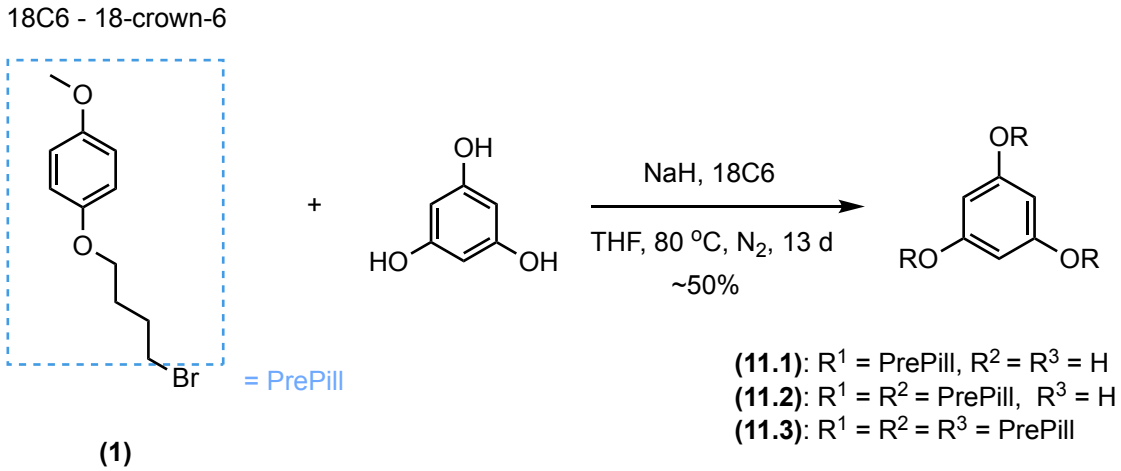

Scheme 2.8: Reaction scheme for the synthesis of the analogue species (**11**). The conversion rate of the starting material according to ^{1}H NMR is $\sim$ 50%, which is quoted here as the different products were not separated.

At the same time a ^{1}H NMR spectrum was acquired, shown in Figure 2.11(a). Two diagnostic peaks were useful for progression monitoring: the aliphatic R-C$\mathbf{H}_2$-Br peak of the starting material, (**1**), at 3.51 ppm (see Appendix Figure A.1 for the ^{1}H NMR spectrum of (**1**)) and the aromatic core peaks of the products, (**11**) at 5.97 ppm. The former exists exclusively in the starting material and the latter exclusively in the products. After 24 h the product aromatic peaks were detected, but the reagent aliphatic peak was also present, suggesting that the reaction was progressing, but not yet finished.

The reaction was continued and monitored daily for another two days, then for another ten days without monitoring, whereupon it was stopped and a final ^{1}H NMR spectrum was taken. The progress of this reaction at those points in time is shown in Figure 2.11(b), (c), and (d). The integrations of the product aromatic peak increases relative to the integrations of the reagent aliphatic peak with time, showing the product being formed and the starting material being consumed. This process is also visible in the coalescence of the two aliphatic peaks (2.08 (R-CH_2-C$\mathbf{H}_2$-CH_2Br), 1.95 (R-C$\mathbf{H}_2$-CH_2-CH_2Br)) of the starting material, (**1**),

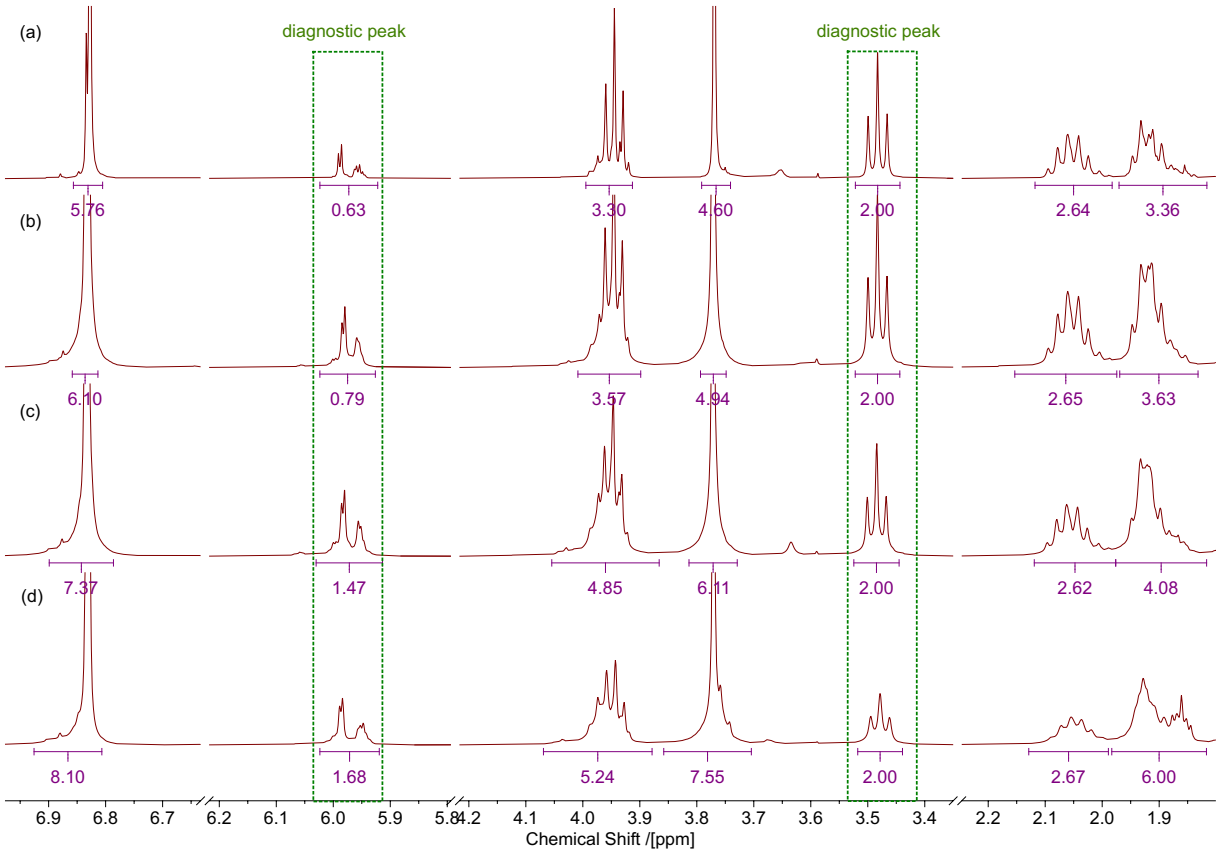

Figure 2.11: ^{1}H NMR spectra for the reaction mixture of (**11**) after (a) 24 h, (b) 48 h, (c) 72 h, (d) 13 d. All peaks are integrated relative to the aliphatic R-C**H**$_2$-Br peak from reactant molecule (**1**) that only appears in the starting material to monitor the progression of reaction.

into one aliphatic peak at 1.93 in (Figure 2.11(d)) (resulting in 3 peaks in that area for this reaction mixture, two for the starting material and one for the product) since their environments are much more similar to each other in the product.

The ratio of the integrations of the diagnostic peaks implies that there is a ∼50% conversion of starting materials to products, at both the three (c) and thirteen (d) day points. From this we can infer that an equilibrium is being approached and it's unlikely that the reaction would proceed significantly further. This synthetic route was not deemed suitable due to the low conversion of this test reaction.

The apparent absence of the tris-substituted species is interesting. Despite the same ratio of starting materials being used, the A2 attempt between 4-bromobutane-pillar[5]arene (**2**) and phloroglucinol (Scheme 2.7) gave mostly the tris-substituted product. With the data

obtained for this experiment it is, however, not actually possible to rule out that the absence of the tris-substituted species in MS is due to reasons of instability during ionisation or difficulties during vaporisation. If we assume that the tris-substituted product is not present, then we can subtract the integrations of the starting material, (**1**), from the reaction mixture integrations (when normalised against the peak which only appears for the starting material), and roughly deduce that the bis-substituted product is the majority product. However, with the uncertainties present in manually integrating peaks on a ^{1}H NMR spectrum, it is not advisable to narrow down the believed ratios any more than this.

Due to time constraints, this route was not pursued further, despite the cautiously positive results. Had it been continued, trying to improve the conversion of starting material to product by adding further equivalents of NaH to the reaction after ∼50% conversion could make this a suitable synthesis after-all. Another promising set of conditions was also found after the discontinuation of this route. Zn powder was reported to catalyse the reaction of phloroglucinol (and other alcohols) with *N*-bromobutane in high yields and with selectivity over the number of substitutions that occurred based on the ratios of starting materials.[117] This reaction does not require anhydrous conditions or reagents that are liable to degrade over time, and the Zn powder can be reused multiple times without loss of activity and hence it would be very interesting to attempt the synthesis of the analogue species (**11**) this way.

This would, of course, have to be also then attempted on 4-bromobutane-pillar[5]arene (**2**) rather than the precursor. That could prove challenging, as the one thing that became clear through these syntheses and those described in the next chapter, is that reactions involving pillar[5]arene based compounds are difficult to successfully perform in high yields. Sometimes this can be due to ineffective reactions, as was the case for amino bis-pillar[5]arene (**3**), other times this can be due to the difficulties in purification. The synthesis of any substituted pillar[5]arene results in a product that is difficult to separate from the majority unsubstituted pillar[5]arene produced at the same time. Hence, most syntheses performed here had to contend with pillar[5]arene impurities. Working with mixtures of desired pillar[5]arenes and pillar[5]arene impurities, both of which drag on silica during chromatography due to their host-guest chemistry leads to large losses in material as crude products need to be purified

multiple times to achieve a pure compound. Low yields this early on in a multi-step synthesis make its success unlikely, so other handcuff synthesis methods were explored in parallel to this one and will be discussed in the next chapter (3).

2.3 Conclusions and future work

2.3.1 Other linkers

Click chemistry could be an alternative way of joining pillar[5]arenes to a linker that would allow for different types of reactions to the ones already attempted. The bromide functional group of 4-bromobutane-pillar[5]arene (**2**) can be converted to an azide with very high yields, though care has to be taken to work on small scales to avoid generating diazidomethane.[48] Such an azide-substituted pillar[5]arene could then react with a bis-alkyne linker, e.g. a bis-propargyl-aromatic ester generated from Boc-5-aminoisophthalic acid (**7**). The reaction of isophthalic acid with propargyl bromide has over 80% yields in the literature, while similar reactions with alcohols have much lower yields,[118] so phloroglucinol would be a worse linker to explore here. Such a synthesis is proposed in Scheme 2.9. A species with four pillar[5]arene moieties has been generated using a similar synthesis route.[119]

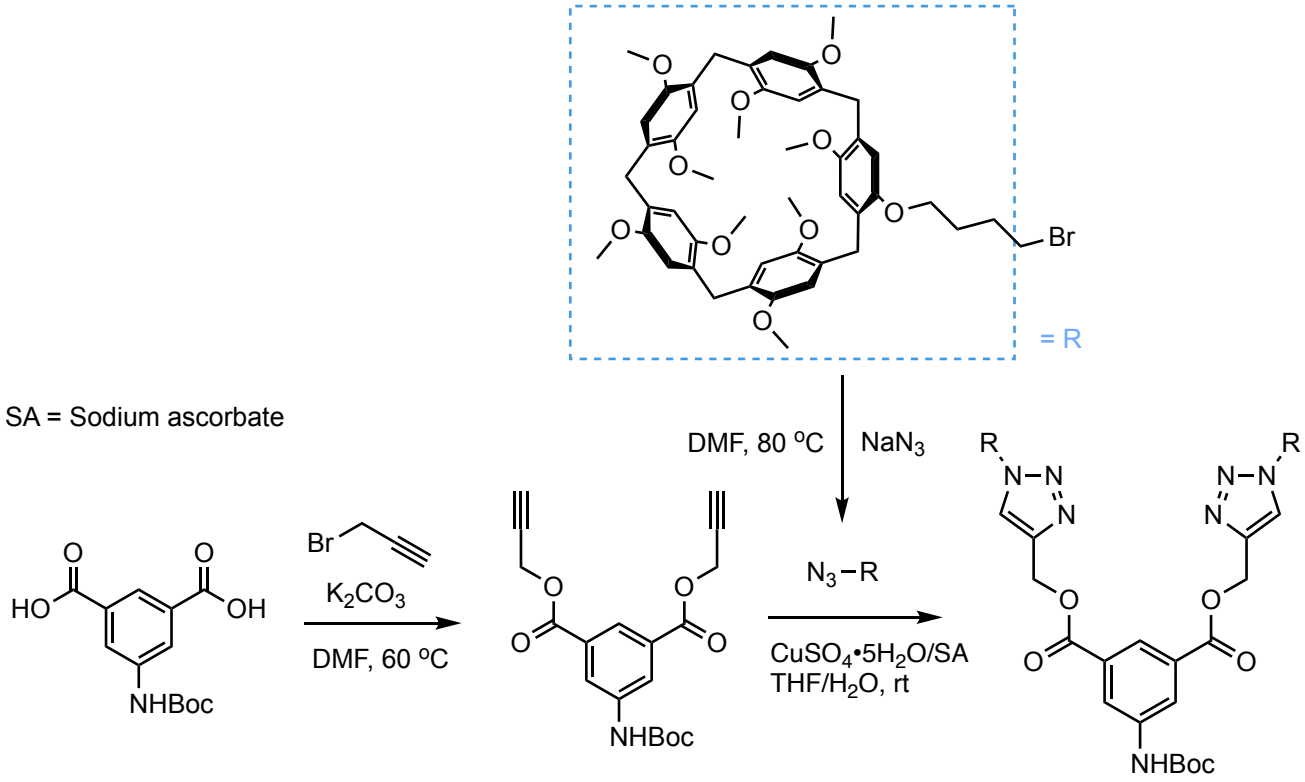

Scheme 2.9: Reaction scheme for the synthesis of a proposed bis-pillar[5]arene species based on click chemistry.

An alternative way of using click chemistry to achieve this would be to have the alkyne groups on the pillar[5]arene and azide groups on the linker as shown in Scheme 2.10. An *n*-butyne substituted pillar[5]arene has not been reported yet, though similar pillar[5]arenes have been made through demethylation of pillar[5]arene and then addition of a suitably functionalised species,[120,121] or through cocyclisation.[122] The cocylisation-based synthesis for 3-butene-substituted pillar[5]arene (**13**) optimised in Chapter 3.2.1 gives better yields than any of the works cited here and should be applicable to 4-bromobut-1-yne just as much as it is to 4-bromobut-1-ene. This could then be combined with a diazidoamine if one could be synthesised similarly to diazidoalkanes.[123–125]

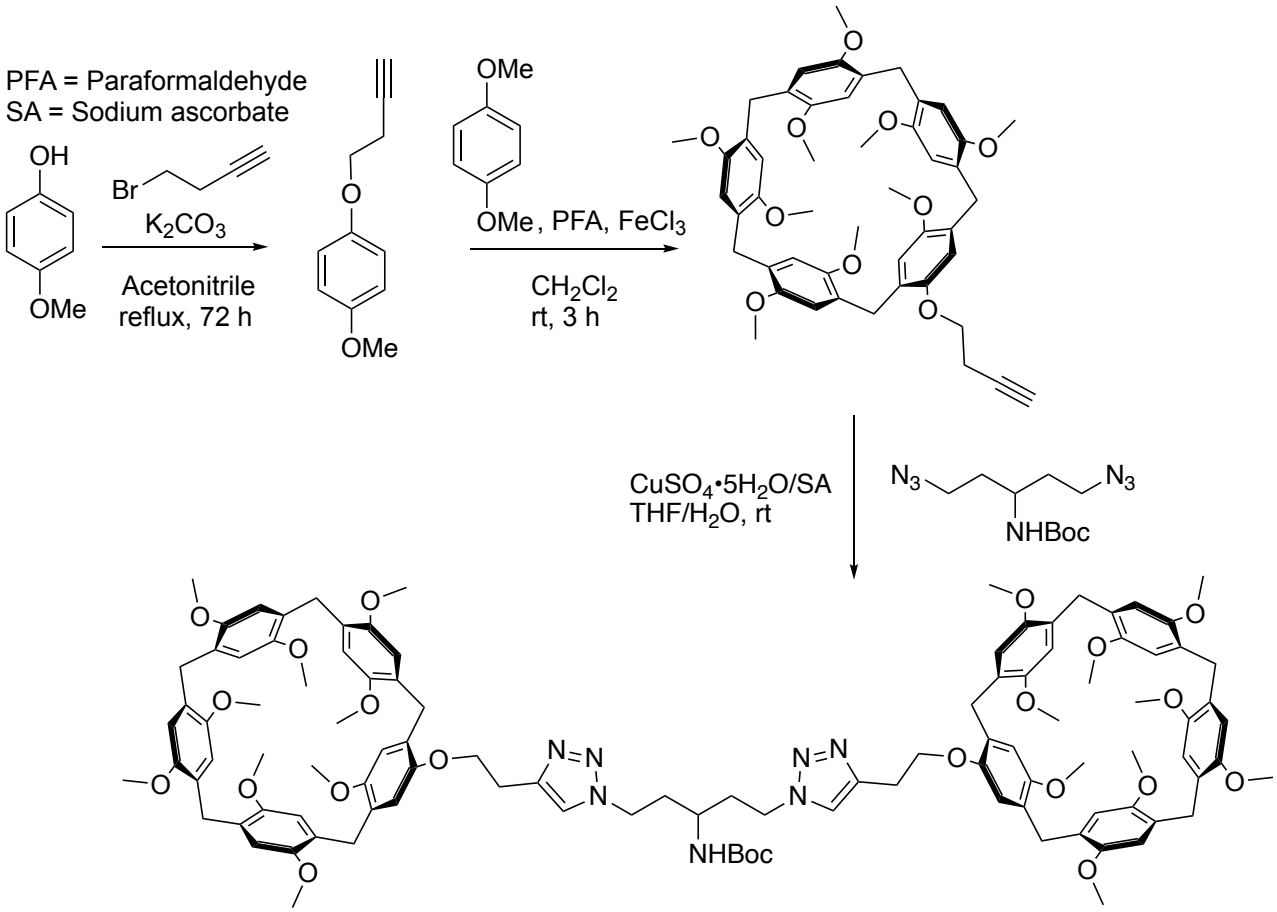

Scheme 2.10: Reaction scheme for the synthesis of a proposed bis-pillar[5]arene species based on click chemistry.

2.3.2 Proposed assembly of triple decker handcuff

Despite attempts involving multiple synthetic routes, the synthesis of a triple decker handcuff was unsuccessful. If a bis-pillar[5]arene species with a free amine group is synthesised in the future, the remaining steps to producing a triple decker handcuff are as follows: synthesise the handcuff body, synthesise the handcuff rod, thread component molecules together and then stopper them in place.

To synthesise the handcuff body, the bis-pillar[5]arene species can be reacted with PTCDA [126] as shown in Scheme 2.11 to give the handcuff body.

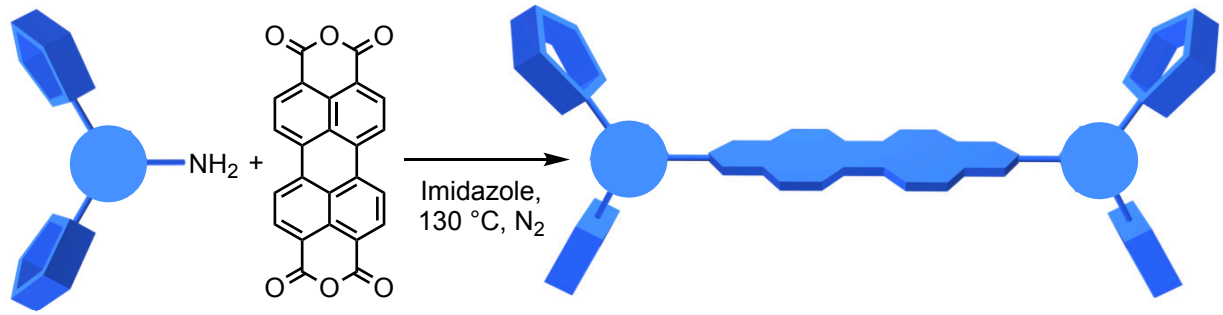

Scheme 2.11: Proposed reaction scheme for the synthesis of the handcuff body once a bis-pillar[5]arene species is synthesised.

To synthesise a handcuff rod, which contains a PDI core with aliphatic groups capped by imidazole moieties, those aliphatic chains need to be synthesised first. [39] A twelve carbon aliphatic chain was chosen to approximately mimic the length of the handcuff body on each side of the PDI core. The synthesis of the eight carbon analogue and then its reaction with PTCDA to give a similar handcuff rod is described in Chapter 3.2.3.

Once all the individual parts of this triple decker rotaxane handcuff are synthesised, they can be mixed together to achieve threading, then a stopper can be added to prevent dethreading as shown in Scheme 2.12. A similar handcuff rotaxane formation is described in Chapter 3.2.4.

This triple decker handcuff rotaxane would have then been investigated with cyclic voltammetry to elucidate its electrochemical properties.

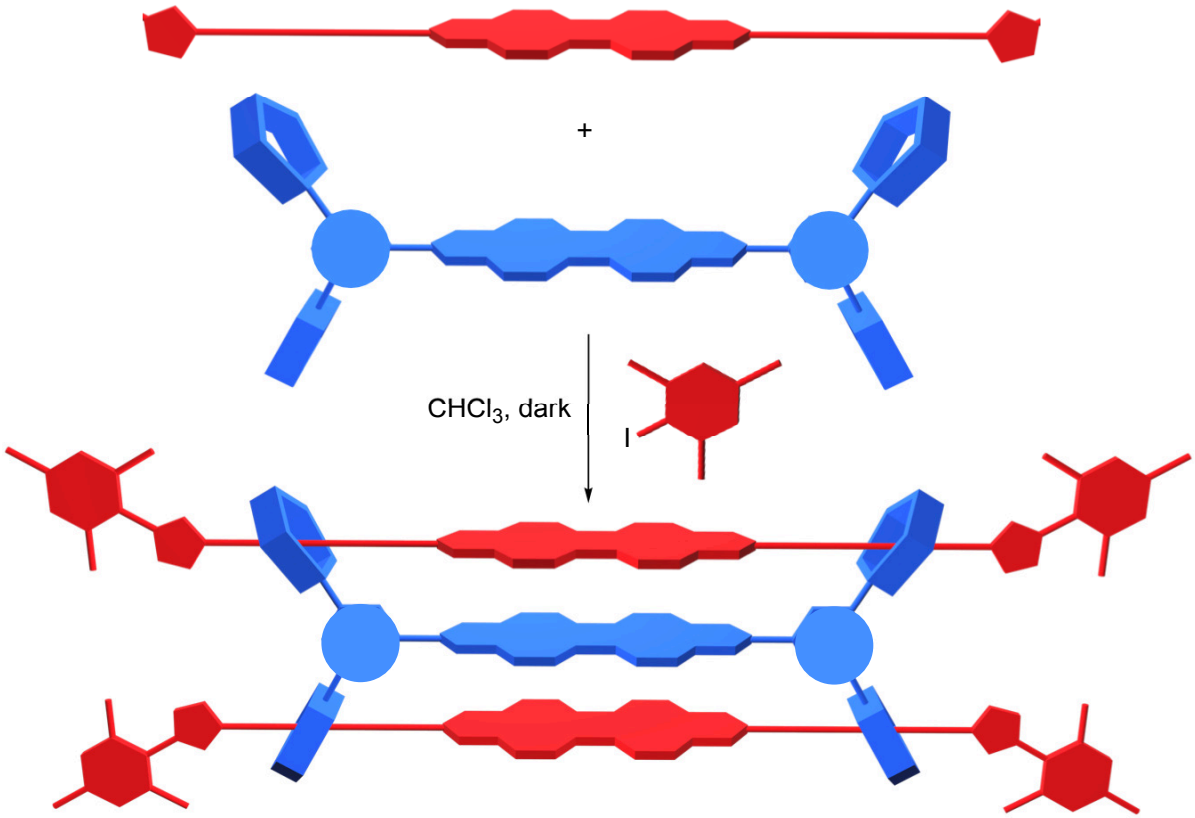

Scheme 2.12: proposed reaction scheme for the synthesis of the triple decker handcuff rotaxane.

2.3.3 Conclusions

A triple decker handcuff synthesis was attempted in this work. The most crucial step, the synthesis of a bis-pillar[5]arene linker that can also react with PTCDA was unsuccessful and hence the envisaged triple decker handcuff was never made. The original amino bis-pillar[5]arene (**3**) designed for the triple decker handcuff was based on doubly alkylating one end of ethylenediamine with 4-bromobutane-pillar[5]arene (**2**). This type of linker should have been flexible, nucleophilic and easy to modify, but it only gave mono-substituted species when attempted on the desired starting materials and many side products when attempted on a simpler analogue. To circumvent both of those issues, an oxybenzaldehyde-substituted pillar[5]arene could be combined with ethylene diamine twice over two reductive aminations to give amino bis-pillar[5]arene (**3**).

The second species, amido bis-pillar[5]arene (**8**), was based on two amide couplings of 5-aminoisophthalic acid with 4-aminobutane-pillar[5]arene (**6**). This should have been a more reliable reaction than the alkylation for the previous species at the cost of less flexibility. Unfortunately the reaction procedure with thionyl chloride as a coupling agent yielded a difficult to separate mixture of the mono- and bis-substituted products with a conversion of ∼50%. Attempts with other coupling agents (CDI) were also unsuccessful, although EDC seems like a promising coupling agent to circumvent these issues.

The final species that was attempted here, ether bis-pillar[5]arene (**10**), was based on an ether synthesis between phloroglucinol and 4-bromobutane-pillar[5]arene (**2**). This reaction suffered from mixtures of mono-, bis-, and tris-substituted products, then from poor yields. Upon change of base, more promising results were obtained, but ultimately not good enough to continue at that stage.

Based on these results however, it might be more worthwhile to try the click chemistry routes suggested in Section 2.3.1. Alternatively, an even more radical change might be necessary to bring a triple decker handcuff into existence. Instead of the tetrakis-pillar[5]arene species proposed here, a tetrakis-imidazole-capped-alkane species could be made as the handcuff rod. This could be paired with two bis-pillar[5]arene handcuff bodies in an inversion of the handcuff body and rod roles proposed in this work so far. This modification would avoid the need for reacting a linker with two pillar[5]arene species. The handcuff body from the PDI-PDI handcuff[39] could be used. It would still require a linker to link the four imidazole-capped-alkane species to PTCDA, but perhaps having fewer pillar[5]arene-based reactions would be advantageous.

3 Synthesis of [2]handcuff rotaxane

3.1 Synthesis of tetrazine handcuff

While the work discussed thus far was based on symmetric PDI-PDI templating interactions between the handcuff rod and body, combinations of PDIs with other moieties are also interesting and have been explored within the group, e.g. PDI-NDI,[39] or PDI-naphthalene,[40] the latter of which has been discussed in the Introduction (1.4.2). In this chapter we hence consider the synthesis of a PDI-tetrazine handcuff as no handcuffs containing tetrazine motifs were found in the literature, though a [3]pseudo-rotaxane,[127] Metal-Organic Frameworks (MOF)s[128–130] and cages based on it do exist.[131,132] This dearth of tetrazine containing interlocked molecules was deemed necessary to rectify, especially since similarly to PDIs, tetrazines are interesting electrochemically, as they can be reversibly reduced to radical anions.[55] Just like for the PDI-PDI handcuff (see Introduction 1.4.2), it should be possible to hold a PDI core and a tetrazine core in proximity to each other in a fixed orientation using mechanical bonds and explore their through-space interactions (e.g. π, cation-π and anion-π interactions) in detail to see what effects this proximity has on the paramagnetism, emission and aggregation properties of these compounds.

Furthermore, this research could shed further light on the reactivity of tetrazines. They can take part in Inverse Electron-Demand Diels-Alder (IEDDA) reactions as tetrazines serve as a 4π-reagent when coupled with a 2π dienophiles such as alkenes or alkynes. This reaction is catalyst free, with conditions that are often benign, which reduces toxicity issues, and is very fast, which is convenient and more sustainable.[133] Diels-Alder *exo* vs *endo* selectivity is influenced by π-π interactions, and it is likely that IEDDA reactions are also influenced in this way. Synthesising PDI-tetrazine handcuffs and manipulating their electronic properties, then performing IEDDA reactions on them would help elucidate these effects.

The handcuff was designed to be a 'double decker' as opposed to the thus far considered 'triple decker' handcuffs, or between one bis-pillar[5]arene handcuff body and one rod, one with a PDI core and the other with an aromatic tetrazine core. For this synthesis, a body with a tetrazine core and a rod with a PDI core was chosen as shown in Figure 3.1, because

the PDI rod was already reported, although the opposite design should be just as interesting as discussed at the end of this section. In either case, the stacking interactions between the PDI core and the tetrazine core should facilitate association in the threading step of the synthesis.

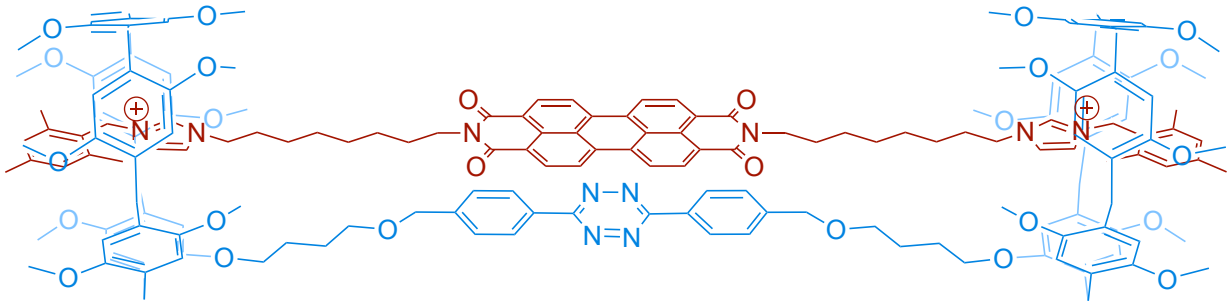

Figure 3.1: Double Decker Handcuff with a tetrazine and PDI core.

Unlike the PDI cores discussed so far, tetrazine cores need to be synthesised from scratch, as reasonably priced precursors such as tetrazine synthons are not commercially available. Furthermore, as tetrazine is poorly soluble in organic solvents, it would not be easy to attach two pillar[5]arenes to an already formed tetrazine core to form a handcuff body. Instead, the approach taken was to join two nitrile-substituted pillar[5]arenes via the modified Pinner synthesis method.[58]

3.1.1 Synthesis of nitrile substituted pillar[5]arene

Benzonitrile was chosen to create a tetrazine core that would stack well with a PDI core as the created tetrazine would be a part of an extended conjugated network. The benzonitrile identified for this purpose was 4-(hydroxymethyl)benzonitrile. It would be combined with 4-bromobutane-pillar[5]arene (**2**) to give benzonitrile-pillar[5]arene (**12**) using the Williamson ether synthesis,[134] as shown in Scheme 3.1.

Sodium hydride was added to a solution of the commercially available 4-(hydroxymethyl)-benzonitrile. To this reaction mixture 4-bromobutane-pillar[5]arene (**2**) was added to give a mixture of substitution and elimination products; the desired benzonitrile-pillar[5]arene (**12**) was obtained in a 24% yield and the side product 3-butene-substituted pillar[5]arene (**13**) in a 61% yield. The spectra of the two products are fully assigned in the Appendix (Fig-

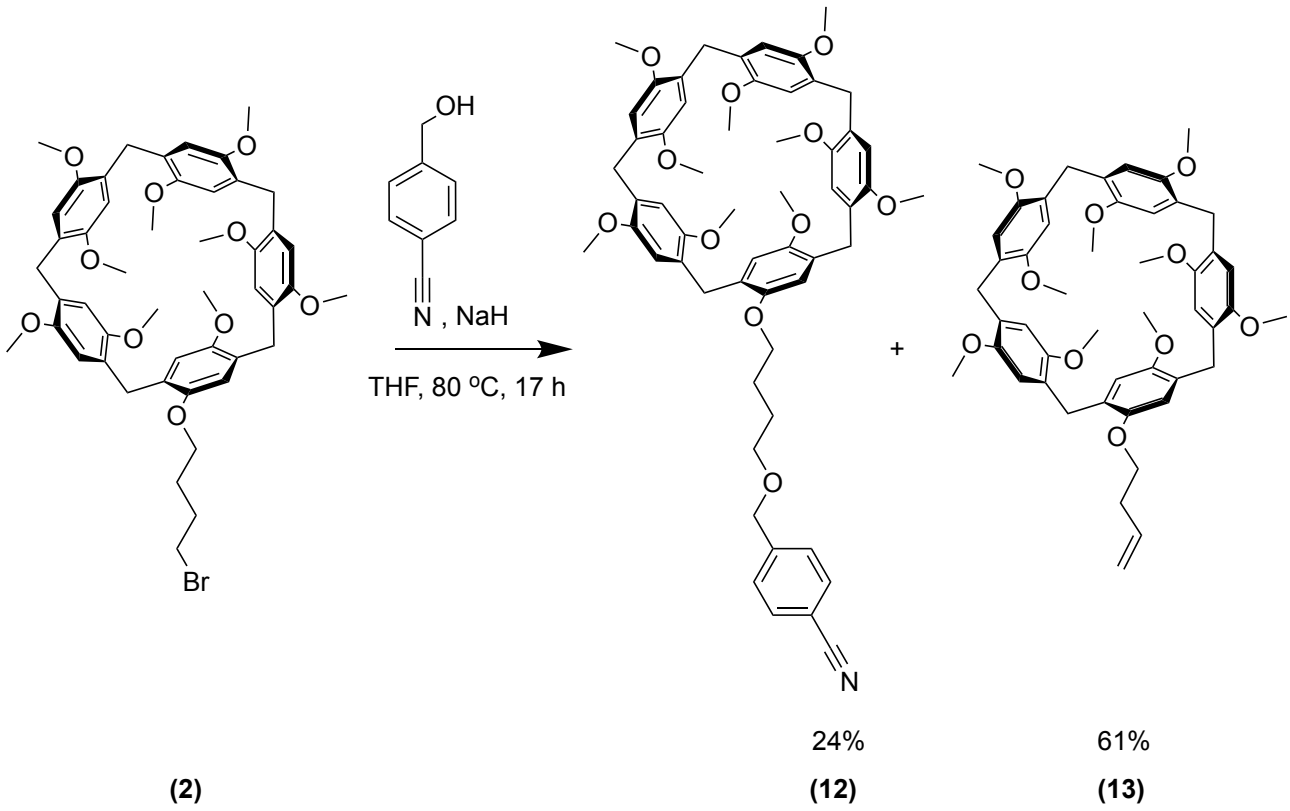

Scheme 3.1: Reaction scheme for the synthesis of benzonitrile-pillar[5]arene (**12**) and 3-butene-substituted pillar[5]arene (**13**).

ure Figures A.20, A.21, A.24 and A.25). Both are novel substituted pillar[5]arenes, though a nitrile-substituted pillar[5]arene (pentakis-acetonitrile-substituted pillar[5]arene[135]) and a quadruply and triply substituted version of 3-butene-substituted pillar[5]arene (**13**) have been reported.[136]

To try and improve yields, a slight modification of this reaction was attempted. The 4-bromobutane-pillar[5]arene (**2**) was stirred with tetrabutylammonium iodide (TBAI) before being added to the 4-(hydroxymethyl)benzonitrile and sodium hydride reaction mixture, but this gave lower yields.

Further attempts to optimise this reaction were carried out on an analogue: 1-(4-bromobutoxy)-4-methoxybenzene (**1**). High-yielding Williamson ether syntheses available in published literature were compared to each other and a selection of facile and cheap preparations[116,137–140] were attempted. The test reactions were performed on small scales. The success of each reaction was judged based on ^{1}H NMR peak ratios of the desired to side

product. To confirm that this was a sensible approximation to make, such a ratio was first obtained for the above where the yields of both are known.

The ^{1}H NMR spectrum for the reaction mixture is shown in Figure 3.2 along with the spectra of the side product 3-butene-substituted pillar[5]arene (**13**), and desired product benzonitrile-pillar[5]arene (**12**) with peaks used to calculate the ratio of desired to side product integrated.

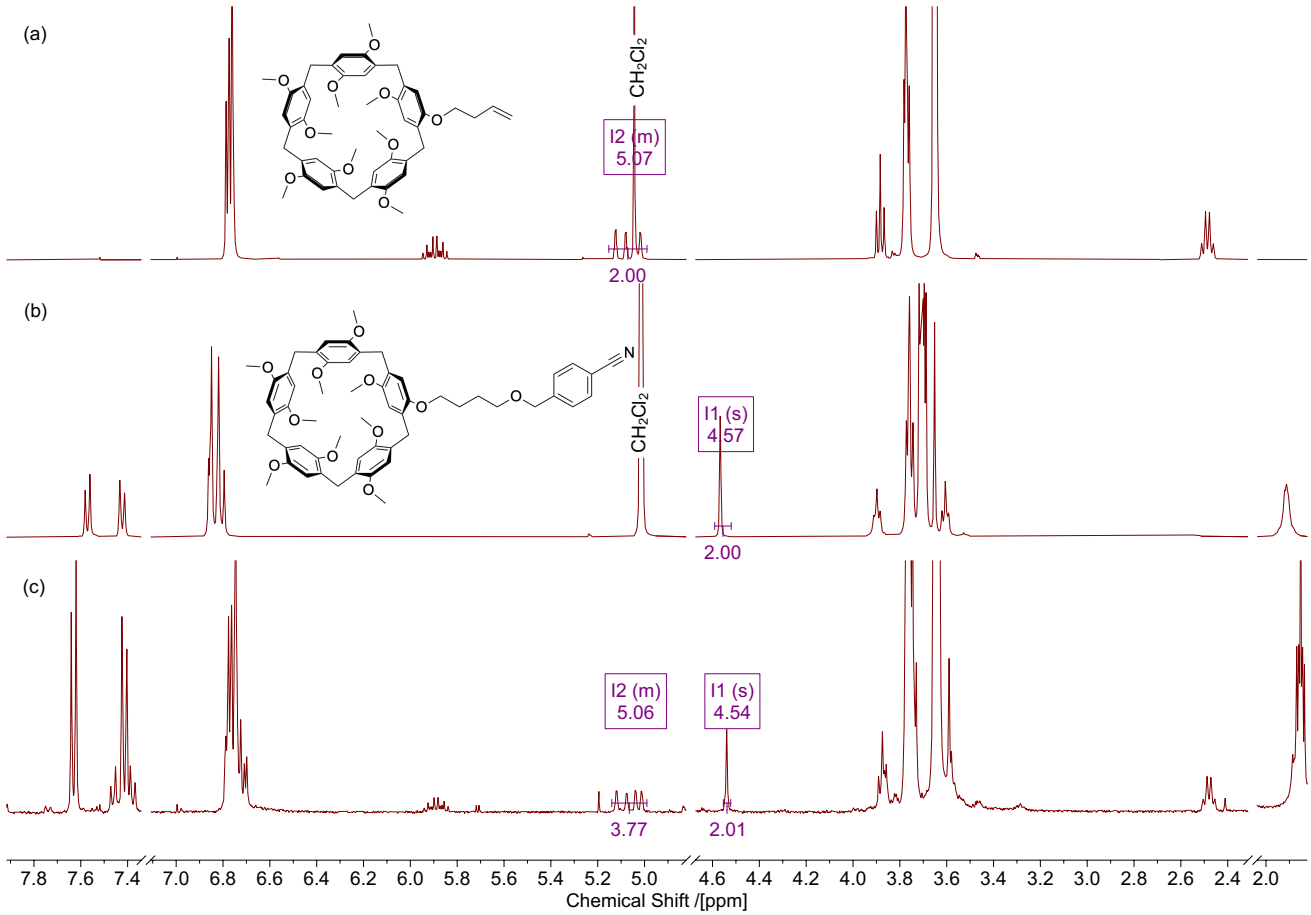

Figure 3.2: ^{1}H NMR (300 MHz, $CDCl_3$ 298 K) spectra of (a) side product 3-butene-substituted pillar[5]arene (**13**), (b) desired product benzonitrile-pillar[5]arene (**12**), and (c) the reaction mixture that contains both compounds with peaks used to calculate the ratio of desired to side product integrated.

Peak I1 was chosen as NC-C_6H_4-C$\mathbf{H}_2$O- is unique to benzonitrile-pillar[5]arene (**12**) (it does not overlap with any other peaks in this mixture, including the starting material's equivalent NC-C_6H_4-C$\mathbf{H}_2$OH peak) and peak I2 was chosen as -CH=C$\mathbf{H}_2$ is unique to 3-

butene-substituted pillar[5]arene (**13**). The integral ratio calculation is explained in the Appendix Section A.2. The calculated molar ratio of desired to side product is 35:65 in the synthetic mixture. The isolated yields of those two products from that reaction were 24% and 61%, which gives them a ratio of 28:72. These ratios obtained through ^{1}H NMR analysis of the reaction mixture and of the isolated products are approximately the same, showing that ^{1}H NMR analysis can be used to quickly determine reaction success.

The reagents and conditions attempted for the synthesis of the analogue species, nitrile-methoxybenzene (**14**), are summarised in Scheme 3.2 as A1 – A5.

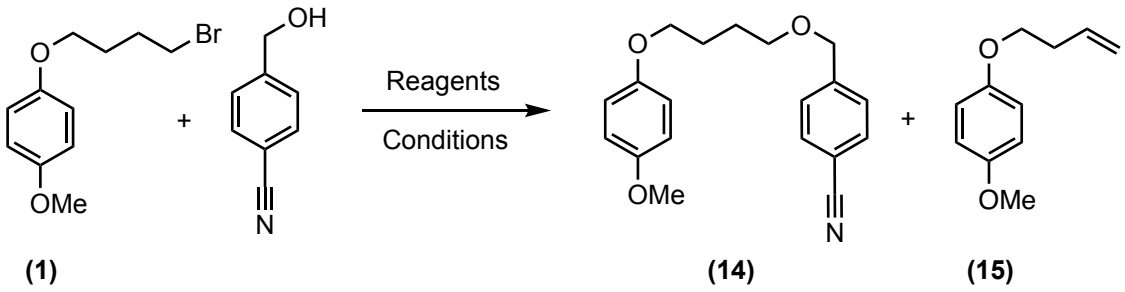

Summary of conditions

Attempt	Reagents	Conditions	Ratio of P:SP
A1	NaH,TBAI	Tolene, N_2, 80 °C	68:32
A2	NaH	THF/DMF, N_2, 80 °C	81:19
A3	NaH,18C6	THF, N_2, 80 °C	100:0
A4	KOH	AcN, N_2, 60 °C	49:51
A5	AgO	$CHCl_3$, N_2, 60 °C	N/A

Scheme 3.2: Reaction scheme for the synthesis of the desired product nitrile-methoxybenzene (**14**) and side product 3-butene-substituted pillar[5]arene (**13**) with the reagents, conditions, and ratio of product to side product (P:SP) enumerated A1 – A5 in the table.

For each attempted optimisation, the ratio of the desired product (**14**) to side product (**15**) was calculated using equations 2 and 3 to assess the results. The analogous ^{1}H NMR peaks as used for this calculation for benzonitrile-pillar[5]arene (**12**) could be used for nitrile-methoxybenzene (**14**) as they also exist for those analogue molecules. The ^{1}H NMR spectra for these attempts (A1 – A5) are shown in Figure 3.3.

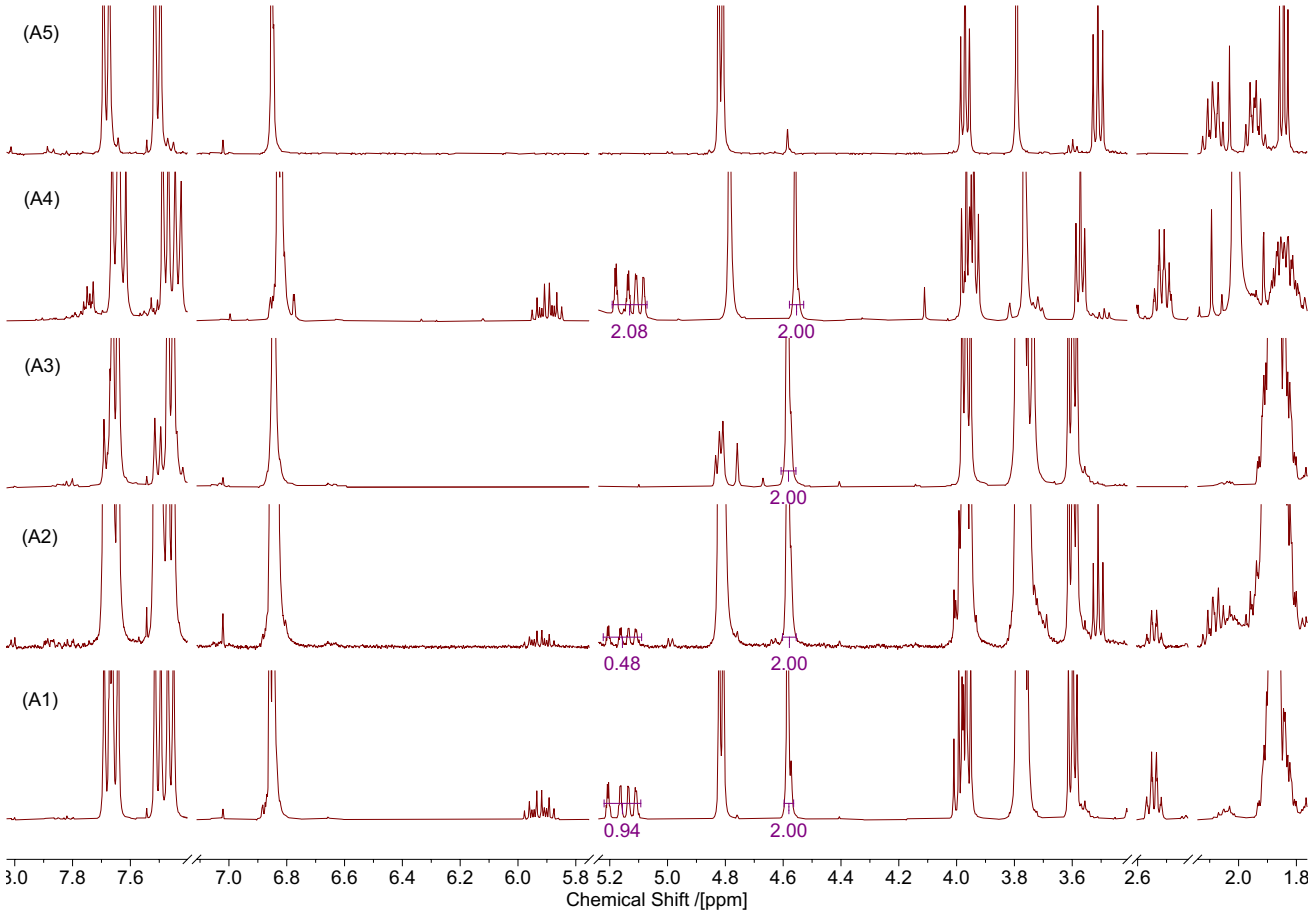

Figure 3.3: ^{1}H NMR (300 MHz, $CDCl_3$ 298 K) spectra of the reaction mixtures for methods A1 – A5 with peaks used to calculate the ratio of desired to side product integrated.

The ratios calculated from these spectra are tabulated in Scheme 3.2 and show that A3 (NaH, 18C6, THF, N_2, 80 °C) gave the best results. It was then applied to the original 4-bromobutane-pillar[5]arene (**2**), but none of the three attempts surpassed a ratio of 44:56, which is not significantly superior to the original ratio of 35:65. The conditions optimised on (**1**) were concluded to be not as optimal for 4-bromobutane-pillar[5]arene (**2**).

While the optimised method A3 in Scheme 3.3 could only efficiently produce nitrile-methoxybenzene (**14**) and not the desired benzonitrile-pillar[5]arene (**12**), this does still present the possibility of rearranging the order of steps in the reaction scheme - first obtaining nitrile-methoxybenzene (**14**) and only then proceeding with the cocyclisation reaction to indirectly obtain benzonitrile-pillar[5]arene (**12**).

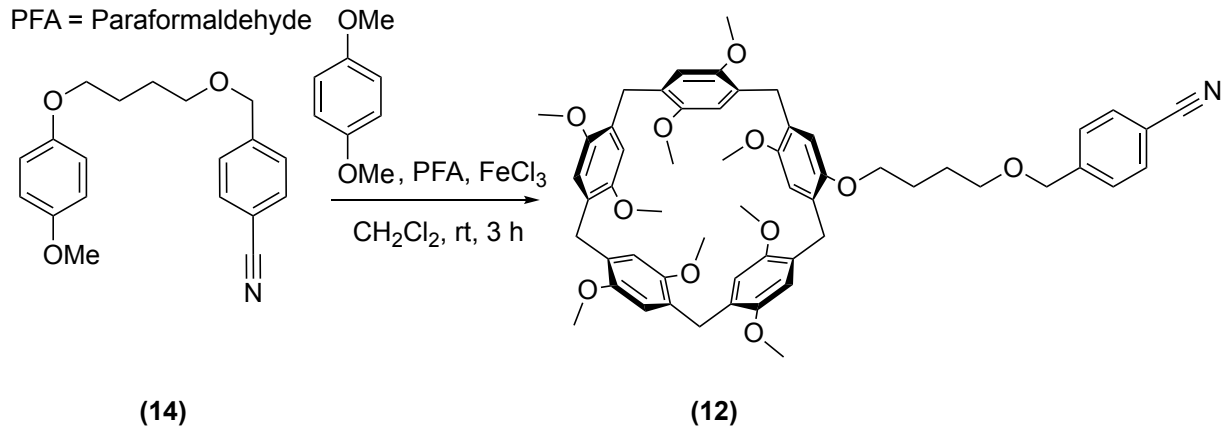

Scheme 3.3: Proposed reaction scheme for the synthesis of the benzonitrile-pillar[5]arene (**12**) from nitrile-methoxybenzene (**14**).

However, since the pillar[5]arene reaction is itself low yielding (20–30%), the nitrile-methoxybenzene (**14**) reaction had to be done on larger scales. Two attempts at scaling the reaction up to 3 g and 1.5 g scales yielded ratios of around 50:50 of the desired to side products, much less than the 100:0 from the previous attempt of the A3 conditions. Attempting to reproduce the original A3 conditions exactly once again resulted in a ratio of $\sim$ 50:50. It remains unclear what caused the anomalously high efficiency in the initial experiment.

Looking back at this work now, a comparison with the same set of conditions used in the previous chapter comes to mind (Scheme 2.8). For phloroglucinol, no elimination products were detected at all. This is likely due to the differences in nucleophilicity and basicity between phenols and benzyl alcohols. Since deprotonated benzyl alcohols are more basic, they would lead to eliminations, while the nucleophilic phenols only give substitution products. Perhaps cynaophenol would have been a more promising species to try in this synthesis.

While this optimisation was underway, an attempt at making the tetrazine handcuff body was made with the small amounts of benzonitrile-pillar[5]arene (**12**) combined from various previous reactions via the modified Pinner synthesis[58] as shown in Scheme 3.4.

Benzonitrile-pillar[5]arene (**12**) was mixed with hydrazine hydrate and sulfur, then oxidised; conditions typically employed for the conversion of benzonitriles to tetrazines.[141–143]

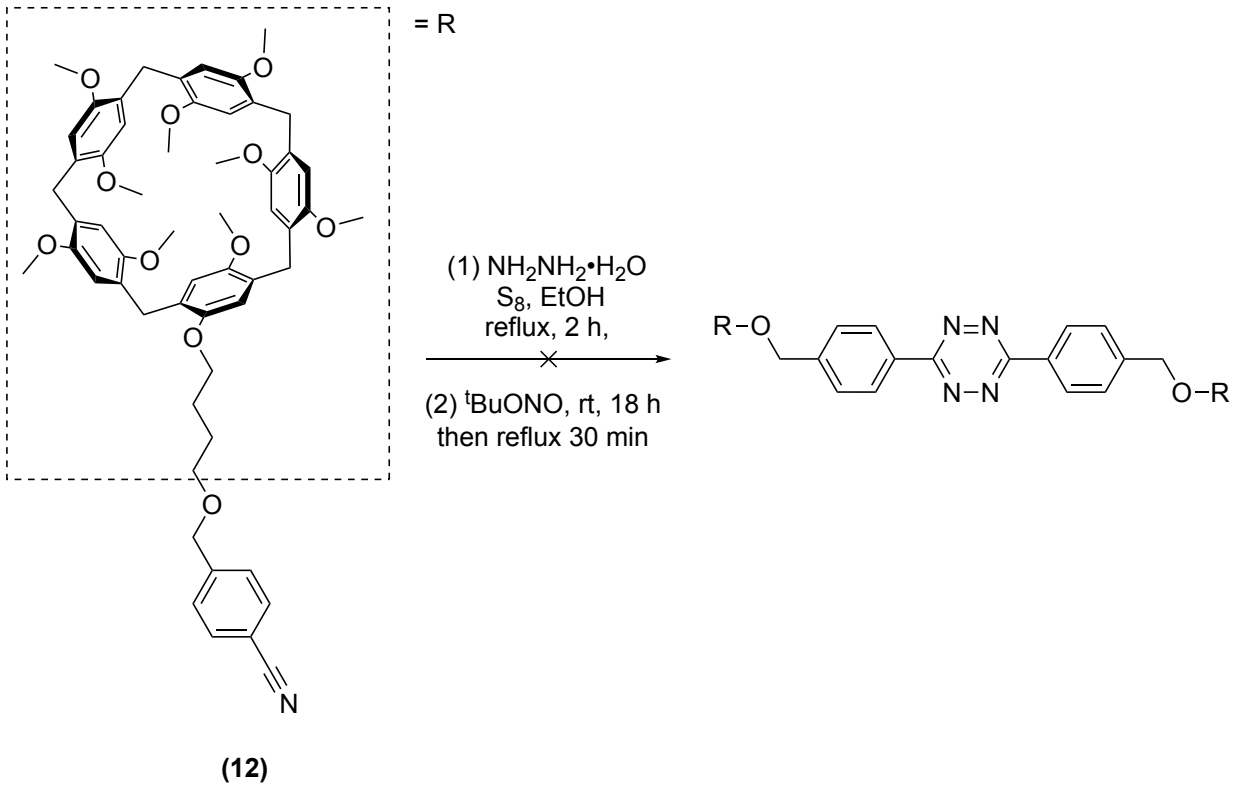

(12)

Scheme 3.4: Reaction scheme for the synthesis of the tetrazine handcuff body.

No tetrazine-containing product was detected using ESI-MS, ^{1}H NMR spectroscopy or MALDI MS. The lack of solubility of benzonitrile-pillar[5]arene (**12**) in ethanol, which was the solvent for this reaction is likely to blame for this. Later, it became apparent that tetrazine formation reactions can be performed in CH_2Cl_2, which would have possibly avoided these issues.[56] However, due to time constraints this synthesis was not pursued further. Had this handcuff synthesis been continued, an aromatic tetrazine substituted with an alkene on each side could be synthesised, which could be coupled to 3-butene-substituted pillar[5]arene (**13**) through alkene metathesis.

Alternatively, synthesising a tetrazine rod with aliphatic-imidazole arms, by modifying an existing benzonitrile-alkane synthesis[144] rather than synthesising a tetrazine body would likely allow for the solubility issues to be overcome. This rod could then be combined with a bis-pillar[5]arene handcuff body. However, perhaps a tetrazine rotaxane with a pillar[5]arene macrocycle should be synthesised first, as a simpler species that would allow for the optimisation of conditions for these compounds.

3.2 Synthesis of the alkene handcuff

Having synthesised a novel substituted pillar[5]arene as a side product, it seemed worthwhile to utilise it in its own [2]handcuff rotaxane synthesis. With this compound a bis-pillar[5]arene handcuff body could be synthesised in one step by joining two moieties of 3-butene-substituted pillar[5]arene (**13**) via an alkene metathesis reaction. This could then be threaded by a rod with a PDI core. The proposed structure of this handcuff is shown in Figure 6.23.

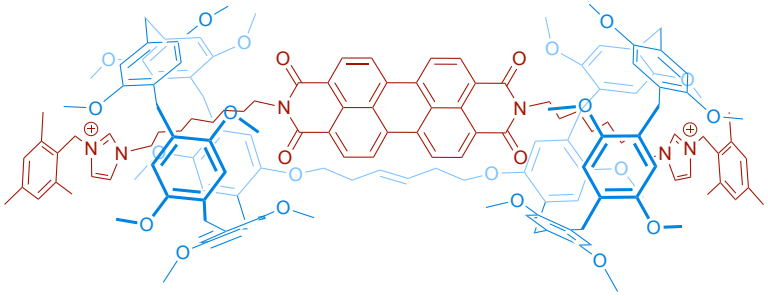

Figure 3.4: [2]handcuff rotaxane with alkene and PDI moieties.

Unlike previously discussed double and triple decker handcuffs, the PDI-alkene handcuff would be mostly or entirely lacking the stacking recognition motif of PDI-PDI or PDI-tetrazine handcuffs and only rely on the rotaxane like templating between a macrocycle and a rod. In this case that would be, alkane-pillar[5]arene templating[49,145,146], imidazole-pillar[5]arene templating[147–149] and favourable entropic effects of displacing solvent molecules from the pillar[5]arene cavity to drive threading. The relative contribution of the entropic effects, however,are likely pretty small compared to the other interactions.[150]

During the synthesis of the similar PDI-based handcuffs previously discussed in the Introduction (1.4.2), it was hypothesised that the synthesis method used only required templating between the host's macrocycles and the rod. The proposed synthesis of the PDI-alkene handcuff is a good way to test this. Because the PDI-alkene handcuff is so similar to the previously synthesised PDI-PDI handcuff, it will allow for a deeper understanding of how important the mutual π-stacking recognition motif is for the synthesis of the handcuff.

3.2.1 Synthesis of substituted pillar[5]arene

A new synthesis route where 3-butene-substituted pillar[5]arene (**13**) is the desired product rather than just a side product was devised and is shown in Scheme 3.5.

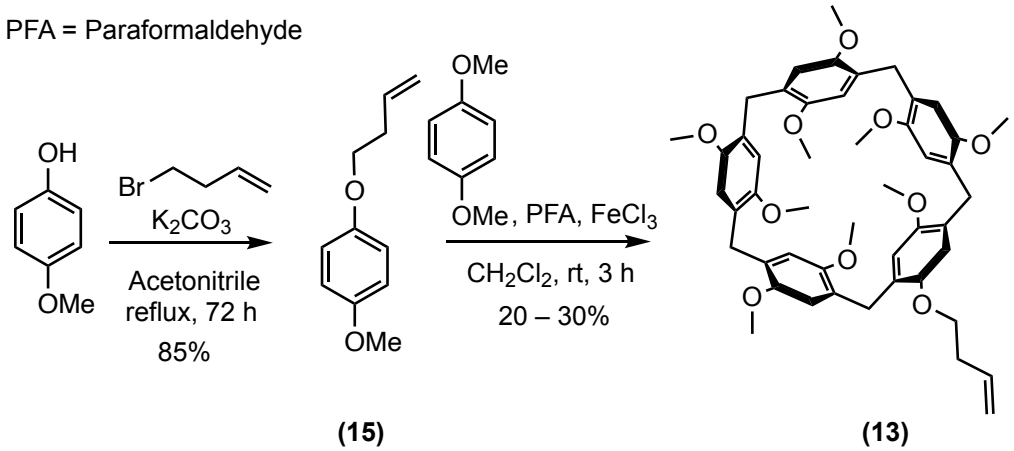

Scheme 3.5: Reaction scheme for the synthesis of the 3-butene-substituted pillar[5]arene (**13**).

Commercially available 4-methoxyphenol and 4-bromobut-1-ene were combined in the presence of potassium carbonate and reacted to give 1-(but-3-en-1-yloxy)-4-methoxybenzene (**15**). The product was characterised with ^{1}H NMR spectroscopy shown in the Appendix in Figure A.22 and Figure A.23. It was then co-cyclised with 1,4-dimethoxybenzene in the presence of iron(III) chloride to give the 3-butene-substituted pillar[5]arene (**13**) and unsubstituted pillar[5]arene (**16**), which were separated using flash column chromatography. The product was characterised with ^{1}H NMR spectroscopy shown in the Appendix in Figure A.24 and Figure A.25.

Yields in the range of 20–30% were obtained for this reaction across several experiments, which is in line with values for similar reactions. The low yields are due to the reaction stoichiometry, which uses a large excess of 1,4-dimethoxybenzne to avoid the formation of multiply-substituted pillar[5]arenes with more than one unit of 1-(but-3-en-1-yloxy)-4-methoxybenzene (**15**), which are more difficult to separate from the desired product than the unsubstituted pillararene. As such, the majority product is unsubstituted pillar[5]arene as identified by ^{1}H NMR spectroscopy shown in the Appendix in Figure A.26. Despite this, multiply-substituted pillar[5]arenes are also formed as confirmed by ^{1}H NMR spectroscopy

shown in the Appendix in Figure A.27.

The redox behaviour of 3-butene-substituted pillar[5]arene (**13**) was investigated by cyclic voltammetry (CV) in CH_2Cl_2 with added $[^nBu_4N][BF_4]$ (0.2 M) as the supporting electrolyte, at ambient temperature and at a scan rate of 0.10 Vs^{-1} as shown in Figure 3.5 and Table 3.2.

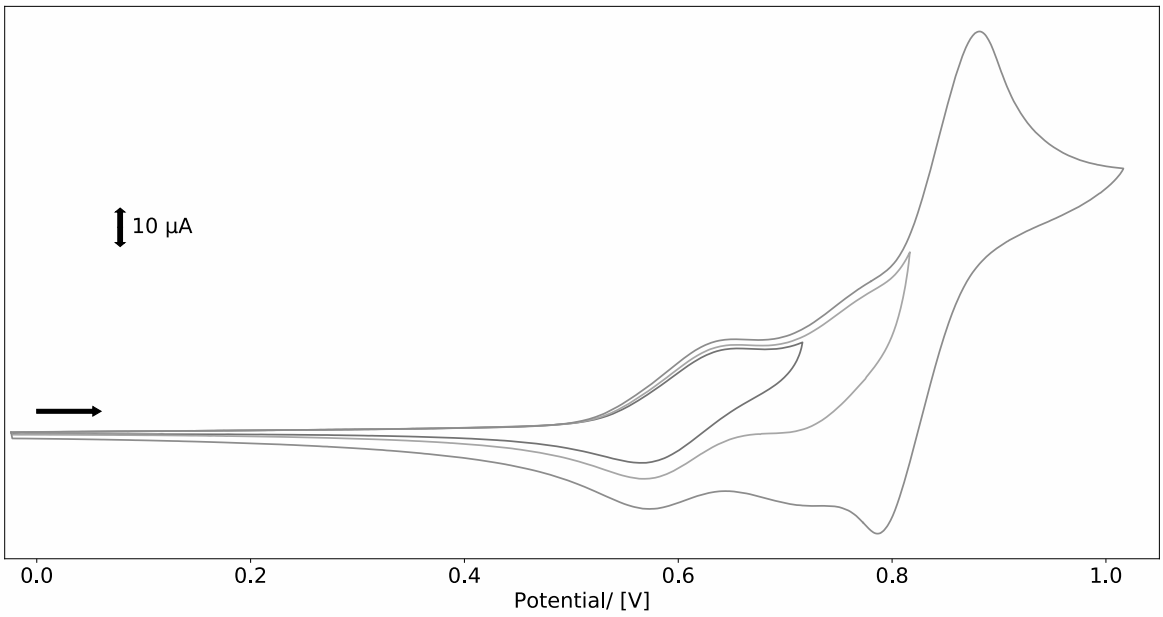

Figure 3.5: CV of 3-butene-substituted pillar[5]arene (**13**) in CH_2Cl_2 containing $[^nBu_4N][BF_4]$ (0.2 M) as supporting electrolyte, at ambient temperature and at a scan rate of 0.10 Vs^{-1}. Potentials reported vs. Fc^+/Fc.

In line with expectations, no redox processes were detected at negative potentials. At positive potentials the first oxidation (at $E_{1/2}$ 0.61 vs. Fc^+/Fc) shows reversible behaviour. The remaining oxidations are poorly resolved and correspond to the loss of multiple electrons. Previous studies[151] indicate that beyond the first oxidation these become a series of closely overlapped multi-electron oxidations. These poorly resolved oxidations were better resolved by square wave voltammetry, shown in Figure 3.6 and Table 3.3 at the end of this chapter.

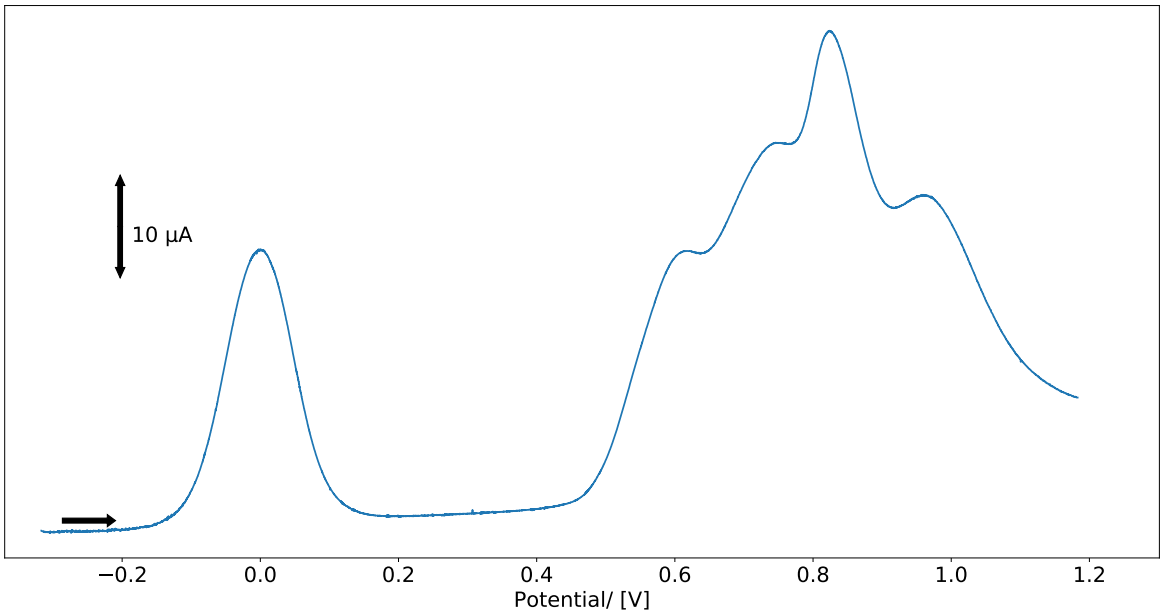

Figure 3.6: Square wave voltammetry of 3-butene-substituted pillar[5]arene (**13**) in CH_2Cl_2 containing $[^nBu_4N][BF_4]$ (0.2 M) as the supporting electrolyte, at ambient temperature. The process is referenced to Fc^+/Fc, at 0 V, added as the internal standard. Potentials reported vs. Fc^+/Fc.

Under UV/vis spectroelectrochemistry experiments, the oxidation processes appear chemically reversible under these conditions as shown in Figure 3.7. These findings are similar to those for pillar[5]arene (**16**) found within our group previously.[151] Neutral, 3-butene-substituted pillar[5]arene (**13**) shows a peak at 295 nm due to presence of aromatic rings and no other features. When a potential of +1.28 V (vs the saturated calomel electrode) was applied to a solution of 3-butene-substituted pillar[5]arene (**13**) in CH_2Cl_2, containing $[^nBu_4N][BF_4]$ (0.2 M) as a supporting electrolyte, oxidation resulted in the emergence of new absorbance bands at 440 and 467 nm. The original band was shifted to 297 nm with no significant loss of intensity observed. When a potential of 0 V was applied, the spectrum of the neutral 3-butene-substituted pillar[5]arene (**13**) was fully regenerated.

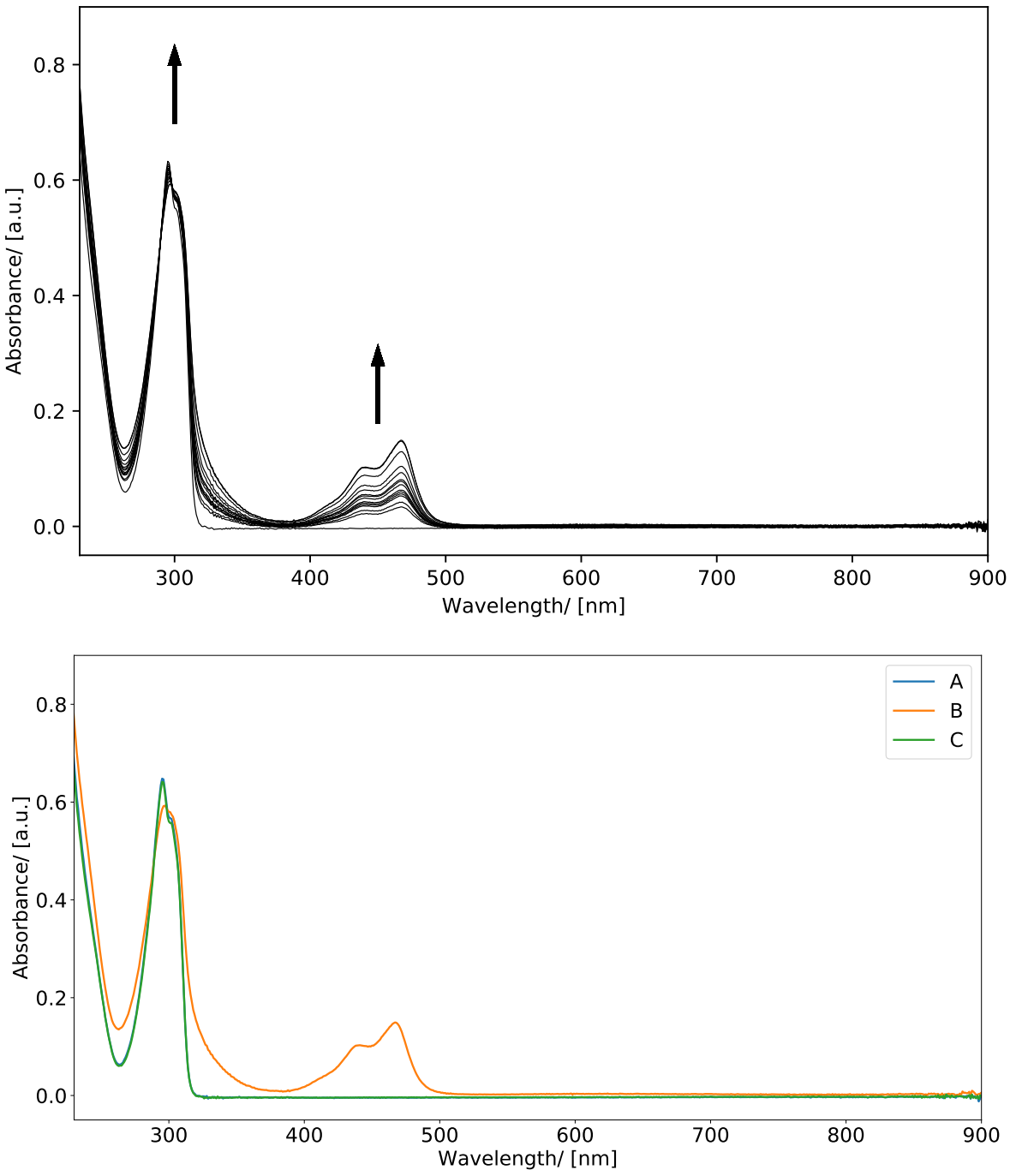

Figure 3.7: UV/vis absorption spectra showing: Top: the inter-conversion of redox states in 3-butene-substituted pillar[5]arene (**13**) between (**13**) and $(\mathbf{13})^{+}$; Bottom: 3-butene-substituted pillar[5]arene (**13**) (A) before oxidation, (B) after oxidation, and (C) after the redox cycle. A is not visible, as it lies exactly beneath C. Spectra were recorded in CH_2Cl_2 containing $[^{n}Bu_4N][BF_4]$ (0.2 M) as the supporting electrolyte at 273 K.

An Electron Paramagnetic Resonance (EPR) spectrum was also recorded for the one-electron oxidised 3-butene-substituted pillar[5]arene (**13**) as shown in Figure 3.8. A simulation was then performed to model the experimental behaviour using a series of 2, 4 and 8 equivalent hydrogens with hyperfine couplings of 1.700, 1.151 and 0.560 $\times$ 10^{-4} cm^{-1}, respectively. The results strongly resemble the EPR spectrum for pillar[5]arene (**16**)[151], and so it is likely also true in the case of 3-butene-substituted pillar[5]arene (**13**) that the unpaired electron is located around the core of a single arene subunit, and this unpaired electron is interacting with each methylene bridge's two equivalent protons, each methoxy group's six equivalent protons, and each adjacent arene group's single proton.

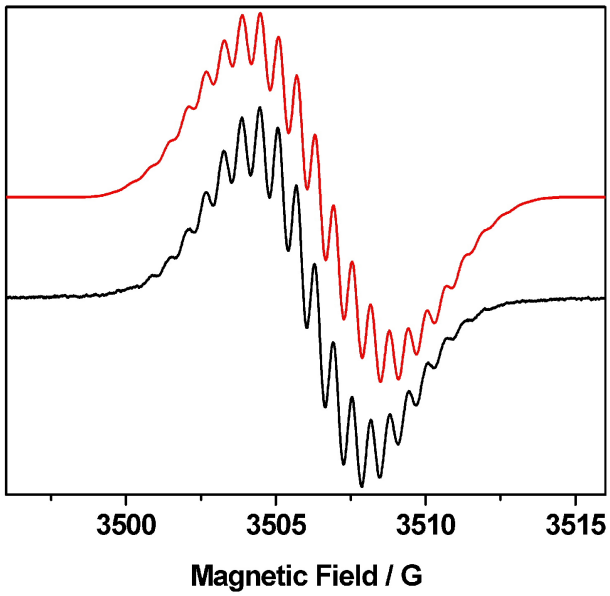

Figure 3.8: Experimental (black) and simulated (red) X-band EPR spectra of 3-butene-substituted pillar[5]arene (**13**). The sample was electrogenerated at 273 K from the parent molecule in CH_2Cl_2 with $[^nBu_4N][BF_4]$ (0.2 M) as the supporting electrolyte. The simulated spectrum was generated using g_{iso} of 2.0038, a_{iso} of 1.700 (2H), 1.151(4H) and 0.560(8H) x 10^{-4} cm^{-1}, a line-width of 0.65 G and a Gaussian line-shape.

Finally, 3-butene-substituted pillar[5]arene (**13**) was crystallised by slow diffusion of hexane into a solution of the compound in chloroform. A single crystal was taken for crystallography and confirmed the compound's structure as shown in Figure 3.9. The butene arm of this macrocycle was observed to be disordered over three positions on two attachment points. A disordered molecule of hexane was also found inside the cavity.

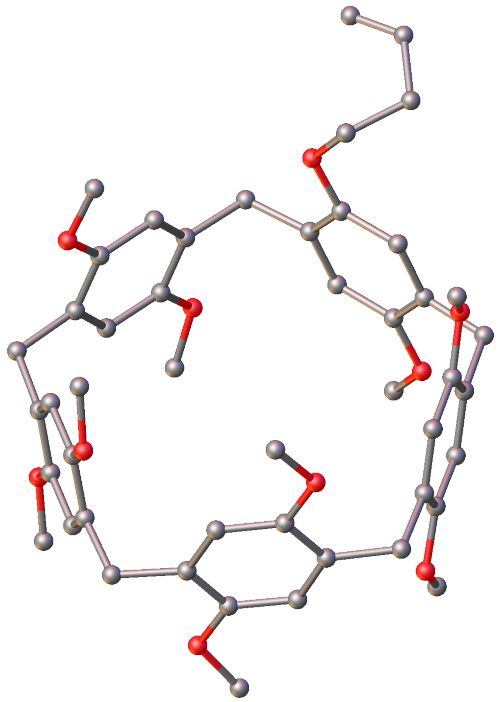

Figure 3.9: X-ray crystal structure of 3-butene-substituted pillar[5]arene (**13**). Grey = carbon, red = oxygen, hydrogen atoms and solvent molecules are omitted for clarity.

3.2.2 Synthesis of the handcuff body

The Hoveyda-Grubbs II catalyst [152] was chosen for the joining of the two 3-butene-substituted pillar[5]arene (**13**) moieties as an easily available option that has been frequently utilised for supramolecular syntheses. [109,153,154] The synthesis of this species is shown in Scheme 3.6.

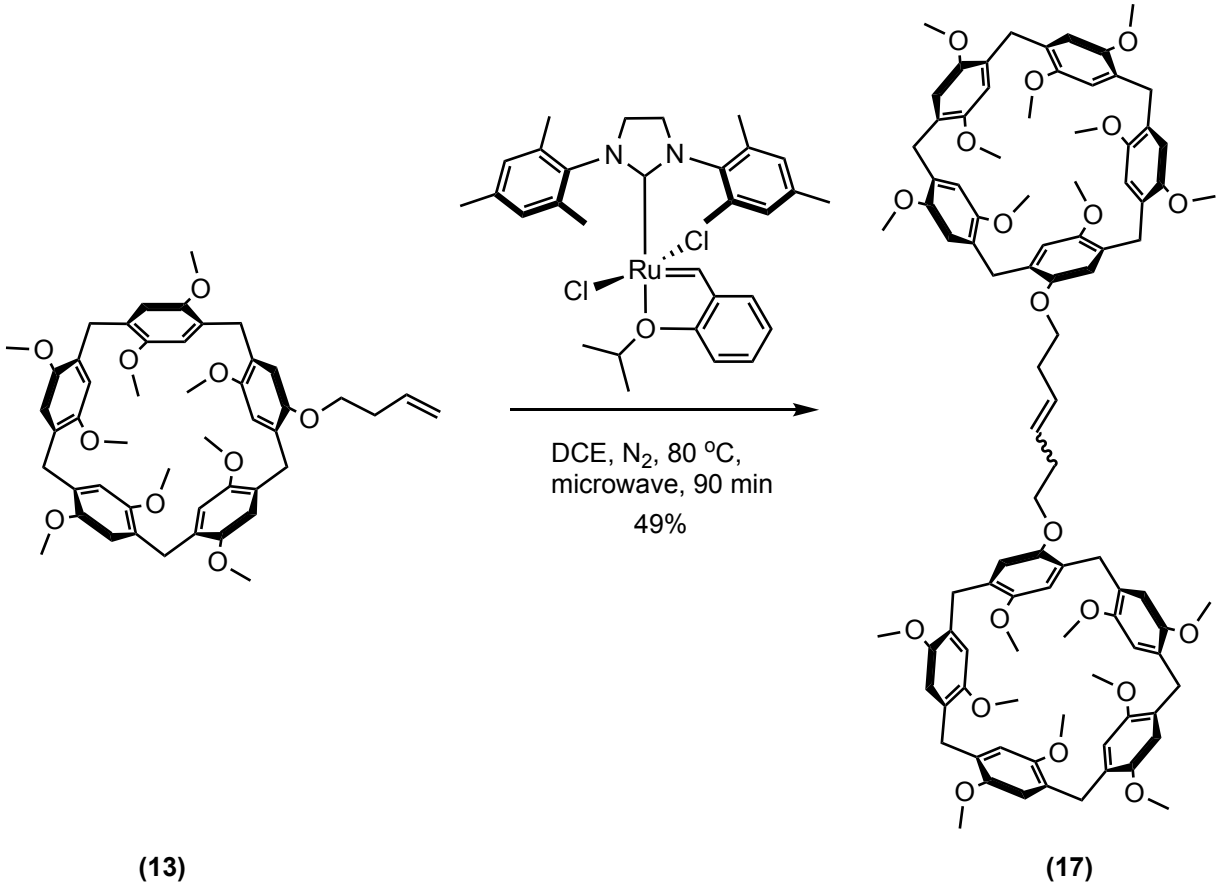

Scheme 3.6: Reaction scheme for the synthesis of the alkene handcuff body (**17**).

The details of this synthesis are adapted from conditions employed for the synthesis of molecular knots using alkene metathesis[155]. The first attempt was performed at 40 °C in CH_2Cl_2, since pillar[5]arenes are most soluble in halogenated solvents like chloroform and CH_2Cl_2, but only yields of around 20% were obtained. Fortunately, 3-butene-substituted pillar[5]arene (**13**) is also soluble in DCE which allowed for this reaction to be conducted at 110 °C in a microwave reactor, and this increased the yields to around 50% after purification using flash column chromatography. The structure of the alkene handcuff body (**17**) was confirmed by ^{1}H NMR spectroscopy shown in the Appendix in Figure A.28 and Figure A.29.

The Hoveyda-Grubbs II catalyst is an *E*-selective catalyst. 3-butene-substituted pillar[5]arene (**13**), as a terminal olefin is a Type I olefin and hence can rapidly homodimerise and then undergo secondary metathesis, which favours the more thermodynamically stable product (*E*). This specific catalyst has been reported to catalyse a metathesis reaction between two Type I olefins in an *E*/*Z* ratio of 7:1.[156] As the alkene peak in the ^{1}H NMR spectrum of 3-butene-substituted pillar[5]arene (**13**) is broad and hence no coupling constant could be obtained, it was assumed that the major product in this reaction is the *E* isomer based on theory.

A ^{1}H DOSY NMR of (**17**) was also attempted since it was possible that the cis/trans alkene versions of this compound would differ enough in size for it to be detectable. The spectrum is shown in the Appendix in Figure A.30, but it does not show two compounds of differing sizes, which could mean that they are of a similar size or that purification removed the *Z* isomer. Since it is likely that the major product was the *E* isomer, the rest of the handcuff synthesis that follows assumes the *E* isomer to be the relevant one.

The redox behaviour of (**17**) was investigated by Cyclic Voltammetry (CV) in CH_2Cl_2, containing [^{n}Bu$_4$N][BF$_4$] (0.2 M) as the supporting electrolyte, at ambient temperature and at 0.10 Vs^{-1} as shown in Figure 3.10 and Table 3.2 at the end of the chapter. Similarly to 3-butene-substituted pillar[5]arene (**13**), no electrochemical processes were detected at negative potentials. At positive potentials the first oxidation (at $E_{1/2}$ 0.62 V vs. Fc^{+}/Fc) shows reversible behaviour. Again, the remaining oxidations are poorly resolved, and correspond to the loss of multiple electrons as this is a complex series of overlapping oxidation processes. These oxidations were better resolved by the square wave voltammetry shown in Figure 3.11 and Table 3.3 at the end of the chapter.

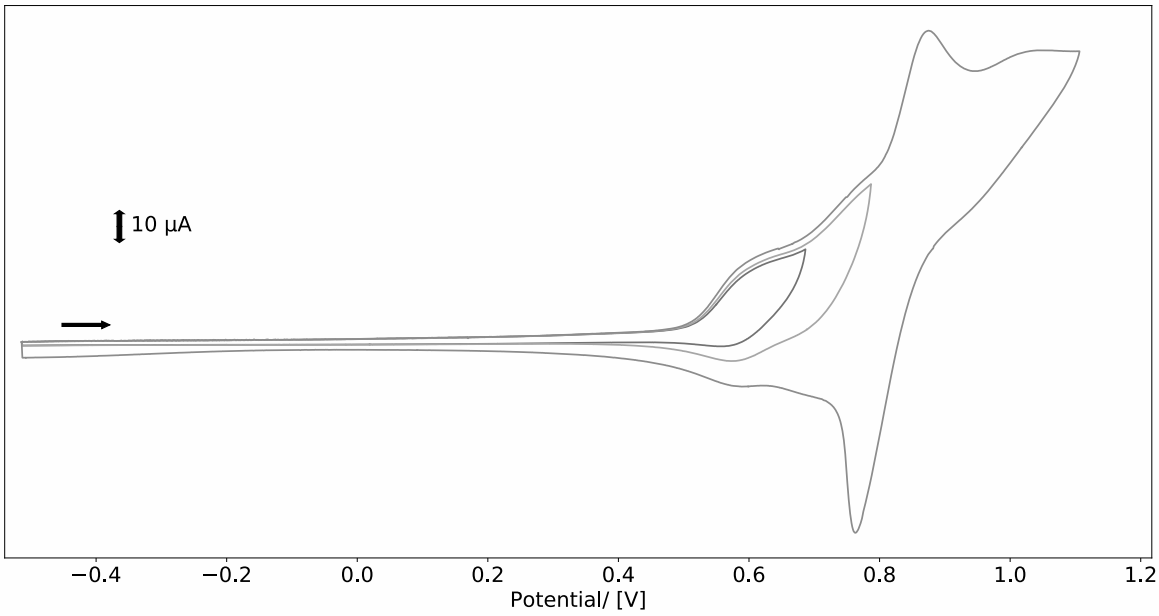

Figure 3.10: Cyclic voltammogram of (**17**) in CH_2Cl_2 containing $[^nBu_4N][BF_4]$ (0.2 M) as supporting electrolyte, at ambient temperature and at 0.10 Vs^{-1}. Potentials reported vs. Fc^+/Fc.

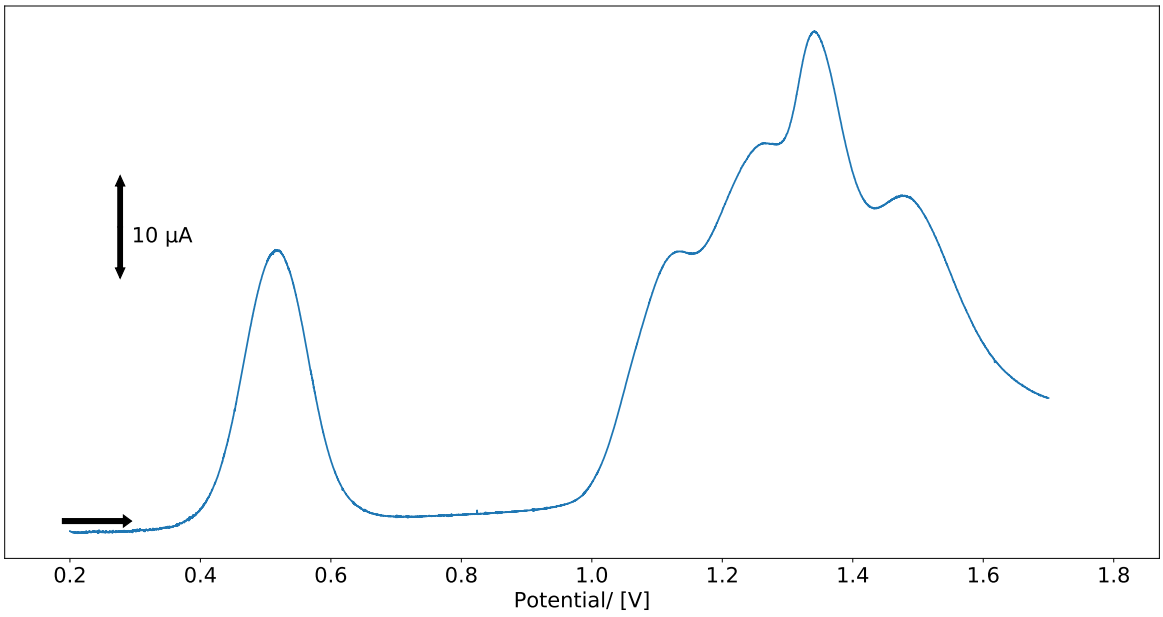

Figure 3.11: Square wave voltammetry of (**17**) in CH_2Cl_2 containing $[^nBu_4N][BF_4]$ (0.2 M) as the supporting electrolyte, at ambient temperature. The process at 0 V is Fc^+/Fc added as the internal standard. Potentials reported vs. Fc^+/Fc.

Overall, the cyclic voltammetry for 3-butene-substituted pillar[5]arene (**13**) and (**17**) are similar to each other, showing that the alkene core does not have a significant effect on the molecular orbitals of the macrocycles since it is both far removed and not active in this potential window, as shown in Figure 3.12.

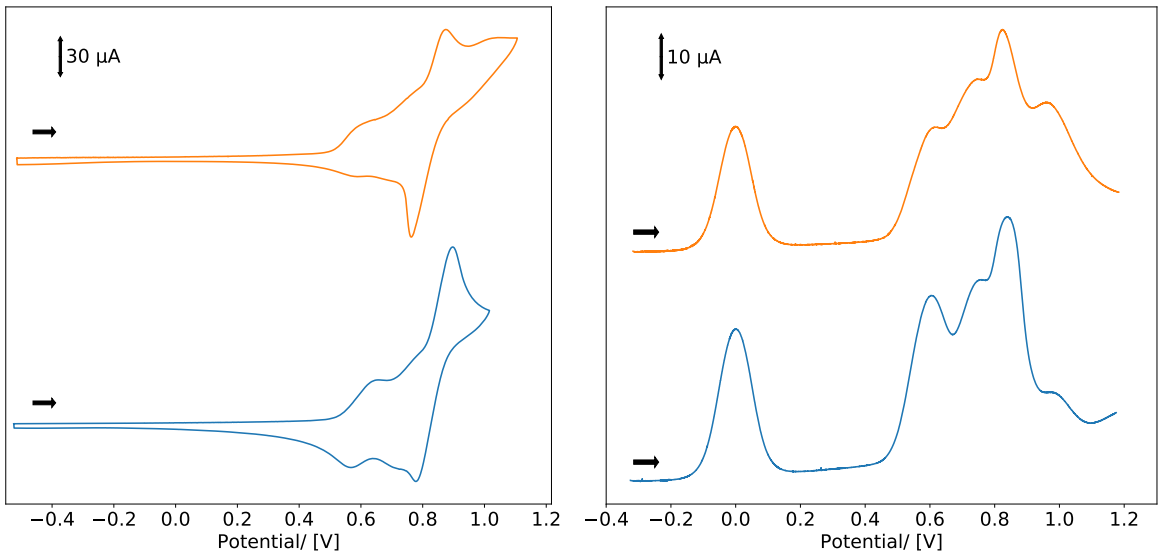

Figure 3.12: Left: cyclic voltammograms, Right: square wave voltammograms of the alkene handcuff body (**17**) (orange) and 3-butene-substituted pillar[5]arene (**13**) (blue) in CH_2Cl_2 containing $[^nBu_4N][BF_4]$ (0.2 M) as supporting electrolyte, at ambient temperature and at 0.10 Vs^{-1}. The square wave process at 0 V is Fc^+/Fc added as the internal standard. Potentials reported vs. Fc^+/Fc.

An attempt at crystallising (**17**) for the purposes of X-ray crystallography was made in the same conditions as for 3-butene-substituted pillar[5]arene (**13**) (slow diffusion of hexane into a solution of the compound in chloroform), but only amorphous solids were obtained which did not diffract.

3.2.3 Synthesis of the handcuff rod

A rod with a PDI core with an 8-imidazolyloctane chain on each side was chosen for ease of comparison to a handcuff rotaxane previously synthesised within the group.[39] Its synthesis is shown in Scheme 3.7.

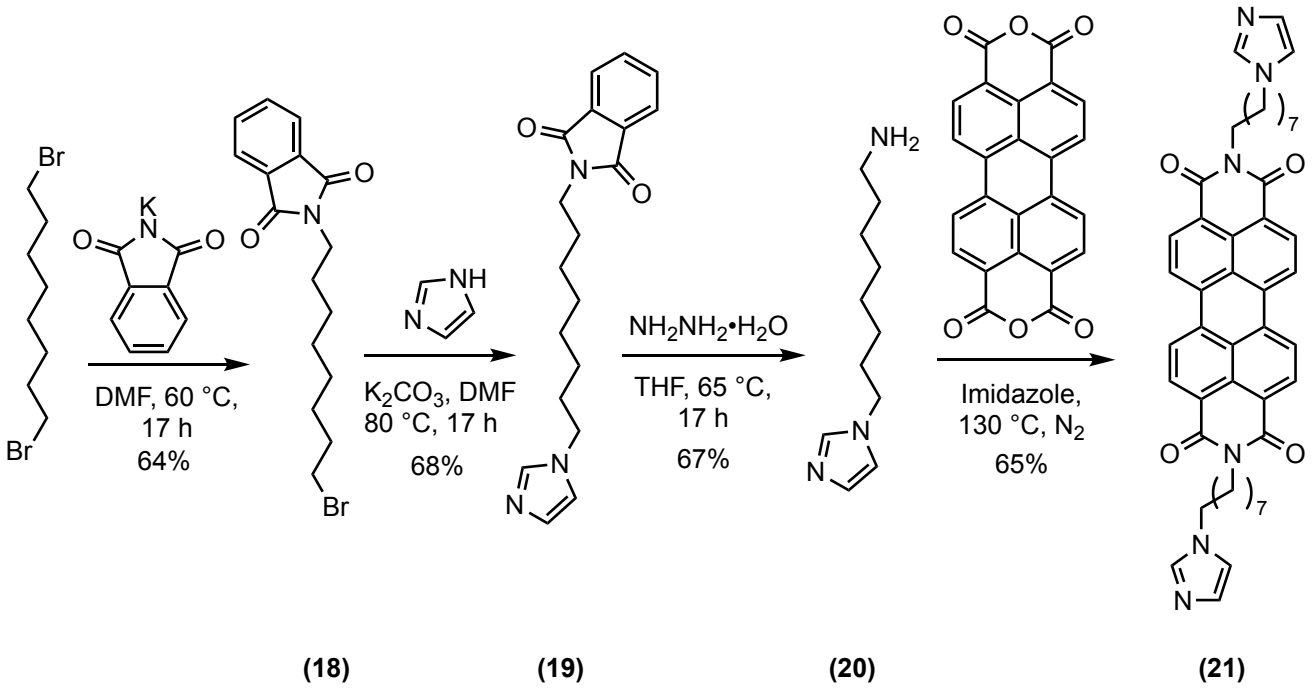

Scheme 3.7: Reaction scheme for the synthesis of the handcuff rod (**21**).

Commercially available 1,8-dibromooctane was mixed with potassium phthalimide to give N-(8-bromooctyl)phthalimide (**18**), which was then mixed with imidazole to give N-(8-imidazolyloctyl)phthalimide (**19**). The phthalimide group was then cleaved using hydrazine hydrate to give 8-(1H-imidazol-1-yl)octan-1-amine (**20**), which was mixed with PTCDA in molten imidazole to afford the handcuff rod (**21**).[126] The successful synthesis of all of these products was confirmed by ^{1}H NMR spectroscopy shown in the Appendix in Figures A.31–A.38.

3.2.4 Alkene handcuff synthesis

Once all the individual parts of this handcuff rotaxane were synthesised, the final threading and stoppering reaction could be undertaken. The synthesis of the alkene handcuff (**23**), which follows the method used earlier in the group[39] is shown in Scheme 3.8.

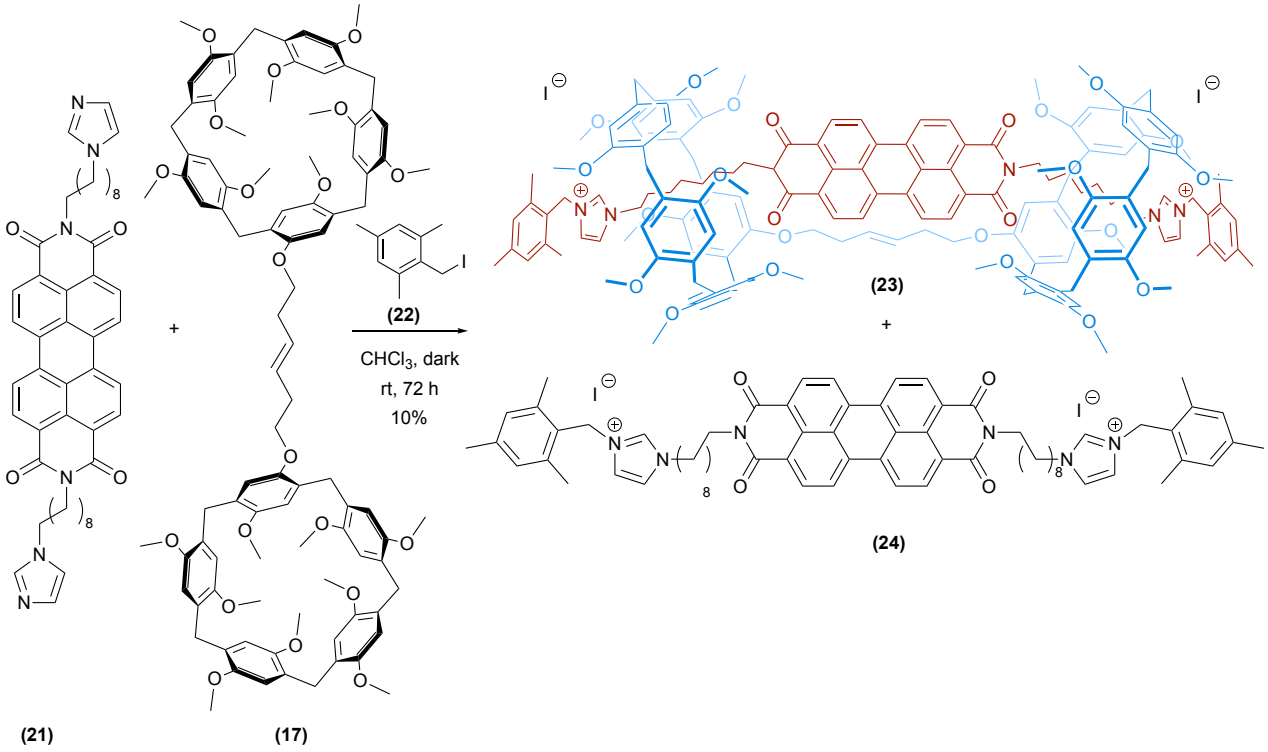

Scheme 3.8: Reaction scheme for the synthesis of the alkene handcuff rotaxane (**23**) and the stoppered rod (**24**).

The handcuff body (**17**) and handcuff rod (**21**) were dissolved in a minimum amount of chloroform ($\sim$ mg/ml scale) to encourage threading. Several cycles of heating close to the boiling point of the solvent, swirling and sonicating the reaction mixture were undertaken, replenishing the chloroform as needed. This method of saturating the solution with both starting materials is crucial for threading to be successful.

Once the starting materials were fully dissolved and assumed to be threaded, the reaction mixture was cooled to -10 °C to discourage kinetic dethreading. At this point the light sensitive stopper group (**22**) was added in the dark and the reaction mixture was gently stirred for 72 hours to yield the handcuff species (**23**). The first sign of an interlocked

pillar[5]arene-alkane species was visible even in the ^{1}H NMR spectrum of the crude reaction mixture, as the rod's alkane proton signals are shifted upfield due to shielding from the pillar[5]arene macrocycles.[49] As there are usually no other peaks in this region, it is easy to observe rotaxane formation even in complex mixtures. This was corroborated with the correct mass found with ESI-MS (m/z calcd for $[M]^{2+}$ (1283.1380); found (1283.1322)). However, both the negative ^{1}H NMR peaks and the correct mass could be observed for a rotaxane where only one end of the rod was threaded through one macrocycle.

The purification of this handcuff proved challenging. The first attempt at flash column chromatography yielded poor results as the crude product adhered strongly to the silica. Once the crude product's iodide counteranions were exchanged with PF_6^-, sticking to the silica was a much smaller issue. The next attempts at synthesis therefore included anion exchange prior to purification. However, even after anion exchange, the purification remained challenging due to the streaking. It was difficult to resolve separate spots or bands on TLC, prep TLC and flash column chromatography alike. The lack of stacking molecular recognition between the body and the rod, and this need for multiple purifications led to yields of 10% being observed for this synthesis.

Despite the difficulties, the presence of the alkene handcuff (**23**) was confirmed by ^{1}H NMR spectroscopy shown in the Appendix in Figures A.41 and A.42. A comparison of the ^{1}H NMR spectra of the alkene handcuff body (**17**), handcuff (**23**) and handcuff rod (**21**) is shown in Figure 3.13 assigned with the help of ^{1}H –^{1}H COSY and NOESY NMR spectra shown in the Appendix in Figures A.43 and A.44.

The upfield shifting of the aliphatic arms of the handcuff rod component is illustrated with dotted lines. The protons which exhibit the largest ppm shifts ($\varkappa$ – 3.71, ι – 3.45 and ϑ – 2.18) can be understood to be within the macrocycle's cavity as they should receive the strongest shielding effect. The proton with a less extreme shift, η – 1.12, is a bit further away from the bulk of the donated electron density, while protons ζ, ε, δ and γ are closest to the PDI core and hence exhibit little shifting. This high degree of symmetry and the integral values for the peaks rule out that this compound could be a rotaxane where only one end of the rod was threaded through one macrocycle.

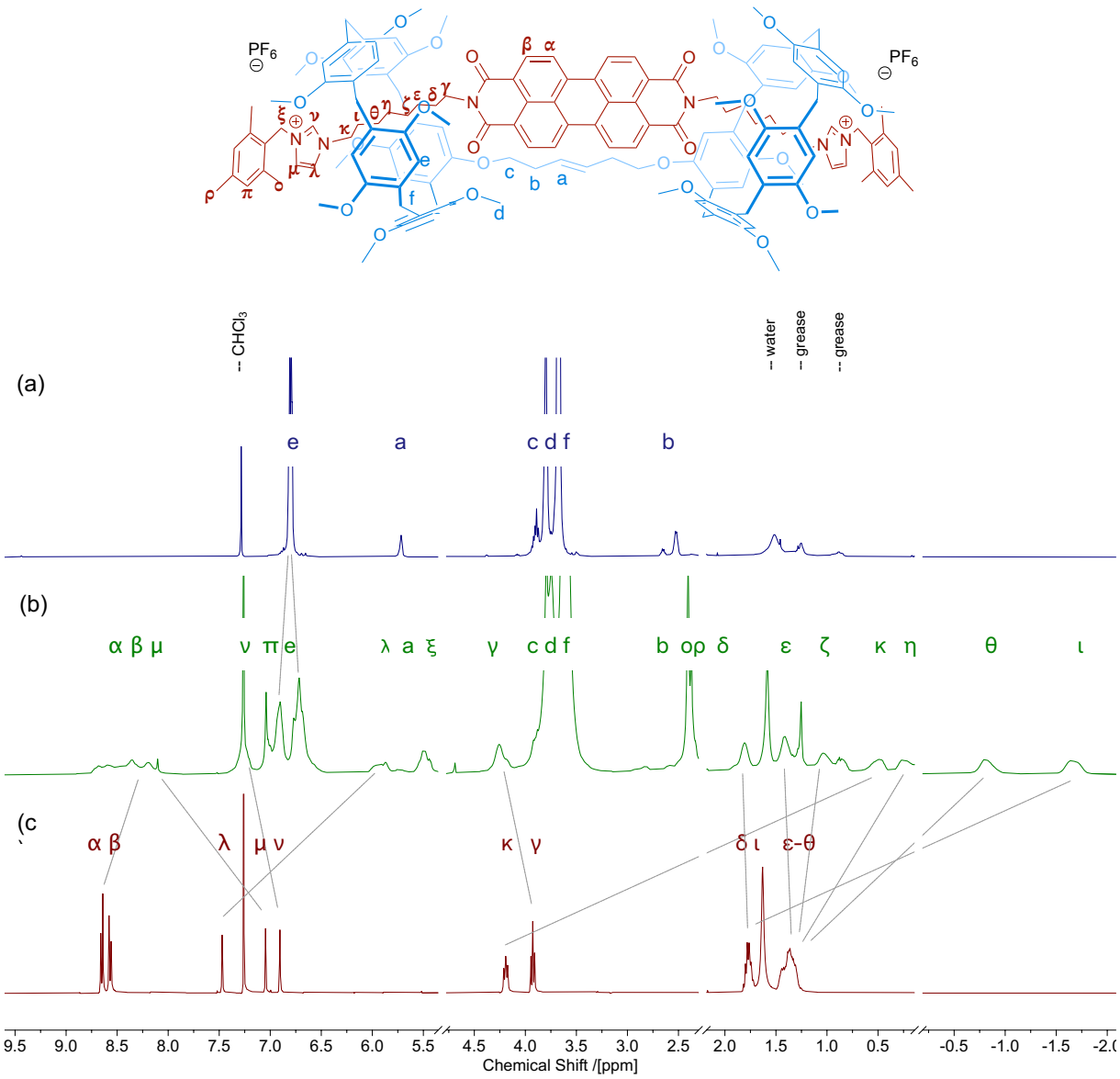

Figure 3.13: ^{1}H NMR (300 MHz, $CDCl_3$ 298 K) spectra of the alkene a) handcuff body (**17**), b) handcuff (**23**) and c) handcuff rod (**24**) showing the characteristic upfield shift of many of the handcuff's aliphatic rod peaks.

A further level of complexity displayed in this spectrum is due to the substituted nature of the pillar[5]arenes. The substitution makes their rims no longer equivalent and threading can occur through either rim. It has been postulated previously that this inequivalency leads to handcuffs with three possible stereoisomers.[33] This was observed in the PDI-PDI handcuff in some ^{1}H NMR peak splittings. It is not possible to determine if this is happening for the PDI-alkene handcuff (**23**) as the corresponding peaks are too broad, but the systems

are very similar.

Even after multiple attempts to purify with prep TLC, flash column chromatography and recrystallisation, it is likely that the sample still contained the stoppered rod (**24**) which was formed as a side product alongside the handcuff. This is most visible in Figure A.41 in peak γ which is integrates to more than 4, and has a shoulder, but other peaks like δ, η, ζ are also affected as shown in the Appendix in Figure A.41. Multiple samples of this handcuff were synthesised and purified separately and then together but it was not possible to obtain a sample with less than approximately 20 – 30 % of the rod also present (as calculated by ^{1}H NMR peak ratio). This suggests that the ∼ 10% yield for this reaction is an overestimate and the true yield is lower than that.

The successful synthesis of this handcuff confirms the hypothesis that this method only requires templating between the body's macrocycles and the rod. However the much lower yields observed (vs the PDI-PDI and PDI-naphthalene handcuffs yields of 81% and 78% respectively both shown in the Introduction Section 1.4.2)[40] do indicate that the stacking interaction between the rod and the body is very important in improving its efficiency. The handcuff body for this handcuff was also shorter (a double bond vs a PDI core), which might have impacted threading efficiency. Furthermore, if the threading is inefficient, more of the stoppered rod is likely formed, which makes the purification harder, further lowering yields.

To complete the comparison with the PDI-PDI and PDI-naphthalene handcuffs, the PDI-alkene handcuff (**23**) was investigated by UV/vis spectroscopy and cyclic voltammetry.

The UV/vis spectrum of (**23**) in CH_2Cl_2 shows three bands of increasing intensity, an absorption profile expected of unaggregated PDIs in solution as shown in Figure 3.14.[39,68]

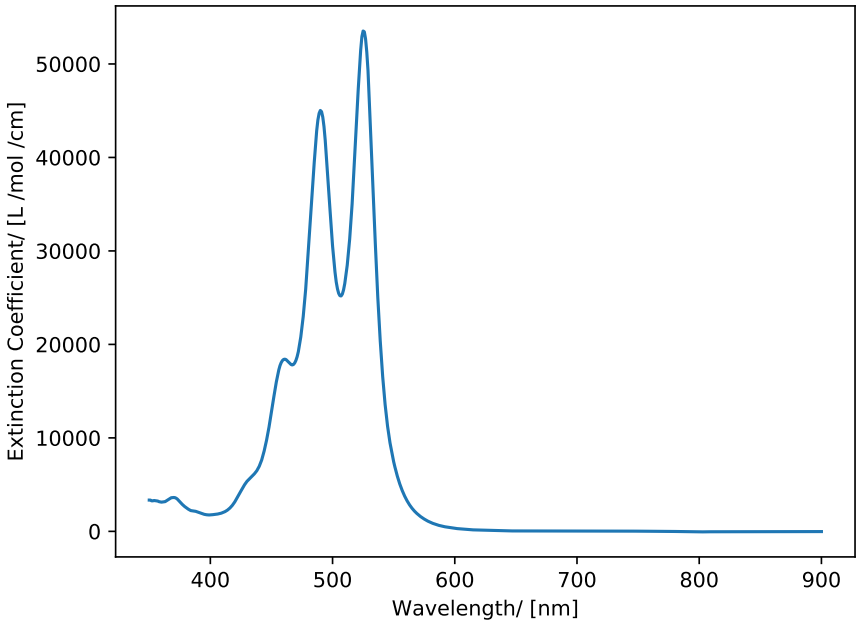

Figure 3.14: UV/vis absorption spectrum of the alkene handcuff (**23**) in CH_2Cl_2.

The spectrum shape looks similar to that of the stoppered rod (**24**) previously obtained within the group, and the peaks appear at similar wavelengths as shown in Table 3.1.

	Wavelength / [nm]
(**24**)	459 489 525
(**23**)	461 491 526

Table 3.1: UV/vis absorption data for the alkene handcuff (**23**) and the stoppered rod (**24**)[39]

This is consistent with the handcuff only containing one PDI core, but does not exclude the presence of a free rod in solution, as mixtures of different PDI species do not display reordering in the intensity of these bands or blue shifts relative to the monomers, which are characteristic of stacking species.[39]

Cyclic (CV) and square-wave (SW) voltammetry in CH_2Cl_2, containing $[^nBu_4N][BF_4]$ (0.2 M) as the supporting electrolyte, at ambient temperature and at 0.10 Vs^{-1} were used to probe how the proximity of a perylene diimide to an alkene affects the PDI molecular orbitals as shown in Figure 3.15.

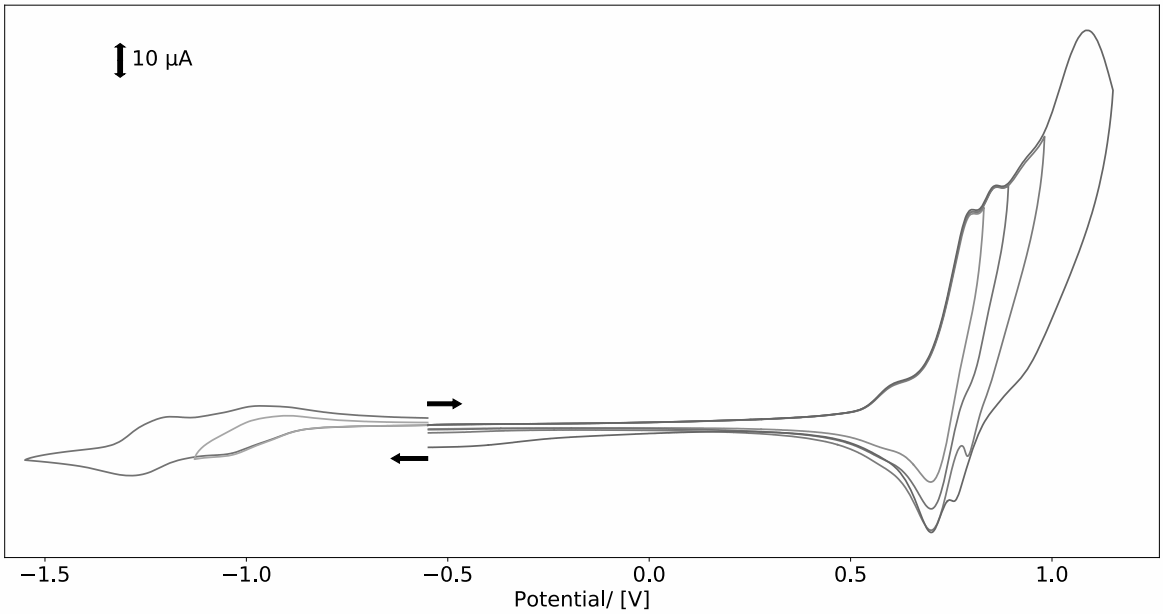

Figure 3.15: Cyclic Voltammogram of the alkene handcuff (**23**) in CH_2Cl_2 containing $[^nBu_4N][BF_4]$ (0.2 M) as supporting electrolyte, at ambient temperature and at 0.10 Vs^{-1}. Potentials reported vs. Fc^+/Fc.

For the PDI-naphthalene handcuff (**25**) (Figure 1.11) the redox-active PDI core links the two pillar[5]arenes to form the body of the handcuff, whilst the rod contains the naphthalene moiety. This contrasts with the PDI-alkene handcuff (**23**) for which it is the rod that contains the redox active PDI core. However, for both handcuffs the non-PDI cores do not interact with the PDI core to extend the molecular orbital system across multiple cores as was supposed to be the case for the triple decker handcuff envisioned in the previous chapter or in the PDI-PDI handcuff.[39]

For the PDI-PDI handcuff, three redox couples were observed, with the first two corresponding to one electron being added to one and then the other PDI core. The third couple corresponded to two electrons being simultaneously added to the PDI cores. The presence of these processes support the existence of an extended molecular orbital system delocalised

over the two PDI cores. The alkene handcuff (**23**) and naphthalene handcuff (**25**) CVs shown in Figure 3.16 do not show those three redox couples which were observed for the PDI-PDI handcuff.

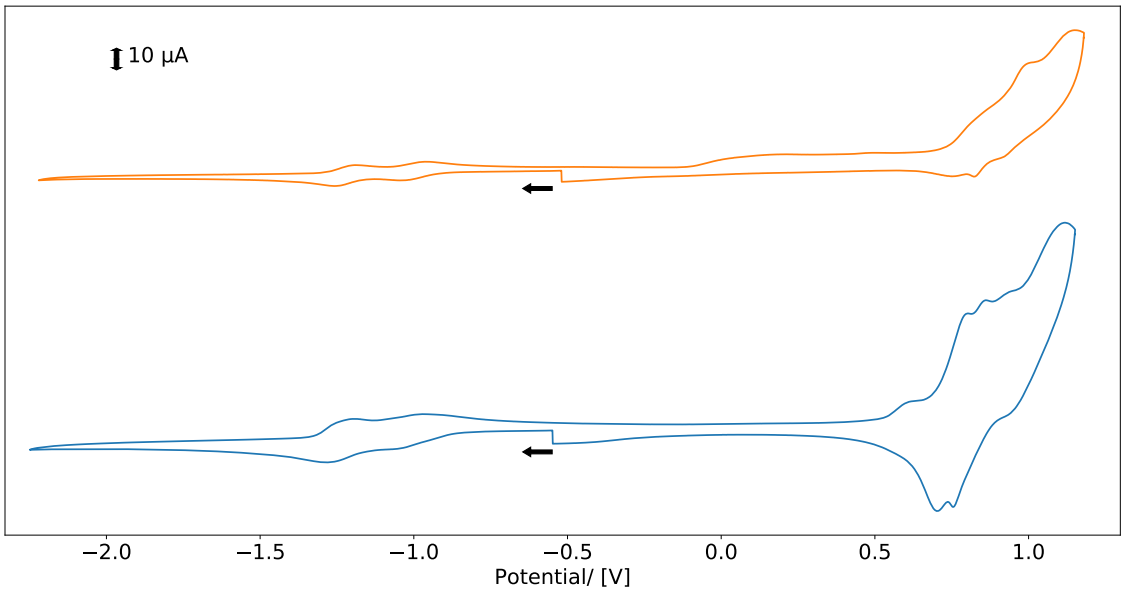

Figure 3.16: Cyclic Voltammograms of the alkene handcuff (**23**) (blue) and a similar handcuff (**25**) (orange) in CH_2Cl_2 at ambient temperature and at 0.10 Vs^{-1}, containing $[^nBu_4N][BF_4]$ (0.2 M) as supporting electrolyte for the former and (0.4 M) for the latter.[40] Potentials reported vs. Fc^+/Fc.

In fact, despite being a complex interlocked molecule, the naphthalene handcuff shows two one-electron reductions (at $E_{1/2}$ -1.00 and -1.22 V vs. Fc^+/Fc) separated by ∼0.2 V as is standard for simple PDI species unsubstituted in the bay regions, such as the alkene handcuff rod (**24**) (reductions at $E_{1/2}$ -0.96 and -1.15 V vs. Fc^+/Fc) as shown in Figure 3.17 and Table 3.2. Despite the similarity in structural features, the reduction signals for the alkene handcuff (**23**) look different, showing what appears to be an overlap of at least three, possibly four reduction processes around two areas of $E_{1/2}$ -1.01 and -1.24 V vs. Fc^+/Fc. Square wave voltammetry for these species was also performed as shown in the same figure, but did not resolve the reduction signals of the alkene handcuff (**23**) any further hence they are quoted as only two peaks in Tables 3.2 and 3.3.

Upon closer inspection, the alkene handcuff (**23**) CV and SW may be interpreted as a combination of the voltammograms for the PDI-naphthalene handcuff (**25**) and the stoppered

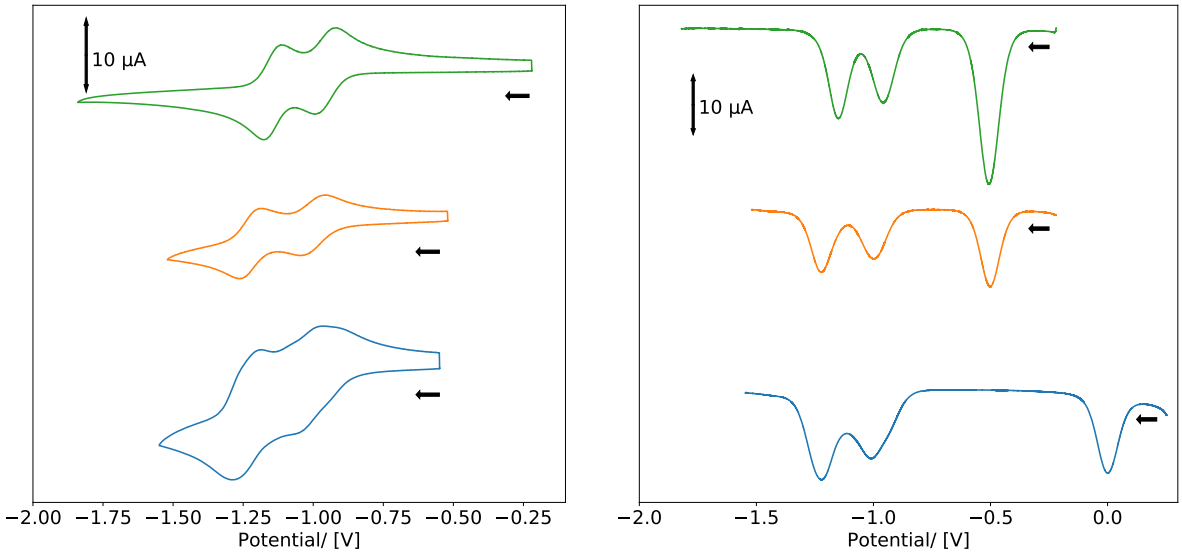

Figure 3.17: Left: cyclic voltammorgram; Right: square wave voltammogram of the alkene handcuff (**23**) (blue), similar handcuff (**25**) (orange) and the stoppered rod (**24**) (green) in CH_2Cl_2 at ambient temperature and at 0.10 Vs^{-1}, containing $[^nBu_4N][BF_4]$ (0.2 M) as supporting electrolyte for the former and (0.4 M) for the latter.[40]. The square wave process at 0 V (blue) is Fc^+/Fc added as the internal standard, and the one at -0.52 V (orange, green) is $[(\eta^5\text{-}C_5Me_5)_2Fe]^+/[(\eta^5\text{-}C_5Me_5)_2Fe]$ also added as the internal standard, later referenced to the Fc+/Fc couple by an independent calibration. Potentials reported vs. Fc^+/Fc.

rod (**24**). This would support observations made during the analysis of the ^1H NMR data where some of the rod appeared present in addition to the handcuff.

Next, the oxidations of the alkene handcuff (**23**) were compared to those of its starting material, the handcuff body (**17**) as shown in Figure 3.18. The first oxidation process (at $E_{1/2}$ 0.61 V vs. Fc^+/Fc) appears very similar to the first oxidation process for the handcuff body (**17**) (at $E_{1/2}$ 0.62 V vs. Fc^+/Fc). The remaining oxidations are poorly resolved and correspond to the loss of multiple electrons, observations consistent with the pillar[5]arene-based starting materials, hence only the first oxidation (Ox A) is quoted for all of these compounds in Table 3.2. The oxidations were better resolved by the square wave voltammetry shown in the same figure.

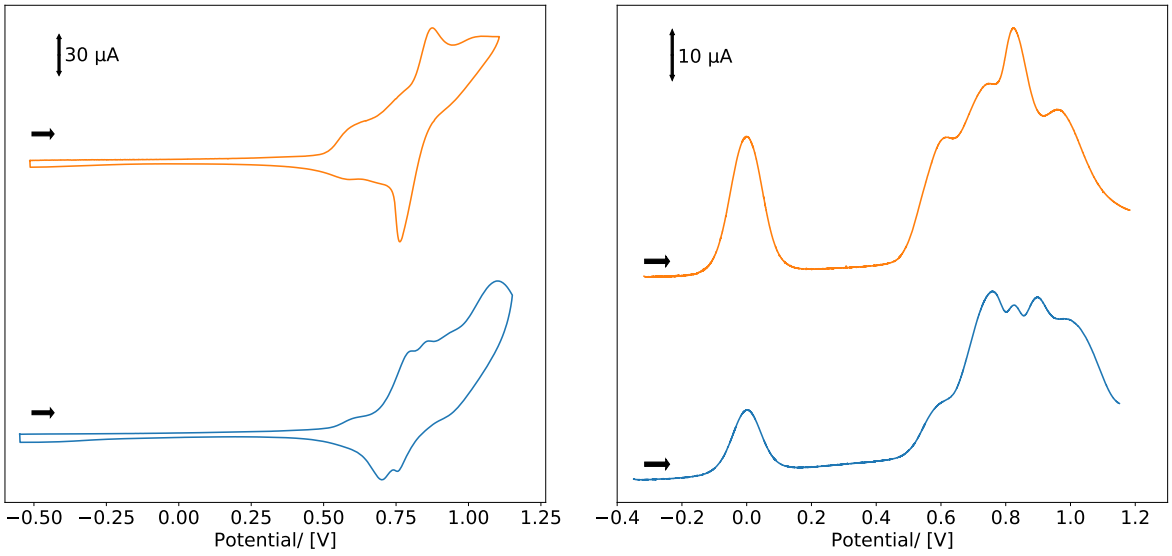

Figure 3.18: Left: cyclic voltammogram; Right: square wave voltammogram of the alkene handcuff (**23**) (blue) and starting material (**17**) (orange) in CH_2Cl_2 containing $[^nBu_4N][BF_4]$ (0.2 M) as supporting electrolyte, at ambient temperature. The square wave process at 0 V is Fc^+/Fc added as the internal standard. Potentials reported vs. Fc^+/Fc.

Overall, the CV oxidations for (**23**) look different to those for 3-butene-substituted pillar[5]arene (**13**) and (**17**). These differences are possibly due to the imidazolium species, which might be reactive in this potential window. This could potentially explain the extra SW peak observed for (**23**) at 0.90 V vs. Fc^+/Fc (Ox D in Table 3.3. Unfortunately, no oxidation experiments on the handcuff rod (**24**) and no SW oxidation experiments on the naphthalene handcuff (**25**) were performed so there are no direct comparisons with the current data.

Compound	Ox A	Red A	Red B
(**13**)	0.61	-	-
(**17**)	0.62	-	-
(**24**)	-	-0.96	-1.15
(**25**)	-	-1.00	-1.22
(**23**)	0.61	-1.01	-1.24

Table 3.2: CV data in V for 3-butene-substituted pillar[5]arene (**13**), handcuff body (**17**), stoppered rod (**24**), naphthalene handcuff (**25**), and alkene handcuff (**23**) in CH_2Cl_2 at ambient temperature, containing $[^nBu_4N][BF_4]$ (0.2 M) as supporting electrolyte for (**13**) (**17**), (**23**), and (0.4 M) for (**24**), (**25**).[40]

Compound	Ox A	Ox B	Ox C	Ox D	Ox E	Red A	Red B
(**13**)	0.61	0.76	0.84	-	0.98	-	-
(**17**)	0.62	0.75	0.82	-	0.96	-	-
(**24**)	-	-	-	-	-	-0.96	-1.15
(**25**)	-	-	-	-	-	-1.00	-1.22
(**23**)	0.61	0.76	0.83	0.90	0.98	-1.01	-1.22

Table 3.3: SW data in V for 3-butene-substituted pillar[5]arene (**13**), handcuff body (**17**), stoppered rod (**24**), naphthalene handcuff (**25**), and alkene handcuff (**23**) in CH_2Cl_2 at ambient temperature, containing $[^nBu_4N][BF_4]$ (0.2 M) as supporting electrolyte for (**13**) (**17**), (**23**), and (0.4 M) for (**24**), (**25**).[40]

3.2.5 Synthesis of a [3]rotaxane through alkene metathesis

A natural next step after synthesising the PDI-alkene handcuff (**23**) was to attempt to cleave the handcuff body to give a [3]rotaxane made of the handcuff rod and two separated macrocycles. A similar reaction has been successful before.[31] To that end the same alkene metathesis conditions as had been utilised to synthesise (**17**) were used on the handcuff and a convenient alkene that was available on hand: 1-(but-3-en-1-yloxy)-4-methoxybenzene (**15**).

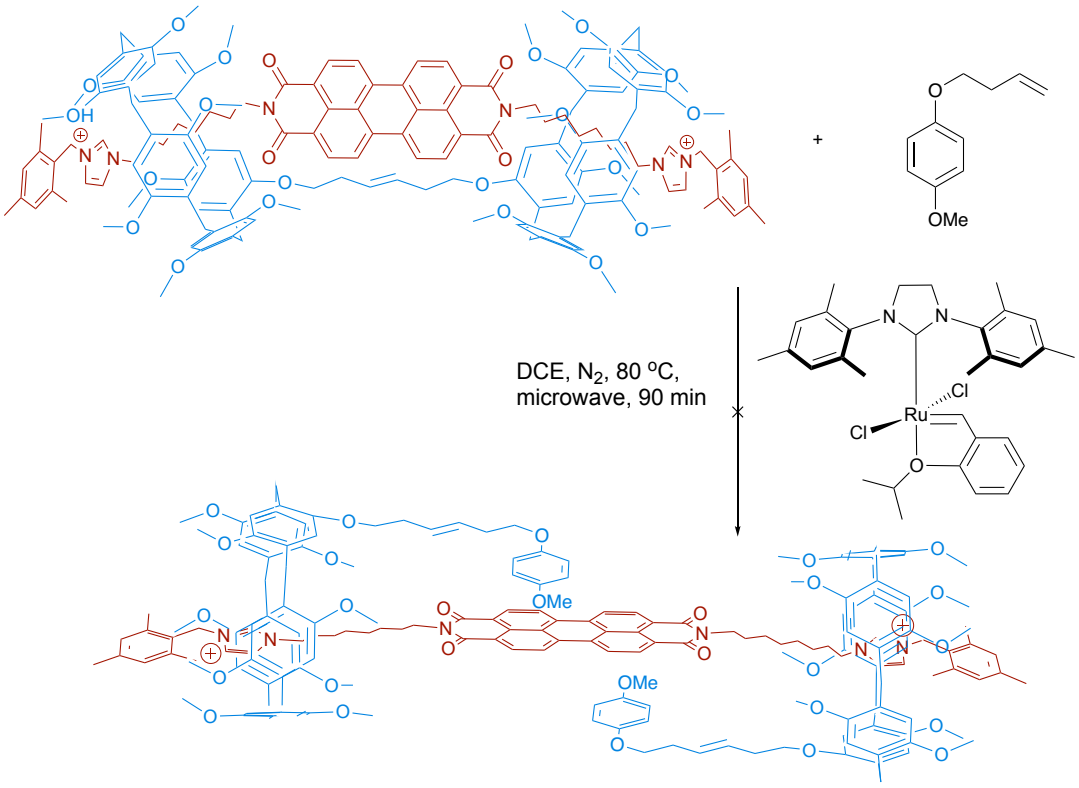

Scheme 3.9: Reaction scheme for the synthesis of a [3]rotaxane from the alkene handcuff rotaxane (**23**).

Unfortunately no products or intermediates of the correct masses were found using MALDI-TOF MS. It is possible that this handcuff and the Hoveyda-Grubbs-II catalyst are both sterically crowded and hence no reaction was observed. Ozonolysis might be a potential pathway to achieving a cleaving of the handcuff body, but it could cleave more than just the desired double bond and hence was not attempted at this time.

3.3 Conclusions

A PDI-tetrazine handcuff synthesis, with a tetrazine bis-pillar[5]arene body and a PDI bis-imidazole rod was attempted. During this process two novel pillar[5]arene species, the desired benzonitrile-pillar[5]arene (**12**) and a side product: 3-butene-substituted pillar[5]arene (**13**) were synthesised. However due to issues with yields for benzonitrile-pillar[5]arene (**12**) and issues with solubility during the tetrazine reaction, a handcuff body was not synthesised. Finding an alternative set of conditions or attempting to make a handcuff with a PDI and pillar[5]arene body and a tetrazine and imidazole rod might make the synthesis of this rod possible.

The side product 3-butene-substituted pillar[5]arene (**13**) was then used, after its synthesis was optimised, to synthesise a PDI-alkene handcuff (**23**). This proved an earlier hypothesis that the described handcuff threading method only required templating between the rod and the macrocycles, but through a comparison with the PDI-PDI and PDI-naphthalene handcuffs previously synthesised within the group, it became apparent that the lack of a stacking interaction which guides the approach of the body and rod, makes this reaction inefficient and the purification of the final handcuff difficult.

The alkene handcuff (**23**) showed a UV/vis absorption profile consistent with an unaggregated PDI in solution. The CV is consistent with a PDI-based species, but different to the PDI-PDI or PDI-naphthalene handcuff voltammograms, likely because up to 30% of the stoppered rod (**21**) was also present in the investigated samples of (**23**).

An attempt at turning the PDI-alkene handcuff (**23**) into a [3]rotaxane through another alkene metathesis reaction was made, but was not successful. Ozonolysis could be another reaction that would cleave the alkene, but it could also damage other parts of the molecule.

4 Introduction to leather

Leather is a historically and culturally important material throughout much of the world, and as such numerous artefacts such as clothing and book covers are made from or contain it. Leathercraft is a diverse and complex topic with both traditional methods and modern industrial techniques, and as such the varieties of produced leather differ considerably from one another. Scientific understanding and analysis of leather is concerned with categorising leathers by what they were made from and how they were processed, determining the chemical composition of each kind, ascertaining how this leads to the physical properties of the objects made from them, and, in particular for the focus of this chapter, deducing why and how these chemicals deteriorate over time so as to better conserve and safely handle historic leather items.

This chapter will begin by introducing what is known about the chemical composition and structure of leather, existing knowledge of its decay routes and what analytical techniques can be employed to study this. This body of knowledge will then be applied to a collection of both modern leather reference samples, as well as deteriorated historic leather book bindings from the Natural History Museum (NHM)'s collection to investigate the chemistry of a particular type of leather deterioration known to conservators as red rot. This work was conducted in part during a five month placement at the NHM in collaboration with scientists there as well as the Business Partnership Unit at the University of Nottingham after being awarded an EPSRC IAA grant of £10 000.

4.1 Leather

The raw starting material from which leather is produced is the skin or hide of various animals such as cows, goats and pigs. As such the discussion of the chemistry of leather begins from the biochemistry of animal skins. Skins are primarily made of long, three-dimensional polymerised amino acid chains linked by peptide bonds. These chains fold and twist through one another to form a complex supramolecular structure that supports and stabilises the material.[157]

The most important chemical in this structure is the protein collagen. Collagen molecules are 280 nm long and 1.4 nm wide triple helices of an amino acid polymer with glycine in every third position, which in the skin naturally align to form bundles of interwoven fibrils. Skin obtained from different animals or indeed different parts of the same animal have different inter- and intra-fibril structure, which can be seen under Scanning Electron Microscopy (SEM) and helps explain the variability in leather's firmness, flexibility, and other physical bulk properties.[158]

It is also important to note that the skins used to make leather consist of multiple layers. The outermost layer, the epidermis, is made up of keratinised cells that are removed along with the hair using an aqueous mixture of lime and sodium sulfide before a skin is tanned. Below the epidermis lies the dermis, termed grain in leather. This layer is made up of fine collagen fibres that give leather a smooth surface. Below the grain, the collagen fibrils grow in width and are called the corium. Finally, towards the bottom, they lie parallel to the surface and form a limiting layer that separates the skin from the flesh. This is illustrated in Figure 4.1. Other steps preceding the tanning include bating which uses ammonium sulfate and makes the skin soft and silky and pickling in acid and sodium chloride.[159]

4.2 Tanning process

Unless stored in protective environments, raw skins are subject to physical damage, chemical reactions and bacterial or fungal attack, leading to gradual decay. Various methods of protecting against these sources of damage to make a durable, stable and useful product have been used throughout human history. Drying out the skins, treating them with oils or fats to imbue the collagen fibre network with hydrophobic properties, applying waxes to provide surface protection and many other approaches have been used. Products of such methods, such as parchment or vellum, are beyond the scope of this work, and this work instead focuses on understanding vegetable tanning of skins to produce leather. Vegetable tanning specifically uses chemicals called tannins as the primary agent for the treatment of animal skins, so an understanding of what tannins are is necessary.[160]

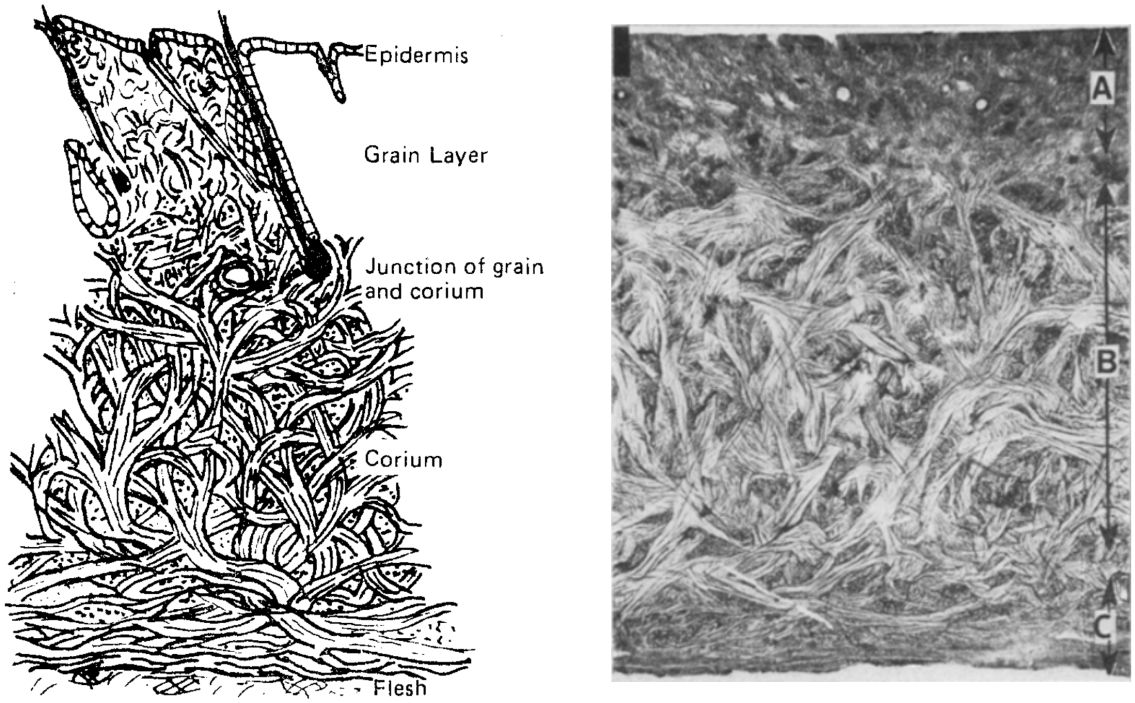

Figure 4.1: Left: diagram showing the cross section structure of cattle skin[159], left: cross section of cattle leather after tanning as seen under a microscope, where A is the grain, B is the corium and C is the limiting flesh layer.[158]

4.2.1 Tannins

Tannins, are large polyphenolic molecules produced by plants and used in their biochemistry to bind to and precipitate proteins, alkaloids and polysaccharides. Of the tannins found in nature, those that do not exceed around 3000 Da are small enough to penetrate the fibre network of a skin and hence be of use to leathercraft.[161]

There are four classes of vegetable tannins; hydrolysable, condensed, complex and phlorotannins[162] but it is only the first two which are relevant to tanning. Hydrolysable tannins are further divided into gallotannins and ellagitannins depending on whether they are esters of gallic acid or hexahydrodiphenoic acid (a precursor of ellagic acid), while condensed tannins are polymers of flavan-3-ol units linked via carbon-carbon single bonds. Both types have a polyol core, (e.g. D-glucose for gallotannins) as shown in Figure 4.2. Hydrolysable tannins come from plants such as sumac, oak, chestnut or valonea, and produce light brown or yellow/green tinted leathers, while condensed tannins are found in mimosa and quebracho for example, and lead to a brown-red colour that darkens when exposed to light. A sin-

gle plant may contain just one type of tannin or a mixture of hydrolysable and condensed tannins.[163–166]

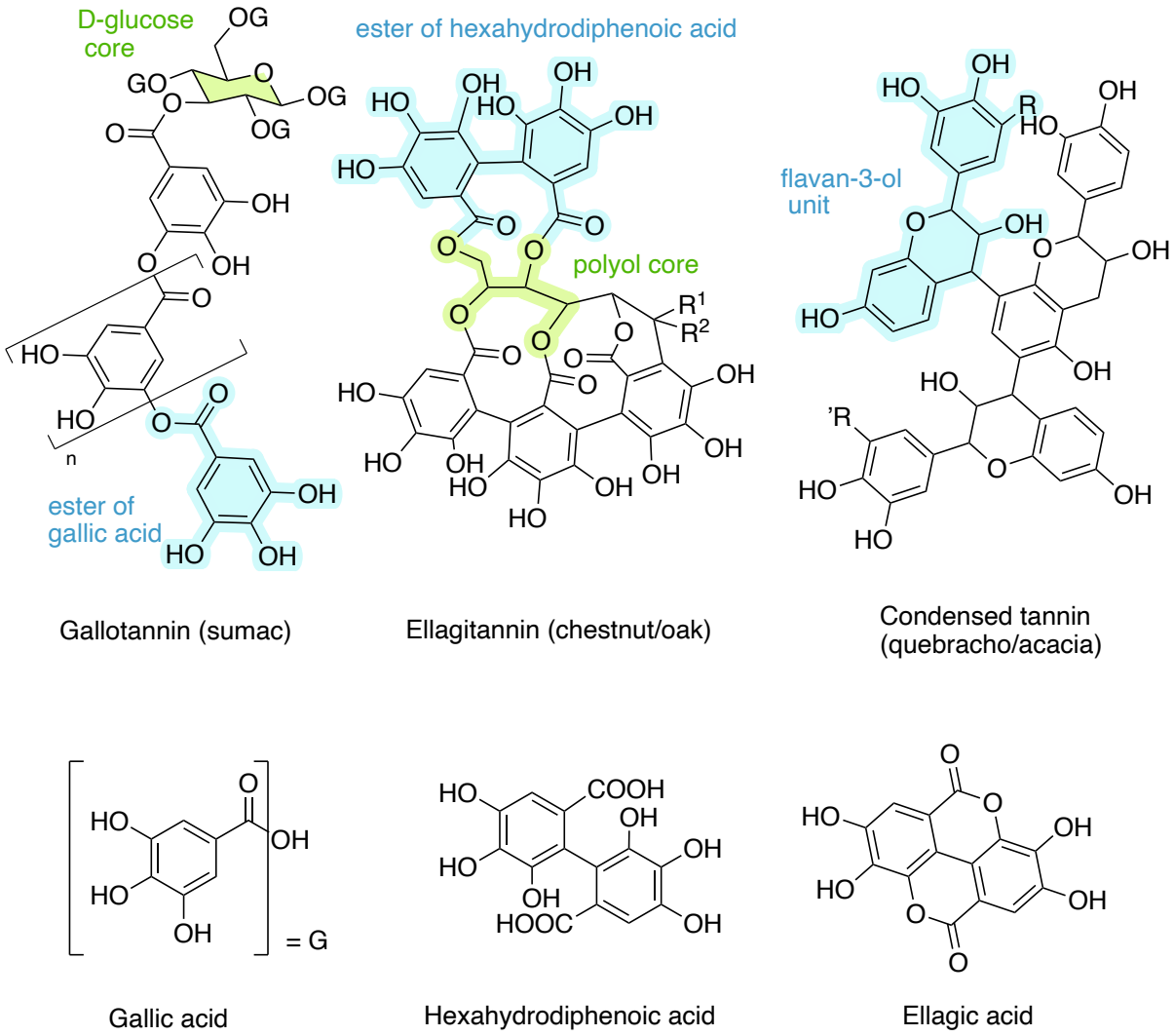

Figure 4.2: Classes of vegetable tannins adapted from Falcão *et al.*[167]

Chemical tests for the presence of different tannin types exist (e.g. the ferric and vanillin tests)[168], but as these stain the leather, they are inappropriate for museum items. Furthermore, the reliability of these tests decreases with degradation, making them doubly unsuitable here. The techniques applied instead in this context are discussed in Section 4.5.1.

The wide range of possible choices of both the animal that the skin is obtained from as well as the plants from which tanning agents are derived, make leather a diverse and versatile material with significant geographic variation based on the locally available raw

materials.[169]. Sources of tannins historically used for leather tanning and their categorisation into the above mentioned types has been investigated by Falcão *et al* and are useful to this work.[163]

Additionally to these vegetable tannins with a long record of historical use, modern industrial methods of producing leather based on mineral tanning agents such as chromium salts, named chrome tanning, are also currently used, but as this work focuses on decay of historic leathers in museums and collections, the majority of which were produced via vegetable tanning,[170,171] this is largely beyond the scope of this work.

4.2.2 Effects of tanning on skins

Each collagen helix is structured such that carboxyl and amine groups are exposed, facing outwards from the helix as shown in Figure 4.3. These present a large number of potential sites for hydrogen bonding to occur. Tanning primarily works by utilising this feature; the large number of densely packed alcohol groups on vegetable tannins allow them to form multiple hydrogen bonds with a unit of the collagen helix. This, combined with their suitable size for this purpose, leads to tannins inserting between adjacent fibres, hydrogen bonding to both, and thus reinforcing the structure of the network via cross-linking. Some bonds with covalent and ionic characteristic may also be formed with certain tannins, leading to even further fortification.[160]

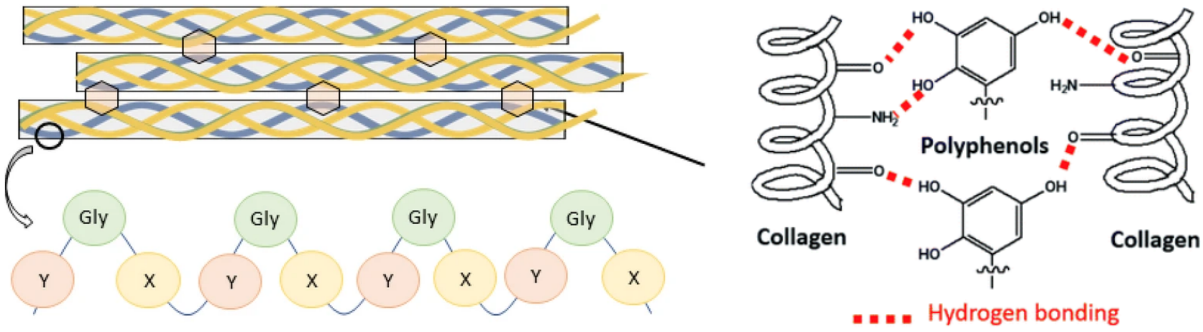

Figure 4.3: The inter- and intra-fibre collagen structure and tannin cross-linking adapted from Dickinson *et al*[172] and Moujahed *et al.*[173]

The amount of tannin required to effectively stabilise the collagen network is between 15% and 40% of the dehydrated mass of the skin depending of the type of leather pro-

duced.[171,174] This permanent change to the skin's large scale structure changes the macroscopic properties of the final leather item, and microscopically makes its chemical components less water soluble, more resistant to microbial attack and less prone to decomposition with heat or just time.[175] Tanning also typically leaves a calcium carbonate residue in the leather, as the calcium hydroxide used in preparing the skin reacts with atmospheric CO_2.[176]

Chromium salt based tanning also works by cross-linking collagen fibres but through chromium complexes forming between the chromium centres of the tannins and the carboxyl groups in the collagen.[157]

4.3 Book Binding

As well as these general properties of leathers, further processing or treatment is also done depending on the intended use of the tanned skin. As this project is concerned with leather-bound historical books, the details of the bookbinding process and how it might effect the final chemistry of the artefacts studied will be reviewed here. Different considerations would influence study of leather used as, for example, clothing, but this is beyond the scope of this work.

Firstly, bookbinding requires a relatively thin leather that can still withstand repeatedly being bent open as a book is used. It hence has to be strong for its thickness, and the grain layer is typically kept to give a distinctive surface texture and pattern for aesthetic reasons. Thicker skins from, for example adult cattle, need to have much of the corium removed to reach an acceptable thickness but this disproportionately reduces its strength. The variation in material properties from location to location on a single animal's skin also leads to considerations in where the skin is taken from, with regions of denser fibre packing and hence higher strength preferred for areas of the book that will be exposed to mechanical stress. Post tanning, dyes are often applied to achieve a desirable colour, and fats are used to soften the final leather for better feel and flexibility. If the tanning process produced an acidic leather, it is neutralised with a weak base such as sodium bicarbonate. Waterproofing may be carried out using silicones, fluorocarbons or other agents. Finally, the finished leather for a book cover may be covered with a suspension of pigments in a resin emulsion to produce

a pleasing effect such as shininess or smoothness as desired. All of these processes may leave residues that affect the results observed when analysing the leather objects in this project and should thus be kept in mind when forming hypotheses or explanations.[177]

4.4 Leather Deterioration

While tanned leather is certainly far more resistant to decomposition than a raw skin, over the timescale of centuries the collagen-tannin network does still gradually deteriorate. The obvious implications of this to conservation of historical leather artefacts has motivated studies of the mechanisms by which deterioration proceeds.[178,179] The two main processes identified as relevant are oxidation and hydrolysis in both the tannins and the collagen peptide chains.[157]

Hydrolysis will be discussed at greater length in Section 4.4.1, but first the effects of oxidation and general deterioration processes is briefly reviewed. Oxidative breakdown of collagen is usually induced by one of several factors. Heat can increase the rate of reaction with atmospheric oxygen and ozone, as well as thermally excite bonds and cause units of a polymer to separate, and in more extreme cases lead to the unwinding of the collagen helix. Light exposure can cause photolysis of C-C bonds in the collagen backbone, and photo-oxidation can form oxygen free radicals and then peroxides that oxidise parts of the leather. Lubricants introduced in the leather making process may contain unsaturated lipids which can autoxidise to produce free radicals and cause oxidative chain reactions throughout the collagen network. All of these factors reduce the amount of intermolecular cross linking that was introduced by tanning, and thus weakens the protections it brought.[160,171]

Once oxidation has left the leather no longer protected by a tightly cross-linked tannin network, both hydrolysis and further oxidation can then go on to disturb the internal structure of the collagen fibres, causing it to denature into disordered, water-soluble gelatin.[180,181] These molecular changes are observed macroscopically as fraying, brittleness and other physical changes to the leather,[182] initially on the surface of the item and then proceeding towards the centre.

Precisely how a given leather sample deteriorates depends largely on environmental conditions[160,171] such as changes in temperature of surroundings, atmospheric pollutants, and pH. Oxidative breakdown is promoted by alkaline conditions while hydrolysis is acid-catalysed.[157,183]

Leathers made from different animals or using different tannins are observed to deteriorate at different rates. For example, leather tanned with condensed tannins more easily absorbs sulfur dioxide up to 6% of its weight[177,184] leading to increased acidic hydrolysis of collagen.[171] Increased thermal degradation is reported in sheep leather.[185,186] Tannins extracted from plants are also naturally impure and depending on the source introduce, among other things, metals including Cu, Fe, Al, Mn or Zn which can catalyse or impede oxidative processes. Leather objects may also deteriorate faster depending on how they were used, with items exposed to perspiration for example containing higher levels of chloride and hence decreased pH.[160]

4.4.1 Red Rot

The particular type of deterioration important for this work is commonly referred to as red rot, owing to the distinctive symptoms of leather that often becomes dry and reddish, or in advanced stages crumbles into a dark powder.[187,188] Despite the possible implications of the word "rot" it is not decay of biological origin. An example of a book suffering from red rot is shown in Figure 4.4.

Past studies have associated red rot with sulfuric acid formed in humid storage conditions from either sulfur introduced in the tanning process, or atmospheric sulphur dioxide permeating the collagen–tannin matrix. Sulfur dioxide is transformed into a trioxide when exposed to light, and this adsorbs onto tannins where it proceeds to react with moisture present in the leather and produces hydronium ions.[160] This can lead to surface pH readings of 3–4[189,190] and leads to hydrolysis of the peptide bonds holding the collagen molecules together, as well as the tannins themselves. As previously noted, as condensed tannin leathers are more prone to absorbing atmospheric sulfur, and as expected red rot is hence more frequently observed in these rather than hydrolysable tannin leathers.[191] The distinctive red colour sometimes

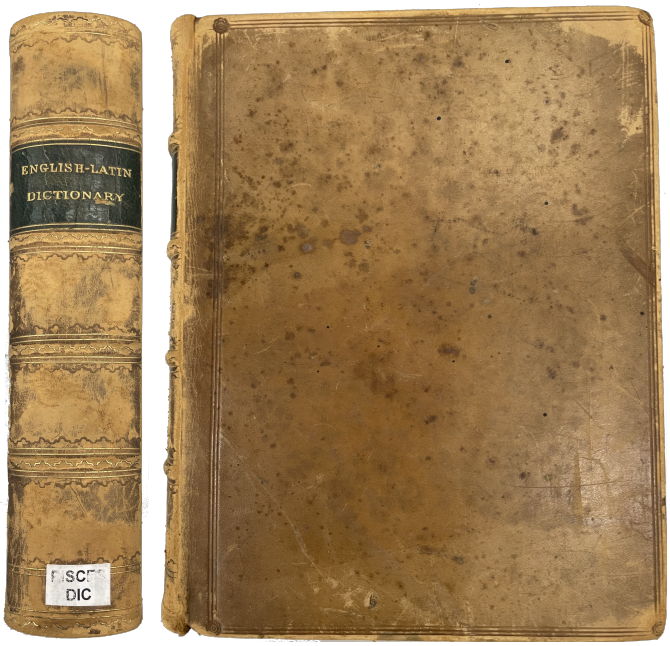

Figure 4.4: Book affected by red rot, especially on the spine.

observed is due to particular decay products of the tannins such as phlobophenes and anthocyadins.[192]

Furthermore, leather items made with condensed tannins from the late 19th and early 20th centuries are thought to be especially vulnerable to red rot due to changes in the tanning process, with more aggressive acids beginning to be used for removing hair from the raw skins. This both increased the acidity of the leather product and destroyed enzymes found in animal skin that offer protection from environmental influences.[193]

For prevention of red rot and other forms of degradation, vegetable-tanned leather is recommended to be stored in a stable environment with less than 0.06 ppb sulfur dioxide, no exposure to electromagnetic radiation with wavelength 100-1000 nm, and relative humidity between 50–55%.[194]

4.5 Analytical techniques

4.5.1 FTIR

Fourier Transform Infrared (FTIR) Spectroscopy is a technique in which the interaction of IR radiation with matter is measured. More specifically, for Attenuated Total Reflectance (ATR)-FTIR Spectroscopy, which is used in this work, the IR radiation interacts with the surface of the sample and is reflected. The reflections are measured and recorded as spectra that can be used to identify or quantify a material, as they identify the chemical bonds inside its molecules.

The FTIR spectra of leather are mostly made up of collagen signals, as that is the most abundant compound within it.[195] For vegetable tanned leathers, a smaller but important component of these spectra are tannin signals. The ATR-FTIR spectrum of a piece of leather is compared with the spectrum of collagen and the tanning agent in Figure 4.5. The leather spectrum contains the signals from both collagen and tannins.

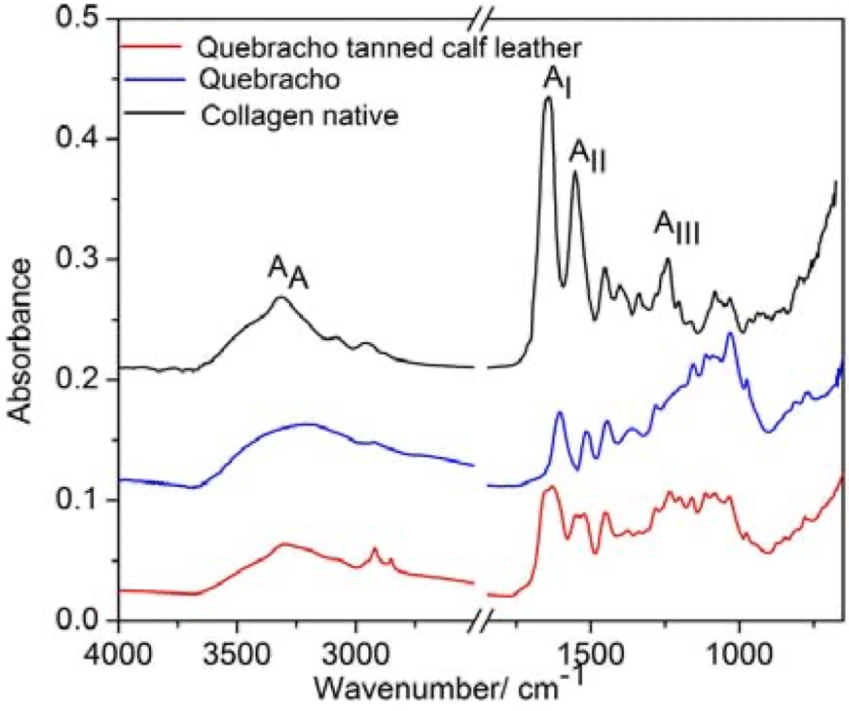

Figure 4.5: The ATR-FTIR spectrum of a piece of leather is compared with the spectrum of collagen and quebracho adapted from Sendrea *et al.*[196]

Because collagen dominates the spectra, when Falcão *et al.* were trying to find out what tannins were used in tanning historical leathers, they decided to extract the samples in water/acetone solutions due to collagen's lack of solubility in that solvent system, and this removed many of the collagen bands. Thanks to this simplification of the spectra, they developed a method for determining if a piece of leather was tanned with condensed or hydrolysable tannins, which is useful to know for leather conservation purposes.[163,167,169]

They extracted tannins from plant powders and leather fibres with aqueous or aqueous-acetone solutions and deposited each liquid sample on the surface of an ATR crystal and evaporated to dryness under nitrogen flow. They then examined the FTIR signals in the region of 1750-700 cm^{-1} of tannins from different plants and compared them against modern and historical leathers to narrow down diagnostic bands.

The diagnostic peaks that this group found are shown as an identification flowchart in Figure 4.6 and are used in the experimental section of this work. The assignments of these peaks are shown in Table 4.1.

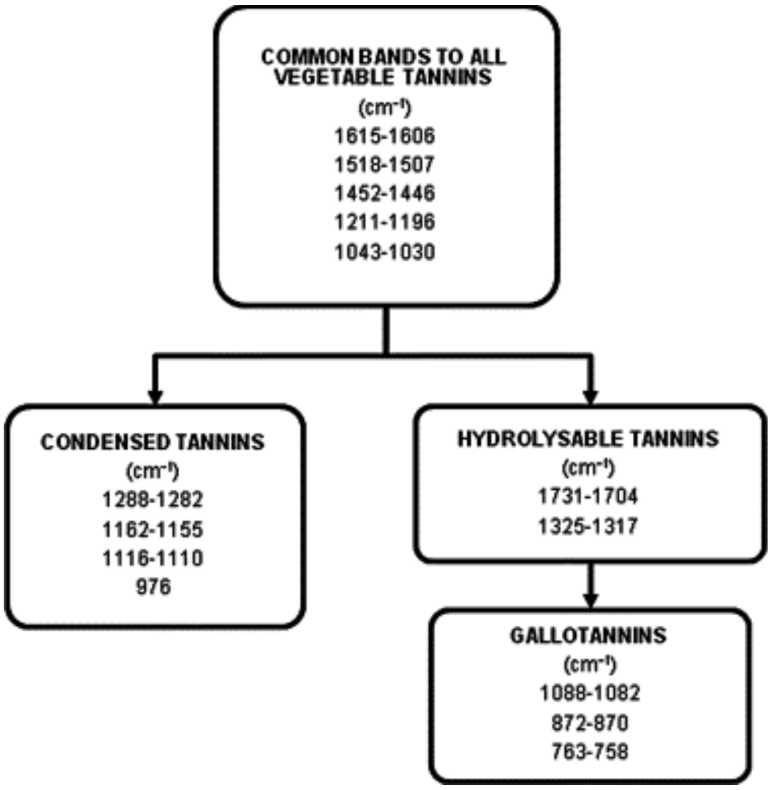

Figure 4.6: Diagram adapted from Falcão *et al.*[167]

Tannin peaks	Assignment
All tannins:	
1615–1606 (m–vs)	ν C=C aromatic ring
1518–1507 (w–m)	ν C=C skeletal ring
1452–1446 (m–s)	ν C=C aromatic ring
1211–1196 (m–vs)	ν aromatic C–OH
1043–1030 (m–vs)	β = C–H deformation
Hydrolysable:	
1731–1704 (m–s)	ν C=O phenolic esters/lactones
1325–1317 (m–s)	ν C–O lactones and O–H deformation
Gallotannins:	
1088–1082 (m)	ν C–O–C aryl phenolic ester
872–870 (w)	γ OH and γ tetrasubsituted aromatic C–H
763–768 (w–m)	ν skeletal (sugar ring breathing vibration)
Condensed:	
1288–1282 (ms–vs)	ν C–O pyran ring/flavonoids
1162–1155 (s)	ν C–O–C cyclic ether
1116–1110 (s–vs)	ν C–O–C cyclic ether
976 (w)	

Table 4.1: Table adapted from Falcão *et al.*[163]

Extraction is a destructive process, so Sebestyén *et al.* later used these assignments on four un-extracted pieces of leather with good results.[197] The ATR attachment only leaves an imprint in the leather, so it is much less destructive. The work in this report continues analysis on many more un-extracted pieces to further understanding of these complex collagen–tannin spectra.

The complexity in the following analysis arises when tannin peaks overlap to some extent with collagen peaks. More specifically for peaks common to all vegetable tannins there is overlap with: amide I at 1650 cm^{-1},[157] amide II at 1550 cm^{-1},[157] deformation of proteins and lipids at 1448 cm^{-1},[198] amide III and glycine/proline chains at 1200 cm^{-1},[199] and carbohydrate residues in collagen at 1031 cm^{-1}.[199] However, the ∼1035 cm^{-1} tannin peak is quite large, while the carbohydrate residue peak present in collagen in the same region is very small[199]. This can be useful for telling apart vegetable and chrome tanned leathers as chrome tanned leathers should not have a large peak there.

For hydrolysable tannin peaks, the ∼1715 cm^{-1} peak doesn't overlap, but the ∼1320 cm^{-1} peak overlaps with proline side chains at 1337 cm^{-1}.[199] For gallotannin peaks, the ∼1085 cm^{-1} peak overlaps with carbohydrate residues in collagen at 1082 cm^{-1},[199] while the remaining peaks don't overlap. Finally, for condensed tannin peaks there are overlaps with: amide III in collagen as well as CH wag from glycine backbone and proline side chains at 1282 cm^{-1},[199] the C–O stretching vibrations of the carbohydrate residues at 1160 cm^{-1},[200] the ν(C-O) ν(C-O-C) carbohydrates at 1121 cm^{-1},[201] and amide III at 974 cm^{-1}.[172] For this reason the analysis of the FTIR will have to be detailed.

Furthermore, FTIR data can also be used to compare concentrations of one species to another within a mixture through comparison of the absorbances of their respective peaks, as concentration and absorbance are related through the Beer–Lambert Law. A ratio of the absorbance of one peak of interest to another is taken and calibrated by inspecting reference samples. For example, as collagen deteriorates, the intensity of the amide I and amide II peaks changes and a ratio of these peaks can be used to quantify deterioration. This has been used in the past to study the deterioration of collagen[202–205] and more specifically collagen in leathers.[196,206] This work aims to find a suitable ratio for evaluating red rot deterioration. Once that is achieved, multivariate analysis could be used to study deterioration[172] or tannins[207] within leathers further.

4.5.2 SEM

Scanning electron microscopy (SEM) is an imaging technique that exploits the wavelengths of electrons (much shorter than that of photons) to allow for the creation of images with nanometre resolution. SEM overlaps with optical microscopy in what it can show for a piece of leather (e.g. grain pattern, grain and corium structure, collagen fibres), but SEM can achieve higher magnifications to elucidate fibril structure and can be coupled with Energy Dispersive X-ray (EDX) analysis to understand the elemental composition of a surface being examined. SEM has been widely used to gain a better understanding of the supramolecular structure of leather.[158,159,208]

Cavities are left behind in the grain layer of a leather when hair is removed during leather-making. These cavities are arranged in different patterns for different animals, as shown in Figure 4.7, and hence can be used to identify the animal of origin when inspected with an optical microscopy or SEM.[158]

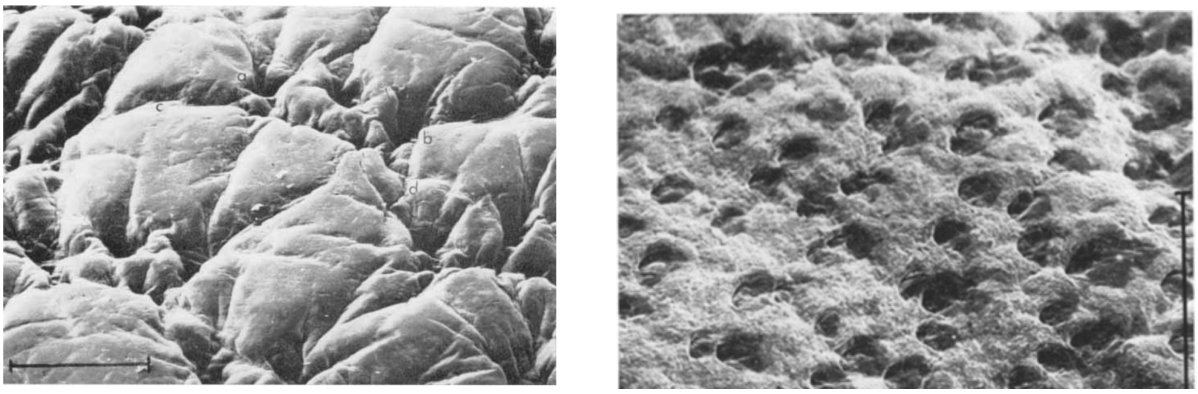

Figure 4.7: SEM of left: goatskin[208] and right: cattle skin[159] showing their different grain patterns.

SEM can also show biological degradation e.g. fungal colonies, as shown in Figure 4.8. These are not related to red rot, but should be ruled out when inspecting deteriorated samples.

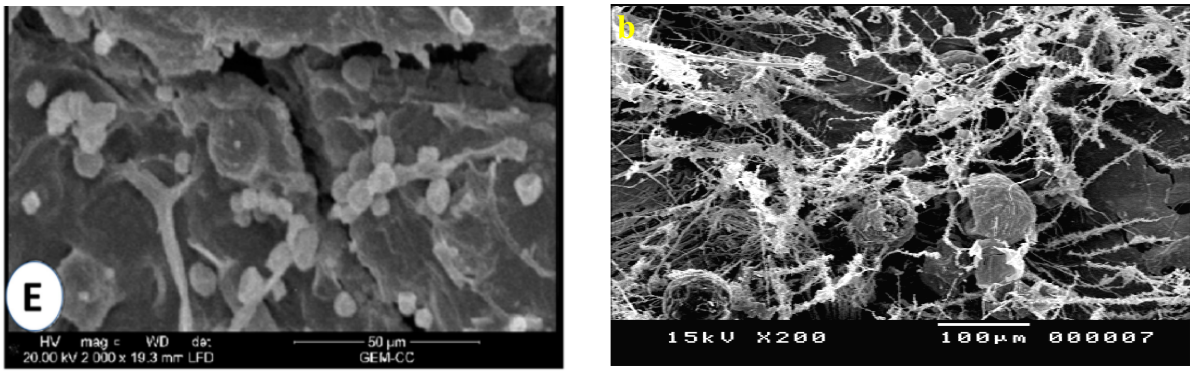

Figure 4.8: SEM of fungal colonies on leather.[209,210]

Most importantly for this work, SEM can help understand the various processes and stages of degradation. Surface erosion, loss of the fibre matrix cohesion, and criss crossing of fibrils is shown in Figure 4.9.

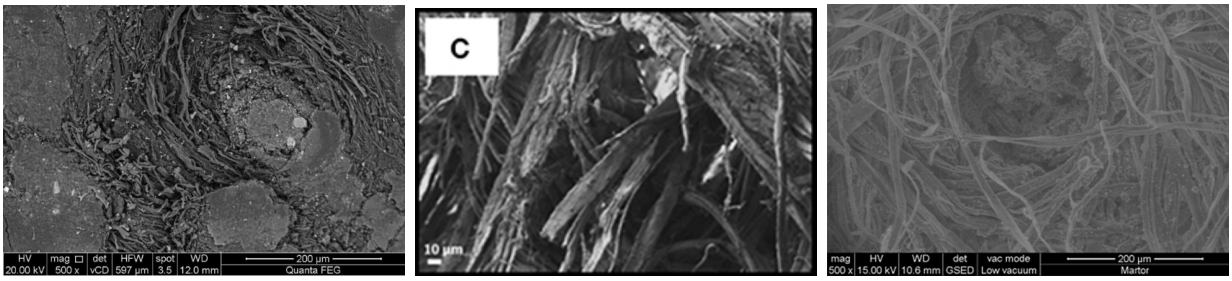

Figure 4.9: SEM of surface erosion, loss of the fibre matrix cohesion, and criss crossing of fibrils.[190,211,212]

Elemental analysis performed with SEM-EDX has previously been useful in determining the identity of a white 'bloom' on a lether book binding as calcium salts of fatty acids as well as silicates,[213] specific inorganic dyes used on the surfaces,[214] and changes in elemental composition of historical vs new leathers.[210]

4.5.3 ICP-OES and ICP-MS

Modern leather manufacturers submit their products to certification processes which include Inductively Coupled Plasma (ICP) analysis to determine if they are safe before being sold. ICP techniques such as Optical Emission Spectroscopy (OES), or Mass Spectrometry (MS) are used to identify what elements are present in a sample (both trace and major elements).

This technique requires liquid samples, so in the case of solid samples such as leather, extractions (suspending samples in solution and analysing species that dissolve) or digestions (fully dissolving a solid sample, usually with strong acids) are necessary. These give rise to two different methods of elemental analysis; extractable elemental content and total elemental content. A plasma torch is then used to vaporise droplets of the liquid sample and ionise them. For OES the ionised gaseous mixture emits photons which can be collected and analysed, while MS analyses atoms based on their mass to charge ratios. These techniques also have different sensitivities of parts per million (ppm) and as low as parts per trillion (ppt) respectively.

The methodology for this process from one commercial certification body, OEKO TEX, was chosen for this project as they publish their certification process openly and provide permissible limits for different types of products to the public based on safety evaluations. For these purposes, heavy metals are the elements tested for, as they can be toxic to humans. The permissible limits of total heavy metal content and extractable heavy metal content in decorative leather items (book bindings fall into this category) according to OEKO TEX are provided in Table 4.2.[215]

Element	Extractable	Total
As	1	100
Pb	1	90
Cd	0.1	40
Hg	0.02	0.5
Cr	200	-
Cr(VI)	3	-
Co	4	-
Cu	50	-
Ni	4	-
Ba	1000	-
Se	100	-

Table 4.2: Permissible limits of extractable heavy metal content for decorative items (category IV) in mg/kg according to OEKO-TEX certification.

While ICP has been previously used to probe elemental make up of historical leathers to help identify pigments,[216,217] no studies focusing on red-rot and ICP have been found.

5 Exploration of red rot

5.1 Aims

After consulting with the Natural History Museum (NHM) on what research would be of help to their conservators, the aims for this project were agreed. They were three-fold. Firstly, to make an initial exploration of health and safety aspects of red rot dust using a range of spectroscopic techniques and, from there, suggest further necessary tests. Secondly, to understand more about the red rot deterioration process by comparing undeteriorated and deteriorated leather samples, also with spectroscopic techniques. Thirdly, to attempt to quantify the degree of deterioration of book bindings suffering from red rot.

The project therefore required collection and categorisation of samples of reference and deteriorated leathers, and access to spectroscopic techniques such as FTIR, SEM-EDX, ICP-OES and ICP-MS. The process of achieving these aims is described below.

5.2 Reference and deteriorated samples

5.2.1 Sample naming conventions

All of the pieces of leather collected for this project from the NHM, Leather Conservation Centre (LCC), Museum of Leathercraft (MOL), Graham Lampard and the University of Northampton (UON) have the prefix RR (red rot) for organisational purposes. A set of modern leathers was gathered as reference samples (R1 – 19) and a set of historical leathers displaying signs of red rot was collected from historic bindings as deteriorated samples (S1 – 24). Within the text they are referred to by their R and S codes respectively (e.g. reference sample R11 or deteriorated sample S10), but in spreadsheets and on spectra they appear as RRR and RRS codes respectively (e.g. RRR11 or RRS10). The deteriorated samples are dated based on the publication information found on one of the first few pages of the book they come from. This is an underestimate of the leather's age, as the leather would have had to be tanned and ready for book binding before that date. However, it is likely that the true date of manufacture is close to the date published as leather was in high demand at the time

and would have been sold and used soon after being made.

Categories of the collected pieces of leather:

- Strips were collected from all reference samples (R1 – 19) and some deteriorated samples (S1, 2, 3, 6, 8, 10, 18) as cuttings from spools or bindings (a few cm × a few cm), which have a grain or top side (TS), a corium or cross section (CS) and a flesh or bottom side (BS).
- Scrapings were collected from all deteriorated samples. They were scraped off of the leather bindings with a spatula and look like powder (P) or clumps of fibres (C).
- Filter Papers (FP) were collected from all deteriorated samples: filter paper was used to wipe powders off of the surface of the leather bindings.

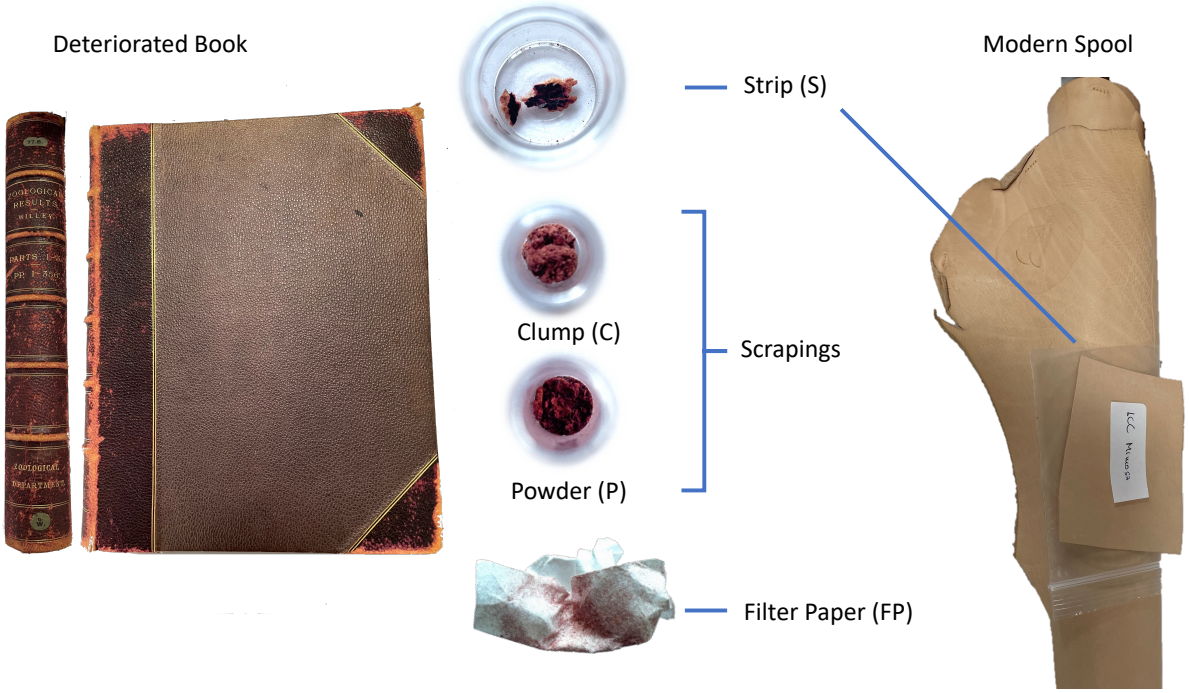

Figure 5.1: Types of reference and deteriorated samples.

5.2.2 Sample metadata

Since it is not usual for information about the binding to be included in a book or records about said book, deteriorated samples have limited metadata associated with them. This means that it is not certain what type of animal the book bindings used in this study are made of. However, most book binding leathers are made of split cattle hide, calfskin, sheep, goat, or pig.[177] For the sake of comparison, reference samples of those types of animals including duplicates, when available were obtained. The type of animal and tannage used for creation of the leather was fully or partially provided for the reference samples collected, though tannage information is often obfuscated, since exact tanning recipes are each tannery's secret.[218]

All the books used to collect samples were categorised into three levels of red rot deterioration: small (S), medium (M), large (L), based on the severity of deterioration over the entire leather-covered area. The metadata along with visual observations is contained in a spreadsheet, which along with photos of the origins (e.g. books, spools, sample booklets) of each sample, and the collected strips, scrapings and filter papers are provided in the electronic appendices. An explanation of the structure of the electronic appendices and a reminder of what the abbreviations mentioned above mean can be found in the Appendix A.6.

5.3 ATR-FTIR

For the ATR-FTIR analysis, a Thermo Fisher Scientific Nicolet iS50 Fourier Transform Infrared (FTIR) Spectrometer equipped with a diamond Attenuated Total Reflectance (ATR) attachment was used. Spectra were acquired on both sides of the strips, on scrapings, and filter papers from 4000 to 400 cm^{-1} by performing 16 scans with a resolution of 4 cm^{-1}. For reasons of non-destructibility and ease of preparation, the ATR-FTIR spectra were recorded on samples with no further preparation. Photos of the ATR-FTIR instrumentation for each test and all of the collected .csv files can be found in the electronic appendices.

OMNIC software was used for processing the spectra and bespoke python scripts utilising standard libraries such as numpy and matplotlib were written to analyse and visualise data.

Original code written for this project can also be found in the electronic appendices. All absorbance spectra are non-normalised. The normalisation applied is explained individually for each transmission spectrum. An example set up for an ATR-FTIR measurement is shown in Figure 5.2.

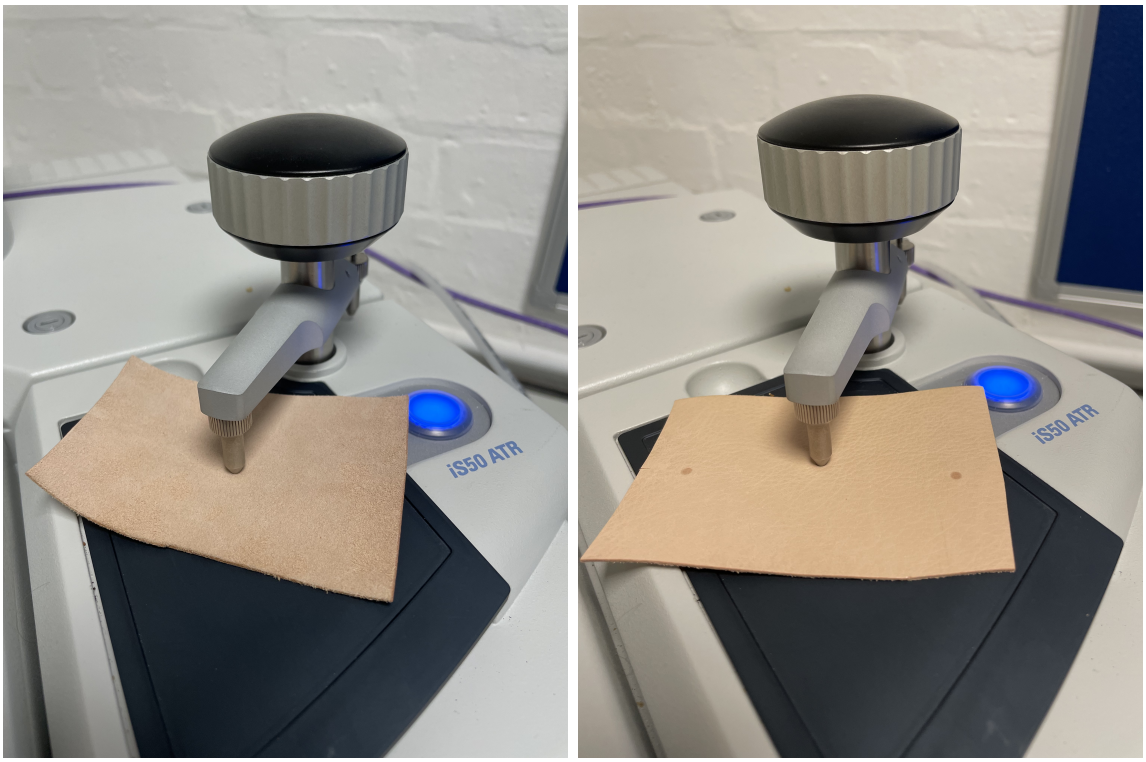

Figure 5.2: ATR-FTIR set up for the grain (TS) and flesh (BS) measurement for sample R15.

Two skiver (goat or sheep), two calf, two goat, two pig, one sheep, and one cattle (R10 - R19) reference samples were chosen for FTIR ATR analysis. Out of the deteriorated samples, two of each degradation classification (S, M, L) were chosen for detailed tests (S1, 2, 3, 6, 10, 18), and two samples treated with Klucel G (a cellulose-based conservation treatment) were chosen (S15, 16) for less detailed tests.

Spectra discussed but not reproduced within the text can be also found within the electronic appendices as pdfs. The collected FTIR spectra were analysed between 1800 and 600 cm^{-1}, as is common for leather. Peaks in the 4000 – 3000 cm^{-1} region are often obscured by water peaks due to leather's absorptive properties.[219] Bulk water content increases further in deteriorated leathers due to the polar groups present in the unfolded collagen structure

which can bind more water.[190]

5.3.1 ATR-FTIR of reference samples

The first obvious difference between the reference and deteriorated sample FTIR spectra was homogeneity. Reference samples have very similar spectra for BS and TS, while samples are more inhomogeneous, as shown in Figure 5.3. This is related to degradation, as structural inhomogeneity of leather has been correlated to these sequential steps: thermal destabilisation of the collagen–tannin matrix, de-tanning, and thermal destabilisation of de-tanned collagen followed by gelatinisation.[220]

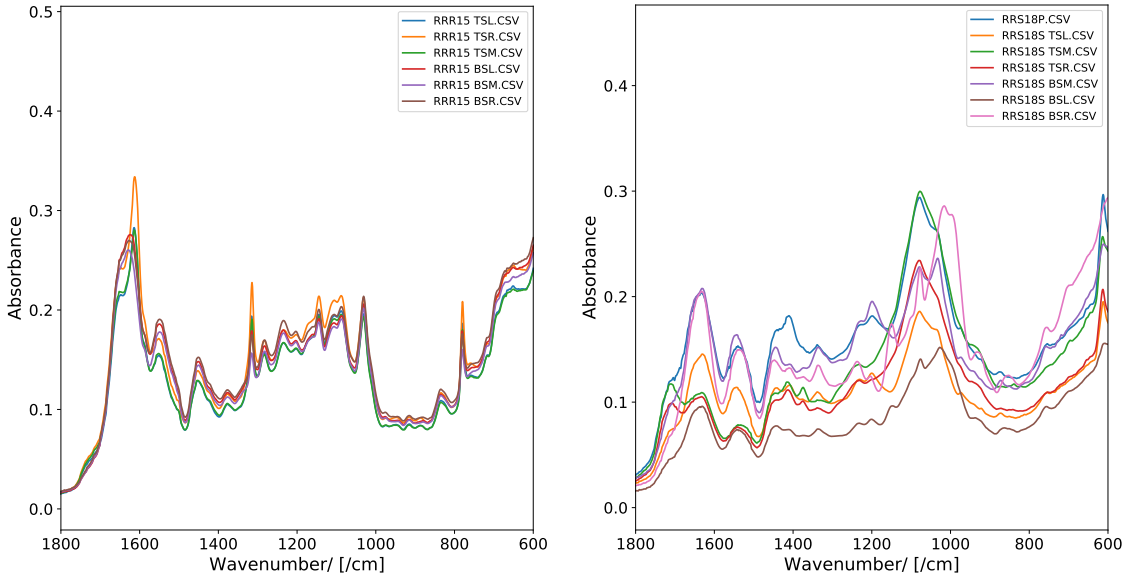

Figure 5.3: FTIR spectra showing the homogeneity in a reference sample (R15) vs inhomogeneity in a deteriorated sample (S18).

The only reference that displayed significant differences between the two sides was R12, as shown in Figure 5.4. This sample is embossed with a straight grain pattern and was likely sanded beforehand to remove the original grain pattern. The embossing process changes the surface of a piece of leather by stamping a pattern into it. As ATR-FTIR is a surface technique, these surface modifications have likely resulted in a different signal, but more testing would be necessary to be sure.

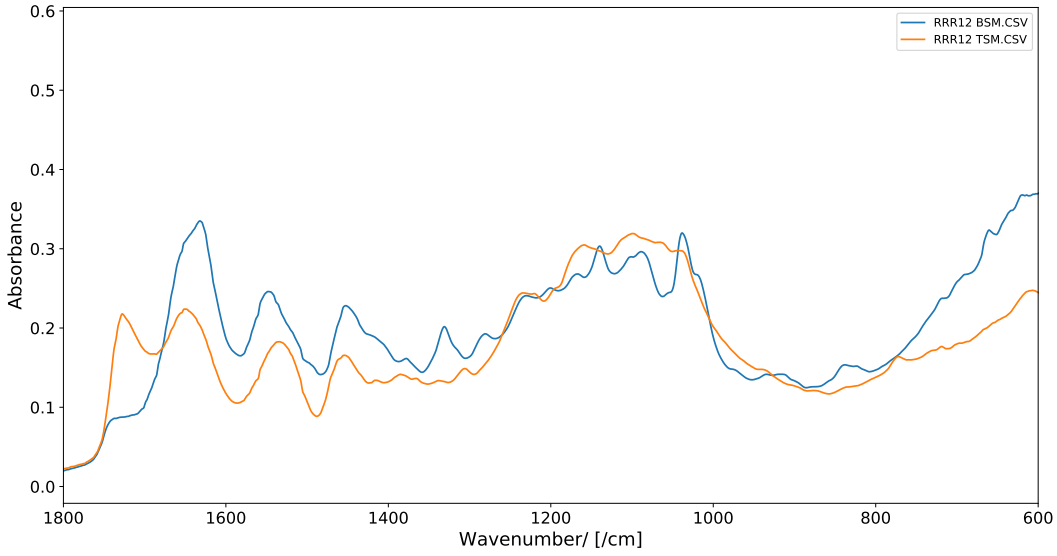

Figure 5.4: FTIR spectrum of the flesh (BS) and grain (TS) side of R12.

Next, the reference samples collected were compared to each other, e.g. R17 and R18. They are very similar in appearance and mechanical properties, with a thickness of around 2 mm, and are both goat samples likely tanned with sumac. Their FTIR spectra are qualitatively very similar, with most of the same peaks appearing in both spectra, but with slight intensity differences between them.

As explained in the Introduction (4.5.1), it is possible to differentiate between condensed and hydrolysable tannins based on their FTIR spectra through qualitative analysis.[167,169,197] Reference samples R17 and R18 were concluded to have been tanned using vegetable tanning methods, as the peaks common to all vegetable tanned leathers were found (red dotted lines). Furthermore, hydrolysable (blue dotted lines) and gallo-(purple dotted lines) tannin peaks were found; however, condensed tannin peaks (green dotted lines) were not present or only faintly visible as shoulders, as shown in Figure 5.5. It is not possible to rule a contributing condensed tannage out completely, as many collagen and tannin peaks broadly overlap, making the small peaks hard to assign. A mostly hydrolysable tannage is consistent with the information on these samples provided by the LCC, as sumac contains hydrolysable gallotannins.[163]

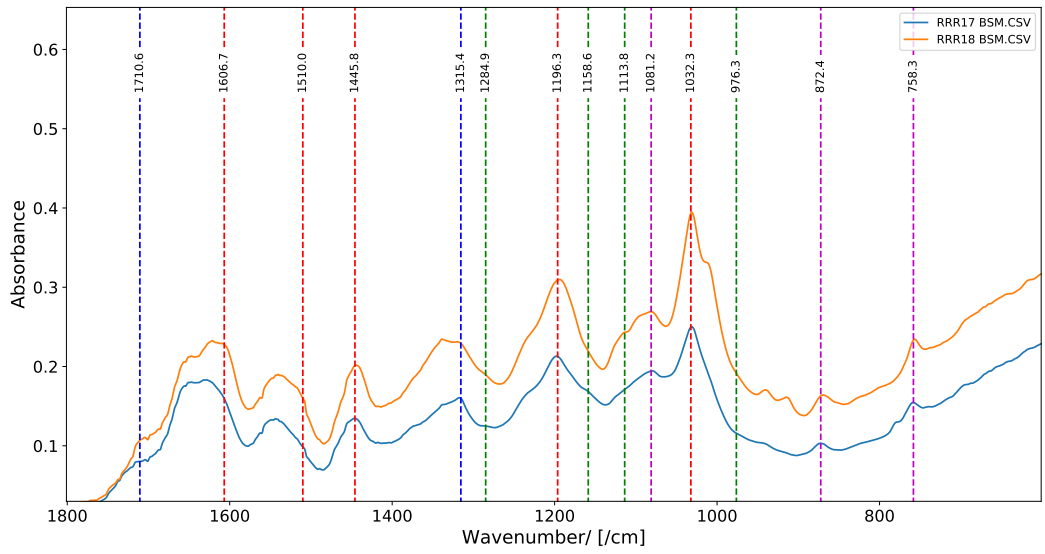

Figure 5.5: FTIR spectrum of the flesh side (BS) of R17 and R18 and assignments for vegetable (red), hydrolysable (blue), gallo- (purple) and condensed (green) tannins. The first two vegetable peaks at 1607 and 1510 cm^{-1} are visible as shoulders on the collagen amide I and II bands usually centred around 1630 and 1540 cm^{-1}.These spectra show clear hydrolysable and gallo- tannin peaks but display only faint condensed tannin peaks if present.

Reference samples R13 and R16 have very similar FTIR spectra, but differ in appearance; brown in colour and 0.5 mm thick vs tan and 1 mm thick. Such differences are expected of leathers produced from pig and calf respectively. However, the fact that the FTIR spectra are so similar, does showcase the difficulty in differentiating between collagen taken from different sources – the differences are often too subtle for a qualitative assessment and need, for example, a deconvolution of the amide I band to be differentiated. [220]

Upon careful examination of the FTIR spectrum shown in Figure 5.6, R13 contains a few peaks that R16 lacks (1725, 1314, 758 cm^{-1}), which are diagnostic of hydrolysable and more specifically, gallo- tannins (blue and purple dotted lines). This is consistent with the information provided about R13 as a sumac, tara and myrobalan tanned leather. Both reference samples also show peaks consistent with condensed tannins (green dotted lines), which matches the information provided about R16, as a mimosa tanned leather, but not about R13. Perhaps R13 was originally tanned with a condensed tannin and later retanned with hydrolysable tannins as is common practice in industry, and hence shows both.

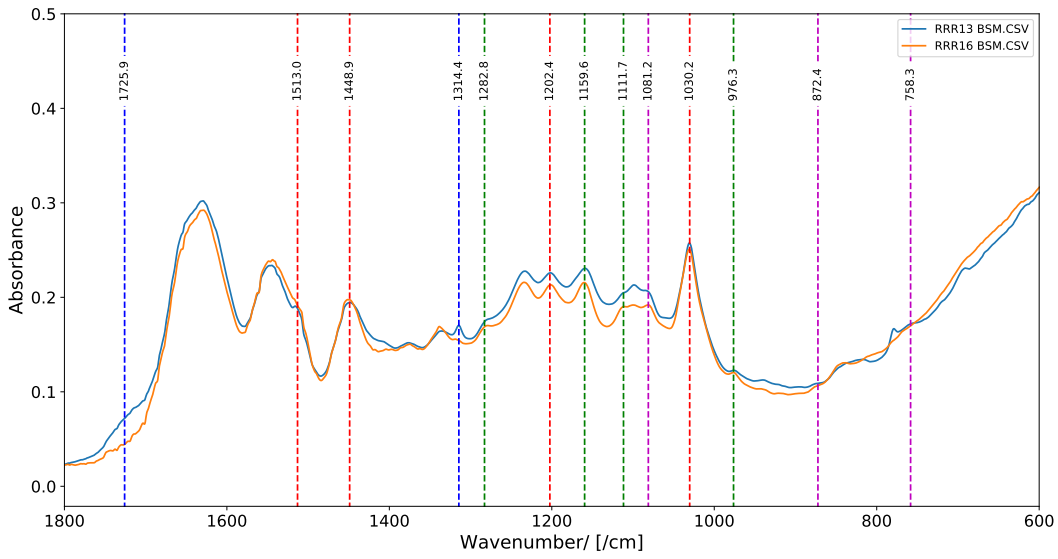

Figure 5.6: FTIR spectrum of the flesh side (BS) of R13 and R16 and assignments for vegetable (red), hydrolysable (blue), gallo- (purple) and condensed (green) tannins. The $\sim$1610 cm^{-1} peak of vegetable tannins is not visible even as a shoulder under the collagen amide I band. These spectra show clear hydrolysable and gallo- tannin peaks for R13 and a lack of those peaks for R16.

Reference samples R12 and R15 show somewhat similar FTIR spectra, but differ in appearance. R12 is black and 0.5 mm thick, while R15 is tan and 1 mm thick. The former is sheepskin, while the latter is calf. The tannages for these reference samples are harder to analyse, as shown in Figure 5.7. The hydrolysable peak at 1728 cm^{-1} is only present for R12 and not for R15 but the other hydrolysable peak at 1317 cm^{-1} is present for both. It is perhaps only present in R15 due to some other structural feature and not hydrolysable tannins. Most of the gallotannin peaks are absent for both reference samples, while condensed peaks are more visible for R15. This is broadly in line with the provided information of R12 being a sumac, tara, myrobalan tanned leather (hydrolysable gallotannins), though the gallotannin peaks are mostly absent. Perhaps the surface black dye is adding an additional layer of complexity to the spectrum. R15 peaks are also in line with being mimosa tanned (condensed). However, based on the difficulty with these assignments, it might not always be possible to determine tannin type on un-extracted pieces of leather.

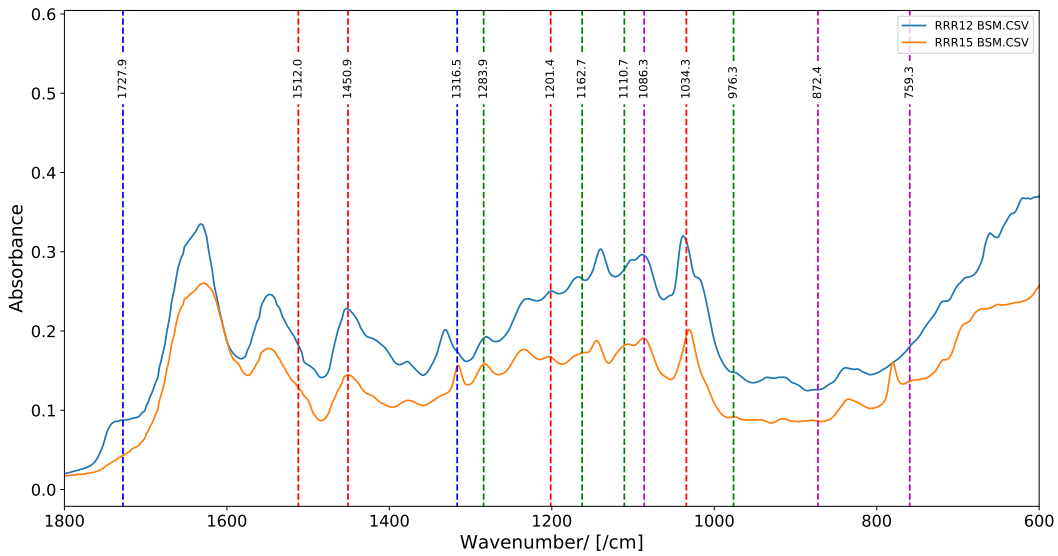

Figure 5.7: FTIR spectrum of the flesh side (BS) of R12 and R15 and assignments for vegetable (red), hydrolysable (blue), gallo- (purple) and condensed (green) tannins. The $\sim$1610 cm^{-1} peak of vegetable tannins is not visible even as a shoulder under the collagen amide I band. These spectra show some hydrolysable peaks for R12 and condensed peaks for R15.

Reference samples R14 and R19 display somewhat similar spectra, but are different in appearance, with R14 being a medium tan in colour and 2.5 mm in thickness cow leather and R19 being a dark tan in colour and 3 mm in thickness pig leather with a very visible grain pattern. These reference samples did not come with more information than vegetable tanned, so they are appropriate for testing the method for determination of tanning type described above on samples of known tannage type.

Both reference samples show the vegetable tannin peaks. Both also show hydrolysable peaks, but gallotannins are more uncertain, though the peak at 757 cm^{-1} looks pronounced for R14 (similarly to R17 and R18), which perhaps suggests that R14 was tanned with hydrolysable gallotannins, while R19 was tanned with hydrolysable ellagitannins. The condensed peaks are subdued for both, so perhaps both samples have been in contact with condensed tannins, but they contributed less to the final tannage.

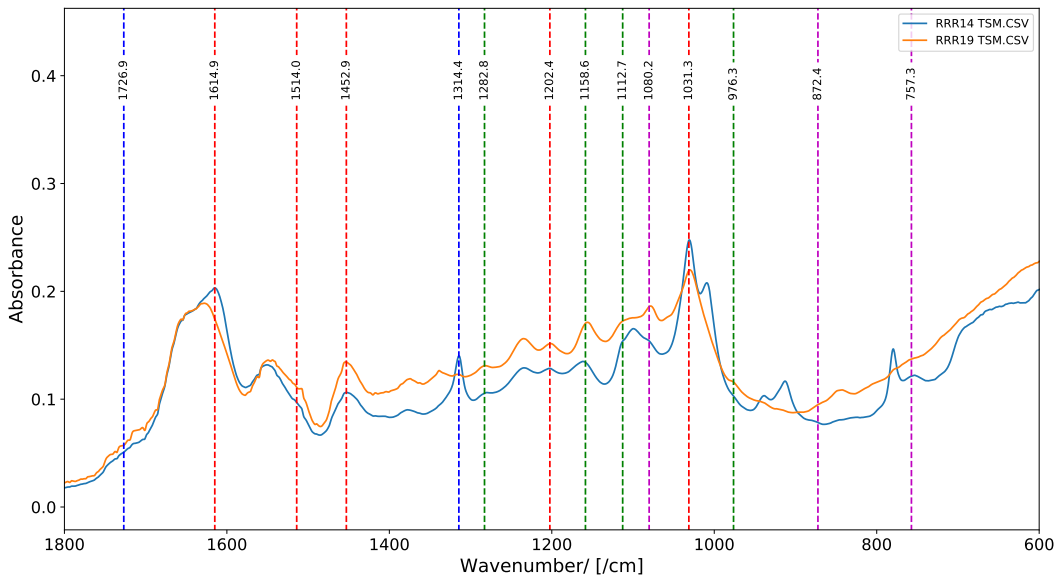

Figure 5.8: FTIR spectrum of the grain side (TS) of R14 and R19 and assignments for vegetable (red), hydrolysable (blue), gallo- (purple) and condensed (green) tannins. The $\sim$1610 cm^{-1} peak of vegetable tannins is not visible even as a shoulder under the collagen amide I band for R19. These spectra show clear hydrolysable peaks and suppressed condensed peaks.

Reference samples R10 and R11 are both skivers (young sheep or goats), with R10 being dark brown and 0.5 mm thick, and R11 being tan, lightly painted and embossed, and 0.5 mm thick. These samples are from the 1900s, but they have been kept in a pristine sample book that has been rarely opened and hence show no signs of deterioration despite being of a similar age to the deteriorated samples. Due to the lack of observed deterioration and the qualitative similarities of their spectra to R17 and R18, they have been treated as equivalent to the modern leather reference samples. Both reference samples show qualitatively similar FTIR spectra, displaying vegetable tannin peaks, as shown in Figure 5.9. Both also show clear hydrolysable and gallo- peaks, but condensed tannin peaks are not present in either, suggesting a hydrolysable gallotannin tannage. The similarity to R17 and R18 might suggest that these were goat skivers and that goat collagen does look identifiably different to the remaining sheep, pig and cattle collagen types studied here.

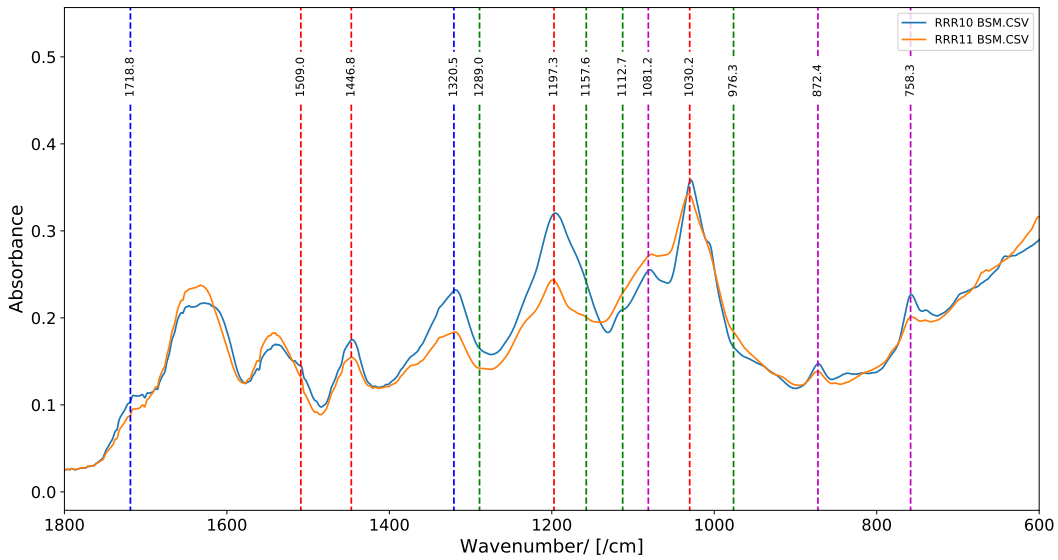

Figure 5.9: FTIR spectrum of flesh side (BS) of R10 and R11 and assignments for vegetable (red), hydrolysable (blue), gallo- (purple) and condensed (green) tannins. The ∼1610 cm^{-1} peak of vegetable tannins is not visible even as a shoulder under the collagen amide I band. These spectra show clear hydrolysable and gallotannin peaks and a lack of condensed peaks.

In almost all cases it was possible to determine whether a piece of un-deteriorated leather was tanned using condensed or hydrolysable tanning methods, and the hydrolysable category could often be split further into gallo- or ellagi- tannins without the need for extraction. It also seems that goat leathers display spectra different enough to pig, sheep and cattle to make qualitative identification possible in some cases. Both of these are however hard to reliably conclude on such small sample sizes. This is especially true when taking into account anomalous dispersion with a diamond ATR crystal, which causes red shifts with respect to the band positions of spectra collected in transmission mode. For future work, it will be important to use the same set up to analyse pure collagen, tannins and any other relevant compounds to confirm their peak positions more accurately.[176]

5.3.2 ATR-FTIR of deteriorated samples

For the deteriorated samples scrapings were collected to test whether they would be as good as strips, in case that is all that was available, but also because they are primarily composed of the corium. The grain layer is very thin and hence contributes little to the overall volume of scrapings. The corium might not display surface dyes or treatments[221] and hence be easier to analyse or have a different level of deterioration than the grain and flesh.

For S1, the scrapings are most similar to the most deteriorated grain samples as shown in Figure 5.10, which is consistent with them having been obtained mostly from the surface and having been subjected to mechanical destruction as part of the scraping process. This is useful to understand, as depending on available instruments and permissions obtained from specimen owners it might be necessary to work with only pieces that have fallen off the bindings of their own accord and cannot be reattached during consolidation.

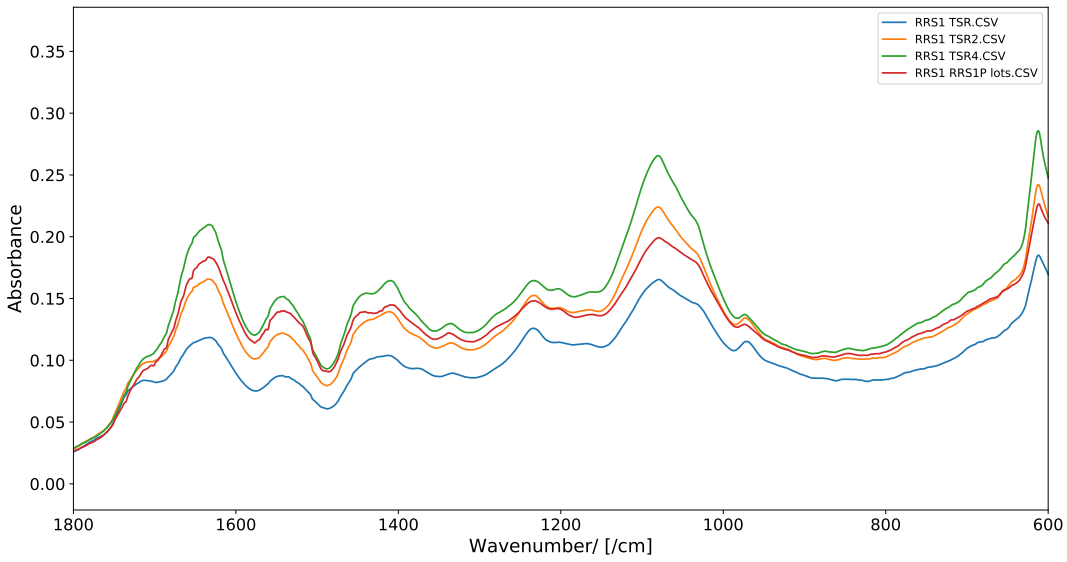

Figure 5.10: FTIR spectrum showing the similarity between grain (TS) and scrapings for S1.

S1 shows vegetable tannin peaks, as shown in Figure 5.11. In fact, all the sample spectra display the vegetable tannin peaks other than the ~1610 cm^{-1} peak, which is not visible even as a shoulder under the collagen amide I peak. For deteriorated samples, this is to be expected, as the 1651 cm^{-1} component is correlated with denatured collagen which increases

with deterioration.[220] These will not be pointed out for each sample going forward.

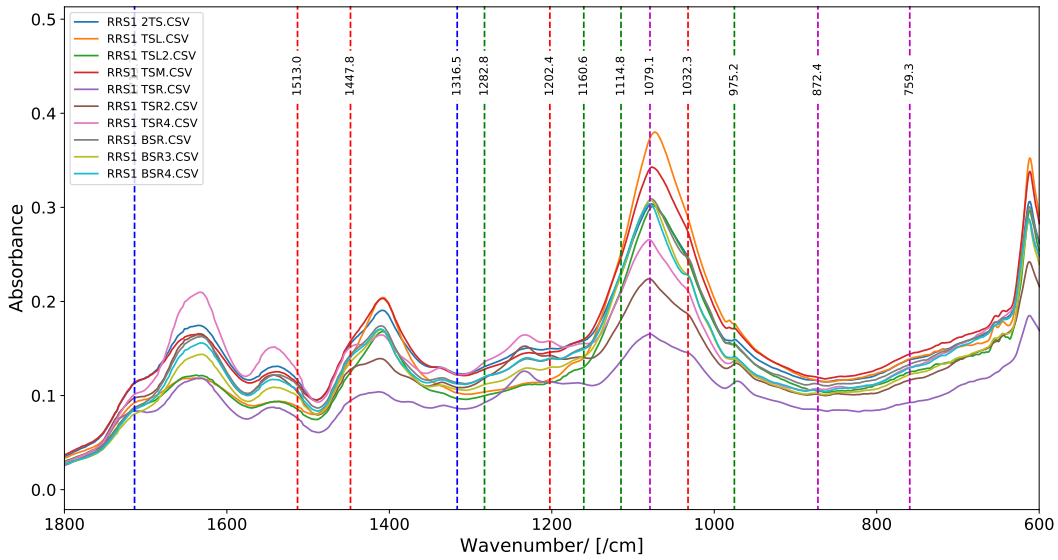

Figure 5.11: FTIR spectra of flesh (BS) and grain (TS) sides of S1. The ∼1715 cm^{-1} hydrolysable peak is present. Gallotannin peaks are possibly present though ∼871 cm^{-1} and ∼760 cm^{-1} are faint. Meanwhile, condensed peaks are mostly or entirely absent.

S1 is possibly a hydrolysable tanned leather, as one correct peak is present, while condensed peaks are mostly or entirely absent. Out of the hydrolysable peaks ∼1715 cm^{-1} is clearly visible, while ∼1320 cm^{-1} isn't. Since it is rare to see overlaps with collagen peaks in the 1700s cm^{-1} area, this peak is taken as diagnostic for hydrolysable tannins even if the second peak is uncertain. It is hard to determine if gallotannins are present or not. For any sample, the ∼1085 cm^{-1} gallotannin peak overlaps with a collagen peak at 1080 cm^{-1}, so is not enough to be diagnostic, and for S1 the other two gallotannin peaks are very small. This sample is too deteriorated to reliably be assigned a tannage.

The peak at 1080 cm^{-1} dominates the S1 spectra, relegating the usually dominant fifth vegetable tannin peak at 1030 cm^{-1} to a small shoulder. This is not something observed in the reference samples. If this is a collagen based peak, then its increased size might be due to a deterioration based structure change. This seems likely since it is strongly present in all deteriorated sample spectra and changes in intensities of collagen amide sub-bands are documented.[222]

To quantify this effect, a ratio of the absorbances at 1030 cm^{-1} and 1080 cm^{-1} for the grain and flesh side of multiple locations for one piece and then for all reference samples in one flesh and grain location each was taken, as calculated in the electronic appendices and shown in Tables 5.1 and 5.2. FTIR peak ratios are often used to quantify degradation in leather.[196,206,222]

The three ratios for R15 were the same to two decimal places for the BS (1.12) and TS (1.06) respectively. They are shown to three decimal places in the table to display the small differences between locations on the same sample. This is in line with the previous statement about the homogeneity of undeteriorated samples.

Name	ratio
R15 TSL	1.057
R15 TSR	1.063
R15 TSM	1.060
R15 BSL	1.122
R15 BSM	1.118
R15 BSR	1.116

Table 5.1: The ratio of the peak at 1030 cm^{-1} to the peak at 1080 cm^{-1} for three locations each (L - left, M - middle, R - right) for the grain (TS) and flesh (BS) sides of R15.

Henceforth ratios will be displayed to two decimal places, to avoid focusing on the small inhomogeneities present in even the least deteriorated piece of leather. Based on the R15 results the assumption that undeteriorated pieces of leather display ratios which are the same to two decimal places across different locations for a given side was made. Hence, in interests of limited time, the remaining reference samples were only scanned in one location each per side. However, it would be prudent to examine a larger number of pieces in this way to confirm that this assumption is true.

Focusing on Table 5.2, all of the ratios for the flesh side (BS) are above 1, though R12 and R15 are closer to 1 than the other reference samples. R12 could be explained through the mechanical strain that the surface modifications have had on the overall structure, but R15 is an anomaly. The flesh side (BS) ratios are generally higher than the grain side (TS) ratios, which would be consistent with the grain side being the side usually more exposed to the atmosphere and touch and hence more prone to degradation. Alternatively, it could

be an intrinsic property difference between the two sides or even both of those effects at the same time. Further investigation of this difference is recommended. The R12 TS ratio is the only ratio below 1, which is again likely caused by its weakened structure. Another departure from the trends are that the ratios for R16 and R18 TS are higher than for their BS ratios.

Name	BS ratio	TS ratio
R10	1.4	1.31
R11	1.25	1.24
R12	1.04	0.90
R13	1.26	1.14
R14	1.79	1.61
R15	1.12	1.06
R16	1.31	1.40
R17	1.28	1.27
R18	1.46	1.60
R19	1.15	1.18

Table 5.2: The ratio of the peak at 1030 cm^{-1} to the peak at 1080 cm^{-1} for the grain (TS) and flesh (BS) sides of each reference sample.

This 1030/1080 ratio was also then calculated for the S1 spectra (electronic appendices). The S1 ratios are a lot more variable than the ratios for R15 and overall lower (below 1) than those of the reference samples, ranging from 0.73 to 0.87. In fact, S1 is so inhomogeneous that rotating the sample in place (as far as that was possible with human precision) under the ATR attachment changed the ratio from 0.87 to 0.82. It is likely that a small shift in the strip's position occurred during rotation.[223] (Photos of exact sample positions for measurements are in the electronic appendices). This inhomogeneity might also be the reason the grain ratios are not smaller than the flesh ratios, in contrast with most of the reference samples.

The S10 sample is another very deteriorated sample, as can be seen on the photo shown in Figure 5.12, where the tan powdery areas have almost completely obscured the original brown leather. Despite this serious level of deterioration, the spectra display hydrolysable and gallo- tannin peaks clearly, so are easy to assign. Even if the peak at 1080 cm^{-1} is an overlapped tannin and collagen peak enlarged by deterioration, the second and third gallotannin peaks are isolated from other collagen peaks (as discussed in 4.5.1) and hence good diagnostic peaks for gallotannins. Condensed tannins are a minor component if present

at all. This suggests that S10 was tanned with hydrolysable gallotannins.

The spectra are inhomogeneous overall, which is consistent with an advanced level of degradation. The TS is more inhomogeneous than BS which is consistent with it being more exposed to the atmosphere and touch. Those conclusions are also confirmed by the 1030/1080 ratios, which are lower for the TS (0.76 – 0.86) than the BS (0.99 – 1.05), with the TS placing far below 1.

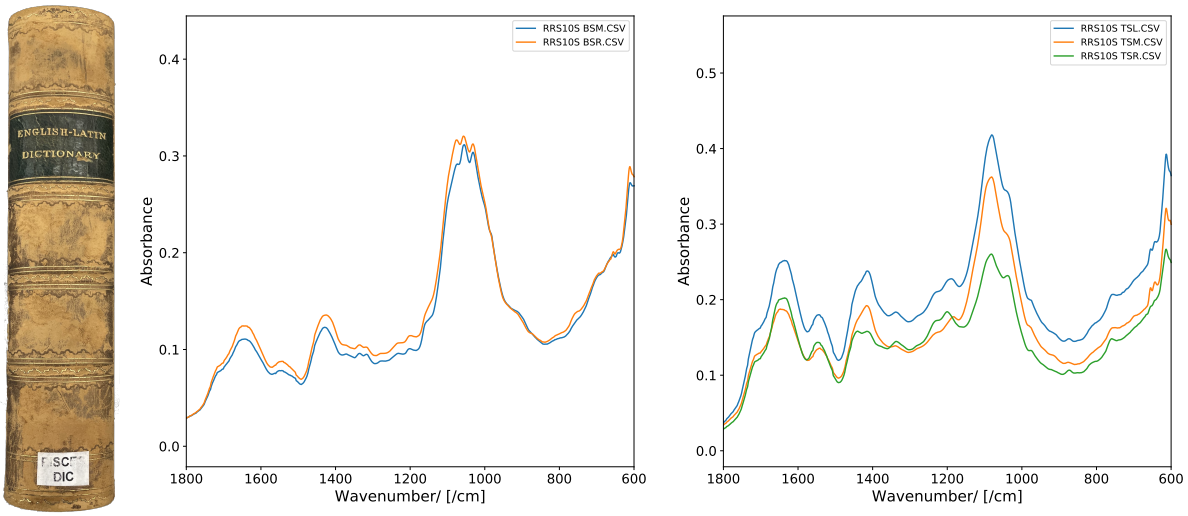

Figure 5.12: Photo of the spine of S10; FTIR spectra of the flesh (BS) vs grain (TS) side of S10 displaying higher level of homogeneity for the former than for the latter

The spectrum of the scrapings (C) qualitatively looks like the spectra of the TS, as shown in Figure 5.13 and its ratio (0.81) also falls within the TS range. A new type of sample (P) was tested for this binding. The library book code was stuck onto this book with some sticky tape, which came off of the book with a layer of the deteriorated leather stuck to it. This sticky tape was placed under the ATR attachment as with all the previous samples and gave a spectrum that qualitatively resembled the BS spectra, but was more intense and resolved, as shown in Figure 5.13 despite being taken from the cover (TS) of this book. This is consistent with the hypothesis that the TS becomes more deteriorated, as it is more exposed, and this small part of it, which was protected by sticky tape has deteriorated less. If further investigated this could lead to some coatings that could be applied to the leather to keep it from deteriorating.

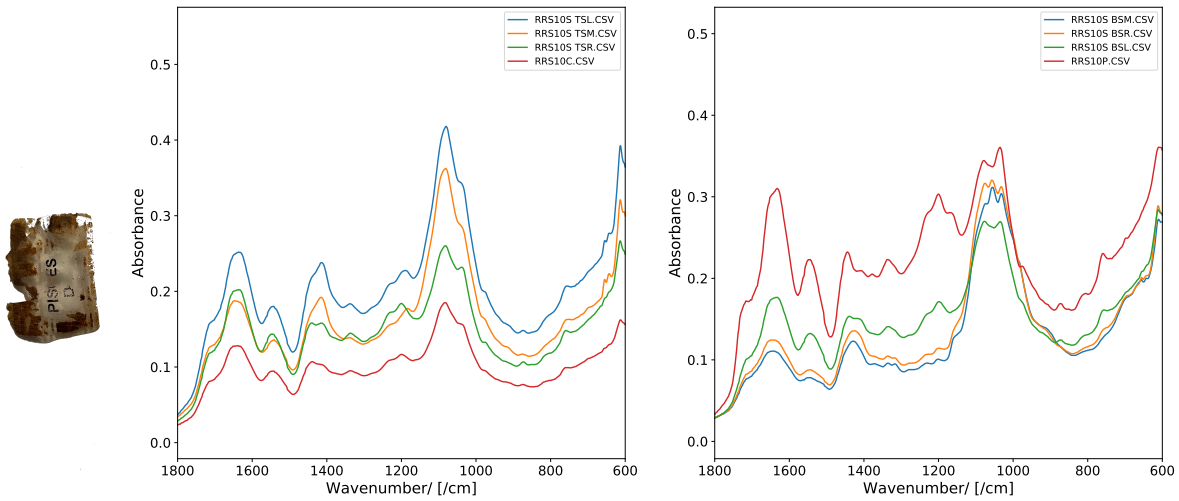

Figure 5.13: Photo of RRS10P; FTIR spectra of the grain (TS) side of S10 and C showing similarity; FTIR of the flesh (BS) side of S10 and P showing similarity.

The S6 sample was the least deteriorated sample available. In fact, it might not be suffering from red rot at all, as the smell associated with red rot degradation was hard to detect. Qualitatively, the S6 spectra look like the reference spectra identified as goat origin and in particular like R10, as shown in Figure 5.14. They display hydrolysable and gallotannin peaks clearly. Condensed tannin peaks are a minor component more visible in TS, which might signify that the dye is condensed tannin based.[221] Perhaps, this book was bound in goat origin leather tanned with hydrolysable gallotannins.

The S6 scrapings (C) give a less intense signal than the strip, unlike in S1 where they are similar in intensity. This is consistent with the S6 strip being in an un-deteriorated state, while the scrapings are much more deteriorated since the process of obtaining the scrapings mechanically destroys the collagen and tannin structures. For S1, the strips are deteriorated enough to be crumbling off of the surface and hence there isn't much difference between them and the scrapings. However, the S6 scrapings do resemble the TS once rescaled so that the most and least intense peaks are normalised from 0 – 100 transmittance, as shown in Figure 5.14. That figure also shows a third type of sample (FP), which was collected by wiping a piece of filter paper against the surface of the binding, to keep the books as intact as possible. A clean piece of filter paper was used as the background and subtracted from this spectrum. The signal for FP was much less intense than even that for the scrapings. When rescaled, it

became clear that FP samples would not be enough for the planned analysis, as they were not comparable to the strips and scrapings and are hence not discussed any further.

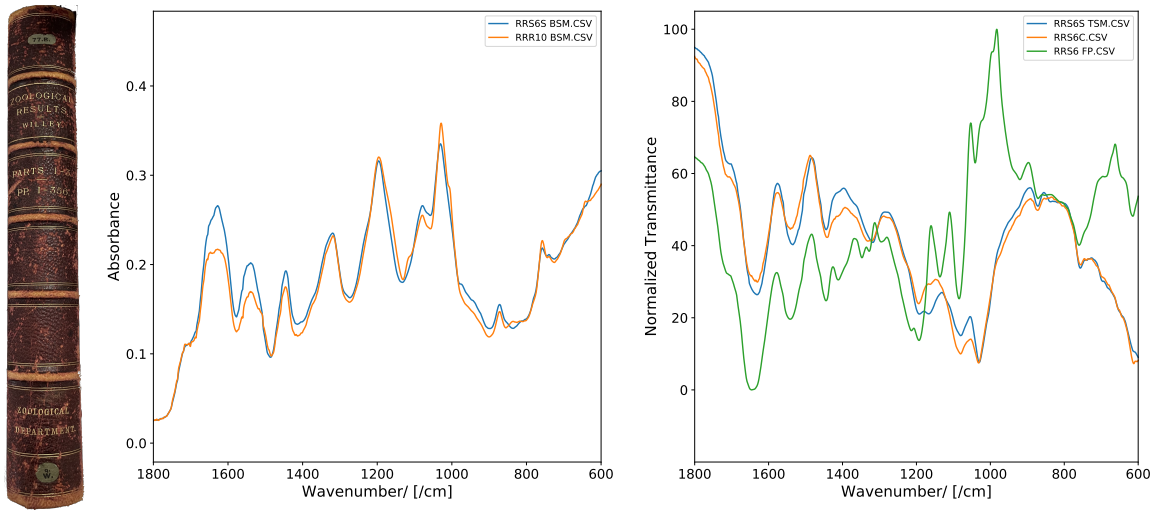

Figure 5.14: Photo of the spine of S6; FTIR spectra of the flesh side of S6 in comparison with R10; FTIR spectra of the grain side in comparison with scrapings and filter paper sample of S6.

The 1030/1080 BS ratios are (1.22 – 1.26), higher than TS ratios (1.14 – 1.17), but both above 1. The spectra are also very homogenous with BS being slightly more homogenous than TS. They resemble the reference samples in that, which is consistent with S6 being the least deteriorated-looking sample. The scrapings have the lowest ratio (1.03) of the S6 samples, which is consistent with them being most damaged.

The S3 spectra display hydrolysable tannin peaks. The gallo- and condensed tannin peaks are a minor component if present at all. By process of elimination, it is possible that this leather was therefore tanned with ellagitannins. Moreover, the grain side is dyed an intense black (unlike the light brown flesh side) which might be why its FTIR signals display peaks not observed for its flesh side or for the heretofore examined leathers; most notably a very large peak at 1014 cm^{-1}, as shown in Figure 5.15.

The unusual results for the TS extend to the 1030/1080 ratios, which are above 1 (1.01 – 1.13) and higher than for BS (0.78 – 0.86). BS ratios are quite low, which in conjunction with the presence of the smell associated with red rot and the ease with which pieces of the grain layer flaked off of the surface of the binding prompted a reclassification of this sample from

the original S to current L. The reason for the original classification was that the saturated layer of dye on the surface of the binding did not display the usual red rot powderiness, as can be seen in Figure 5.15.

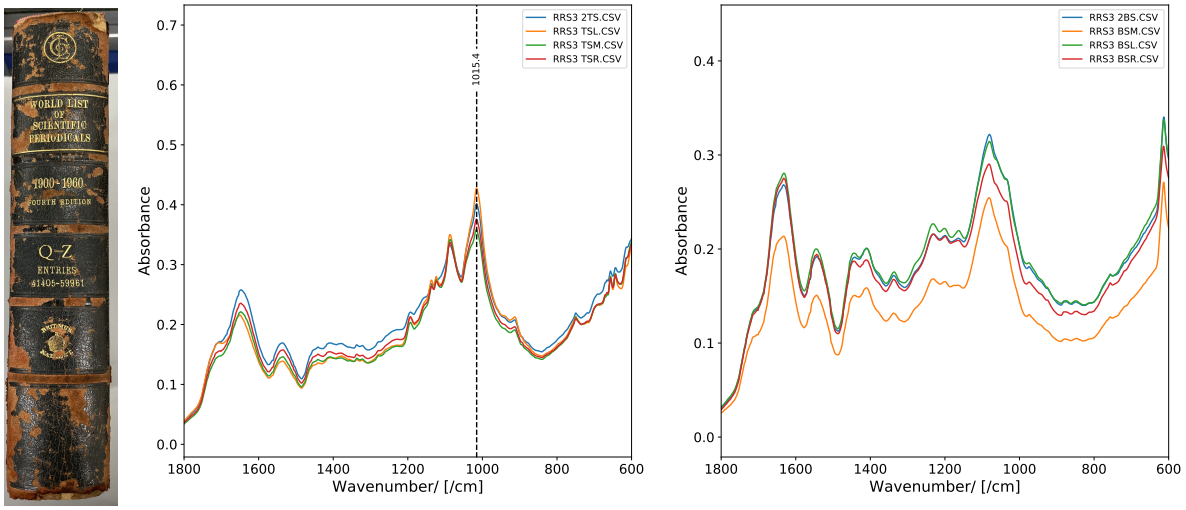

Figure 5.15: Photo of the spine of S3 showing the black dye and flaking, and FTIR spectra of the grain vs flesh side of S3 displaying higher level of homogeneity for the former than for the latter.

This initial confusion over the deterioration classification, the high 1030/1080 TS ratios and the fact that the TS spectra appear homogenous unlike the BS spectra, as shown in Figure 5.15, suggests that a thick layer of dye on the surface of a binding keeps the collagen and tannin structure from deteriorating. Since this is only true for the surface of the binding, however, the corium and flesh layers, which the dye does not reach, deteriorate, as expected. This would also explain the ease with which only the topmost, dyed grain layer flakes off of the binding.

The spectrum of the scrapings is slightly lower intensity than the spectra for the BS but it does resemble them strongly, even without rescaling. This is in line with the new classification of this sample, as very deteriorated and confirms that scrapings could be used if strips were unavailable.

S2 is another deeply dyed sample like S3, as shown in Figure 5.16. The S2 spectra display hydrolysable and gallo- tannin peaks clearly, while condensed tannin peaks are a minor component if present at all. This suggests that S2 was likely tanned with hydrolysable gallotannins. The very large peak at 1014 cm^{-1} visible for S3 is not present for S2, suggesting that that peak is particular to the black dye.

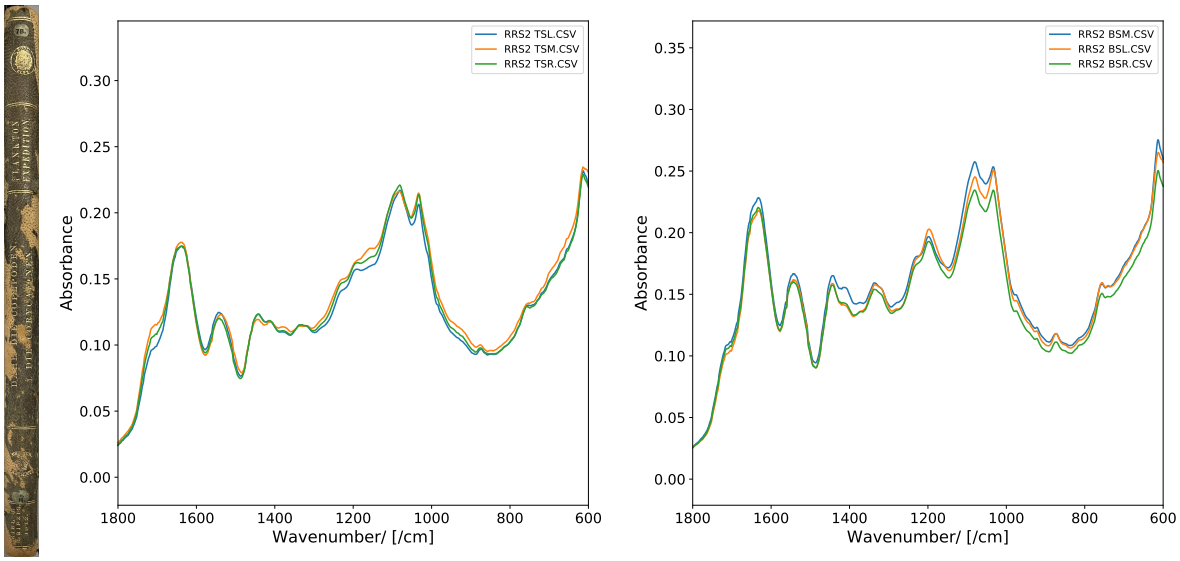

Figure 5.16: Photo of the spine of S2 showing the green dye and flaking and FTIR spectra of the grain vs flesh side of S2 displaying higher level of homogeneity for the former than for the latter.

The 1030/1080 ratios are lower for the TS (0.94 – 0.99) than for the BS (0.97 – 1.02) and close to 1, which is consistent with TS being more deteriorated, but the overall sample being only moderately deteriorated (M).

Similarly to S3, the TS is overall slightly more homogenous than the BS and visually a similar flaking effect of the green dye can be observed on the surface of the binding, as shown in Figure 5.16. Perhaps dying a cover green requires less coating than black, which would explain why the S2 TS FTIR spectrum is more similar to the usual leather spectra than that of S3. S2 is also less deteriorated than S3. These factors in combination could explain why the dye effect is less pronounced here.

As with S3, the spectrum of the S2 scrapings looks qualitatively like the BS spectra, but need rescaling like the spectrum for S6 for finer analysis, as the S2 strips are only moderately deteriorated.

S18 spectra display hydrolysable and gallo- tannin peaks clearly. Condensed tannins are a minor component if present at all. This suggests a hydrolysable gallotannin based tannage. The 1030/1080 ratios for TS (0.81 – 0.89) are lower than BS (1.03 – 1.19) and below 1 for TS but above 1 for BS. This is consistent with a moderately deteriorated sample.

The edges of the flesh side (BS) for S18 give spectra that look quite similar to the S3 TS spectra, as shown in Figure 5.17. In particular, S18 also shows a strong peak at 1014 cm^{-1}. The binding for S18 is very dark in colour, similarly to S3, adding weight to the hypothesis that these features are associated with strong dyes. That this effect is observed for the BS and not the TS, is unexpected. A closer examination of the S18 piece shows that the TS is missing dye in many places, and the light brown corium layer usually found below the grain is visible. It is likely that the TS spectra taken for this piece have avoided the dyed grain and captured the undyed corium. Meanwhile, the BS is also a very dark colour, suggesting that it too was dyed, unlike in the case of S3 where the BS remained undyed. That accounts for the dye effect observed for the edges of this piece. The 1030/1080 ratios for the edges are also the highest, which is in line with the S3 TS ratios.

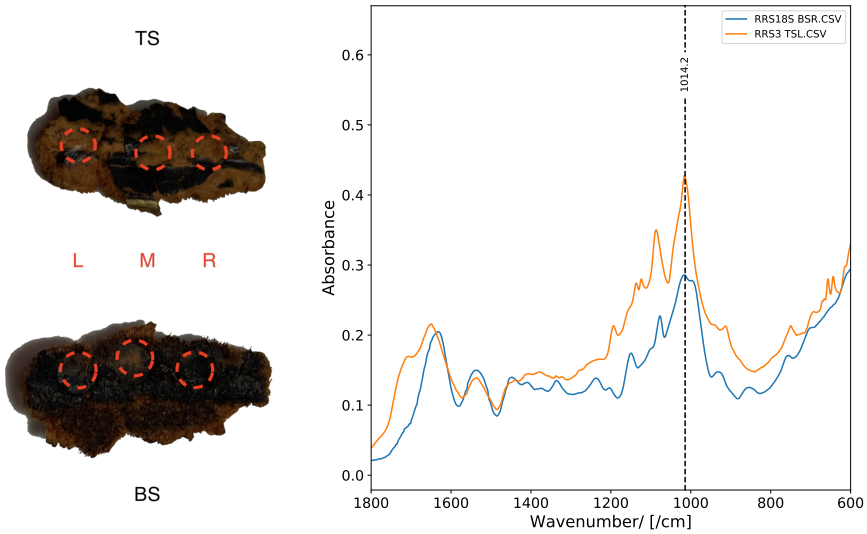

Figure 5.17: Photo of the strip on both TS and BS of S18 used for FTIR experiments with positions (left - L, middle - M, and right - R) the ATR attachment scanned circled in red; FTIR spectrum of S18 BSR in comparison with S3 TSL.

However, one spectrum from the middle of the flesh (BS) side for S18 looks similar to those of S2 instead, as shown in Figure 5.18. The middle part of the S18 piece is more light brown than the rest, and hence likely showing the undyed corium below, but on the flesh side this time. The low 1030/1080 ratio (1.03) for this part is also consistent with the lack of dye.

The spectrum of the scrapings (P) qualitatively looks like the spectrum for the TS, as shown in Figure 5.18, which is consistent with the TS spectra actually showing the corium, as surface scrapings would include mostly upper corium, as the grain is only a thin layer on top of it.

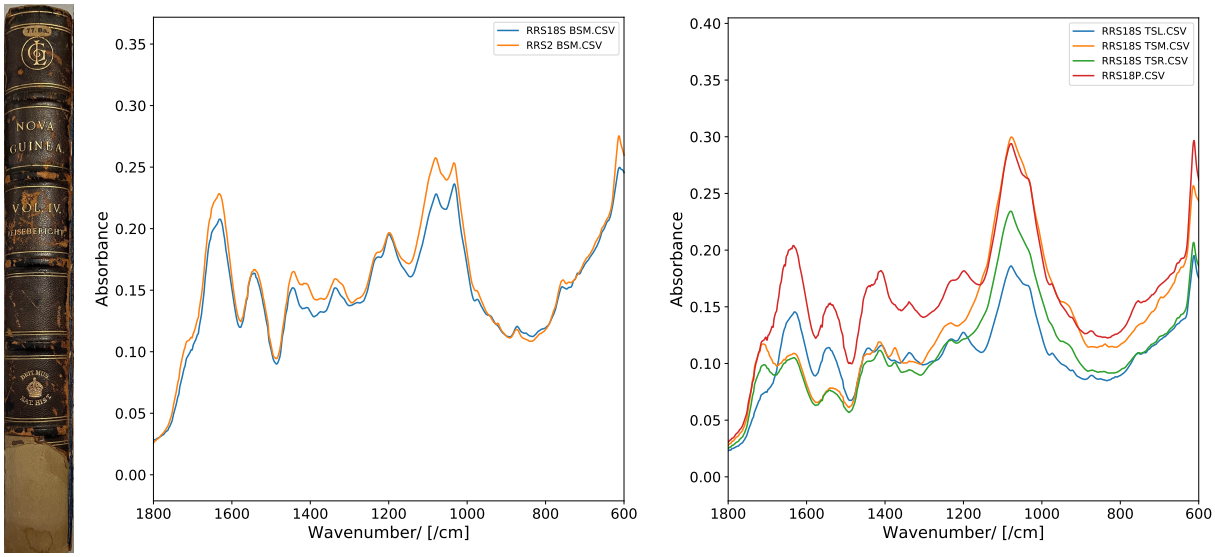

Figure 5.18: Photo of the spine of S18; FTIR spectrum of S18M BS in comparison with S2 BSM; FTIR spectra of the TS and scrapings of S18.

Samples S16 and S15 are still part of the NHM collection and hence only tiny pieces, equivalent to scrapings, that fell off while handling were collected. Both spectra show the first but not second hydrolysable peak. The gallotannin second and third peaks are also very faint, while condensed peaks are prominent, making it likely that these samples are condensed or at least of mixed hydrolysable/condensed tannage. These are the first such mixed tannages observed among these samples. The 1030/1080 ratio for S15 is 0.95 and 1.00 for S16. Despite both of these bindings having been dyed black, as previously mentioned scrapings are mostly composed of the corium and hence are unlikely to show the dye effect.

Finally, both of these samples have been treated with Klucel G - a cellulose based treatment used in leather conservation. The FTIR spectrum for Klucel G was also obtained and is shown along with the spectra of S15 and S16 in Figure 5.19. The Klucel G peaks are not visible in the S15 and S16 spectra, suggesting that this treatment either doesn't penetrate into the corium, or that it might have been scraped away during normal use.

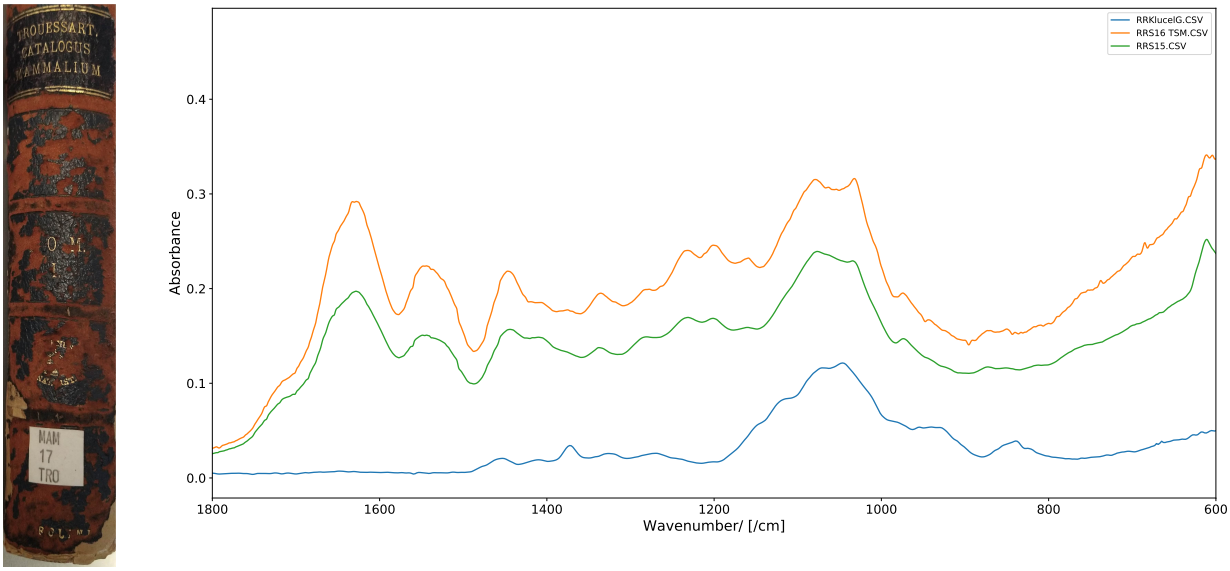

Figure 5.19: A photo of the cover of S16; FTIR spectra of the scrapings of S15 and S16, as well as for Klucel G.

5.3.3 Conclusion

A summary of all of the findings about tannage and 1030/1080 ratios discussed above can be found in Table 5.3. The tannages for most samples could be determined with the method developed on the reference samples. The most common tannage within the sample data set is hydrolysable gallotannin. Leathers tanned with hydrolysable tannins have been shown to be less prone to red rot than those tanned with condensed tannins[224], so this seemed surprising at first. However, condensed samples could have not lasted at all to this day and the NHM collection could be biased due to availability of tannins or tanner preference.

Sample	Tannage	Deterioration	TS range	BS range	Scrapings
S1	Unknown	L	0.76 - 0.87	0.73 - 0.79	0.89
S2	Gallotannin	M	0.94 - 0.99	0.97 - 1.02	1.00
S3	Ellagitannin	L	1.01 - 1.13	0.78 - 0.86	0.90
S6	Gallotannin	S	1.14 - 1.17	1.22 - 1.26	1.03
S10	Gallotannin	L	0.76 - 0.86	0.86 - 0.99	0.81
S15	Mixed	M	N/A	N/A	0.95
S16	Mixed	M	N/A	N/A	1.00
S18	Gallotannin	M	0.84 - 0.89	1.03 - 1.19	0.88

Table 5.3: The proposed tannages, deterioration levels, and ratios of the peak at 1030 cm^{-1} to the peak at 1080 cm^{-1} for each sample.

Some tannin peaks used for identification are present as shoulders and hence hard to assign, which could be improved by using 1st and 2nd derivatives. However, due to the data having been collected at 16 sample scans per spectrum, no matter the accuracy of the finite difference method used on the data, the resulting derivatives are incredibly messy. At such a low scan number the data's signal to noise ratio is too low, and calculating derivatives hugely amplifies high frequency noise and makes differentiating signal from noise impossible. It would be prudent to collect data with higher numbers of sample scans and analyse it with derivatives to confirm these findings.

Another check needed to validate these results would be to remove the collagen peak overlaps with the tannin peaks. This could be done through obtaining ATR-FTIR collagen spectra and subtracting them from the leather spectra or through extracting the tannins from the leathers into solution. Both would be interesting to see.

When looking at the entire 1030/1080 ratio data set and discounting the S3 TS due to its strong dye effect, the ranges for different degradation levels are, as shown in Table 5.4. These ratios could be used to determine degradation classifications for leather bindings, which should prove useful to conservators.

However, these ratios are somewhat imprecise due to the differences between types of animal of origin, tannage, and especially strong dyes. Therefore at present, these ratios should be used in conjunction with other observations and only when a thorough analysis of a number of positions on a piece can be performed.

	TS	BS	Scrapings
S	1.14 - 1.17	1.22 - 1.26	1.03
M	0.84 - 0.99	0.97 - 1.19	0.88 - 1.00
L	0.76 - 0.87	0.73 - 0.99	0.81 - 0.90

Table 5.4: The proposed ratio ranges of the peak at 1030 cm^{-1} to the peak at 1080 cm^{-1} for different degradation levels.

In addition, the 1030/1080 ratios are not precise without deconvolution, as has been previously done by others in such circumstances.[206,225,226] Hence they are examined in this work as a quick proof of principle. Since it looks like there is a pattern worth investigating here, these peaks should be deconvoluted and identified and then tried out on more samples.

Furthermore, while a general degradation pattern has clearly been identified here, it might not be red rot specific. No historic, but definitely unaffected by red rot bindings were analysed in this study, since they are considered more valuable and hence not open to destructive analysis. Having extensively compared different types of samples using FTIR, it is clear that a lot can be gleaned from studying pieces that have fallen off and cannot be reattached, but also that entire books can be subjected to the ATR attachment. This method is non-destructive, with only a small imprint of the ATR attachment left behind in the leather surface after testing. To determine if the above observations are red rot specific, historic books of various levels of degradation, but which are not suffering from red rot should be examined.

During this project, it also became apparent that red rot degrading leather emits a hard to describe but characteristic smell.[160] A different method of identifying red rot degradation and even classifying the level of such degradation worth exploring is gas chromatography (GC). No studies of red rot degraded leathers with GC were found within the literature, but GC has been used on modern collagen-based materials.[227–229]

5.4 SEM

For the Scanning Electron Microscopy (SEM) analysis a JEOL JSM–IT500 scanning electron microscope was used. Samples were prepared on 10 mm aluminium stubs and attached with an adhesive carbon tab without coating. The strip samples were cut into three pieces to show the grain (TS), flesh (BS), and cross section (CS), while scrapings (C and P) were either placed onto the adhesive directly or the adhesive was lightly pressed to the surface of a book binding taking away with it some material. Imaging was conducted at a range of distances matching specimen heights and an electron gun accelerating potential of 15 kV. Qualitative X-ray microanalysis was carried out using an Oxford Instruments XMax 80 solid state Energy Dispersive Spectrometer (EDS) detector, controlled by Aztec software Version 5.0. No corrections or additional measurements that would allow for quantification were performed.[230] All of the images and spectra obtained can be found in the electronic appendices. An example set up for an SEM measurement is shown in Figure 5.20.

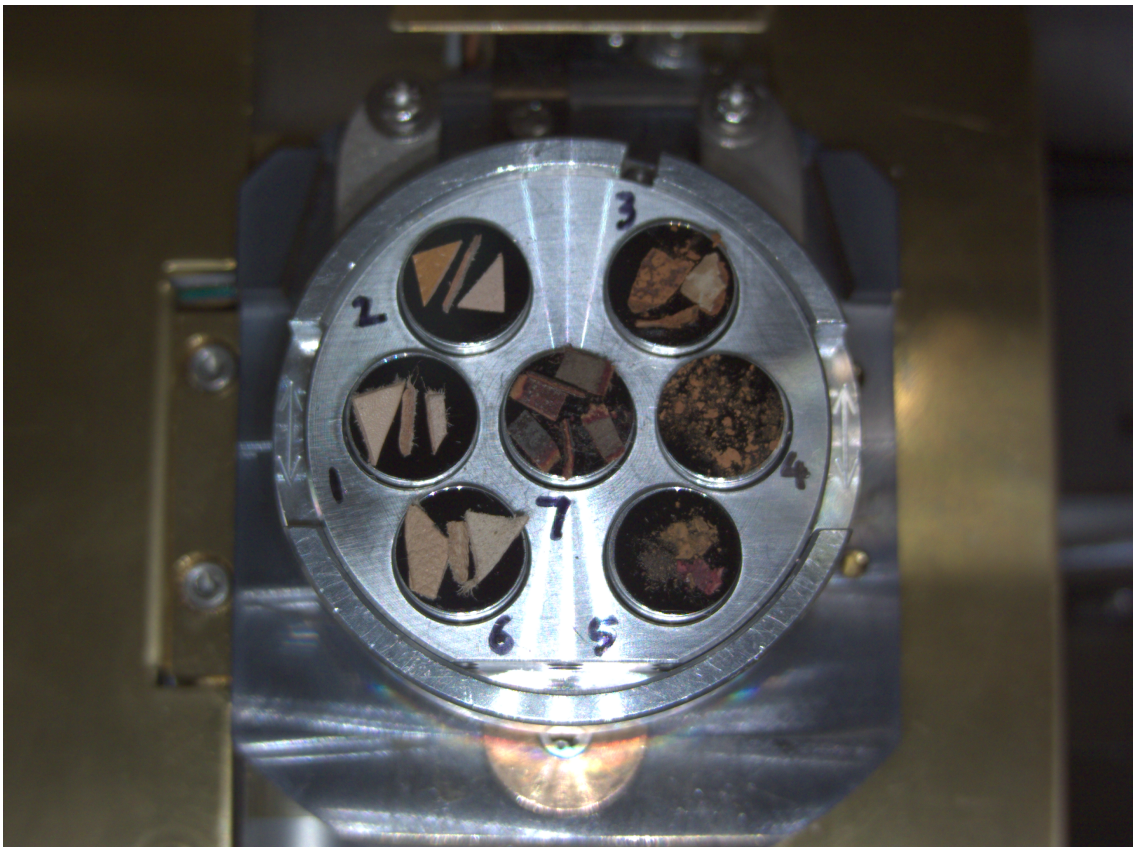

Figure 5.20: SEM set up showing samples attached to stubs with adhesive.

One of each type of animal was chosen for reference sample testing (R12, 13, 15, 17). Out of deteriorated samples, at least two samples of each degradation classification (S,M,L) were chosen for detailed tests (S1 – 4, 6, 8, 10, 18, 20), and two samples treated with Klucel G (S15, S16).All collected SEM and EDX data is included in the electronic appendix folders as image files. Fungi colonies were not identified in any of the deteriorated leathers, as was expected from these samples.[210] This confirms the long established treatment of red rot as a different process to bio-deterioration.

5.4.1 SEM of reference samples

An example set of TS, CS, and BS images for R15 is shown in Figure 5.21. The grain pattern is clearly visible on the reference samples (Figure5.21 left) and can be used to identify the animal of origin for a piece of leather. R15 was confirmed as calf leather when compared to the literature.[208,231,232]

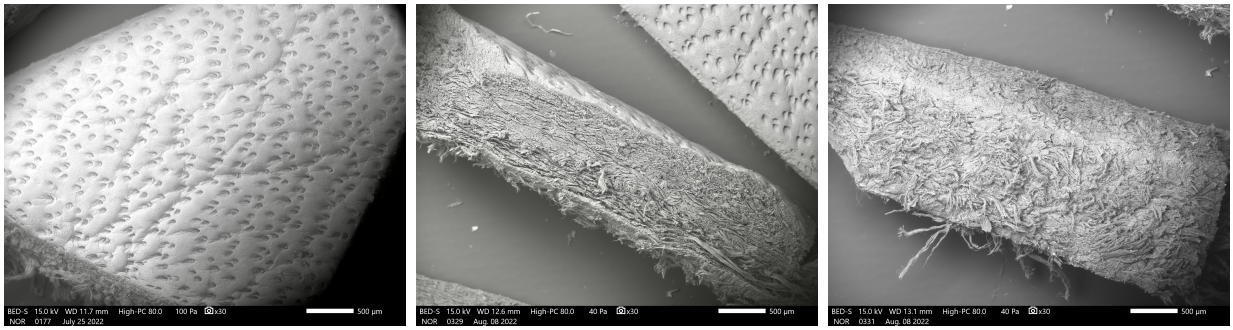

Figure 5.21: SEM of R15 showing left: the grain (TS), middle: cross section (CS), and right: flesh (BS) sides.

The cross sections of the reference samples show a very ordered structure of the collagen fibre matrix. The largest bundles are seen in the centre of the corium and they become more horizontal, forming a limiting layer below which the muscles would have been (Figure5.21 middle). The fibre bundles can also be clearly seen on the flesh side (Figure5.21 right). However, they get progressively smaller as they approach the grain, where they form a layer of tightly-woven, fine fibres that cannot be resolved without staining.[158] This network of collagen fibres is most clearly visible in R17 as shown in Figure 5.22.

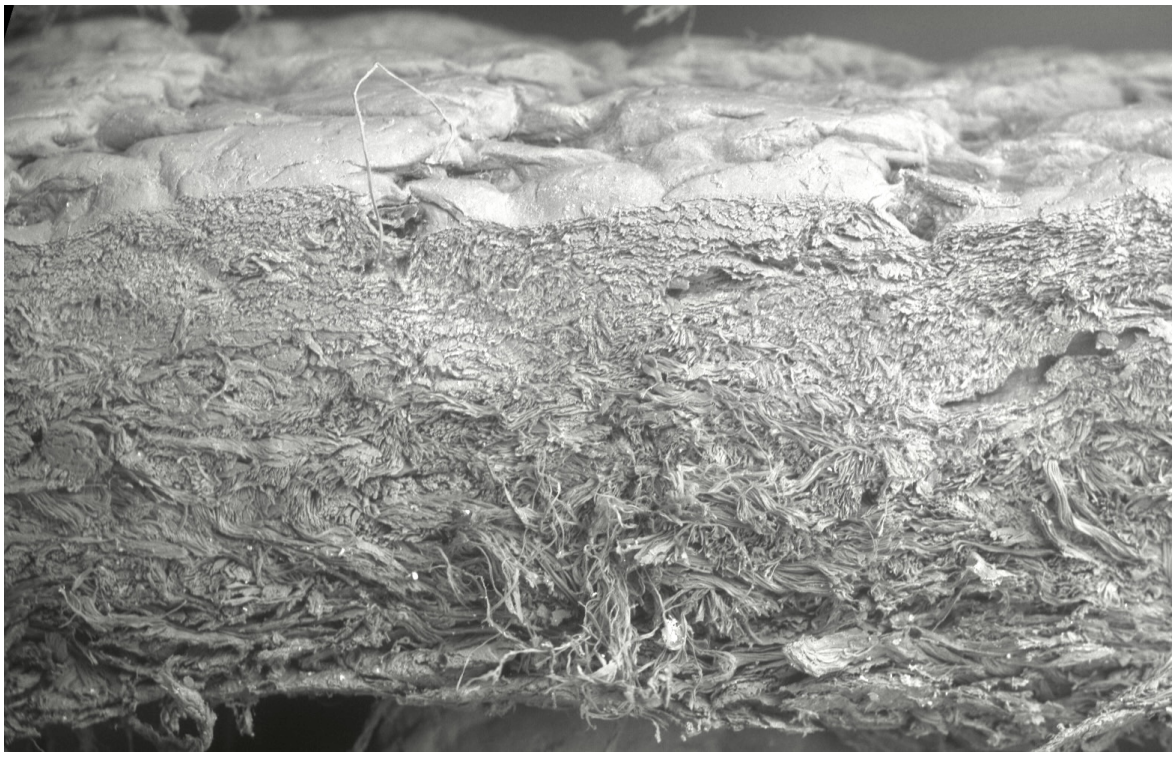

Figure 5.22: A zoom into an SEM image of R17 showing the cross section. Taken from A.47.

R12 was the only reference sample that did not display a grain pattern, likely because it has been sanded and embossed, as shown in Figure 5.23. The cross section also looks more disordered than for the other samples, which could be due to loss of structural integrity during embossing or due to the fragility of the leather itself, if for example it was taken from a young animal. This is consistent with observations made about R12 in the FTIR section.

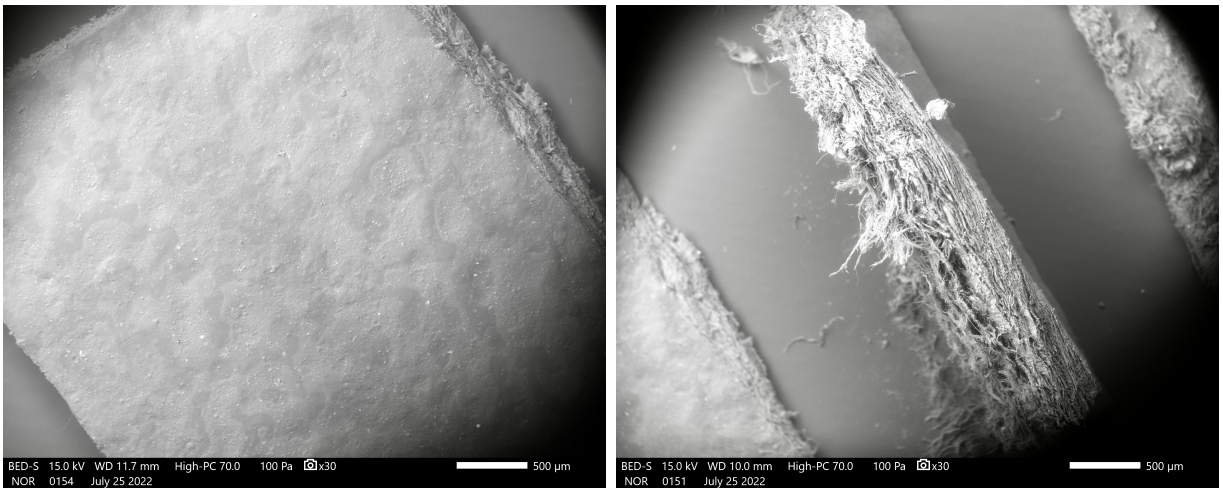

Figure 5.23: SEM of R12 showing left: the grain (TS), right: the cross section (CS).

5.4.2 SEM-EDX of reference samples

The grain (TS), corium (CS) and flesh (BS) side of each strip was then subjected to EDX analysis. All examined samples contain mostly C, O, and N, which is expected of a collagen-based material. The other most common elements are: Na, Mg, Al, Si, P, S, Cl, Ca with K and Fe sometimes present. All of these elements are expected due to the various leather-making processes described in the Introduction (4.1). R12 was the only reference sample that showed the presence of Cr, as shown in the SEM-EDX in Figure 5.24. This suggests that it was chrome tanned before being retanned with vegetable tannins.

All reference samples also sometimes show bright 'specks' among the collagen fibres, as can be seen in the centre of the SEM image from the top of Figure 5.24. When these white specks are subjected to EDX analysis they show presence of Si, Al, Na and/or Ca which are either absent or much less visible in spectra taken from other areas of the sample. Many specks also show an increased presence of O (compare spectrum 1 with spectrum 3). These could be silicates and/or salts of fatty acids which are likely present due to leather-making processes or as part of dust and dirt.[190,210,213] A spreadsheet with the elements detected in each area, with the specks highlighted is available in the electronic appendices.

Finally, Ti was found in R13. Titanium and combined chrome-titanium tanning is an area that is an actively explored area of research[233–236] and hence it is possible that the detected Ti comes from the tanning method. Despite R13 being a sample from J Hewit & Sons, which prides itself on not using heavy metals such as Cr or Ti in their tanning, the leathers they purchase often come already tanned and are only retanned by them. Hence it is difficult to rule out titanium tanning in this case.

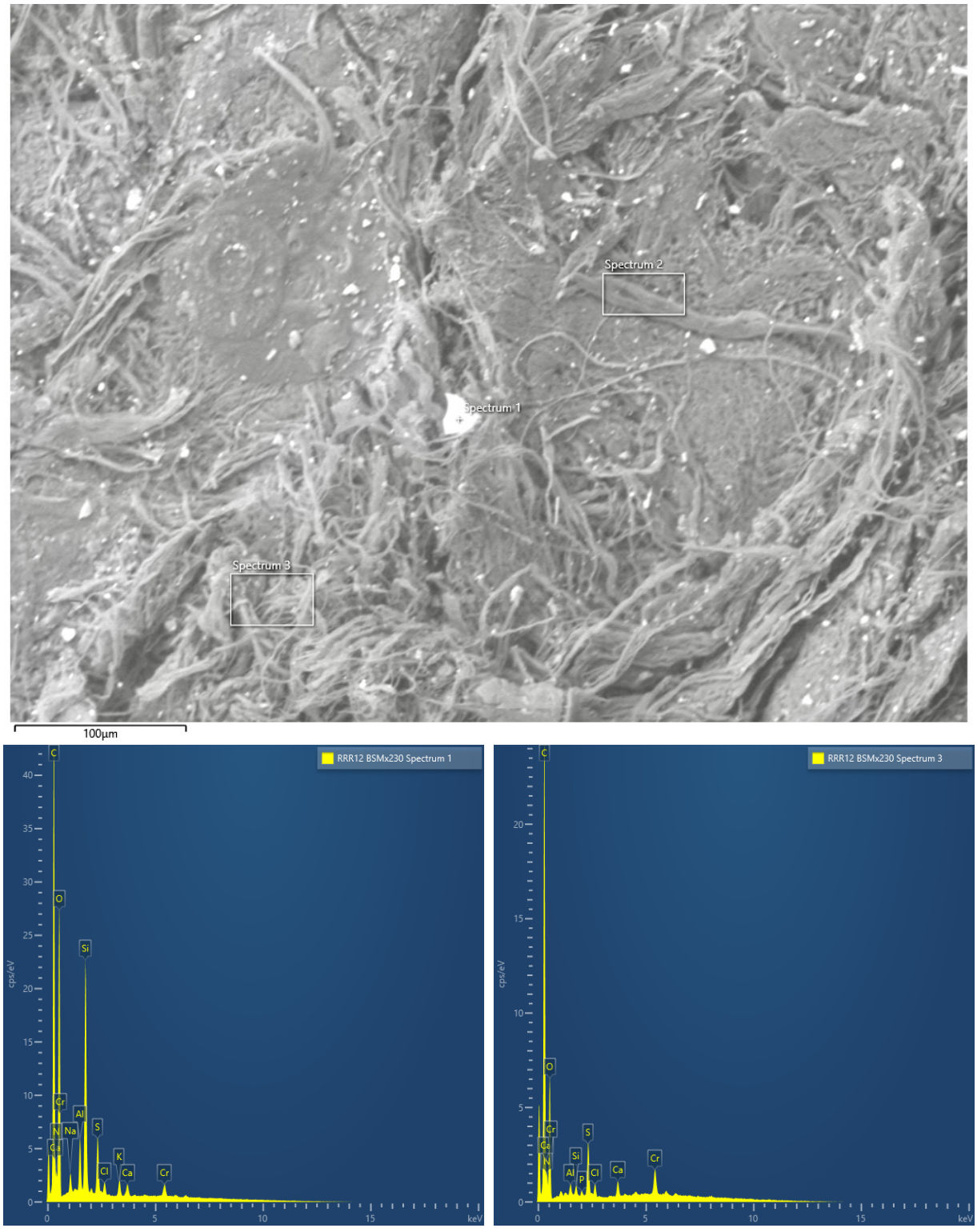

Figure 5.24: Top: SEM of R12 showing where EDX spectra were taken from; bottom left: EDX spectrum 1, bottom right: EDX spectrum 3. Spectrum 2 can be found in A.48.

5.4.3 SEM of deteriorated samples

The SEM images of the grain (TS) of deteriorated samples S6, S2 and S10, which show increasing (S, M, L) levels of degradation, are shown in Figure 5.25. S6 shows a smooth top layer broken up by cracks and some gaps. For S2, the top layer is partially missing, exposing the collagen fibrils beneath. For S10 what looks like a powdery surface to the naked eye looks fibrous under SEM. This is in great contrast to the reference samples which show a smooth and unbroken top layer with a visible grain pattern. The deteriorated samples do not display a grain pattern which is understandable for the samples that have eroded and deformed, but even the least deteriorated S6 is lacking a grain pattern.

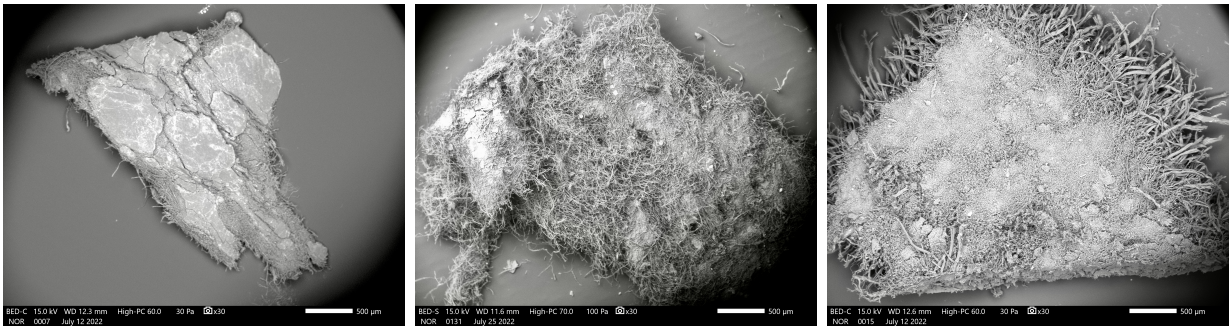

Figure 5.25: SEM of the grain (TS) of deteriorated samples. Left: S6, middle: S2, right: S10.

Red rot is characterised by the leather surface cracking and then turning into a powder (4.4.1). This powder that comes off the leather upon touch was analysed. It was confirmed to be made of segmented collagen fibres of varying lengths and thicknesses. When compared to the fibres found in the flesh side (BS) of the same sample, they are on average clearly much shorter and thinner, as shown in Figure 5.26.

The cross sections of deteriorated samples shown in Figure 5.27 illustrate what happens to the collagen fibres in the corium during deterioration. The very ordered fibrillar network displayed by the reference sample cross sections is still somewhat visible in S6. In S2 a loss of the fibre matrix cohesion can be observed due to partial unwinding of collagen fibres and in S8 the grain layer is splitting away from the corium and the fibrils appear to be melting together or gelatinising.

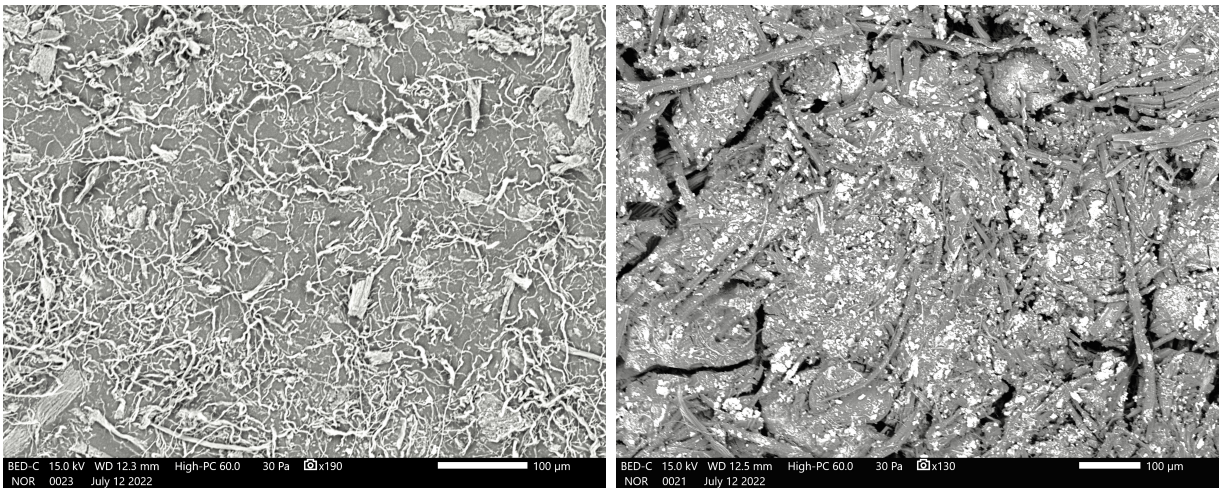

Figure 5.26: SEM of deteriorated sample S10. Left: scrapings (P), right: flesh side (BS)

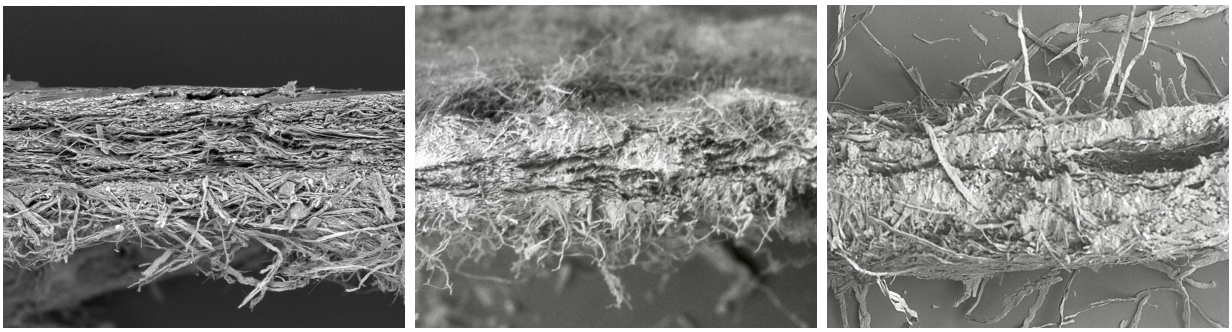

Figure 5.27: SEM of the cross section of deteriorated samples left: S6, middle: S2, right: S8.

Finally, the flesh side of the deteriorated samples, shown in Figure 5.28 shows long, thick and ordered fibrils for S6, cohesion loss and criss crossing in S2 and S3, and some gelatinisation present in S3 as well.

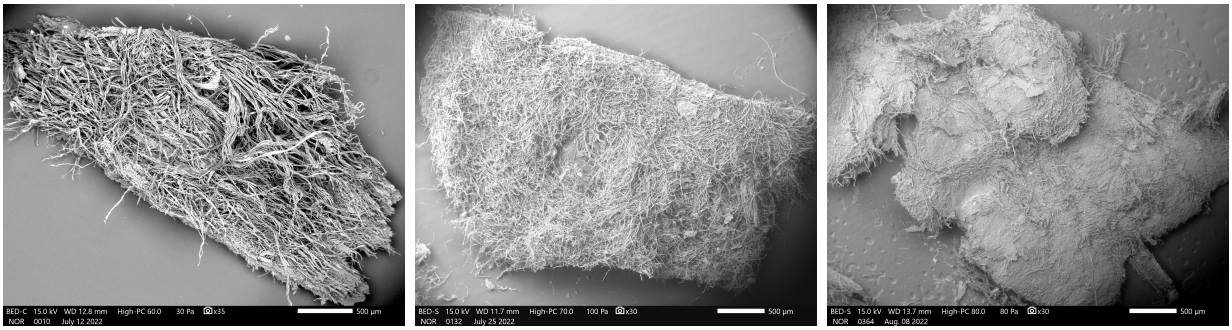

Figure 5.28: SEM of the flesh (BS) of deteriorated samples left: S6, middle: S2, right: S3.

Some deteriorated samples like S1 or S8 have a layer of paper stuck to the flesh side (BS). Paper is a cellulose-based material with a supramolecular fibre matrix, somewhat similar to that of leather. Paper has its own set of deterioration processes though they are also hydrolysis- and oxidation-based. The solutions to those problems are different.[237] The details of those problems and solutions both are beyond the scope of this work. The paper fibres can be clearly seen on SEM, as shown in Figure 5.29 in contrast with the leather fibres.

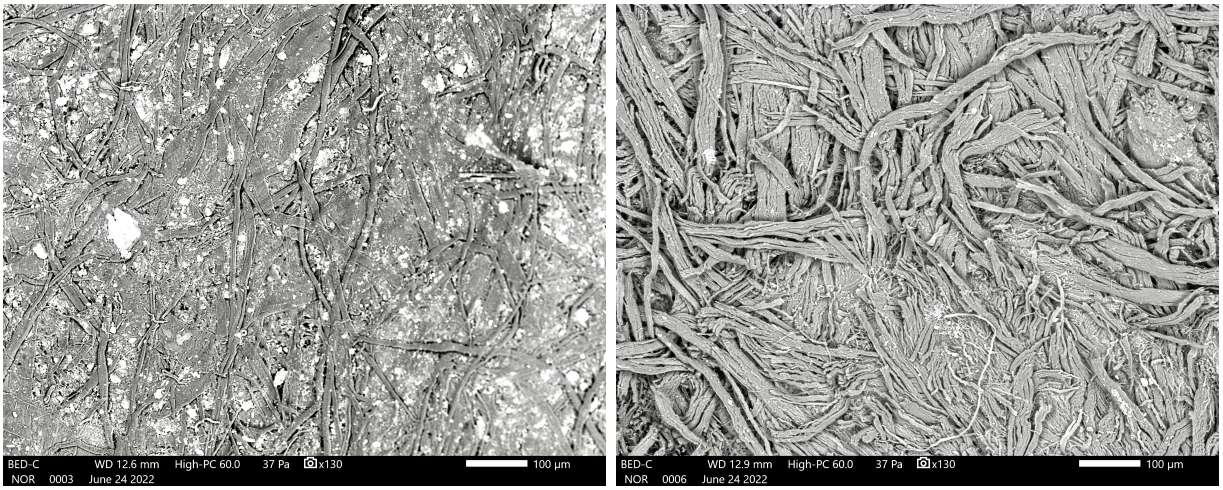

Figure 5.29: SEM of the deteriorated sample S1. Left: flesh side (BS) with paper stuck to it, right: grain (TS) with no paper.

Similarly to what was found in the FTIR results, S3 and S18 look unusually intact in some ways. S3 shows a smooth and intact top layer on the grain (TS) with some cracks, as shown in Figure 5.30. It resembles S6 more than any of the other deteriorated samples. S18 shows such a layer on both the grain (TS) and the flesh (BS) sides, as shown in the same figure, though the edges of the flesh side show fraying as well. A smooth layer on the flesh side is quite unusual - neither the reference samples, nor the other deteriorated samples show that. This is however consistent with the hypothesis postulated in the FTIR section, that the TS for both S3 and S18 and the BS for S18 have a thick layer of dye on top. In both deteriorated samples the dye gives a smooth surface layer, which resembles an undeteriorated sample, while the fibres underneath display more deterioration.

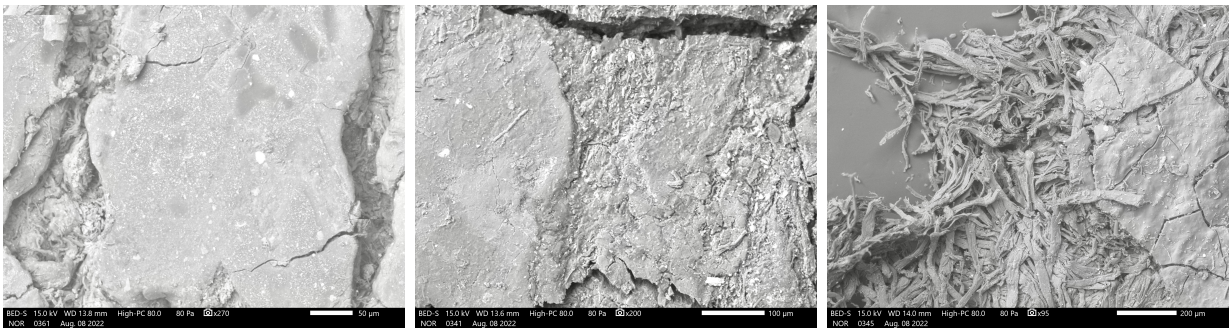

Figure 5.30: SEM of deteriorated samples left: S3 grain (TS), middle: S18 grain (TS), right: S18 flesh (BS).

Similarly to what was seen in the FTIR section, the S16 and S15 scrapings do not look different to other leather samples despite having been treated with Klucel G in the past.

SEM images of deteriorating samples of leather found in the literature have shown eroding surfaces like these,[211,238,239] and a similar effect was even achieved on new leathers through the use of mechanical force.[159] Loss of the order in the fibre matrix cohesion has also been observed previously,[212,220,240] as well as the criss-crossing.[190,241,242] This suggests that these features are common to most types of leather deterioration which are not biologically based, such as hydrolysis or oxidation (4.4), and not just red rot.

5.4.4 SEM-EDX of deteriorated samples

SEM-EDX analysis was performed on the deteriorated samples. Frequently detected elements are as follows: C, N, O, Na, Mg, Al, Si, P, S, Cl, Ca, K and sometimes Fe and Cu, which is comparable to the reference samples. Many of the EDX spectra for the more deteriorated samples show a much smaller diversity of elements, which is consistent with a slow loss of material, leaving behind only the collagen fibres. The presence of Fe and Cu in some samples can be explained by the marbling baths sometimes used for leather decoration containing iron and copper sulfate.[243] This could have contributed to deterioration of the leathers, as the presence of metal ions can cause damage in a few different ways: through catalysing oxidation reactions, through reacting with tannins and causing detanning and by crystallising as salts and loosening the collagen network.[243] Cr was not found in any deteriorated sample, which is in line with the expectations that these books predate chrome tanning.

Overall, more bright specks are visible in the deteriorated samples than in the reference samples. Crystalline deposits are called 'spues' in the leather trade and happen when unbound species within the leather migrate to its surface due to cyclical changes in environmental conditions.[244] S6 is a good illustration of this. While no specks were visible on the intact top layer of the grain, the exposed fibres of the corium and flesh side exhibit many bright spots, as shown in Figure 5.31.

When analysed these specks are confirmed to sometimes be made of Si, Al, O, and K, likely silicates, as discussed previously. There are also a lot of Ca specks. Calcium hydroxide is used in the liming baths during leather manufacture and it can react with CO_2 in the atmosphere to give calcium carbonate. Powdered gypsum ($CaSO_4$) was also sometimes used to remove fat,[174] or created when sulfate ions react with calcium milk used in the unhairing process.[243] Either source of Ca can also saponify when near fatty acids (present in oils used to treat leather surfaces).[176] S6 also shows one Na and Cl speck, which is much rarer, but likely due to sodium chloride used in curing.[245] The scrapings (P and C) show some specks as well, but fewer than strips. This is presumably due to there being less material overall for the scrapings. More deteriorated samples show fewer specks, likely because the spues that have migrated to the surface, could detach from the leather more easily.

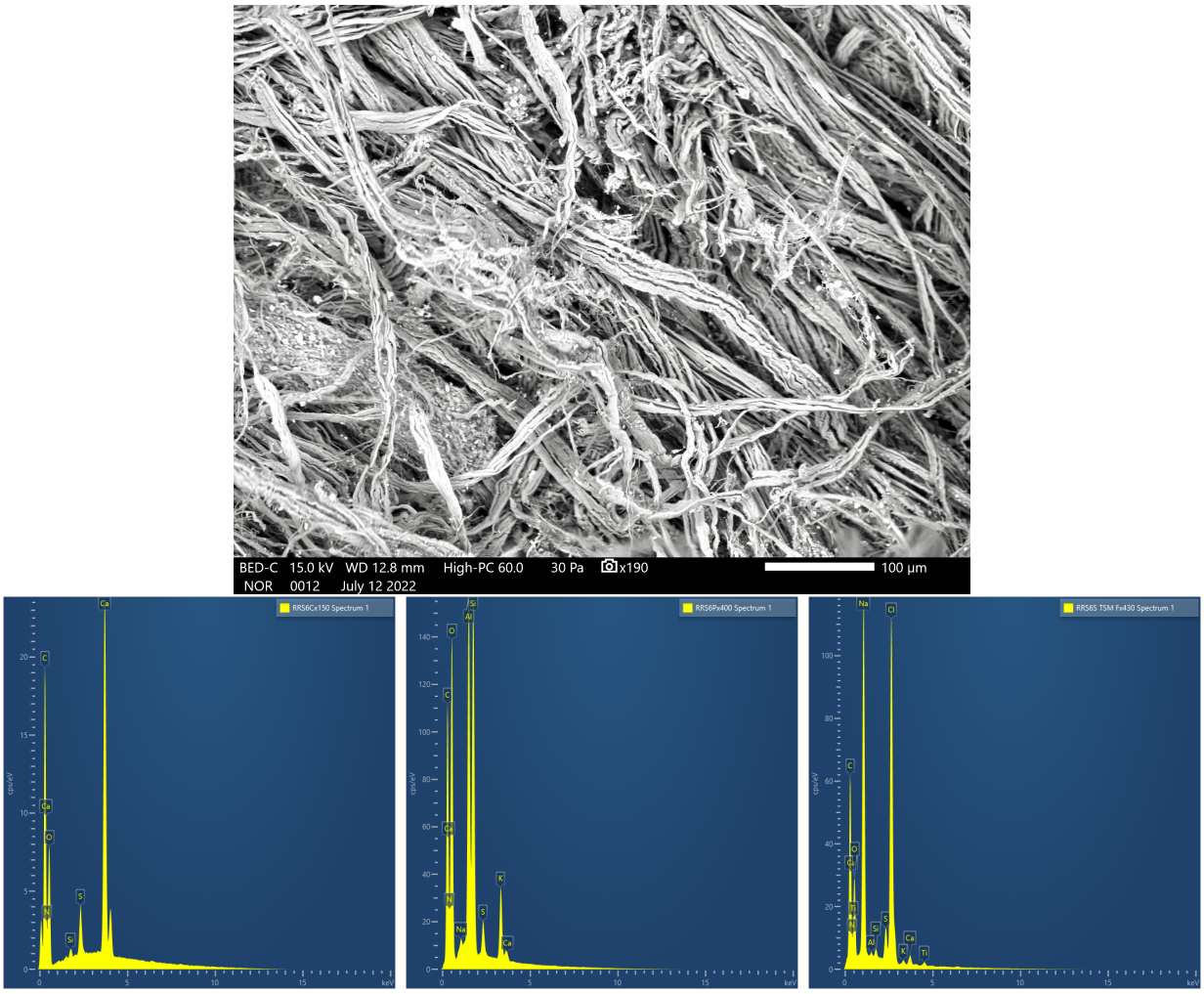

Figure 5.31: Top: SEM of the flesh side (BS) of deteriorated samples S6. Bottom: SEM-EDX of the specks found on the fibres of S6 showing left: Ca speck, middle: Si, Al, O and K speck, right: Na and Cl speck.

More interestingly, Ti was found in S3, as shown in Figure 5.32. S3 is a much older sample than R13 (a reference sample containing Ti), as the book it came from was published in 1965, which predates the early patents for use of Ti in leather tanning. For leathers of such age it is more likely that Ti was used in a dye, perhaps titanium dioxide, frequently used to lighten other dyes.[246] Titanium dioxide has also been used in disinfection of parchments and leather bindings,[247,248] so it could have been used in conservation.

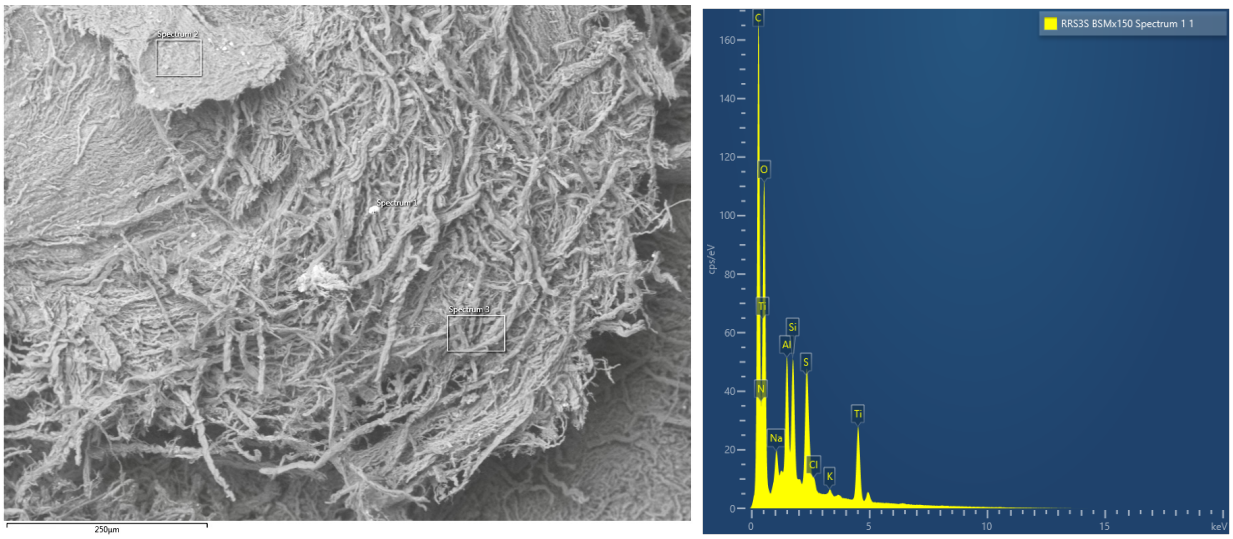

Figure 5.32: SEM of the flesh side (BS) of S3 and SEM-EDX of the speck. The speck is labelled Spectrum 1 on the SEM image. Spectra 2 and 3 can be found in A.49.

Finally, Ba was detected in S2 and S16, as shown in Figure 5.33. Ba has been found in leathers before, likely as a component of the pigments used to dye or paint them.[214,217] The two bindings that contain Ba are not the same colour (green and black) and the most well known use of Ba in pigmentation is barium white, so again it might have been used to lighten the colour. Alternatively, barium hydroxide has been used in paper conservation for purposes of deacidification, which could be another source.[249]

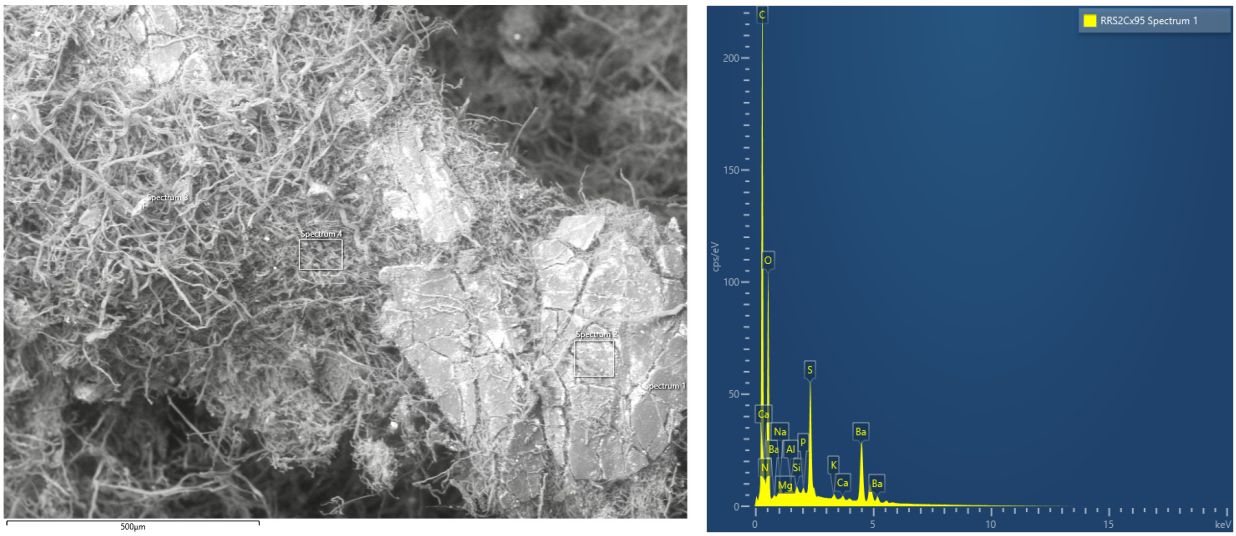

Figure 5.33: SEM of a scraping (C) of S2 and SEM-EDX Spectrum of the speck. The speck is labelled Spectrum 1 on the SEM image. Spectra 2, 3, and 4 can be found in A.50.

5.4.5 Conclusion

Leather book bindings suffering from red rot appear similar to those suffering of other types of non-biological deterioration. The powder that comes off of the leather upon touch is made of collagen fibres with occasional specks mostly made up of calcium salts or silicates. However, these findings would benefit from being compared to historical book bindings which are not suffering from red rot as well as to modern book bindings. A calibration with standards would allow for more precision when determining the chemical make up of the surfaces with SEM-EDX, which could allow for more understanding of the deterioration processes, through for example, a comparison of sulfur content between deteriorated samples, as sulfur presence is linked to red rot.

As for conservation purposes, the surface dye effect observed with FTIR and SEM suggests that protecting the leather from the elements might be beneficial, but that doing so only to the surface is not enough and it would need to penetrate into the corium to have satisfactory results. However, this might be challenging to develop without negatively impacting the feel of the leather, which is an important part of a leather book binding. This is not the focus of this project, but various coatings for leather are being investigated in the wider literature.[224,242,250]

5.5 ICP Analysis

5.5.1 ICP-OES

An attempt at measuring the total metal content for pieces of leather was made. For initial experiments, 100 mg of R15 was left stirring in nitric acid overnight, and the digestion looked successful, however, a precipitate was formed upon dilution. Since the solution did not retain all of the matter, testing this sample would not give meaningful results. Aqua regia did not digest the entire sample even after a few weeks and leaving the sample in the original nitric acid for a week also did not avoid precipitation. A microwave digestion could be successful, but it was deemed too dangerous.[251] Due to these problems, total metal content was not assessed and extractable heavy metal content was assessed instead. Fortunately, total metal content is the less useful measure of the two for this work, as the book bindings are touched by people rather than consumed, therefore it is more important to know what can be extracted from the leathers into human sweat than what exactly is present in total.

Next, the extractable heavy metal content was assessed. OEKO TEX (see Section 4.5.3) uses ISO methodology[252,253] for this purpose. It requires 2 g of leather in 100 ml of artificial sweat solution or 1 g in 50 ml. The latter was chosen to preserve resources, however, even 1 g is a large proportion of the entire binding, as leather is not a dense material. Therefore only four deteriorated samples were available for testing (S3, 5, 6, 21), S6 having a degradation classification of S, while the others are L. To complement these, four reference samples, one of each type of animal were also tested (R12, 13, 15, 17).

The ISO methodology was followed during sample preparation. Leathers with water content above 30% need to be dried according to said methodology, but vegetable tanned leathers do not exceed that limit in the current atmospheric conditions within the UK,[219] therefore drying was deemed unnecessary. Measurements without humidity errors could be obtained if the samples were dried to ensure the lowest permissible elements are definitely within regulations, in the future.

A gram of each sample, cut into small pieces (∼5 mm × 2 mm) was weighed out and stirred in 50 ml of an artificial sweat solution (per litre: 0,5 g of L-histidine monohydrochloride

monohydrate; 5 g of sodium chloride; 2,2 g of sodium dihydrogen phosphate dihydrate) for 4 h. The leather pieces were then filtered out and the solution was acidified with 2.5 ml of nitric acid (70%). The solutions obtained are shown in Figure 5.34.

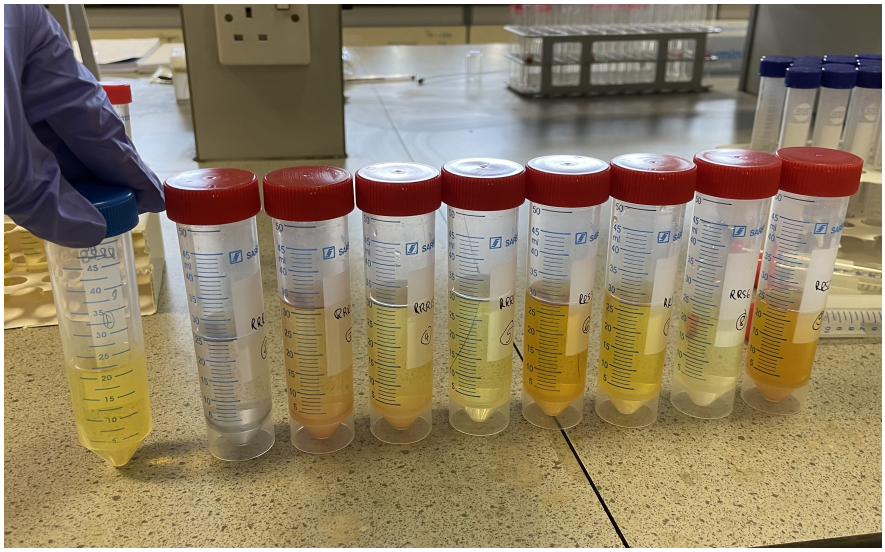

Figure 5.34: Solutions of extracted reference and deteriorated leathers.

An Optima 2000 ICP-OES spectrometer (PerkinElmer, MA, USA) in the axial view mode was used for elemental analysis. Operating conditions, accessories, and spectral lines monitored are summarised as follows: plasma power of 1300 W, signal integration time (5 s), and processed in peak area mode, using 7 points/peak for integration. The injector tube was made of alumina and had an internal diameter of 2 mm. Argon was used as the plasma (15 L/min), auxiliary (0.2 L/min) and nebuliser gas (0.6 L/min). Nitrogen was used as purging gas (2 L/min) in the optical system of the spectrometer. The analytical wavelengths were (nm): Ba–233.527, Cd–214.44, Co–228.616, Cr–267.716, Cu–327.393, Ni–221.648, Pb(II)-220.353. A multi-element standard with Ag, Al, B, Ba, Bi, Ca, Cd, Co, Cr, Cu, Fe, Ga, In, K, Li, Mg, Mn, Na, Ni, Pb, Sr, Tl, Zn, in the range 1 – 100 mg/L (0, 1, 5, 20, 40, 60, 100 and 10 as quality control mg/L) was used for calibration. The measured mass fractions were then corrected to account for the dilutions according to Equation 1.[254]

$$w_x = \frac{w_{x,i} - w_{b,i}}{m} \times V_1 \times F_d \tag{1}$$

Where w_x is the mass fraction of the metal extracted from the leather (mg/kg), $w_{x,i}$ is

the concentration of the metal in question determined by the instrument (mg/L), $w_{b,i}$ is the concentration of the blank (artificial sweat solution) determined by the instrument (mg/L), m is the mass of the sample (g), V_1 is the volume of the artificial sweat solution (ml), F_d is the dilution factor derived from the acidification or any further dilutions.

Out of the heavy metals that OEKO-TEX publishes permissible limits for As, Cr(VI), Hg and Se were the only metals not included in this test, as they were not present in the multi-element standard used. Cr(VI) can be present in chrome tanned leathers in very small amounts, as it exists in an equilibrium with Cr(III), but it is not relevant to vegetable tanned leathers which do not contain large amounts of chromium.[255]

The machine calibration combined with the correction to the measured mass fractions means that the range of corrected mass fractions that can be reliably measured is $\sim$ 52.5 – 5250 mg/kg.

No elements other than Cr for reference samples R12 and R15 were detected within those limits, as shown in Table 5.5.

Sample ID	Element	w_x (mg/kg)
R12	Cr	94.4
R15	Cr	79.7

Table 5.5: Corrected mass fractions (w_x) of detected elements extracted from leather samples using an artificial sweat solution. Remaining results can be found in the electronic appendices.

All samples are therefore within the OEKO-TEX Cr limits of 200 mg/kg. The high levels of Cr in R12 and R15 could mean that they were originally chrome tanned before being re-tanned with vegetable tanning methods if the metadata classifying them as vegetable tanned is assumed to be correct. The analysis of the SEM-EDX results has already flagged R12 as containing Cr, but for R15 it did not show much presence of Cr. Chrome tanned leather has been reported to have mass fractions of extractable Cr between 50 - 500 mg/kg.[255] Both R12 and R15 fall within that range. As SEM-EDX was not able to identify R15 as a sample with significant Cr content, it is an unsuitable technique for telling apart chrome and vegetable tanned leathers.

The only other limit tested for that is also above the lowest reliable range of detectable mass fractions of $\sim$ 52.5 mg/kg for this method is Ba at 1000 mg/kg. Since Ba was not detected, all samples are also within the safe limits for Ba. Since the remaining elements were not detected at this sensitivity, the extracts will need to be tested with a different technique.

5.5.2 ICP-MS

Multi-element analysis of diluted solutions was undertaken by ICP-MS (Thermo-Fisher Scientific iCAP-Q). Samples were introduced (flow rate 1.2 ml/min) from an autosampler (Cetac ASX-520) incorporating an ASXpress rapid uptake module through a perfluoroalkoxy (PFA) Microflow PFA-ST nebuliser. Sample processing was undertaken using Qtegra software utilising external cross-calibration between pulse-counting and analogue detector modes when required. Internal standards, used to correct for instrumental drift, were introduced to the sample stream on a separate line (equal flow rate) via the ASXpress unit or added directly to calibration standards and samples and introduced on a single line. Internal standards included combinations of Sc (10), Ge (10), Rh (5), Re (5) and Ir (5) µg/L. The matrices used for internal standards, calibration standards and sample diluents are typically either 2% Primar grade HNO_3 (Fisher Scientific, UK) with 4% methanol (to enhance ionisation of some elements). A multi-element solution with Ag, Al, As, Ba, Be, Cd, Ca, Co, Cr, Cs, Cu, Fe, K, Li, Mg, Mn, Mo, Na, Ni, P, Pb, Rb, S, Se, Sr, Ti, Tl, U, V and Zn, in the range 0 – 100 µg/L (0, 20, 40, 100 µg/L) was used.

Hg was not tested for due to the high carryover effect, which can cause problems for future measurements with this machine.[256] Alternative equipment such as the DMA-80 is available, but requires a different preparation method and was hence not explored in this work.

The leather extracts needed to be diluted fifty-fold for ICP MS due to the very high concentrations of Na $\sim$ 2300 mg/L in the artificial sweat solution. High concentrations of Na reduce the ionisation rate of the elements in the plasma making the internal STD correction not reliable which is an analytical limitation of the technique. If the mass fractions of any

of the elements of interest fall below the limit of detection (LOD) as a result of this dilution then another technique will be necessary to measure them.

To determine the LOD, the artificial sweat solution was tested four times as a blank for all of the elements and the mean (μ) and standard deviation (σ) of these results were used to calculate the LOD $= \mu + 3\sigma$ and limit of quantification (LOQ) $= \mu + 10\sigma$.[257] The LOD for Cd is below but within the order of magnitude of the very low permissible limit of extraction for leather (0.1 mg/kg) after the dilutions. The remaining LODs are at least an order to several orders of magnitude higher.

The detected mass fractions were corrected according to Equation 1 and are shown in Table 5.6. Mass fractions measured for the samples that fall below the LOD are denoted as <LOD in the table.

	Cr	Co	Ni	Cu	As	Se	Cd	Ba	Pb
R12	160	0.0540	0.348	1.32	0.0353	<LOD	0.0224	0.804	0.111
R13	21.9	0.0426	0.274	1.67	0.0488	<LOD	<LOD	5.21	54.2
R15	132	0.0263	0.438	1.83	0.0396	<LOD	0.0276	1.24	0.686
R17	1.51	0.0446	0.516	2.85	0.0327	<LOD	0.0343	1.68	1.88
S3	7.75	0.0882	0.646	7.78	0.526	0.0784	0.316	6.99	71.0
S5	0.986	0.161	0.439	3.50	1.08	0.0570	0.0918	2.06	20.0
S6	0.337	0.481	0.515	5.32	1.26	0.0178	0.0994	3.18	8.09
S21	1.71	0.0907	0.375	3.34	14.2	0.0581	0.520	3.33	8.92
Limits	200	4	4	50	1	100	0.1	1000	1

Table 5.6: Corrected mass fractions (w_x) of detected elements extracted from leather samples using an artificial sweat solution and the OEKO-TEX permissible limits in mg/kg.

As was already established with ICP-OES, all of the reference samples are within the permissible Cr and Ba limits, with R12 and R15 showing the highest mass fractions of Cr. Ni, Cu, and As were detected far below the permissible limits. Se is also definitely within the permissible limits, as the mass fractions fall below the LOD, it is even possible that none is present in solution. Co is a bit more complex, as the measured mass fractions fall above the LOD but below the LOQ for R13, R15, and R17. This makes the mass fractions for those reference samples less certain, but they are definitely present. However, considering that the permissible limit is two orders of magnitude higher than the detected mass fractions it is very unlikely that it is exceeded. Hence, it is likely that all the reference samples fall within the

permissible Co limit. Pb is a more worrying case; R12 and R15 fall within the permissible limit, while R17 exceeds it, and R13 exceeds it by far. Finally, R13 is below LOD for Cd, but R12, R15, and R17 are above LOD and below LOQ and since they are within the order of magnitude of the permissible limit, it is not certain if those values are actually within it or not. Cd and Pb are hence a possible concern for these reference samples, but a different technique might prove more useful for Cd.

Similarly, the deteriorated samples were also all within the Cr and Ba limits. Ni and Cu were detected far below the permissible limits. The Se values are within permissible limits for S3, S5, and S21, but below the LOQ for S6. Following similar logic to above though, all of the samples should fall far below the permissible Se limits. S3 falls below the permissible limit for As, but S5, S6 and S21 are above it. S5 and S6 are very close to the Cd permissible limit, while S3 and S21 exceed it and all deteriorated samples exceed the Pb permissible limit, so it appears that these deteriorated samples may have unsafe levels of As, Cd, and Pb.

The extractable content of other elements (B, Na, Mg, P, S, K, Ca, Ti, Li, Be, Al, V, Mn, Fe, Zn, Rb, Sr, Mo, Ag, Cs, Tl, U) was measured at the same time as the heavy metals. Mg, K, Ca, Ti, Al and Zn were detected for all samples and Ag for some, confirming some of the SEM-EDX detections. Na and P could not be quantified, as they are present in large quantities in the artificial sweat solution. The mass fractions for S come out to a few thousand mg/kg for the reference samples, while for the deteriorated samples they are in the tens of thousands. The mass fraction for the least deteriorated sample, S6, is 13k while the more deteriorated S5 and S21 are above 20k. S3 has so far been classified as very degraded (L) but its S mass fractions is only 15k, which could be due to the dye effect. An interesting pattern emerges here, but four deteriorated samples is far too few for any certainty. As S content could be related to red rot (4.4.1), this idea should be further pursued but perhaps a less destructive technique such as X-ray photoelectron spectroscopy (XPS) which only requires a small amount of material could be used. The mass fraction data for ICP-OES and MS can be found in the electronic appendices.

5.5.3 Conclusion

With this, the methodology for assessing extractable heavy metal content in deteriorated leather samples for most elements of concern is developed. Application of the OEKO-TEX and ISO methodologies to testing for the safety of leather-based objects has not previously been attempted on historic samples. Due to the need for large dilutions to avoid matrix effects arising from high concentrations of electrolytes[258] in combination with the low permissible limits set for Cd and Hg, a different technique is necessary for those two elements. Further research into Atomic Absorption Spectroscopy (AAS) for these purposes is recommended. Furthermore, more repeats for these samples should be run and more different samples should be tested to confirm these results, as a single test is insufficient to be certain of the veracity of these results.

The results are, however, concerning enough to continue testing or to warrant precautions when handling these samples and the books they come from. The typical precaution which reduces skin contact with harmful materials is to cover relevant body parts with personal protective equipment (PPE) in the form of gloves (e.g. natural rubber gloves).[259] Care should be taken to not touch exposed skin (e.g. face) or eyes with gloved hands. Regardless of its chemical composition, exposure to any dust in excessive amounts can cause skin irritation, eye damage and respiratory problems. To assess this the extent of dust present in the air in libraries containing deteriorating leather-bound tomes, air sampling may be needed and PPE such as gloves, coveralls, goggles and a respirator that fit the wearer, might need to be provided in line with the findings of such an assessment.[260] Furthermore, leathers can emit volatile organic compounds (VOCs), which could be harmful and should be separately investigated.[261,262]

5.6 Conclusions and future work

Upon inspection of reference and deteriorated leather samples with ATR-FTIR spectroscopy, it became clear that deteriorated leathers display greater spatial inhomogeneity of spectral features than fresh leathers. Based on previous work in the literature, ATR-FTIR was then used to make the first substantial investigation into distinguishing between types of tannins in leathers in a non-destructive way. Following these promising initial results, more robust detection methods such as 2nd derivatives and deconvolution should be used to verify these claims. Furthermore, a new ratio of peaks was developed as a way of categorising the level of deterioration and should be investigated further after deconvolution of peaks. Such a ratio could be widely applicable to leather-bound tomes, however as dye effects can disrupt it care needs to be taken. Such analysis can be performed on whole books, strips or scrapings, which makes it versatile, but at this stage measurements from multiple locations are needed to perform it. Finally, as these findings might not be specific to red rot affected books, a comparison with non-red rot affected books of historical origin is called for.

SEM analysis was also performed on reference and deteriorated samples. It revealed the difficulty in finding the grain pattern that could identify the animal origin of a tome. The characteristic red rot powder which detaches from the leather and covers nearby surfaces was shown to be made mostly of short and thin collagen fibres, with few silicate or calcium based specks present. Both FTIR and SEM analysis led to the conclusion that a thick top layer of dye can keep the collagen fibres it affects more intact, but the fibres below it deteriorate as usual. This likely means that any conservation treatments would benefit from permeating the entirety of the leather, to avoid the flaking off of the top protected layer, when the lower layers lose their cohesion. Furthermore, red rot deterioration observed with SEM for these bindings, such as surface erosion, criss-crossing of fibres, and loss of matrix cohesion, looked very similar to non-red rot deterioration (hydrolysis, oxidation and gelatinisation).

At this stage, due to the lack of clear visual or spectroscopic markers for red rot, it appears that a more characteristic feature of red rot affected leathers than the appearance or chemical make up of the collagen-tannin matrix, might be their smell. Gas chromatography analysis of the distinctive smell should be performed, as it could reveal something particular

to red rot that has been missed so far.

Finally, elemental analysis of a few samples using ICP-OES and ICP-MS was performed. It is advantageous to perform such analysis on artificial sweat solution extracts of leathers, rather than on fully dissolved leathers, as it is difficult to fully digest pieces of leather for total heavy metal content analysis. Furthermore, ICP-OES is not sufficiently sensitive to test for elements other than Cr and Ba, which have much higher permissible limits than other elements such as As, Pb, Co, Cu and Ni. For those elements ICP-MS is recommended and a methodology for using it on historical leathers was described here. This is however a destructive technique that requires a large sample mass, and it is still insufficiently sensitive for Cd and Hg. Nevertheless, levels above the permissible limits of As, Cd, and Pb were detected for several samples, hence further tests into heavy metal content, air-sampling, and VOC analysis inside enclosed spaces that store deteriorating leather bindings, as well as appropriate precautions in the form of PPE, are recommended.

6 Experimental

6.1 General equipment

^{1}H and ^{13}C NMR spectra were recorded using either a Bruker DPX300, AV400 or DPX400 machines at room temperature. Chemical shifts are reported with respect to the $CDCl_3$ residual peak at 7.26 ppm for ^{1}H spectra and 77.00 ppm for ^{13}C spectra or with respect to the DMSO residual peak at 2.50 ppm for ^{1}H spectra and 39.50 ppm for ^{13}C spectra. For ^{1}H NMR spectroscopy, splitting patterns are described using the following abbreviations H - number of hydrogen atoms in an environment, s = singlet, d = doublet, t = triplet, q = quartet, m = multiplet, br = broad; coupling constant (J in Hz).

Electrospray ionisation mass spectra (ESI-MS) were recorded with a Bruker MicroTOF using methanol or acetonitrile as the solvent. MALDI-TOF mass spectra were recorded with a Bruker Ultraflex III mass spectrometer using trans-2-[3-(4-tert-butylphenyl)-2-methyl-2-propenylidene]-malononitrile as the matrix.

Cyclic voltammetry was carried out using an Autolab PGSTAT20 potentiostat under an argon atmosphere using a three-electrode arrangement in a single compartment cell. Glassy carbon was used as the working electrode, platinum wire as the secondary electrode and a saturated calomel reference electrode, chemically isolated from the test solution via a fritted bridge tube containing electrolyte solution, in the cell. An analyte concentration of 1 mM was used with $[^{n}Bu_4N][BF_4]$ (200 mM) as a supporting electrolyte. Redox potentials are referenced to the ferrocenium/ferrocene couple, which was implemented as an internal reference. No compensation was applied for internal resistance.

UV/vis spectroelectrochemical measurements were performed using an optically transparent quartz electrochemical cell, with a 0.5 mm path length. A three-electrode configuration of a platinum/rhodium gauze working electrode, platinum wire secondary electrode and a silver/silver chloride reference electrode (chemically isolated via a fritted bridge tube) were used in the cell. The potential at the working electrode was regulated with a Sycopel Scientific Ltd DD10M potentiostat and the spectra recorded with a Perkin Elmer 16 spectrophotometer. Temperature control was achieved with a stream of chilled nitrogen gas

(cooled by passing through a tube submerged in liquid nitrogen) across the surface of the cell, adjusting the flow rate as necessary in response to a temperature sensor (±0.1 °C). [^{n}Bu$_4$N][BF$_4$] (200 mM) was used as the supporting electrolyte for the experiments.

Bulk electrolysis was performed under an argon atmosphere at 0 °C in a two-component cell: a platinum/rhodium gauze working electrode and secondary electrode are separated by a glass frit. A silver/silver chloride reference electrode was bridged to the test solution through a vycor frit, oriented at the centre of the working electrode. The working electrode compartment, containing analyte (1 mM), was stirred rapidly with a magnetic stirrer bar during electrolysis. [^{n}Bu$_4$N][BF$_4$] (200 mM) was used as the supporting electrolyte for the experiments. After electrolysis was completed, the prepared solution was transferred by cannula to a quartz EPR tube for analysis on a Bruker EMX spectrometer. Solution phase (fluid) spectra were recorded at room temperature Spectra were simulated when possible using WIN EPR SimFonia software.

6.2 1-(4-bromobutoxy)-4-methoxybenzene (1)

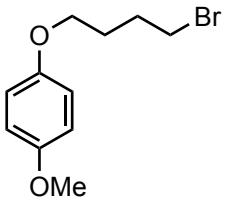

Original method: To a suspension of potassium carbonate (6.30 g, 45.6 mmol) in 1,4-dibromobutane (6.0 ml, 50 mmol), a solution of 4-methoxyphenol (3.76 g, 30.2 mmol) in 70 ml acetone was added dropwise. The reaction mixture was heated at 65 °C and stirred for 24 h. It was then cooled to r.t. and the excess solid potassium carbonate was filtered out. The solvent was then removed under reduced pressure and the resulting oily mixture was dissolved in 100 ml dichloromethane and washed with 100 ml of water, then 100 ml of brine. The organic layer was then dried over magnesium sulphate, which was then filtered out. The solvent was then removed under reduced pressure. The resulting oily mixture was then dripped into cold hexane forming white iridescent precipitate, which was removed and confirmed to be the dimer side product (1,4-bis(4-methoxyphenoxy)butane). The solvent was

removed from the hexane solution and the resulting oily liquid was frozen solid. This solid was washed with 3 × 20 ml of cold hexane under reduced pressure giving a white crystalline solid (1.78 g, 6.90 mmol, 23%) ^{1}H NMR (300 MHz, Chloroform-d) δ 6.85 (4 H, s), 3.97 (2 H, t, J 6.1), 3.79 (3 H, s), 3.51 (2 H, t, J 6.6), 2.14 - 2.03 (2 H, m), 1.99 - 1.87 (2 H, m). ^{13}C NMR (75 MHz, Chloroform-d) δ 153.8, 153.0, 115.4, 114.7, 67.5, 55.8, 33.5, 29.5, 28.0.

New method: 4-methoxyphenol (2.48 g, 20.0 mmol), 1,4-dibromobutane (9.50 ml, 80.1 mmol), potassium carbonate (8.49 g, 61.4 mmol) and potassium iodide (3.36 g, 20.2 mmol) were mixed in acetone (400 ml). The reaction mixture was heated at reflux and stirred for 48h. It was then cooled to r.t. and the excess potassium carbonate was filtered out. The solvent was then removed under reduced pressure and the resulting oily mixture was purified using flash column chromatography (silica, 60:40 CH_2Cl_2: Cyclohexane) to give a colourless solid (2.26 g, 16.4 mmol, 82%).

6.3 4-bromobutane-pillar[5]arene (2)

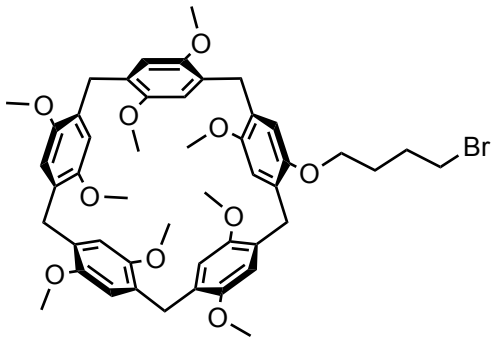

A solution of 1,4-dimethoxybenzene (13.3 g, 96.0 mmol), 1-(4-bromobutoxy)-4-methoxybenzene (1.56 g, 6.04 mmol) and paraformaldehyde (8.71 g, 290 mmol) in 900 ml dichloromethane was stirred for 10 min in an oven dried flask under N_2. To this reaction mixture anhydrous iron(III)chloride (2.53 g, 15.1 mmol) was added and stirred at room temperature for 3 h. The reaction mixture was then quenched with water (500 ml) and extracted with water 200 ml × 3. The organic layer was then concentrated under reduced pressure and silica was added to form a viscous suspension. The entirety of the solvent was then removed under reduced pressure. The resulting solid was dry loaded for the purposes of flash column chromatography (silica, CH_2Cl_2) to give an orange crude product which was further repeatedly purified

in combination with similar samples from repeated reactions using flash column chromatography (silica, CH_2Cl_2) to give a pale cream powder in approximately 20–30% yield over all reactions. ^{1}H NMR (300 MHz, Chloroform-d) δ 6.85 - 6.62 (m, 1H), 3.82 (t, J = 6.1 Hz, 2H), 3.77 (d, J = 3.5 Hz, 10H), 3.68 - 3.61 (m, 27H), 3.49 (q, J = 6.1 Hz, 2H), 1.68 (dq, J = 8.3, 6.3 Hz, 2H), 1.62 - 1.50 (m, 2H). ^{13}C NMR (75 MHz, Chloroform-d) δ 151.0, 150.9, 150.8, 150.0, 128.7, 128.4, 128.4, 128.4, 128.3, 128.2, 115.0, 114.5, 114.2, 114.1, 114.0, 113.9, 67.6, 56.2, 56.1, 55.9, 33.3, 29.9, 29.9, 29.7, 29.0, 28.5. ESI-HRMS m/z calc'd for $[M+H]^+$ (871.3051); found (871.3010).

6.4 *N*-Boc-ethylenediaminobutane-pillar[5]arene (3.1)

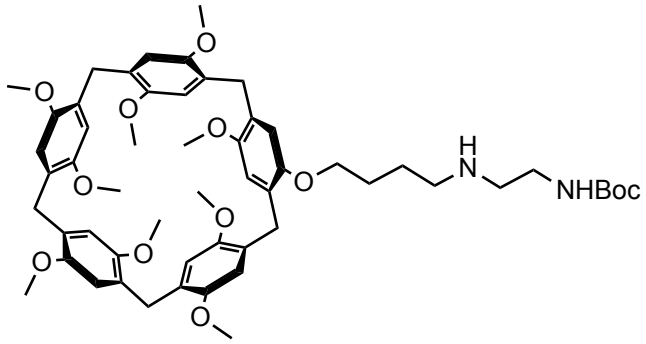

To a solution of 4-bromobutane-pillar[5]arene (**2**) (2.13 g, 0.810 mmol) in DMF (125 ml), *N*-Boc-ethylenediamine (0.058 g, 0.362 mmol) and potassium carbonate (0.322 g, 2.33 mmol) were added. The mixture was heated at 135 °C and stirred for 24 h. The reaction mixture was then cooled to r.t. then the solvent was removed under reduced pressure. The cream solid was then dissolved in 40 ml of chloroform and washed with water 3 × 40 ml. The solvent was then removed under reduced pressure to give a cream solid. The crude product was then purified using flash column chromatography to give a yellow oil (20.0 mg, 0.0210 mmol, 3%), which was confirmed to be the mono-alkylated species. ^{1}H NMR (300 MHz, Chloroform-d) δ 6.94 - 6.56 (m, 10H), 4.04 (s, 2H), 3.92 (d, J = 5.9 Hz, 2H), 3.80 - 3.74 (m, 10H), 3.68 (dd, J = 9.5, 4.1 Hz, 25H), 2.39 - 2.23 (m, 2H), 2.21 - 2.09 (m, 2H) 1.83 (s, 4H). ^{13}C NMR (75 MHz, Chloroform-d) δ 150.9, 128.4, 114.3, 67.6, 64.2, 55.9, 39.9, 29.5, 28.6, 26.3, 25.9.

6.5 Attempt at *N*-Boc-ethylenediamino-bis-hexane (4)

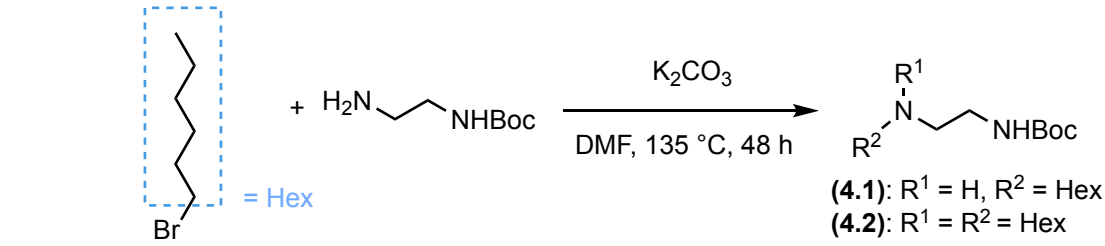

To a solution of bromohexane (0.500 g, 3.03 mmol) in DMF (100 ml), *N*-Boc-ethylenediamine (0.164 g, 1.01 mmol) and potassium carbonate (0.900 g, 6.06 mmol) were added. The mixture was heated at 135 °C and stirred for 48 h. The reaction mixture was then cooled to r.t. then the solvent was removed under reduced pressure. The yellow solid was then dissolved in 40 ml of chloroform and washed with water 3 × 40 ml. The solvent was then removed under reduced pressure to give a dark orange oil. MALDI: mono- (**4.1**) (m/z calc'd for $[M+H]^+$ (245.2224); found (245.2208)) and bis-alkylated (**4.2**) (m/z calc'd for $[M+H]^+$ (329.3163); found (329.3169)).

6.6 4-phthalimidobutane-pillar[5]arene (5)

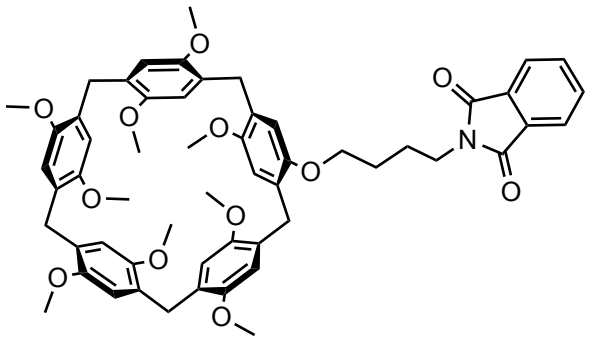

To a solution of 4-bromobutane-pillar[5]arene (**2**) (3.42 g, 3.92 mmol) in DMF (50 ml), potassium phthalimide (1.05 g, 5.67 mmol) was added. The reaction mixture was heated at 60 °C and stirred for 17 h. It was then cooled to r.t. and the solvent was removed under reduced pressure. The yellow solid was dissolved in 40 ml dichloromethane and extracted with brine. The organic layer was then dried over magnesium sulfate. The solvent was then removed under reduced pressure to give a yellow solid, which was then purified using flash column chromatography (silica, dichloromethane) to give a yellow solid (3.01 g, 3.21 mmol,

82%). ^{1}H NMR (400 MHz, Chloroform-d) δ 7.85 (dd, J = 5.5, 3.0 Hz, 2H), 7.72 (dd, J = 5.4, 3.0 Hz, 2H), 6.80 – 6.67 (m, 10H), 3.86 (t, J = 6.2 Hz, 2H), 3.81 – 3.73 (m, 12H), 3.68 – 3.56 (m, 27H), 1.98 – 1.89 (m, 2H), 1.88 – 1.80 (m, 2H). ^{13}C NMR (101 MHz, Chloroform-d) δ 168.4, 150.8, 134.0, 132.1, 128.3, 128.3, 128.2, 128.2, 123.2, 114.2, 114.1, 114.0, 114.0, 67.9, 55.8, 55.8, 55.8, 55.7, 37.8, 29.8, 29.7, 27.2, 25.6.

6.7 4-aminobutane-pillar[5]arene (6)

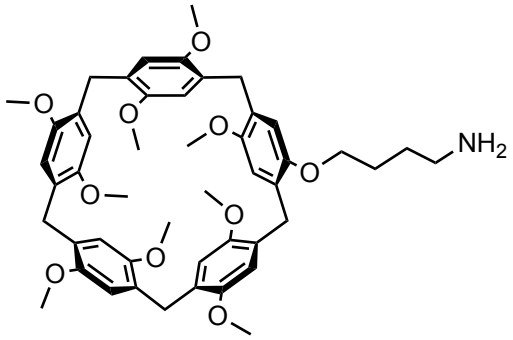

A mixture of 4-phthalimidobutane-pillar[5]arene (**5**) (1.22 g, 1.30 mmol) and NH_2NH_2 (0.417 g, 13.0 mmol) was heated at 65 °C in MeOH (50 ml) for 17 h. The solvent was removed using filtration and the solid was dissolved in CH_2Cl_2 and washed with saturated Na_2CO_3 then dried over magnesium sulfate. The solvent was then removed under reduced pressure to give a white solid (1.32 g, 1.64 mmol, 46%). ^{1}H NMR (400 MHz, Chloroform-d) δ 6.90 – 6.69 (m, 10H), 3.91 – 3.73 (m, 14H), 3.75 – 3.54 (m, 27H), 2.02 – 1.77 (m, 4H), 1.72 – 1.55 (m, 2H). ^{13}C NMR (101 MHz, Chloroform-d) δ 150.9, 150.8, 128.4, 114.0, 68.2, 55.9, 55.9, 55.9, 55.9, 55.8, 55.7, 53.3, 29.6, 29.5, 26.8. ESI-HRMS m/z calc'd for $[M+H]^+$ (808.4055); found (808.4092).

6.8 Boc-5-aminoisophthalic acid (7)

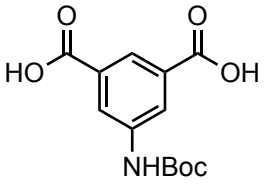

A mixture of 5-aminoisophthalic acid (5.65 g, 31.5 mmol), and NaOH (2.75 g, 69 mmol) was stirred in 1:1 DMF:water (50 ml) at 0 °C. Di-tert-butyl dicarbonate (7.01 g, 32.0 mmol) was added to this suspension. The reaction mixture was warmed to room temperature and stirred overnight, then the product was precipitated through the addition of 3M HCl (25 ml). The product was filtered out and washed with water then dried to give an off-white product without need for further purification (5.75 g, 21.1 mmol, 67%). ^{1}H NMR (400 MHz, DMSO) δ 13.16 (s, 2H), 9.78 (s, 1H), 8.31 (d, J = 1.6 Hz, 2H), 8.08 (t, J = 1.5 Hz, 1H), 1.56 – 1.40 (m, 10H). ^{13}C NMR (101 MHz, Chloroform-d) δ 167.0, 153.2, 140.7, 132.1, 124.0, 123.0, 80.2, 28.5, 27.3. ESI-HRMS m/z calc'd for $[M+Na]^{+}$ (304.0792); found (304.0780).

6.9 Attempt at amido bis-pillar[5]arene (8)

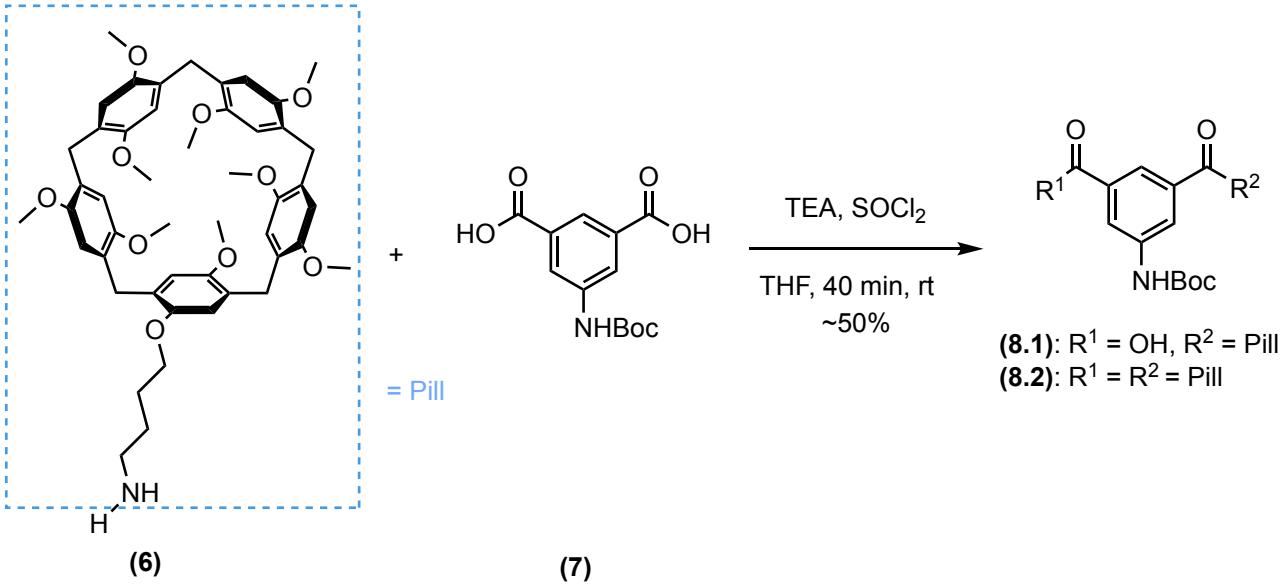

(6) **(7)**

Boc-5-aminoisophthalic acid (**7**) (0.061 g, 0.216 mmol), 4-aminobutane-pillar[5]arene (**6**) (0.384 g, 0.476 mmol) and thriethylamine (88 mg, 0.865 mmol) were dissolved in anhydrous

THF. Thionyl chloride (0.064 g, 0.540 mmol) was added to this solution at room temperature. The mixture was stirred for 40 minutes, then another aliquot of thionyl chloride and 4-aminobutane-pillar[5]arene (**6**) was added. The solvent was then removed under reduced pressure. The resulting solid was then extracted from sodium bisulfite 5% solution in water, then from sodium hydroxide solution, then dried over magnesium sulfate. The solvent was then removed under reduced pressure. The crude product was purified using flash column chromatography (silica, CH_2Cl_2 with 1% acetone) to give a brown solid (60 mg) which was likely to be a mixture of the starting material 4-aminobutane-pillar[5]arene (**6**), the mono (**8.1**) and di-substituted (**8.2**) products. (**8.1**): MALDI m/z calc'd for [M] (1069.4703); found (1070.467),and (**8.2**): MALDI m/z calc'd for [M] (1759.8129); found (1860.781)

6.10 Attempts at amido bis-octane (9)

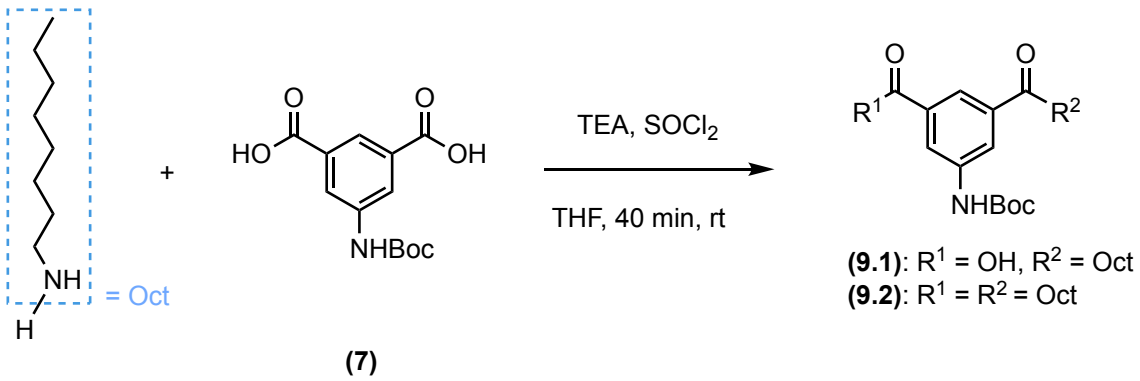

$SOCl_2$ coupling: Boc-5-aminoisophthalic acid (**7**) (0.100 g, 0.3566 mmol), octylamine (0.101 g, 0.783 mmol) and thriethylamine (0.216 g, 2.14 mmol) were dissolved in anhydrous THF. Thionyl chloride (0.093 g, 0.783 mmol) was added to this solution at room temperature. The mixture was stirred for 40 minutes, then another aliquot of thionyl chloride and octylamine was added three times. The solvent was then removed under reduced pressure. The resulting solid was then extracted from sodium bisulfite 5% solution in water, then from sodium hydroxide solution, then dried over magnesium sulfate. The solvent was then removed under reduced pressure. ESI-MS of (**9.1**): (m/z calc'd for $[M+H]^+$ (393.2384); found (393.2385));(**9.2**): (m/z calc'd for $[M+H]^+$ (504.3796); found (504.3777)).

CDI coupling: CDI (0.105 g, 0.647 mmol) was added portionwise to a solution of Boc-5-aminoisophthalic acid (**7**) (0.100 g, 0.356 mmol) in DCM (50 ml) at room temperature and the mixture was stirred for 1 hour, then octylamine (0.084 g, 647 mmol) was added and the reaction mixture was stirred for another 24 hours. Another aliquot of Boc-5-aminoisophthalic acid (**7**) and CDI was added and the reaction was stirred for another 24 hours. The solvent was then removed. ESI-MS (**9.1**) (m/z calc'd for $[M+Na]^+$ (415.2209); found (415.2203)).

6.11 Ether tris-pillar[5]arene (10.3)

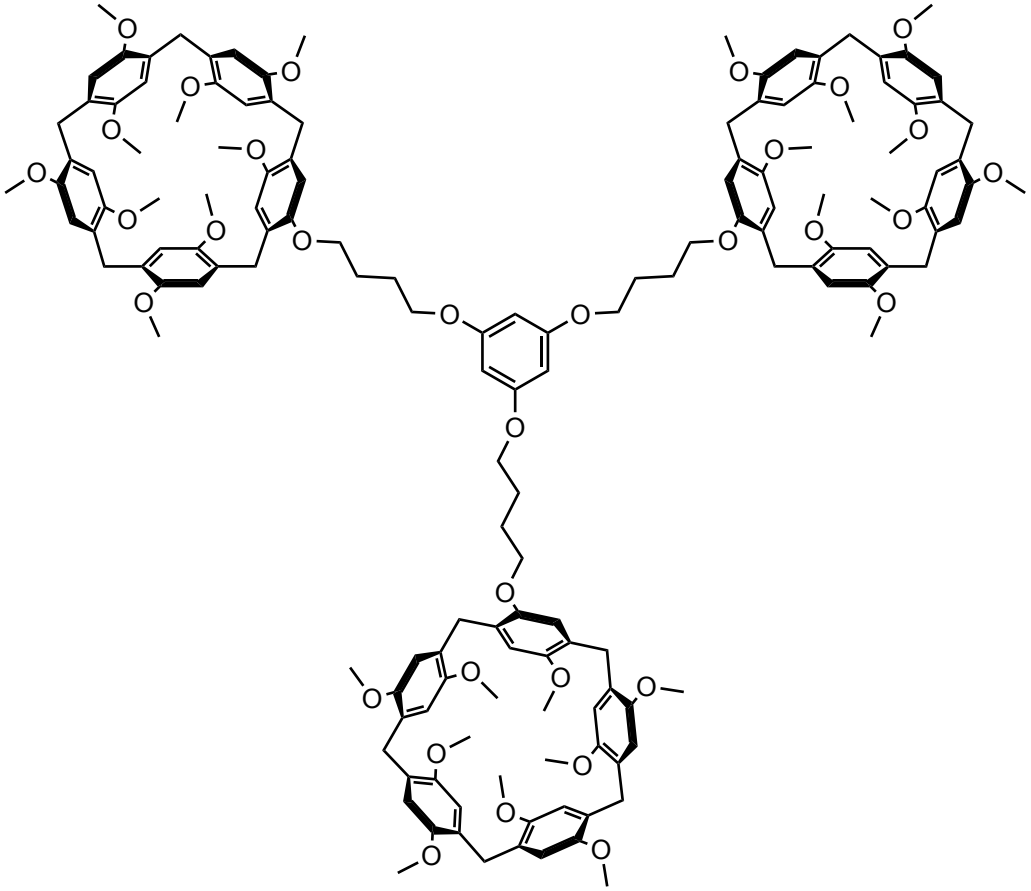

Attempt 1: 4-bromobutane-pillar[5]arene (**2**) (0.512 g, 0.588 mmol), phloroglucinol (0.024 g, 0.192 mmol) and potassium carbonate (0.158 g, 1.14 mmol) were mixed in DMF 50 ml at 80 °C for 48 h. The reaction mixture was then cooled and the solvent was removed under reduced pressure. The sticky oil was then extracted from CH_2Cl_2, water and brine then dried with magnesium sulfate. The solvent was again removed under reduced pressure to give

an orange solid, which was purified using flash column chromatography (silica, CH_2Cl_2) to give a white solid (40 mg) which was identified as a mixture of the mono- (**10.1**), di- (**10.2**), and tri-substituted (**10.3**) products as discussed in 2.2.5. Mono- (**10.1**): MALDI m/z calc'd for [M] (916.4034); found (916.450). Di- (**10.2**): MALDI m/z calc'd for [M] (1706.7751); found (1706.956). Tri- (**10.3**): MALDI m/z calc'd for [M] (2497.1468); found (2497.052).

Attempt 2: 4-bromobutane-pillar[5]arene (**2**) (0.502 g, 0.577 mmol), phloroglucinol (0.037 g, 0.294 mmol) and potassium carbonate (0.234 g, 1.69 mmol) were mixed in acetone (50 ml) at 70 °C for 6 d. The reaction mixture was then cooled and the solvent was removed under reduced pressure. The sticky oil was dissolved in CH_2Cl_2 and washed with water and brine then dried with magnesium sulfate. The solvent was again removed under reduced pressure to give an orange solid, which was purified using flash column chromatography (silica, CH_2Cl_2) to give a white solid (0.233 g, 0.0893 mmol, 31%) identified as the tri-substituted (**10.3**) product. ^{1}H NMR (400 MHz, Chloroform-d) δ 6.83 – 6.74 (m, 30H), 6.10 (s, 3H), 4.03 – 3.94 (m, 6H), 3.94 – 3.87 (m, 6H), 3.83 – 3.74 (m, 30H), 3.72 – 3.56 (m, 81H), 2.06 – 1.90 (m, 12H). ^{13}C NMR (101 MHz, Chloroform-d) δ 162.6, 160.9, 150.9, 150.8, 128.3, 128.2, 128.2, 128.2, 128.2, 114.2, 114.2, 114.1, 114.1, 67.6, 55.9, 55.8, 36.3, 29.7, 29.7, 29.5, 26.6, 26.4. MALDI m/z calc'd for [M] (2497.1468); found (2497.816).

6.12 Attempt at ether bis-pillar[5]arene analogue (11)

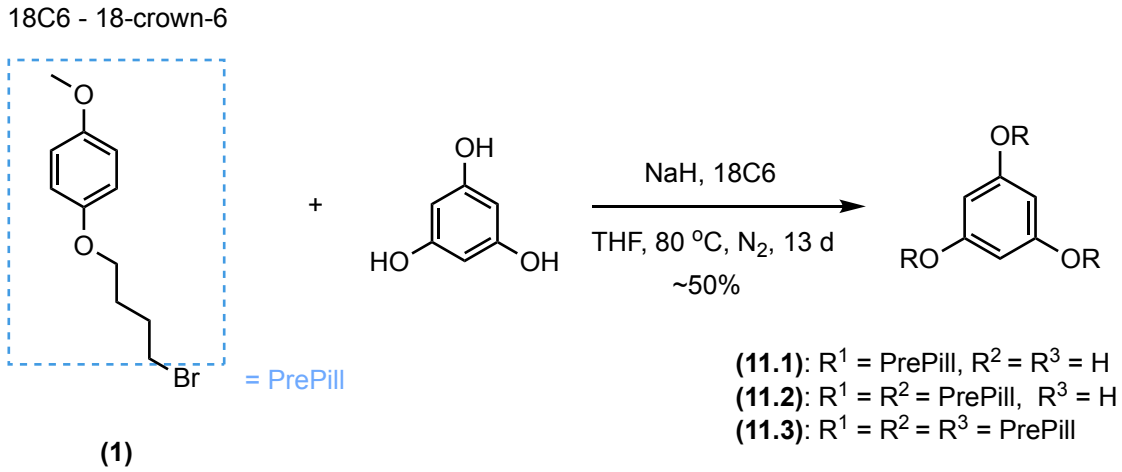

A flame dried flask was charged with phloroglucinol (41 mg, 323 mmol) and anhydrous THF (1.3 ml) under an atmosphere of N_2 at 0 °C. Sodium hydride 60 % dispersion in mineral

oil (10 mg, 0.250 mmol) was added, followed by (**1**) (102 mg, 0.388 mmol) and 18-crown-6 (1.00 mg, 0.00194 mmol). The reaction mixture was then refluxed at 80 °C for 13 days. An aliquot of this reaction mixture was removed and extracted from CH_2Cl_2 and water, concentrated and subjected to ^{1}H NMR to determine the conversion rate of 50% of starting material to products in lieu of a yield, as this reaction mixture was never purified. Mono- (**11.1**): ESI-HRMS m/z calc'd for $[M+Na]^+$ (327.1203); found (327.1215). Di- (**11.2**): ESI-HRMS m/z calc'd for $[M+Na]^+$ (505.2197); found (505.2207).

6.13 Benzonitrile-pillar[5]arene (12)

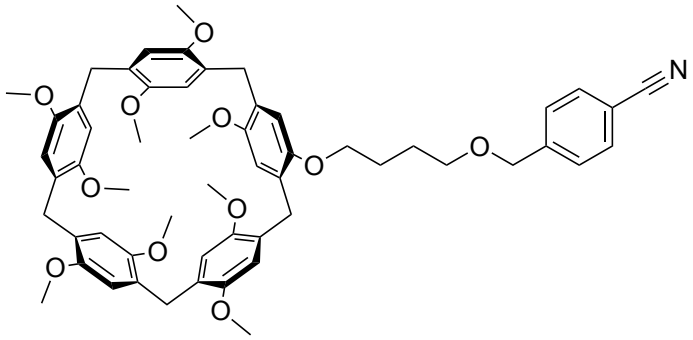

A flame dried flask was charged with 4-(hydroxymethyl)benzonitrile (66.0 mg, 0.551 mmol) dissolved in anhydrous THF (20 ml) from a departmental still, under an atmosphere of N_2 then cooled to 0°C. Sodium hydride (60 % dispersion in mineral oil) (26.0 mg, 1.10 mmol) was added to this solution and kept cool for 30 min. A solution of 4-bromobutane-pillar[5]arene (**2**) (200 mg, 0.229 mmol) dissolved in anhydrous THF (5 ml) was then added dropwise to the reaction mixture. The mixture was brought to reflux and left stirring overnight. The reaction mixture was then cooled, quenched with concentrated ammonium chloride (5 ml) and diethyl ether (5 ml), then washed with water and brine. It was then dried over sodium sulfate, concentrated *in vacuo* and purified using flash column chromatography (CH_2Cl_2) to give a colourless solid (50 mg, 0.054 mmol, 24%) ^{1}H NMR (400 MHz, Chloroform-d) δ 7.57 (d, J = 8.2 Hz, 2H), 7.42 (d, J = 8.0 Hz, 2H), 6.90 – 6.77 (m, 10H), 4.57 (s, 2H), 3.93 – 3.86 (m, 2H), 3.79 – 3.72 (m, 10H), 3.73 – 3.63 (m, 27H), 3.64 – 3.57 (m, 2H), 1.97 – 1.86 (m, 4H). ^{13}C NMR (101 MHz, Chloroform-d) δ 150.60, 150.58, 150.53, 149.71, 144.07, 132.22, 128.45, 128.38, 128.34, 128.32, 128.28, 128.21, 128.18, 127.62,

118.86, 114.62, 113.83, 113.79, 113.76, 113.73, 113.68, 113.65, 113.59, 111.23, 71.98, 70.74, 68.08, 55.77, 55.74, 55.68, 55.66, 55.56, 29.60, 29.54, 29.37, 29.32, 26.77, 26.67. ESI-HRMS m/z calc'd for $[M+H]^+$ (924.4317); found (924.4305).

6.14 3-butene-substituted pillar[5]arene (13)

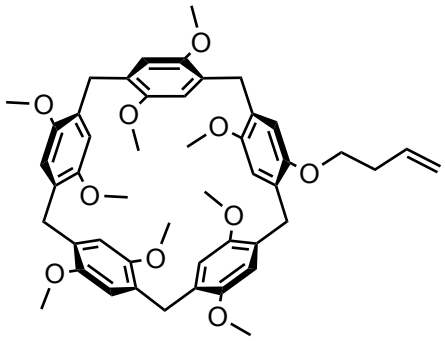

A mixture of 1-(but-3-en-1-yloxy)-4-methoxybenzene (**15**) (1.90 g, 10.7 mmol), dimethoxy benzene (13.5 g, 97.8 mmol) and formaldehyde (8.82 g, 293 mmol) was stirred inCH_2Cl_2 (700 ml) in an oven dried flask under N_2 for 10 min. Iron (III) chloride (2.56 g, 15.3 mmol) was then added to the reaction mixture which was left stirring at room temperature for 3h. The reaction was then quenched with water (700 ml). The organic phase was separated out and washed with water (300 ml) and brine (300 ml) then dry loaded onto silica. The mixture was purified using flash column chromatography (silica, CH_2Cl_2) to give a cream coloured solid which is a ∼20:80 mixture of 3-butene-substituted pillar[5]arene (**13**) and pillar[5]arene (**16**). This mixture was further repeatedly purified in combination with similar samples from repeated reactions using flash column chromatography (silica, CH_2Cl_2) to give a lightly cream coloured solid in approximately 20–30% yield over all reactions. ^{1}H NMR (400 MHz, Chloroform-d) δ 6.80 – 6.73 (m, 10H), 5.89 (ddt, J = 17.0, 10.1, 6.7 Hz, 1H), 5.15 – 4.97 (m, 2H), 3.88 (t, J = 6.6 Hz, 2H), 3.81 – 3.74 (m, 10H), 3.64 (dd, J = 4.3, 1.7 Hz, 28H), 2.48 (qt, J = 6.6, 1.5 Hz, 2H). ^{13}C NMR (101 MHz, Chloroform-d) δ 150.84, 150.82, 150.79, 149.94, 128.46, 128.30, 128.27, 128.23, 128.21, 128.20, 128.15, 115.15, 114.20, 114.15, 114.10, 114.07, 67.84, 55.85, 55.83, 55.79, 55.77, 55.75, 34.20, 29.72, 29.69, 29.65, 29.62. ESI-HRMS m/z calc'd for $[M+Na]^+$ (813.3609); found (813.3656). Crystal Data: orthorhombic, space group $Pna2_1$ (no. 33), a = 35.9157(3) Å, b = 12.0571(1) Å, c = 11.4426(1) Å, V = 4955.09(7) Å^3,

Z = 5, T = 120(10) K, μ(Cu Kα) = 0.637 mm^{-1}, D_{calc} = 1.164 g/cm^3, 87942 reflections measured (7.74° ≤ 2Θ ≤ 145.06°), 9751 unique (R_{int} = 0.0226, R_{sigma} = 0.0104) which were used in all calculations. The final R_1 was 0.0458 (I>=2u(I)) and wR_2 was 0.1314 (all data).

6.15 Attempts at nitrile-methoxybenzene (14)

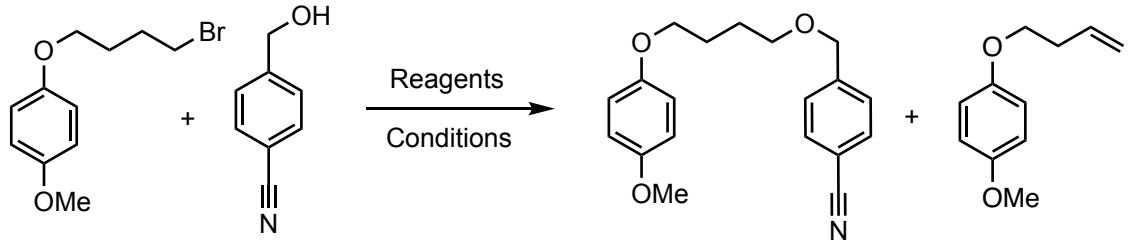

(1) **(14)** **(15)**

Summary of conditions

Attempt	Reagents	Conditions	Ratio of P:SP
A1	NaH,TBAI	Tolene, N_2, 80 °C	68:32
A2	NaH	THF/DMF, N_2, 80 °C	81:19
A3	NaH,18C6	THF, N_2, 80 °C	100:0
A4	KOH	AcN, N_2, 60 °C	49:51
A5	AgO	$CHCl_3$, N_2, 60 °C	N/A

Attempt 1: A flame dried flask was charged with sodium hydride 60 % dispersion in mineral oil (10 mg, 0.250 mmol) and anhydrous toluene (0.24 ml) under an atmosphere of N_2. This mixture was stirred for 15 min before adding 4-(hydroxymethyl)benzonitrile (58.0 mg, 0.484 mmol) dissolved in anhydrous toluene (0.24 ml). The reaction mixture was left stirring overnight then (**1**) (50.0 mg, 0.194 mmol) and TBAI (4.00 mg, 0.0100 mmol) dissolved in anhydrous toluene (0.8 ml) was added to it. The reaction mixture was refluxed at 80 °C for 17 hours. The solvent was then removed under reduced pressure.

Attempt 2: A flame dried flask was charged with 4-(hydroxymethyl)benzonitrile (58.0 mg, 0.484 mmol) and (**1**) (50.0 mg, 0.194 mmol) and anhydrous THF (5.4 ml) and DMF (1ml) under an atmosphere of N_2. This mixture was stirred at 0 °C and sodium hydride 60 % dispersion in mineral oil (10 mg, 0.250 mmol) was added to it. The reaction mixture was stirred at room temperature for 25 min then heated to reflux at 80 °C and left heating overnight. The solvent was then removed under reduced pressure.

Attempt 3: A flame dried flask was charged with 4-(hydroxymethyl)benzonitrile (58.0 mg, 0.484 mmol) and anhydrous THF (2 ml) under an atmosphere of N_2 at 0 °C. Sodium hydride 60 % dispersion in mineral oil (10 mg, 0.250 mmol) was added, followed by (**1**) (50.0 mg, 0.194 mmol) and 18-Crown-6 (1.00 mg, 0.00194 mmol). The reaction mixture was then refluxed at 80 °C overnight. The solvent was then removed under reduced pressure.

Attempt 4: A flask was charged with 4-(hydroxymethyl)benzonitrile (58.0 mg, 0.484 mmol), (**1**) (50.0 mg, 0.194 mmol) and potassium hydroxide (41.0 mg, 0.736 mmol) in acetonitrile (20 ml) and refluxed at 90 °C overnight under an atmosphere of N_2. The solvent was then removed under reduced pressure.

Attempt 5: A flame dried flask was charged with 4-(hydroxymethyl)benzonitrile (58.0 mg, 0.484 mmol), silver oxide (0.193 mg, 0.833 mmol), molecular sieves 3 Å(200 mg) and anhydrous chloroform (2 ml) under an atmosphere of N_2 . This mixture was stirred for an hour. A solution of (**1**) (50.0 mg, 0.194 mmol) in anhydrous chloroform (1 ml) was added to the reaction mixture over 30 min. The reaction mixture was then refluxed at 60 °C overnight. The solvent was then removed under reduced pressure.

6.16 1-(but-3-en-1-yloxy)-4-methoxybenzene (15)

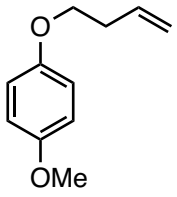

A mixture of 4-methoxyphenol (2.76 g, 22.2 mmol), 4-bromobut-1-ene (6.00 g, 44.4 mmol) and potassium carbonate (7.68 g, 55.5 mmol) in acetonitrile (50 ml) was refluxed in the dark for 3 days. The progression of the reaction was monitored using NMR and further aliquots of 4-bromobut-1-ene were added when it was no longer visible on NMR until a stable ratio of product to phenol starting material of ∼85:15 was achieved. The reaction mixture was cooled and the solids removed by filtration. The remaining reaction mixture was concentrated *in vacuo* and then purified using flash column chromatography (silica, 60:40 CH_2Cl_2: Cyclohexane gradually increased to 100%CH_2Cl_2) to give a colourless liquid (3.36

g, 18.9 mmol, 85%). ^{1}H NMR (400 MHz, Chloroform-d) δ 6.84 (d, J = 1.6 Hz, 4H), 5.91 (ddt, J = 17.0, 10.3, 6.7 Hz, 1H), 5.21 – 5.06 (m, 2H), 3.97 (t, J = 6.7 Hz, 2H), 3.77 (s, 3H), 2.52 (qt, J = 6.7, 1.4 Hz, 2H). ^{13}C NMR (101 MHz, Chloroform-d) δ 153.84, 153.06, 134.60, 116.92, 115.62, 114.64, 77.04, 67.95, 55.74, 33.79.

6.17 Alkene handcuff body (17)

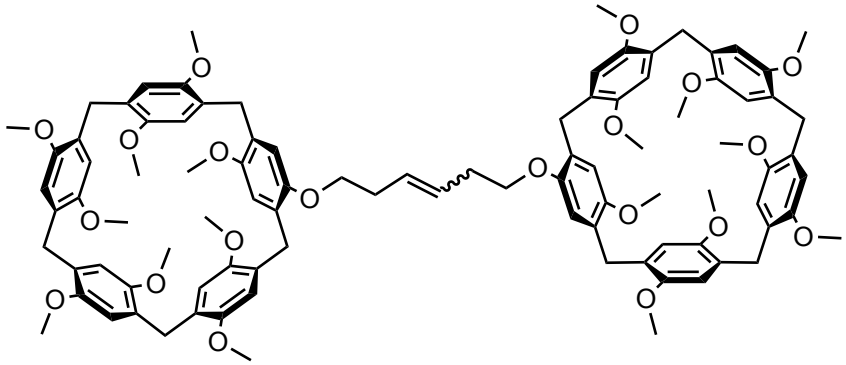

A solution of 3-butene-substituted pillar[5]arene (**13**) (500 mg, 0.633 mmol) in dry DCE (40 ml) was added to a flame dried microwave flask. The solution was then degassed with N_2 for 10 min. To the degassed solution HG-II (40.0 mg, 0.0638 mmol) was added under N_2. The reaction mixture was then irradiated with a CEM batch reactor at 110 °C for 90 min. The solvent was then removed *in vacuo* and the crude product was purified using flash column chromatography with a solvent gradient (silica, 100% CH_2Cl_2 gradually mixed to 2% Acetone in 98% CH_2Cl_2) to give a cream coloured powder (241 mg, 0.155 mg, 49%) . ^{1}H NMR (400 MHz, Chloroform-d) δ 6.88 – 6.69 (m, 20H), 6.04 – 5.62 (m, 2H), 3.93 – 3.80 (m, 4H), 3.82 – 3.70 (m, 20H), 3.71 – 3.55 (m, 54H), 2.69 – 2.45 (m, 4H). ^{13}C NMR (101 MHz, Chloroform-d) δ 150.77, 150.75, 149.90, 128.77, 128.52, 128.31, 128.28, 128.25, 128.22, 128.20, 128.18, 115.16, 114.12, 114.08, 114.04, 114.01, 113.99, 113.97, 68.29, 55.80, 33.31, 29.63. ESI-HRMS m/z calc'd for $[M+Na]^+$ (1575.7014); found (1575.6806).

6.18 N-(8-bromooctyl)phthalimide (18)

Potassium phthalimide (1.14 g, 6.12 mmol) and 1,8-dibromooctane (5.04 g, 18.4 mmol) was suspended in DMF (125 ml) and stirred overnight. The solvent was then removed under

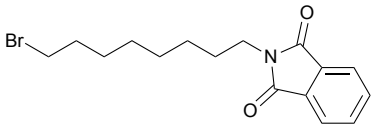

reduced pressure. The reaction mixture was then dissolved in EtOAc and washed with water, saturated NH_4Cl and brine. The organic fraction was reduced under pressure and frozen. The frozen liquid was then broken up into small pieces and filtered under reduced pressure and washed with cold hexane, which gave a white solid (1.32 g, 3.93 mmol, 64%). ^{1}H NMR (400 MHz, Chloroform-d) δ 7.83 (dd, J = 5.4, 3.0 Hz, 2H), 7.70 (dd, J = 5.4, 3.0 Hz, 2H), 3.67 (t, 2H), 3.38 (t, J = 6.9 Hz, 2H), 1.83 (p, J = 6.9 Hz, 2H), 1.71 – 1.62 (m, 2H), 1.47 – 1.24 (m, 8H). ^{13}C NMR (101 MHz, Chloroform-d) δ 168.48, 132.18, 132.17, 123.17, 37.99, 33.96, 32.74, 28.95, 28.59, 28.53, 28.06, 26.72. ESI-HRMS m/z calc'd for $[M+H]^+$ (338.0677); found (338.0750).

6.19 N-(8- imidazolyloctyl)phthalimide (19)

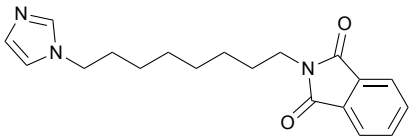

N-(8-bromooctyl)phthalimide (**18**) (1.00 g, 2.97 mmol), potassium carbonate (0.616 g, 4.46 mmol) and imidazole (0.405 g, 5.95 mmol) was suspended in DMF (10 ml) and stirred at 80 °C overnight. The reaction mixture was then filtered and the solvent was removed from the filtrate under reduced pressure. The crude product was purified using flash column chromatography (silica, CH_2Cl_2 with 2% MeOH) to give a white product (0.651 g, 2.00 mmol, 68%). ^{1}H NMR (400 MHz, Chloroform-d) δ 7.83 (dd, J = 5.4, 3.0 Hz, 2H), 7.70 (dd, J = 5.5, 3.0 Hz, 2H), 7.45 (s, 1H), 7.04 (s, 1H), 6.89 (s, 1H), 3.90 (t, J = 7.2 Hz, 2H), 3.67 (t, J = 7.3 Hz, 2H), 1.79 – 1.73 (m, 2H), 1.69 – 1.60 (m, 2H), 1.35 – 1.27 (m, 8H). ^{13}C NMR (101 MHz, Chloroform-d) δ 168.48, 137.07, 133.89, 132.16, 129.38, 123.18, 46.99, 37.93, 31.03, 28.88, 28.88, 28.48, 26.66, 26.45. ESI-HRMS m/z calc'd for $[M+H]^+$ (326.1790); found 326.1863.

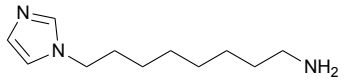

6.20 8-(1H-imidazol-1-yl)octan-1-amine (20)

N-(8- imidazolyloctyl)phthalimide (**19**) (0.502 g, 1.54 mmol) was dissolved in ethanol (20 ml) and refluxed with hydrazine monohydrate (0.467 g, 9.33 mmol) under an N_2 atmosphere overnight. The reaction mixture was then cooled and 4M HCl (6 ml) was added. This reaction mixture was refluxed for a further 6h. The formed solid was then filtered out, then the solution was concentrated under reduced pressure. The solution was basified with 2M NaOH and then extracted with CH_2Cl_2. The organic layer was dried with sodium sulfate and the solvent was removed under reduced pressure to afford a crude product, which was taken to the next step without purification (0.201 g, 1.03 mmol, 67 %). ^{1}H NMR (400 MHz, Chloroform-d) δ 7.46 (s, 1H), 7.05 (s, 1H), 6.89 (s, 1H), 3.91 (t, J = 7.1 Hz, 2H), 2.10 – 1.94 (m, 2H), 1.82 – 1.71 (m, 2H), 1.60 – 1.46 (m, 2H), 1.31 – 1.26 (m, 8H). The ^{13}C NMR was too contaminated to assign. ESI-HRMS m/z calc'd for $[M+H]^+$ (196.1735); found (196.1764).

6.21 Alkene handcuff rod (21)

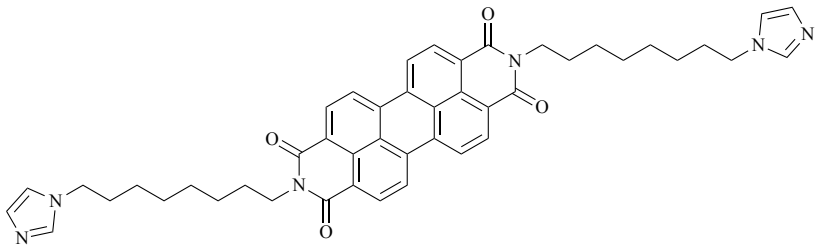

PTCDA (101 mg, 0.257 mmol) and 8-(1H-imidazol-1-yl)octan-1-amine (**20**) (100 mg, 0.512 mmol) were mixed in DMF (7 ml) under N_2. The reaction mixture was heated at 160 °C overnight. It was then cooled, filtered and the solid was washed with acetone to give (125 mg, 0.167 mmol, 65%) of the red product. ^{1}H NMR (400 MHz, Chloroform-d) δ 8.65 (d, J = 7.9 Hz, 4H), 8.57 (d, J = 8.1 Hz, 4H), 7.47 (s, 2H), 7.05 (d, J = 1.1 Hz, 2H), 6.91 (t, J = 1.3 Hz, 2H), 4.19 (t, J = 7.7 Hz, 4H), 3.93 (t, J = 7.2 Hz, 4H), 1.77 (h, J = 8.5, 8.0 Hz, 8H), 1.47 – 1.29 (m, 16H). MALDI m/z calc'd for [M] (746.358); found (746.539).

6.22 2,4,6- trimethylbenzyl iodide (22)

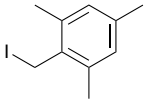

Mesitylmethanol (1.02 g, 6.65 mmol) was dissolved in dry dioxane (10 ml). To this solution potassium iodide (1.10 g, 6.65 mmol) and $BF_3.Et_2O$ (0.945 g, 6.65 mmol) were added. The reaction mixture was stirred at room temperature in the dark for 4h. The reaction mixture was then quenched with ice water and extracted with diethyl ether. The organic layer was then dried over anhydrous magnesium sulfate and the solvent was removed under reduced pressure. The crude product was purified using distillation to give (1.23 g, 4.75 mmol, 71%) of pale yellow product. ^{1}H NMR (400 MHz, Chloroform-d) δ 6.85 (s, 2H), 4.53 (d, J = 38.5 Hz, 2H), 2.36 (d, J = 12.7 Hz, 6H), 2.27 (d, J = 3.7 Hz, 3H). ^{13}C NMR (101 MHz, Chloroform-d) δ 137.83, 136.83, 129.42, 21.09, 19.26, 3.95.

6.23 Alkene handcuff (23)

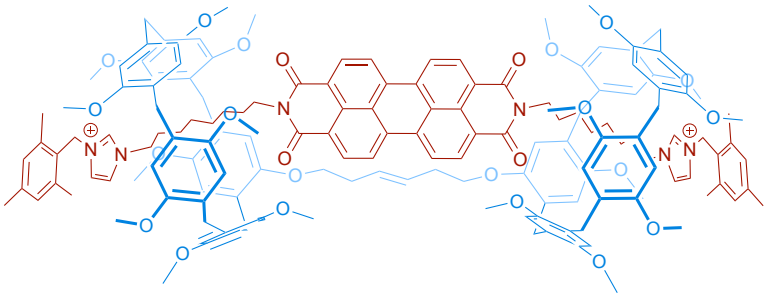

A solution of the alkene handcuff body (**17**) (100 mg, 0.0644 mmol) and the handcuff rod (**21**) (51.0 mg, 0.0683 mmol) was prepared in a minimum amount of chloroform (∼5 ml) and was alternately heated and sonicated to ensure maximum saturation. The chloroform was replenished if necessary. The solution was then cooled at -10 °C for half an hour before 2,4,6-trimethylbenzyl iodide (**22**) (42.0 mg, 0.162 mmol) was added in the absence of light. The reaction mixture was then stirred in the dark and allowed to slowly reach room temperature then left to continue for 3 days. The solvent was then removed *in vacuo*. The resulting red solid was dissolved in hot ethanol (125 ml) to which ammonium hexafluorophosphate (101 mg, 620 mmol) was added. The mixture was allowed to cool, forming red precipitate.

The precipitate was compacted on a centrifuge and the solvent decanted. The solid was then suspended in methanol (125 ml), the mixture sonicated, centrifuged and the solvent decanted three more times before being dried and giving a red solid. This crude product (57.0 mg, 0.0200 mmol, 31%) was purified using column chromatography (silica, chloroform, gradually mixed to 15% methanol in chloroform) to give a red solid (0.0140 mg, 0.00491 mmol, 8%). ^{1}H NMR (400 MHz, Chloroform-d) δ 8.78 – 8.13 (m, 10H), 7.20 (s, 2H), 7.04 (s, 4H), 6.95 – 6.59 (m, 20H), 6.07 – 5.88 (m, 2H), 5.85 – 5.60 (m, 2H), 5.57 – 5.41 (m, 4H), 4.26 (s, 4H), 3.99 – 3.40 (m, 78H), 2.96 – 2.56 (m, 4H), 2.39 (d, J = 13.1 Hz, 18H), 1.81 (s, 4H), 1.42 (s, 4H), 1.03 (s, 4H), 0.48 (s, 4H), 0.25 (s, 4H), -0.81 (s, 4H), -1.66 (s, 4H). ^{13}C NMR (101 MHz, Chloroform-d) δ 163.34, 162.86, 151.24, 150.68, 150.34, 140.18, 138.18, 138.01, 133.66, 132.13, 131.39, 130.11, 130.01, 129.09, 128.91, 128.26, 125.39, 123.31, 121.38, 116.05, 115.04, 114.07, 113.94, 113.64, 68.32, 58.50, 58.01, 55.75, 55.53, 47.94, 47.41, 40.55, 33.71, 31.94, 30.79, 30.18, 29.38, 29.09, 28.84, 28.21, 27.83, 26.72, 25.96, 25.44, 21.17, 21.04, 19.56, 19.51. ESI-HRMS m/z calc'd for $[M]^{2+}$ (1283.1380); found (1283.1322).

A Appendix

A.1 Index

An index connecting all of the compounds synthesised in this work with the data obtained for each. Some data is not available (N/A) for some compounds.

Compound No	Scheme	Experimental Section	NMR	MS	Other
(1)	2.1	6.2. Lit.[79]	A.1, A.2	N/A	
(2)	2.1	6.3. Lit.[49]	A.3, A.4	6.3	
(3)	2.2	6.4. Lit.[84–87]	A.5, A.6, A.7	N/A	
(4)	2.3	6.5. Lit.[84–87]	A.8, A.9	6.5	
(5)	2.4	6.6. Lit.[97]	A.10, A.11	N/A	
(6)	2.4	6.7. Lit.[97]	A.12, A.13	6.7	
(7)	2.5	6.8. Lit.[98]	A.14, A.15	6.8	
(8)	2.5	6.9. Lit.[263]	A.16	2.5	
(9)	2.6	6.10. Lit.[99,263]	A.17	6.9	
(10)	2.7	6.11. Lit.[103–105]	A.18, A.19	2.9	
(11)	2.8	6.12.	2.11	6.12	
(12)	3.1	6.13. Lit.[134]	A.20, A.21	6.13	
(13)	3.5	6.14. Lit.[49]	A.24, A.25, A.27	6.14	CV: 3.5, SW: 3.6, SEC: 3.7, EPR: 3.8, XRC: 3.9
(14)	3.2	6.15. Lit.[116,137–140]	3.3	N/A	
(15)	3.5	6.16. Lit.[79]	A.22, A.23	N/A	
(16)	1.15	N/A Lit.[44]	A.26	N/A	CV, SW: A.45, SEC, EPR: A.46
(17)	3.6	6.17. Lit.[155]	A.28, A.29, A.30	6.17	CV: 3.10, SW: 3.11
(18)	3.7	6.18. Lit.[126]	A.31, A.32	6.18	
(19)	3.7	6.19. Lit.[126]	A.33, A.34	6.19	
(20)	3.7	6.20. Lit.[126]	A.35, A.36	6.20	
(21)	3.7	6.21. Lit.[126]	A.37, A.38	6.21	
(22)	3.8	6.22. Lit.[126]	A.39, A.40	N/A	
(23)	3.8	6.23. Lit.[39]	A.41, A.42, A.43, A.44	3.8	UV: 3.14, CV: 3.15
(24)	3.8	6.23. Lit.[39]	N/A	N/A	CV, SW: 3.17
(25)	1.11	N/A Lit.[40]	N/A	N/A	CV, SW: 3.17

A.2 NMR Peak ratio calculation

This ^{1}H NMR spectrum is a mixture of compound A and compound B in the stroichiometric ratio of x parts A to y parts B. Let us identify two peaks in the ^{1}H NMR spectrum with integrations I_1 and I_2, which respectively are present solely in compound A and compound B and not in both. Furthermore, the number of hydrogens contributing to peak 1's integration due to compound A is H_{A1} while peak 2's integration is influenced by H_{B2} hydrogens from B.

We can then infer that

$$I_1 \propto xH_{\mathrm{A1}}\,,$$
$$I_2 \propto yH_{\mathrm{B2}}\,.$$

Which we can combine to produce

$$\frac{x}{y} = \frac{I_1 H_{\mathrm{B2}}}{I_2 H_{\mathrm{A1}}}\,. \tag{2}$$

Denoting $r = x/y$ we can then find the percentage of the mixture which is A and B as

$$\text{Percentage of A} = \frac{100x}{x+y} = \frac{100r}{1+r}\,,$$
$$\text{Percentage of B} = \frac{100y}{x+y} = \frac{100}{1+r}\,,$$

and a ratio in terms of A:B as

$$\frac{100r}{1+r} : \frac{100}{1+r} \tag{3}$$

A.3 ^{1}H NMR spectra

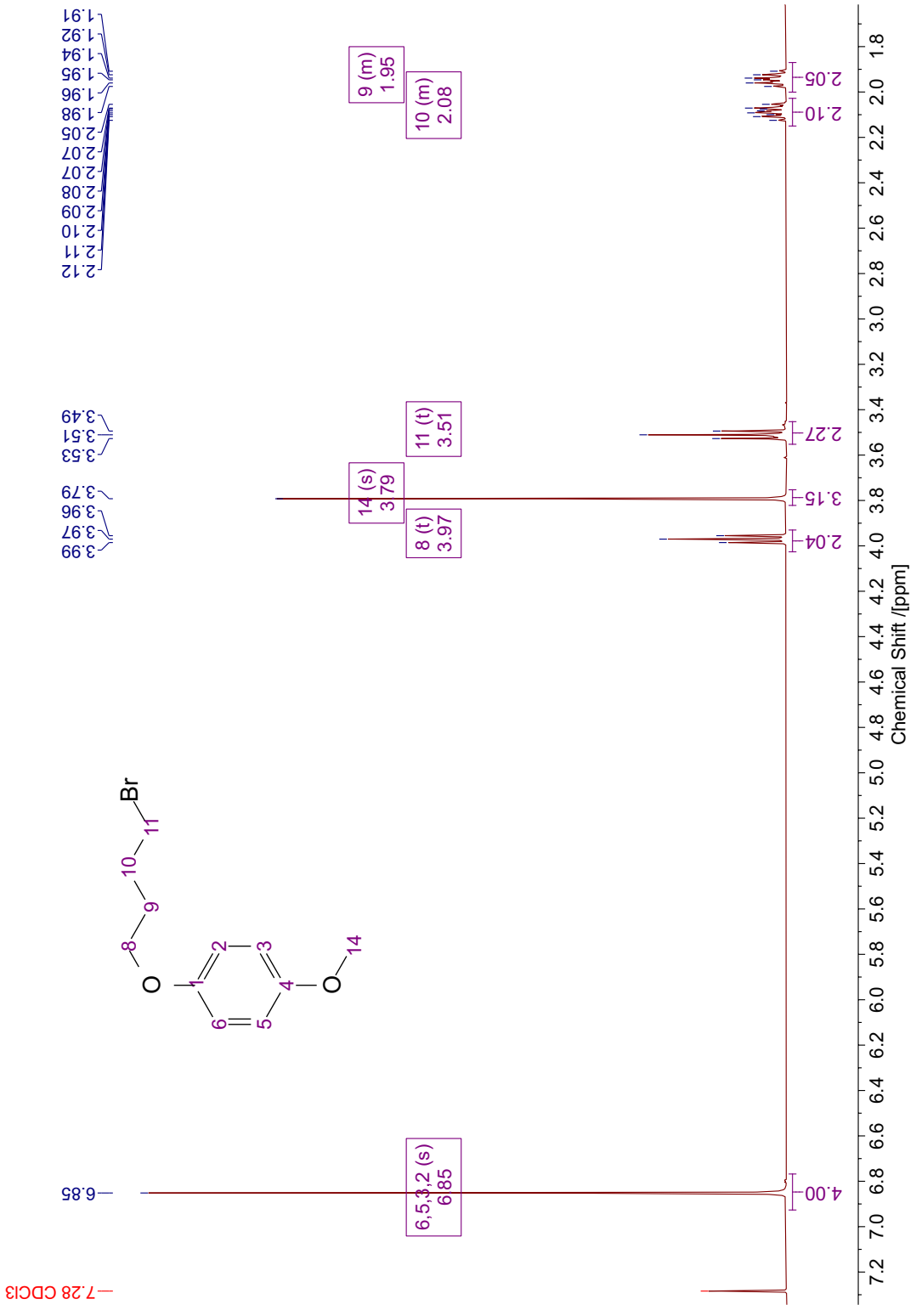

Figure A.1: ^{1}H NMR spectrum of 1-(4-bromobutoxy)-4-methoxybenzene (**1**).

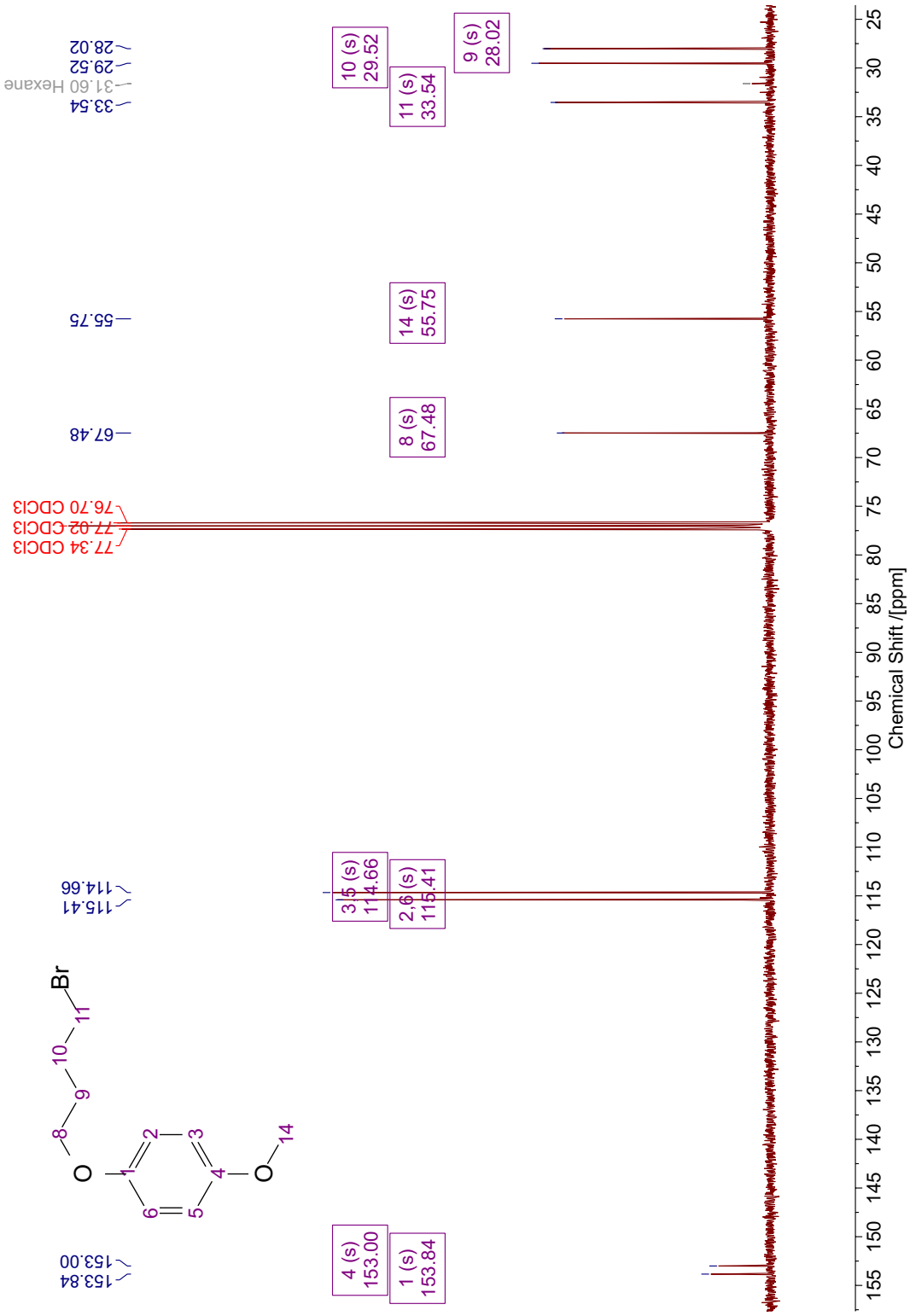

Figure A.2: ^{13}C NMR spectrum of 1-(4-bromobutoxy)-4-methoxybenzene (**1**).

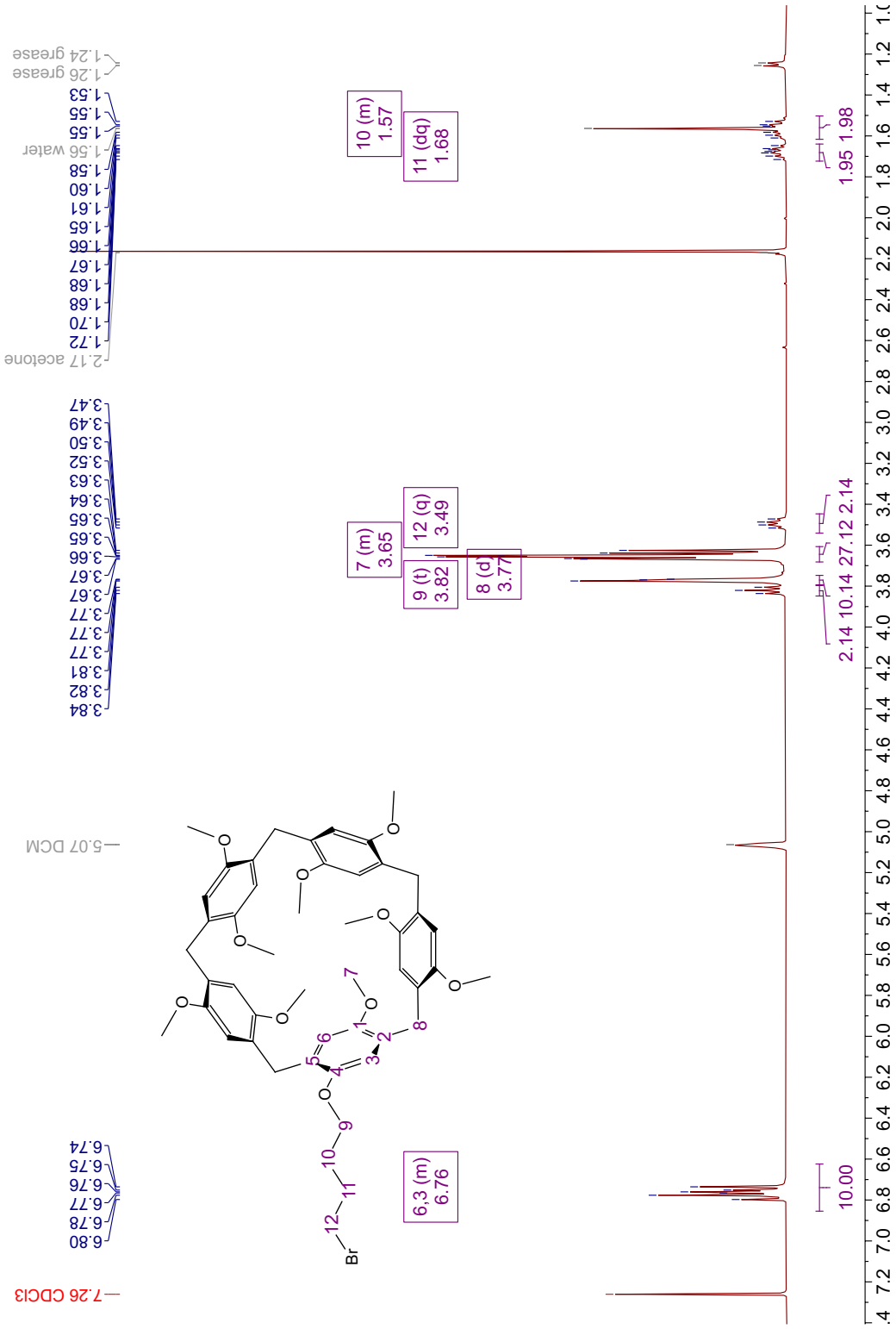

Figure A.3: ^{1}H NMR spectrum of 4-bromobutane-pillar[5]arene (**2**).

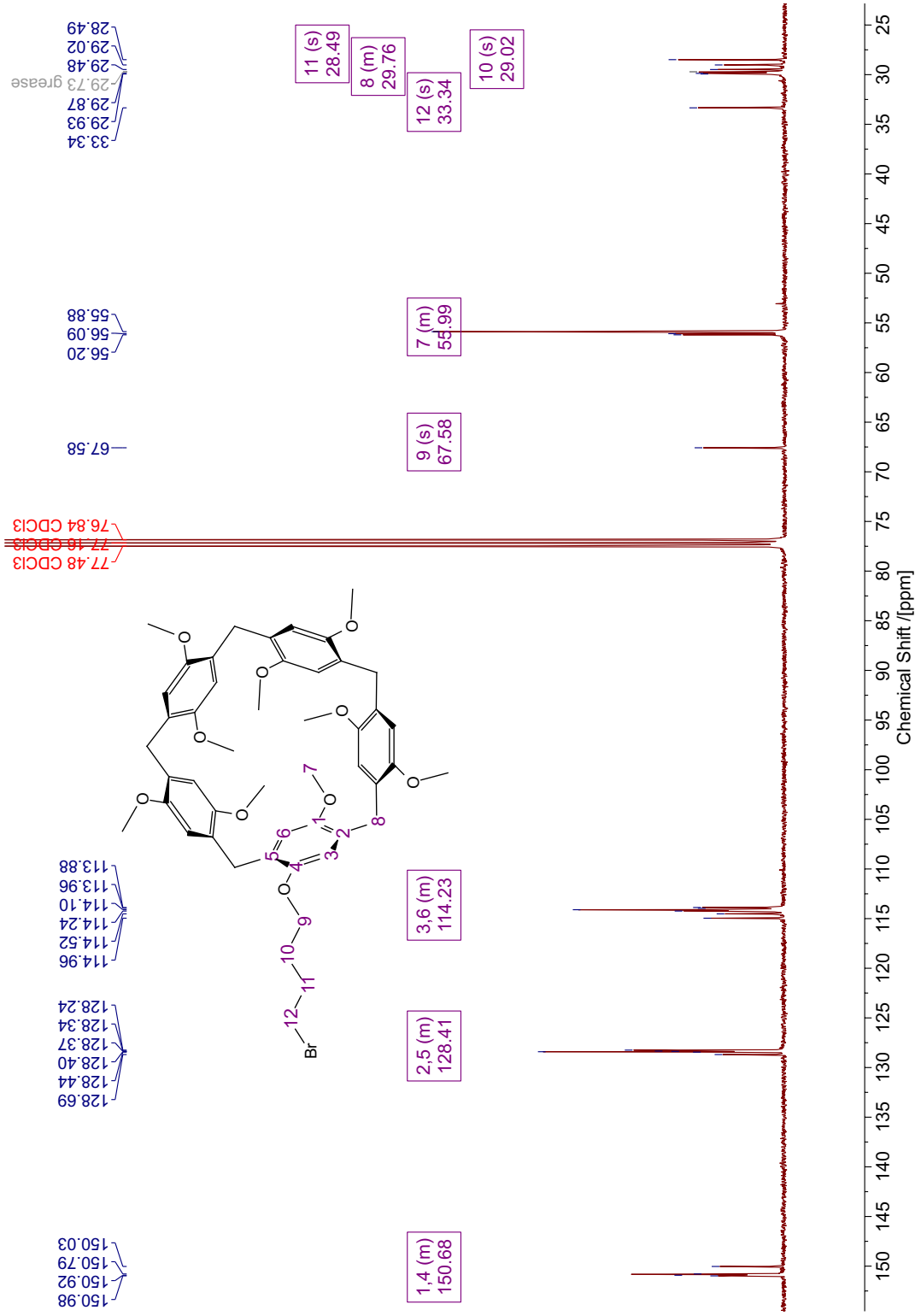

Figure A.4: ^{13}C NMR spectrum of 4-bromobutane-pillar[5]arene (**2**).

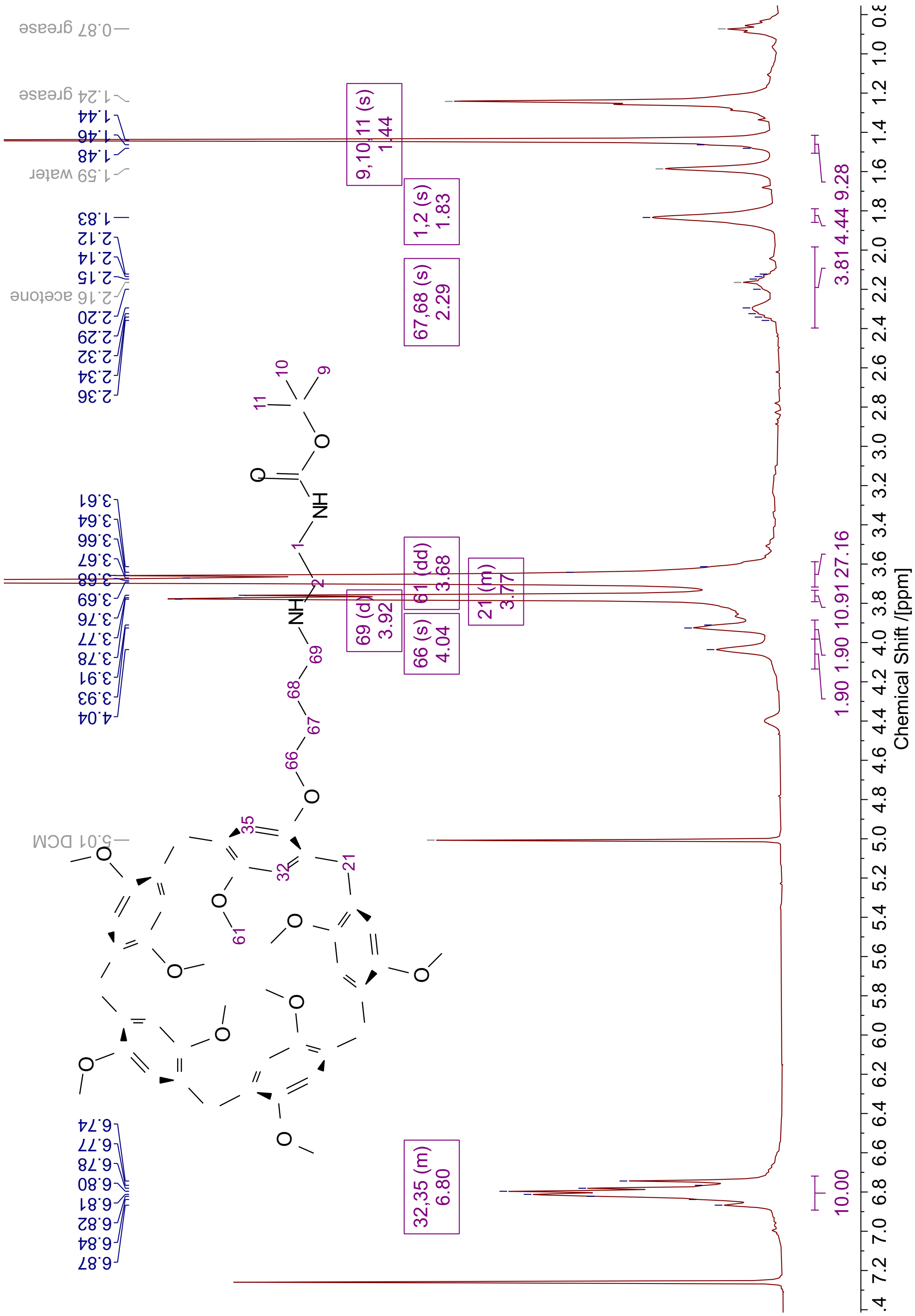

Figure A.5: ^{1}H NMR spectrum of *N*-Boc-ethylenediaminobutane-pillar[5]arene (**3.1**).

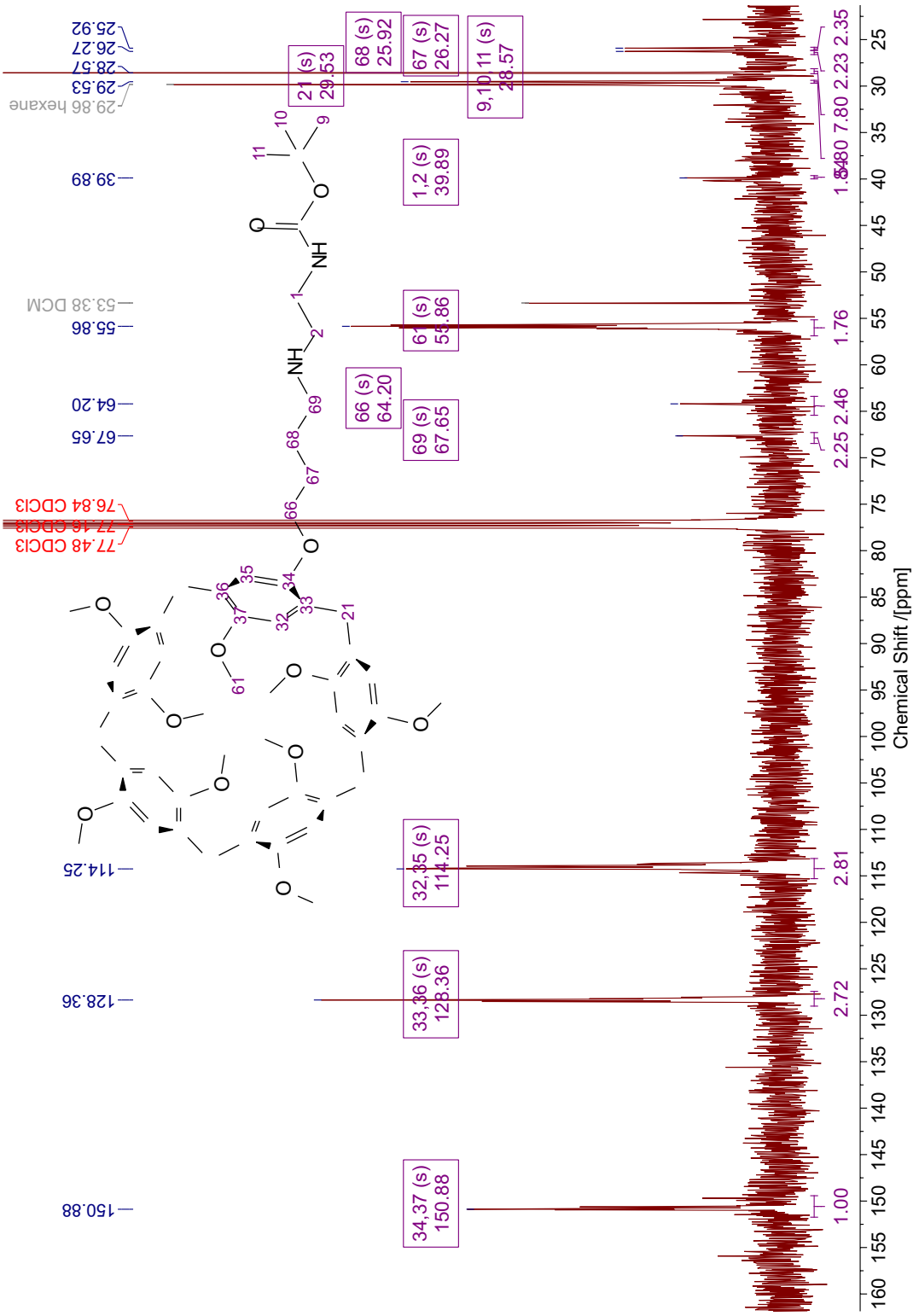

Figure A.6: ^{13}C NMR spectrum of *N*-Boc-ethylenediaminobutane-pillar[5]arene (**3.1**).

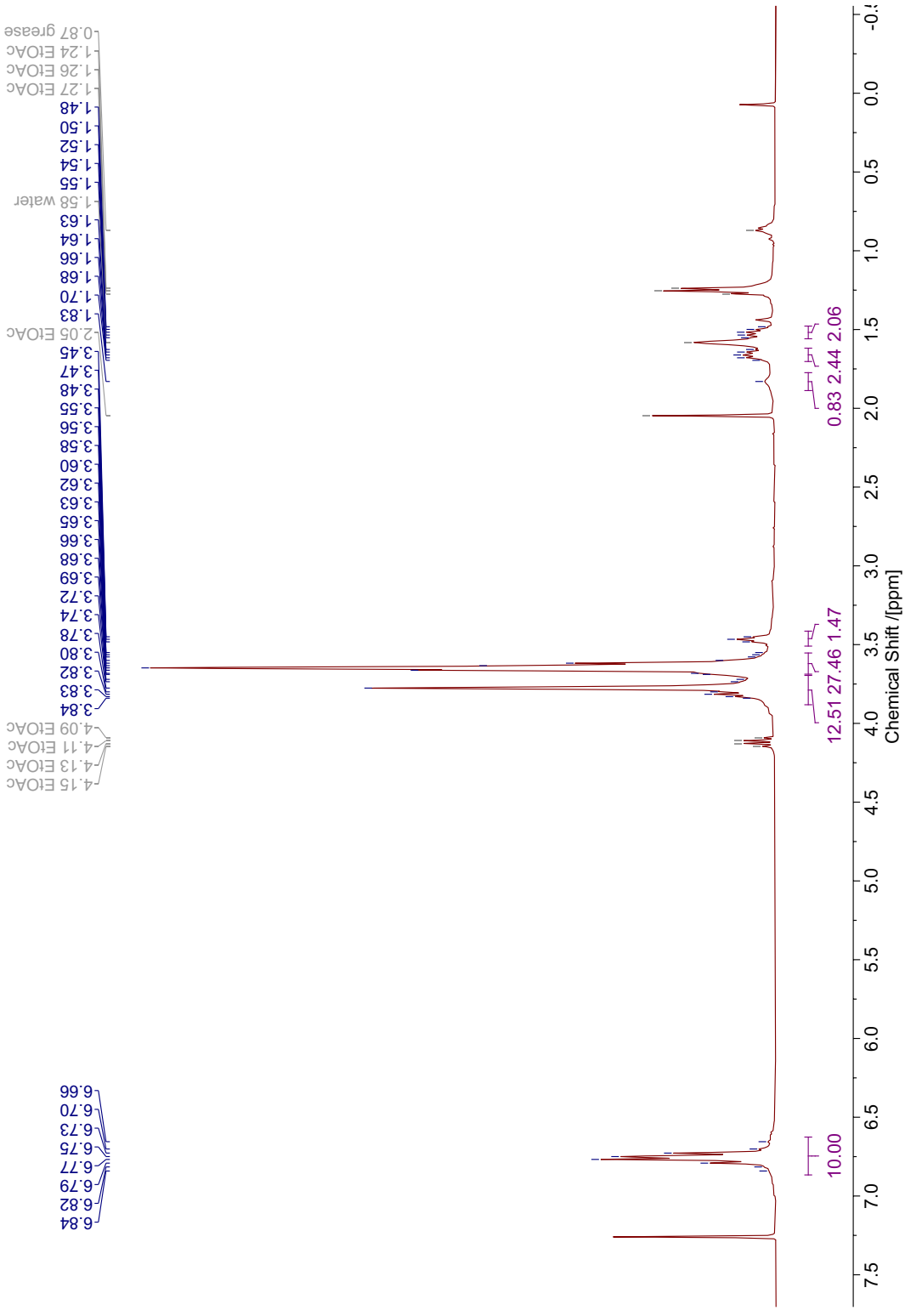

Figure A.7: ^{1}H NMR spectrum of *N*-Boc-ethylenediaminobutane-pillar[5]arene (**3.1**) after its decomposition.

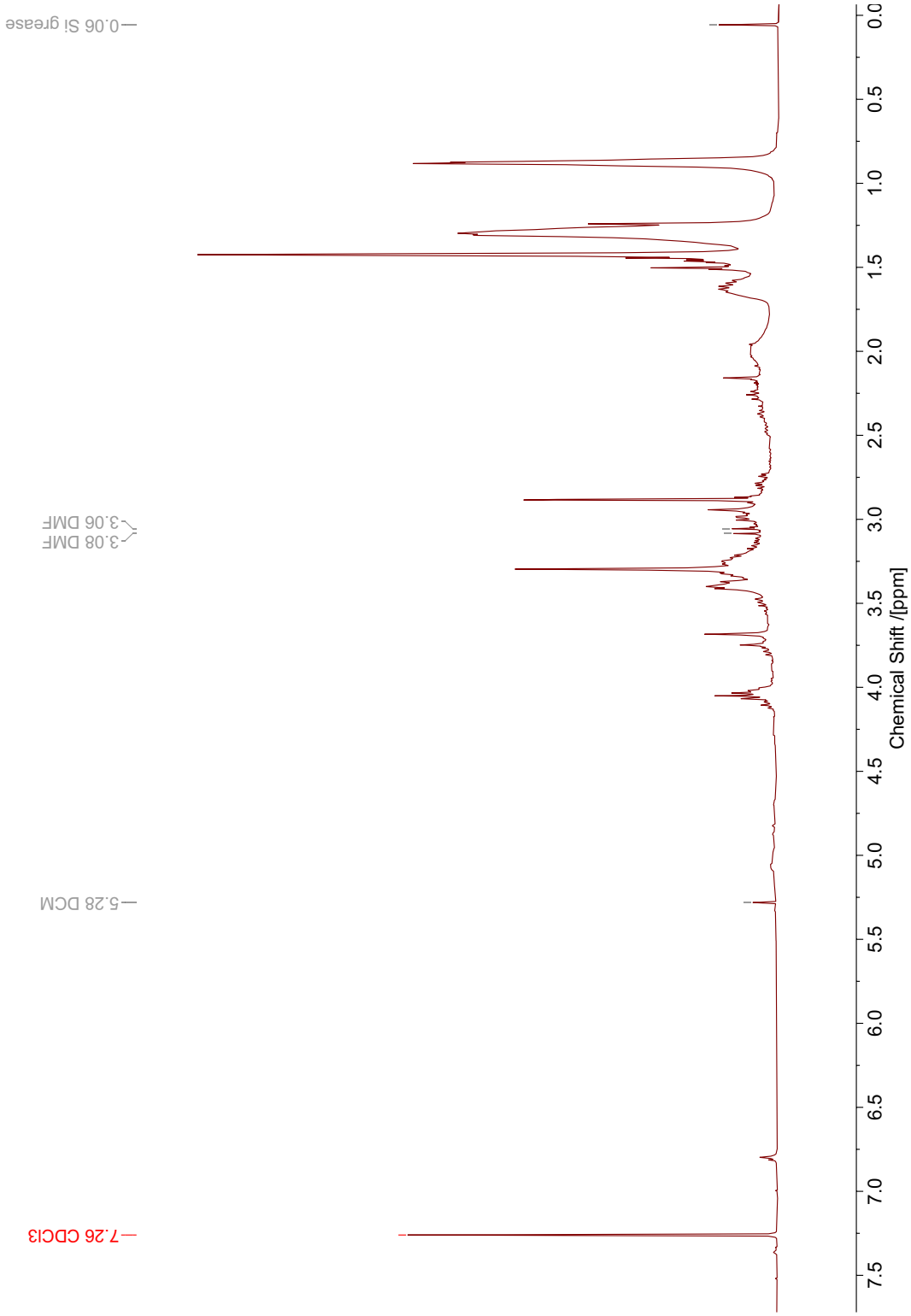

Figure A.8: ^{1}H NMR spectrum of tthe attempt at N -Boc-ethylenediamino-bis-hexane (**4**).

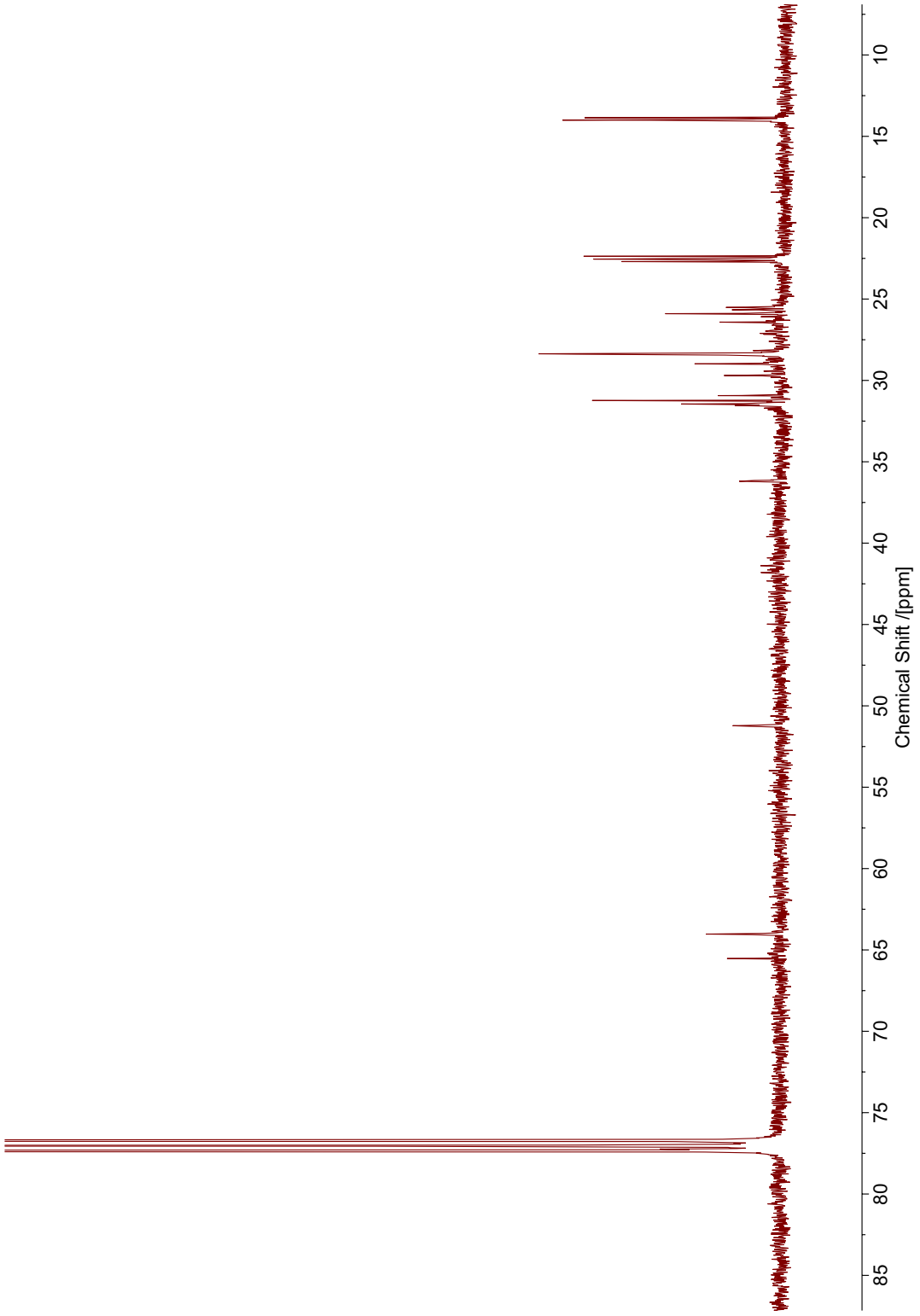

Figure A.9: ^{13}C NMR spectrum of the attempt at N -Boc-ethylenediamino-bis-hexane (**4**).

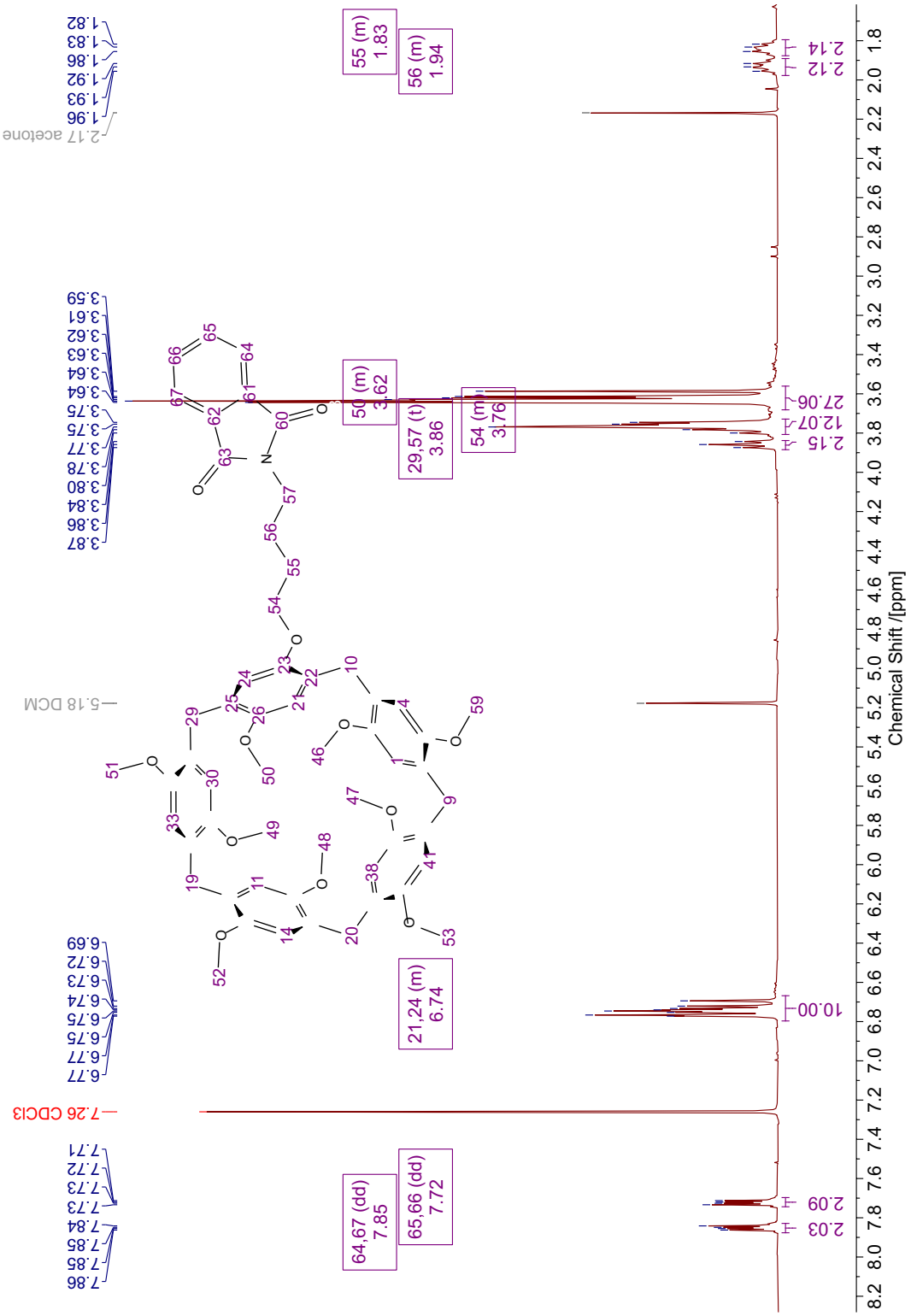

Figure A.10: ^{1}H NMR spectrum of 4-phthalimidobutane-pillar[5]arene (**5**).

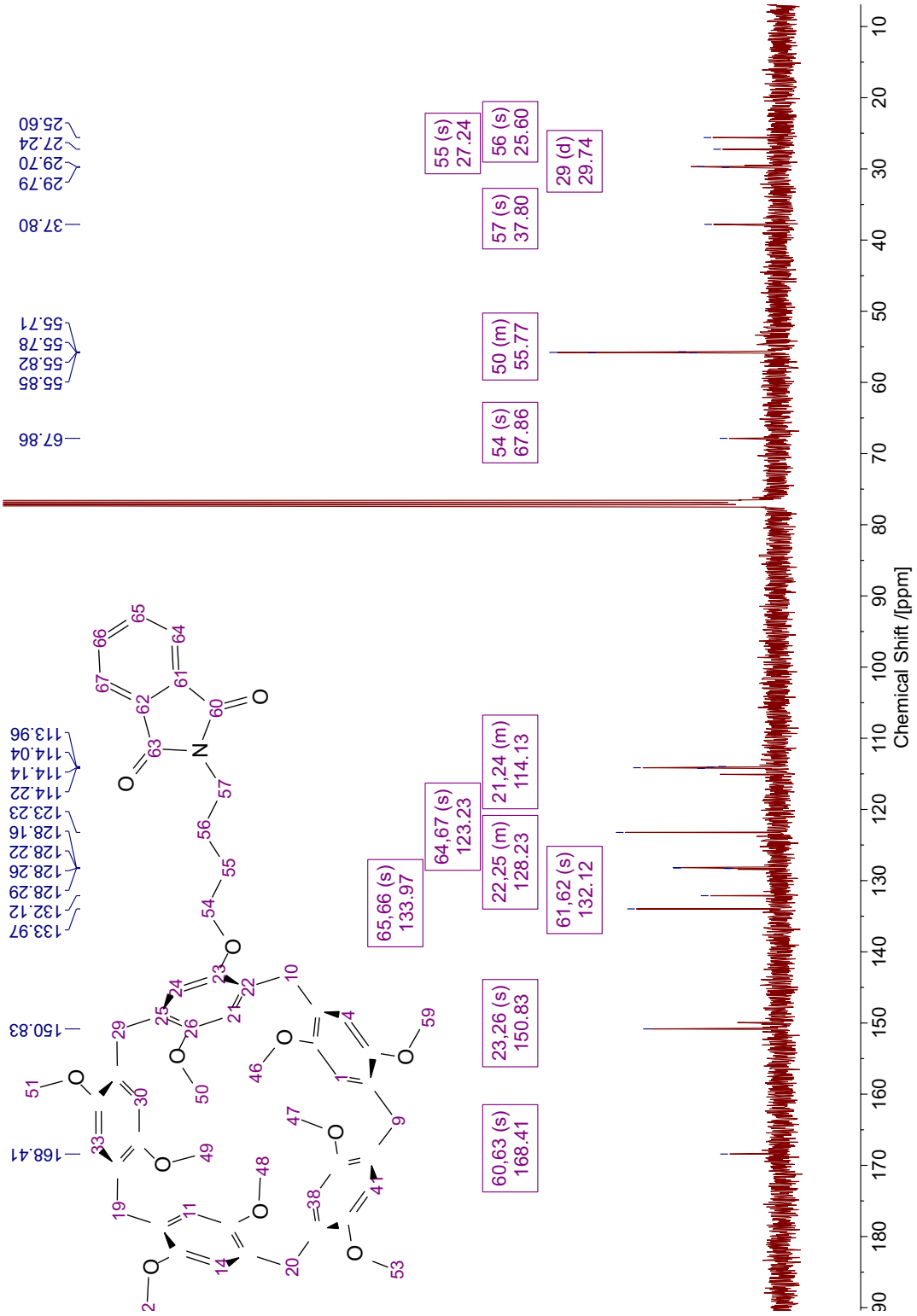

Figure A.11: ^{13}C NMR spectrum of 4-phthalimidobutane-pillar[5]arene (**5**).

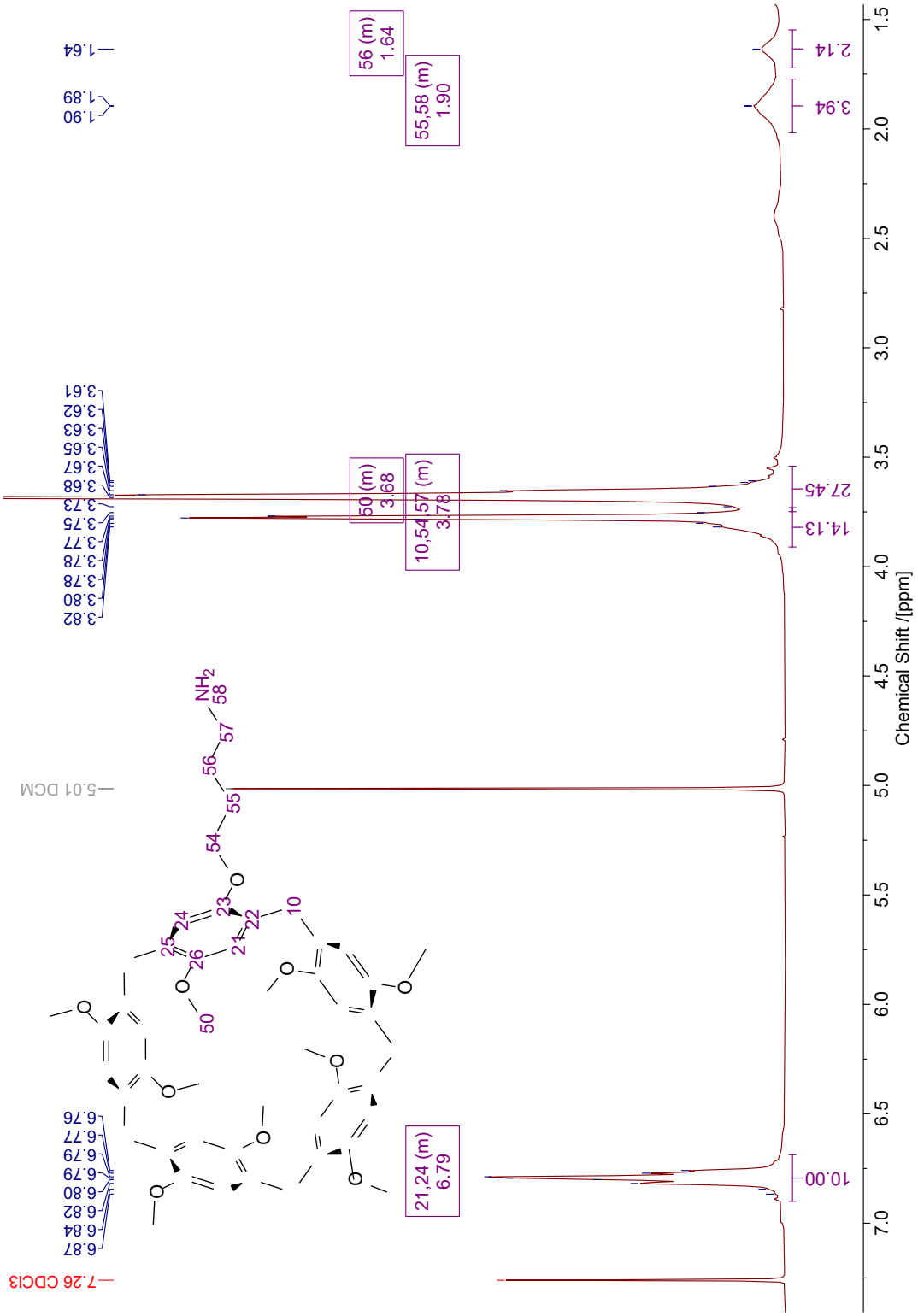

Figure A.12: ^{1}H NMR spectrum of 4-aminobutane-pillar[5]arene (**6**).

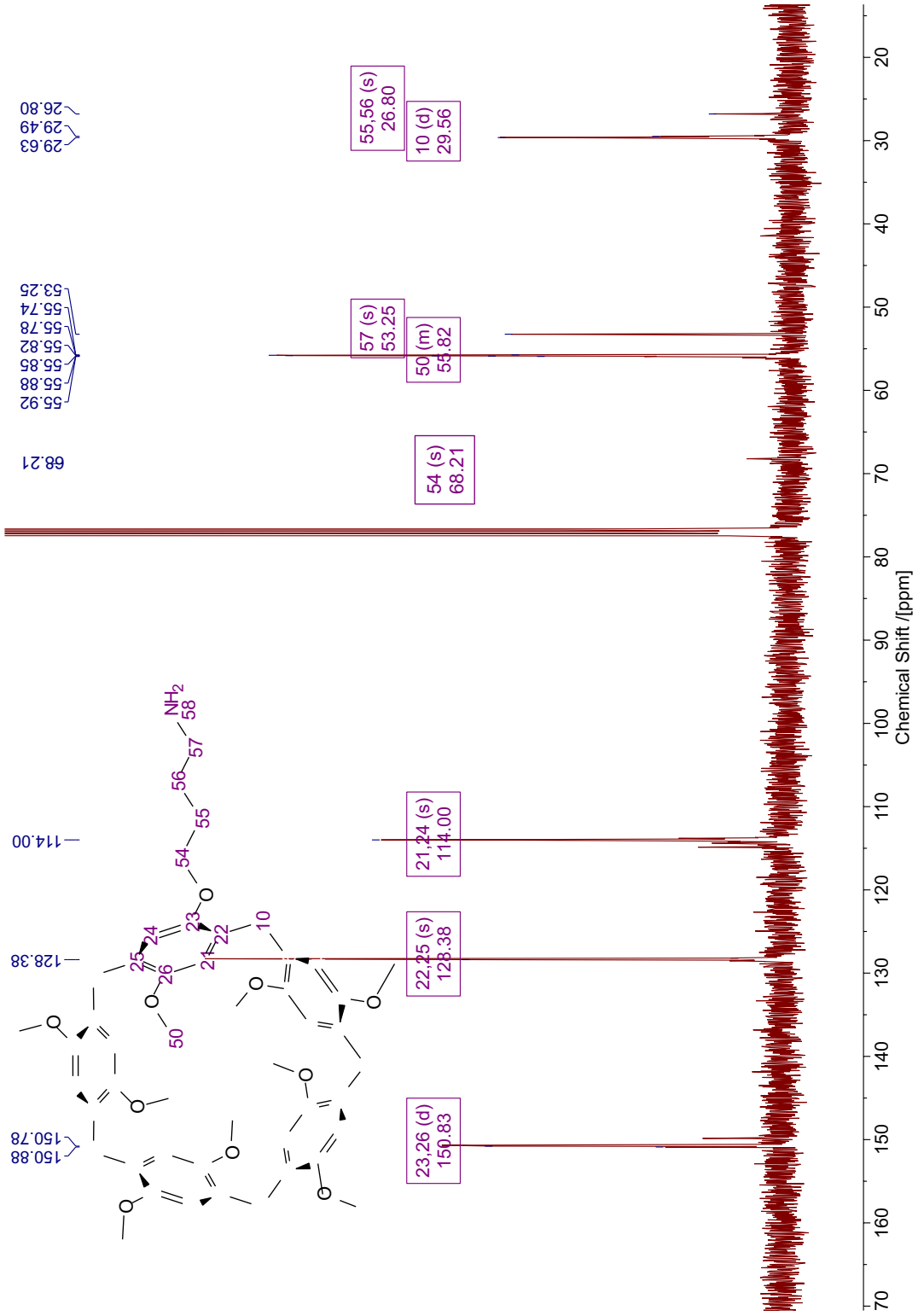

Figure A.13: ^{13}C NMR spectrum of 4-aminobutane-pillar[5]arene (**6**).

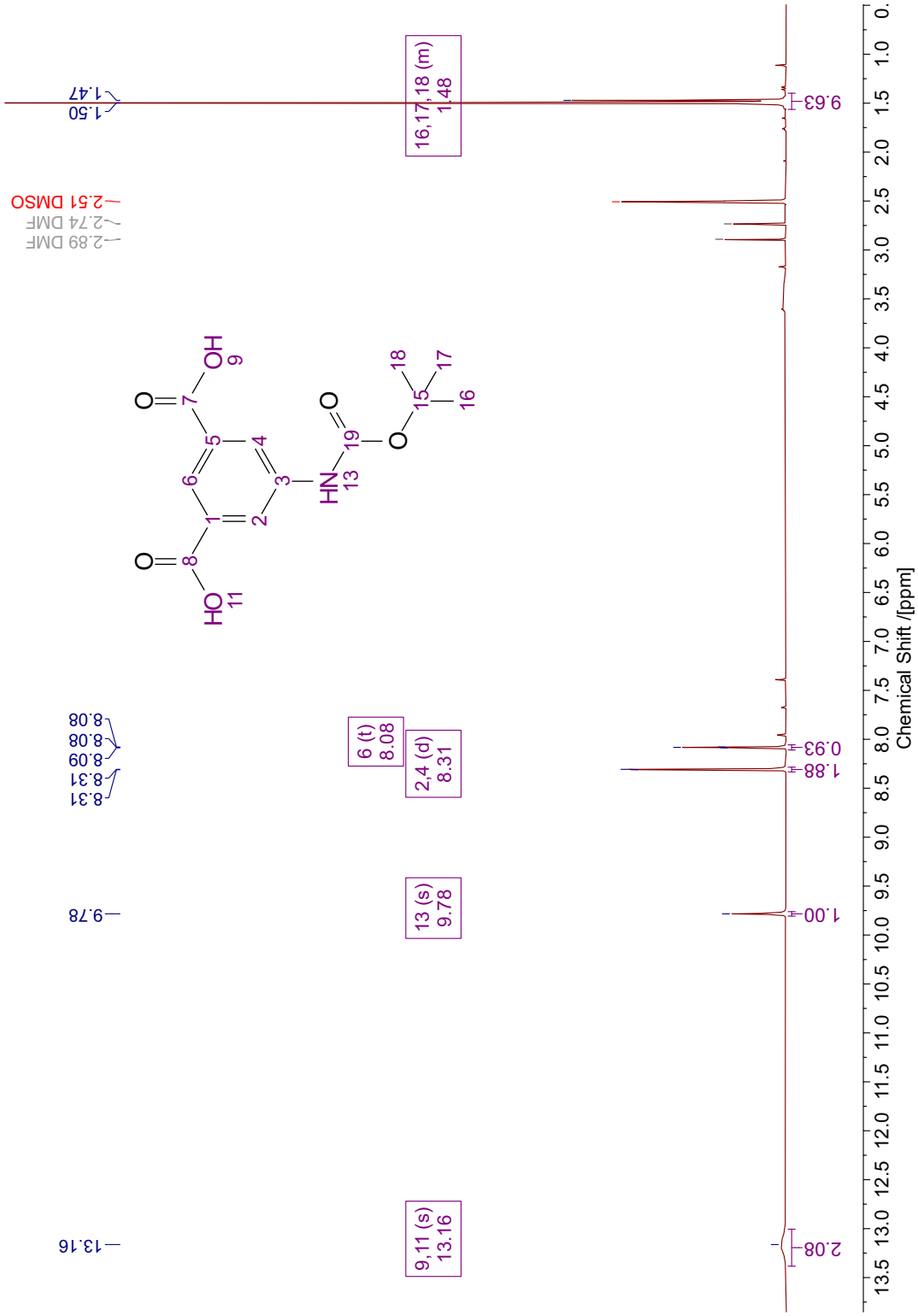

Figure A.14: ^{1}H NMR spectrum of Boc-5-aminoisophthalic acid (**7**).

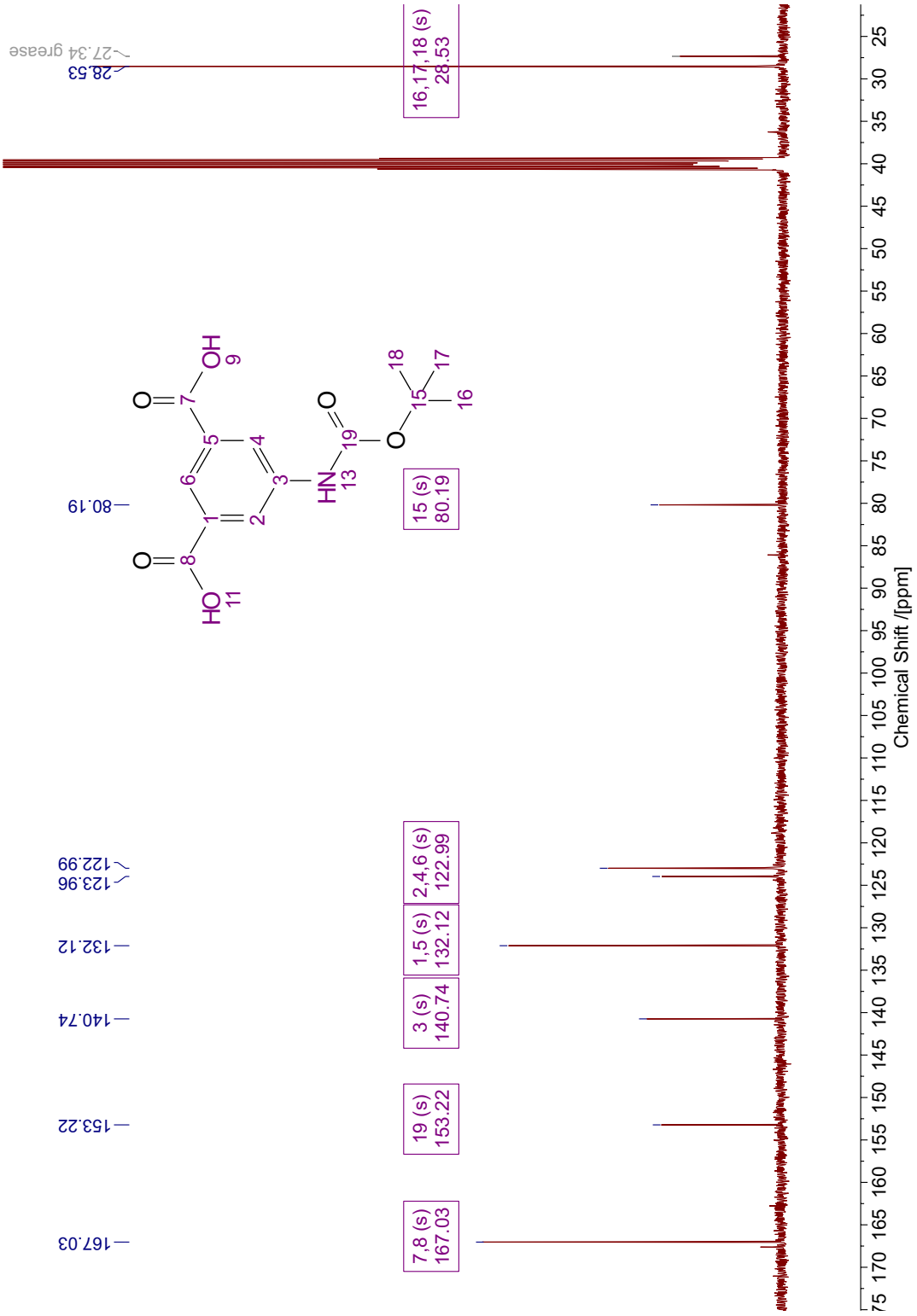

Figure A.15: ^{13}C NMR spectrum of Boc-5-aminoisophthalic acid (**7**).

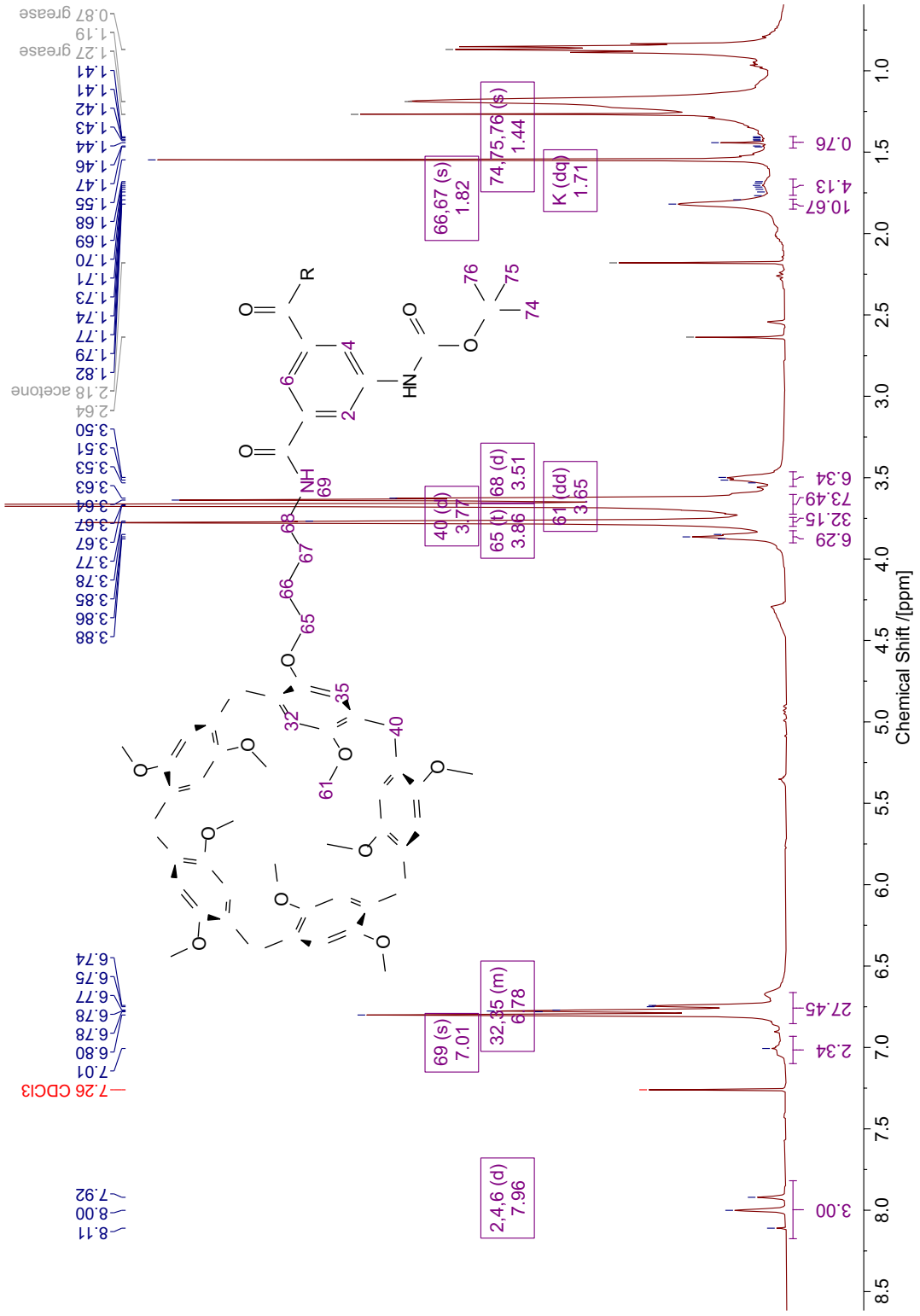

Figure A.16: ^{1}H NMR spectrum of amido bis-pillar[5]arene (**8**).

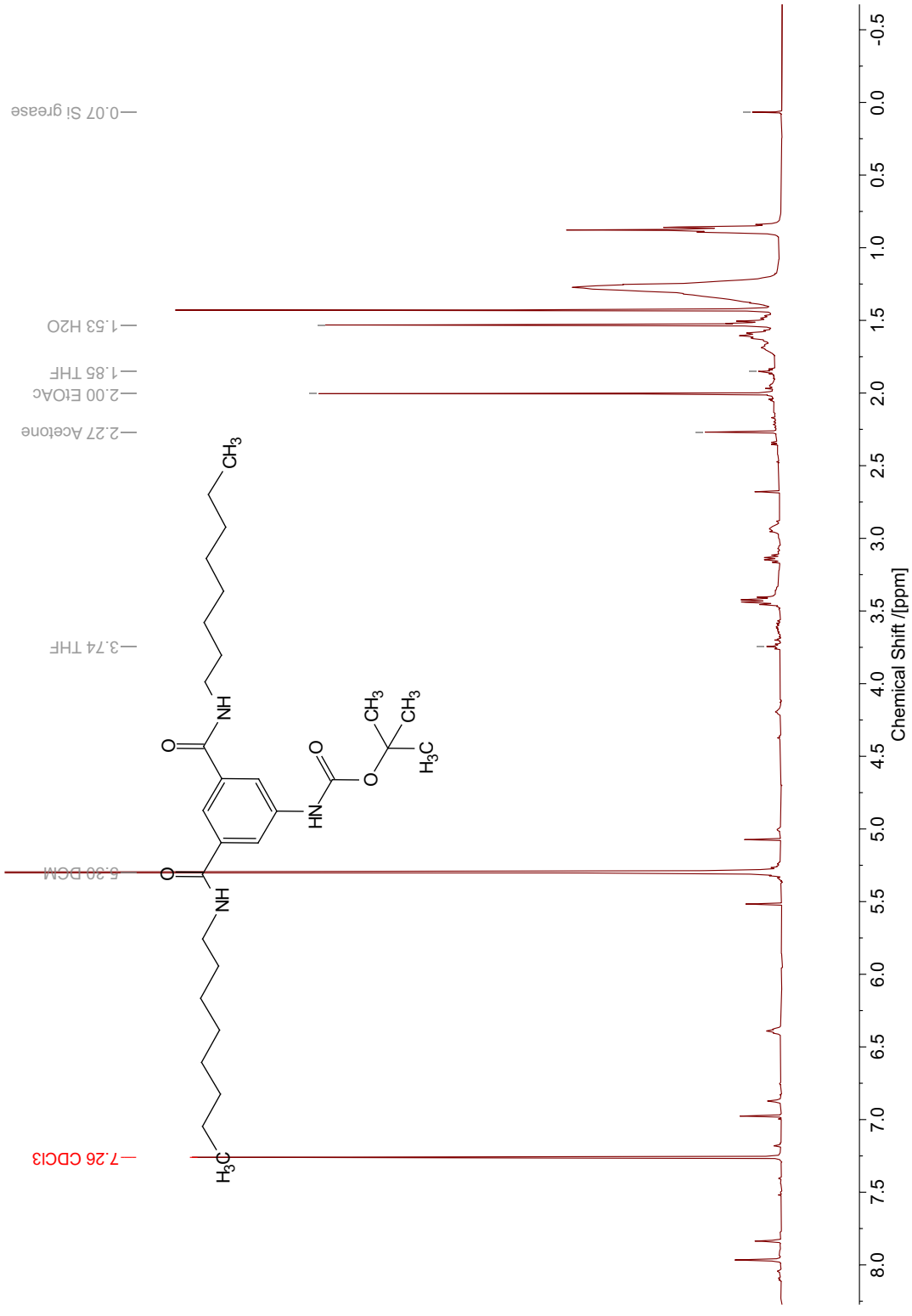

Figure A.17: ^{1}H NMR spectrum of (**9**). Unassigned as it is a mixture of products or rotamers.

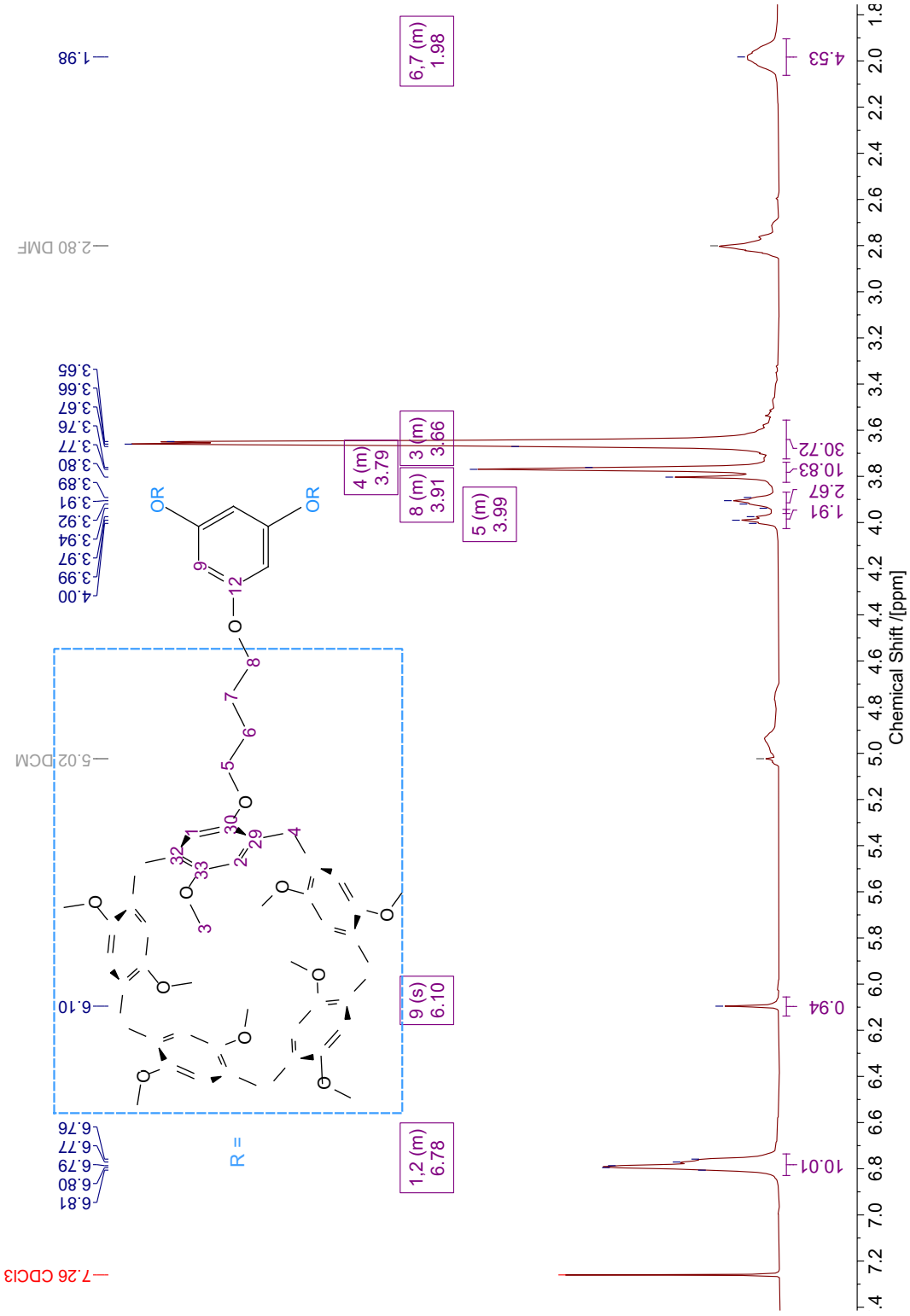

Figure A.18: ^{1}H NMR spectrum of ether tris-pillar[5]arene (**10.3**).

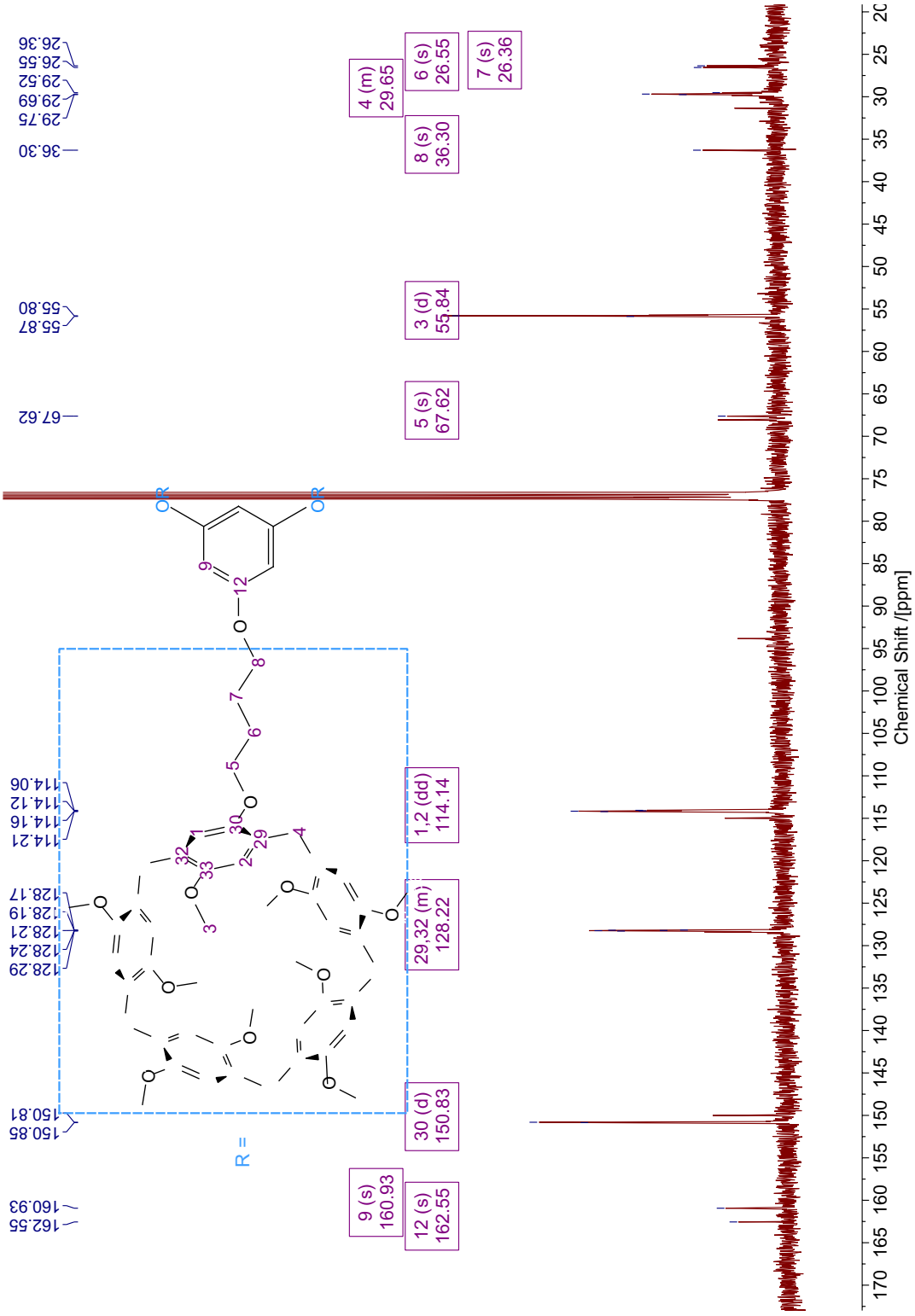

Figure A.19: ^{13}C NMR spectrum of ether tris-pillar[5]arene (**10.3**).

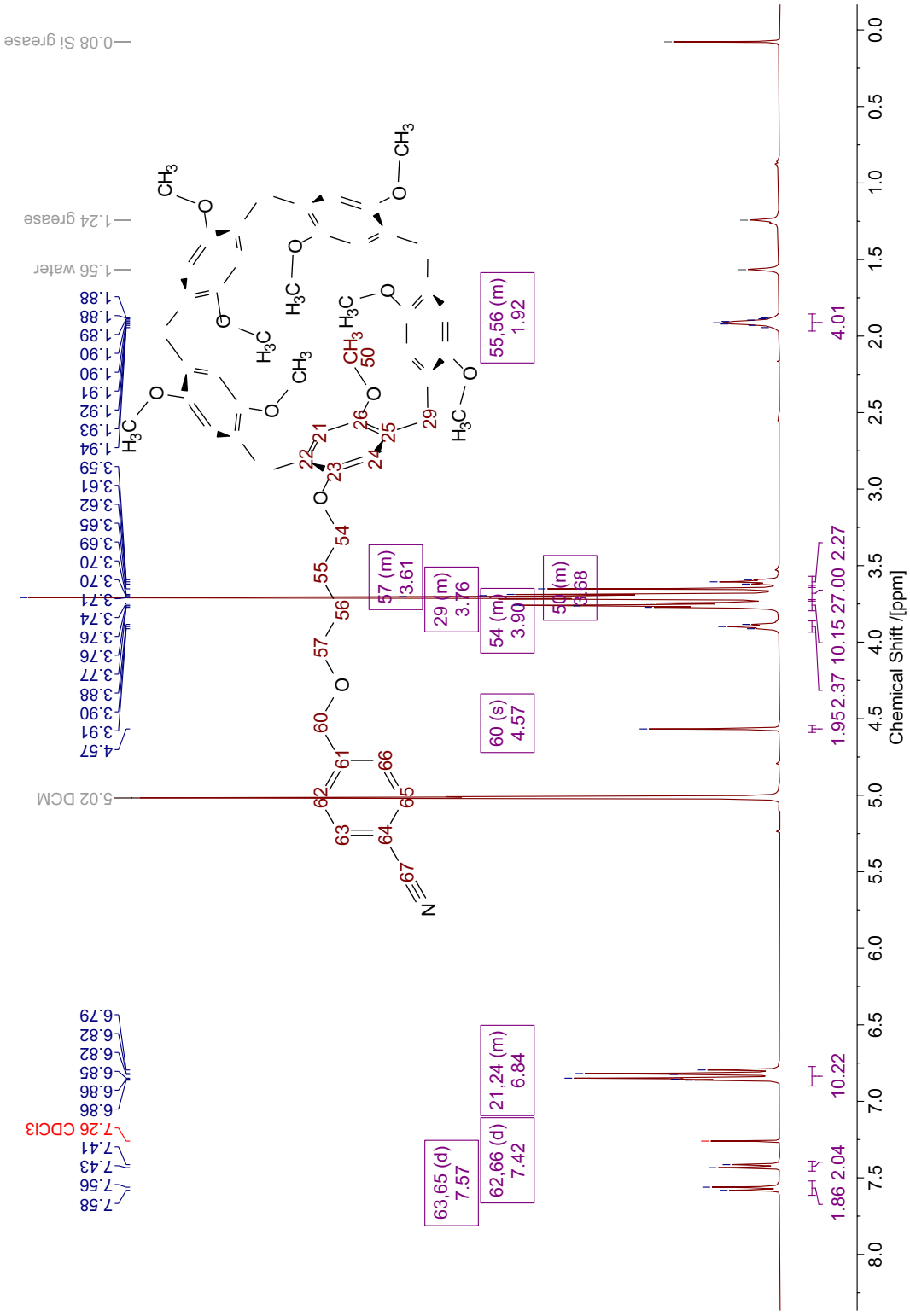

Figure A.20: ^{1}H NMR spectrum of benzonitrile-pillar[5]arene (**12**).

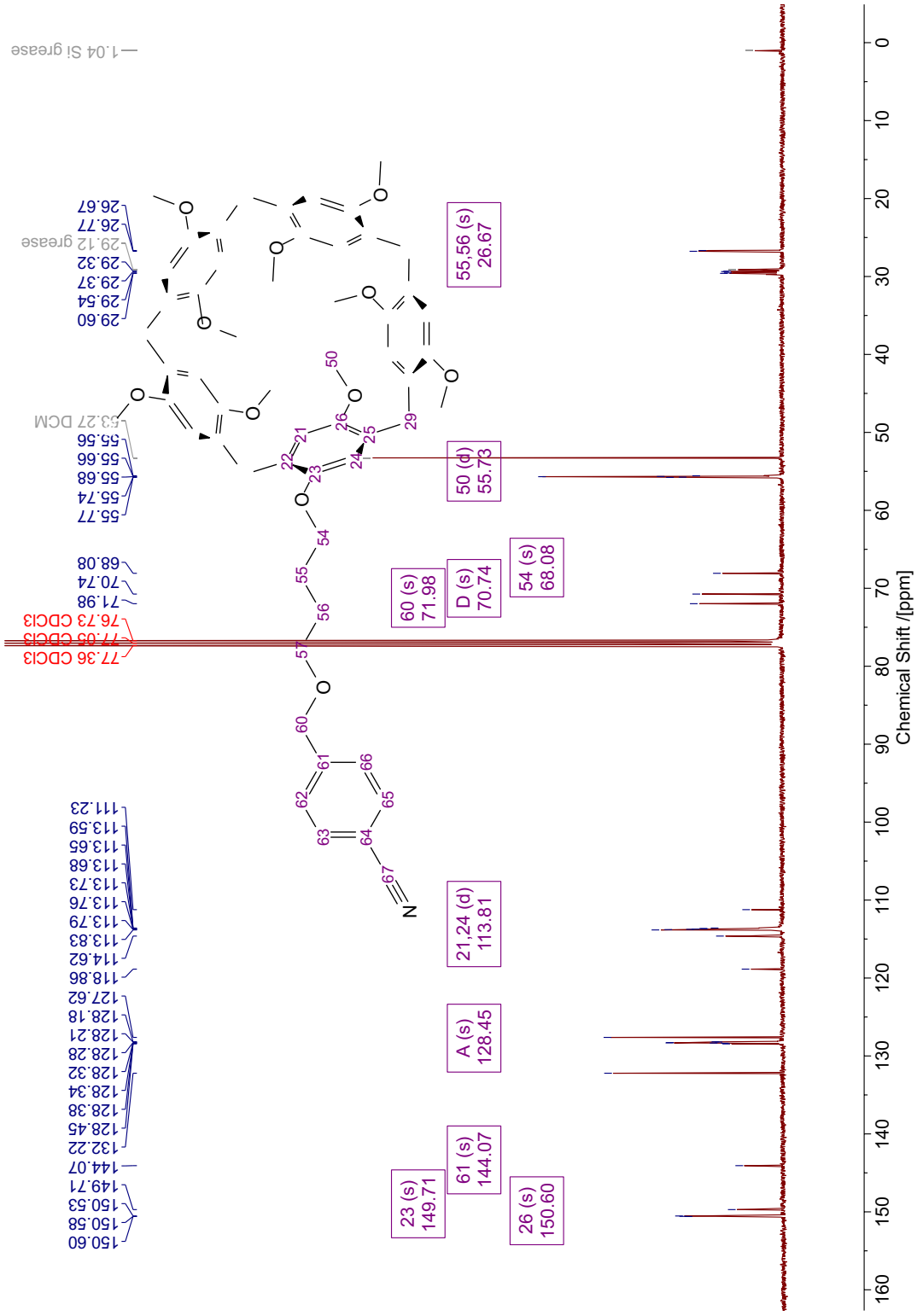

Figure A.21: ^{13}C NMR spectrum of benzonitrile-pillar[5]arene (**12**).

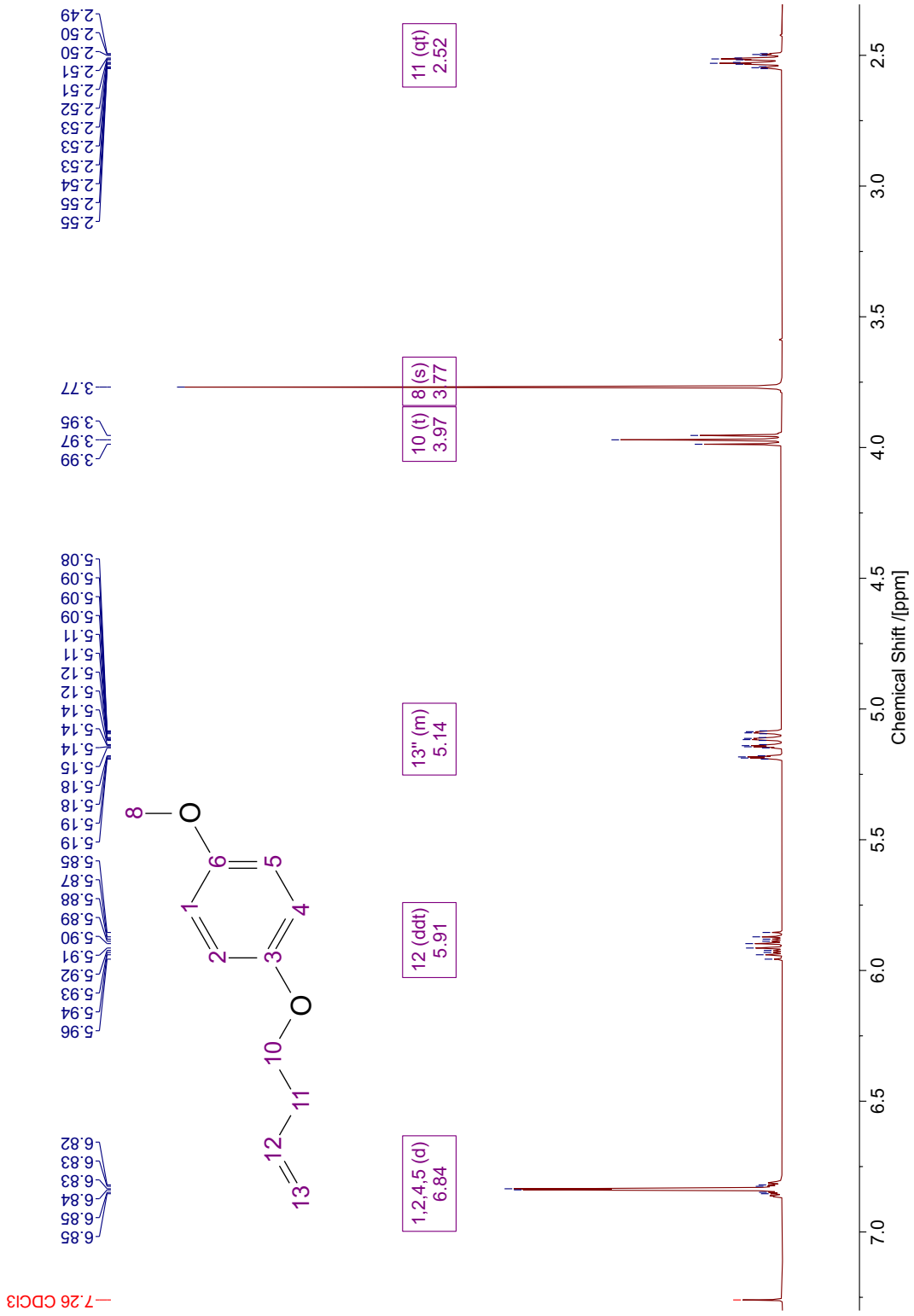

Figure A.22: ^{1}H NMR spectrum of 1-(but-3-en-1-yloxy)-4-methoxybenzene (**15**).

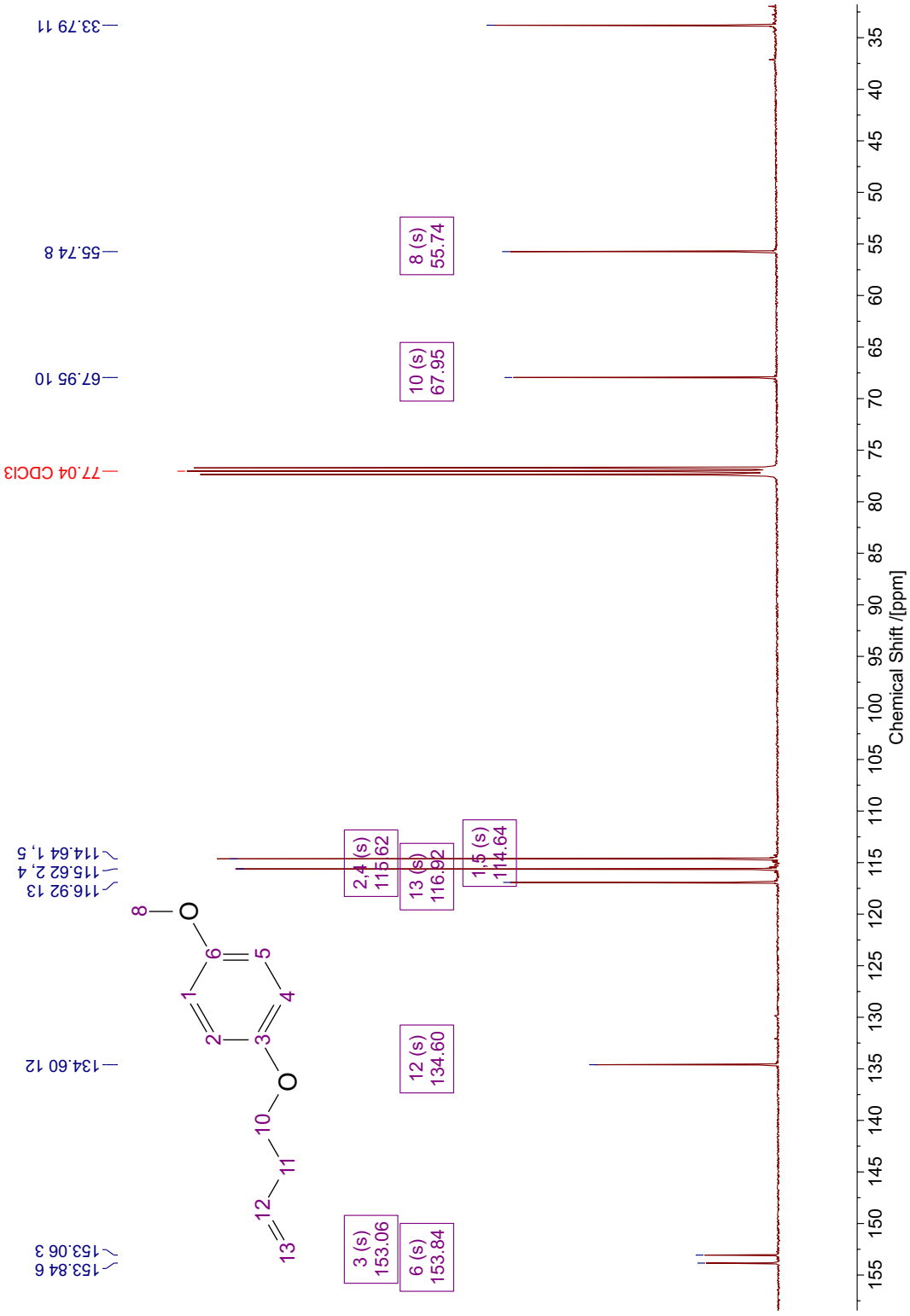

Figure A.23: ^{13}C NMR spectrum of 1-(but-3-en-1-yloxy)-4-methoxybenzene (**15**).

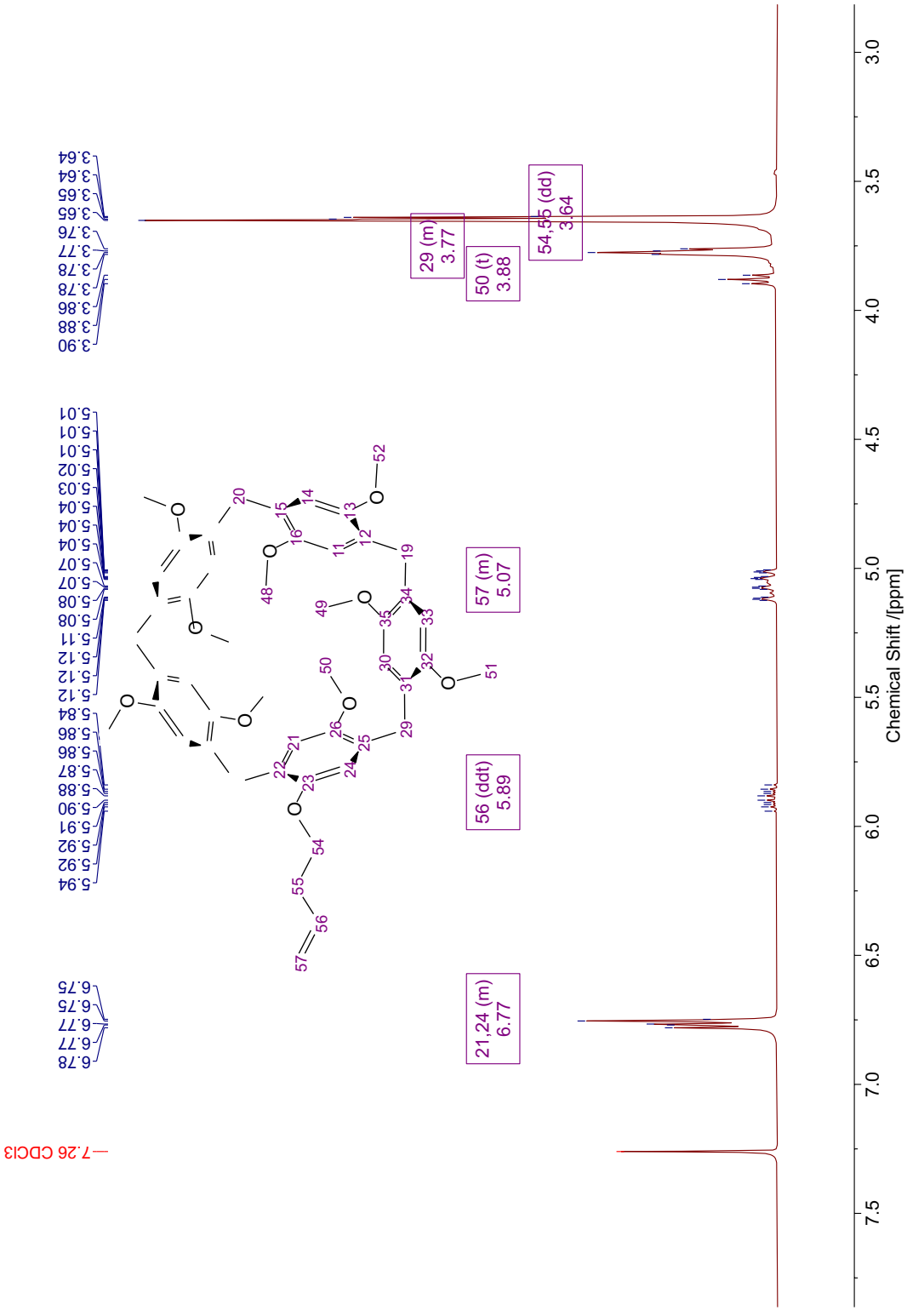

Figure A.24: ^{1}H NMR spectrum of 3-butene-substituted pillar[5]arene (**13**).

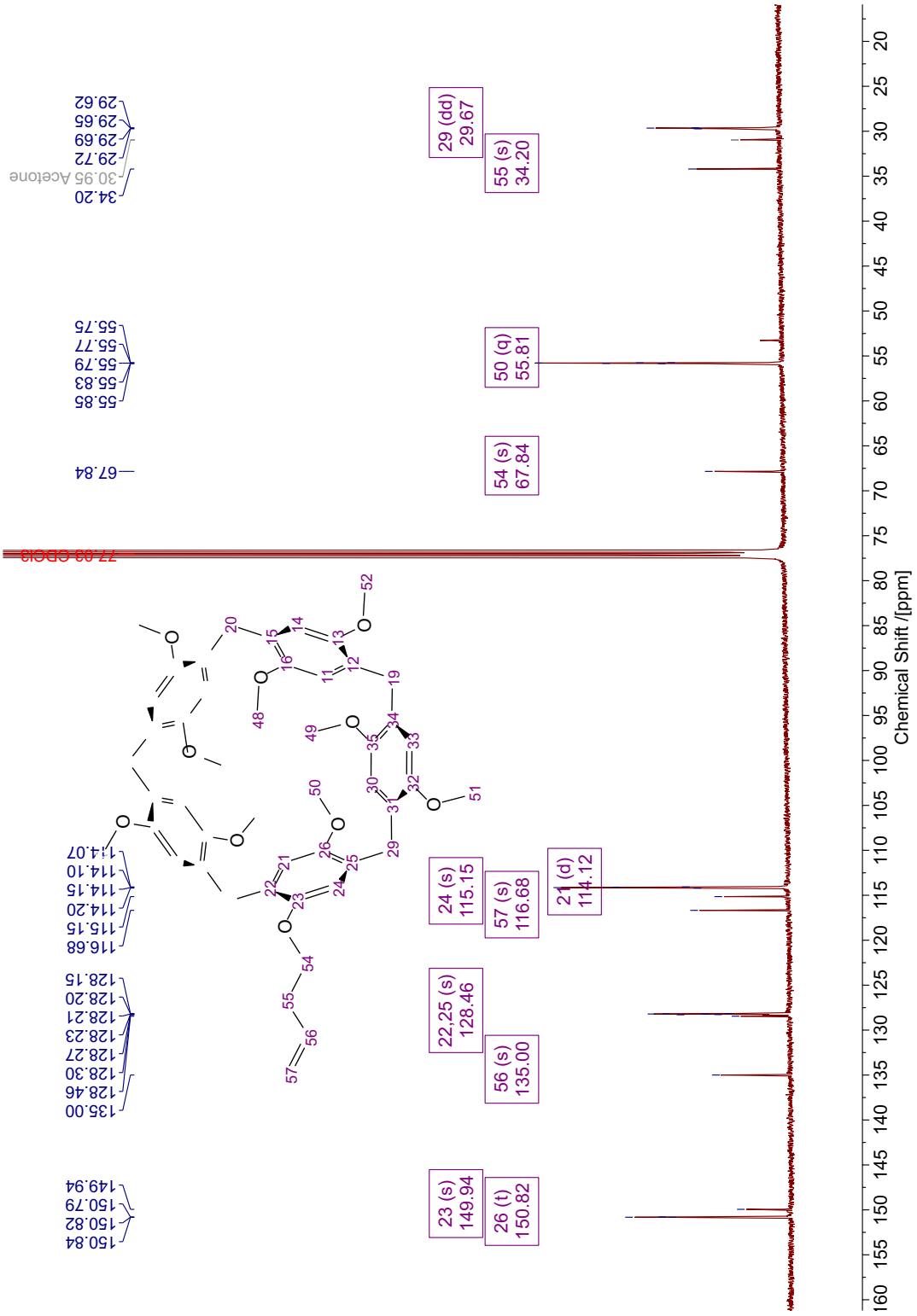

Figure A.25: ^{13}C NMR spectrum of 3-butene-substituted pillar[5]arene (**13**).

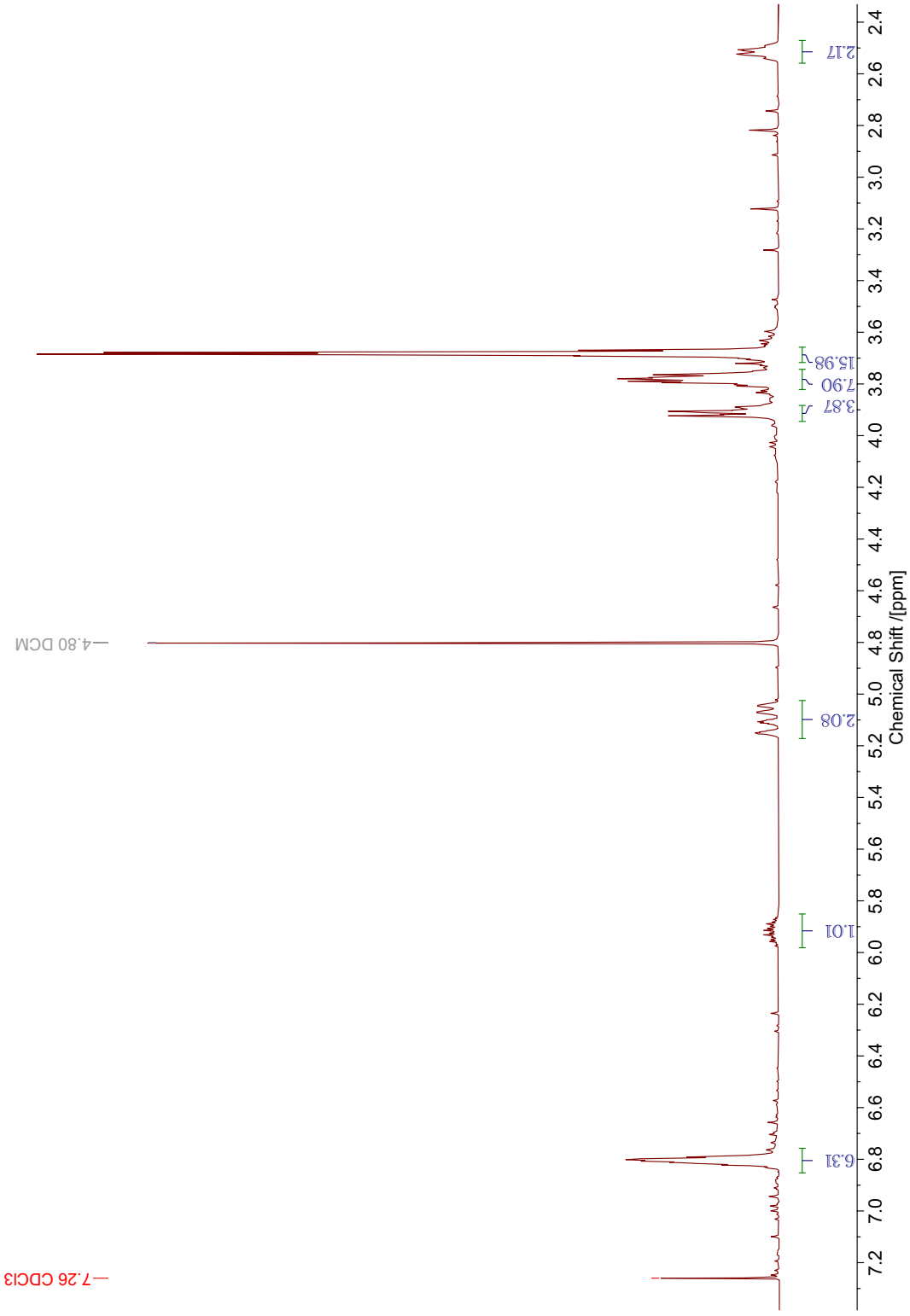

Figure A.26: ^{1}H NMR spectrum of pillar[5]arene (**16**) obtained as a side product when making 3-butene-substituted pillar[5]arene (**13**).

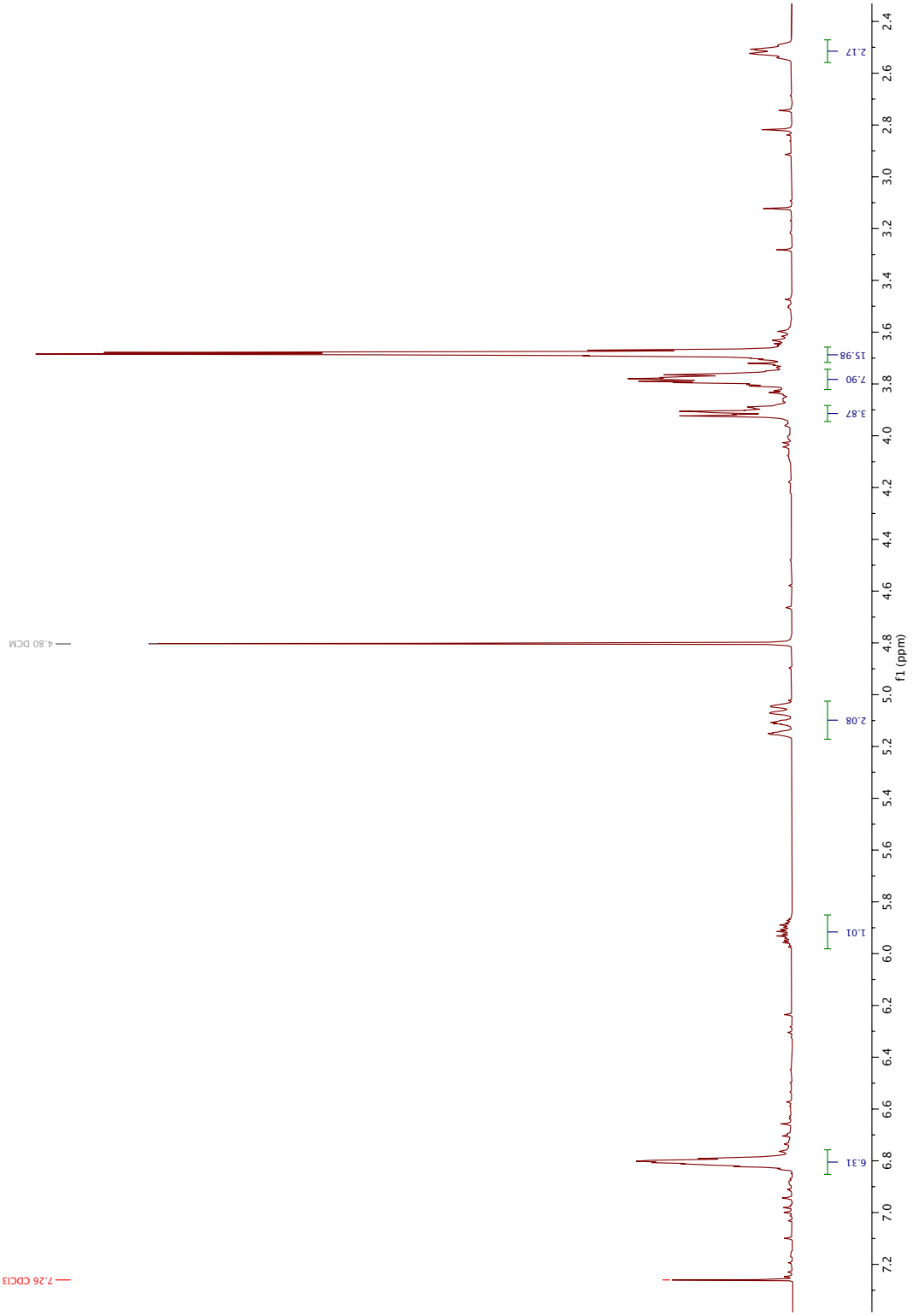

Figure A.27: ^{1}H NMR spectrum of multi 4-alkene substituted DMPillar[5]arene. The leftmost peak (aromatic 10H) should integrate to 10 against the next peak along (alkene 1H), but is closer to 6. There are more alkene protons than expected. In conjunction with multiple spots on tlc, this is likely a mixture of substituted DMPillar[5]arenes.

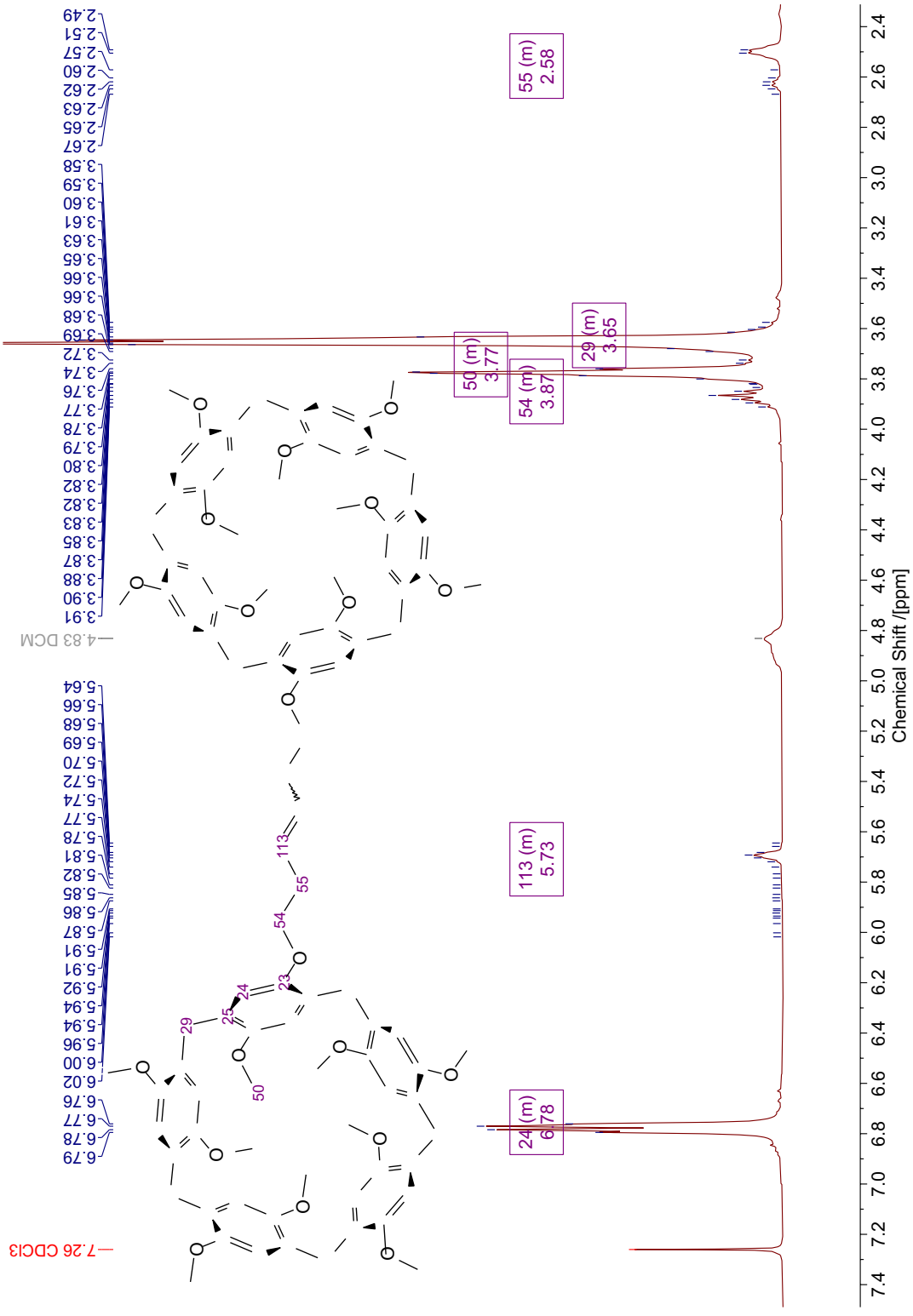

Figure A.28: ^{1}H NMR spectrum of the alkene handcuff body (**17**).

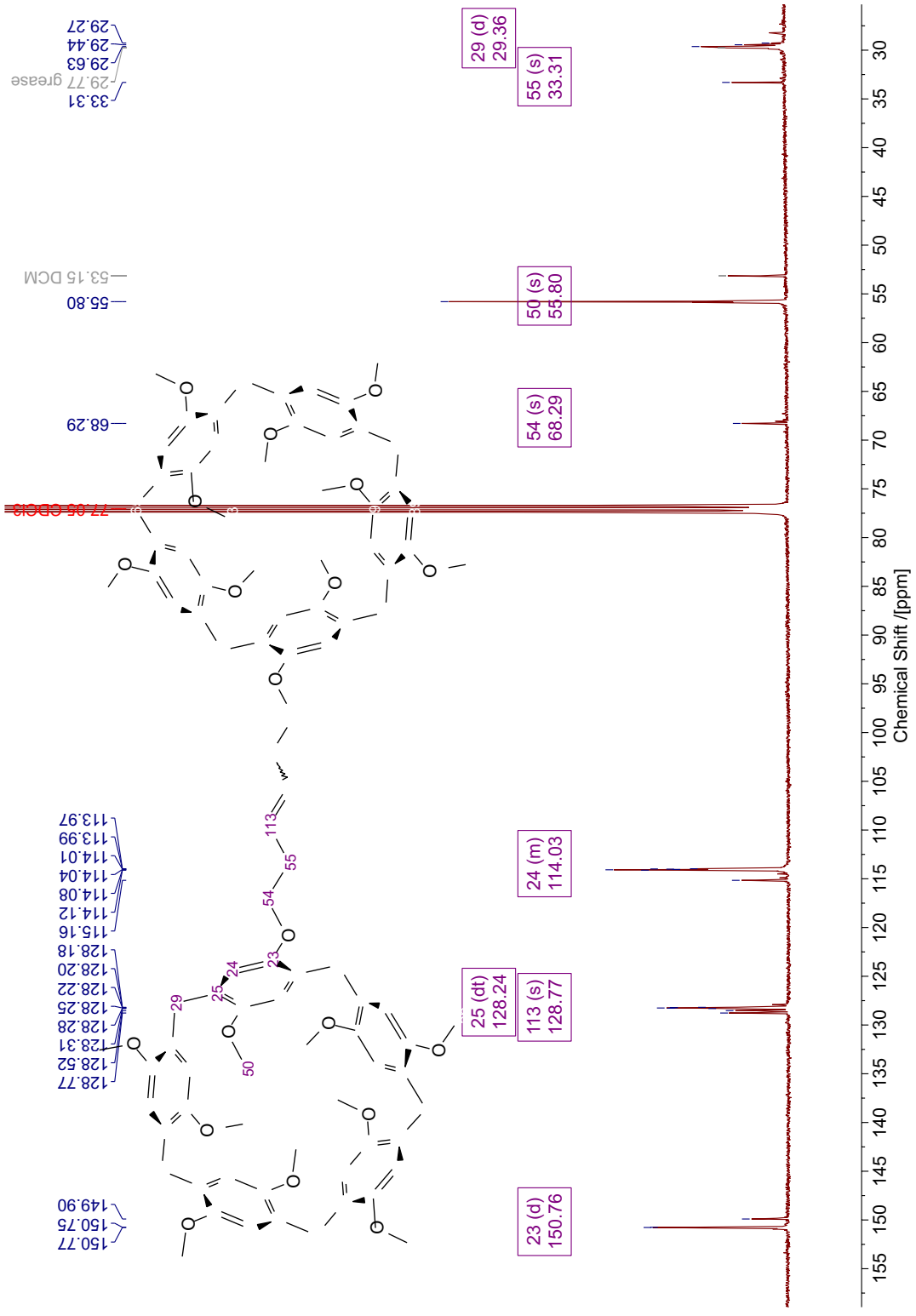

Figure A.29: ^{13}C NMR spectrum of the alkene handcuff body (**17**).

Figure A.30: DOSY NMR spectrum of the alkene handcuff body(**17**).

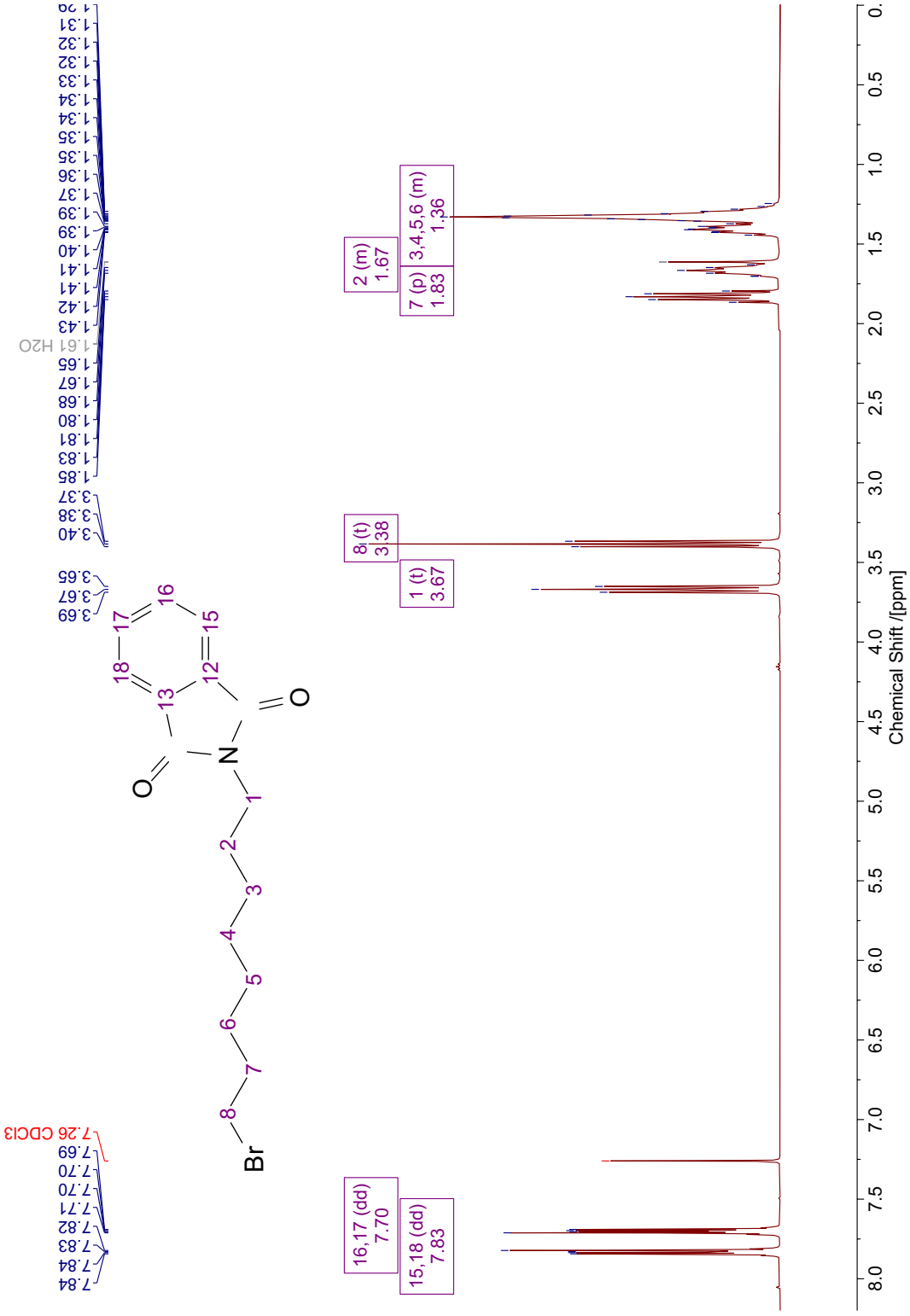

Figure A.31: ^{1}H NMR spectrum of the N-(8-bromooctyl)phthalimide (**18**).

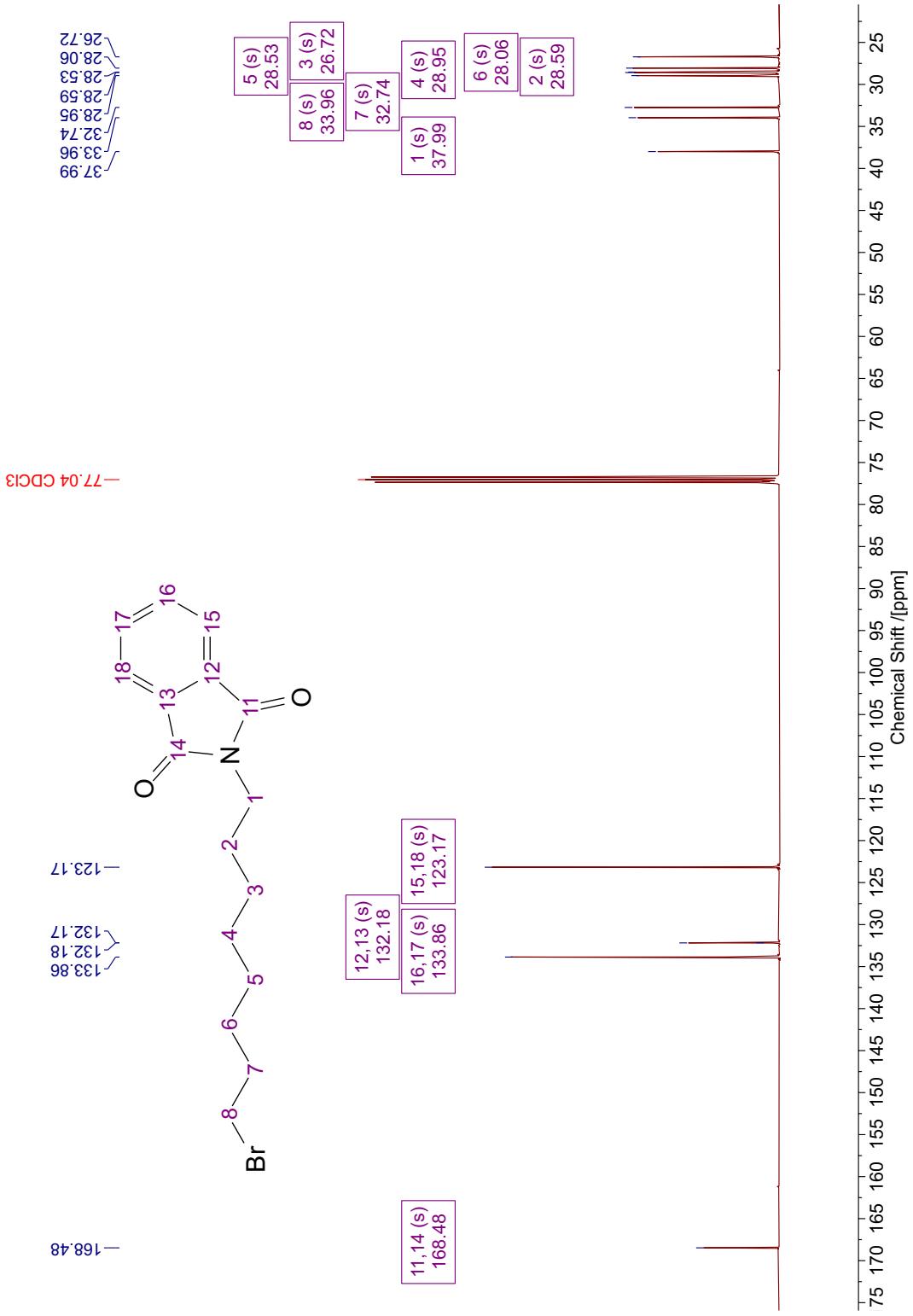

Figure A.32: ^{13}C NMR spectrum of the N-(8-bromooctyl)phthalimide (**18**).

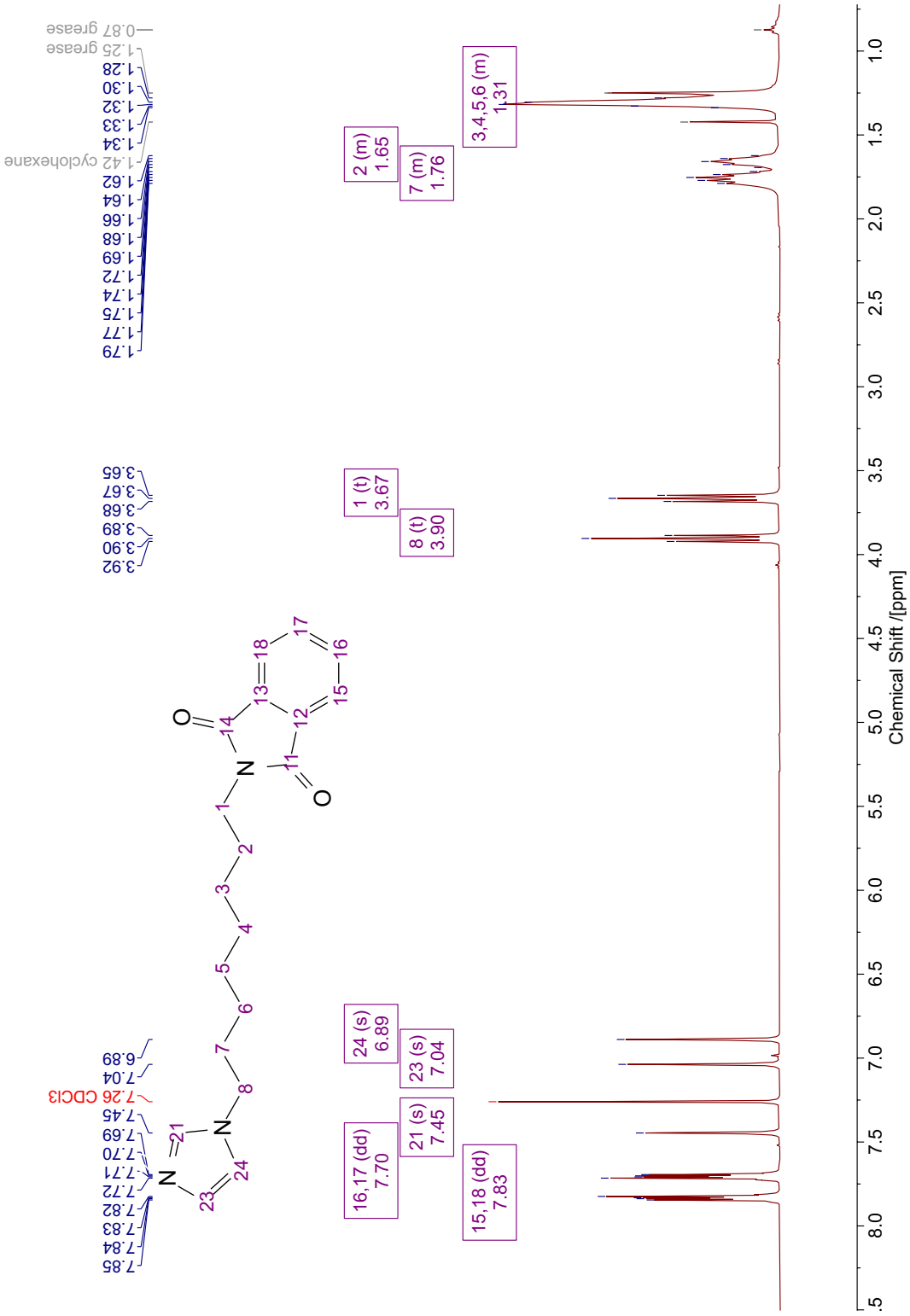

Figure A.33: ^{1}H NMR spectrum of the N-(8- imidazolyloctyl)phthalimide (**19**).

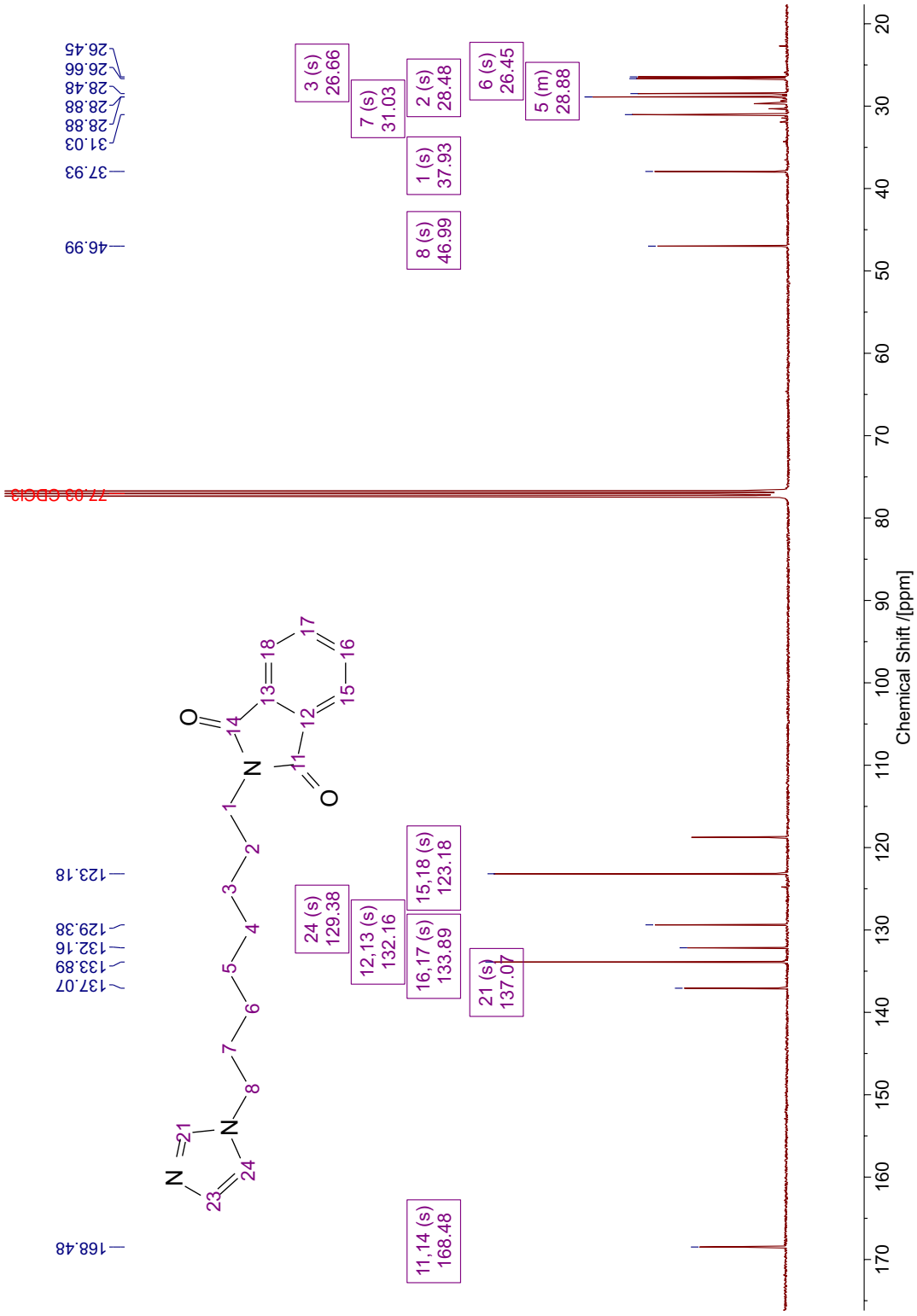

Figure A.34: ^{13}C NMR spectrum of the N-(8- imidazolyloctyl)phthalimide (**19**).

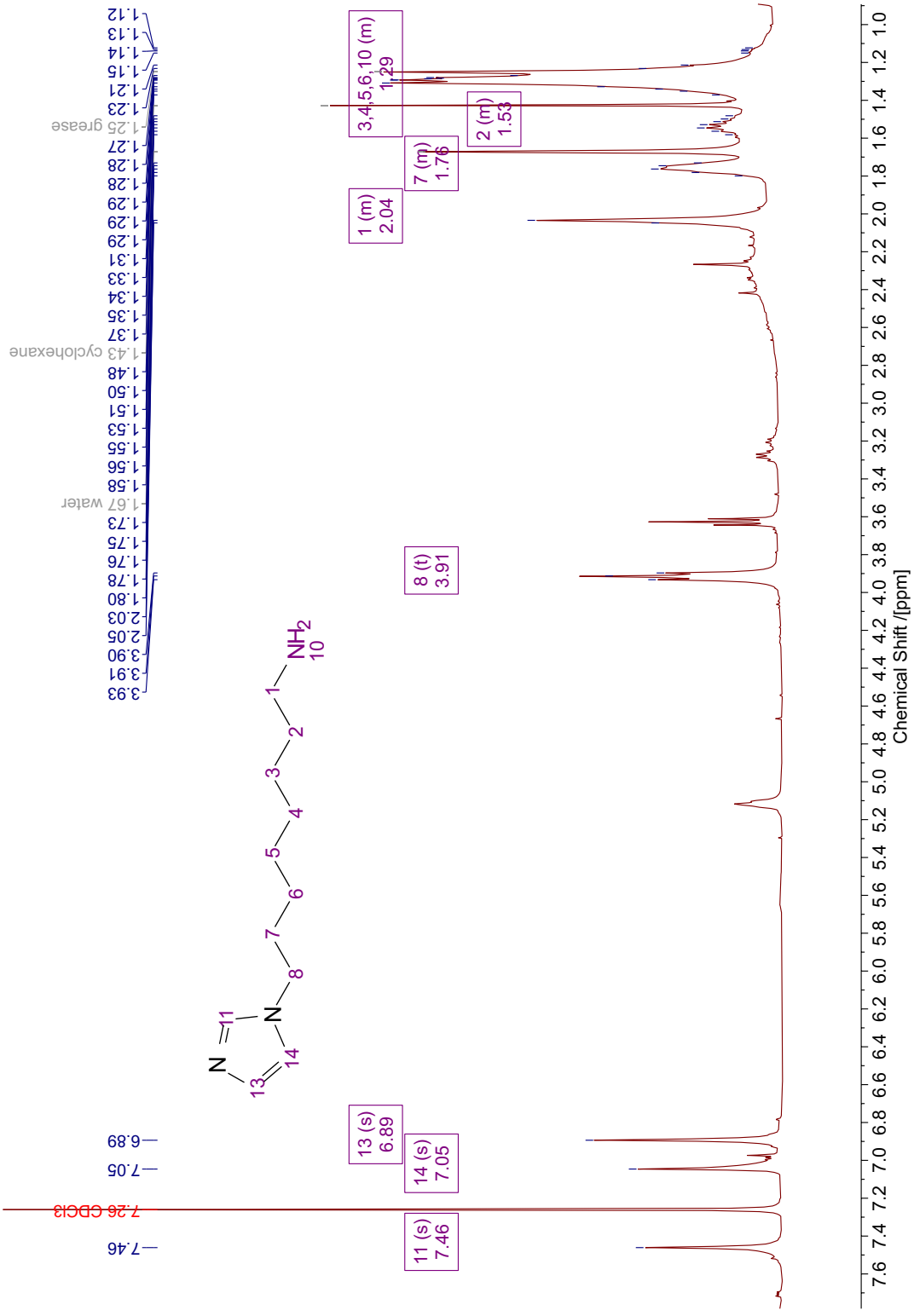

Figure A.35: ^{1}H NMR spectrum of the 8-(1H-imidazol-1-yl)octan-1-amine (**20**) with some starting material contamination.

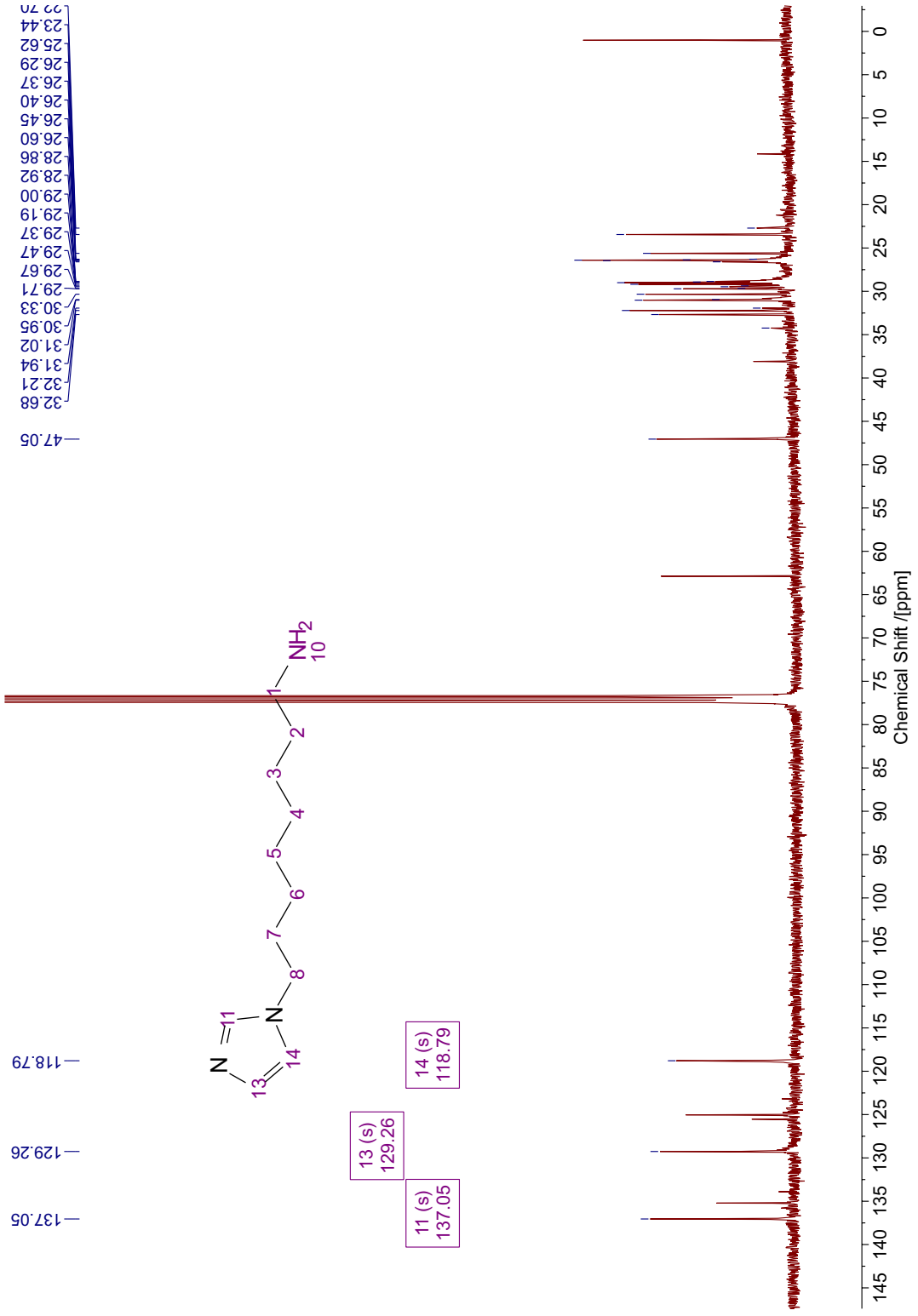

Figure A.36: Unassigned ^{13}C NMR spectrum of the 8-(1H-imidazol-1-yl)octan-1-amine (**20**) with some starting material contamination.

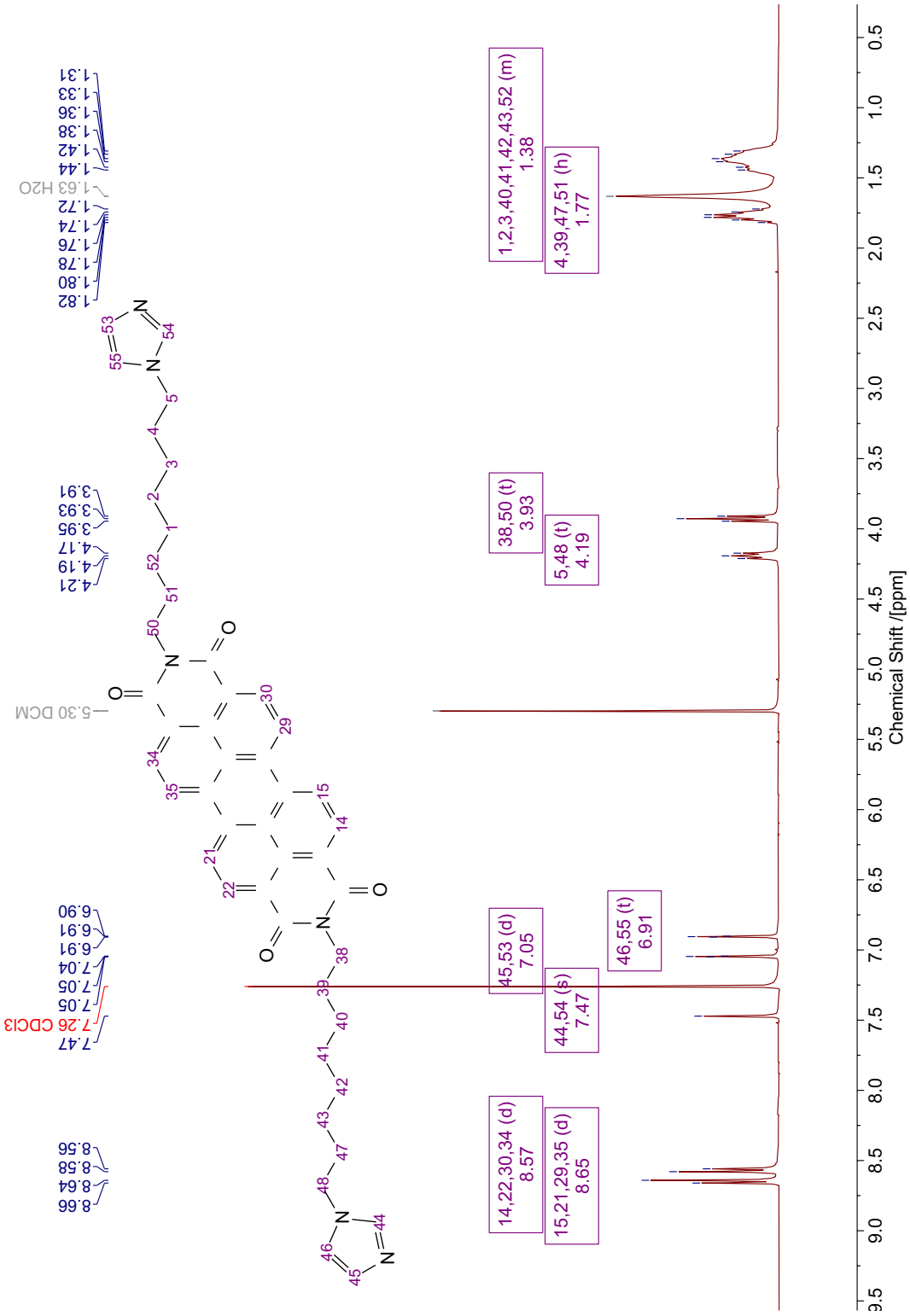

Figure A.37: ^{1}H NMR spectrum of the alkene handcuff rod (**21**).

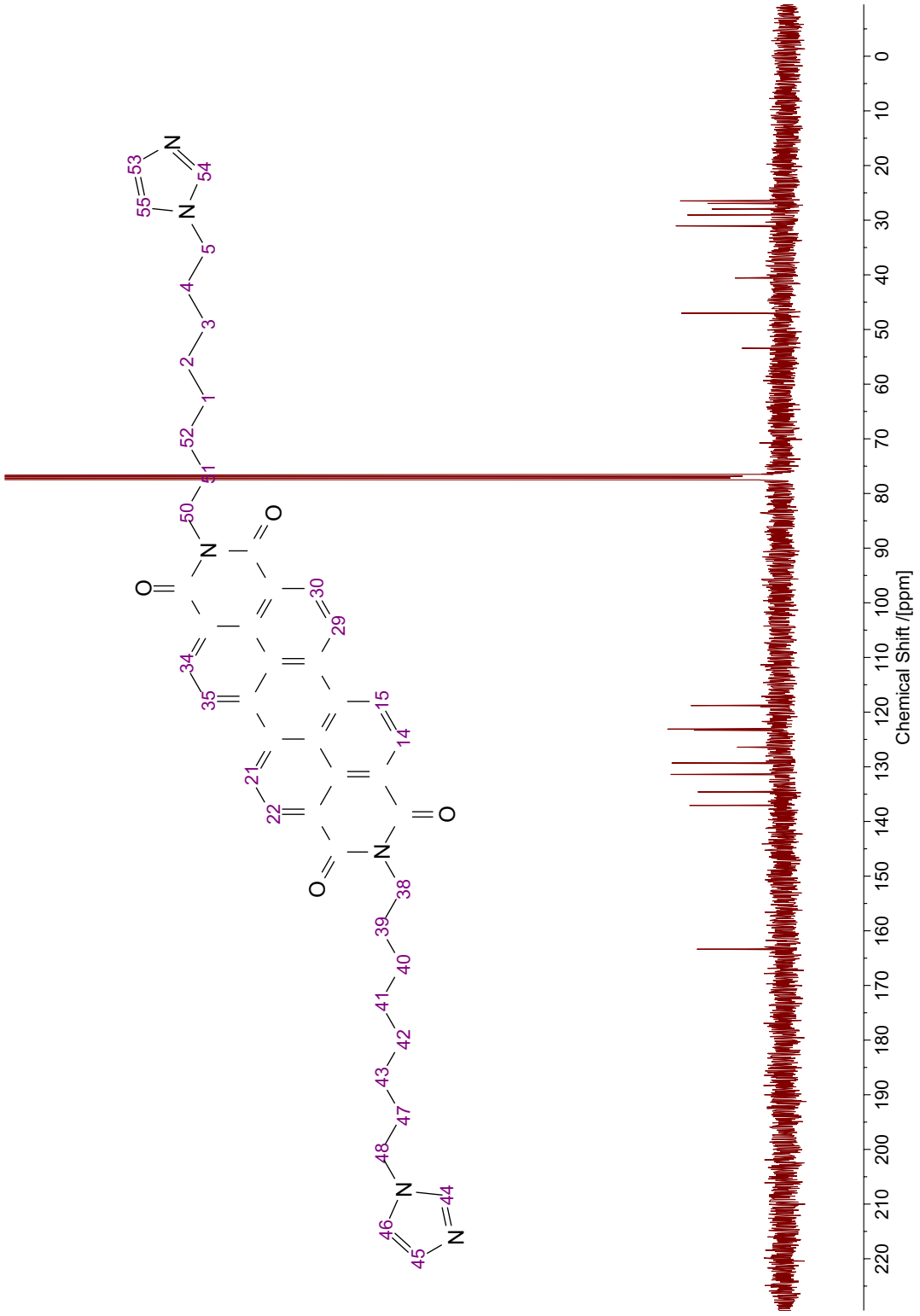

Figure A.38: ^{13}C NMR spectrum of the alkene handcuff rod (**21**).

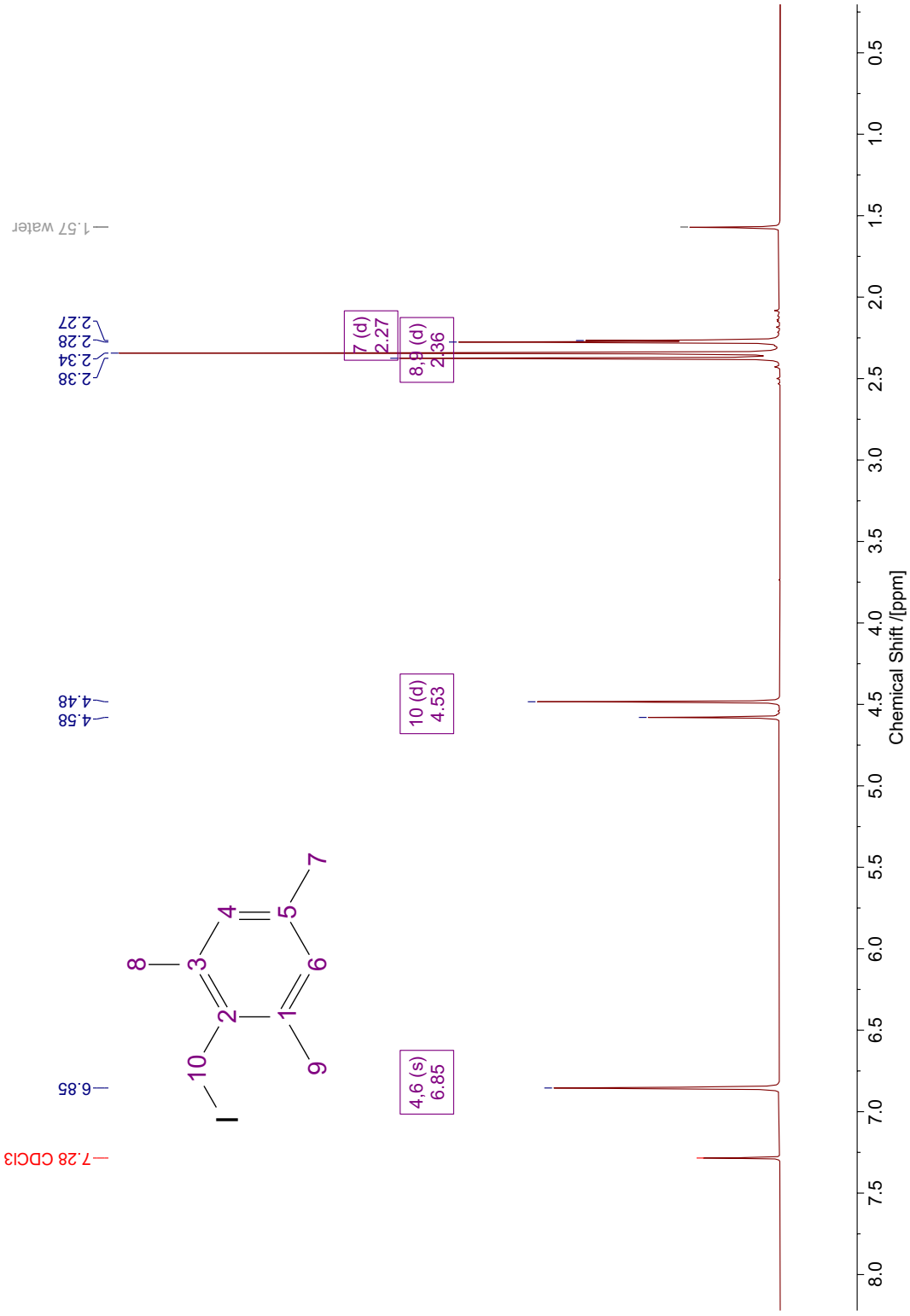

Figure A.39: ^{1}H NMR spectrum of the alkene handcuff stopper (**22**).

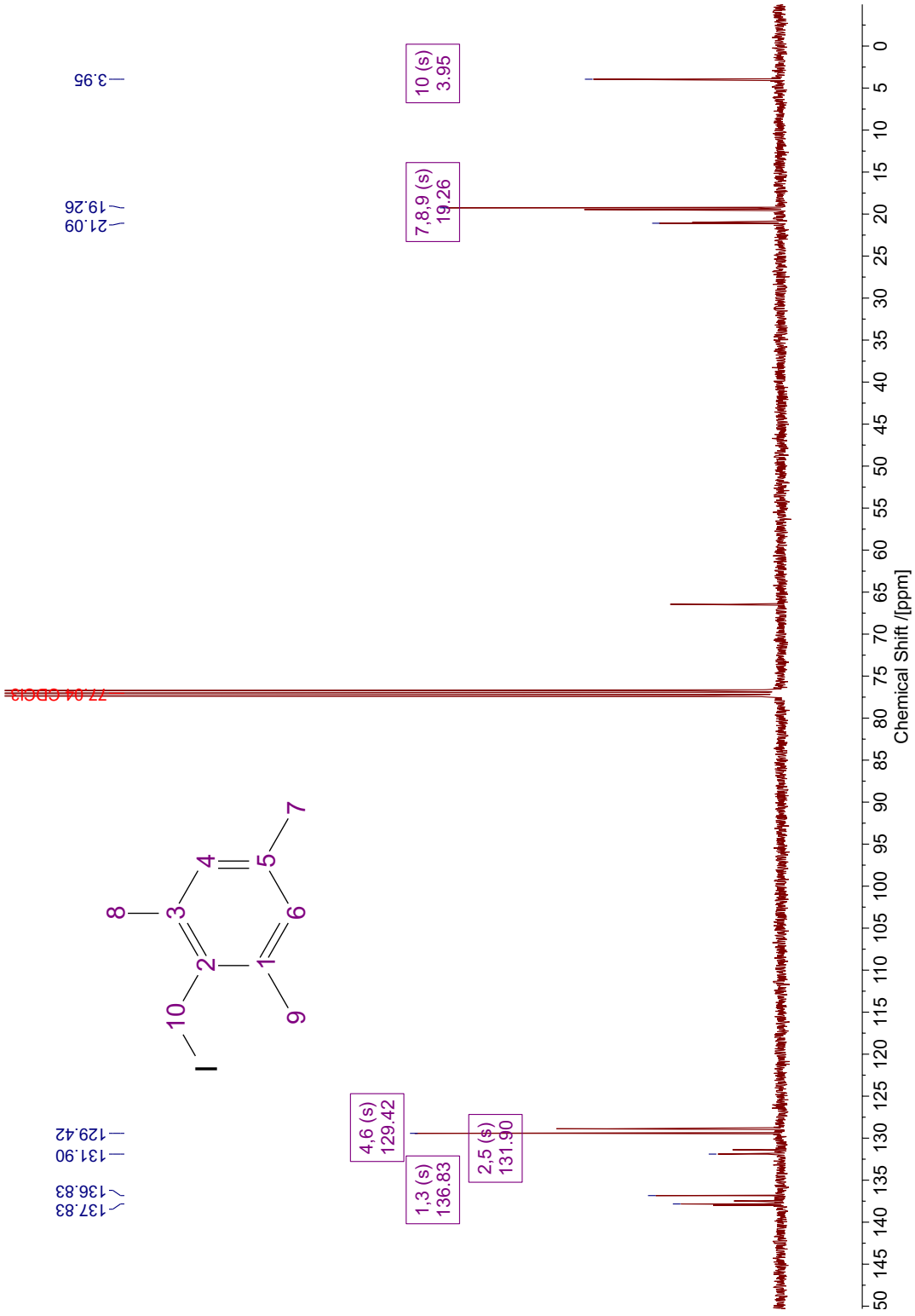

Figure A.40: ^{13}C NMR spectrum of the alkene handcuff stopper (**22**).

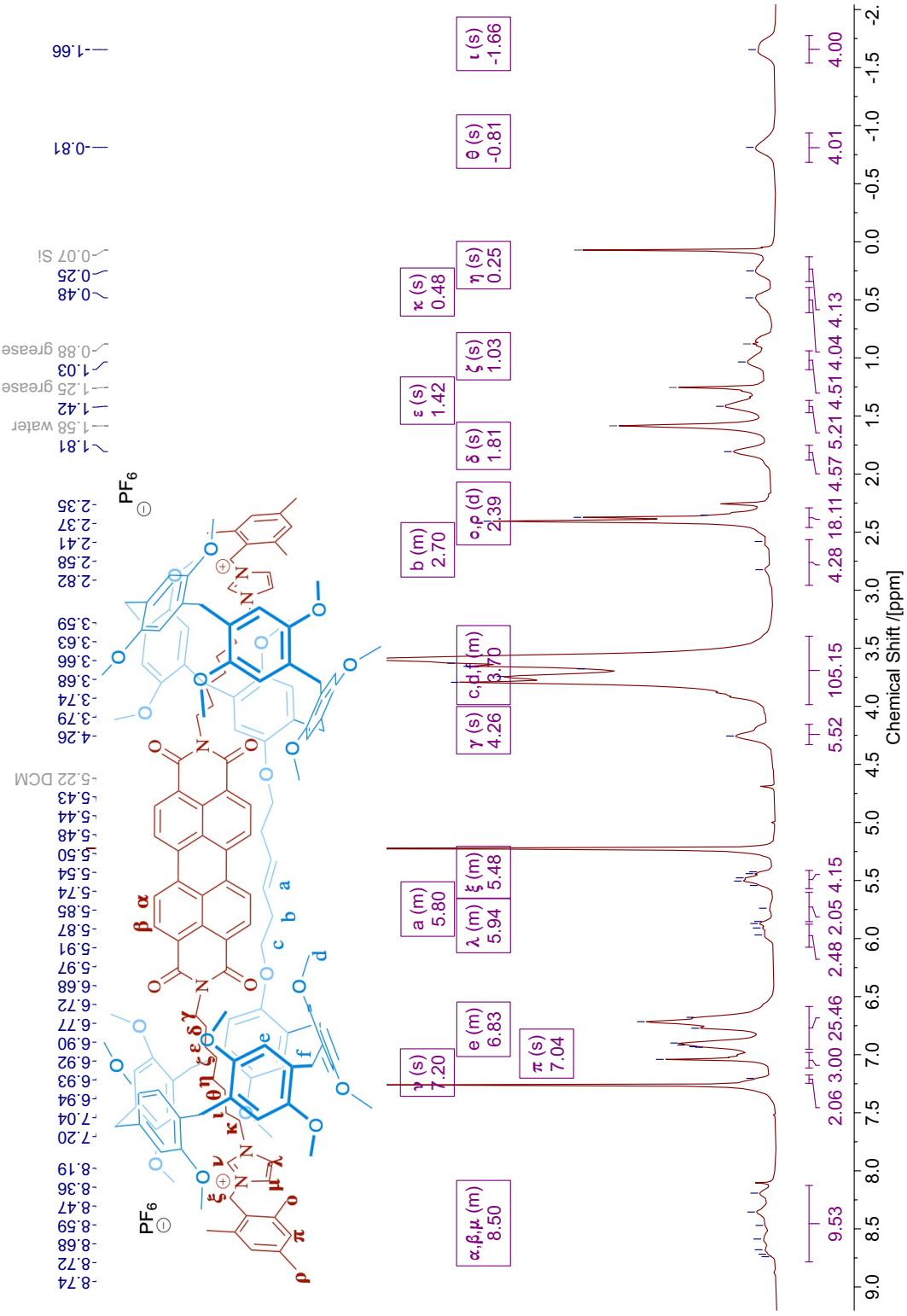

Figure A.41: ^{1}H NMR spectrum of the alkene handcuff (**23**).

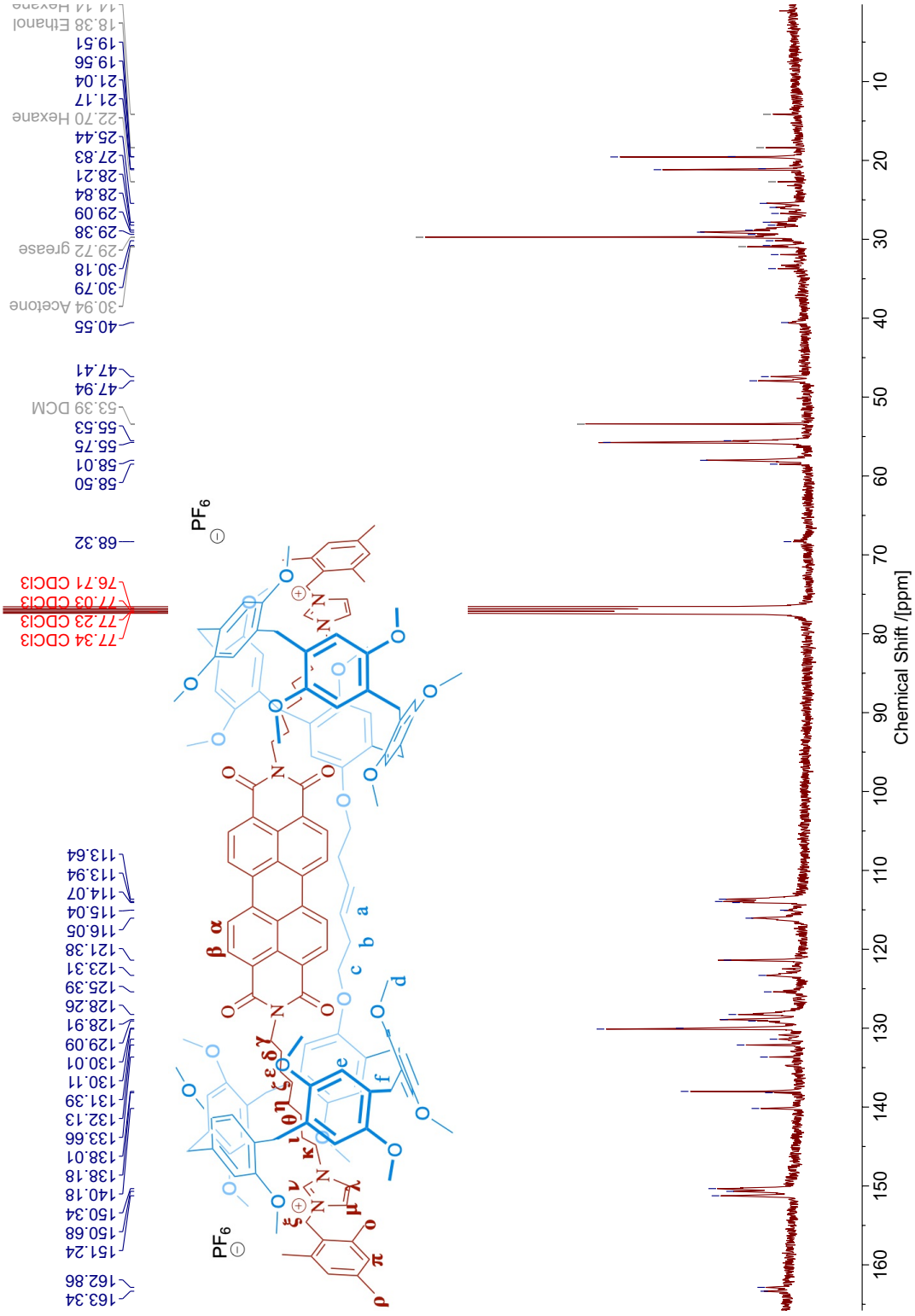

Figure A.42: ^{13}C NMR spectrum of the alkene handcuff (**23**).

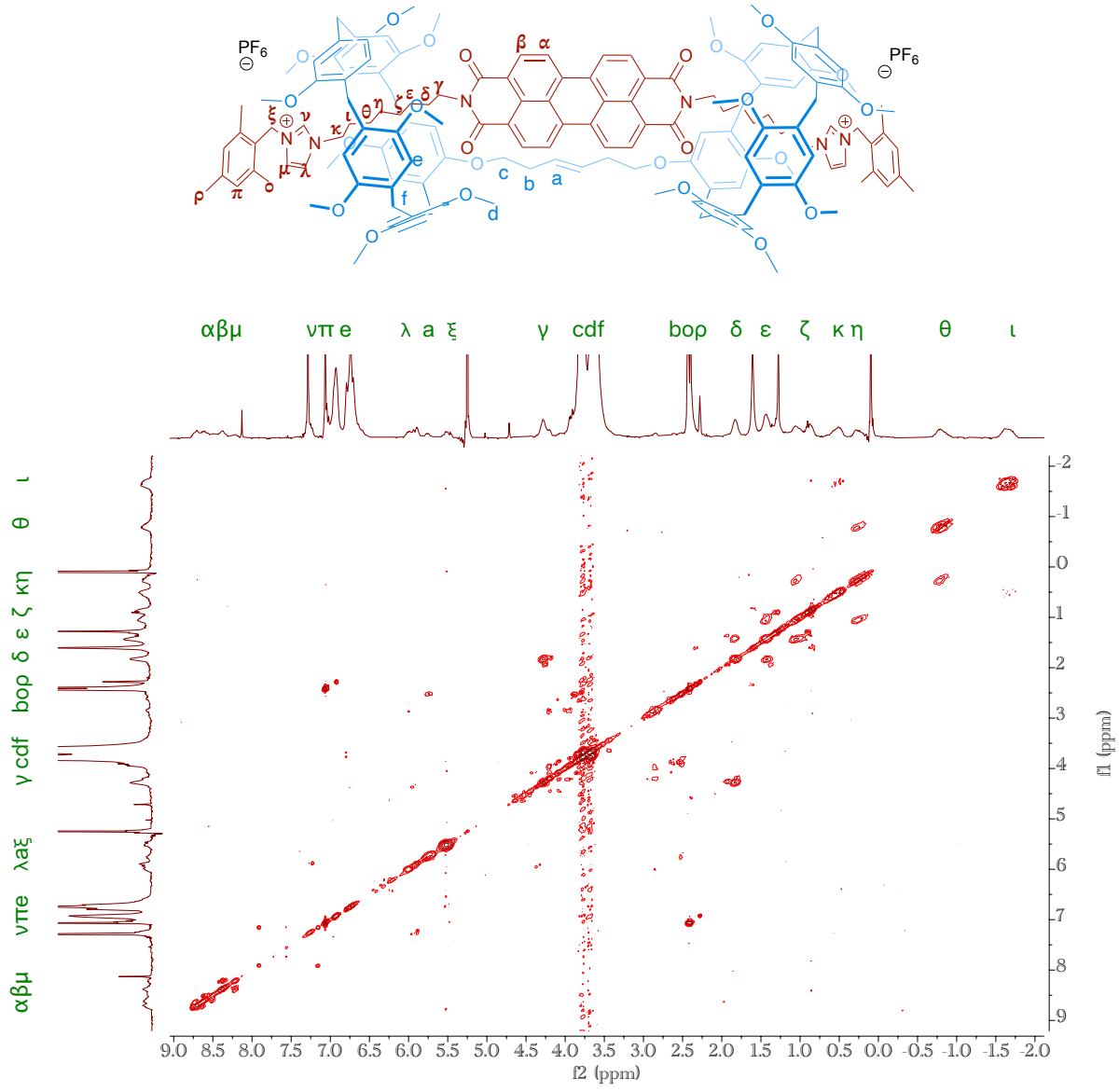

Figure A.43: ^{1}H –^{1}H COSY NMR (300 MHz, $CDCl_3$ 298 K) spectrum of the alkene handcuff (**23**).

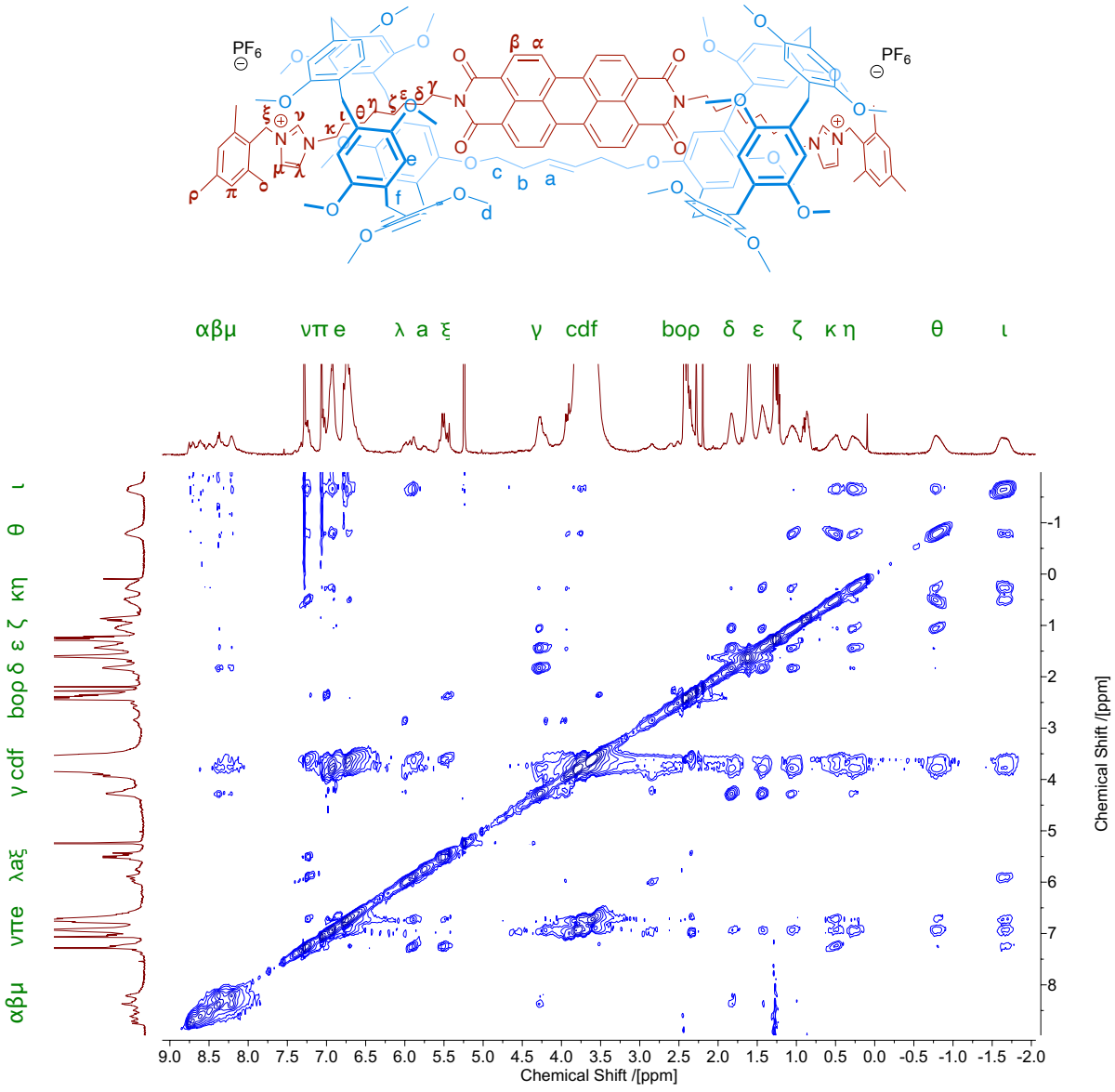

Figure A.44: ^{1}H –^{1}H NOESY NMR spectrum of the alkene handcuff (**23**).

A.4 Crystallography

Empirical formula	$C_{42.8}H_{52.15}O_8$
Formula weight	694.656
Temperature/K	120(10)
Crystal system	orthorhombic
Space group	$Pna2_1$
a/Å	35.9157(3)
b/Å	12.0571(1)
c/Å	11.4426(1)
α/°	90
β/°	90
γ/°	90
Volume/Å^3	4955.09(7)
Z	5
ρ_{calc} g/cm^3	1.164
μ/mm^{-1}	0.637
F(000)	1871.0
Crystal size/mm^3	0.2 × 0.1 × 0.05
Radiation	Cu Kα (λ = 1.54184)
2Θ range for data collection/°	7.74 to 145.06
Index ranges	-43 ≤ h ≤ 42, -14 ≤ k ≤ 14, -14 ≤ l ≤ 14
Reflections collected	87942
Independent reflections	9751 [R_{int} = 0.0226, R_{sigma} = 0.0104]
Data/restraints/parameters	9751/20/640
Goodness-of-fit on F^2	1.039
Final R indexes [I>=2σ(I)]	R_1 = 0.0458, wR_2 = 0.1306
Final R indexes [all data]	R_1 = 0.0463, wR_2 = 0.1314
Largest diff. peak/hole / e Å^{-3}	0.42/-0.29
Flack parameter	0.434(19)

Table A.1: Crystal data and structure refinement for 3-butene-substituted pillar[5]arene (**13**).

Experimental

Single crystals of 3-butene-substituted pillar[5]arene (**13**) were obtained through slow vapour diffusion from chloroform into hexane. A suitable crystal was selected and mounted in fomblin oil on a mitegen loop on a GV1000, TitanS2 diffractometer. The crystal was kept at 120(10) K during data collection. Using Olex2, the structure was solved with the olex2.solve structure solution program using Charge Flipping and refined with the olex2.refine refinement package using Gauss-Newton minimisation.

A.5 Reproduced data for pillar[5]arene (16)

Data for pillar[5]arene (**16**) as a comparison with 3-butene-substituted pillar[5]arene (**13**) discussed in this work. Figures adapted from Champness et al[151].

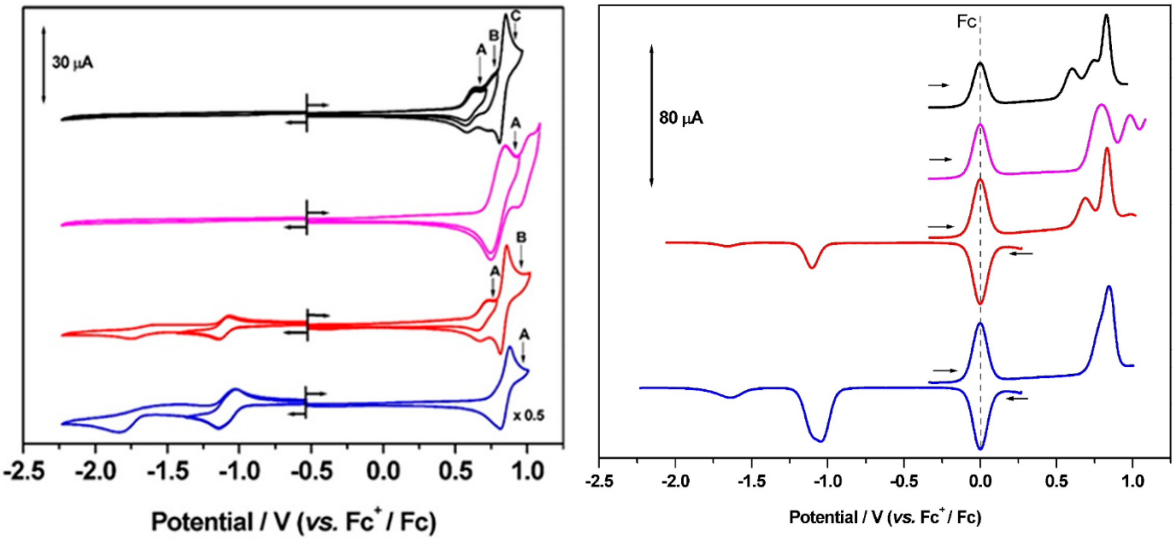

Figure A.45: Left: cyclic voltammogram; right: square wave voltammogram of pillar[5]arene (**16**) (black trace) in CH_2Cl_2 containing $[^nBu_4N][BF_4]$ (0.4 M) as supporting electrolyte, at ambient temperature and at 0.10 Vs^{-1}.

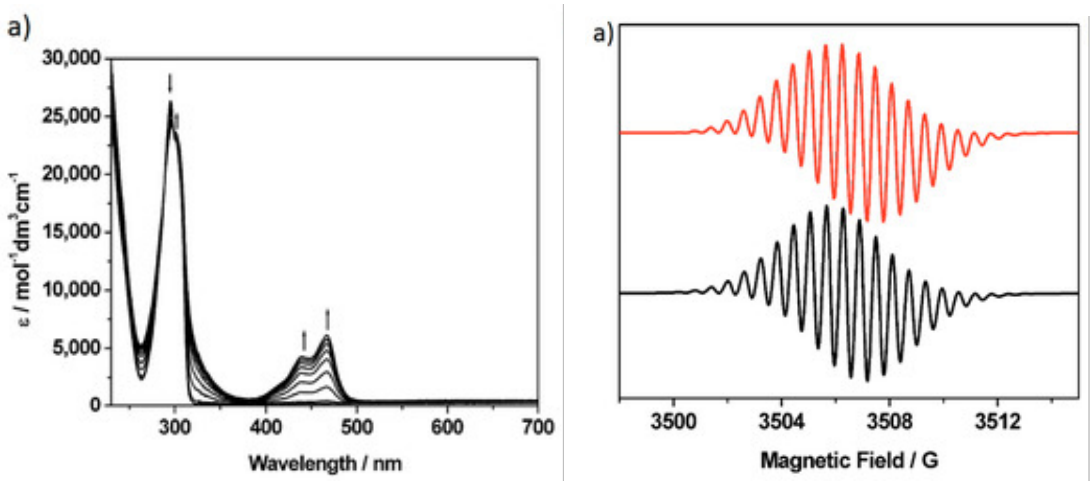

Figure A.46: Left: UV-vis absorption spectra showing the inter-conversion of redox states in pillar[5]arene (**16**) between P5A and $[P5A]^+$; right: experimental (black) and simulated (red) X-band EPR spectra of $[P5A]^+$. Both spectra were recorded in CH_2Cl_2 containing $[^nBu_4N][BF_4]$ (0.4 M) as supporting electrolyte at 273 K. The simulated EPR spectrum was generated using g_{iso} of 2.0038, a_{iso} of 1.720 (2H), 1.136(4H) and 0.570(8H) x 10^{-4} cm^{-1}, a line-width of 0.25 G and a Gaussian line-shape.

Chemical Science

ROYAL SOCIETY OF CHEMISTRY

PERSPECTIVE

View Article Online
View Journal | View Issue

Cite this: *Chem. Sci.*, 2022, **13**, 3915

All publication charges for this article have been paid for by the Royal Society of Chemistry

Received 28th January 2022
Accepted 27th February 2022

DOI: 10.1039/d2sc00568a

rsc.li/chemical-science

Mechanically interlocked molecular handcuffs

Nicholas Pearce, [a] Marysia Tarnowska, [b] Nathan J. Andersen, [b] Alexander Wahrhaftig-Lewis, [a] Ben S. Pilgrim *[b] and Neil R. Champness *[a]

The field of mechanically interlocked molecules that employ a handcuff component are reviewed. The variety of rotaxane and catenane structures that use the handcuff motif to interlock different components are discussed and a new nomenclature, distilling diverse terminologies to a single approach, is proposed. By unifying the interpretation of this class of molecules we identify new opportunities for employing this structural unit for new architectures.

1. Introduction

The design of mechanically interlocked molecular components and architectures that resemble real-world objects is often a pursuit of the supramolecular chemist, as evidenced in the constructions of molecular knots,[1] Borromean rings,[2] and complex higher-order catenanes such as olympiadane which resembles the Olympic rings.[3] The field has developed rapidly over the past few years and has recently been termed molecular nanotopology.[4] Indeed, frequently when it comes to the nomenclature of such complex mechanically interlocked molecules, these structures have their names derived from the objects that their structure resembles. One example that fits this vernacular convention is molecular handcuffs, where the name perhaps implies their structure of a bis(macrocyclic) host 'arresting' a guest molecule.

In this review we seek to explore the diversity of structures based on molecular handcuffs and related systems, introducing the reader to these fascinating molecular structures and their utility in studying complex interactions. We also present a new convention for the naming of these intricate and complex structures. Whilst several attempts have been made to introduce a systematic nomenclature to the world of mechanically locked molecules,[5,6] including recommendations by IUPAC,[5] a widespread adoption of any naming convention has yet to occur. Although the name 'molecular handcuff' is open to interpretation, and at times even conflicts with other naming conventions, we hope in this review article to make some headway towards defining what qualifies as a molecular handcuff. In simplistic terms a handcuff molecule consists of two molecular components: a host component with a structure of two joined macrocycles; and a guest component that is threaded through each of the host's two rings, as a doubly mechanically interlocked molecule. In this simple sense the molecule resembles real-world handcuffs, which are two joined metal rings that can be used to restrain a prisoner. As with all areas of

[a]School of Chemistry, University of Birmingham, Edgbaston, Birmingham, B15 2TT, UK. E-mail: n.champness@bham.ac.uk
[b]School of Chemistry, University of Nottingham, University Park, Nottingham, NG7 2RD, UK. E-mail: ben.pilgrim@nottingham.ac.uk

Nicholas Pearce is a post-doctoral researcher at the University of Birmingham whose current work is based around constructing mechanically interlocked molecules featuring redox and photo active components. He obtained his PhD at the University of Nottingham under the supervision of Prof. Neil Champness studying the effects of sulfur atom substitution on rylene diimide systems.

Marysia completed their MSc at Nottingham University in 2017, working on the synthesis of rotaxanes and catenanes based on pillar[5]arene and imidazole-containing alkane chain systems, as well as their manipulation, leading to very basic molecular machine properties. In 2018 Marysia joined the Champness group to begin a PhD. Their research, now continued in the Pilgrim group, focuses on supramolecular handcuff structures based on pillar[5]arene, perylene diimide (PDI) and imidazole-containing systems.

chemistry, our imagination is not restrained to the real-world and therefore the term molecular handcuff may be applied to ring systems of two or more joined loops, and molecular handcuffs may form multiple mechanical bonds with a single axle molecule.

Broadly, mechanically interlocked molecules are classified into two main categories: catenanes and rotaxanes. Molecular handcuffs too, can be divided into these two classes. For handcuff rotaxanes, the guest 'axle' does not form a closed macrocyclic loop but should penetrate both host macrocycles (Fig. 1a). The analogy with real world handcuffs is clearest in the case of handcuff rotaxanes, where the handcuffs represent the bis(macrocyclic) species and the person's arms correspond to the threaded dumbbell molecule. In this physical analogy, the arrestee's wrists serve as the recognition sites for the handcuff clips. In the case of handcuff catenanes (Fig. 1b), a bis(macrocyclic) molecule is threaded through both of its macrocycles by another macrocyclic guest molecule. This guest species may assume the form of a bis(macrocycle) itself, so both bis(macrocycles) are mutually interlocked as a cyclic bis[2]catenane.

The diversity of mechanically interlocked molecules invokes topological and architectural considerations, especially when it comes to rationalising their structure and nomenclature. As such, we have chosen to omit certain examples from this review that do not follow either a topological or architectural approach to the goal of achieving a handcuff structure. Generally, those mechanically interlocked molecules that employ a host molecule with a cryptand or cage-like structure,[7,8] have been excluded, since the cavity of these hosts typically presents only one guest recognition site and demonstrating that multiple rings have been threaded is debatable (or that multiple

Nathan Andersen studied Chemistry at Nottingham Trent University, completing his master's research under the supervision of Dr Gareth Cave, where he examined the chromatographic properties of surface modified silica-gels. He then moved to the University of Nottingham to join the Champness group for his doctoral studies, as part of the low-dimensional materials and interfaces programme, looking at chromophore interactions across mechanically interlocked molecules. His work continued as part of the Pilgrim group, where he focused on the synthesis of asymmetric rylene based rotaxanes.

Ben S. Pilgrim is a Research Fellow and Group Leader in the Green Chemicals Beacon of Excellence at the University of Nottingham, UK. He studied for his MChem at St John's College, Oxford University, UK from 2005–2009. Ben completed his doctoral studies with Timothy Donohoe in 2013 and then moved to the University of Cambridge, UK on a Herchel Smith Research Fellowship with Jonathan Nitschke on metal–organic cages. In 2016, Ben was awarded a Royal Commission for the Exhibition of 1851 Research Fellowship, and in 2019 moved to Nottingham to start his own lab in supramolecular organic chemistry. His current research interests include supramolecular catalysis, developing responsive supramolecular systems, and designing new synthetic routes to interlocked molecules.

Alexander Wahrhaftig-Lewis obtained his undergraduate degree in Chemistry from the University of Nottingham in 2018, completing his Masters' year research project with Professor Neil Champness. He is currently studying towards his PhD at the University of Birmingham, also within the Champness research group. His research is primarily focused on the synthesis and analysis of substituted pillar[5]arenes and the development of new organic linkers for metal organic frameworks.

Neil R. Champness is the Norman Haworth Professor of Chemistry at the University of Birmingham having moved from the University of Nottingham, UK in 2021. After completing his PhD at the University of Southampton, UK, with Bill Levason he moved to Nottingham in 1995, being appointed Chair of Chemical Nanoscience in 2004. His research spans chemical nanoscience and all aspects of molecular organization, including surface supramolecular assembly, the synthesis of mechanically interlocked molecules and supramolecular chemistry in the solid-state using crystal engineering approaches.

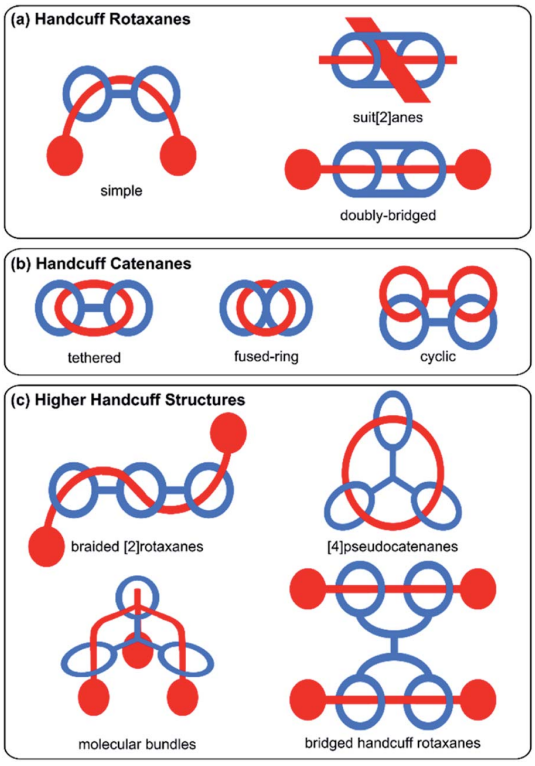

Fig. 1 Schematic representation of the types of handcuff mechanomolecules reviewed in this work.

mechanical bonds are present) from a strictly topological standpoint. We have also chosen to omit unimolecular species such as pretzelanes,[9,10] which resemble handcuffs that are 'arresting' themselves, as well as bis(macrocyclic) hosts that serve multiple guests, where the handcuff is serving as a tether between the two ensnared guests. We have, however, included higher order handcuff structures: species that comprise an oligo(macrocyclic) host to a single guest molecule that threads each of the host's macrocycles, since these species are analogous to handcuffs that would be used to arrest an entity with additional arms. These structures are clearly related to the other forms of molecular handcuffs, since in every case, the parent compound can be reduced to a handcuff system by rationalisation of the oligo(macrocyclic) host as a bis(macrocycle) that possesses additional complexity (Fig. 1c).

Considering these factors, this review aims to comprehensively survey the molecular design and synthesis of mechanically-bonded handcuff architectures as well as providing an insight into their properties and functions. We have framed our discussion of molecular handcuffs against other naming conventions, where relevant, to draw comparisons between the taxonomy of mechanically interlocked molecules, as well as to inform the reader of handcuff examples that have been alternatively categorized. We have used a new terminology to describe handcuffed structures of the form (x) handcuff [y]rotaxane/catenane. In this naming system x refers to the number of threaded macrocyclic hosts that are joined in the handcuff component of the mechanically interlocked molecule. Thus, if two macrocycles are joined, as in the simplest handcuff systems, then $x = 2$; if there are three joined macrocycles then $x = 3$ and so forth. If only two rings of a tris(macrocyclic) host are occupied by the guest, the result would be a (2)handcuff. The second term, y, refers to the number of mechanically bonded components of the rotaxane, or catenane, following the well-established protocols in the field.[5] Examples discussed throughout this article will make it clear how this terminology has been applied and where additional descriptors are required. Our discussion of handcuff architectures has been divided into three main classes based upon their structure: (i) handcuff rotaxanes, (ii) handcuff catenanes and (iii) higher order handcuff architectures (Fig. 1), and each class will be discussed in turn.

2. Handcuff rotaxanes

Perhaps the most straightforward form of molecular handcuffs to rationalise are handcuff rotaxanes that consist of a bis(macrocyclic) component that forms two mechanical bonds with a single axle component that has threaded through each macrocycle. Invoking our proposed nomenclature described above, such a system would be termed a (2)handcuff [2]rotaxane and is the closest parallel to 'real-world' handcuffs: the bis(macrocyclic) host reflects the pair of handcuffs and the molecular axle can be thought of as the person trapped within them. Indeed the most common form of molecular handcuffs are (2)handcuff [2]rotaxanes. An alternative name for this type of bridged macromolecule was proposed by Vögtle,[11] who pioneered some of the early work into handcuff rotaxanes. He suggested 'Bonnanes' after the city of Bonn in which they were based, the former bridge capital of Germany, to reflect the bridge between the pair of macrocycles.

A unique opportunity afforded by handcuff rotaxanes that does not exist for simpler [2]rotaxanes is the possibility of mechanically bonding the system with a single stopper group that lies between both macrocycles. If the system is rigid enough, dethreading can still be prevented by a sufficiently bulky central group, without the need for the axle to possess stoppers at each terminus. This principle is well demonstrated by 'suit[n]anes', a term proposed by Stoddart[12] to describe a molecular body encapsulated within a molecular suit in which n limbs are protruding. In the case of a suit[2]ane, two limbs of a central axle (the 'torso') protrude from a bis(macrocyclic) host that is typically connected with two covalent bridges (the 'suit'). Due to the great similarity between suitanes and handcuff rotaxanes, we reason that suitanes are a form of handcuff rotaxane and will discuss them as part of this section.

2.1 Strategies for handcuff rotaxane synthesis

Much as there are different mechanisms by which [2]rotaxanes can be prepared (for example: capping, slipping, ring-clipping and templating), several strategies towards the synthesis of handcuff rotaxanes have been demonstrated that include the

linking of macrocycles in a 2-ring [3]rotaxane; the linking of axles in a 2-axle [3]rotaxane; as well as the more traditional threading followed by stoppering method. Although to date the number of different synthetic approaches that have been realised in pursuit of handcuff rotaxane synthesis is quite small, we note that other methods are viable, including both ring-clipping and templating. For example, consider the case of ring-clipping; the precursor to the bis(macrocyclic) species might exist as a double clamp like molecule that associates with two active sites on a separate axle molecule; the handcuff rotaxane could then be generated by simultaneous ring closing reactions. Similarly, with suitably designed molecular components, concurrent active-templating reactions could be used to end-cap a central axle within the cavities of a bis(macrocylic) catalyst. Since these methods of handcuff synthesis have yet to be achieved, we will duly focus on those strategies which do have a literature precedent and describe them in more detail.

2.1.1 Linking synthesis. One of the earliest examples of a handcuff rotaxane-like molecule came from the Stoddart group in 2005, who employed a dialkylammonium axle that formed a pseudo[3]rotaxane with two crown ether hosts bearing olefin groups, which could then be coupled by olefin cross metathesis to afford a pseudo(2)handcuff [2]rotaxane.[13] Also in 2005 the Stoddart group reported a strategy for the reaction of dialdehyde and diamine compounds that are designed to clip around dialkyl-ammonium containing dumbbells, forming imine bonds under thermodynamic control.[14] Amongst a number of examples, the authors described a 'cyclic [4]rotaxane' which contains two handcuff molecules but as each of these do not bind to the same axle component the molecule does not fit our definition of a mechanically interlocked handcuff structure.

Soon afterwards, Sato and Takata also used the strategy of covalently linking the macrocycles of a [3]rotaxane to form a true (2)handcuff [2]rotaxane.[15] Two dibenzo[24]crown-8 (DB24C8) macrocycles functionalised with methacrylate groups on each of the benzene rings were threaded onto a dialkylammonium axle and end-capped, producing a [3]rotaxane (Fig. 2a). Connection between the wheels was subsequently

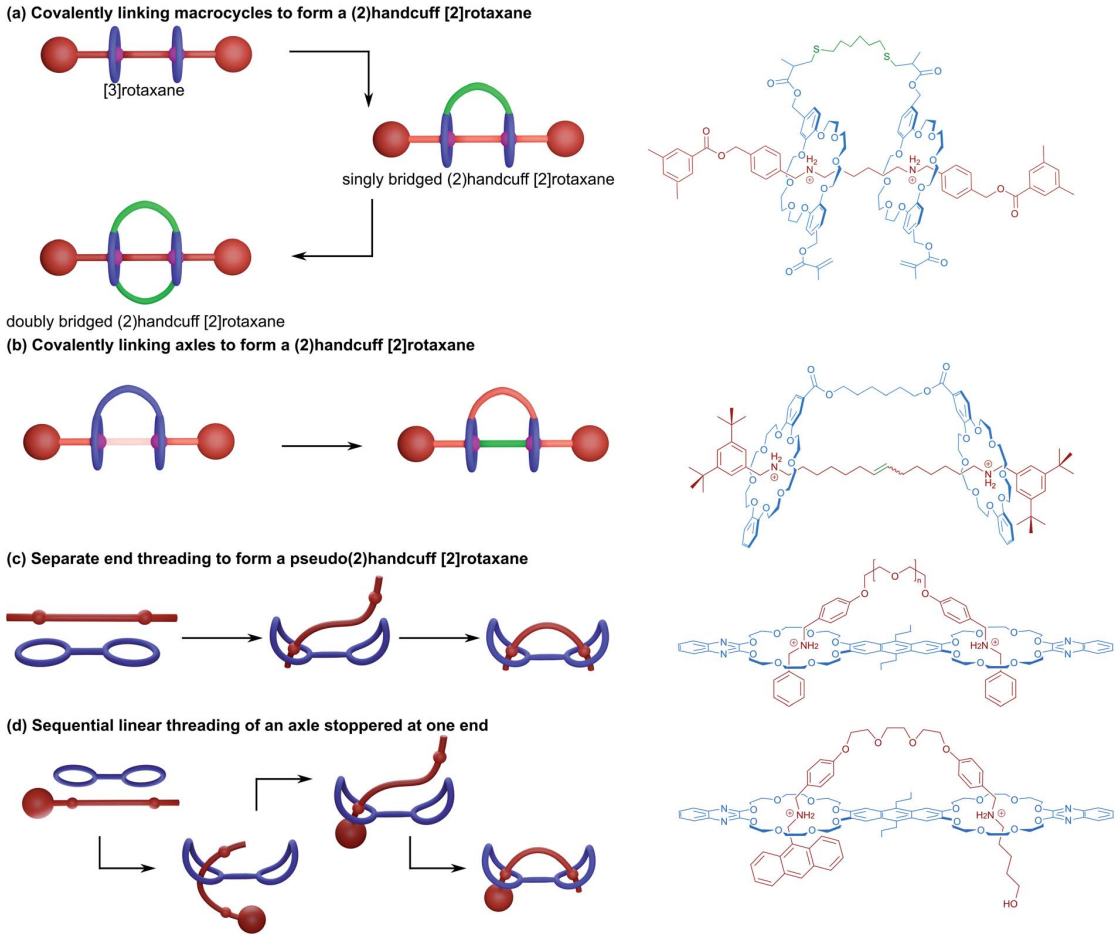

Fig. 2 Methods of (2)handcuff [2]rotaxane synthesis. (a) Linking macrocycles; (b) linking axles; (c) separate end threading; and (d) leading end threading.

achieved by two conjugate additions of hexanedithiol to this [3]rotaxane, forming the singly bridged handcuff compound as the main product when using lower reactant concentration. When the initial concentration of reactants was increased, an additional tether between the remaining methacrylate groups on the other side of the macrocycles is able to react, forming a doubly bridged (2)handcuff [2]rotaxane. Interestingly, when the conjugate addition reaction was performed on free macrocycle no bis(macrocyclic) product was detected, instead only a polymer was observed, revealing both the advantages of organising reactive components with mechanical bonds and the control over the chemistry provided through a handcuffing strategy.

The related approach of threading two axles through each ring of a bis(macrocycle) prior to linking the axles together was exhibited by Iwamoto and co-workers.[16,17] DB24C8 macrocycles were linked with ester groups and threaded with half-dumbbell alkylammonium axles bearing terminal olefins. The pre-organisation of these components permitted linking of the axles with an olefin metathesis reaction, producing the handcuff rotaxane (Fig. 2b). Ultimately the authors were interested in pursuing a high yielding synthesis of a [3]rotaxane, which could be produced directly from the handcuff by using a saponification reaction to remove the bridge between the macrocycles. The rationale of temporarily tethering the macrocycles and proceeding *via* a handcuffed intermediate proved advantageous towards overcoming the entropic limitations of directly coupling two pseudo[2]rotaxanes, where the labile macrocycles could more easily slip away prior to the metathesis reaction.

2.1.2 Threading synthesis. The majority of examples of (2)handcuff [2]rotaxanes have been formed by employing a threading and end capping process. Typically, in this procedure an axle molecule that bears two host recognition sites is mixed with a bis(macrocycle) and the two components are allowed to associate before both ends of the axle are reacted with sterically encumbering stopper groups. The recognition sites of each component must be at an appropriate spacing to permit the threading interactions, or the tethers linking each recognition unit ought to offer enough conformational flexibility such that a bimolecular association is possible. The mechanism of threading can vary between systems: the axle molecule may thread outwardly, with each end separately piercing each macrocycle (this is necessarily the case if the axle contains a central group too large to pass through either macrocycle); or by a leading end of the axle first threading one macrocycle, then the other.

A detailed study into the thermodynamic and kinetic effects of these different threading mechanisms in pseudo(2)handcuff [2]rotaxanes has been published by the Schalley group.[18] For homodivalent (symmetrical) pseudorotaxanes utilising ammonium/crown ether recognition, two mechanistic steps are involved: (i) the threading of one ammonium arm of the axle into one crown ether, followed by (ii) the threading of the second arm into the remaining crown (Fig. 2c). The Schalley group showed that if a pseudo[3]rotaxane comprised of two ammonium axles and a bis(crown ether) is mixed with a pseudo [3]rotaxane made from a divalent ammonium axle and two crown ethers, the mixture will form an equilibrium that shifts towards the formation of the pseudo(2)handcuff [2]rotaxane product where the divalent ammonium axle is associated with the bis(crown ether), and the remaining monovalent components form pseudo[2]rotaxanes. Thus, for handcuff rotaxanes, the second threading event becomes favourable due to a chelate cooperativity. Furthermore, the effects on binding of the axle to the bis(macrocyclic) host can be pronounced by additional favourable interactions between the spacer groups of the host and guest entities. If the spacer is 'non-innocent' and participates in a binding interaction or is the correct length to modulate additional favourable interactions, an enhanced chelate cooperativity is observed, representing additional thermodynamic effects upon threading.

On the other hand, Schalley and co-workers[18] were able to force sequential linear threading of a divalent ammonium axle that was stoppered at one end through a heterodivalent bis(crown ether) with two different cavity sizes. In this case threading now involves three steps: (i) threading of the leading end of the axle into the larger crown ether cavity up to the first ammonium recognition site, (ii) migration of the larger crown ether along the axle to the second ammonium station and lastly, (iii) the threading of the leading end of the axle into the smaller crown ether cavity (Fig. 2d). The different cavity sizes allowed for the kinetics of each threading step to be monitored independently, with (i) occurring on the millisecond timescale, (ii) on the second timescale and (iii) on the order of minutes. Differences in spacer length were also considered, the authors this time finding that longer spacers were more able to overcome the activation enthalpy of the second threading event, where strain in the transition state presents a barrier to handcuff formation. Consequently, the kinetically optimum spacer length may be different to the thermodynamically ideal option. Importantly, the authors conclude that whilst longer spacers can be slightly less favourable due to entropic effects, this effect is only slight, and that long, flexible tethers between binding sites remain potent to the assembly of handcuff species. A similar study into this sequential 'inchworm' mechanism of threading has been recently published by Chen and co-workers,[19] also utilising multivalent ammonium axle/crown ether host binding interactions. Through a combination of NMR spectroscopy and molecular dynamics simulations, a study into the kinetics of threading the three station axle through either bis(macrocyclic) or tris(macrocyclic) hosts was performed. The results supported those of Schalley and co-workers, confirming that whilst the first threading event is very fast, it was considerably slower for the additional threading steps to occur, due to a gradual decrease in the freedom of movement of both host and guest components imposing a significant entropic effect upon the system. When a more conformationally flexible guest was used, complete threading was achieved more quickly, accompanied by an increase in the proportion of complexed components, establishing how important axle flexibility can be in the successful synthesis of handcuff rotaxanes.

2.2 Chemical topology in handcuff rotaxane systems

The arrangement of components within handcuff rotaxanes can lead to deeper structural complexity in the form of topological isomerism. This topoisomerism may become apparent in the relative orientation of the two macrocycles (especially if chiral or cone-shaped macrocycles are used), or in the way the axle weaves around the host before threading. For heterodivalent bis(macrocycles) and directional axles, the order in which each ring is threaded also affords the possibility of topoisomerism. In this section some of the ways in which the topology of handcuff rotaxanes has been studied will be explored.

2.2.1 Stereoisomerism in handcuff rotaxanes. One of the first reported syntheses of a (2)handcuff [2]rotaxane came from the Vögtle group in 2006 who were investigating covalent reactions of rotaxanes for further preparative chemistry.[11] Vögtle and coworkers first prepared a [3]rotaxane that consisted of two sulfonamide containing macrocycles about a single axle (Fig. 3a). By reaction of the sulfonamide groups with a dihaloalkane tether, a covalent bridge was installed between the two macrocycles, forming a handcuff rotaxane by a linking synthesis. Due to the presence of one sulfonamide group per macrocyclic ring, the possibility of cyclodirectionality is introduced depending on the whether the sequence of sulfonamide and amide groups occurs in a clockwise or anticlockwise manner about the axle. Since an achiral axle was employed, cyclochirality[20] is only manifested in the relative orientation of the two macrocycles, both in the parent [3]rotaxane and the handcuff rotaxane: a *meso* form of the handcuff exists where both macrocycles share the same orientation and a pair of enantiomers (D and L forms) arise if the macrocycles have opposite directionality. All three cyclodiastereoisomeric forms were detected and separation proved to be possible. The chirality of the parent [3]rotaxane was more pronounced in the CD spectra of the enantiomers than in the handcuff form where the wheels could not rotate freely with respect to each other due to the tether, a finding which may be of significance in the creation of molecular motors or ratchets where controlled rotational motion is essential.

A study by Tokunaga and co-workers[21] examined the formation of a helically chiral (2)handcuff [2]rotaxane from achiral components. A calix[4]arene frame was used to orthogonally position two crown ether macrocycles, which were attached to alternating subunits of the calixarene. A bis-ammonium axle was complexed with the bis(calix-crown ether) and stoppered (Fig. 3b). Given the orthogonal orientation of the macrocycles, following the first ammonium/crown ether binding, the second threading event can occur from either side of the other macrocycle. Since threading from either direction is equally likely, a racemic mixture of the two helical handcuff enantiomers is produced, which could be separated by chiral HPLC. As with the cyclodirectional macrocycles of Vögtle's system, chirality was only induced when both wheels are threaded.

Tokunaga and co-workers also reported an alternative approach to introducing chirality to handcuff rotaxanes.[22] In this later example a (2)handcuff [2]rotaxane was prepared using a handcuff molecule comprising two crown ethers linked through a biphenyl group combined with a symmetrical bis-ammonium salt. The resulting species exhibits both mechanically planar and axial chirality.

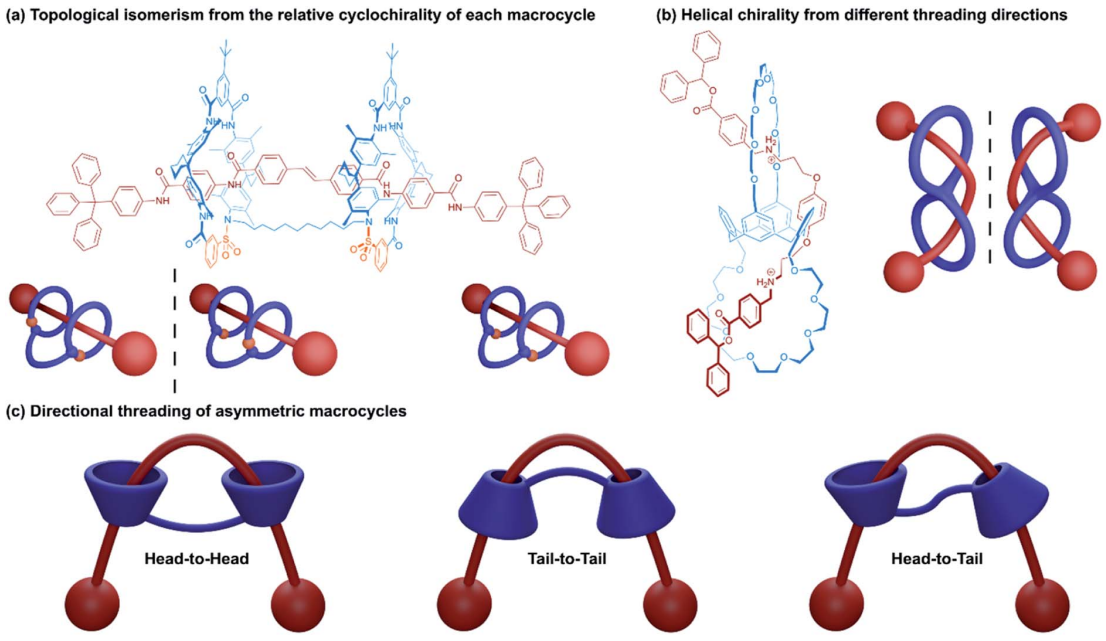

Fig. 3 Topological isomerism in (2)handcuff [2]rotaxanes. (a) Relative cyclochirality of each macrocycle; (b) helical chirality resulting from direction of threading; (c) directional threading of asymmetric macrocycles.

Another form of stereoisomerism in handcuff rotaxanes can be instituted using non-symmetrical macrocycles. Neri and coworkers note that for a bis(macrocycle) with cone-shaped calix[6]arene hosts, three stereoisomeric handcuff rotaxanes are possible with head-to-head, tail-to-tail and head-to-tail relative orientations of the calix-wheels (Fig. 3c).[23] Taking advantage of the "*endo*-alkyl rule",[24] the preference for directional threading of a calixarene by an alkylbenzylammonium guest to have the benzene ring of the guest on the phenol rim side of the calixarene, Neri and coworkers were able to synthesise a (2)handcuff [2]rotaxane with exclusively tail-to-tail orientational isomerism. Knowledge of synthetic strategies such as this can be valuable in the construction of molecular architectures with higher-order topologies, without the concern of generating undesired mechanoisomers.

2.2.2 Mechanical bond location. Described in the Introduction to this section, handcuff rotaxanes allow for the prospect of forming a mechanically bonded system where only one stopper group is required. Dethreading of the bis(macrocycle) can be limited if the axle molecule is sufficiently long that one of the macrocycles would have to pass over a sterically demanding blocking group located at the axle's centre. Indeed, this principle has been demonstrated by Chen and co-workers,[25] who were able to synthesise a pseudo(2)handcuff [2]rotaxane by complexing a triptycene derived bis(crown ether) host and a dibenzylammonium guest that contained a central anthracenyl unit too large to pass through the crown cavity. Despite lacking terminal blocking groups on the threaded axle, the stability of the complex was confirmed by NMR and fluorescence spectroscopy, as well as through an X-ray crystal structure. The guest molecule was modified further to present terminal propargyl groups, for subsequent reaction of the handcuff complex. Instead of a reaction with bulky stoppering groups, Chen decided to combine the propargyl-handcuff with a diazide using a copper-catalysed azide–alkyne Huisgen cycloaddition or 'click' reaction to form a polyhandcuff rotaxane, averaging seven handcuff monomer units (Fig. 4a). To our knowledge, this is the only example of a polyhandcuff rotaxane, and it stands to reason that the bis(crown ether) hosts must be truly mechanically bonded since the axle is comprised of numerous repeating blocking anthracenyl moieties.

Stoddart introduced us to the concept of suitanes in 2006 [12] as a mechanically interlocked molecular architecture in which a central molecular body is encompassed by a close fitting molecular 'suit' that is distinguishable from capsules and carceplexes by the protruding limbs of the central body. In pursuit of this molecular composition, Stoddart and co-workers assembled a pseudo[3]rotaxane from two [24]crown-8 rings bearing aldehyde groups and a dibenzylammonium axle. The ammonium recognition sites of the axle were separated by a bis(anthracenyl) core, able to prohibit further movement of the macrocycles. A dynamic covalent chemistry approach was used to connect the two macrocycles in the pseudo[3]rotaxane with imine bonds through the reaction of the aldehyde groups with two equivalents of *p*-phenylenediamine, forming the suitane. Computational force-field modelling, coupled with solid-

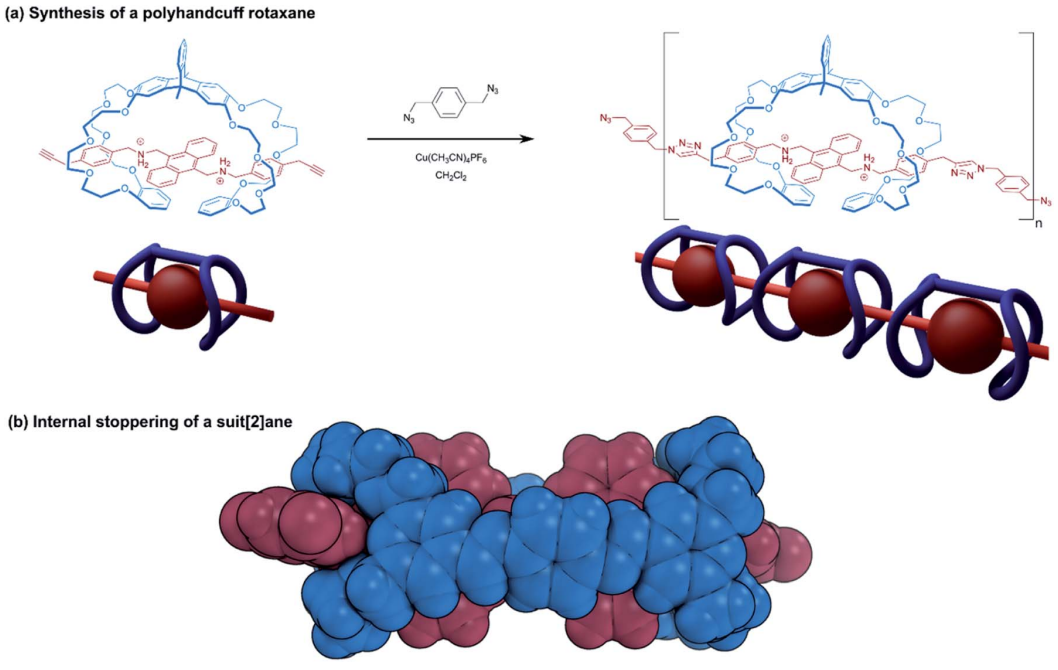

Fig. 4 Handcuff rotaxanes with sterically limiting groups placed between the two macrocycles. (a) Synthesis of a polyhandcuff rotaxane; (b) single crystal X-ray structure of a suit[2]ane.

state structural data of the suitane from single crystal X-ray crystallography indicate that supplementary interactions between the phenylene linker and the anthracenyl core play a role in further stabilising the structure (Fig. 4b). Moreover, the integrity of the suitane's mechanical bonds was evidenced by the lack of any free host or guest present in a sample of the suitane that had been heated for 30 days. Comparing the suitane's synthetic strategy with the linking synthesis of Sato and Takata[15] (see Section 2.1.1), reveals many similarities between the suitane and doubly-bridged handcuff rotaxanes: the difference in mechanical bond location is somewhat superficial to the overall structure; the deeper principles of rational molecular design and supramolecular chemistry unite suitanes and handcuffs.

In suitanes and doubly-bridged handcuff rotaxanes, the second connecting bridge between the macrocycles creates a third macrocyclic unit, the aperture of which lies perpendicular to those of the original macrocycles. The different composition of the third macrocycle endows it with different chemical properties to the two flanking macrocycles and thus, may provide the possibility of different host–guest chemistry. The threading modes of a macrotricyclic host consisting of two DB24C8 macrocycles, wherein one pair of benzene rings formed part of a triptycene bridge and the other pair an anthracene bridge, was examined by Chen and co-workers.[26] The aliphatic paraquat derivative, 1,1′-di(6-hydroxyhexyl)-4,4′-bipyridinium formed complexes with the macrotricyclic host where each hydroxyhexyl tail participated in a threading interaction with each DB24C8 host, and could later be stoppered to form the corresponding (2)handcuff [2]rotaxane. Modification of the viologen to replace the hydroxyhexyl groups with a bulkier substituent that could not thread the crown cavity still allowed for construction of a [2]rotaxane, in this case however, it was the third macrocylic cavity, circumscribed by the triptycene and anthracene bridges that was threaded, and no handcuff was formed. A related structure published by Chiu and co-workers,[27] complexed a bridged DB24C8 macrotricyclic cage with an alkylammonium axle to form a [2]rotaxane. The axle only contained one ammonium recognition site and consequently only one crown ether was threaded. Despite certain topological similarities between this rotaxane and handcuff structures, from a supramolecular standpoint, the mechanical bond location sets this structure apart from true handcuff species.

A conceptually related strategy has been reported recently by Pöthig and co-workers.[28] In their system they assemble a [2]rotaxane using a macrocyclic component based on a so-called 'pillarplex', a complex in which two imidazolium containing macrocycles are linked through the formation of bis-N-heterocyclic carbene silver(I) moieties. This cylindrical macrocycle is threaded by simple a diamine rod which can be stoppered through amide bond formation. Interestingly, the silver cations can be removed by addition of acid leading to the formation of a [3]rotaxane in which the two imidazolium-containing macrocycles are separated from each other. The process is reversible establishing a mechanism for conversion between [2] and [3]rotaxanes. The system has clear parallels to the suitane structures described above.

2.3 Controlling motion in handcuff rotaxanes

Precise control over molecular motion is one of the most significant attributes of mechanically interlocked supramolecular chemistry. Compared to covalent chemistry, the freedom of movement permitted by the mechanical bond allows for the construction of more advanced molecular machines.[29] In the field of rotaxanes, perhaps the most prevalent example of controlling molecular motion leading to a machine-like application is the construction of bistable molecular switches.[30] The position of the macrocycle along an axle containing two chemically distinct stations can be reversibly controlled by external stimuli that favour interactions between one station over the other. In [2]rotaxane switches, typically the motion of the components is purely relative: the ring moving along the axle is indistinguishable from the axle moving through the ring. This is not necessarily the case in switches built using handcuff rotaxanes, where conformational rigidity of either the bis(macrocyclic) component or the axle means that more substantial rearrangement might be imposed on just one of the molecular species for the system to move between its two states. We will demonstrate this principle in detail by first considering motion in switchable (2)handcuff [2]rotaxane systems built around conformationally restrictive bis(macrocycles).

2.3.1 Rigidity in the bis(macrocyclic) component. An early doubly-bridged handcuff rotaxane was reported in 2007 by Chiu and co-workers[31] that could undergo translational motion of the host about the axle in response to various stimuli. The system incorporated a macrotricyclic host; where two DB24C8 moieties were bridged with bicyclo[2.2.2]octyl linkers to form a rigid cage-like structure; and an axle with central pyridinium sites and terminal benzylammonium stoppers (Fig. 5a). Translation of the host to one end of the axle could be achieved by increasing affinity of the host for the ammonium stations, which proved to be possible through three mechanisms: (i) altering the polarity of the solvent, (ii) changing the counterions, or by (iii) lowering the pH. Decreasing the affinity of the host for the ammonium stations (*e.g.*, by increasing the pH), saw the position of the host return to the centre of the axle and occupy both pyridinium stations.

A subsequent collaboration between Chao and Chiu[32] used the same macrotricyclic host with a restructured axle that contained central alkylammonium stations and pyridinium stoppers. Synthesised and crystallised as the PF_6^- salt, the crown ethers interact with the central alkylammonium stations, and the axle can adopt a linear 'stretched' conformation (Fig. 5b). Upon the addition of four equivalents of tetrabutylammonium fluoride, the axle rearranges to allow for interaction between the pyridyl and crown ether groups, established by changes to the NMR spectrum of the handcuff that showed the extrusion of the central aliphatic chain through the flanking macrocycles with changes to the shifts of the pyridinium and aliphatic chain protons, indicating complexation. The authors advocate that this rearrangement is due to disruption of hydrogen bonds between the ammonium centres and crown ethers by the fluoride ions, leading to a more favourable interaction with the pyridinium units. As the fluoride salt, the axle of the handcuff is

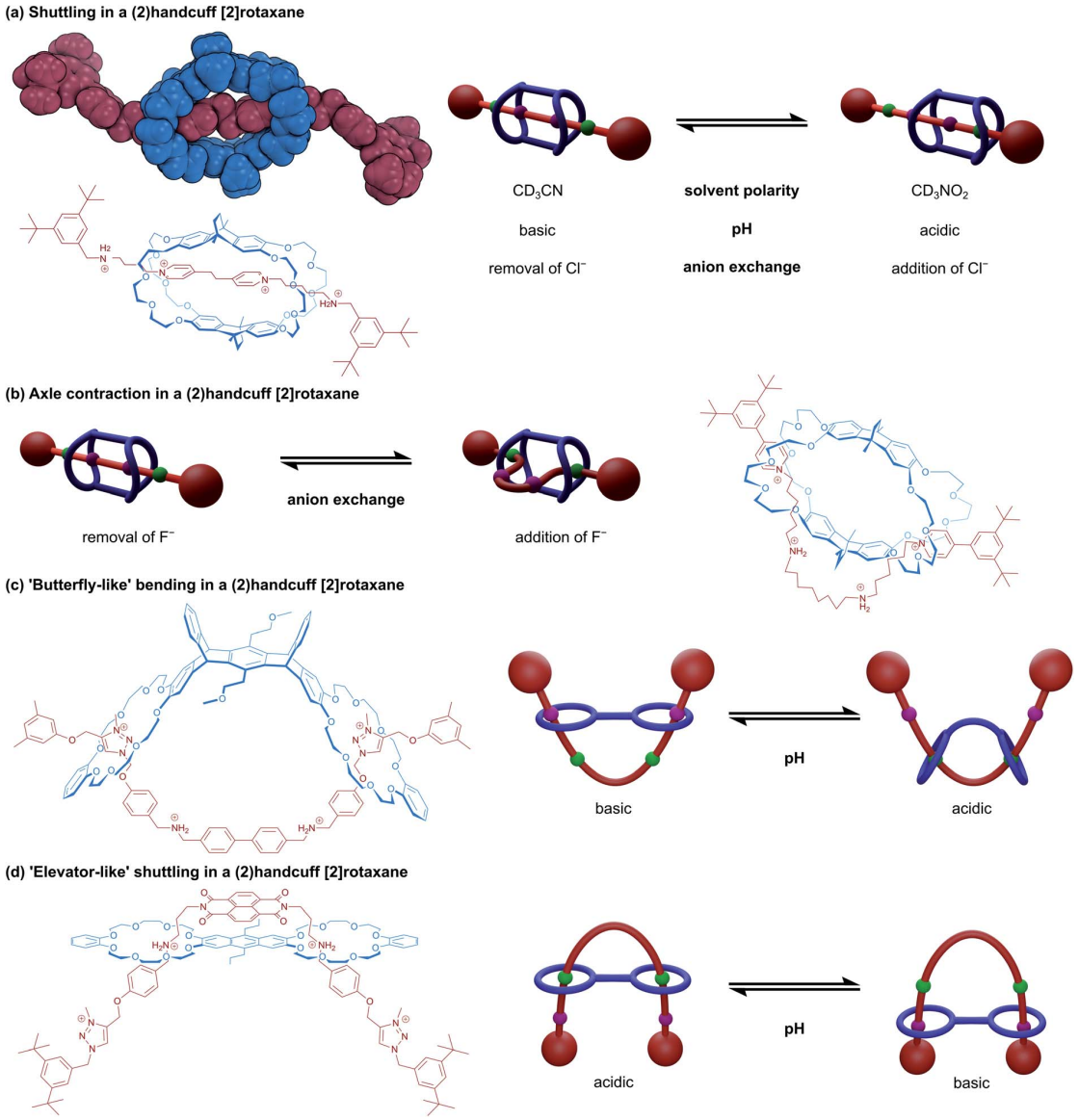

Fig. 5 Controllable motion in (2)handcuff [2]rotaxanes. (a) Shuttling motion including a view of the single crystal X-ray structure; (b) axle contraction; (c) 'butterfly-like' bending; (d) 'elevator-like' shuttling.

considerably shorter end-to-end since the central portion must move out through the aperture of the remaining (non-crown) ring, dubbed the 'contracted' form. The rigidity of the bridges connecting the crown ethers prohibits expansion of the host to accommodate this change. The length change between stretched and contracted states was calculated through molecular dynamics simulations as 36%, which is greater than in human muscle. Precipitation of the fluoride with calcium tetrafluoroborate restored the stretched conformation of the handcuff.

A very similar study into a handcuff rotaxane derived molecular muscles was published by Qu and co-workers.[33] An anthracene bridged bis(crown ether) was complexed with an axle containing a central ferrocene unit, that was flanked by benzylammonium groups and capped with triazolium based stoppers. Under acidic conditions, the protonated ammonium groups interact strongly with the crown ethers and under basic conditions, the outmost triazolium moieties are preferred over the deprotonated benzylamines. Here, a length change of 15.8 Å or 48% is reported, facilitated by mutual rotation of the two cyclopentadienyl rings of the ferrocene, displaying a combination of both translational and rotary motion in a single-molecule system. Chen and co-workers also employed an axle composed of central benzylammonium recognition sites and

flanking triazolium stoppers in an acid/base switchable (2)handcuff [2]rotaxane.[34] Some key differences are that the DB24C8 macrocycles were connected as part of a larger, pentiptycene based scaffold, and secondly the central benzylammonium sites were directly adjoined as *p*-biphenyl (Fig. 5c). In this instance, although switching from ammonium to triazolium stations does cause a similar bending of the axle, a concomitant distortion of the pentiptycene host is required. This opening out of the bis(macrocycle) was likened to that of "a butterfly spreading its wings" and represents another form of controllable motion available to handcuff systems.

Elevator-like motion has also been described for handcuff rotaxanes. A two station benzylammonium/triazolium axle with a central naphthalene diimide (NDI) was complexed with an anthracene bridged bis(crown ether) by Liu and co-workers (Fig. 5d).[35] At low pH, the inner benzylammonium groups are protonated and interact with the crown ethers, which also brings the axle's NDI and host's anthracenyl chromophores in close proximity (3.9 Å), quenching the fluorescence of the system. A charge transfer band can be observed in the absorption spectrum of the handcuff that is not present for either isolated component. Addition of base to the handcuff moves the bis(crown ether) elevator platform to the triazolium stations and separates the anthracenyl and NDI chromophores to a distance of 12.4 Å. Interestingly, we note that although Liu[35] used the same bis(macrocycle) as Qu,[33] the computationally calculated structures of the systems exhibit markedly different conformations of the bis(macrocycle). In Liu's work, the bis(macrocycle) possesses an almost planar conformation, which means the axle must adopt a U-shaped conformation to thread through both rings, and the two arms of the axle serve as the elevator 'shaft'. On the other hand, in the system described by Qu, the crown ether units curl round and allow the axle to thread both rings whilst remaining roughly linear and stretched out. We reason that the size and charge complementarity between the two central components in Liu's handcuff may account for the conformational differences that lead to the dissimilarities in reported motion.

2.3.2 Rigidity in the threaded component. When a more conformationally restrictive axle is used in a handcuff rotaxane system, it is instead the bis(macrocyclic) element that may have to endure structural rearrangement to allow for motion between stations along the axle. Sauvage and co-workers[36,37] prepared a [3]rotaxane that used a linear rod-like axle whose central portion contained eight *para*-connected aromatic rings (Fig. 6). The central four rings provided a dual 2,2-bipyridine

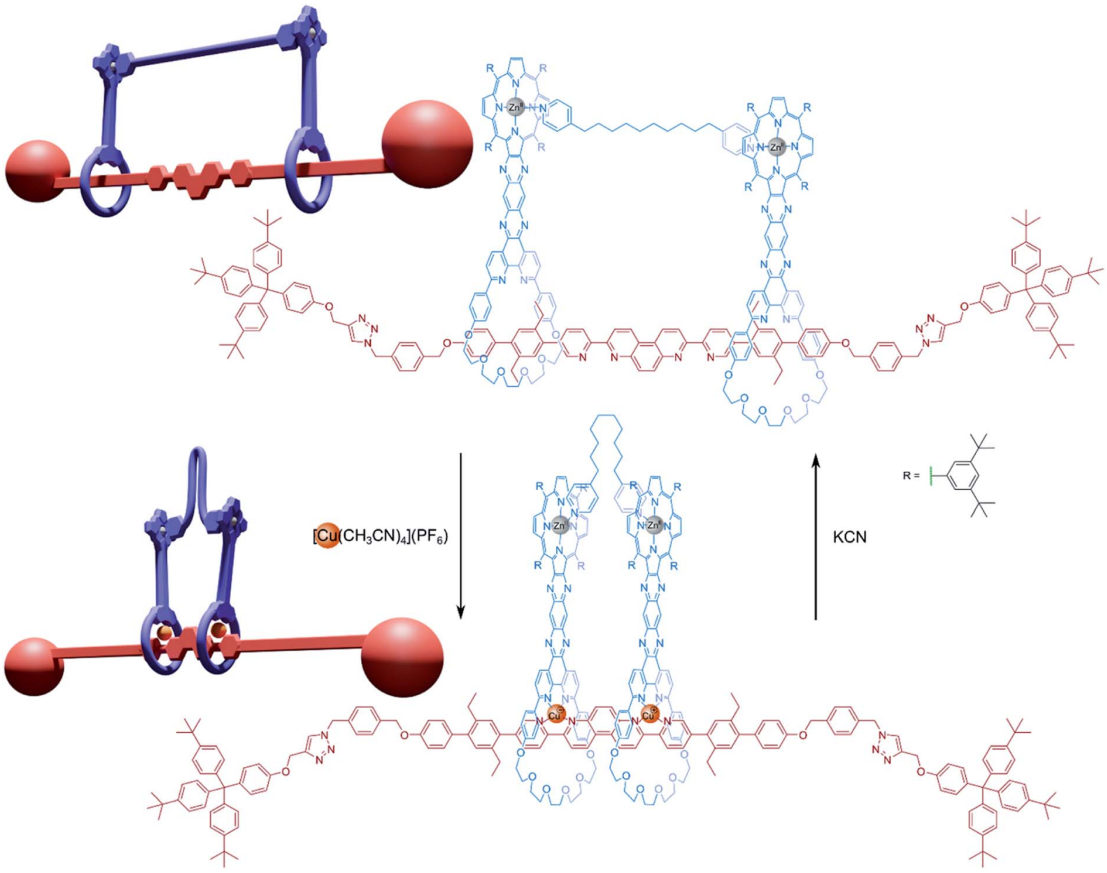

Fig. 6 Compressor/extensor or accordion-like motion about a rigid axle.

functionality from a 4,7-phenanthroline nucleus, allowing metal-templated complexation with 1,10-phenanthroline-based macrocycles, and the system was then stoppered using a 'click' reaction that introduced triazole stations to the axle as well as the encumbering end caps. The macrocycles of the [3]rotaxane also bore zinc-porphyrin functional groups that were connected directly to the phenanthroline moieties by a fused ring arrangement.

This [3]rotaxane could be converted into a handcuff rotaxane by using a linking synthesis to bridge the zinc-porphyrin centres with various dipyridyl ligands. When the rotaxane is complexed with copper(I), the positions of the two porphyrin plates are controlled by the geometry of the central axle, which forms coordination complexes with through its bipyridyl units with the phenanthroline groups of each macrocycle. Since the position of the macrocycles is rigidly defined, the linking dipyridyl tethering molecule must adopt a conformation to fit in the available space between the two porphyrin plates and may have to fold or compress considerably. If the copper(I) centres are removed, the macrocycles become free to glide along the 80 Å axle and the tether can extend to a preferred conformation that will instead determine the separation of the macrocyclic 'wheels'. Sauvage found that this [3]rotaxane architecture could form handcuff compounds with tethers ranging from 2.8 Å (DABCO) to 18 Å (1,10-di(4-pyridyl)decane). In the case of the 18 Å tether, the metalated form of the handcuff complex becomes destabilised due to distortions imposed on the tethering molecule, however, the tether is still able to bind. As such, the authors rationalised the motion exhibited by this structure as functioning as a reversible 'compressor/extensor', or perhaps like an accordion.

2.3.3 Redox control over handcuff systems. Mechanically binding molecules together as handcuffs is an efficient strategy for the positioning interesting molecular species close in space, whilst still allowing for free movement as required. Schalley and co-workers[38] prepared a (2)handcuff [2]rotaxane from a tetrathiafulvalene (TTF) based bis(macrocycle) and an NDI equipped with the appropriate benzylammonium recognition sites. The absorption spectrum of the resulting handcuff displayed a strong intramolecular charge-transfer between the electron donating TTF unit and the electron accepting NDI, which may have helped the self-assembly process. Electrochemical investigations of the NDI-TTF handcuff revealed that the compound was stable across five redox states, and this redox stability was improved greatly over the free axle and wheel components, although the first oxidation potential (associated with the TTF chromophore) occurred at higher potential, due to stabilisation of the neutral state by intramolecular charge-transfer and the already dicationic nature of the handcuff. The optimised geometries of all five redox states of the complex were computed, finding that the separation between the NDI and TTF planes increases with both oxidation and reduction as the attractive charge-transfer interaction is lost.

Champness and co-workers[39] also prepared redox active handcuff rotaxanes that positioned perylene diimide (PDI) chromophores in close proximity by means of pillar[5]arene/imidazolium rotaxane formation. The PDI units of axle and host species communicate strongly with π-stacking interactions, especially visible in the emission spectrum of the handcuff, which displayed an excimer-like profile, indicating electronic coupling between the two π-systems. This handcuffed compound was also stable across multiple redox states and capable of accepting four electrons. Spectroelectrochemical measurements of the two-electron reduced PDI–PDI handcuff unveiled a unique absorption profile for a PDI-based molecule that was assigned to the formation of a π-dimer that is not seen for rigidly spaced PDI–PDI dimers. The addition of two more electrons to the handcuff resulted in the loss of interaction between the two PDI units. A similar NDI–PDI handcuff rotaxane was also synthesised in which the addition of four electrons could be achieved in independent steps. Although features in the absorption and EPR spectra of the one-electron reduced NDI–PDI handcuff show little evidence of charge hopping between the two chromophores, this does seem to be possible for the two-electron reduced handcuff: EPR activity is lost, and the absorption profile is distinct from those of typical NDI^- and PDI^- chromophores. The strategy of molecular handcuffs provided a unique opportunity to probe interactions between redox centres that was enhanced by the flexibility granted to the system from the use of mechanical, not covalent bonds.

3. Handcuff catenanes

The natural partner to handcuff rotaxanes are handcuff catenanes, where the bis(macrocyclic) species is threaded through each ring by another single macrocycle. Following our suggested terminology, this arrangement would be called a (2)handcuff [2]catenane, reflecting that a two-ringed host is threaded by a second guest molecule. Since a handcuff catenane is the topological result of covalently connecting the two outer rings in a linear [3]catenane, the name pseudo[3]catenanes, introduced by Becher[40] is also used occasionally in the literature. Interestingly, despite being a viable synthetic strategy for the synthesis of handcuff catenanes, we have not found any examples of handcuff catenanes that were constructed in this manner.

We also consider the mutual interlocking of two separate bis(macrocyclic) species to be a form of (2)handcuff [2]catenane: a two-ringed component is threaded through each macrocycle by a single species (that happens to also have bis(macrocyclic) structure), and two mechanical bonds are present in the form of the intertwined rings of a catenane, so the structure must qualify as both a (2)handcuff and a [2]catenane. This molecular architecture is most commonly referred to as a cyclic bis[2]catenane and we expand our discussion of handcuff catenanes to include these interesting arrangements.

3.1 Linear handcuff catenanes

Much as described for handcuff rotaxanes in Section 2.1, one might imagine different synthetic routes could be employed to produce a handcuff catenane. The catenane counterpart to the rotaxane 'linking synthesis' would involve covalently bridging two macrocycles in a [3]catenane to form the bis(macrocycle); whereas a threading synthesis would proceed as it does for

a handcuff rotaxane, but instead of introducing stopper groups to the pseudo(2)handcuff [2]catenane, the ends of the threaded component are joined to each other, forming the third macrocycle. The latter case of threading a bis(macrocycle) is considerably more common amongst literature examples, though some differences arise from the connectivity of the two macrocycles. The two rings might be fused together by a central molecular species that serves as the recognition site for the thread, such that encircling this central species is accompanied by a concomitant threading of both macrocycles. Alternatively, the two macrocycles might be separated by a non-interacting tether and it is more important for the threading species to have affinity for the macrocyclic loops to ensure that threading occurs prior to the macrocyclisation step.

3.1.1 Fused-ring handcuff catenanes. The earliest synthesis of a (2)handcuff [2]catenane was reported by Becher and co-workers in 1995.[40] Taking advantage of the tendency of TTF to form a strongly associated 1 : 1 charge-transfer complex with cyclobis(paraquat-*p*-phenylene), a bis(macrocycle) was designed around the TTF unit that would maximise π–π interactions with the paraquat species (Fig. 7a). Thus, macrocycles were formed by equipping a tetrathiolated TTF with glycolic loops, bridged by hydroquinone or anthraquinone spacers, that would lead to a separation between the TTF and these electron rich spacers of approximately 7 Å, optimal for binding the paraquat cyclophane. Unlike Schalley's TTF-based bis(macrocycle)[38] where each end of the TTF unit was part of a separate macrocycle, in Becher's system, the macrocycles were connected across the long axis of the TTF centre, leading to *cis*/*trans* isomers that could interconvert in solution. Handcuff catenanes were synthesised *via* the reaction of the precursor components of cyclobis(paraquat-*p*-phenylene) in the presence of the TTF bis(macrocycle). For the hydroquinone-spaced bis(macrocycle), both *cis* and *trans* isomers of the handcuff were obtained, which could be separated from each other and characterised independently. These isomers did not interconvert, even in the presence of trifluoroacetic acid, indicating that the paraquat cyclophane inhibits TTF protonation that would lead to isomerisation. The oxidation potentials of the TTF centre increase for the handcuff catenanes compared to the free bis(macrocycles) due to charge transfer between the cyclobis(paraquat-*p*-phenylene) and the encircled TTF, though no significant difference was noted for the *cis* and *trans* isomers, implying that the change in handcuff configuration does not greatly affect its electron donating ability.

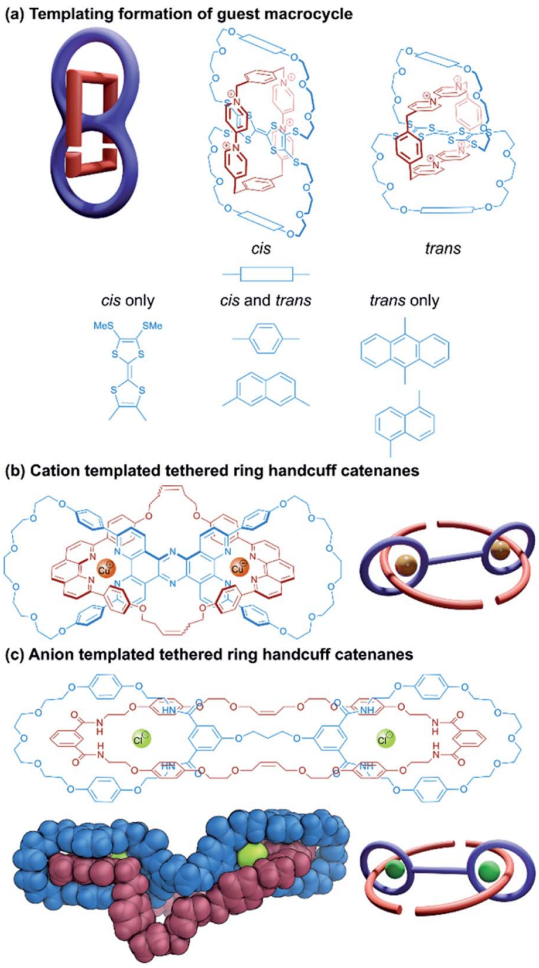

Fig. 7 Structures of (2)handcuff [2]catenanes. (a) Fused-ring catenanes synthesised by templating the formation of the guest macrocycle; (b) tethered-ring handcuff catenanes synthesised through copper(I)-phenanthroline templating; (c) tethered-ring handcuff catenanes synthesised through chloride-amide hydrogen bond templating including a view of the single crystal X-ray structure.

The handcuff catenane containing anthraquinone spacers was only obtained as the *trans* isomer, the yield of which was greatly improved by repeating the reaction at high (10 kbar) pressure. A supplementary study by Li and Becher[41] replaced the anthraquinone moieties with further TTF units, which CPK modelling determined would allow for essential π–π donor–acceptor interactions only when the central bis-loop TTF unit was in the *cis*-configuration.

This proved to be true experimentally, and the corresponding handcuff catenane was obtained solely as the *cis*-isomer, whose D_{2h} symmetry was readily identifiable by ^{1}H NMR spectroscopy. On the other hand, the anthraquinone *trans*-isomer possesses D_2 symmetry and a strong temperature dependence is seen in the ^{1}H NMR spectrum.[40] Handcuff catenane formation was also explored with bis(macrocycles) incorporating 1,5- and 2,7-dioxynaphthalene spacing units.[42] The 1,5-dioxynaphthalene containing bis(macrocycle) efficiently and exclusively formed the *trans*-isomer in 48% yield, whereas its constitutional isomer containing 2,7-dioxynaphthalene formed a mixture of handcuff isomers in a lower overall yield of 28%. CPK modelling showed only the *trans*-configuration of the bis(macrocycle) containing 1,5-dioxynaphthalene spacers can adopt an energetically favourable conformation for the self-assembly process; the 2,7-variant must twist into an energetically unfavourable state to achieve a suitable orientation for handcuff catenane formation.

Finally, Li and Becher[43] examined the effect of modification to the cyclobis(paraquat-*p*-phenylene) component of their handcuff catenane systems by replacement of the phenylene

linkers in the cyclophane with tetrafluorophenylene. Compared to the highly efficient *trans*-handcuff catenane formation for the 1,5-dioxynaphthalene spaced bis(macrocycle),[42] the introduction of fluorine reduces the efficiency of the self-assembly process and also reverses the configurational selectivity. When both phenylene linkers are tetrafluorophenylene linkers, the *cis*-handcuff is the major product; when only one phenylene linker is fluorinated, the *trans*-isomer is still preferred over the *cis*-configuration in a 5 : 3 ratio, contrasting the exclusively *trans*-arrangement for unfluorinated cyclobis(paraquat-*p*-phenylene). In this case, π–π interactions between the threading species and the loops of the bis(macrocyclic) host become more relevant, as the electron deficient tetrafluorobenzene forms donor–acceptor stacking interactions with the electron rich 1,5-dioxynaphthalene units.

3.1.2 Tethered-ring handcuff catenanes. In designing handcuff catenanes in which the two macrocycles of the bis(macrocyclic) component are separated spatially by a covalent tether that does not contain a useful chemical recognition site, some mechanism must be put in place to ensure the threading species passes through the macrocycles and remains there until the final macrocycle has been synthesised. To this effect, Sauvage and co-workers used an ion templating strategy in the self-assembly of a pseudo[3]rotaxane,[44,45] where allylic ends of the two threaded species could be coupled together with simultaneous ring-closing metathesis (RCM) reactions (Fig. 7b). A bis(macrocycle) was designed with back-to-back chelating phenanthroline units that could take advantage of the templating effect of copper(I) cations to hold two phenanthroline threads within each of its cavities. The ends of these threads were held in close proximity, so the olefin metathesis reactions that form the final macrocycle proceeded efficiently, although no diastereomeric selectivity was reported. Despite the aromatic link between the two copper centres in the handcuff complex, no electronic communication between them was found by electrochemical analysis.

A very similar approach towards handcuff synthesis was realised by Beer and co-workers,[46] who employed a chloride anion template to organise isophthalamide components in a suitable orientation for RCM reactions to afford a handcuff catenane (Fig. 7c). Elucidation of the single crystal structure of the handcuff revealed the importance of the chloride template by the orthogonal arrangement of isophthalamide recognition sites in the host bis(macrocycle) and guest macrocycle. In the solid state, bunching of the ethereal portions of the guest macrocycle and bis(macrocyclic) tether occurs creating a crypt-and-like cavity, which the authors propose might serve as a useful cationic binding site. Overall, this might allow the handcuff catenane to function as an ion-pair receptor.

3.1.3 Chemical topology in handcuff catenanes. As with handcuff rotaxanes (see Section 2.2), handcuff catenanes also offer the possibility of topological isomerism as the components orient themselves around and through each other. Stoddart and co-workers have demonstrated such topological isomerism in the self-assembly of a (2)handcuff [2]catenane comprised of two fused cyclobis(paraquat-*p*-phenylene) cyclophanes through which a bis-1,5-dioxynaphtho[50]crown-14 macrocycle was threaded (Fig. 8).[47] The synthesis of this handcuff catenane is unique in that the guest naphtho-macrocycle templates the formation of the bis(macrocyclic) host. Similar

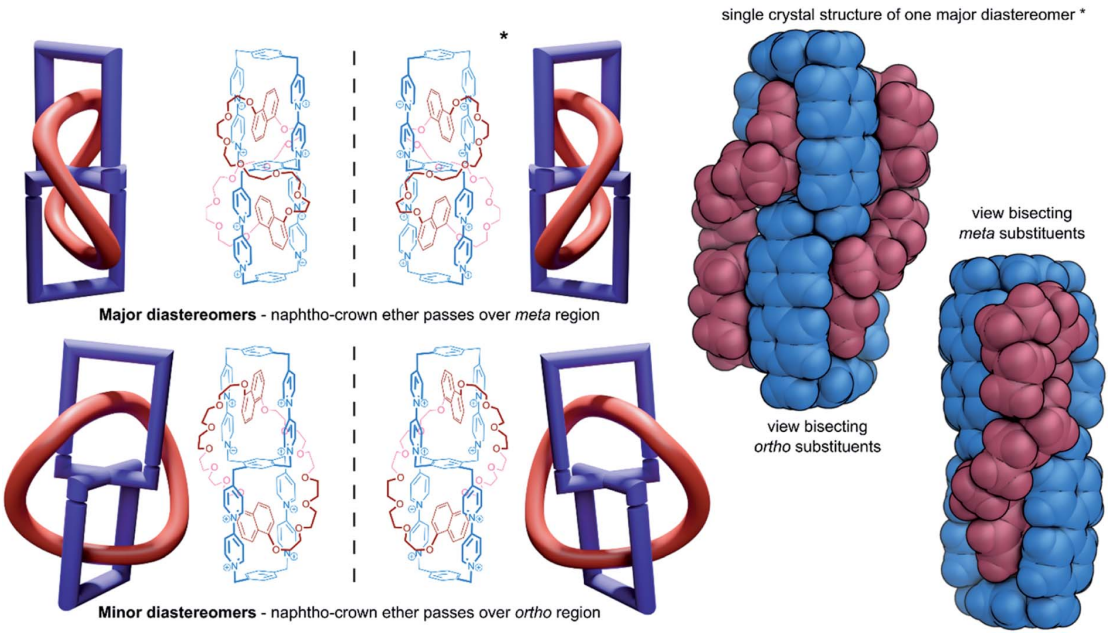

Fig. 8 Chemical topology in handcuff catenanes governed by the large macrocycle orientation, with two views of the single crystal X-ray structure of the major diastereoisomer.

to the chiral handcuff rotaxane reported by Tokunaga,[21] a pair of mirror-image enantiomers are formed depending on which direction the crown ether threads through the cavity of the second paraquat box of the bis(macrocycle). Unlike Tokunaga's system where the two rings of the bis(macrocycle) were fused orthogonally, in Stoddart's bis(macrocycle), the two cyclophane rings are fused about a phenyl ring, at 60° to each other, allowing the large macrocycle to wind about its host in two distinct paths. The naphtho-crown ether may pass over the central phenyl ring of the bis(macrocycle) through the small gap between the cyclophanes (designated the '*ortho*-region'), or through the large gap (the '*meta*-region'), creating a pair of topological diastereoisomers that cannot interconvert without the breaking of a covalent bond. Single crystal structure determination of the handcuff catenane ascertained that the major product of the synthesis was the *meta* isomer, which co-crystallised as an enantiomeric pair. Careful analysis of the handcuff in the solution state by NMR spectroscopy indicated the presence of another molecular species, whose identity was assumed to be the *ortho*-topological isomer. Interestingly, DFT calculations predict that in a vacuum the *ortho*-isomer is slightly favoured energetically, whereas under a solvation model the *meta*-isomer is thermodynamically preferred, matching the experimental outcome. Compared with handcuff rotaxanes, studies into the chemical topology offered by their catenane counterparts are much rarer. Many of the same opportunities for mechanoisomerism exist that may be explored in the future.

3.2 Cyclic handcuff catenanes

Cyclic bis[2]catenanes are mutually interlocked bis(macrocyclic) systems akin to two pairs of handcuffs that are arresting each other. Cyclic handcuff catenanes are topologically distinguished from linear (2)handcuff [2]catenanes, which are made from a total of three macrocycles instead of four. Here we note that related cyclic [2]rotaxane systems, or [c2] daisy chain rotaxanes,[48–50] are the only remaining example of two-component doubly mechanically bonded structures, though in this case the absence of a bis(macrocyclic) species from their structure precludes them from classification as handcuff molecules. Preparation of cyclic bis[2]catenanes may follow many of the same design and construction principles seen already for handcuff rotaxanes and linear handcuff catenanes: *i.e.*, a bis(macrocycle) must form two mechanical bonds with a single guest species, though new synthetic avenues are also opened as a result of their homodimeric nature.

3.2.1 Cyclic handcuff catenanes with simple tethers. Some of the earliest examples of cyclic bis[2]catenanes that have been reported were side products in the attempted synthesis of pretzelanes,[9,10] interlocked structures based upon [2]catenanes whose rings are also linked covalently. Vögtle and co-workers prepared a [2]catenane system from macrocycles that contained sulfonamide groups,[9] offering a reactive site for further functionalisation. Alkylation with a suitable difunctional reagent did succeed in intramolecularly linking the two catenated rings, producing the pretzelane target, but also afforded a cyclic bis[2]catenane product where pairs of [2]catenanes are linked through reaction with two of the tethering molecules. Stoddart and co-workers also produced a cyclic bis[2]catenane as a side product of a pretzelane synthesis.[10] An electron rich dioxynaphtho-crown ether was functionalised with a *p*-xylylene dibromide derivative that is capable of reacting to form the familiar electron deficient macrocycle cyclobis(paraquat-*p*-phenylene) cyclophane, when combined with its bis(paraquat-*p*-phenylene) precursor (Fig. 9a). The dioxynaphthalene group templates the formation of the cyclophane, so if the cyclisation occurs intramolecularly a pretzelane forms and intermolecular reactions lead to cyclic (or linear) catenane oligomers. Experimentally, the cyclic bis[2]catenane was favoured over the pretzelane with respective isolated yields of 20% and 14% for the two compounds. Stoddart's cyclic crown ether/paraquat cyclophane handcuff represents the only example of a bis[2]catenane where the bis(macrocyclic) component contains two different types of macrocycle.

Yano and co-workers have also reported several cyclic bis[2]catenanes as side products of poly[2]catenane synthesis, where [2]catenanes bearing reactive groups have been linked by further covalent coupling reactions.[51–53] In some cases two complementary [2]catenanes were joined directly, for example, [2]catenanes containing pendent carboxylic acid groups were combined with [2]catenanes bearing pendent phenol or aniline moieties to form ester-bridged or amide-bridged polycatenanes and cyclic handcuffs.[53] In another instance, a simple ditopic bisalkyne linker was employed as a means of linking [2]catenane monomers with pendent azide groups through a 'click' reaction (Fig. 9b).[51]

A targeted approach to cyclic handcuff catenane synthesis was reported by Fujita and co-workers as a method of producing exceptionally large 'ultramacrocycles'.[54] Taking advantage of the reversible 'magic-ring' catenation exhibited by palladium clipped macrocycles when exposed to polar solvents,[55] a bis(macrocycle) was prepared that tethered two of these palladium macrocycles together (Fig. 9c). The addition of water to a DMSO solution of the palladium-bis(macrocycle) induced catenation of the coordination rings as cyclic handcuff dimers, confirmed by mass spectrometry and DOSY spectroscopy. The authors suggest that their technique of using reversible catenation overcomes some of the entropic disadvantages of uniting large components by providing a comparably large reaction centre. Due to the labile nature of the mechanical bonds in this system, this study represents an example of molecular handcuffs that can be unlocked and relocked at will.

Stang and co-workers have also recently reported a cyclic bis[2]catenane platinum metallacage that can be transformed between locked and unlocked topologies by guest exchange, concentration and solvent stimuli (Fig. 9d).[56] The cyclic bis[2]catenane formed at much lower concentrations than homologous [2]catenane monomers of the untethered macrocycle, due to the synergistic effect of multiple catenation events.

Dynamic ring formation has also been used by Chiu and co-workers in the fabrication of cyclic bis[2]catenanes.[57] The group had previously developed a [2]catenane synthesis that uses sodium ions to template the orthogonal alignment of two di(ethylene glycol) diamines which are then cyclised through

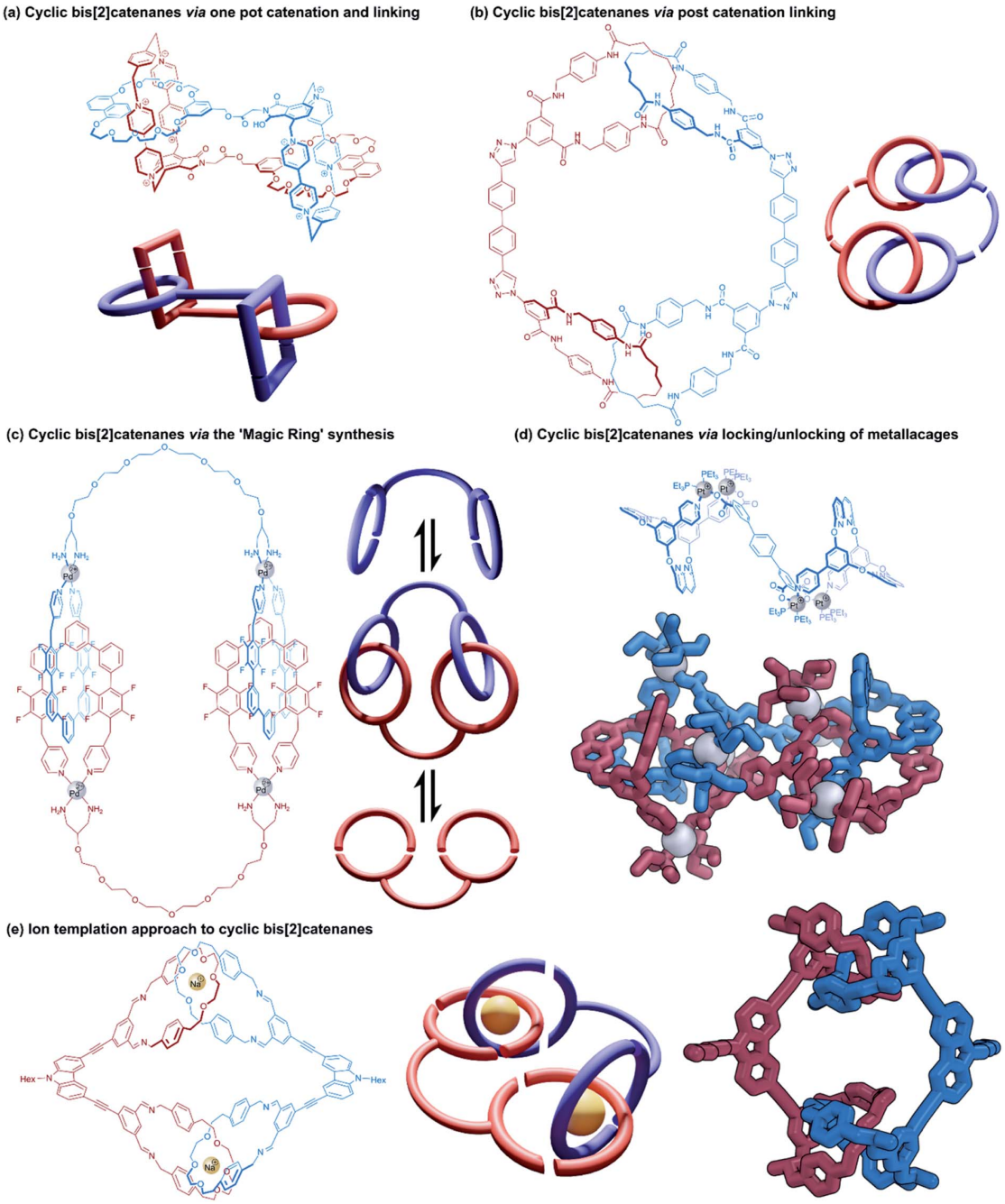

Fig. 9 Cyclic bis[2]catenanes. (a) A one-pot approach with simultaneous catenation and linking; (b) post-catenation linking of [2]catenanes through azide–alkyne cycloadditions; (c) a 'magic ring' synthesis using the reversible ring locking/unlocking of Pd(II) macrocycles; (d) using the reversible locking/unlocking of metallacages. Hydrogen atoms have been omitted on the representation of the single crystal X-ray structure; (e) templation around sodium ions to construct cyclic bis[2]catenates. The crystal structure of the reduced and methylated form without sodium ions. Hydrogen atoms have been omitted on the representation of the single crystal X-ray structure.

condensation with isophthalaldehyde units.[58] Chiu constructed a tetraaldehyde species that consisted of two rigid dialdehyde arms held at ~90° to each other, to counteract the linearly functionalised catenane structural motif. Condensation of this tetraaldehyde with the protocatenane template gave a cyclic bis[2]catenane product (Fig. 9e), as well as cyclic trimers and tetramers.[57] Reduction of the imine groups to amines locked the structure in place and allowed for purification of the handcuff.

3.2.2 Cyclic handcuff catenanes with macrocyclic tethers. Another approach taken in the synthesis of cyclic bis[2]catenanes has been demonstrated by Böhmer and co-workers, based upon dimeric tetraurea calix[4]arene capsules.[59] A calix[4]arene was functionalised on its wide rim with urea groups that lead into terminal octenyl residues. Under a solvent template, two such calix[4]arenes form hydrogen-bonded dimers and olefin metathesis was employed to form covalent connections between the octenyl residues. When the metathesis reaction unites adjacent residues of just one calix[4]arene, a cyclic bis[2]catenane product is obtained; though side products are possible if connections form between the two different calix[4]arene monomers in the dimeric capsule. Any *cis*/*trans* isomeric complications were removed by subsequent hydrogenation. Once mechanically bonded, the capsule can be closed (Fig. 10a) and opened (Fig. 10b) by changing solvent due to the relative stability of the hydrogen-bonded seam in solvents of differing polarity. This allows for the release and exchange of guest molecules.

The yield of the cyclic bis[2]catenane handcuff was greatly improved by first ensuring one of the calix[4]arenes was already connected as the bis-loop derivative before forming the handcuff, avoiding any possible cross-connection between the two monomeric units.[60] This strategy also allowed for the formation of heterodimeric capsules, with different loop sizes.[61] When the pairs of loops of the second calix[4]arene monomer are closed by the metathesis reaction, this may occur in either direction (that is to say a particular thread may react with its clockwise or anticlockwise neighbour). In the homodimeric handcuff capsule, this leads to an enantiomeric pair of topological isomers of the resulting bis[2]catenane with D_2 point group symmetry. However, the point group symmetry is reduced to C_2 when the cyclodirectionality of the hydrogen-bonded urea belt (which is kinetically stable) is considered (Fig. 10c). The parent heterodimeric handcuff capsule possess C_2 point group symmetry. The cyclodirectionality of the hydrogen-bonded urea here adds an independent element of chirality but does not change the point group and so two diastereomeric pairs of enantiomers are observed (Fig. 10d).

Böhmer and co-workers were able to chromatographically resolve the two enantiomers of various capsules with a chiral stationary phase. The reversible opening of the capsule combined with the chirality might lead to useful applications of these handcuff molecules in the discrimination of chiral guest moieties.

Chas and Ballester[62] built upon Böhmer's earlier calix[4]arene capsule work and created heterodimeric handcuff capsules built from interlocked calix[4]arene and calix[4]pyrrole hemispheres. The substitution of one of the calix[4]arenes with a calix[4]pyrrole provides different functionality to each interior pole of the capsule. Amine oxide guest molecules were found to interact strongly with the capsule; the pyrrole portion forms hydrogen bonds with the *N*-oxide and the calixarene provides stabilising C–H–π interactions. Stabilisation of particularly reactive *N*-oxide guests was also possible by confinement within the handcuff capsule.[63] The polarised inner space also permitted co-encapsulation of ion pairs; experiments with both

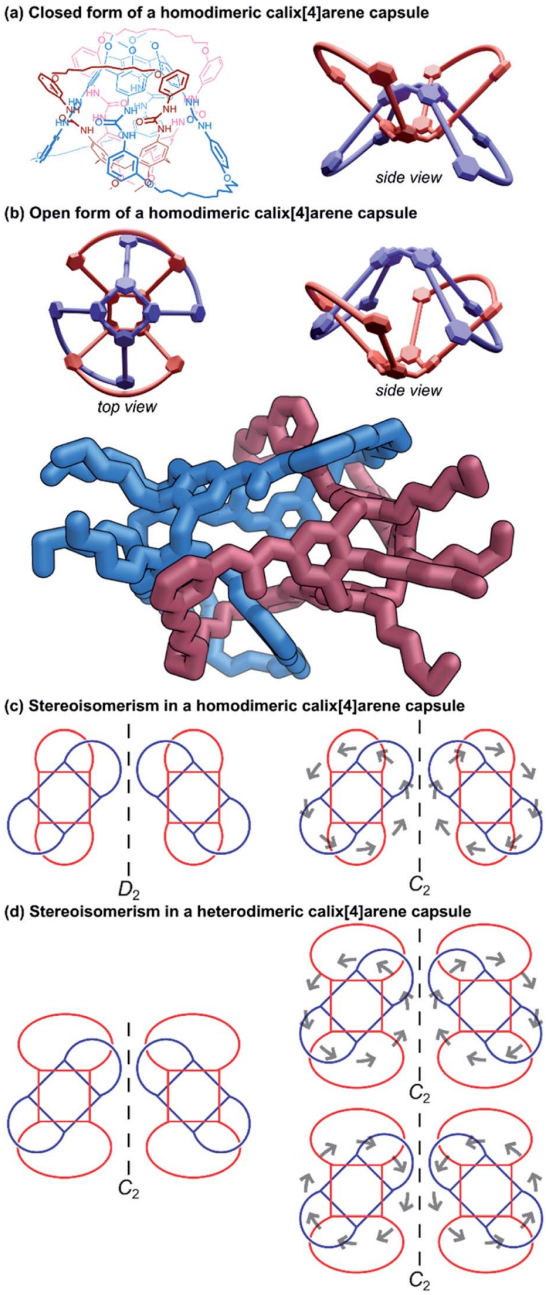

Fig. 10 Cyclic (2)handcuff [2]catenanes synthesised *via* dimeric calix[4]arene capsules. (a) Chemical structure and schematic representation of such a handcuff in the closed form; (b) schematic representations and a crystal structure representation of the open form. Hydrogen atoms have been omitted on the representation of the single crystal X-ray structure; (c) stereoisomerism possible in a homodimeric handcuff capsule, with grey arrows indicating the direction of the hydrogen bonding in the urea belt; (d) stereoisomerism possible in a heterodimeric handcuff capsule, with grey arrows indicating the direction of the hydrogen bonding in the urea belt.

tetramethylammonium chloride and tetraethylphosphonium chloride salts showed complete encapsulation of both ions of the salt.[62] The co-encapsulation of such guests might allow for the possibility of using this architecture as a vessel for certain chemical reactions. More recent work performed by Ballester and co-workers[64] examined the use of the calix[4]arene/calix[4]pyrrole handcuff to encapsulate a series of alkylated *N*,*N*-dimethylamine *N*-oxide guests where the non-methyl alkyl group varied in length from C1 to C10. Smaller *N*-oxides were co-encapsulated with a solvent molecule which would occupy the calixarene hemisphere; larger *N*-oxide molecules occupied the entire cavity by themselves, with the alkyl chain undergoing severe coiling to fit into the capsule. Competitive addition of shorter *N*-oxides to capsules hosting longer ones saw the complete replacement of the longer guest with the shorter one, even if it also meant entropic costs associated with encapsulating a solvent molecule as well, revealing the capsule's ability to stabilise sterically demanding *gauche* states of coiled aliphatic chains. Furthermore, the advantages of the handcuff topology were established by comparing host properties against an analogous non-interlocked capsule. The largest guest that could be trapped without the supporting mechanical bonds bore just a C5 chain, thus, the mechanical bonds helped stabilise against the thermodynamic instability of the multiple *gauche* interactions present for the convoluted aliphatic chains.

4. Higher handcuff architectures

Finally, we turn our attention to molecular handcuffs of a higher order; species that possess not only the doubly interlocked handcuff motif described thus far but carry further complexity in the form of additional mechanical bonds. As an example, a molecular structure comprising a four ring system that is able to lock on to a guest molecule with four separate 'limbs' would be analogous to a harness style restraint that simultaneously binds the wrists and ankles. This arrangement would be called a (4)handcuff [2]rotaxane under our nomenclature, since the hosting component has four occupied rings.

Developments in the field of mechanically interlocked chemistry have allowed for the construction of many intricate molecular architectures. Within this section we describe supramolecular bundles, pseudo[4]catenanes, as well as examples of handcuff systems that involve more than just two components. The limit to the complexity that can be achieved by molecular handcuffing is still far from becoming realised.

4.1 Threefold interlocked handcuff structures

Beginning our exploration of higher order handcuffs are structures that involve expansion of the bis(macrocyclic) component to a three-loop tris(macrocycle). The arrangement of the three macrocycles within the host offers a new avenue of topological considerations: the three rings may be coplanar or orthogonal to a common plane (or perhaps neither), likewise the three rings might be arranged linearly or branching from a central point. These differences in host topology can have a profound effect on the structure of the guest molecule, which could thread all rings from the same side, as is the case for supramolecular bundles, or pass through the rings in sequence from one end to the other, like a braid. The relationship between tris(macrocyclic) systems and (2)handcuffs should be apparent when considering the threading of the guest component. If during association of the two components the guest fails to thread through the third macrocycle, the resulting supramolecule would still bear all the hallmarks of a traditional (2)handcuff. As such, we reason that whether the third macrocycle is threaded or not, the resulting structure should be considered part of the handcuff family of supramolecules.

4.1.1 Handcuff rotaxanes with three mechanical bonds – (3)handcuff [2]rotaxanes. The first host–guest inclusion complex using a tris(macrocyclic) host and trivalent guest was reported by Stoddart and co-workers.[65] A triphenylene core was used to fuse three benzo[24]crown-8 macrocycles and a trifurcated guest was made from three dibenzylammonium cations linked in the *meta* positions around a central benzene core. The resulting 1 : 1 assembly of these components was termed a 'supramolecular bundle'. The collective stabilising π–π interactions between the cores of the two components as well as hydrogen bonding between the crown ether and ammonium recognition sites meant that the compound retained its integrity in the solution phase, despite the lack of stoppering groups, although dethreading could be stimulated by the addition of base. Rotaxane variants based on the same tritopic recognition motif were later constructed by post-assembly stoppering[66] and by templating formation of the tris(macrocycle) with the trisammonium guest in a triple ring closing metathesis reaction.[67]

A study into the kinetics of the multivalent bundle threading was also performed with a related guest molecule that contained dicationic viologen units instead of the dibenzylammonium recognition sites.[68] Threading of two of the viologen arms into the receptor proceeded almost instantly, whereas the third threading event was considerably slower, eventually equilibrating to the fully threaded complex after ten days. Schalley and co-workers also evaluated the thermodynamic threading behaviour of trivalent pseudorotaxanes constructed from a tris(tetralactam) host and a trifurcated axle with three bisamide arms using NMR and ITC experiments.[69] The second binding event was found to exhibit a slightly positive cooperativity, the third binding event, however, was non-cooperative due to unfavourable strain, perhaps due to a slight mismatch in the size of the receptor and guest. The preorganisation of the host and guest components still ultimately ensures formation of the completely threaded complex, and after stoppering with copper-catalysed azide–alkyne Huisgen cycloaddition reactions gives the (3)handcuff [2]rotaxane (Fig. 11a).

Stoddart and co-workers also constructed (3)handcuff [2]rotaxane supramolecular bundles with axles whose arms contained both dibenzylammonium and viologen stations (Fig. 11b).[70,71] These elevators could be operated as bistable rotaxanes. Through the addition of base the dibenzylammonium sites are deprotonated and the tris(macrocyclic) 'platform' moves along the axle to the viologen stations, travelling a distance of 0.7 nm. Subsequent protonation of the ammonium stations by acidification restabilised the platform in its upper position. The

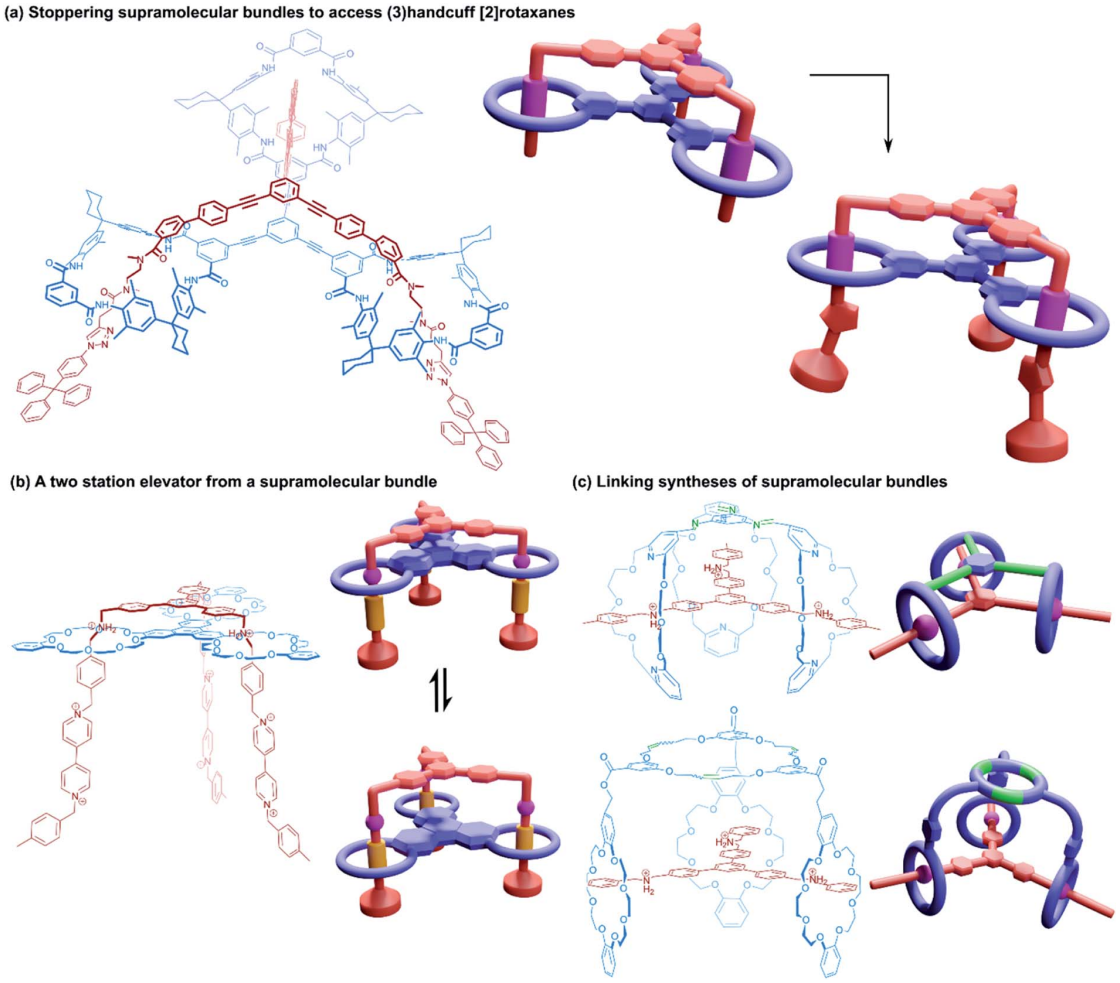

Fig. 11 (3)Handcuff [2]rotaxanes. (a) The stoppering of a supramolecular bundle made from a tris(tetralactam) host *via* azide–alkyne cycloadditions to give a (3)handcuff [2]rotaxane; (b) a two station molecular elevator with a platform that moves between viologen and dibenzylammonium stations; (c) linking synthesis of supramolecular bundles using olefin metathesis and imine formation.

authors estimate that the downward force exerted by the tris(macrocyclic) platform is around 200 pN, roughly one order of magnitude larger than forces provided by linear motors such as the muscle protein myosin.[72] Interestingly, the motion of the host appears to follow a three-step pathway rather than moving smoothly in a concerted process. Schalley and co-workers also constructed a switchable (3)handcuff [2]rotaxane elevator based upon the tris(tetralactam) host and a trifurcated axle with bisamide and triazole stations.[69] The addition of chloride to the rotaxane caused a shift in binding from the bisamide to triazole sites, which can be completely reversed by precipitation of the chloride using sodium tetraphenylborate.

Alternative approaches to (3)handcuff [2]rotaxane synthesis have also been reported that make use of a linking approach (see Section 2.1.1) to covalently join three macrocycles together in a pseudo[4]rotaxane. In a collaboration between Stoddart and Grubbs,[73] the familiar 1,3,5-tris(dibenzylammonium) axle self-assembled with three equivalents of a dibenzo[24]crown-8 derivative that bore two olefinic side arms. A simultaneous olefin metathesis reaction was able to link the three threaded macrocycles, forming a cyclic trimer of the crown ether monomers and yielding the (3)handcuff [2]rotaxane (Fig. 11c). In the absence of the template this unique cyclisation could not occur, and no trimers were formed. A dynamic covalent strategy in tandem with the tritopic template approach was used to link together formyl appended dipyrido[24]crown-8 macrocycles through reaction with 1,3,5-triaminobenzene to form imine bonds (Fig. 11c).[74] The short bridging unit between the three macrocycles constrained the system rigidly enough to provide mechanical bonding, even without the need for conventional stoppers, akin to suitanes (see Section 2.2). Indeed, a suit[3]ane was also synthesised through the reaction of two 1,3,5-triaminobenzene caps with three dipyrido[24]crown-8 rings that were functionalised on both pyridine units with formyl moieties

in the presence of the trisammonium template. Chan and co-workers also created a suit[3]ane by linking together the three macrocyclic monomers with coordination bonds.[75] A dibenzo [24]crown-8 macrocycle was functionalised with four terpyridine groups, two for each of the macrocycle's benzene rings. Coordination of these ligands with cadmium(II) ions generated a metalloprism 'suit' that could encapsulate a tris(ammonium) guest molecule, connected to a central 1,3,5-substituted benzene core by flexible aliphatic chains (Fig. 12a). Encapsulation of the guest component further stabilised the complex.

So far all the axle components of the (3)handcuff [2]rotaxanes described have had a radially branched structure, where identical recognition sites extend as spokes from a central unit. In contrast, a linear threadlike component with three ammonium recognition sites was used by Tian and co-workers in the construction of a handcuff rotaxane with a braided topology.[76] A tris(macrocycle) with a central DB24C8 unit and smaller flanking benzo[21]crown-7 macrocycles was mixed with the flexible tris(ammonium) axle, which self-assembled into the fully threaded pseudo[2]rotaxane, with subsequent introduction of phenyl stoppers (Fig. 12b). Since the phenyl rings of the axle are too large to pass through the cavity of the benzo[21]crown-7 macrocycles, the mechanism of threading cannot proceed *via* a single leading end passing in turn through all three macrocycles, but the central DB24C8 must at least be threaded ahead of one of the smaller outer macrocycles in order to produce the (3)handcuff.

A linear thread was also used by Meng and Chen to fabricate a molecular pulley based upon a triply interlocked [2]rotaxane.[77] A triptycene core connected three DB24C8 macrocycles so that the planes of the macrocycles were rotated 120° with respect to each other. An axle molecule made of alternating dibenzylammonium and triazole stations, stoppered at one end, was able to thread sequentially through the host's three rings, following the inchworm mechanism described earlier.[19] Once fully associated the axle was stoppered on its leading end (introducing a third triazole group as part of the reaction) to give a (3)handcuff [2]rotaxane. Methylation of the triazole stations created cationic triazolium recognition sites (Fig. 13a). The thread of the system could be pulled through by deprotonation of the ammonium sites, causing the macrocycles to favour the triazolium stations and subsequently retracted by reprotonating, similar to the motion of a rope about a pulley. The unique pulley geometry combines the linear translocation of a [2]rotaxane with the rotary motion typical of a [2]catenane.

4.1.2 Handcuff catenanes with three mechanical bonds – (3)handcuff [2]catenanes. The work of the Chen group has also extended to producing triply interlocked catenane structures based upon the triptycene tris(macrocycle) described above. Their first (3)handcuff [2]catenane was synthesised from a triple olefin metathesis reaction from a pseudo[4]rotaxane precursor.[78] The triptycene tris(macrocycle) was threaded through each cavity by a dibenzylammonium thread functionalised with terminal olefin groups. The tris(macrocycle)

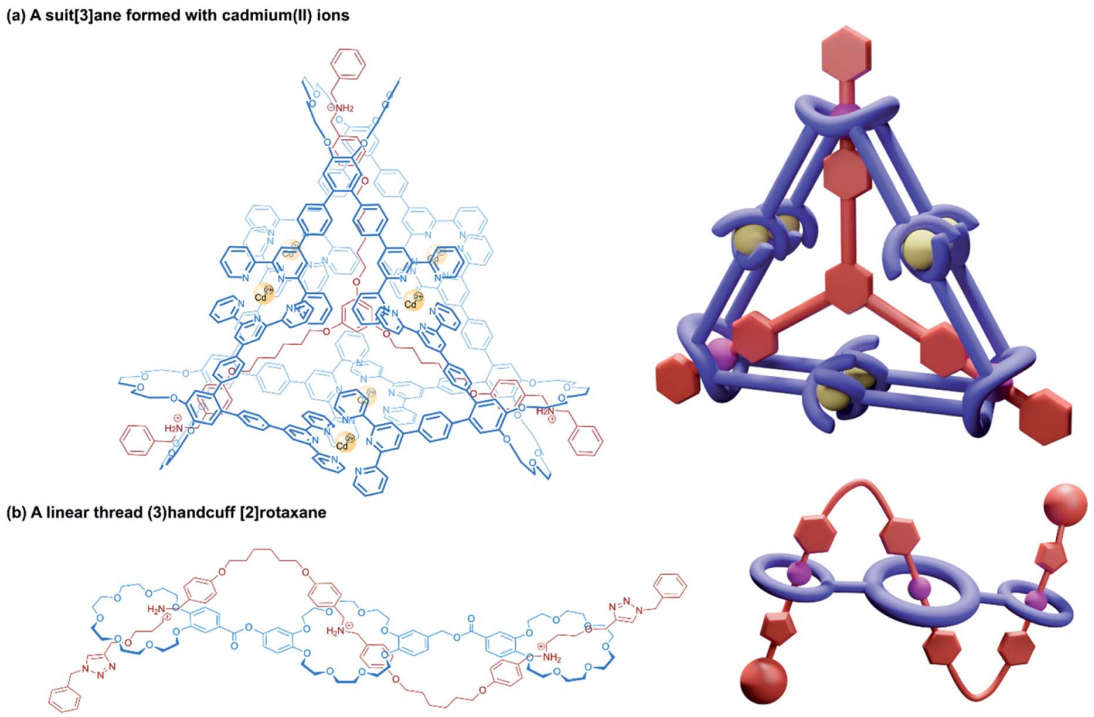

Fig. 12 Other approaches to (3)handcuff [2]rotaxanes. (a) A suit[3]ane formed from the coordination of terpyridine groups to cadmium(II) ions; (b) a braided (3)handcuff [2]rotaxane architecture.

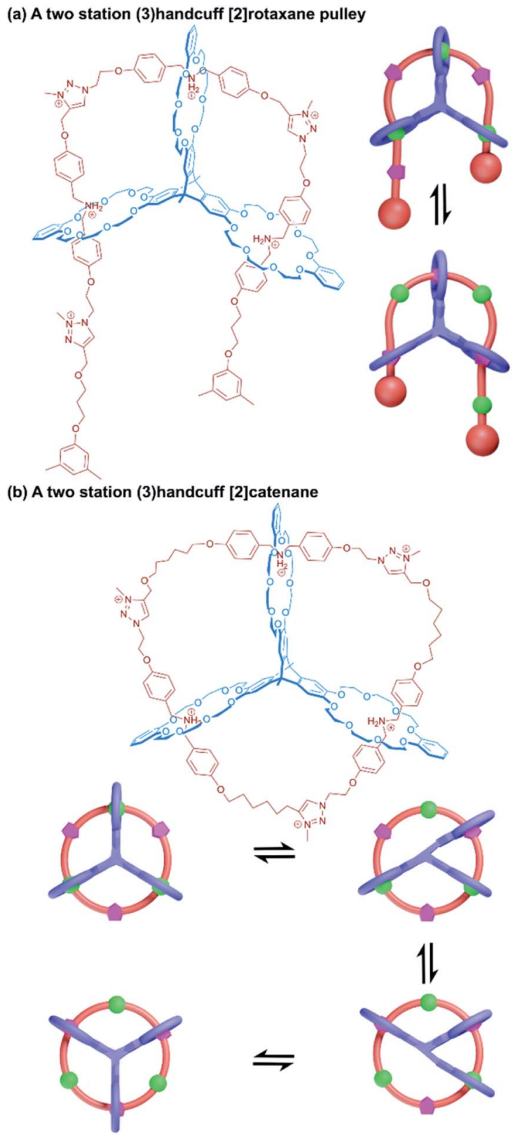

Fig. 13 Two station (3)handcuffs based upon a tris(macrocycle) derived from a triptycene core. (a) A [2]rotaxane pulley with dibenzylammonium and triazolium stations; (b) stepwise motion of the macrocycles in a (3)handcuff [2]catenane between dibenzylammonium and triazolium stations.

positioned the olefin termini of the threads in close proximity, facilitating the ring-closing metathesis reaction and any isomeric complications were removed by hydrogenation. This method of handcuff catenane synthesis is very similar in approach to the (2)handcuff [2]catenane work of Sauvage[44,45] and Beer[46] outlined in Section 3.1.2, where the large guest macrocycle is formed by multiple olefin metathesis reactions. The crystal structure of the (3)handcuff [2]catenane showed three large cavities formed by the space between the triptycene core of the host and the large guest macrocycle. Later work demonstrated it was also possible to produce the same (3)handcuff [2]catenane architecture by starting with an olefin-terminated tris(benzylammonium) strand.[79] Interestingly, if this strand was already conjoined as a macrocycle and later mixed with the tris(macrocyclic) host, a reversible ring-opening ring-closing metathesis reaction could be stimulated by the addition of Grubbs II catalyst, forming the triply catenated product in high yield. A chiral variation was also reported,[80] where the tris(macrocycle) was modified with (*R*)-1,1′-binaphthyl moieties. Post-synthetic *N*-acylation of the tris(ammonium) thread created stopper units that limited rotation of the large macrocycle. Compared to the unthreaded host, the guest's presence greatly reduced the Cotton effect of the binaphthyl chromophore at 241 nm, but increased the effect at 248 nm, possibly indicative of chirality transfer to the large threaded macrocycle.

More recently, Chen and co-workers developed a (3)handcuff [2]catenane from a pyrazine extended version of their triptycene tris(crown ether) and a thread made from alternating dibenzylammonium and methyltriazolium stations.[81] Familiar to us from related systems, deprotonation of the ammonium sites caused rotation of the thread so that the triazolium stations associated with the cavities of the tris(macrocyclic) host, which could be reversed by reprotonation. The switching between these two states also corresponded with a change in emission intensity from the central quinoxaline fluorophore. A detailed investigation into the relative motion of the two components revealed that a stepwise motion was generated by the appropriate stimulus; with the crown ether moieties migrating one at a time to their new stations through a series of four stable states (Fig. 13b). This stepwise motion also supports the one-ring-at-a-time observation of motion in the molecular elevator described in the previous section.[71]

4.2 Fourfold interlocked handcuff structures

Increasing the ring count of the host component from three to four boosts the topological possibilities of the resulting handcuff systems as new connective opportunities are available for arranging the rings before even considering their three-dimensional orientations. Fortunately for our discussion, the difficulties of synthesising such highly intricate topological systems have limited the structures of (4)handcuff systems presently realised to those that contain a tetrakis(macrocyclic) host with four rings branching symmetrically from a central nucleus.

4.2.1 Handcuff rotaxanes with four mechanical bonds – (4) handcuff [2]rotaxanes. Quadruply interlocked [2]rotaxanes were first reported by Böhmer and co-workers[82,83] who made use of the well-defined hydrogen-bonded arrangement between two urea functionalised calix[4]arenes (see Section 3.2.2) to organise the components for mechanical bonding. In the first instance,[82] a tetraloop calixarene was prepared by olefin metathesis of an tetra-bis(alkenyl) functionalised calix[4]arene,[84] where adjacent alkenyl arms were coupled to produce the four new macrocycles. When mixed with a second calix[4]arene derivative carrying four pendent alkylmaleimide arms in apolar solvents, heterodimeric capsules of the two calixarenes formed, with the

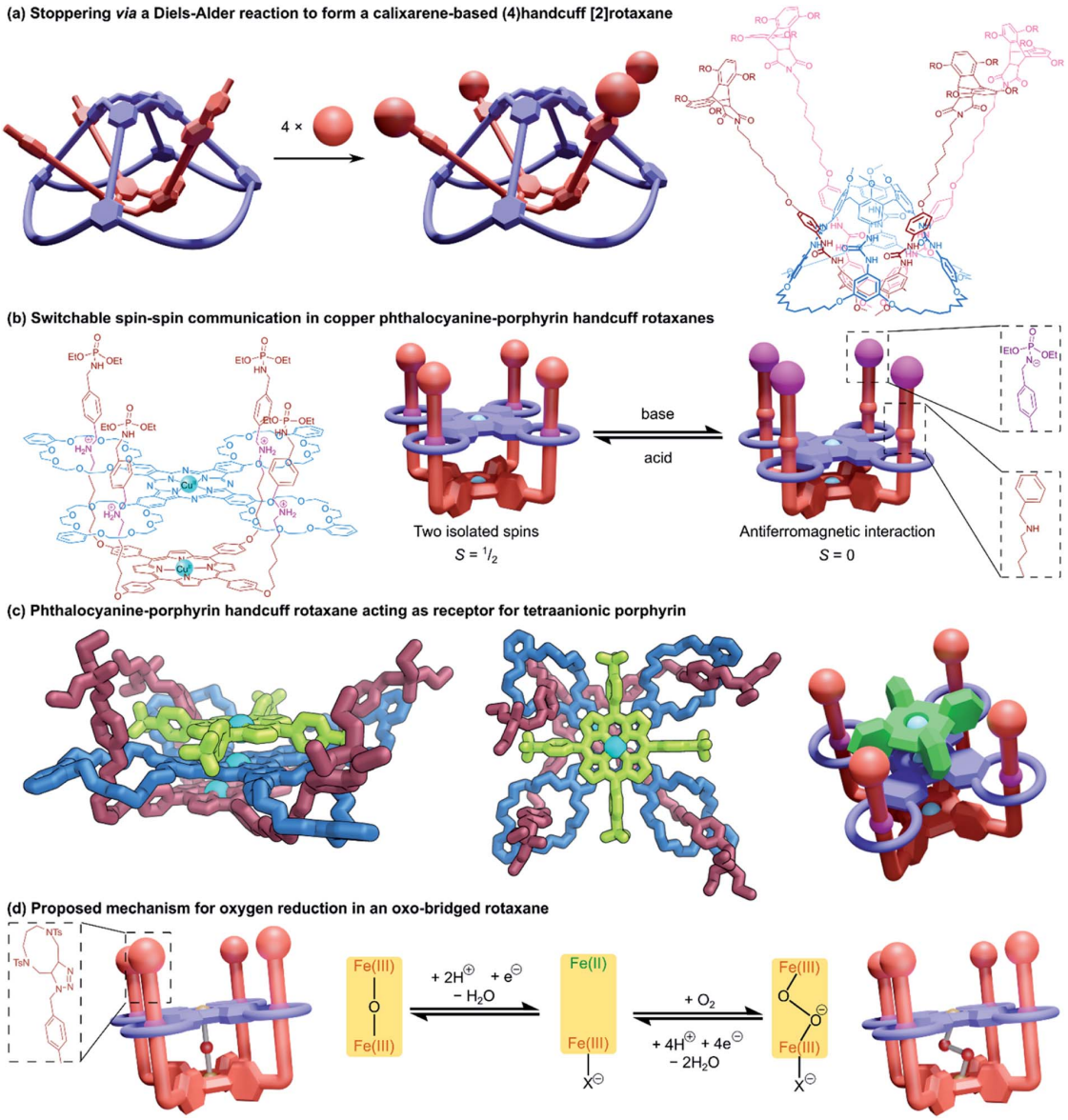

Fig. 14 Structures of (4)handcuff [2]rotaxanes. (a) Diels–Alder reactions between maleimide and anthracene units to stopper a dimeric calix[4]arene capsule; (b) Addition of acid or base to a copper phthalocyanine–porphyrin handcuff rotaxane moves the handcuff position along the axle and controls the spin–spin communication between the metal centres; (c) a phthalocyanine–porphyrin handcuff rotaxane acting as a receptor for a third tetraanionic porphyrin. Hydrogen atoms have been omitted on the two views of the single crystal X-ray structure; (d) proposed mechanism for oxygen reduction in an oxo-bridged handcuff rotaxane.

alkylmaleimide arms threaded through each of the four loops of the host component (Fig. 14a). This pseudo(4)handcuff [2]rotaxane could then be stoppered through a Diels–Alder reaction between the maleimide groups and 1,4,5,8-tetraalkoxyanthracene. In the other instance,[83] the tetraloop host was created by ring closing around the four armed guest calixarene in a heterodimeric capsule of the two calix[4]arenes. This alternative pathway allowed for the use of a shorter axle component and smaller threaded macrocycles. The more tightly knitted (4)handcuff [2]rotaxane was stable in solvents that would typically break the hydrogen bonded seam between the two calixarene hemispheres and exchange of solvent molecules entrapped within the capsule was completely suppressed. As such the authors compared this fourfold rotaxane to a mechanically bonded equivalent of a hemicarcerand.

Tanaka and co-workers employed mechanical bonding as a method of cofacially stacking dimers of porphyrin and phthalocyanine chromophores.[85] A phthalocyanine unit with

four peripheral DB24C8 macrocycles and a porphyrin substituted with four benzylammonium arms formed a pseudorotaxane complex that was locked with the introduction of phosphoramidate stopper groups to the threaded arms of the porphyrin (Fig. 14b). Both porphyrinic centres were then metallated with copper(II). In the fully protonated (4)handcuff [2]rotaxane, the two copper centres do not interact and the EPR spectrum of the complex shows two isolated doublet ($S = 1/2$) spins. When deprotonated by strong base, the two copper centres move closer together, allowing an antiferromagnetic ($S = 0$) interaction between the spins. The switchable spin–spin communication afforded by this mechanically interlocked architecture was recognised as valuable progress towards spintronic nanomachines.

Subsequent work exploited the size and charge complementarity between the porphyrin–phthalocyanine (4)handcuff and a tetraanionic porphyrin to form a three membered columnar array,[86] sandwiching the tetrakis(macrocyclic) phthalocyanine between the two porphyrin species (Fig. 14c). The identity of the metal centres of each member of the (4) handcuff assembly could be programmed, either by pre-metallating the components prior to rotaxane self-assembly,[87] or by site specific metallation of either component.[88] The phthalocyanine host selected for manganese(II) ions, the porphyrin guest showed selectivity for iron(II) and nickel(II) ions. Complexation of the rotaxane to the tetraanionic porphyrin expanded the heterometallic array to a third metal ion. The spin–spin communication of paramagnetic copper(II) ions confined within the central phthalocyanine moiety could be programmed by the identity of metal centres in the surrounding porphyrins.[89] Similarly, the electrochemical properties of the (4)handcuff [2]rotaxane were affected by the charge density of the metal within the electrostatically bonded porphyrin.[90]

The close-stacked but flexible arrangement of metal centres within the porphyrin–phthalocyanine could also be exploited for catalytic purposes. Metallation with iron(II) followed by aerobic oxidation afforded a μ-oxo-bridged complex that showed efficient catalytic reduction of oxygen to water (Fig. 14d).[91] The structural adaptability provided by the mechanical bonds suitably accommodated peroxide and superoxide intermediates in the proposed catalytic pathway. A μ-nitrido-bridged diiron version of the (4)handcuff showed oxidative properties towards methane and ethane in the presence of hydrogen peroxide.[92] The catalytic potency was enhanced by the addition of a tetraanionic porphyrin cofactor, which caused electronic perturbation of the metallic active sites. For greater detail, an in-depth review of their fourfold rotaxane work was recently published by Yamada and Tanaka within the context of face-to-face assemblies of porphyrinoids.[93]

A related (4)handcuff [2]rotaxane has been reported[94] that combines a resorcinarene-based cavitand with four crown ether macrocyclic appendages with a porphyrin decorated with four imidazolium arms. Similar in architecture to Tanaka's (4)handcuff [2]rotaxanes, the authors compared the cavitand to a "bowl" and the porphyrin component to the lid of that bowl.

4.2.2 Handcuff catenanes with tetrakis(macrocyclic) hosts – (4)handcuff [2]catenanes. Catenane structures based upon the tetraloop calixarene described above have also been synthesised by the Böhmer group.[95–97] The assembly of heterodimeric capsules between the tetraloop calix[4]arene and calix[4]arenes substituted with four terminal olefin groups allowed for a ring closing metathesis reaction to occur between the adjacent alkenyl residues, forming a multiply catenated architecture.

The two newly created macrocyclic rings each formed mechanical bonds with two of the loops in the tetrakis(macrocyclic) calixarene template, resulting in a cyclic catenane topology (Fig. 15a). The structure resembles a pair of (2)handcuff [2]catenanes with separate covalent connections between the bis(macrocyclic) components and threaded guests, or rather, the structure could be reduced to two discrete (2)handcuff [2]catenane molecules by cutting along a mirror plane perpendicular to the interlocked rings. A crystal structure confirmed the interlocked arrangement of the two calixarene hemispheres.[96] Catenated homodimers of the tetraloop calixarene were also synthesised by starting with a tetra(bis)alkenyl guest. A total of eight catenated rings can be seen in the crystal structure of the compound (Fig. 15b).[95] Starting with the open-loop form of the tetraloop species was also considered as a synthetic route to both these structures, although it proved much more effective to form the tetrakis(macrocyclic) host first due to limiting the number of 'wrong' connections between the terminal olefinic side-chains during the ring-closing metathesis reaction. As with the rotaxane analogue above, the tight-knit structure of the capsule provided a cavity for (almost) permanent guest inclusion; the strength of the inclusion could be modulated by the number of catenated rings, and by their length.[96]

Tanaka and co-workers have also reported a multiply interlocked catenane derived from their porphyrin–phthalocyanine model.[98] A pseudorotaxane consisting of the tetrakis(macrocyclic) phthalocyanine threaded with a porphyrin substituted with long alkylammonium arms that terminated in benzaldehyde residues underwent reaction with pyrrole, creating a new porphyrin cap from the benzaldehyde arms and locking the structure as a catenane (Fig. 15c). The movement of the phthalocyanine component along the alkylammonium arms allowed for the invasion of two dianionic porphyrins, which could occupy the space between the phthalocyanine platform and the porphyrin end caps. As a trinuclear copper(II) complex, the spin–spin communication could be modulated by pH, or switched off by the intercalation of dianionic porphyrins.

4.3 Three component handcuffs – (*n*)handcuff [3]rotaxanes

We conclude our discussion of higher order handcuff architectures with a few examples of handcuff rotaxanes that contain more than two distinct components that are interlocked by the handcuff motif *i.e.*, each threadlike component must form at least two mechanical bonds with its host. Sauvage and co-workers synthesised a tetrakis(macrocyclic) porphyrin with each loop containing a 1,10-phenanthroline group.[99] An axle molecule was designed with a central bis-3,8-(*o*-pyridyl)-4,7-phenanthroline fragment, such that the gathering and threading effect of copper(I) would associate each axle molecule with two of the macrocycles of the porphyrin host. The

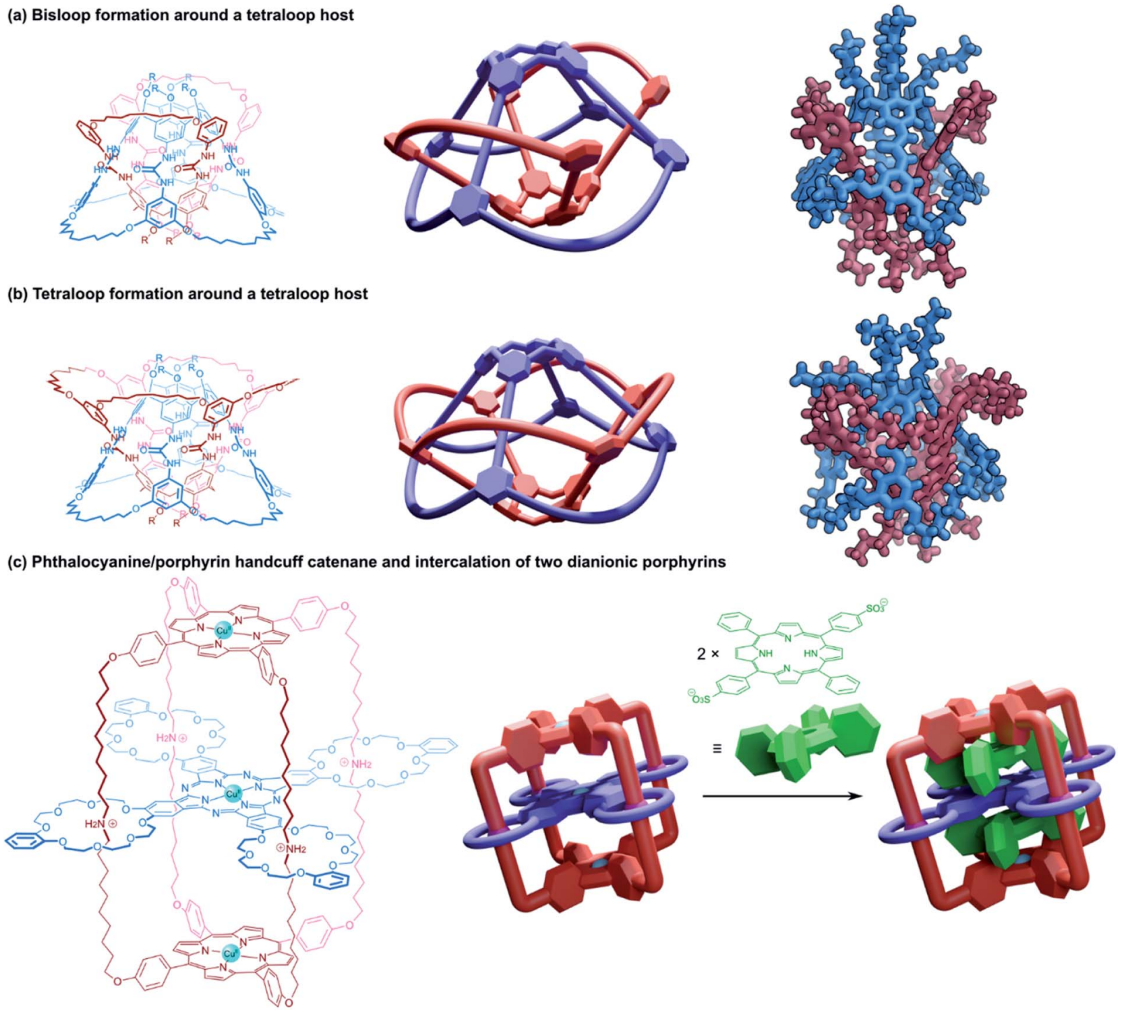

Fig. 15 Structures of (4)handcuff [2]catenanes. (a) Bisloop formation around a tetraloop host synthesised *via* olefin metathesis/hydrogenation, with a view of the single crystal X-ray structure; (b) tetraloop formation around a tetraloop host synthesised *via* olefin metathesis/hydrogenation, with a view of the single crystal X-ray structure; (c) a quadruply interlocked phthalocyanine/porphyrin handcuff into which two dianionic porphyrins could intercalate.

pseudo[3]rotaxane underwent reaction with encumbering stopper groups to generate a [3]rotaxane species that resembles two (2)handcuff [2]rotaxanes that are connected by linking the tether between the bis(macrocyclic) host of two separate molecules (Fig. 16a).

Tanaka and co-workers published a method of repetitive stepwise handcuff rotaxane formation that begins with a *trans*-A_2B_2 porphyrin functionalised with two benzylammonium arms (Fig. 16b).[100] A *trans*-bis(macrocylic) porphyrin could then be threaded on to this axle as a (2)handcuff [2]rotaxane after stoppering. The remaining *meso* positions of the bis(macrocyclic) porphyrin were then converted into new benzylammonium arms and the threading-stoppering sequence of reactions could be repeated to add more porphyrin layers. In principle, this 'daisy-chain' strategy of oligomeric (2)handcuff [2]rotaxane synthesis could be extended to any number of porphyrin layers. The control of sequence offered by this approach for a similar metalloporphyrin assembly presents great opportunity to develop molecular wires and unique spintronic devices.

Finally, we turn our attention to a handcuff [3]rotaxane synthesised by the Tanaka group in 2016.[101] Their fourfold rotaxane approach was repeated with a porphyrin axle, decorated in each of its *meso* positions with long arms containing two alkylammonium stations (Fig. 16c). This axle was able to assemble into a 1 : 2 complex with two equivalents of their tetra(macrocyclic) phthalocyanine host; the first phthalocyanine moving along the axle to the second set of alkylammonium stations to allow a second phthalocyanine to thread onto the axle before stoppering. Electrochemical measurements of the [3]rotaxane indicated substantial electronic interaction between the components, especially the two phthalocyanine hosts. When both phthalocyanines were added as their copper(II)

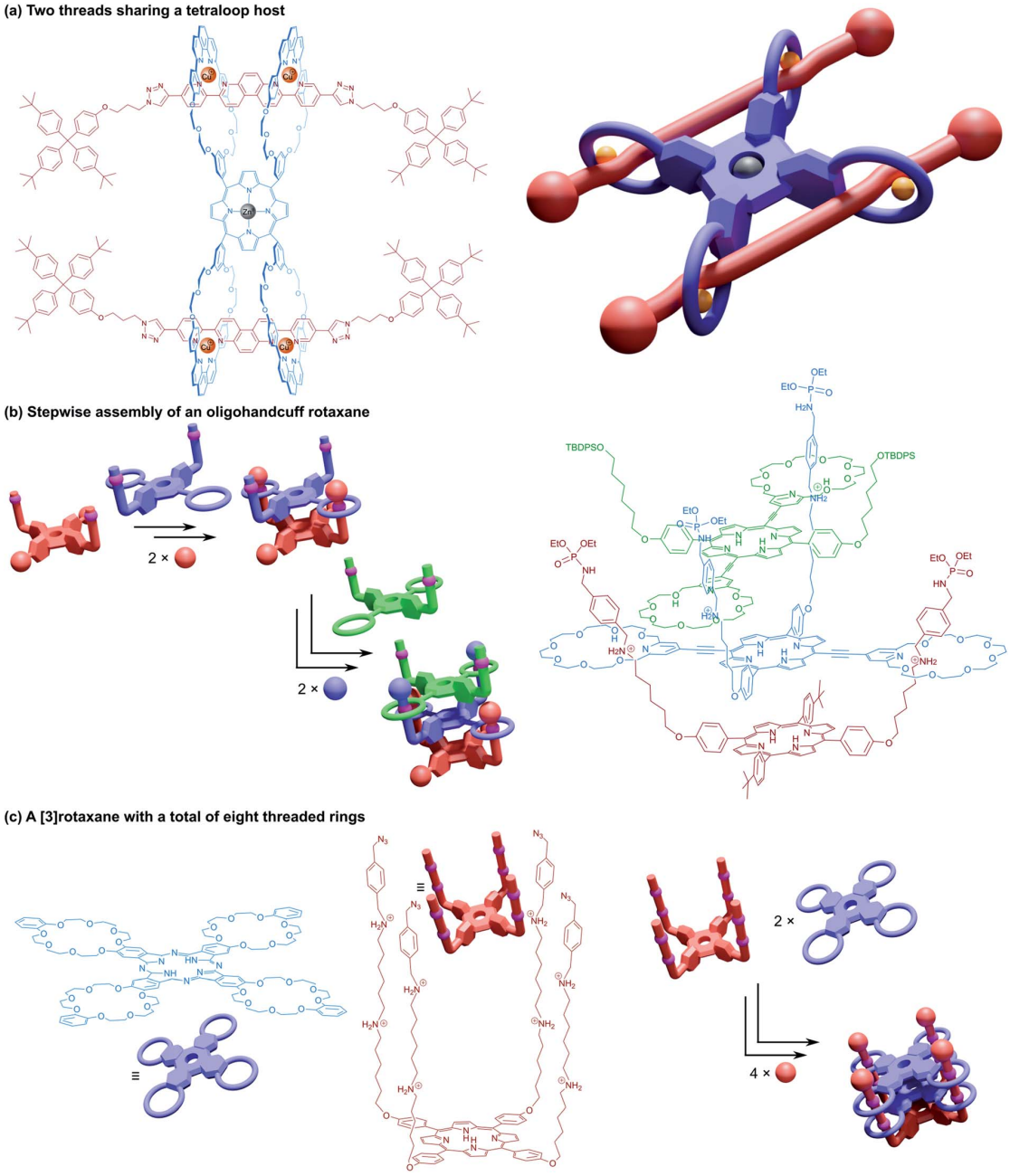

Fig. 16 Structures of multiple component handcuff rotaxanes. (a) Two threads sharing a tetraloop host held in place with copper(I) phenanthroline coordination before stoppering; (b) stepwise assembly and stoppering of an oligohandcuff rotaxane; (c) two tetrakis(macrocyclic) hosts threaded onto a single tetrafurcated axle.

complexes, the trimeric assembly displayed an antiferromagnetic interaction in its protonated form, contrasting the spin–spin interaction of the analogous dimeric stack.[85] This three component architecture comprising a total of eight threaded rings represents the most complicated molecular handcuff species we have encountered to date, and likely one of the most intricate mechanically bonded systems currently achieved.

5. Conclusions

In this article we have attempted to bring together the variety of mechanically interlocked molecules that employ the use of a molecular handcuff motif. One issue we have encountered in doing so, is the variation and breadth of terminology that has been used to discuss these topologically related structures. The

diffuse terminology that has been employed in the field has perhaps obscured the commonalities in approaches that have been used across these molecular systems. We have attempted to bring together systems which are conceptually associated, and in doing so have introduced a new nomenclature that can be employed to compare and contrast this range of structures. We anticipate that our new terminology will aid researchers to describe their structures more readily, and to identify related structures for comparison.

Many successful strategies have been developed to synthesise molecular handcuffs that build upon traditional mechanically interlocked techniques. The advancement of handcuffed structures has led to unique examples of topological chirality,[102] as well as unique control of relative motion, seen in examples of elevators[35,69–71] and pulleys.[77] The precise but flexible arrangement of molecular fragments offered by handcuff rotaxane formation has enabled unprecedented investigation of molecular interactions, whether through communication between redox active chromophores,[35,38,39] or through programmable spin–spin interactions across nearby metal cations.[85,89,98,101] These studies illustrate the exceptional power of the handcuff scaffold as a tool for positioning chemical entities, where the adaptable, flexible nature of the mechanical bond prevails over the more restricting covalent counterpart.

Another feature of reviewing the variety of handcuff structures is to draw out synergies between different systems. We hope that readers of this article will see new approaches to the expansion of available handcuff architectures. Indeed, it becomes apparent that the use of handcuffs to assemble new molecular constructs is perhaps only limited by our imagination. As such, we wish to stimulate our readers' creativity and encourage researchers within this field to explore the use of handcuffs in their own mechanically interlocked designs.

Author contributions

M. T., N. J. A., and A. W.-L., contributed equally to the writing of this manuscript. Figures were created by M. T., N. J. A., and A. W.-T. with direction from all authors. All authors conceived the idea and created the outline with equal contributions and the text was compiled and refined by N. P. with input and direction from B. S. P. and N. R. C.

Conflicts of interest

There are no conflicts to declare.

Acknowledgements

N. P., A. W.-L. and N. R. C. would like to thank the University of Birmingham for funding. N. R. C. gratefully acknowledges the support of the UK Engineering and Physical Sciences Research Council (EP/S002995/1) for an Established Career Fellowship. M. T. would like to thank the School of Chemistry, University of Nottingham for funding. N. J. A. would like to thank the EPSRC Low-Dimensional Materials & Interfaces DTP for funding. B. S. P. would like to thank the Green Chemicals Beacon of Excellence, University of Nottingham for his Nottingham Research Fellowship.

References

1 S. D. P. Fielden, D. A. Leigh and S. L. Woltering, *Angew. Chem., Int. Ed.*, 2017, **56**, 11166–11194.
2 S. J. Cantrill, K. S. Chichak, A. J. Peters and J. F. Stoddart, *Acc. Chem. Res.*, 2005, **38**, 1–9.
3 D. B. Amabilino, P. R. Ashton, A. S. Reder, N. Spencer and J. F. Stoddart, *Angew. Chem., Int. Ed.*, 1994, **33**, 1286–1290.
4 Q.-H. Guo, Y. Jiao, Y. Feng and J. F. Stoddart, *CCS Chem.*, 2021, **3**, 1542–1572.
5 A. Yerin, E. S. Wilks, G. P. Moss and A. Harada, *Pure Appl. Chem.*, 2008, **80**, 2041–2068.
6 O. Safarowsky, B. Windisch, A. Mohry and F. Vögtle, *J. Prakt. Chem.*, 2000, **342**, 437–444.
7 M. Zhang, K. Zhu and F. Huang, *Chem. Commun.*, 2010, **46**, 8131–8141.
8 G. H. Clever and M. Shionoya, *Chem.–Eur. J.*, 2010, **16**, 11792–11796.
9 R. Jäger, T. Schmidt, D. Karbach and F. Vögtle, *Synlett*, 1996, **1996**, 723–725.
10 Y. Liu, P. A. Bonvallet, S. A. Vignon, S. I. Khan and J. F. Stoddart, *Angew. Chem., Int. Ed.*, 2005, **44**, 3050–3055.
11 M. Radha Kishan, A. Parham, F. Schelhase, A. Yoneva, G. Silva, X. Chen, Y. Okamoto and F. Vögtle, *Angew. Chem., Int. Ed.*, 2006, **45**, 7296–7299.
12 A. R. Williams, B. H. Northrop, T. Chang, J. F. Stoddart, A. J. P. White and D. J. Williams, *Angew. Chem., Int. Ed.*, 2006, **45**, 6665–6669.
13 S. J. Cantrill, R. H. Grubbs, D. Lanari, K. C. F. Leung, A. Nelson, K. G. Poulin-Kerstien, S. P. Smidt, J. F. Stoddart and D. A. Tirrell, *Org. Lett.*, 2005, **7**, 4213–4216.
14 F. Aricó, T. Chang, S. J. Cantrill, S. I. Khan and J. F. Stoddart, *Chem.–Eur. J.*, 2005, **11**, 4655–4666.
15 T. Sato and T. Takata, *Tetrahedron Lett.*, 2007, **48**, 2797–2801.
16 H. Iwamoto, Y. Yawata, Y. Fukazawa and T. Haino, *Chem. Lett.*, 2010, **39**, 24–25.
17 H. Iwamoto, Y. Yawata, Y. Fukazawa and T. Haino, *Supramol. Chem.*, 2010, **22**, 815–826.
18 W. Jiang, K. Nowosinski, N. L. Löw, E. V. Dzyuba, F. Klautzsch, A. Schäfer, J. Huuskonen, K. Rissanen and C. A. Schalley, *J. Am. Chem. Soc.*, 2012, **134**, 1860–1868.
19 Z. Meng, B.-Y. Wang, J.-F. Xiang, Q. Shi and C.-F. Chen, *Chem.–Eur. J.*, 2016, **22**, 15075–15084.
20 O. Lukin and F. Vögtle, *Angew. Chem., Int. Ed.*, 2005, **44**, 1456–1477.
21 T. Tsukamoto, R. Sasahara, A. Muranaka, Y. Miura, Y. Suzuki, M. Kimura, S. Miyagawa, T. Kawasaki, N. Kobayashi, M. Uchiyama and Y. Tokunaga, *Org. Lett.*, 2018, **20**, 4745–4748.
22 S. Tajima, A. Muranaka, M. Naito, N. Taniguch, M. Harada, S. Miyagawa, M. Ueda, H. Takaya, N. Kobayashi, M. Uchiyama and Y. Tokunaga, *Org. Lett.*, 2021, **23**, 8678–8682.

23 R. Ciao, C. Talotta, C. Gaeta, L. Margarucci, A. Casapullo and P. Neri, *Org. Lett.*, 2013, **15**, 5694–5697.
24 C. Talotta, C. Gaeta, T. Pierro and P. Neri, *Org. Lett.*, 2011, **13**, 2098–2101.
25 F. Zeng, Z. Meng, Y. Han and C.-F. Chen, *Chem. Commun.*, 2014, **50**, 7611–7613.
26 Y.-K. Gu, Y. Han and C.-F. Chen, *Supramol. Chem.*, 2015, **27**, 357–363.
27 C.-J. Chuang, C.-C. Lai, Y.-H. Liu, S.-M. Peng and S.-H. Chiu, *Chem.–Eur. J.*, 2012, **18**, 16698–16707.
28 P. J. Altmann and A. Pöthig, *Angew. Chem., Int. Ed.*, 2017, **56**, 15733–15736.
29 J. F. Stoddart, *Angew. Chem., Int. Ed.*, 2017, **56**, 11094–11125.
30 S. Erbas-Cakmak, D. A. Leigh, C. T. McTernan and A. L. Nussbaumer, *Chem. Rev.*, 2015, **115**, 10081–10206.
31 C.-F. Lin, C.-C. Lai, Y.-H. Liu, S.-M. Peng and S.-H. Chiu, *Chem.–Eur. J.*, 2007, **13**, 4350–4355.
32 C.-J. Chuang, W.-S. Li, C.-C. Lai, Y.-H. Liu, S.-M. Peng, I. Chao and S.-H. Chiu, *Org. Lett.*, 2009, **11**, 385–388.
33 H. Li, X. Li, Y. Wu, H. Ågren and D.-H. Qu, *J. Org. Chem.*, 2014, **79**, 6996–7004.
34 Y.-X. Ma, Z. Meng and C.-F. Chen, *Org. Lett.*, 2014, **16**, 1860–1863.
35 Z.-J. Zhang, M. Han, H.-Y. Zhang and Y. Liu, *Org. Lett.*, 2013, **15**, 1698–1701.
36 J. Frey, C. Tock, J.-P. Collin, V. Heitz and J.-P. Sauvage, *J. Am. Chem. Soc.*, 2008, **130**, 4592–4593.
37 J.-P. Collin, J. Frey, V. Heitz, J.-P. Sauvage, C. Tock and L. Allouche, *J. Am. Chem. Soc.*, 2009, **131**, 5609–5620.
38 H. V. Schröder, H. Hupatz, A. J. Achazi, S. Sobottka, B. Sarkar, B. Paulus and C. A. Schalley, *Chem.–Eur. J.*, 2017, **23**, 2960–2967.
39 L. Yang, P. Langer, E. S. Davies, M. Baldoni, K. Wickham, N. A. Besley, E. Besley and N. R. Champness, *Chem. Sci.*, 2019, **10**, 3723–3732.
40 Z.-T. Li, P. C. Stein, N. Svenstrup, K. H. Lund and J. Becher, *Angew. Chem., Int. Ed.*, 1995, **34**, 2524–2528.
41 Z.-T. Li and J. Becher, *Chem. Commun.*, 1996, 639–640.
42 Z.-T. Li, P. C. Stein, J. Becher, D. Jensen, P. Mørk and N. Svenstrup, *Chem.–Eur. J.*, 1996, **2**, 624–633.
43 Z.-T. Li and J. Becher, *Synlett*, 1997, **1997**, 557–560.
44 J. Frey, T. Kraus, V. Heitz and J.-P. Sauvage, *Chem. Commun.*, 2005, 5310–5312.
45 J. Frey, T. Kraus, V. Heitz and J.-P. Sauvage, *Chem.–Eur. J.*, 2007, **13**, 7584–7594.
46 N. H. Evans, C. J. Serpell and P. D. Beer, *Angew. Chem., Int. Ed.*, 2011, **50**, 2507–2510.
47 K. J. Hartlieb, A. K. Blackburn, S. T. Schneebeli, R. S. Forgan, A. A. Sarjeant, C. L. Stern, D. Cao and J. F. Stoddart, *Chem. Sci.*, 2014, **5**, 90–100.
48 M. C. Jiménez, C. Dietrich-Buchecker and J.-P. Sauvage, *Angew. Chem., Int. Ed.*, 2000, **39**, 3284–3287.
49 L. Fang, M. Hmadeh, J. Wu, M. A. Olson, J. M. Spruell, A. Trabolsi, Y.-W. Yang, M. Elhabiri, A.-M. Albrecht-Gary and J. F. Stoddart, *J. Am. Chem. Soc.*, 2009, **131**, 7126–7134.
50 A. Goujon, T. Lang, G. Mariani, E. Moulin, G. Fuks, J. Raya, E. Buhler and N. Giuseppone, *J. Am. Chem. Soc.*, 2017, **139**, 14825–14828.
51 T. Hagiwara, M. Yamazaki, T. Suzuki, T. Sawaguchi and S. Yano, *Polymer*, 2011, **52**, 5426–5430.
52 T. Hagiwara, M. Yamazaki, T. Sawaguchi and S. Yano, *Trans. Mater. Res. Soc. Jpn.*, 2008, **33**, 1269–1272.
53 T. Hagiwara, M. Yamazaki, T. Sawaguchi and S. Yano, *J. Res. Inst. Sci. Technol., Nihon Univ.*, 2011, **2011**, 124.
54 A. Hori, T. Sawada, K.-i. Yamashita and M. Fujita, *Angew. Chem., Int. Ed.*, 2005, **44**, 4896–4899.
55 A. Hori, A. Akasaka, K. Biradha, S. Sakamoto, K. Yamaguchi and M. Fujita, *Angew. Chem., Int. Ed.*, 2002, **41**, 3269–3272.
56 Y. Wang, Y. Zhang, Z. Zhou, R. T. Vanderlinden, B. Li, B. Song, X. Li, L. Cui, J. Li, X. Jia, J. Fang, C. Li and P. J. Stang, *Nat. Commun.*, 2020, **11**, 2727.
57 Y.-W. Wu, S.-T. Tung, C.-C. Lai, Y.-H. Liu, S.-M. Peng and S.-H. Chiu, *Angew. Chem., Int. Ed.*, 2015, **54**, 11745–11749.
58 S.-T. Tung, C.-C. Lai, Y.-H. Liu, S.-M. Peng and S.-H. Chiu, *Angew. Chem., Int. Ed.*, 2013, **52**, 13269–13272.
59 M. O. Vysotsky, M. Bolte, I. Thondorf and V. Böhmer, *Chem.–Eur. J.*, 2003, **9**, 3375–3382.
60 A. Bogdan, M. O. Vysotsky, T. Ikai, Y. Okamoto and V. Böhmer, *Chem.–Eur. J.*, 2004, **10**, 3324–3330.
61 O. Molokanova, A. Bogdan, M. O. Vysotsky, M. Bolte, T. Ikai, Y. Okamoto and V. Böhmer, *Chem.–Eur. J.*, 2007, **13**, 6157–6170.
62 M. Chas and P. Ballester, *Chem. Sci.*, 2012, **3**, 186–191.
63 A. Galán, G. Gil-Ramírez and P. Ballester, *Org. Lett.*, 2013, **15**, 4976–4979.
64 A. Galan, M. Espelt and P. Ballester, *Supramol. Chem.*, 2016, **28**, 455–463.
65 V. Balzani, M. Clemente-León, A. Credi, J. N. Lowe, J. D. Badjić, J. F. Stoddart and D. J. Williams, *Chem.–Eur. J.*, 2003, **9**, 5348–5360.
66 J. D. Badjić, V. Balzani, A. Credi, J. N. Lowe, S. Silvi and J. F. Stoddart, *Chem.–Eur. J.*, 2004, **10**, 1926–1935.
67 J. D. Badjić, S. J. Cantrill, R. H. Grubbs, E. N. Guidry, R. Orenes and J. F. Stoddart, *Angew. Chem., Int. Ed.*, 2004, **43**, 3273–3278.
68 J. D. Badjić, S. J. Cantrill and J. F. Stoddart, *J. Am. Chem. Soc.*, 2004, **126**, 2288–2289.
69 L. Kaufmann, N. L. Traulsen, A. Springer, H. V. Schröder, T. Mäkelä, K. Rissanen and C. A. Schalley, *Org. Chem. Front.*, 2014, **1**, 521–531.
70 J. D. Badjić, V. Balzani, A. Credi, S. Silvi and J. F. Stoddart, *Science*, 2004, **303**, 1845–1849.
71 J. D. Badjic, C. M. Ronconi, J. F. Stoddart, V. Balzani, S. Silvi and A. Credi, *J. Am. Chem. Soc.*, 2006, **128**, 1489–1499.
72 J. E. Molloy and C. Veigel, *Science*, 2003, **300**, 2045–2046.
73 H. Hou, K. C. F. Leung, D. Lanari, A. Nelson, J. F. Stoddart and R. H. Grubbs, *J. Am. Chem. Soc.*, 2006, **128**, 15358–15359.
74 B. H. Northrop, F. Aricó, N. Tangchiavang, J. D. Badjić and J. F. Stoddart, *Org. Lett.*, 2006, **8**, 3899–3902.
75 Y.-C. Wang, Y.-P. Liang, J.-Y. Cai, Y.-J. He, Y.-H. Lee and Y.-T. Chan, *Chem. Commun.*, 2016, **52**, 12622–12625.

76 C. Gao, Z.-L. Luan, Q. Zhang, S.-J. Rao, D.-H. Qu and H. Tian, *Org. Lett.*, 2017, **19**, 3931–3934.
77 Z. Meng and C.-F. Chen, *Chem. Commun.*, 2015, **51**, 8241–8244.
78 X.-Z. Zhu and C.-F. Chen, *J. Am. Chem. Soc.*, 2005, **127**, 13158–13159.
79 Y. Jiang, X.-Z. Zhu and C.-F. Chen, *Chem.–Eur. J.*, 2010, **16**, 14285–14289.
80 X.-Z. Zhu and C.-F. Chen, *Chem.–Eur. J.*, 2006, **12**, 5603–5609.
81 Z. Meng, Y. Han, L.-N. Wang, J.-F. Xiang, S.-G. He and C.-F. Chen, *J. Am. Chem. Soc.*, 2015, **137**, 9739–9745.
82 C. Gaeta, M. O. Vysotsky, A. Bogdan and V. Böhmer, *J. Am. Chem. Soc.*, 2005, **127**, 13136–13137.
83 O. Molokanova, M. O. Vysotsky, Y. Cao, I. Thondorf and V. Böhmer, *Angew. Chem., Int. Ed.*, 2006, **45**, 8051–8055.
84 M. O. Vysotsky, A. Bogdan, L. Wang and V. Böhmer, *Chem. Commun.*, 2004, 1268–1269.
85 Y. Yamada, M. Okamoto, K. Furukawa, T. Kato and K. Tanaka, *Angew. Chem., Int. Ed.*, 2012, **51**, 709–713.
86 Y. Yamada, N. Mihara, S. Shibano, K. Sugimoto and K. Tanaka, *J. Am. Chem. Soc.*, 2013, **135**, 11505–11508.
87 Y. Yamada, N. Mihara and K. Tanaka, *Dalton Trans.*, 2013, **42**, 15873–15876.
88 N. Mihara, Y. Yamada and K. Tanaka, *Bull. Chem. Soc. Jpn.*, 2017, **90**, 427–435.
89 N. Mihara, Y. Yamada, K. Furukawa, T. Kato and K. Tanaka, *Dalton Trans.*, 2018, **47**, 7044–7049.
90 N. Mihara, Y. Yamada, S. Akine, K. Sugimoto and K. Tanaka, *Chem. Commun.*, 2017, **53**, 2230–2232.
91 N. Mihara, Y. Yamada, H. Takaya, Y. Kitagawa, S. Aoyama, K. Igawa, K. Tomooka and K. Tanaka, *Chem.–Eur. J.*, 2017, **23**, 7508–7514.
92 Y. Yamada, K. Morita, N. Mihara, K. Igawa, K. Tomooka and K. Tanaka, *New J. Chem.*, 2019, **43**, 11477–11482.
93 Y. Yamada and K. Tanaka, *J. Inclusion Phenom. Macrocyclic Chem.*, 2020, **96**, 197–213.
94 T.-H. Chiang, C.-Y. Tsou, Y.-H. Chang, C.-C. Lai, R. P. Cheng and S.-H. Chiu, *Org. Lett.*, 2021, **23**, 5787–5792.
95 L. Wang, M. O. Vysotsky, A. Bogdan, M. Bolte and V. Böhmer, *Science*, 2004, **304**, 1312–1314.
96 O. Molokanova, G. Podoprygorina, M. Bolte and V. Böhmer, *Tetrahedron*, 2009, **65**, 7220–7233.
97 A. Bogdan, Y. Rudzevich, M. O. Vysotsky and V. Böhmer, *Chem. Commun.*, 2006, 2941–2952.
98 Y. Yamada, R. Itoh, S. Ogino, T. Kato and K. Tanaka, *Angew. Chem., Int. Ed.*, 2017, **56**, 14124–14129.
99 C. Roche, J.-P. Sauvage, A. Sour and N. L. Strutt, *New J. Chem.*, 2011, **35**, 2820–2825.
100 Y. Yamada, M.-a. Okada and K. Tanaka, *Chem. Commun.*, 2013, **49**, 11053–11055.
101 Y. Yamada, T. Kato and K. Tanaka, *Chem.–Eur. J.*, 2016, **22**, 12371–12380.
102 E. M. G. Jamieson, F. Modicom and S. M. Goldup, *Chem. Soc. Rev.*, 2018, **47**, 5266–5311.

A.6 Electronic Appendices

The electronic appendices can be found here. The included README which can serve as an explanation of the structure of the electronic appendices is reproduced below:

A.6.1 Artefact Data

Folder : All the deteriorated artefacts were photographed before sample collection or analysis, and the pictures can be found in this folder. For deteriorated samples (S), the spine, the cover (b), and the title page (c) of the book when available are given. For reference samples (R) the spool or sample book the sample originates from is shown.

Sample Data.xlsx : Information about each deteriorated and reference sample (such as age, colour, etc) and the Electronic Appendix Inventory Sheet.

Electronic Appendix Inventory Sheet : Ticked boxes for if the photos a-c are present

A.6.2 Photos of Samples

Folder : Photographs of the samples removed from the artefacts above, in the form they were taken for analysis.

A.6.3 FTIR

FTIR Results Folder : Contains all the csv format data obtained from the IR machine measurements of the samples.

FTIR Setup Folder : Photographs of the sample placed in the IR machine to make a measurement.

Electronic Appendix Inventory Sheet : Ticked boxes for if data is present and if setup is present in above folders

FTIR Processed Data/Tannin assignments S.xlsx : FTIR detections of tannin types in deteriorated samples

FTIR Processed Data/FTIRPeakRatios1030vs1080.xlsx : Measuring deterioration of samples by comparing ratios of collagen and tannin FTIR peaks

FTIR Processed Data/FTIR1030vs1080RBS.pdf and FTIR1030vs1080RTS.pdf : As above but for the BS and TS of reference samples.

A.6.4 SEM

SEM Results Folder : Images of samples. Typically a small zoom factor (x30 or x45 for example) shows the whole sample. Files with A are annotations of these which show where larger zoom factor images were taken from, which are then shown in separate images.

SEM-EDX Folder : Spectra taken of SEM images with names corresponding to those in SEM folder. One image showing where spectra were taken, and then one file per spectrum.

Electronic Appendix Inventory Sheet : List of samples with SEM taken, all magnifications they are taken at, and below those how many spectra at that magnification are present.

SEM Processed Data/SEM Elemental Composition.xlsx : Summary of SEM-EDS spectra, what elements are in each sample and how much.

SEM Samples Folder : photographs of the samples used for SEM, in boxes or on pucks

A.6.5 ICP

ICP Results: Contains all of the ICP-OES and ICP-MS data obtained from the respective machines.

ICP Processed Data: Contains all of the ICP-OES and ICP-MS data processed as described in the thesis.

ICP Setup: Contains pictures taken while preparing samples.

A.6.6 Loose .py files

Code written to process the ICP and FTIR data.

A.6.7 Abbreviations in file names

RRS - red rot deteriorated sample

RRR - red rot reference sample

BS - bottom side

TS - top side

CS - cross section

L - left

R - right

M - middle

E - edge

F - fibres

S - strip

C - clump

P - powder

FP - filter paper

A.7 Additional SEM and SEM-EDX

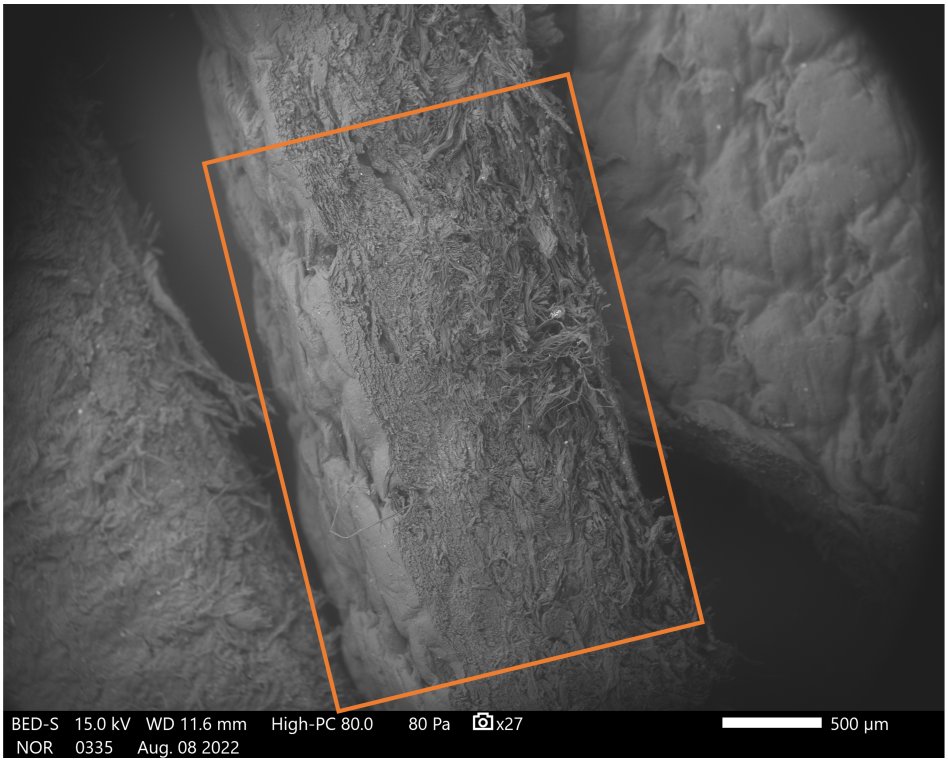

Figure A.47: The original SEM image of R17 with the area that the zoom was taken from for Figure 5.22 in the main text highlighted in orange.

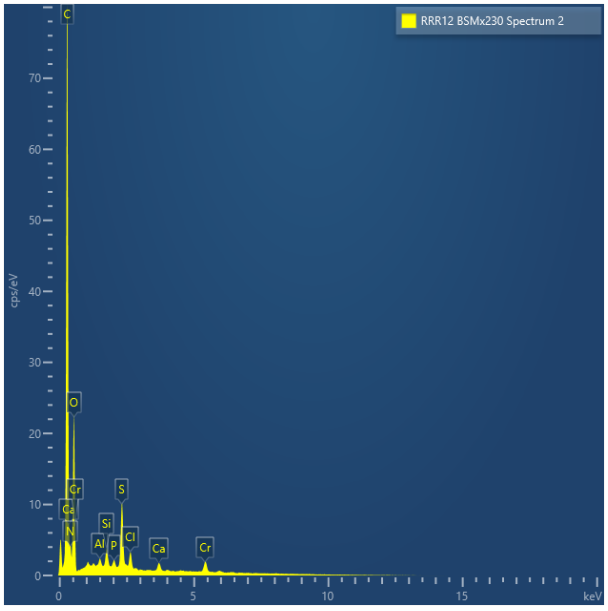

Figure A.48: EDX spectrum 2 from Figure 5.24 in the main text.

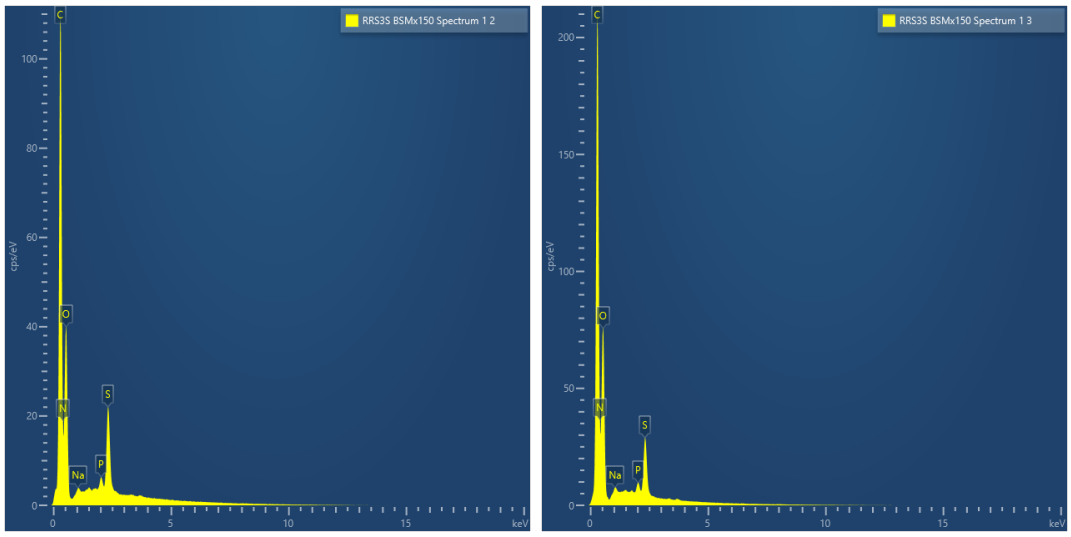

Figure A.49: Remaining SEM-EDX for Figure 5.32.

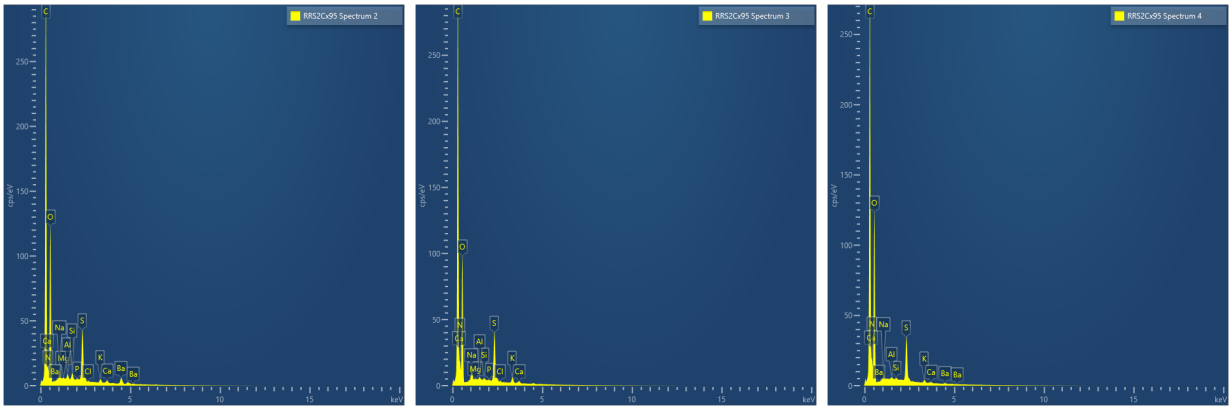

Figure A.50: Remaining SEM-EDX for Figure 5.33.

References

[1] J.-M. Lehn, *Supramol. Chem.*, 2008, **260**, 1762–1763.

[2] D. B. Amabilino and J. F. Stoddart, *Chem. Rev.*, 1995, **95**, 2725–2828.

[3] S. Erbas-Cakmak, D. A. Leigh, C. T. McTernan and A. L. Nussbaumer, *Chem. Rev.*, 2015, **115**, 10081–10206.

[4] M. J. Langton, F. Keymeulen, M. Ciaccia, N. H. Williams and C. A. Hunter, *Nat. Chem.*, 2016, **9**, 1–5.

[5] E. R. Kay and D. A. Leigh, *Angew. Chem. Int. Ed. Engl.*, 2015, **54**, 10080–10088.

[6] A. Coskun, M. Banaszak, R. D. Astumian, J. F. Stoddart and B. A. Grzybowski, *Chem. Soc. Rev.*, 2012, **41**, 19–30.

[7] D. J. Cram, *Angew. Chemie Int. Ed. English*, 1988, **27**, 1009–1020.

[8] C. J. Pedersen, *Angew. Chemie Int. Ed. English*, 1988, **27**, 1021–1027.

[9] J.-M. Lehn, *Angew. Chemie - Int. Ed.*, 1988, **27**, 89–112.

[10] J. P. Sauvage, *Angew. Chemie - Int. Ed.*, 2017, **56**, 11080–11093.

[11] J. F. Stoddart, *Angew. Chemie - Int. Ed.*, 2017, **56**, 11094–11125.

[12] B. L. Feringa, *Angew. Chemie - Int. Ed.*, 2017, **56**, 11060–11078.

[13] C. J. Bruns and J. F. Stoddart, *The Nature of the Mechanical Bond: From Molecules to Machines*, John Wiley & Sons, Inc., Hoboken, NJ, USA, 2016, pp. 1–761.

[14] N. H. Evans and P. D. Beer, *Self-Assembled Links: Catenanes*, John Wiley & Sons, Ltd, Chichester, UK, 2012.

[15] E. Wasserman, *J. Am. Chem. Soc.*, 1960, **82**, 4433–4434.

[16] G. Schill and A. Luttringhaus, *Angew. Chemie Int. Ed. English*, 1964, **3**, 546–547.

[17] C. O. Dietrich-Buchecker, J. P. Sauvage and J. P. Kintzinger, *Tetrahedron Lett.*, 1983, **24**, 5095–5098.

[18] G. Gil-Ramirez, D. A. Leigh and A. J. Stephens, *Angew. Chemie - Int. Ed.*, 2015, **54**, 6110–6150.

[19] v. W. C. M stone at the English language Wikipedia [GFDL (http://www.gnu.org/copyleft/fdl.html), CC-BY-SA-3.0 (http://creativecommons.org/licenses/by-sa/3.0/) or GFDL (http://www.gnu.org/copyleft/fdl.html)], *No Title*, 2007.

[20] P. R. Ashton, T. T. Goodnow, A. E. Kaifer, M. V. Reddington, A. M. Z. Slawin, N. Spencer, J. F. Stoddart, C. Vicent and D. J. Williams, *Angew. Chemie Int. Ed. English*, 1989, **28**, 1396–1399.

[21] M. Fujita, F. Ibukuro, H. Hagihara and K. Ogura, *Nature*, 1994, **367**, 720–723.

[22] G. Barin, R. S. Forgan and J. F. Stoddart, *Proc. Math. Phys. Eng. Sci.*, 2012, **468**, 2849–2880.

[23] M. Xue, Y. Yang, X. Chi, X. Yan and F. Huang, *Chem. Rev.*, 2015, **115**, 7398–7501.

[24] I. T. Harrison and S. Harrison, *J. Am. Chem. Soc.*, 1967, **89**, 5723–5724.

[25] G. Schill and H. Zollenkopf, *Justus Liebigs Ann. Chem.*, 1969, **721**, 53–74.

[26] H. Ogino, *J. Am. Chem. Soc.*, 1981, **103**, 1303–1304.

[27] P. L. Anelli, N. Spencer and J. F. Stoddart, *J. Am. Chem. Soc.*, 1991, **113**, 5131–5133.

[28] C. Wu, P. R. Lecavalier, Y. X. Shen and H. W. Gibson, *Chem. Mater.*, 1991, **3**, 569–572.

[29] N. Pearce, M. Tarnowska, N. J. Andersen, A. Wahrhaftig-Lewis, B. S. Pilgrim and N. R. Champness, *Chem. Sci.*, 2022, **13**, 3915–3941.

[30] T. Sato and T. Takata, *Tetrahedron Lett.*, 2007, **48**, 2797–2801.

[31] H. Iwamoto, Y. Yawata, Y. Fukazawa and T. Haino, *Chem. Lett.*, 2010, **39**, 24–25.

[32] H. Iwamoto, Y. Yawata, Y. Fukazawa and T. Haino, *Supramol. Chem.*, 2010, **22**, 815–826.

[33] R. Ciao, C. Talotta, C. Gaeta, L. Margarucci, A. Casapullo and P. Neri, *Org. Lett.*, 2013, **15**, 5694–5697.

[34] L. Kaufmann, N. L. Traulsen, A. Springer, H. V. Schröder, T. Mäkelä, K. Rissanen and C. A. Schalley, *Org. Chem. Front.*, 2014, **1**, 521–531.

[35] M. Radha Kishan, A. Parham, F. Schelhase, A. Yoneva, G. Silva, X. Chen, Y. Okamoto and F. Vögtle, *Angew. Chemie - Int. Ed.*, 2006, **45**, 7296–7299.

[36] O. Safarowsky, B. Windisch, A. Mohry and F. Vögtle, *J. für Prakt. Chemie*, 2000, **342**, 437–444.

[37] T. Tsukamoto, R. Sasahara, A. Muranaka, Y. Miura, Y. Suzuki, M. Kimura, S. Miyagawa, T. Kawasaki, N. Kobayashi, M. Uchiyama and Y. Tokunaga, *Org. Lett.*, 2018, **20**, 4745–4748.

[38] H. V. Schröder, H. Hupatz, A. J. Achazi, S. Sobottka, B. Sarkar, B. Paulus and C. A. Schalley, *Chem. - A Eur. J.*, 2017, **23**, 2960–2967.

[39] L. Yang, P. Langer, E. S. Davies, M. Baldoni, K. Wickham, N. A. Besley, E. Besley and N. R. Champness, *Chem. Sci.*, 2019, **10**, 3723–3732.

[40] P. Langer, *Ph.D. thesis*, University of Nottingham, 2019.

[41] C. Roche, J. P. Sauvage, A. Sour and N. L. Strutt, *New J. Chem.*, 2011, **35**, 2820–2825.

[42] Y. Yamada, M. A. Okada and K. Tanaka, *Chem. Commun.*, 2013, **49**, 11053–11055.

[43] C. Talotta, C. Gaeta and P. Neri, *Org. Lett.*, 2012, **14**, 3104–3107.

[44] T. Ogoshi, S. Kanai, S. Fujinami, T.-a. Yamagishi and Y. Nakamoto, *J. Am. Chem. Soc.*, 2008, **130**, 5022–5023.

[45] M. Holler, N. Allenbach, J. Sonet, J.-F. Nierengarten, J. He, Z. Abliz, W. Chen and F. Huang, *Chem. Commun.*, 2012, **48**, 2576–2578.

[46] T. Ogoshi, M. Hashizume, T.-a. Yamagishi, Y. Nakamoto, Y. Nakamoto, R. Salvio, A. Sartori and R. Ungaro, *Chem. Commun.*, 2010, **46**, 3708.

[47] T. Ogoshi, K. Demachi, K. Kitajima and T.-a. Yamagishi, *Chem. Commun.*, 2011, **47**, 7164.

[48] N. L. Strutt, R. S. Forgan, J. M. Spruell, Y. Y. Botros and J. F. Stoddart, *J. Am. Chem. Soc.*, 2011, **133**, 5668–5671.

[49] L. Liu, D. Cao, Y. Jin, H. Tao, Y. Kou and H. Meier, *Org. Biomol. Chem.*, 2011, **9**, 7007–7010.

[50] F. Würthner, C. R. Saha-Möller, B. Fimmel, S. Ogi, P. Leowanawat and D. Schmidt, *Chem. Rev.*, 2016, **116**, 962–1052.

[51] X. Zhan, A. Facchetti, S. Barlow, T. J. Marks, M. A. Ratner, M. R. Wasielewski and S. R. Marder, *Adv. Mater.*, 2011, **23**, 268–284.

[52] A. M. Brouwer, *Pure Appl. Chem.*, 2011, **83**, 2213–2228.

[53] F. Yukruk, A. L. Dogan, H. Canpinar, G. Dicle and E. U. Akkaya, 2005.

[54] F. Würthner, *Chem. Commun.*, 2004, 1564–1579.

[55] F. Miomandre and P. Audebert, *J. Photochem. Photobiol. C Photochem. Rev.*, 2020, **44**, 100372.

[56] G. Clavier and P. Audebert, *Chem. Rev.*, 2010, **110**, 3299–3314.

[57] A. Pinner, *Berichte der Dtsch. Chem. Gesellschaft*, 1893, **26**, 2126–2135.

[58] N. Abdel, M. Kira and M. Tolba, *Tetrahedron Lett.*, 1968, **9**, 3871–3872.

[59] P. E. Hartnett, A. Timalsina, H. S. Matte, N. Zhou, X. Guo, W. Zhao, A. Facchetti, R. P. Chang, M. C. Hersam, M. R. Wasielewski and T. J. Marks, *J. Am. Chem. Soc.*, 2014, **136**, 16345–16356.

[60] J. Zhang, F. Bai, Y. Li, H. Hu, B. Liu, X. Zou, H. Yu, J. Huang, D. Pan, H. Ade and H. Yan, *J. Mater. Chem. A*, 2019, **7**, 8136–8143.

[61] J. D. Yuen, V. A. Pozdin, A. T. Young, B. L. Turner, I. D. Giles, J. Naciri, S. A. Trammell, P. T. Charles, D. A. Stenger and M. A. Daniele, *Dye. Pigment.*, 2020, **174**, 108014.

[62] H. Langhals, A. Hofer, S. Bernhard, J. S. Siegel and P. Mayer, *J. Org. Chem.*, 2011, **76**, 990–992.

[63] K. M. Lefler, K. E. Brown, W. A. Salamant, S. M. Dyar, K. E. Knowles and M. R. Wasielewski, *J. Phys. Chem. A*, 2013, **117**, 10333–10345.

[64] E. A. Margulies, L. E. Shoer, S. W. Eaton and M. R. Wasielewski, *Phys. Chem. Chem. Phys.*, 2014, **16**, 23735–23742.

[65] H. Langhals and R. Ismael, *European J. Org. Chem.*, 1998, 1915–1917.

[66] P. Spenst and F. Würthner, *Angew. Chemie - Int. Ed.*, 2015, **54**, 10165–10168.

[67] K. E. Brown, W. A. Salamant, L. E. Shoer, R. M. Young and M. R. Wasielewski, *J. Phys. Chem. Lett.*, 2014, **5**, 2588–2593.

[68] S. Yagai, T. Seki, T. Karatsu, A. Kitamura and F. Würthner, *Angew. Chemie - Int. Ed.*, 2008, **47**, 3367–3371.

[69] T. Seki, A. Asano, S. Seki, Y. Kikkawa, H. Murayama, T. Karatsu, A. Kitamura and S. Yagai, *Chem. - A Eur. J.*, 2011, **17**, 3598–3608.

[70] J. Gorman, S. R. E. Orsborne, A. Sridhar, R. Pandya, P. Budden, A. Ohmann, N. A. Panjwani, Y. Liu, J. L. Greenfield, S. Dowland, V. Gray, S. T. J. Ryan, S. De Ornellas, A. H. El-Sagheer, T. Brown, J. R. Nitschke, J. Behrends, U. F. Keyser, A. Rao, R. Collepardo-Guevara, E. Stulz, R. H. Friend and F. Auras, *J. Am. Chem. Soc.*, 2022, **144**, 368–376.

[71] C. Gao, L. Xue, Y. Chen and X. Li, *Colloid Polym. Sci.*, 2015, **293**, 35–48.

[72] B. Carlotti, I. K. Madu, H. Kim, Z. Cai, H. Jiang, A. K. Muthike, L. Yu, P. M. Zimmerman and T. Goodson, *Chem. Sci.*, 2020, **11**, 8757–8770.

[73] S. J. Hauschildt, Z. Wu, D. Uersfeld, P. Schmid, C. Götz, V. Engel, B. Engels, K. Müllen and T. Basché, *J. Chem. Phys.*, 2022, **156**, 044304.

[74] H. Yoo, H. W. Bahng, M. R. Wasielewski and D. Kim, *Phys. Chem. Chem. Phys.*, 2012, **14**, 2001–2007.

[75] H. Liu, L. Shen, Z. Cao and X. Li, *Phys. Chem. Chem. Phys.*, 2014, **16**, 16399–16406.

[76] C. Lin, T. Kim, J. D. Schultz, R. M. Young and M. R. Wasielewski, *Nat. Chem.*, 2022, **14**, 786–793.

[77] K. Müllen and G. Klarner, *Electronic Materials: The Oligomer Approach*, wiley, 2007, pp. 1–599.

[78] N. Pearce, K. E. Reynolds, S. Kayal, X. Z. Sun, E. S. Davies, F. Malagreca, C. J. Schürmann, S. Ito, A. Yamano, S. P. Argent, M. W. George and N. R. Champness, *Nat. Commun.*, 2022, **13**, 1–10.

[79] T. B. Wei, L. H. Qi, Q. P. Zhang, W. H. Zhang, H. Yao, Y. M. Zhang and Q. Lin, *New J. Chem.*, 2020, **44**, 12531–12537.

[80] Y. Guan, P. Liu, C. Deng, M. Ni, S. Xiong, C. Lin, X. Y. Hu, J. Ma and L. Wang, *Org. Biomol. Chem.*, 2014, **12**, 1079–1089.

[81] X. Cheng, H. Li, F. Zheng, Q. Lin, Y. Zhang, H. Yao and T. Wei, *Dye. Pigment.*, 2016, **127**, 59–66.

[82] Y. Wu, H. Qin, J. Shen, H. Li, X. Shan, M. Xie and X. Liao, *Chem. Commun.*, 2022, **58**, 581–584.

[83] S. Aivali, L. Tsimpouki, C. Anastasopoulos and J. K. Kallitsis, *Molecules*, 2019, **24**, 4406.

[84] S. Sau and R. Banerjee, *Eur. J. Med. Chem.*, 2014, **83**, 433–447.

[85] Q. Lou, L. Ji, W. Zhong, S. Li, S. Yu, Z. Li and X. Meng, *Molecules*, 2014, **19**, 8803–8819.

[86] S. R. Yasa, S. S. Kaki, Y. Poornachandra, C. G. Kumar and V. Penumarthy, *Bioorganic Med. Chem. Lett.*, 2016, **26**, 1978–1982.

[87] M. Hebda, M. Bajda, A. Wieckowska, N. Szałłaj, A. Pasieka, D. Panek, J. Godyń, T. Wichur, D. Knez, S. Gobec and B. Malawska, *Molecules*, 2016, **21**, 410.

[88] F. Kilchmann, M. J. Marcaida, S. Kotak, T. Schick, S. D. Boss, M. Awale, P. Gönczy and J. L. Reymond, *J. Med. Chem.*, 2016, **59**, 7188–7211.

[89] L. Fang, Y. Hu, Q. Li, S. Xu, M. K. Dhinakarank, W. Gong and G. Ning, *Org. Biomol. Chem.*, 2016, **14**, 4039–4045.

[90] P. Chen, Y. Zhou and J. Yang, *Chem. Commun.*, 2017, **53**, 1144–1147.

[91] T. B. Wei, J. D. Ding, J. F. Chen, B. B. Han, X. M. Jiang, H. Yao, Y. M. Zhang and Q. Lin, *New J. Chem.*, 2018, **42**, 1271–1275.

[92] L. H. Qi, J. D. Ding, X. Q. Ma, X. W. Guan, W. Zhu, H. Yao, Y. M. Zhang, T. B. Wei and Q. Lin, *Soft Matter*, 2019, **15**, 6836–6841.

[93] A. Arulkashmir, B. Jain, J. C. John, K. Roy and K. Krishnamoorthy, *Chem. Commun.*, 2014, **50**, 326–328.

[94] F. Rigodanza, E. Tenori, A. Bonasera, Z. Syrgiannis and M. Prato, *European J. Org. Chem.*, 2015, **2015**, 5060–5063.

[95] X. Liu, A. Roberts, A. Ahmed, Z. Wang, X. Li and H. Zhang, *J. Mater. Chem. A*, 2015, **3**, 15513–15522.

[96] B. Zhang, W. Liu, Y. Liu, Z. Suo, L. Feng, F. Xing and S. Zhu, *RSC Adv.*, 2019, **9**, 24638–24645.

[97] S. Gabriel, *Berichte der Dtsch. Chem. Gesellschaft*, 1887, **20**, 2224–2236.

[98] J. Bitta and S. Kubik, *Org. Lett.*, 2001, **3**, 2637–2640.

[99] E. J. E. Freyne, T. P. S. Perera, B. Antonius and E. Al, *Quinazoline derivatives*, 2016, https://worldwide.espacenet.com/patent/search/family/033493782/publication/US9273013B2?q=pn{%}3DUS9273013B2.

[100] K. M. Engstrom, A. Sheikh, R. Ho and R. W. Miller, *Org. Process Res. Dev.*, 2014, **18**, 488–494.

[101] L. Shao, J. Sun, B. Hua and F. Huang, *Chem. Commun.*, 2018, **54**, 4866–4869.

[102] W. Ali, W. Gong, M. Hassan, W. Qu, L. Liu and G. Ning, *Chinese Chem. Lett.*, 2021, **32**, 371–374.

[103] E. K. Ryu, Y. S. Choe, K. H. Lee, Y. Choi and B. T. Kim, J. Med. Chem., 2006, pp. 6111–6119.

[104] Y. H. Jong, L. A. Arnold, F. Zhu, A. Kosinski, T. J. Mangano, V. Setola, B. L. Roth and R. K. Guy, *J. Med. Chem.*, 2009, **52**, 3892–3901.

[105] F. Yang, X. Jiang, J. Li, Y. Wang, Y. Liu, M. Bi, C. Wu, Q. Zhao, W. Chen, J. Yin, J. Zhang, Y. Xie, T. Hu, M. Xu, S. Guo, Z. Wang, Y. He and J. Shen, *Bioorganic Med. Chem. Lett.*, 2016, **26**, 3141–3147.

[106] D. L. Comins and S. P. Joseph, in *Encycl. Reagents Org. Synth.*, John Wiley & Sons, Ltd, Chichester, UK, 2001.

[107] V. Balzani, M. Clemente-León, A. Credi, J. N. Lowe, J. D. Badjić, J. F. Stoddart and D. J. Williams, *Chem. - A Eur. J.*, 2003, **9**, 5348–5360.

[108] J. D. Badjić, V. Balzani, A. Credi, J. N. Lowe, S. Silvi and J. F. Stoddart, *Chem. - A Eur. J.*, 2004, **10**, 1926–1935.

[109] J. D. Badjić, S. J. Cantrill, R. H. Grubbs, E. N. Guidry, R. Orenes and J. F. Stoddart, *Angew. Chemie - Int. Ed.*, 2004, **43**, 3273–3278.

[110] J. D. Badjić, S. J. Cantrill and J. F. Stoddart, *J. Am. Chem. Soc.*, 2004, **126**, 2288–2289.

[111] J. D. Badjic, V. Balzani, A. Credi, S. Silvi and J. F. Stoddart, *Science (80-.).*, 2004, **303**, 1845–1849.

[112] J. D. Badjic, C. M. Ronconi, J. F. Stoddart, V. Balzani, S. Silvi and A. Credi, *J. Am. Chem. Soc.*, 2006, **128**, 1489–1499.

[113] H. Hou, K. C. Leung, D. Lanari, A. Nelson, J. F. Stoddart and R. H. Grubbs, *J. Am. Chem. Soc.*, 2006, **128**, 15358–15359.

[114] B. H. Northrop, F. Aricó, N. Tangchiavang, J. D. Badjić and J. F. Stoddart, *Org. Lett.*, 2006, **8**, 3899–3902.

[115] H. Zhang, K. T. Nguyen, X. Ma, H. Yan, J. Guo, L. Zhu and Y. Zhao, *Org. Biomol. Chem.*, 2013, **11**, 2070–2074.

[116] R. J. Mandle and J. W. Goodby, *Chem. - A Eur. J.*, 2019, **25**, 14454–14459.

[117] S. Paul and M. Gupta, *Tetrahedron Lett.*, 2004, **45**, 8825–8829.

[118] S. H. Sonawane, M. Anniyappan, J. Athar, S. Banerjee and A. K. Sikder, *RSC Adv.*, 2016, **6**, 8495–8502.

[119] J. Wu, S. Sun, X. Feng, J. Shi, X. Y. Hu and L. Wang, *Chem. Commun.*, 2014, **50**, 9122–9125.

[120] P. Xin, H. Kong, Y. Sun, L. Zhao, H. Fang, H. Zhu, T. Jiang, J. Guo, Q. Zhang, W. Dong and C. P. Chen, *Angew. Chemie - Int. Ed.*, 2019, **58**, 2779–2784.

[121] H. Tian, R. Li, P. H. Lin and K. Meguellati, *New J. Chem.*, 2020, **44**, 10628–10632.

[122] K. Wang, C. Y. Wang, Y. Zhang, S. X. A. Zhang, B. Yang and Y. W. Yang, *Chem. Commun.*, 2014, **50**, 9458–9461.

[123] J. W. Lee, S. I. Jun and K. Kim, *Tetrahedron Lett.*, 2001, **42**, 2709–2711.

[124] J. R. Thomas, X. Liu and P. J. Hergenrother, *J. Am. Chem. Soc.*, 2005, **127**, 12434–12435.

[125] S. Roe, M. Gunaratnam, C. Spiteri, P. Sharma, R. D. Alharthy, S. Neidle and J. E. Moses, *Org. Biomol. Chem.*, 2015, **13**, 8500–8504.

[126] N. Pearce, E. S. Davies, W. Lewis and N. R. Champness, *ACS Omega*, 2018, **3**, 14236–14244.

[127] C. R. Benson, A. I. Share, M. G. Marzo and A. H. Flood, *Inorg. Chem.*, 2016, **55**, 3767–3776.

[128] M. Vinu, K. Sivasankar, S. Prabu, J. L. Han, C. H. Lin, C. C. Yang and J. Demel, *Eur. J. Inorg. Chem.*, 2020, **2020**, 461–466.

[129] B. Lerma-Berlanga, C. R. Ganivet, N. Almora-Barrios, S. Tatay, Y. Peng, J. Albero, O. Fabelo, J. González-Platas, H. García, N. M. Padial and C. Martí-Gastaldo, *J. Am. Chem. Soc.*, 2021, **143**, 1798–1806.

[130] B. Lerma-Berlanga, C. R. Ganivet, N. Almora-Barrios, R. Vismara, J. A. Navarro, S. Tatay, N. M. Padial and C. Martí-Gastaldo, *Angew. Chemie - Int. Ed.*, 2022, **61**, e202208139.

[131] D. A. Roberts, B. S. Pilgrim, J. D. Cooper, T. K. Ronson, S. Zarra and J. R. Nitschke, *J. Am. Chem. Soc.*, 2015, **137**, 10068–10071.

[132] D. A. Roberts, B. S. Pilgrim, G. Sirvinskaite, T. K. Ronson and J. R. Nitschke, *J. Am. Chem. Soc.*, 2018, **140**, 9616–9623.

[133] H. Sun, Q. Xue, C. Zhang, H. Wu and P. Feng, *Org. Chem. Front.*, 2022, **9**, 481–498.

[134] B. S. Pilgrim, *Ph.D. thesis*, University of Oxford, 2013.

[135] P. Demay-Drouhard, K. Du, K. Samanta, X. Wan, W. Yang, R. Srinivasan, A. C. Sue and H. Zuilhof, *Org. Lett.*, 2019, **21**, 3976–3980.

[136] M. Guo, X. Wang, C. Zhan, P. Demay-Drouhard, W. Li, K. Du, M. A. Olson, H. Zuilhof and A. C. Sue, *J. Am. Chem. Soc.*, 2018, **140**, 74–77.

[137] S. Drescher and B. Dobner, *Synth. Commun.*, 2014, **44**, 564–573.

[138] J. Hanna, H. Okamura, T. Usui and H. Iino, *Benzothienobenzothiophene Derivative, Organic Semiconductor Material, And Organic Transistor*, 2017, https://worldwide.espacenet.com/publicationDetails/biblio?CC=JP{&}NR=2017066089{&}KC={&}FT=E{&}locale=en{_}EP.

[139] Y. Luo, D. Tang, W. Zhu, Y. Xu and X. Qian, *J. Mater. Chem. C*, 2015, **3**, 8485–8489.

[140] E. S. H. Ashry, L. F. Awad, N. Rashed, A. AbdelRahman and H. A. Rasheed, *Nucleosides, Nucleotides and Nucleic Acids*, 2008, **27**, 309–317.

[141] R. E. Sammelson, M. M. Olmstead, M. J. Haddadin and M. J. Kurth, *J. Org. Chem.*, 2000, **65**, 9265–9267.

[142] W. X. Hu, G. W. Rao and Y. Q. Sun, *Bioorganic Med. Chem. Lett.*, 2004, **14**, 1177–1181.

[143] A. V. Polezhaev, N. A. Maciulis, C. H. Chen, M. Pink, R. L. Lord and K. G. Caulton, *Chem. - A Eur. J.*, 2016, **22**, 13985–13998.

[144] F. Fouad, B. Ellman, S. Bunge, P. Miller and R. Twieg, *Mol. Cryst. Liq. Cryst.*, 2013, **582**, 34–42.

[145] X. B. Hu, L. Chen, W. Si, Y. Yu and J. L. Hou, *Chem. Commun.*, 2011, **47**, 4694–4696.

[146] S. Dong, C. Han, B. Zheng, M. Zhang and F. Huang, *Tetrahedron Lett.*, 2012, **53**, 3668–3671.

[147] C. Li, L. Zhao, J. Li, X. Ding, S. Chen, Q. Zhang, Y. Yu, X. Jia, M. F. Parisi, M. Baller, S. Magonov, S. D. Solares, W. A. Goddard, C.-M. Ho and J. F. Stoddart, *Chem. Commun.*, 2010, **46**, 9016.

[148] S. Dong, J. Yuan and F. Huang, *Chem. Sci.*, 2014, **5**, 247–252.

[149] Y. Zhou, K. Jie, C. Thompson, N. Li and Y. Yao, *Tetrahedron Lett.*, 2015, **56**, 2091–2093.

[150] K. Kanagaraj, M. Alagesan, Y. Inoue and C. Yang, in *Compr. Supramol. Chem. II*, Elsevier, 2017, pp. 11–60.

[151] N. Pearce, E. S. Davies and N. R. Champness, *Molecules*, 2020, **25**, 1627.

[152] S. B. Garber, J. S. Kingsbury, B. L. Gray and A. H. Hoveyda, *J. Am. Chem. Soc.*, 2000, **122**, 8168–8179.

[153] T. J. Kidd, D. A. Leigh and A. J. Wilson, *J. Am. Chem. Soc.*, 1999, **121**, 1599–1600.

[154] J. A. Wisner, P. D. Beer, M. G. Drew and M. R. Sambrook, *J. Am. Chem. Soc.*, 2002, **124**, 12469–12476.

[155] D. A. Leigh, J. J. Danon, S. D. Fielden, J. F. Lemonnier, G. F. Whitehead and S. L. Woltering, *Nat. Chem. 2020 132*, 2020, **13**, 117–122.

[156] A. K. Chatterjee, T. L. Choi, D. P. Sanders and R. H. Grubbs, *J. Am. Chem. Soc.*, 2003, **125**, 11360–11370.

[157] R. R. Ali Hassan, *Spectrosc. Lett.*, 2019, **52**, 288–296.

[158] B. M. Haines and J. R. Barlow, *J. Mater. Sci.*, 1975, **10**, 525–538.

[159] M. Dempsey, *J. Mater. Sci.*, 1974, **9**, 651–657.

[160] M. Kite and R. Thomson, *Conservation of Leather and Related Materials*, Elsevier Butterworth-Heinemann, 2006, pp. 1–340.

[161] A. D. Covington and W. R. Wise, *Tanning Chemistry*, The Royal Society of Chemistry, 2020.

[162] K. Khanbabaee and T. van Ree, *Nat. Prod. Rep.*, 2001, **18**, 641–649.

[163] L. Falcão and M. E. M. Araújo, *Molecules*, 2018, **23**, 1081.

[164] M. König, E. Scholz, R. Hartmann, W. Lehmann and H. Rimpler, *J. Nat. Prod.*, 1994, **57**, 1411–1415.

[165] P. Comandini, M. J. Lerma-García, E. F. Simó-Alfonso and T. G. Toschi, *Food Chem.*, 2014, **157**, 290–295.

[166] D. G. Reid, S. L. Bonnet, G. Kemp and J. H. Van Der Westhuizen, *Phytochemistry*, 2013, **94**, 243–248.

[167] L. Falcão and M. E. M. Araújo, *Vib. Spectrosc.*, 2014, **74**, 98–103.

[168] L. Falcão and M. E. M. Araújo, *J. Cult. Herit.*, 2011, **12**, 149–156.

[169] L. Falcão and M. E. M. Araújo, *J. Cult. Herit.*, 2013, **14**, 499–508.

[170] E. May and M. Jones, *Conservation Science*, Royal Society of Chemistry, 2007.

[171] R. Larsen, *Chimia (Aarau).*, 2008, **62**, 899–902.

[172] E. Dickinson and K. E. High, *Herit. Sci.*, 2022, **10**, 1–13.

[173] S. El Moujahed, F. Errachidi, H. Abou Oualid, A. V. Botezatu-Dediu, F. Ouazzani Chahdi, Y. Kandri Rodi and R. M. Dinica, *RSC Adv.*, 2022, **12**, 4175–4186.

[174] R. Reed, *J. Archaeol. Sci.*, 1974, **1**, 298–300.

[175] A. Watt, *The Art of Leather Manufacture*, BiblioBazaar, Reprint edn., 1885.

[176] A. Vichi, G. Eliazyan and S. G. Kazarian, *ACS Omega*, 2018, **3**, 7150–7157.

[177] B. M. Haines, in *Conserv. Libr. Arch. Mater. Graph. Arts*, Elsevier, 1987, pp. 239–264.

[178] R. S. Thomson, *Am. Leather Chem. Assoc.*, 2002, **97**, 307–320.

[179] R. Rabee, M. F. Ali, A. G. A. Fahmy and S. F. Halim, *Adv. Mater. Res.*, 2014, **1064**, 15–20.

[180] L. Gonzalez, M. Wade, N. Bell, K. Thomas and T. Wess, *Appl. Spectrosc.*, 2013, **67**, 158–162.

[181] C. Carsote, C. Şendrea, M. C. Micu, A. Adams and E. Badea, *Radiat. Phys. Chem.*, 2021, **189**, 109712.

[182] V. Plavan, L. Miu and N. Gavrilyuk, *Procedia Chem.*, 2013, **8**, 279–283.

[183] C. N. Calnan and B. M. Haines, *Leather : its composition and changes with time*, The Leather Conservation Centre, 1991, p. 90.

[184] R. Larsen and L. Rahme, *Læder, pergament og skind: fremstilling, historie og nedbrydning*, Det Kongelige Danske Kunstakademi, Konservatorskolen, 1999.

[185] C. Carşote, E. Badea, L. Miu and G. D. Gatta, *J. Therm. Anal. Calorim.*, 2016, **124**, 1255–1266.

[186] E. Badea, C. Şendrea, C. Carşote, A. Adams, B. Blümich and H. Iovu, *Microchem. J.*, 2016, **129**, 158–165.

[187] J. S. Rogers and W. Beebe, *Leather bookbindings : how to preserve them*, U.S. Department of Agriculture, Washington D.C., 1956, vol. 398.

[188] J. W. Waterer, *Stud. Conserv.*, 1972, **17**, 206.

[189] V. Dirksen, *J. Conserv. Museum Stud.*, 1997, **3**, 6.

[190] E. Badea, C. Carşote, E. Hadîmbu, C. Şendrea and M. C. Lupaș, *Herit. Sci.*, 2019, **7**, 1–14.

[191] A. B. Strzelczyk, J. Kuroczkin and W. E. Krumbein, *Int. Biodeterior.*, 1987, **23**, 3–27.

[192] M.-L. E. Florian, *Leather Conserv. News*, 1985, **2**, 1–5.

[193] H. A. B. van Soest, T. Stambolov and P. B. Hallebeek, *Stud. Conserv.*, 1984, **29**, 21.

[194] L. Ludwick, *Ph.D. thesis*, 2013.

[195] D. Pellegrini, M. Corsi, M. Bonanni, R. Bianchini, A. D'Ulivo and E. Bramanti, *Dye. Pigment.*, 2015, **116**, 65–73.

[196] C. Sendrea, C. Carsote, E. Badea and A. Adams, *Bull., Ser. B*, 2016, **78**, year.

[197] Z. Sebestyén, E. Badea, C. Carsote, Z. Czégény, T. Szabó, B. Babinszki, J. Bozi and E. Jakab, *J. Anal. Appl. Pyrolysis*, 2022, **162**, 105428.

[198] M. Mehta, R. Naffa, C. Maidment, G. Holmes and M. Waterland, *J. Leather Sci. Eng.*, 2020, **2**, 1–15.

[199] M. Jackson, L. P. Choo, P. H. Watson, W. C. Halliday and H. H. Mantsch, *BBA - Mol. Basis Dis.*, 1995, **1270**, 1–6.

[200] L. Rieppo, S. Saarakkala, T. Närhi, H. J. Helminen, J. S. Jurvelin and J. Rieppo, *Osteoarthr. Cartil.*, 2012, **20**, 451–459.

[201] A. Martínez Cortizas and O. López-Costas, *Sci. Rep.*, 2020, **10**, 17888.

[202] P. L. Gordon, C. Huang, R. C. Lord and I. V. Yannas, *Macromolecules*, 1974, **7**, 954–956.

[203] M. G. Haugh, M. J. Jaasma and F. J. O'Brien, *J. Biomed. Mater. Res. - Part A*, 2009, **89**, 363–369.

[204] F. Pati, B. Adhikari and S. Dhara, *Bioresour. Technol.*, 2010, **101**, 3737–3742.

[205] S. B. Botta, P. A. Ana, M. O. Santos, D. M. Zezell and A. B. Matos, *J. Biomed. Mater. Res. - Part B Appl. Biomater.*, 2012, **100 B**, 1009–1016.

[206] Y. Zhang, Z. Chen, X. Liu, J. Shi, H. Chen and Y. Gong, *J. Cult. Herit.*, 2021, **48**, 205–210.

[207] F. D. S. Grasel, M. F. Ferrão and C. R. Wolf, *Spectrochim. Acta Part A Mol. Biomol. Spectrosc.*, 2016, **153**, 94–101.

[208] M. Dempsey, *J. Pathol.*, 1979, **128**, 151–157.

[209] G. Abdel-Maksoud, M. Abdel-Nasser, M. H. Sultan, A. M. Eid, S. H. Alotaibi, S. E.-D. Hassan and A. Fouda, *Life*, 2022, **12**, 1821.

[210] M. Mansour, R. Hassan and M. Salem, *Egypt. J. Archaeol. Restor. Stud.*, 2017, **7**, 1–10.

[211] R. R. Ali Hassan, *J. Inst. Conserv.*, 2019, **42**, 210–225.

[212] M. Vadrucci, G. De Bellis, C. Mazzuca, F. Mercuri, F. Borgognoni, E. Schifano, D. Uccelletti and C. Cicero, *Front. Mater.*, 2020, **7**, year.

[213] B. Pemberton and P. Nel, *AICCM Bull.*, 2008, **31**, 28–35.

[214] T. D. Chaplin, R. J. Clark and M. Martinón-Torres, *J. Mol. Struct.*, 2010, **976**, 350–359.

[215] OEKO-TEX, *Standard STANDARD 100 by OEKO-TEX OEKO-TEX-International Association for Research and Testing in the Field of Textile and Leather Ecology OEKO-TEX*, 2021, www.oeko-tex.com.

[216] F. Valentini, M. Bicchieri, A. Calcaterra and M. Talamo, *Electroanalysis*, 2017, **29**, 2873–2881.

[217] T. Delbey, J. P. Holck, B. Jørgensen, A. Alvis, V. H. Smith, G. M. Kavich, K. A. Harmon, B. F. Dorch and K. L. Rasmussen, *Herit. Sci.*, 2019, **7**, year.

[218] F. Belussi and S. R. Sedita, *Econ. e Polit. Ind.*, 2008, **35**, 51–72.

[219] W. Evans and C. Critchfield, *Bur. Stand. J. Res.*, 1933, **11**, 147.

[220] G. Vyskočilová, C. Carşote, R. Ševčík and E. Badea, *Herit. Sci.*, 2022, **10**, 1–14.

[221] A. Koochakzaei and S. Mallakpour, *Archaeometry*, 2022, 1–14.

[222] M. Unal, H. Jung and O. Akkus, *J. Bone Miner. Res.*, 2016, **31**, 1015–1025.

[223] R. R. Ali Hassan, *J. Cult. Herit.*, 2016, **21**, 786–795.

[224] A. Lama, A. P. M. Antunes, A. D. Covington, J. Guthrie-Strachan and Y. Fletcher, *J. Inst. Conserv.*, 2015, **38**, 172–187.

[225] S. C. Boyatzis, G. Velivasaki and E. Malea, *Herit. Sci.*, 2016, **4**, 1–17.

[226] O. S. Rabotyagova, P. Cebe and D. L. Kaplan, *Mater. Sci. Eng. C*, 2008, **28**, 1420–1429.

[227] E. Chorier, N. Blanc, J. C. Cannot and A. Berthod, *J. Am. Leather Chem. Assoc.*, 2014, **109**, 322–329.

[228] T. Sawoszczuk, J. Syguła-Cholewińska and J. M. del Hoyo-Meléndez, *J. Chromatogr. A*, 2015, **1409**, 30–45.

[229] M. Stanca, C. Gaidau, C. A. Alexe, I. Stanculescu, S. Vasilca, A. Matei, D. Simion and R. R. Constantinescu, *Materials (Basel).*, 2021, **14**, year.

[230] V. Galván Josa, G. Castellano and S. R. Bertolino, *Radiat. Phys. Chem.*, 2013, **88**, 32–37.

[231] Y. Kumazawa, Y. Taga, K. Iwai and Y. I. Koyama, *J. Agric. Food Chem.*, 2016, **64**, 6051–6057.

[232] J. A. Ebsen, K. Haase, R. Larsen, D. V. P. Sommer and L. Ø. Brandt, *J. Cult. Herit.*, 2019, **39**, 21–31.

[233] B. Peng, B. Shi, D. Sun, Y. Chen and D. C. Shelly, *Ultrason. Sonochem.*, 2007, **14**, 305–313.

[234] A. C. Adiguzel Zengin, M. Crudu, S. S. Maier, V. Deselnicu, L. Albu, G. Gulumser, B. O. Bitlisli, B. Basaran and M. M. Mutlu, *Ekoloji*, 2012, **21**, 17–25.

[235] M. Seggiani, M. Puccini, S. Vitolo, C. Chiappe, C. S. Pomelli and D. Castiello, *Clean Technol. Environ. Policy*, 2014, **16**, 1795–1803.

[236] M. M. Mutlu, M. Crudu, S. S. Maier, D. Deselnicu, L. Albu, G. Gulumser, B. O. Bitlisli, B. Basaran, C. C. Tosun and A. C. Adiguzel Zengin, *Ekoloji*, 2014, 83–90.

[237] G. Poggi, M. C. Sistach, E. Marin, J. F. Garcia, R. Giorgi and P. Baglioni, *J. Cult. Herit.*, 2016, **18**, 250–257.

[238] R. R. A. Hassan, M. F. Ali, A. G. A. Fahmy, H. M. Ali and M. Z. Salem, *J. Chem.*, 2020, **2020**, year.

[239] F. Helmi, W. Wahba, A. Brania, M. Abdelnasser and M. Elkobasy, *Adv. Res. Conserv. Sci.*, 2021, **2**, 40–52.

[240] Y. Hu, J. Liu, G. Han, X. Li, Z. Zhang, X. Zheng, F. Wang, Y. Pei, Y. Lei and K. Tang, *J. Cult. Herit.*, 2022, **53**, 118–126.

[241] E. Badea, L. Miu, P. Budrugeac, M. Giurginca, A. Mašić, N. Badea and G. Della Gatta, *J. Therm. Anal. Calorim.*, 2008, **91**, 17–27.

[242] M. Bicchieri, F. Valentini, F. Pascalicchio, M. L. Riccardi, P. Colaizzi, C. Del Re and M. Talamo, *J. Cult. Herit.*, 2018, **33**, 1–9.

[243] M. Ohlídalová, I. Kučerová, V. Brezová, Z. Cílová and A. Michalcová, *J. Cult. Herit.*, 2017, **24**, 86–92.

[244] W. McLean, *Ski. Deep*, 1996, **2**, 19.

[245] X. Li, Y. N. Wang, J. Li and B. Shi, *J. Am. Leather Chem. Assoc.*, 2016, **111**, 230–237.

[246] D. P. Nikolova and M. P. Velcheva, *Restaurator*, 1996, **17**, 203–213.

[247] G. De Filpo, A. M. Palermo, R. Munno, L. Molinaro, P. Formoso and F. P. Nicoletta, *Int. Biodeterior. Biodegrad.*, 2015, **103**, 51–58.

[248] M. Ignat, L. Miu, E. Hadimbu, C. Șendrea, M. C. Micu, S. M. Păunescu, I. M. Caniola and E. Badea, ICAMS Proc. Int. Conf. Adv. Mater. Syst., 2020, pp. 501–506.

[249] F. Gay and M. Ballarin, *Lect. Notes Comput. Sci. (including Subser. Lect. Notes Artif. Intell. Lect. Notes Bioinformatics)*, 2014, **8740**, 290–299.

[250] O. A. Mohamed, A. B. Moustafa, M. A. Mehawed and N. H. El-Sayed, *J. Appl. Polym. Sci.*, 2009, **111**, 1488–1495.

[251] 21/30441409 DC, *BS EN ISO 17072-2. Leather. Chemical determination of metal content. Part 2. Total metal content*, BSI.

[252] BS EN ISO 17072-1:2019 - TC, *Tracked Changes. Leather. Chemical determination of metal content. Extractable metals*, BSI.

[253] BS EN ISO 4044:2017 - TC, *Tracked Changes. Leather. Chemical tests. Preparation of chemical test samples*, BSI.

[254] E. Bielak and E. Marcinkowska, *Sci. Rep.*, 2022, **12**, 5061.

[255] D. Tegtmeyer and M. Kleban, *Chromium and Leather Research A balanced view of scientific facts and figures*, 2013, https://iultcs.org/wp-content/uploads/2020/07/IUR-1{_}Chromiumandleatherresearch{_}Abalancedviewoffacts{_}Aug-2013{_}corr-1.pdf.

[256] J. Lallo, *Spectroscopy*, 2015, **30**, 2–6.

[257] P. Gaines, *ICP Operations Guide: Part 7: Linearity and Detection Limits*, https://www.inorganicventures.com/icp-guide/linearity-and-detection-limits.

[258] I. Rezić and M. Zeiner, *Monatshefte fur Chemie*, 2009, **140**, 325–328.

[259] U.K Health and Safety Executive (HSE), *Selecting protective gloves for work with chemicals*, Hse technical report, 2000.

[260] U.K Health and Safety Executive (HSE), *Dust in the workplace General principles of protection Guidance Note EH44 (Fourth edition)*, 2013.

[261] J. Wang, Z. Ma, L. Chen, H. Sun and W. Fan, Key Eng. Mater., 2018, pp. 32–35.

[262] P. Čech and J. Stádník, *Polish J. Environ. Stud.*, 2021, **30**, 4945–4955.

[263] A. Leggio, E. L. Belsito, G. De Luca, M. L. Di Gioia, V. Leotta, E. Romio, C. Siciliano and A. Liguori, *RSC Adv.*, 2016, **6**, 34468–34475.